Heinrich Heine
Universität
Düsseldorf

Lantibiotic resistance in human pathogens

Inaugural-Dissertation

zur Erlangung des Doktorgrades
der Mathematisch-Naturwissenschaftlichen Fakultät
der Heinrich-Heine-Universität Düsseldorf

vorgelegt von

Julia Gottstein

aus Bonn

Düsseldorf, 14.09.2023

From the Institute of Biochemistry

at the Heinrich Heine University Duesseldorf

Published by permission of the Faculty of Mathematics and Natural Science at the Heinrich Heine University Duesseldorf

Supervisor: Prof. Dr. Sander Smits
Co-supervisor: Prof. Dr. Holger Gohlke

Date of oral examination: 23.10.2023

“A hero is not the one who never falls, she is the one who gets up, again and again, never losing sight of her dreams” - Naruto

火影は オレの夢 だから - Naruto

Abstract

The development of resistance in human pathogens against antibiotics threatens increasingly global public health. Therefore, it is necessary to investigate antibiotic alternatives, the mode of action of new potential drugs, and the pathogens' resistance mechanism to find new treatment options. One of the most crucial antibiotic targets is peptidoglycan synthesis (PGN) which exclusively occurs in bacteria. Antimicrobial peptides (AMPs), targeting PGN- synthesis such as nisin and colistin, are considered promising alternatives against multidrug-resistant bacteria. Despite this, human pathogenic bacteria conferring resistance against these compounds evolved, by expressing a membrane-traversing ATP-binding cassette transporter of the bacitracin efflux (BceAB) type. In the human pathogen *Streptococcus agalactiae* COH1, the upregulation of the genes located within nisin resistance operon confers resistance against the antimicrobial peptide nisin. The proteins expressed are the serine protease *Sa*NSR, cleaving the 6 last amino acids of nisin, the two-component system *Sa*NsrK and *Sa*NsrR, and the BceAB transporter *Sa*NsrFP.

In this thesis, the BceAB transporter was shown to be actively involved in sensing the antibiotic, defends the cell wall by an ATP-hydrolysis-dependent mechanism that separates bacitracin from the cell wall precursor, and initiates a secondary defense mechanism that leads to cell wall modification.

The large extracellular domain of *Sa*NsrP was expressed, purified and characterized and the interaction with bacitracin was confirmed. This supports the described mechanism of *Sa*NsrFP which involves sensing an antibiotic attack via its large extracellular domain.

Within the scope of this work, compounds were screened to identify high affinity binding inhibitors which act specifically against NSR and NsrFP. In a primary screen, one potential compound (an indole-urea derivative) was discovered that is able to specifically inhibit both resistance proteins while not influencing the growth of the sensitive bacterial strain. This compound needs to be optimized for future experiments as it showed moderate µM activity.

Zusammenfassung

Die Zunahme antibiotikaresistenter Krankheitserreger bedroht die öffentliche Gesundheit weltweit. Um neue Behandlungsmöglichkeiten zu finden, ist es daher notwendig, Antibiotika-Alternativen, die Wirkungsweise neuer potenzieller Medikamente und den Resistenzmechanismus der Erreger zu untersuchen. Einer der wichtigsten Angriffspunkte für Antibiotika ist die Peptidoglykan-Synthese (PGN), die ausschließlich in Bakterien stattfindet. Antimikrobielle Peptide (AMPs), die wie Nisin und Colistin auf die PGN-Synthese abzielen, gelten als vielversprechende Alternativen gegen multiresistente Bakterien. Trotzdem haben humanpathogene Bakterien, gegen diese Wirkstoffe zum Beispiel durch Expression eines membranständigen ATP-bindenden Kassettentransporters vom Typ Bacitracin Efflux (BceAB) Resistenzen entwickelt. Im humanen Erreger *Streptococcus agalactiae* COH1 verleiht die Expression des Nisin-Resistenz-Operons eine Resistenz gegen das antimikrobielle Peptid Nisin. Es besteht aus einer Serinprotease *Sa*NSR, die die letzten 6 Aminosäuren von Nisin spaltet, einem Zweikomponentensystem *Sa*NsrK und *Sa*NsrR sowie einem BceAB-Transporter *Sa*NsrFP.

In dieser Arbeit wurde gezeigt, dass der BceAB-Transporter aktiv an der Erkennung des Antibiotikums beteiligt ist, die Zellwand durch einen ATP-Hydrolyse-abhängigen Mechanismus verteidigt, der Bacitracin vom Zellwandvorläufermolekül abtrennt, und einen sekundären Verteidigungsmechanismus initiiert, der zu Zellwandmodifikationen führt.

Ein weiteres Ziel dieser Studie war die stabile Expression, Reinigung und Charakterisierung eines kürzeren Konstrukts der großen extrazellulären Domäne von *Sa*NsrP. Dies wurde erfolgreich durchgeführt, und die Interaktion mit Bacitracin konnte mittels Tyrosinfluoreszenz und MALS bestätigt werden. Dieses bestätigt, dass *Sa*NsrFP aktiv bei der Antibiotika-Erkennung involviert ist, indem es über seine große extrazelluläre Domäne das Antibiotikum Bacitracin bindet. Im Rahmen dieser Arbeit wurden zudem Verbindungen gescreent, um hochaffine Bindungsinhibitoren zu identifizieren, die spezifisch gegen *Sa*NSR und *Sa*NsrFP wirken. In einem ersten Screening wurde eine potenzielle Verbindung (ein Indol-Harnstoff-Derivat) entdeckt, die in der Lage ist, beide Resistenzproteine

spezifisch zu hemmen, ohne das Wachstum des Kontroll-Bakterienstamms zu beeinflussen. Diese Verbindung muss für künftige Experimente optimiert werden, da sie im mikromolaren Bereich Aktivität zeigte.

Table of Contents

Abbreviations

3D	three-dimensional
Å	Angström
ADP	Adenosine-5-diphosphate
AMP	antimicrobial peptide
ATP	Adenosine triphosphate
B. subtilis	*Bacillus subtilis*
C. difficile	*Clostridioides difficile*
Dha	dehydroalanine
DMSO	Dimethylsulfoxide
DNA	Desoxyribonucleic acid
ECD	extracellular domain
GlcNAc	N-acetylglucosamine
HK	Histidine kinase
HPLC	high pressure liquid chromatography
HRP	Horseradish peroxidase
IC_{50}	Half maximal inhibitory concentration
IMHK	Intramembrane histidine kinase
K_D	dissociation constant
kDa	kilo Dalton
L. lactis	*Lactococcus lactis*
Lan	lanthionine
L-PG	Lysyl-phosphatidylglycerol
LTA	Lipoteichoic acid
mRNA	messenger ribonucleic acid
MALS	Multi-angle light scattering
MeLan	Methyl-lanthionine
µM	micromolar
mM	milli molar
MRSA	Methicillin-resistant factor protein
MurNAc	N-acetylmuramic acid
NBD	nucleotide-binding domain

Ni	nickel
NICE	nisin controlled gene expression
nm	nano meter
nM	nanomolar
NRP	Non-ribosomally synthesized peptide
NSR	nisin resistance protein
NTA	Nitrilotriacetic acid
PBP	Penicillin-binding proteins
PGN	peptidoglycan
PTM	Post-translational modification
RiPP	Ribosomally synthesized and posttranslationally modified peptide
RP	reverse phase
RNA	ribonucleic acid
RR	response regulator
SEC	Size exclusion chromatography
S. aureus	*Staphylococcus aureus*
S. gallinarum	*Staphylococcus gallinarum*
S. mutants	*Streptococcus mutans*
S. agalactiae	*Streptococcus agalactiae*
Sa	*Streptococcus agalactiae*
S.coelicolor	*Streptomyces coelicolor*
S. venezuelae	*Streptomyces venezuelae*
TCS	two-component system
TMD	trans membrane domain
TMH	trans membrane helix
UP	undecaprenyl phosphate
UPP	undecaprenyl pyrophosphate
UDP	uridine diphosphate
WTA	Wall teichoic acid

Amino acid	Three letter code	One letter code
Alanine	Ala	A
Arginine	Arg	R
Asparagine	Asn	N
Aspartic Acid	Asp	D
Cysteine	Cys	C
Glutamic Acid	Glu	E
Glutamine	Gln	Q
Glycine	Gly	G
Histidine	His	H
Isoleucine	Ile	I
Leucine	Leu	L
Lysine	Lys	K
Methionine	Met	M
Phenylalanine	Phe	F
Proline	Pro	P
Serine	Ser	S
Threonine	Thr	T
Tryptophan	Trp	W
Tyrosine	Tyr	Y
Valine	Val	V

List of Tables and Figures

1 Introduction

1.1 Antimicrobial Peptides

Antimicrobial peptides are natural products that are part of the innate immune system and can be isolated from organisms across all kingdoms of life (Chen and Lu, 2020, Malmsten, 2014). They are short, amphipathic oligopeptides of 5 to 100 amino acids with a positive net charge ranging from +2 to +11 (Pasupuleti *et al.,* 2012; Bin Hafez *et al.,* 2021). Over 3000 antimicrobial peptides have been identified so far and via bioinformatic peptide mining tools like BAGEL4, RIPPMiner or RODEO even more will be discovered (van Heel *et al.,* 2018, Montalban-Lopez *et al.,* 2021, Chen and Lu, 2020). Antimicrobial peptides are of high pharmaceutical interest due to the fact that they can have antibacterial (Diep and Nes, 2002, Malmsten, 2014), antifungal (Buda De Cesare *et al.,* 2020, Makwana *et al.,* 2023), antiviral (Fu *et al.,* 2021, Urmi *et al.,* 2023), antiparasitic (Rojas-Pirela *et al.,* 2023, Chen *et al.,* 2023a) even antitumor (Liu *et al.,* 2022, Pandit *et al.,* 2011), and antinociception activity (Iorio *et al.,* 2014, Green and Olivera, 2016).

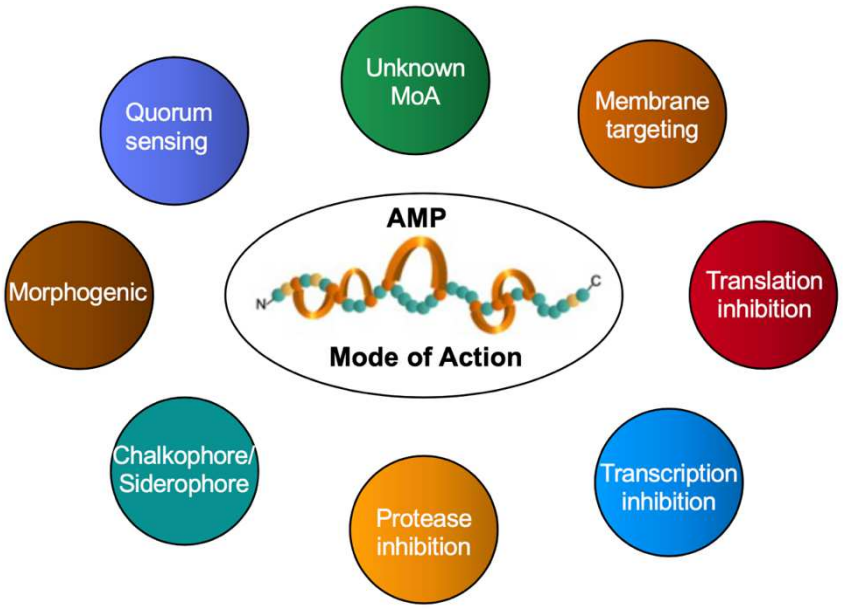

Figure 1: Mode of actions of antimicrobial peptides. The image was modified from (Ongpipattanakul *et al.,* 2022)

These peptide antibiotics can target the membrane, inhibit transcription, translation, and proteases, or function as chalko-or siderophores but there are

still peptides with unknown modes of action (Figure 1) (Ongpipattanakul *et al.,* 2022, Chen and Lu, 2020, Arnison *et al.,* 2013, Rushworth *et al.,* 2022, Schmidt *et al.,* 2005).

Based on their synthesis, the peptides can be divided into two major classes: ribosomally synthesized and post-translationally modified peptides (RiPP) and non-ribosomally synthesized peptides (NRP) (Montalban-Lopez *et al.,* 2021). The latter type of biosynthesis does not require mRNA, thus, resulting peptides can contain non-proteinogenic amino acids and fatty acids besides other post-translational modifications (PTM) (Marahiel and Essen, 2009, Schwarzer *et al.,* 2003). Well-known examples of non-ribosomally synthesized peptide antibiotics are bacitracin and vancomycin (Economou *et al.,* 2013, Schwarzer *et al.,* 2003). RiPPs will be discussed more in detail in section 1.2.1.

In the past several decades, bacteria have become increasingly multidrug-resistant, posing a severe threat to global health, thus antimicrobial peptides have gained importance. Interestingly, bacteria represent also an important source of antimicrobial peptides.

1.2 Bacteriocins and their Classification

AMPs of bacterial origin are referred to as bacteriocins. They are synthesized by Gram-positive and Gram-negative bacteria under specific stress conditions. Targeted are often closely related species (Smits *et al.,* 2020, Diep and Nes, 2002) while producing strains have specialized mechanisms to confer immunity against their own bacteriocin (Alkhatib *et al.,* 2012, Draper *et al.,* 2008). An advantage of bacteriocins is their antibacterial activity in the nanomolar range (Antoshina *et al.,* 2022, Reiners *et al.,* 2017). Bacteriocins can be classified according to their structural characteristics, biosynthetic pathway, phylogenetic affiliation of their producing strain, mode of action, and posttranslational modification (Arnison *et al.,* 2013, Klaenhammer, 1993).

1.2.1 Bacteriocins from Gram-negative bacteria

Colicins are high molecular mass (30-80 kDa) proteins encoded on a plasmid and produced by many *E. coli* strains (Cascales *et al.,* 2007). They consist of three

different functional domains: 1) a translocation domain at the N-terminus, mediating transport across the outer membrane, 2) a receptor binding domain, and 3) a C-terminal pore-forming domain (Wiener *et al.,* 1997). Regulation of the production of the bacteriocin is mediated by the SOS response regulon which is activated in response to DNA damage in bacteria. Colicins can kill their target cells via three possible mechanisms: 1) by forming pores in the inner membrane of the target bacteria, 2) by degrading the peptidoglycan, or 3) by nuclease activity (Upatissa and Mitchell, 2023, Cascales *et al.,* 2007).

Microcins are low molecular weight (<10 kDa) and ribosomally synthesized bacteriocins produced by *Enterobacteriaceae* (Cascales *et al.,* 2007). They can be either encoded within a plasmid or on the chromosome and can be divided into two classes: Class I consists of small-sized (<5kDa), heavily post-translationally modified peptides and class II are either unmodified, minimally modified, and larger microcins (Cole *et al.,* 2022, Markovic *et al.,* 2022). Class II microcins are produced as precursor peptides, containing an N-terminal secretion signal sequence fused to the core microcin peptide. Maturation and transport occur via C39 peptidase-containing ABC transporters, a membrane fusion protein, and TolC, an outer membrane efflux protein (Cole *et al.,* 2022). Once processed and matured, the AMP is able to induce pore-formation, nuclease activity, inhibition of replication, and protein synthesis (Severinov *et al.,* 2007, Markovic *et al.,* 2022).

1.2.2 Bacteriocins from Gram-positive bacteria

Bacteriocins from Gram-positive bacteria can be divided into three distinct classes: Class I contains small (≤10kDa) peptides that are post-translationally modified by specific enzymes, whose genes are also located in the peptide biosynthetic gene clusters, so-called RiPPs (Cotter *et al.,* 2013, Antoshina *et al.,* 2022, Alvarez-Sieiro *et al.,* 2016). RiPPs are usually located with their modification enzymes in a gene cluster on the genome or on mobile gene elements (Arnison *et al.,* 2013, Bartholomae *et al.,* 2017). The biosynthetic gene cluster contains genes that code for enzymes, which catalyze the PTMs, a two-component system (TCS; optional), an exporter protein, a peptidase (optional), and a self-defense system that protects the producer against its own antimicrobial peptide (Hudson and Mitchell, 2018, Bartholomae *et al.,* 2017). The biosynthesis

of RiPPs at the ribosomes depends on mRNA and results first in a precursor peptide, ranging from 20 to 110 aa residues. This precursor contains an N-terminal leader peptide and a C-terminal core peptide (Figure 2) (Arnison *et al.,* 2013, Oman and van der Donk, 2010, Lagedroste *et al.,* 2020). The leader peptide is essential to keep the peptide in an inactive state and for the recruitment of the PTM-enzymes as well as further processing steps and export (van der Meer *et al.,* 1994, Abts *et al.,* 2013, Mavaro *et al.,* 2011, Lagedroste *et al.,* 2021). Only the core peptide is modified at specific amino acids which most frequently are cysteine residues in RiPP. Thus, the thiol group is converted to form for example (methyl-)lanthionine rings which are characteristic of lanthionine-containing peptides (Arnison *et al.,* 2013). Lanthipeptides are a large subgroup of class I bacteriocins and are mainly produced by lactic acid bacteria. Some well-studied examples are nisin, mersacidin and lacticin 3147. Further subclassification of class I bacteriocins depends on the type of posttranslational modification present in the peptide.

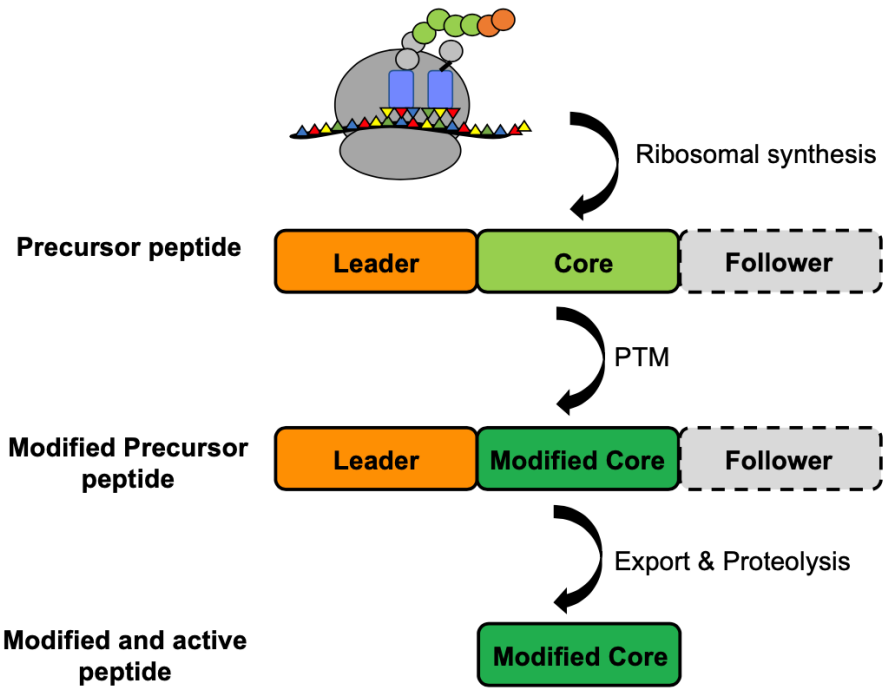

Figure 2: RiPP biosynthesis pathway. Peptides are synthesized at the ribosomes as precursor peptides. They can be subdivided in leader-peptide (orange), core peptide (light green), and in some cases, there is a follower peptide (grey) attached. Post-translational modifications are only installed within the core peptide. After the export, activation of the peptide

is achieved when the leader peptide is cleaved off. Scheme of biosynthesis pathway was modified from (Tung and van der Donk, 2021). Image created with Powerpoint 16.72.

Class II bacteriocins are defined as heat-stable unmodified peptides with a molecular mass ≤10kDa (Cotter *et al.,* 2013, Alvarez-Sieiro *et al.,* 2016). Subgroups are pediocin-like peptides, two peptides bacteriocin, leaderless or single peptides (Antoshina *et al.,* 2022, Nissen-Meyer *et al.,* 2009). The activity of these peptides is based on their ability to insert into membranes, inducing membrane depolarization and cell death. Well-known examples are Lactococcin A and pediocin PA1.

In class III large, heat-labile bacteriocins with molecular masses ≥10 kDa are divided into two subclasses: bacteriolysins, which function as peptidoglycanases, and non-lytic bacteriocins which inhibit carbohydrate transport, replication of DNA, or synthesis of proteins (Zimina *et al.,* 2020, Cotter *et al.,* 2013).

This classification system is based on the antimicrobial activity of the bacteriocin but one of its weaknesses is the exclusion of lanthipeptides without antimicrobial activity. Furthermore, the increasing number of newly, via genome mining tools, discovered structurally diverse peptides made it necessary to establish another classification system. The new classification system was introduced in 2013 and is based on the characteristics of the modification enzymes (Arnison *et al.,* 2013) which will be further discussed in section 1.3.

1.3 Lanthipeptides

Lanthipeptides are mainly found in Gram-positive bacteria but are not restricted to them as they also occur in Gram-negative and cyanobacteria (Tracanna *et al.,* 2017, Li *et al.,* 2010, Wang *et al.,* 2023). In general, peptides of this class contain two specific amino acid modifications, the bis-amino-bis acids lanthionine (Lan) or 3-methyllanthionine (MeLan)(Newton *et al.,* 1953, Ingram, 1969). The PTM is a two-step reaction, catalyzed by one or two enzymes. In the first step, serine and threonine residues are dehydrated to form the unsaturated **α**, **β** amino acids 2,3-didehydroalanine (Dha) and 2,3-didehydrobutyrine (Dhb) (Gross and Morell, 1967, Gross and Morell, 1968). Subsequently, these amino acids form (methyl-) lanthionine rings with a cysteine residue via a Michael-type condensation. Lanthipeptides are typically synthesized as inactive precursors containing an N-

terminal leader peptide and a core peptide. Only the core peptide undergoes posttranslational modifications, not the leader peptide, which is recognized by the modification enzymes and the exporting ATP-binding cassette (ABC) transporter. In the last maturation step, the leader peptide is cleaved off by specific or nonspecific peptidases, releasing the active lanthipeptide (Gross and Morell, 1967, Corvey *et al.,* 2003).

1.3.1 The Classification of Lanthipeptides

The nomenclature of the biosynthetic gene cluster of lanthipeptides is based on the generic locus symbol *lan* and Lan for the proteins. Each individual gene and protein product from the lanthipeptide gene cluster derives its name from the produced lanthipeptide (e.g., nis / Nis for nisin) and a capital letter, which refers to the protein function within the biosynthetic cluster (i.e. A stands for the pre-lanthipeptide, B for the dehydratase, C for the cyclase, etc.).

Lanthipeptides can be categorized into five different classes based on the characteristics of their modification enzymes (Figure 3) (Smits *et al.,* 2020, Xu *et al.,* 2020, Ortiz-Lopez *et al.,* 2020, Arnison *et al.,* 2013). In class I the dehydration and the cyclization are catalyzed by a LanB enzyme and a LanC enzyme which form a complex in the cell. After maturation, the modified precursor peptide is secreted by the transporter LanT and activated by cleaving off the leader peptide by a specific protease LanP (Lagedroste *et al.,* 2017, Montalban-Lopez *et al.,* 2018). Lanthipeptides of this class are i.e nisin (Figure 4), gallidermin, and subtilin which show antimicrobial activity in the low nanomolar range against Gram-positive bacteria (Reiners *et al.,* 2017).

In class II, these enzymatic modification reactions are performed by a single, bifunctional protein LanM which contains a dehydratase domain and a LanC-like cyclase domain. Subsequently, the pre-peptide is exported by LanT and the leader is cleaved off (Repka *et al.,* 2017, Chatterjee *et al.,* 2005). Prominent examples of this class are mersacidin (Figure 4), lacticin 481, actagardine, and cinnamycin.

The class III (LanKC) and class IV lanthipeptide (LanL) modification-enzymes consist of a lyase-, kinase-, and a C-terminal cyclase domain. The difference

between both classes is that the cyclase domain of LanKC is not Zn^{2+} dependent while in LanL the cyclase function relies on Zn^{2+}, similarily to LanC (Kodani *et al.,* 2004, Goto *et al.,* 2010, Xu *et al.,* 2020). Labyrinthopeptin A2, SapB and SapT are representatives of class III without antimicrobial activity. Venezuelin is part of class IV lanthipeptides (Figure 4).

In class V, a tri-protein synthetase composed of LanK, LanX and LanY catalyze the Ser/Thr dehydration and cyclization (Xu *et al.,* 2020, Ortiz-Lopez *et al.,* 2020). In 2020, Cacaodin (Figure 4) was identified as a class V lanthipeptide (Ortiz-Lopez *et al.,* 2020).

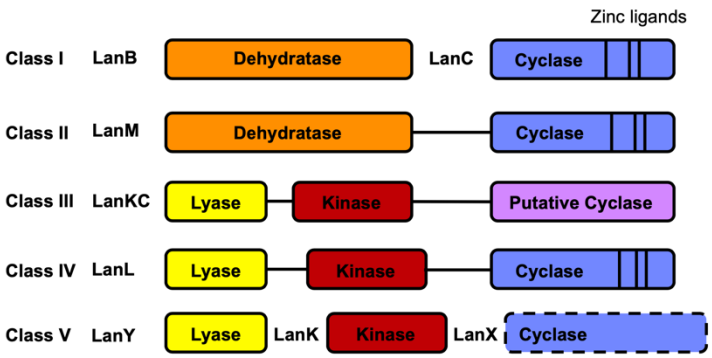

Figure 3: Classification of Lanthipeptides. Based on the biosynthetic enzymes for PTM, lanthipeptides can be subdivided into five different classes. In class I two enzymes catalyze the dehydration of Ser/Thr and the cyclization. LanM of class II is a fused protein of a dehydratase domain and a cyclase domain. Class III LanKC consisting of a lyase, kinase, and a putative cyclase domain, catalyzes the dehydration reaction and cyclization. Class IV LanL differs only from its LanC-like cyclase domain. In class V three different proteins install the modifications. Class I, III, and IV cyclization reactions depend on zinc as a ligand (black vertical lines). Class V cyclase domain has not yet been identified. Image modified from (Pei *et al.,* 2022) and created with Powerpoint 16.72.

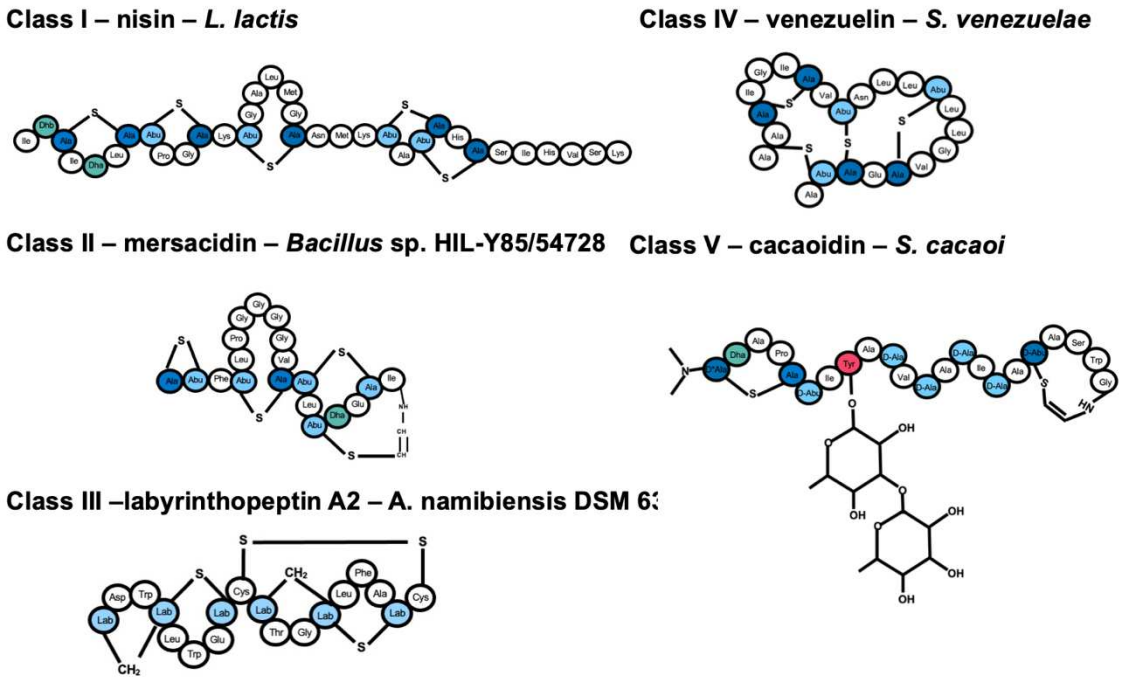

Figure 4: Schematic structure of representative lanthipeptides from each class. Unusual amino acids are highlighted in each structure. The most famous example of a class I lanthipeptide is nisin A. Class II and class III lanthipeptides are represented by mersacidin and labyrinthopeptin A2. An example of class IV and V lanthipeptides are venezuelin and cacaoidin. Image created with Powerpoint 16.72.

1.3.2 Bacitracin

Bacitracin is an antimicrobial peptide produced by *Bacillus subtilis* and *Bacillus licheniformis* by nonribosomal peptide synthases and contains D- and L-amino acids (Konz *et al.,* 1997, Nakano and Zuber, 1990). The peptide antibiotic shows a spectrum of activities e.g., bacitracin acts as a redox agent, binding divalent ions, in its metal-free form bacitracin inhibits bacterial subtilisin-type proteases, it can also inhibit protein disulfide isomerases and most importantly shows antimicrobial activity. Bacitracin binds undecaprenyl pyrophosphate (UPP) which is a lipid carrier that transports cell-wall precursor from the cell´s cytoplasm to its exterior. The bound UPP cannot be dephosphorylated which blocks its regeneration, resulting in the accumulation of intracellular peptidoglycan precursor (Storm, 1974, Storm and Strominger, 1973, Economou *et al.,* 2013, Kingston *et al.,* 2014). This leads to cell wall destabilization and growth inhibition, consequently leading to cell death. The status quo is that bacitracin forms a compact ternary 1:1:1 antibiotic-metal-lipid complex, creating a highly amphipathic structure that enhances membrane-binding affinity (Economou *et al.,* 2013). Due to the stabilizing effect and increased antimicrobial activity, a zinc-

bacitracin (Zn-bacitracin) complex has been commonly used in medical antibiotic formulations (Lightbown *et al*., 1964, Rietkotter *et al*., 2008).

Bacitracin has been used for medical applications for more than 70 years in human and veterinary medicine and also as an animal-feed additive (Johnson *et al.,* 1945, Lightbown *et al.,* 1964). Long-term usage of bacitracin in animals has led to the development of resistance genes in microorganisms, e.g., in bacteria (Manson *et al.,* 2004, Ohki *et al.,* 2003, Radeck *et al.,* 2016, Ma *et al.,* 2019).

1.3.3 Nisin

Nisin A from *Lactococcus lactis* was discovered as the first natural nisin variant in 1928 and is one of the best-studied antimicrobial peptides (Rogers, 1928, Field *et al.,* 2023). Up until now, 14 natural nisin variants are known (Figure 5): nisin Z from *Lactococcus lactis* NIZO 221 86 strain (Mulders *et al.,* 1991), nisin Q from *Lactococcus lactis* 61-14 (Zendo *et al.,* 2003), nisin U and U2 from *Streptococcus uberis* 42 and D536 (Wirawan *et al.,* 2006), nisin F from *Lactococcus lactis* F10 (de Kwaadsteniet *et al.,* 2008), nisin P from *Streptococcus gallolyticus* subsp. *Pasteurianus (Zhang et al., 2012, Wu et al., 2014)*, nisin H from *Streptococcus hypintestinalis* DPC 6484 (O'Connor *et al.,* 2015), nisin O1 to O4 from *Blautia obeum* A2-162 (Hatziioanou *et al.,* 2017), LanA1-4 from *Blautia producta* BP_{SCSK} (Kim *et al.,* 2019), nisin J from *Staphylococcus capitis* APC 2923 (O'Sullivan *et al.,* 2020), Kunicin A from *Apilactobacillus kunkeei* FF30-6 (Zendo *et al.,* 2020), nisin G from *Streptococcus salivarius* DPC6487 (Lawrence *et al.,* 2022) and nisin E from *Streptococcus equinus* APC4007 (Sugrue *et al.,* 2023). Nisin and its variants exhibit activity against a wide range of Gram-positive bacteria including clinically relevant *Staphylococcus aureus*, *Clostridium difficile*, *Bacillus cereus*, *Listeria monocytogenes,* and other streptococci, staphylococci, enterococci. Its high potency against multidrug-resistant bacteria has ignited an interest in its potential use as a biotherapeutic in human and animal health. Thus, it has been shown for nisin to be effectively used to treat atopic dermatitis (Valenta *et al.,* 1996), respiratory tract infections (De Kwaadsteniet *et al.,* 2009), staphylococcal mastitis (Cao *et al.,* 2007), sexually-transmitted infections (Aranha *et al.,* 2004), and gastrointestinal illnesses like colon infections (Kim *et al.,* 2003) and stomach ulcers (Dubois, 1995). Furthermore, recent microbiome-based studies have revealed the beneficial effect that nisin-producing bacteria have on the

gastrointestinal microbiome due to the inhibition of MDR pathogens (Heilbronner *et al.,* 2021, Garcia-Gutierrez *et al.,* 2019).

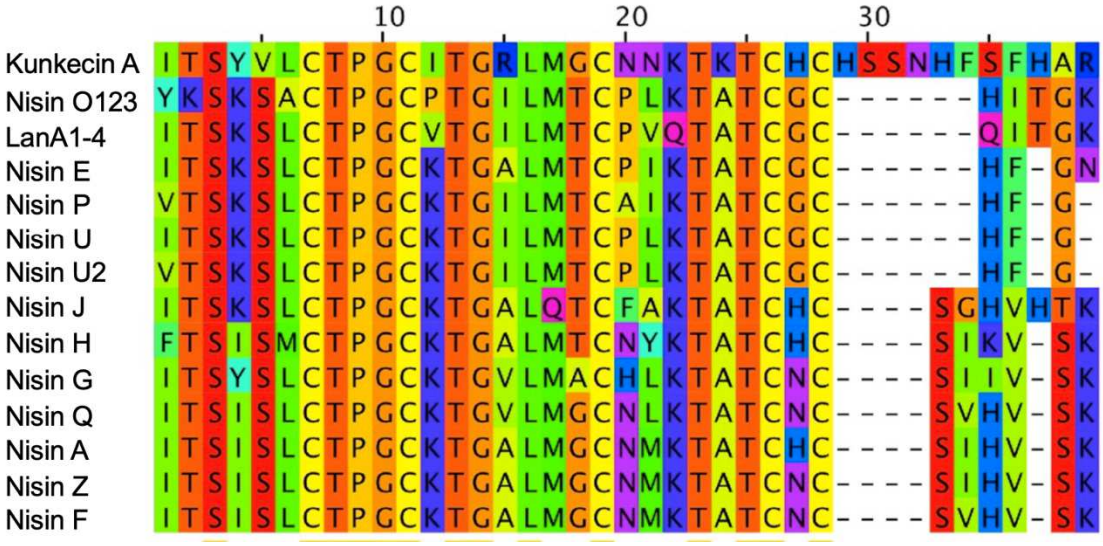

Figure 5: Overview of natural nisin variants. Sequence alignment of the natural nisin variants Kuncicin A, Nisin O1-3, nisin P, nisin U and U2, nisin J, nisin H, nisin Q, nisin A, nisin Z and nisin F. Alignment was created with Clustal Omega and via Jalview 2.11.0 the Taylor color code was applied (Taylor, 1997, Waterhouse *et al.,* 2009, Sievers *et al.,* 2011). Image was modified from (Field *et al.,* 2023).

Nisin consists of 34 amino acids and is an amphipathic peptide with a hydrophobic N-terminus and a hydrophilic C-terminus (Figure 6a). The structure of mature nisin, which was solved in 1991 via NMR spectroscopy, comprises three different parts (van de Ven, 1992). The N-terminus contains the (methyl-lanthionine rings A, B, and C and is involved in the binding of nisin to the cell wall precursor lipid II (Hsu *et al.,* 2004). A flexible hinge region connects the N-terminus with the last intertwined rings D and E of the C-terminus and grants the peptide flexibility which plays a crucial role during pore formation

The high antimicrobial activity of nisin is based on two modes of action of the peptide (Figure 6b & c). First, nisin binds specifically with its N-terminal lanthionine rings the cell wall precursor lipid II, thus inhibiting cell wall synthesis (Figure 6b). The second functionality is facilitated by the flexible hinge region which allows nisin to insert the rings D and E in the membrane which leads to pore formation (Figure 6c). Eight nisin and four lipid II molecules make up one pore of 2-2.5nm diameter, consequentially to the rapid efflux of cell content and eventually cell death (Bierbaum and Sahl, 2009, Breukink and de Kruijff, 2006).

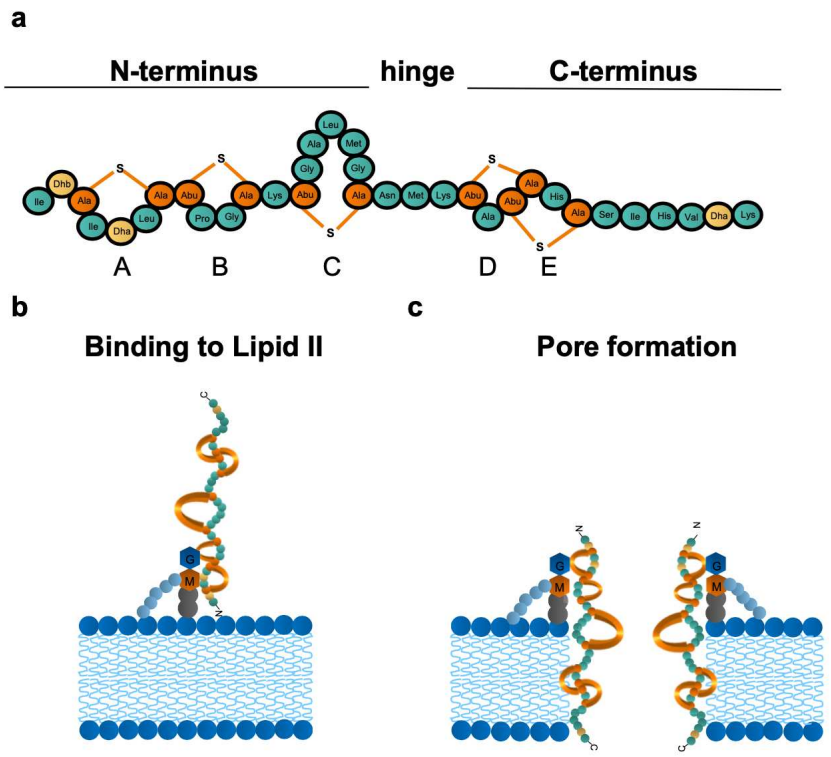

Figure 6: Schematic representation of nisin A and its dual mode of action. a) Nisin with its five characteristic lanthionine rings: Ring A-C are part of the N-terminus and the C-terminus comprises ring D & E. **b)** The N-terminal rings A & B of nisin bind lipid II. **c)** Pore formation of nisin. By binding lipid II and flipping the hinge region inside of the membrane. Pores have a diameter of 2-2.5 nm. Created with Powerpoint 16.72.

1.3.4 The nisin biosynthetic gene cluster

The nisin gene cluster in *L. lactis* contains eleven genes for synthesis, modification, transport self-immunity, and regulation: *nis*ABTCIPRKFEG (Figure 7) (Kuipers *et al.,* 1993, Siegers and Entian, 1995). Nisin is part of class I lanthipeptides with antimicrobial activity, thus termed as a lanthionine-containing antibiotic- short lantibiotic (Ingram, 1969). It is synthesized ribosomally as an unmodified precursor peptide consisting of an N-terminal leader peptide (23 amino acids) and a C-terminal core peptide of 34 amino acids. The core peptide of the precursor is post-translationally modified by two distinct modification enzymes, namely the dehydratase NisB and the cyclase NisC (Koponen *et al.,* 2002). They catalyze the dehydration of serines and threonine residues and the cyclization, generating one lanthionine- and four methyl-lanthionine rings. Subsequently, the modified nisin peptide is exported by NisT (Qiao and Saris, 1996). In the final step, NisP cleaves off the leader peptide to release the mature biologically active peptide (van der Meer *et al.,* 1993, Lagedroste *et al.,* 2017, Qiao and Saris, 1996)

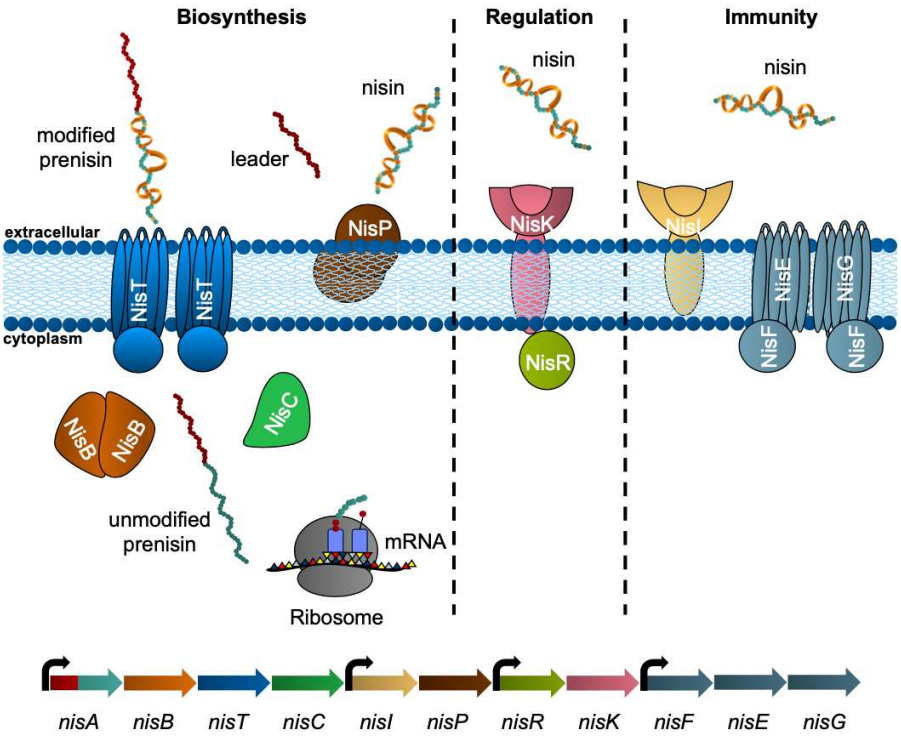

Figure 7: The nisin system. The nisin operon consists of 11 genes encoding biosynthesis, regulation, and immunity proteins. They comprise the lantibiotic nisin (red-green), the modification enzymes NisB (orange) and NisC (green), the exporter NisT (blue), the peptidase NisP, the TCS NisK and NisR and the lipoprotein NisI and ABC transporter NisFEG. Modified from (Abts, 2014) and created with Powerpoint 16.72.

1.3.5 Nisin bioengineering

The emergence of multi-drug resistance pathogens has challenged the effectiveness of commonly used antibiotics, resulting in an urgent need for new antimicrobial compounds. Lantibiotics are very promising alternatives due to their various advantages. An important advantage is that they are gene encoded which facilitates genetic manipulation. Nisin, as the most prominent representative of lantibiotics has been subjected to bioengineering in order to enhance its functional characteristics (Zheng *et al.,* 2022, Zaschke-Kriesche *et al.,* 2019b, Zaschke-Kriesche *et al.,* 2019a, Desmond *et al.,* 2022, Lagedroste *et al.,* 2019). All generated mutants together are beginning to form a blueprint of residues and domains essential for structure-activity relationships related to nisin biosynthesis, antimicrobial spectrum and activity, immunity or resistance proteins, solubility, or heat stability (Field *et al.,* 2023). Here, the focus will be on nisin variants that were successfully optimized in their characteristics in comparison to wild-type nisin A.

The substitution of N-terminal isoleucin 1 for an aromatic amino acid (I1W and I1F) led to a variant with superior antimicrobial activity against lactococcal strains expressing either one of the nisin immunity (nisI, nisFEG) or nisin resistance proteins (NSR, NsrFP)(Lagedroste *et al.,* 2019)

Also, when the threonine at position 2 was changed to a serine/ dehydroalanine nisin activity was improved against nonpathogenic target organisms (Kuipers *et al.,* 1995).

Two variants of nisin generated via saturation mutagenesis at positions 4-6 ($_4$KSI$_6$ and $_4$KFI$_6$) exhibited higher activity against several nonpathogenic strains (Rink et al. 2007) (Rink *et al.,* 2007). Notably, a few natural variants as well as novel nisin-like peptides like agalacticin and maddinglicin contain a lysine at position 4 (van Heel *et al.,* 2016).

The nisin I4V variant exhibited improved antimicrobial and antibiofilm activity against different strains of *Staphylococcus pseudintermedius (*Field *et al.,* 2015*).*

The ring C nisin variant M17Q performed better than nisin A at reducing biofilms of *Staphylococcus epidermidis* from medical device -related materials and significantly reduced viable cells in simulated wound experiments (Twomey *et al.,* 2020)

The hinge region of nisin consists of a 3-amino acid linker region which provides conformational flexibility between the N- and C-termini of nisin. This is critical for antimicrobial activity since after the interaction of the two N-terminal rings of nisin with lipid II, the flexible hinge region allows the insertion of the C-terminal domain into the membrane (Wiedemann *et al.,* 2001, Breukink and de Kruijff, 2006). Zhou *et al.,* (Zhou *et al.,* 2015) demonstrated that both shortened hinge peptides (-1 amino acid) and extended hinge peptides (+2 amino acids) displayed a higher efficacy against several target strains like *L. lactis, E. faecalis, L. monocytogenes,* and *B.cereus.*

Similarly, the extended hinge variant $_{20}$NMKIV$_{24}$ exhibited increased activity against lactococcal strains expressing the nisin immunity proteins (NisI and NisFEG) and the nisin resistance proteins (*Sa*NSR and *Sa*NsrFP)(Zaschke-Kriesche *et al.,* 2019b)

The C-terminus of nisin A, consisting of rings D and E with a six amino acid tail, is crucial for pore formation. It plays an important role in recognition by the nisin resistance protein NSR (Khosa *et al.,* 2016a). By treating an NSR-expressing lactococcal strain with a nisin variant lacking both rings or only ring E, it was demonstrated that NSR-provided resistance can be bypassed. Furthermore, it was shown that both rings are involved to ensure the exact coordination of the nisin cleavage point serine 29 at the enzymatic active site (Khosa *et al.,* 2016c).

Based on this, a nisin derivative (S29P) was identified. This variant displayed in comparison to nisin A a 20-fold increase in specific activity against NSR-producing strains (Field *et al.,* 2019). In the same study, a similar variant with an additional I30V substitution proved to be more stable.

Alternatively, the replacement of Cys 28 with proline resulted in a variant, that was more effective against NSR-producing strains while antimicrobial activity as well as pore formation ability were comparable to nisin A (Zaschke-Kriesche *et al.,* 2019a).

In a different study, several nisin ring mutants were generated including a variant containing installed rings A-D (CCCCA), A-C variant (CCCAA), a variant lacking the last six amino acids (Nisin 1-28 with 5 rings), and a variant missing the entire C-terminus (Nisin 1-22) (AlKhatib *et al.,* 2014b). Treatment of a lactococcal strain empty vector control strain with the CCCCA mutant, resulted in an 8-fold loss of antimicrobial activity in comparison to the wild-type nisin, while when treated with the CCCAA mutant or the nisin$_{1-28}$ mutant a 20-fold loss was exhibited. The nisin$_{1-22}$ variant without the C-terminus displayed a 25-fold loss of activity. When treating a strain that expressed the immunity conferring ABC transporter NisFEG, it became evident that the deletion of ring E resulted in a decrease of activity of NisFEG by 50%, and additional loss of ring D did not result in further reduction (AlKhatib *et al.,* 2014b). Furthermore, in the same study, the deletion of the final six amino acids reduced the activity of NisFEG to 60 % , whereas the truncated nisin$_{1-22}$ variant reduced the activity to 33%. Thus, it was concluded by the authors that the C-terminus of nisin is essential for its activity and that NisFEG requires the recognition of the C-terminus of nisin in order to provide full immunity (AlKhatib *et al.,* 2014b).

In a later study, the same C-terminal mutants, nisin H and gallidermin were used to treat lactococcal strains expressing *Sa*NsrFP (Reiners *et al.,* 2017). The latter were chosen due to their structural resemblance to nisin from the N-terminal part of the molecule while in the case of gallidermin the C-terminus is structurally distinct. In that study, the authors demonstrated that upon treatment with C-terminal variants of nisin, the fold of resistance of the *Sa*NsrFP-expressing strain increased in comparison when treated with the wild-type nisin (Reiners *et al.,* 2017). Since *Sa*NsrFP was still able to recognize the nisin mutants, gallidermin and nisin H, it was concluded that the N-terminus of the antimicrobial peptide is important for the transporter to be able to confer resistance (Reiners *et al.,* 2017).

For the natural nisin variant nisin H, the substitution of phenylalanine to isoleucine (F1I) resulted in a higher potency against lactococcal strains expressing the immunity proteins NisI, NisFEG, or the resistance proteins *Sa*NSR or *Sa*NsrFP (Reiners *et al.,* 2020).

Up until now, nisin, its variants as well as other antimicrobial peptides have demonstrated their high potential against Gram-positive bacteria. To affect Gram-negative bacteria, antimicrobial peptides need access to the inner membrane to reach their target (Nikaido and Vaara, 1985). Consequently, many antimicrobial peptides display poor activity towards Gram-negative species. However, disruption of the outer membrane with chelating agents e.g. EDTA allowed susceptibility to nisin (Stevens *et al.,* 1991). This indicated that nisin can kill Gram-negative bacteria if it can traverse the outer membrane. Thus, in a different approach anti-Gram negative peptides were fused to the C-terminal end of nisin (Zhou *et al.,* 2016, Li *et al.,* 2018). Several engineered variants were identified that exhibited greater activity against clinically relevant pathogenic Gram-negative bacteria including *E.coli*, *Klebsiella pneumonia*, *Acinetobacter baumanni*, *Pseudomonas aeruginosa* and *Enterobacter aerogenes (*Li *et al.,* 2018*)*.

1.3.6 Other lantibiotics

Lantibiotics show antimicrobial activity and many of these are highly active against multidrug-resistant pathogenic *staphylococci*, *enterococci*, *streptococci*, *clostridia (*Dischinger *et al.,* 2014*),* and some even against Gram-negative

bacteria (Mota-Meira *et al.,* 2000, Vestergaard *et al.,* 2019). They can have multiple modes of action e.g. inhibition of peptidoglycan synthesis, pore formation, or targeting a receptor in the cell wall. Similarly to nisin, subtilin, mersacidin, nukacin ISK-1, plantaricin C, lacticin 3147 and lichenicidin are binding lipid II or other peptidoglycan precursors in order to inhibit peptidoglycan synthesis (Brotz *et al.,* 1998, Wiedemann *et al.,* 2006a, Wiedemann *et al.,* 2006b, Shenkarev *et al.,* 2010, Fujinami *et al.,* 2018). Pore formation or membrane depolarization as a second mode of action can be found apart from nisin also in subtilin, Pep5 and epidermin (Bonelli *et al.,* 2006, Kordel *et al.,* 1989).

Cinnamycin or cinnamycin-like peptides change the phospholipid composition by targeting phosphatidyl ethanolamine, thus inhibiting phospholipase A2 (Marki *et al.,* 1991, Vestergaard *et al.,* 2019). Via this mode of action, the membrane permeability can be increased (Sokolove *et al.,* 1989).

The veterinary medicine, food, and pharmaceutical industry take advantage of the antimicrobial activity of lanthipeptides (Cotter *et al.,* 2013, Piper *et al.,* 2009, Dischinger *et al.,* 2014, Shin *et al.,* 2016, Delves-Broughton *et al.,* 1996). Lantibiotics are potent antibiotic alternatives and some are in preclinical and clinical phases of the development as a pharmaceutical drug. Prominent examples for treatment of clinically important pathogens like *C. difficile*, MRSA, or vancomycin-resistant *enterococci* infections are deoxy-actagardine B (NVB302, by Novacta Biosystems Limited)(Crowther *et al.,* 2013) which is a class II lanthipeptide derivative, the class I lanthipeptide NAI-107 (by NIACON)(Castiglione *et al.,* 2008) or the synthetic class II lanthipeptide mutacin 1140-S (by Organics)(Ghobrial *et al.,* 2009, Sandiford, 2020). Other lanthipeptides with partly even higher activity against MRSA and VRE than the antibiotic vancomycin, are mersacidin, lichenicidin(Bliα and Bliβ), lacticin 3147 (LctA/A2) and epilancin 15X (Brotz *et al.,* 1998, Piper *et al.,* 2009, Begley *et al.,* 2009, Ekkelenkamp *et al.,* 2005). The most active lanthipeptide with the highest potential against important pathogenic bacteria is NAI-107 and its derivatives produced by *Microbiospora sp*. 107891(Jabes *et al.,* 2011, Maffioli *et al.,* 2016). All these examples of pharmaceutically used lanthipeptides showcase the high potency of lantibiotics against clinically relevant pathogenic Gram-positive bacteria.

1.4 Lantibiotic Immunity and Resistance

Lantibiotics target cell wall precursors which are present in all bacteria. This makes lantibiotics very active bactericidal drugs. Thus, lantibiotic producer strains, need an immune or self-resistance system that protects them from killing themselves. Genes encoding for at least one or two immunity proteins are found in class I and II lanthipeptides' gene clusters. This can be a lipoprotein LanI and/or an ABC transporter LanFEG.

1.4.1 The Immunity Protein LanI – NisI

LanI is a peripheral-located protein, anchored to the membrane by a fatty acid chain that is attached to an N-terminal cysteine residue. It was shown that the deletion of *lanI,* in this case nisI, leads to the loss of immunity of the producer strain against its own lanthipeptide (AlKhatib *et al.,* 2014a). NisI grants immunity via two modes of action: first, it binds nisin via its C-terminus (Takala and Saris, 2006, Koponen *et al.,* 2004, AlKhatib *et al.,* 2014a, Hacker *et al.,* 2015, Jeong and Ha, 2018), protecting the cell wall of nisin-producing bacteria and second, by clustering the cells, reducing the available surface for the nisin (AlKhatib *et al.,* 2014a).

LanI genes can be found in gene clusters of lantibiotics that act via pore formation as a main mode of action.

The second line of defense against self-produced lantibiotics are LanFEG-type ABC transporters (Gebhard, 2012). They confer immunity by extruding the lantibiotic from the cytoplasmic membrane into the extracellular medium (Stein *et al.,* 2003, Otto *et al.,* 1998, Alkhatib *et al.,* 2012, Peschel and Gotz, 1996).

1.4.2 ABC transporter

ATP-binding cassette (ABC) transporters represent one of the largest superfamilies of membrane proteins and can be found in eukaryotes, archaea, and bacteria. They exhibit various physiological functions including nutrient uptake, the transport of signaling molecules, or conferring multidrug resistance by defending the cell by its specific resistance mechanism e.g. exporting antibiotics (Holland, 2003, Thomas and Tampe, 2018).

The typical architecture of ABC transporters consists of a homodimeric or heterodimeric transmembrane domain (TMD) of twelve transmembrane helices (TM) and a dimer-forming nucleotide-binding domain (NBD) (Beis, 2015). All of the characteristic sequence motifs of ABC transporters reside within the NBD. These are the Walker A, the Walker B, the H-loop, and the signature motifs the C-loop (LSGGQ) and the D-loop (Schmitt and Tampe, 2002, Zaitseva *et al.,* 2006). The NBDs bind and hydrolyze ATP which provides energy for the transport of a substrate across the membrane.

ABC transporters can be subdivided into seven classes, based on the sequence and structural homology in their TMDs (Thomas and Tampe, 2018). Types I-III import substrates e.g. nutrients, types IV and V function as exporters, while members of class VI function as extractors, and type VII ABC transporters can either be part of efflux pumps, operate as lipoprotein extractors, or regulate cell division.

In 2020 a new classification approach based on the fold of the TMD of the ABC transporter was proposed (Figure 8). Class I and II represent importers that are primarily found in bacteria and contain TMDs of five to ten TM helices (Oldham *et al.,* 2007, Korkhov *et al.,* 2012). Type III transporters uptake specific micronutrients into eubacteria but can be found also in archaea and plants (Xu *et al.,* 2013). Their TMDs consist of a transmembrane component and a membrane-embedded substrate-binding protein (Xu *et al.,* 2013, Thomas and Tampe, 2018) instead of two related TMDs.

Class IV transporters can have either homodimeric, heterodimeric, or single-chain TMDs consisting of six TMHs each. In this group, the ABC transporters can be drug exporters, metal-siderophore importers, ion channels, or regulators (Thomas *et al.,* 2020, Kamimoto *et al.,* 2012, Terasaka *et al.,* 2005, Dawson and Locher, 2006). Type V systems comprise ABCG/ABCA/Wzm type ABC transporter that includes on the one side channel-forming secretion systems in bacteria (Chen *et al.,* 2020) and on the other side importers such as ABCA4 (Quazi *et al.,* 2012). According to Thomas *et al.,* class VI and class VII systems are defined as ABC transporters, exhibiting TMD folds similar to type V systems, but lack an amphipathic N-terminal helix and extracellular reentrant helices between TMH5 and TMH6. Furthermore, MacB as a representative of type VII

ABC transporter contains only four TMHs as well as an additional coupling helix (Thomas *et al.,* 2020, Crow *et al.,* 2017).

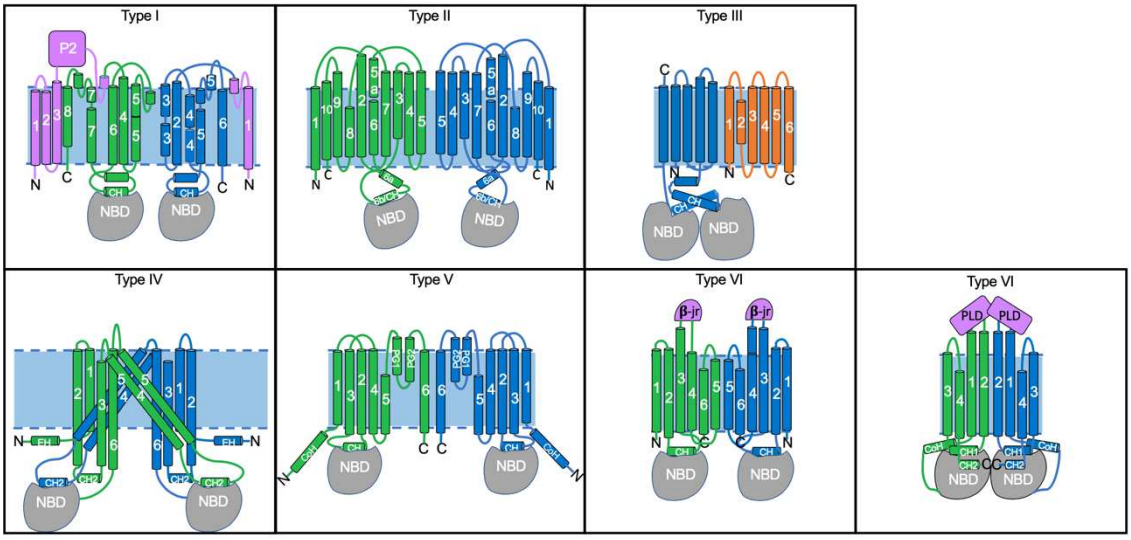

Figure 8: The different types of ABC transporters. Members of the ABC transporter superfamily can be subdivided into distinct types based on their TMD fold. The TMD architecture of each structure is depicted by a topology diagram. The two TMDs of each transporter are highlighted in green and blue, respectively. Substrate-binding components of type I-III folds are shown in orange, and auxiliary domains and additional TM helices are shown in pink. Class I and II represent importers that are primarily found in bacteria and contain TMDs of five to ten TM helices. Prominent examples are the importer $MalFGK_2$ -MalE and the importer $BtuC_2D_2$-F. Type III transporters have TMDs that consist of a transmembrane component and a membrane-embedded substrate-binding protein. An example is the importer EcfTAA´-FoIT. Class IV transporters can have either homodimeric, heterodimeric, or single-chain TMDs consisting of six TMHs each. P-gp, MsbA and CFTR are representatives of this class. Type V systems comprise channel-forming secretion systems in bacteria and on the other side importers such as ABCA4. Other examples are the exporters ABCG5/8 and ABCG2. Class VI and class VII systems are defined as ABC transporters, exhibiting TMD folds similar to type V systems, but lack an amphipathic N-terminal helix and extracellular reentrant helices between TMH5 and TMH6. One example is the extractor $LptB_2FG$ and for class VII the mechanotransmitter MacB. Image was modified from (Thomas *et al*., 2020)

1.4.3 The immunity ABC transporter LanFEG

The LanFEG-type ABC transporters belong to the class IV subfamily of MDR proteins, involved in the efflux of antibiotics, toxins macrolides, or other hydrophilic and hydrophobic compounds. They are encoded in gene clusters of lantibiotics, whose mode of action is to interfere with cell wall synthesis, bind to a specific receptor, or modify the lipid composition of the membranes (Peschel and Gotz, 1996, Altena *et al.,* 2000, Marki *et al.,* 1991). LanFEG-type immunity transporters are homologous to each other and share the same domain organization. Subunits of the LanFEG-type ABC transporters, LanF, LanE, and LanG are encoded on separate genes with a completely assembled transporter in a hypothesized stoichiometry of 2:1:1 (Siegers and Entian, 1995, Chatterjee *et*

al., 2005). LanF proteins are cytoplasmic and dimeric NBDs, providing the energy for substrate transport by hydrolyzing ATP. They share the common conserved ATP-binding cassette motifs but instead of the Q-loop, an E-loop can be found, which is highly conserved in LanFEG-type ABC transporters (Okuda *et al.,* 2010). This loop is thought to be involved in the communication of the NBDs with the TMDs, thus essential for lantibiotic transport (Okuda *et al.,* 2010, Oldham *et al.,* 2008).

LanE and LanG are integral membrane proteins, show high hydrophobicity, and have six putative TM helices (Stein *et al.,* 2005). They are functional heterodimers and are important for substrate binding and translocation (Stein *et al.,* 2003, AlKhatib *et al.,* 2014b, Stein *et al.,* 2005). Furthermore, LanFEG-type transporters confer immunity without any cross-reactivity and thus are specific for their native lantibiotic (Otto *et al.,* 1998). The exact mechanism of how the ABC transporter provides immunity is still unknown. However, several studies have shown data that support an efflux mechanism, where the exporter extrudes the lanthipeptide from the membrane (Stein *et al.,* 2005, Stein *et al.,* 2003, Otto *et al.,* 1998, Okuda *et al.,* 2010).

1.4.4 The ABC transporter NisFEG

NisFEG is the immunity-providing ABC transporter that protects *Lactococcus lactis* from nisin. It is conserved in all species producing nisin and shows similarity with other LanFEG transporters from strains producing other lantibiotics such as subtilin. NisF is the NBD of 25 kDa. The TMD consists of the proteins NisE (28 kDa) and NisG (24 kDa), each containing six predicted TM helices (Figure 9). It has been shown that the deletion of either NisF and NisE leads to a loss of immunity in comparison to the wild type, while mutations of NisG did not show a strong influence on immunity (Siegers and Entian, 1995). NisE and NisG contain conserved tryptophan/aromatic residues, that are hypothesized to be involved in the transport mechanism. In NisE there is a conserved Trp in helix V which is followed by a -PYTY-sequence which is a motif conserved among the immunity genes (Alkhatib *et al.,* 2012). Also, in NisG at the end of helix V, there is a conserved Trp.

NisFEG has been shown to remove nisin from the membrane (Stein *et al.,* 2003). When homologously expressed in *L. lactis*, it is able to confer a seven to eight-

fold of immunity against nisin, which represents 6-8% of immunity in comparison if NisI and NisFEG are together expressed (Stein *et al.,* 2003, AlKhatib *et al.,* 2014b, Koponen *et al.,* 2004, Takala and Saris, 2006, Geiger *et al.,* 2019, Draper *et al.,* 2009). Furthermore, an ATP-hydrolysis deficient mutant was generated by mutating H181 in NisF to alanine, and based on sequence comparison, it was identified to be the H-loop, which is an essential sequence motif present in all ABC transporters. The resulting $NisF_{H181A}EG$ strain still is able to bind ATP but cannot hydrolyze it, thus has lost its immunity (AlKhatib *et al.,* 2014b). In the same study, the authors were able to show via a fluorescence-based assay using a DNA-binding dye that NisFEG withstands pore formation until a concentration of 60 nM. They could also conclude that the immunity ABC transporter recognizes the C-terminus of nisin which is functionally associated with its pore formation mode of action (AlKhatib *et al.,* 2014b).

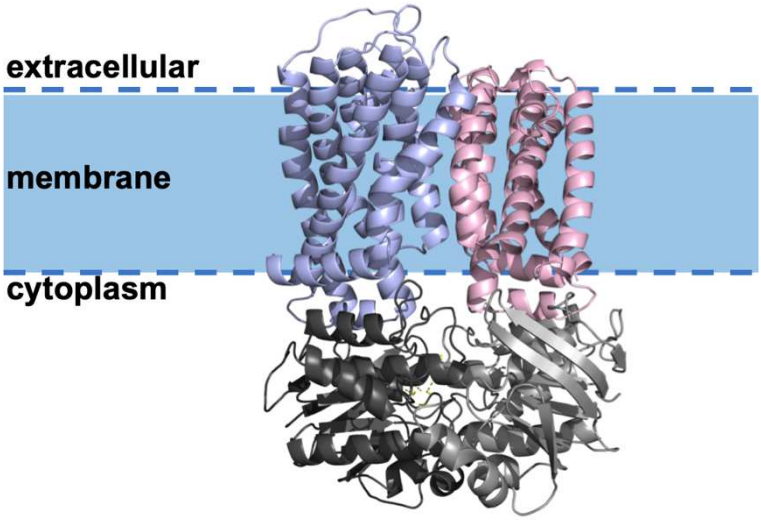

Figure 9: Model of the ABC transporter NisFEG calculated with Topmodel (Mulnaes *et al*., 2020) and was provided by Pablo Cea Medina. Subdomains are highlighted: NisE in light blue, NisG light pink, and the NBDs in black and grey. The image was created using PyMOL 2.3.0 and Powerpoint.

1.4.5 *Streptococcus agalactiae*

Streptococcus agalactiae (Group B streptococcus or GBS) is a Gram-positive pathogen that can asymptomatically colonize rectovaginal niches in women (Raabe and Shane, 2019). GBS infection can lead to invasive GBS disease which is a leading cause of global meningitis, neonatal and infant sepsis, bacteremia, pneumonia, and urinary tract infection in pregnant women and neonates (Chen *et al.,* 2023b, Hall *et al.,* 2017). GBS can be transmitted vertically from colonized mothers to the baby via the genital tract at or just before delivery. This may cause

within the first week of life early-onset invasive neonatal GBS disease (EOD) with symptoms of bacteremia and pneumonia (Schrag *et al.,* 2016, Madrid *et al.,* 2017). Appears a GBS infection later than the first week of life, it is referred to as late-onset disease (LOD), which manifests as bacteremia, urinary tract infection, and meningitis (Berardi *et al.,* 2013, Creti *et al.,* 2021). A report from the World Health Organization (WHO) and the London School of Hygiene & Tropical Medicine (LSHTM) emphasized that GBS infections are the cause of over half a million preterm births, leading to nearly 100,000 newborn deaths, 46,000 stillbirths annually, and significant long-term disability (Hall *et al.,* 2017).

The common treatment for GBS-colonized women or prophylaxis for women with risk factors for EOD is based either on penicillin, ampicillin, and cefazolin (Puopolo *et al.,* 2019). For penicillin-allergic patients, erythromycin and clindamycin are recommended (Puopolo *et al.,* 2019). Due to the overuse of antibiotics in hospitals, cattle production, and agriculture, bacteria develop mechanisms to become resistant. Up-to-date, researchers have informed about clinical isolates of *S. agalactiae* with reduced susceptibility to penicillin G and ampicillin (Mengist *et al.,* 2017, Kasahara *et al.,* 2010), as well as resistance to erythromycin, tetracycline, and clindamycin (Sadowy *et al.,* 2010).

In order to survive in a host and resist, a pathogen like *S. agalactiae* COH1 expresses virulence factors such as the nisin resistance system. Such multi-drug-resistant bacteria are highly problematic and challenge the global health system. Thus, it is of utmost importance to understand the resistance systems of pathogenic bacteria like *S. agalactiae* COH1 and find ways how to bypass them.

1.4.6 The nisin resistance operon

In contrast to the immunity system of lantibiotic-producing strains, non-producing bacteria have developed different mechanisms to prevent growth inhibition or cell death when encountering high levels of lantibiotics in their environment. These mechanisms can be a) modifications of the bacterial cell wall and membrane, leading to a repelling of cationic antimicrobial peptides (Draper *et al.,* 2015, Saar-Dover *et al.,* 2012), or b) based on ABC transporter-mediated detoxification (Gebhard, 2012) c) proteolytic degradation via a peptidase (Sun *et al.,* 2009) d) two-component system mediated resistance (Ohki *et al.,* 2003, Diagne *et al.,* 2022, Dintner *et al.,* 2014).

An example of such a resistance system is the nisin resistance system from *Streptococcus agalactiae* COH1, which encodes for the Bacitracin efflux (BceAB)-type ABC transporter *Sa*NsrFP, the nisin resistance protein *Sa*NSR, and a two-component system: NsrK and NsrR (Figure 10) (Khosa *et al.,* 2013, Khosa *et al.,* 2016c, Khosa *et al.,* 2016a).

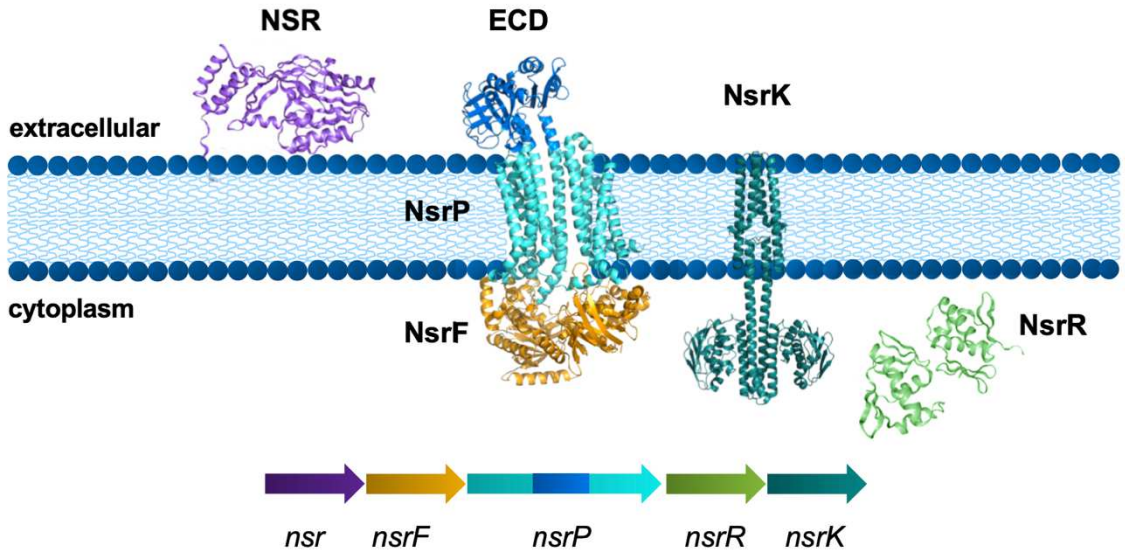

Figure 10: The NSR operon. Encoded are the serine protease *Sa*NSR (purple) (PDB:4Y68 (Khosa *et al.,* 2016a)), the ABC transporter *Sa*NsrFP, consisting of the NBDs *Sa*NsrF (orange), a TMD *Sa*NsrP (light blue) and its ECD (blue), and the two-component system *Sa*NsrR (green) (PDB:5DCM (Khosa *et al.,* 2016b)) and *Sa*NsrK (tealblue).

1.4.5.1 The TCS: NsrK and NsrR

TCS involved in lantibiotic resistance can be subclassified into two groups BceRS-like and LiaRS-like systems. Both types were first discovered in *B. subtilis*. The LiaRS-like TCS consists of three proteins, a kinase (LiaS), a response regulator LiaR, and a negative regulator of LiaR-mediated gene expression (LiaF)(Jordan *et al.,* 2006). A prominent example besides LiaRS from *L. monocytogenes* is VraRS from *S. aureus (*Qureshi *et al.,* 2014).

BceRS-like TCSs comprise a response regulator and an “intramembrane-sensing kinase”, lacking an extracellular domain (Mascher *et al.,* 2003, Dintner *et al.,* 2011).

NsrK belongs to the “intramembrane-sensing kinase” (IMSK) subfamily of histidine kinases. They are characterized by a short N-terminal sensory domain, composed of two TM helices separated by a short loop of less than 25 amino acids (Mascher *et al.,* 2003, Mascher, 2006). Due to their lack of an extracellular domain, they are not able to act as sensors for an antibiotic attack. Thus, it needs

to recruit accessory membrane proteins such as BceAB-type ABC transporter with an extracellular domain that can sense an external trigger (Clemens *et al.,* 2017, Khosa *et al.,* 2013). It has been shown for the IMSK NsaS from *S. aureus* that it controls several genes associated with cell-wall biosynthesis, lipid-modifying enzymes, proteases, and several membrane transporters (Mensa *et al.,* 2014, Bhate *et al.,* 2018). In general, the architecture of this type of kinases can be subdivided into three parts: 1) the TMD domain consisting of two TM helices, 2) the linker domain, and 3) a catalytic domain (Bhate *et al.,* 2018). IM-HKs contain HisKA, and HATPase domains for kinase activity and sometimes a HAMP domain for dimerization (Mascher, 2006). Furthermore, four key structural features were identified for NsaS: 1) it has a short N-terminal amphiphilic helix that anchors its four TM helices into the inner leaflet of the lipid bilayer, where it can sense membrane stress, antibiotic attacks that deform the bilayer or to interact with accessory proteins, 2) there is a break in the helical structure and increased dynamic at the membrane interface 3) the cytoplasmic linker of NsaS is an alpha-helical coiled-coil and 4) forms a dimer (Bhate *et al.,* 2018). The architecture of NsaS can be compared to NsrK since both are intramembrane histidine kinases (Figure 11).

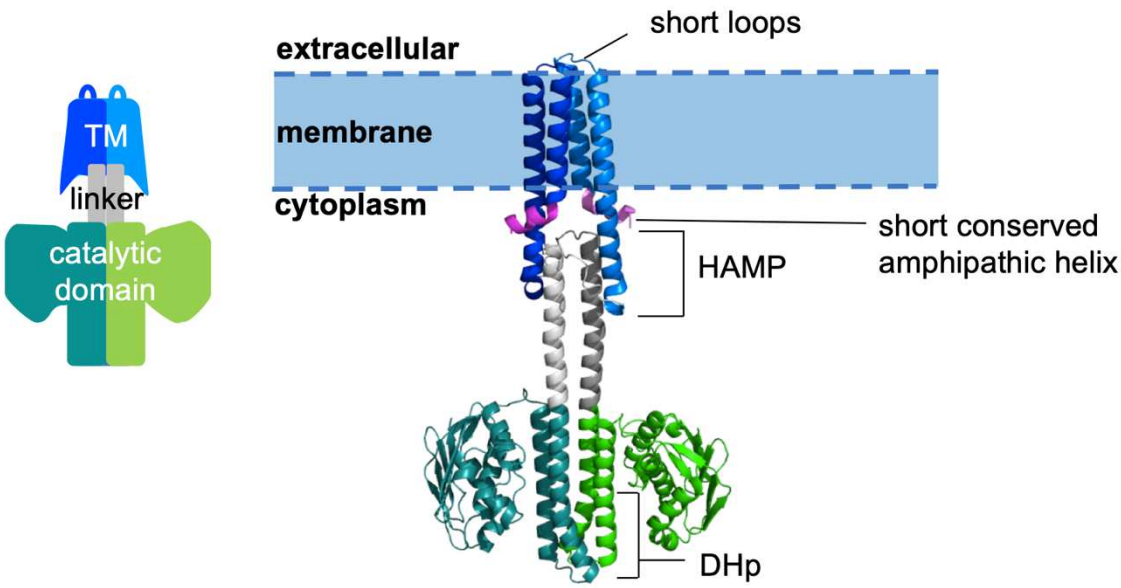

Figure 11: Model of *Sa*NsrK. The intra-histidine kinase *Sa*NsrK can be subdivided into three domains: TM domain (blue), containing the characteristic HAMP transfer domain, a linker domain (grey), and a catalytic domain (green), containing the cytoplasmic dimerization and histidine phosphotransfer domain (DHp). A short amphipathic helix at the N-terminus of the

TMD (pink) is conserved in intramembrane histidine kinases (Bhate *et al.,* 2018). Image created with PyMOL Version 2.3.0 and Powerpoint 16.72.

Furthermore, the involvement of a two-component system in antimicrobial resistance was also shown for *S. pneumoniae,* where it was demonstrated that TCS01 cooperates with a BceAB-type ABC transporter, which was located in a different gene cluster, to sense and induce resistance to structurally unrelated antimicrobial peptides that target precursor of the cell wall (Diagne *et al.,* 2022). For the BceRS-BceAB resistance system in *Bacillus subtilis,* the TCS and ABC transporter was proposed to form a sensory complex (Dintner *et al.,* 2014). It can be hypothesized that *Sa*NsrK shows similar mentioned characteristics.

The response regulators (RRs) of TCS function as phosphorylation-activated switches that regulate e.g., the upregulation of genes (West and Stock, 2001). The general architecture of RRs comprises a receiver domain and an effector domain, that are connected by a flexible linker (Stock *et al.,* 2000). Within the RD is a conserved aspartate residue which is phosphorylated by the histidine kinase upon reception of an external signal. This activates the ED which subsequently binds to specific promotors, initiating transcription of genes (West and Stock, 2001, Mitrophanov and Groisman, 2008). This has been shown for GraSR in *S. aureus* as well as for BceSR in *B. subtilis*, where lantibiotic attack activates the histidine kinase and the corresponding RR BceR and GraR promote the transcription of *gra*XSR, *vra*FG, and *bce*AB genes (Falord *et al.,* 2012, Ohki *et al.,* 2003). A similar function has been postulated for NsrR, where phosphorylation of its RD induces the expression of genes present in the nisin resistance operon (Khosa *et al.,* 2016b)

1.4.5.2 The nisin resistance protein NSR

The nisin resistance protein (NSR) from *S. agalactiae* COH1 is an endopeptidase, belonging to the S41 family of C-terminal processing peptidases (CTPs)(Khosa *et al.,* 2013, Khosa *et al.,* 2015). It is a 35 kDa protein that is highly hydrophobic and anchored via a 21 amino acid residues transmembrane sequence at its N-terminus (Froseth and McKay, 1991). The structure of NSR was solved in 2016 and comprises eleven **β**-strands and eleven **α**-helices that form three domains: an N-terminal helical bundle, the protease cap, and a core domain (Figure 12) (Khosa *et al.,* 2016a). These domains form a hydrophobic tunnel with a width of

10 Å. Using simulation and molecular docking, it was shown that nisin binds with its C-terminal in the tunnel near the catalytic dyad which consists of His_{98} and Ser_{236} (Khosa *et al.,* 2016a). Once nisin has bound, NSR cleaves off its last six amino acids, resulting in a nisin molecule with 100-fold reduced antimicrobial activity and lower affinity towards the cell membrane (Khosa *et al.,* 2013, Khosa *et al.,* 2016a, Sun *et al.,* 2009). Heterologous expression of NSR in *L. lactis* NZ9000 confers 20-fold resistance against nisin (Khosa *et al.,* 2013, Khosa *et al.,* 2016a).

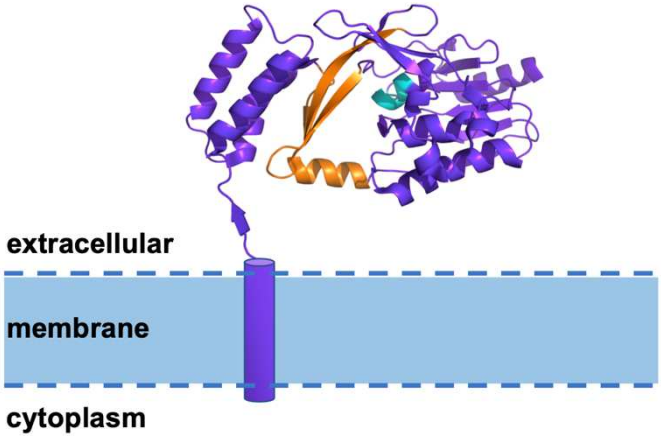

Figure 12: NSR- the nisin resistance protein (PDB ID: 4Y68). The structure of the serine protease NSR is shown. NSR is anchored in the membrane. The residues around the active site are highlighted in light blue, and the protease cap in orange. Image created with PyMOL Version 2.3.0 and Powerpoint 16.72.

1.4.5.3 Bacitracin efflux type ABC transporter

The first BceAB-type ABC transporter was identified in *B. subtilis* which conferred high-level resistance to bacitracin (Ohki *et al.,* 2003). Genomic analysis could show the presence of homologous BceAB transporters mostly in bacteria predominantly found in soil and in human pathogenic bacteria (Gebhard, 2012, Dintner *et al.,* 2011).

Adjacent to the bceAB genes, bceRS genes are located, encoding for a two-component system (TCS) that regulates the expression of transporters. The cognate Bce-TCS system consists of an intramembrane HK BceS that phosphorylates the response regulator BceR (Ohki *et al.,* 2003, Mascher, 2006). It has been shown for biotechnologically and medically relevant Gram-positive bacteria that BceS-like HKs require BceAB-type transporters for antibiotic signaling (Hiron *et al.,* 2011, Dintner *et al.,* 2014, Gebhard, 2012, Revilla-Guarinos *et al.,* 2014).

The structure of BceAB from *B.subtilis* was solved in 2022 at a resolution of 3.8 Å using single particle cryo-EM (George *et al.,* 2022). BceAB consists of two soluble BceA nucleotide-binding domains and one BceB domain with 10 characteristic TM helices (Dintner *et al.,* 2014). TM helices 1 to 4 and 7 to 10 form individual bundles, each representing an FtsX-domain fold like that observed in type VII mechanotransmission ABC transporters (Figure 13a) (Thomas *et al.,* 2020). TM helices 5 and 6 interact with one another and are positioned closer to helices 7-10 than to the other bundle, therefore creating an asymmetric arrangement (George *et al.,* 2022). Furthermore, these helices form together a V-shaped hydrophobic pocket where a lipid could bind (George *et al.,* 2022). The authors were also able to identify a UPP-derivate in this binding site, using liquid chromatography-tandem mass spectrometry. This aligns with the hypothesis that BceB recognizes peptide-lipid complexes such as bacitracin and undecaprenyl pyrophosphate (UPP) (Dintner *et al.,* 2014).

The hallmark for Bce-type transporters is a large extracellular domain (200-250 amino acids long) between TM helices 7 and 8 of BceB (Clemens *et al.,* 2017). The architecture of the ECD can be divided into three domains (Figure 13b): 1) a small alpha beta rich (SABRE) 2) a Porter domain and 3) stalk helices which is a fold similar to those seen in Gram-negative mechanotransmission ABC transporters MacB and LolCDE (George *et al.,* 2022).

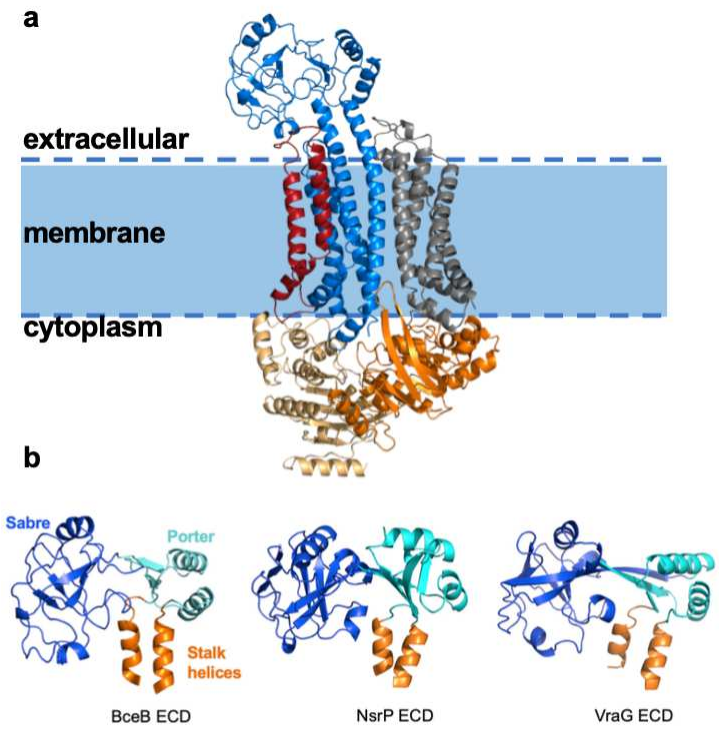

Figure 13: Architecture of the BceAB-type ABC transporter (George *et al.,* 2022) (PDB 7TCG). a) TM Helix bundles 1-4 (grey), TM helix bundles 7-10 (blue), TM helices 5 and 6 (red), and NsrF (light orange/ orange). **b)** ECDs of BceB, NsrP, and VraG in comparison. Subdomains are highlighted: Sabre domain in (blue), Porter domain (cyan), and stalk helices (orange). Models of NsrPECD and VraGECD were created using AlphaFold2 (Jumper *et al.,* 2021). Image created with PyMOL Version 2.3.0 and Powerpoint 16.72.

The ECD shows a very low sequence homology with other Bce-type ECDs (Clemens *et al.,* 2017). It has been proposed that the divergence of this domain directs specificity for resistance against different antimicrobial peptides in different Bce-type transporters (Dintner *et al.,* 2011, Clemens *et al.,* 2017). The status quo is that upon substrate binding e.g., to the ECD of the BceAB-transporter, the signal is transferred to the intramembrane histidine kinase which subsequently phosphorylates its cognate response regulator which induces the expression of the ABC transporter genes. This signal transduction pathway was described e.g. for TCS-Bce systems in *B. subtilis* (BceRS-AB, YxdJK-LM and YvcPQ-RS) (Dintner *et al.,* 2011, Dintner *et al.,* 2014, Staron *et al.,* 2011), in *S. aureus* (GraRS-VraFG, NsaRS-BraDE) (Cho *et al.,* 2021, Bhate *et al.,* 2018). The direct interaction of BceS and BceAB was shown in *B. subtilis*, where BceB, in order to initiate antibiotic resistance needs to form a complex with BceS (Dintner *et al.,* 2014).

Furthermore, it was found that ATP hydrolysis by BceA plays a crucial role in antimicrobial signaling (Rietkotter et al., 2008). Additionally, this type of signaling

is not possible in the absence of the transporter BceAB which strongly indicates that the transporter contains the sensor domain of this system (Revilla-Guarinos *et al.,* 2014, Bernard *et al.,* 2007). Furthermore, the binding of AMP LL-37 to the ECD of the homologous transporter VraG was described in *S. aureus* (Cho *et al.,* 2021). Several putative mechanisms for BceAB-type transporters have been proposed, ranging from AMP export, AMP removal from the membrane, flipping UPP to an ATP hydrolysis-driven mechanism, in which the target-AMP complex is recognized by the BceAB transporter and UPP is physically released from the bound bacitracin (Gebhard and Mascher, 2011, Kingston *et al.,* 2014, Kobras *et al.,* 2020). The expression of the BceAB-type transporter in *B. subtilis* is known to confer resistance against bacitracin and other antibiotics such as mersacidin, plectasine, and actagardine (Ohki *et al.,* 2003, Staron *et al.,* 2011).
Very recently, the structure of BceAB in complex with its cognate histidine kinase BceS was published, showing that the interaction of BceS via its TM helices with the TM helices of BceB is mediated by membrane lipids (George and Orlando, 2023). Furthermore, the authors demonstrate by performing ATPase assays on detergent-solubilized and purified BceAB and BceAB-BceS complex, that the activation of BceS requires BceAB and that both proteins regulate each other due to the significantly reduced maximal ATPase activity from the complex in comparison to the sole BceAB transporter. Via mutational experiments on BceS and testing the effect with ATPase assays, the strong influence of the conformation of BceS on the ATPase activity of the BceAB was demonstrated. In these experiments, the E115K variant of BceS reduced the ATPase activity of the complex while adding an H124Q mutation resulted in ATPase activity compared to the WT complex (George and Orlando, 2023).

1.4.5.4 The BceAB-type transporter *Sa*NsrFP

The nisin resistance operon is found in the clinically-relevant pathogen *S. agalactiae* COH1 (Khosa *et al.,* 2013, Alkhatib *et al.,* 2012) and is similar to the operon of BceAB from *B. subtilis*. It encodes for a BceAB- type transporter and a TCS. The only difference to the *bce* operon is that there is an additional gene encoding the membrane-embedded nisin resistance protein.
*Sa*NsrFP consists of an NBD *Sa*NsrF (28 kDa) which contains the typical ABC transporter signature motifs (Khosa *et al.,* 2013). The TMD domain *Sa*NsrP (74

kDa) comprises 10 TM helices. Similarily to BceAB, the TM helices 1 to 4 and 7 to 10 form individual bundles, each representing an FtsX-domain fold like that observed in type VII mechanotransmission ABC transporters (Thomas *et al.,* 2020). TM helices 5 and 6 interact with one another and are positioned closer to helices 7-10 than to the other bundle, therefore creating an asymmetric arrangement (Figure 14). Between helix 7 and 8, there is a large ECD of 221 amino acids. This ECD is the hallmark of BceAB-type transporters and is hypothesized to be involved in substrate binding and sensing (Ohki *et al.,* 2003, Clemens *et al.,* 2017, Khosa *et al.,* 2013). This aligns well with the fact that intramembrane HKs lack an extracellular domain to sense extracellular stimuli and with the observation of previous studies that demonstrated that *Sa*NsrFP does not need its cognate TCS system in order to provide resistance (Reiners *et al.,* 2017). If expressed in the nisin-sensitive *L. lactis* NZ9000 strain NsrFP conferred a 16-fold resistance against nisin A, and a 12-fold resistance against nisin H and gallidermin. Furthermore, using a Sytox-fluorophore-based assay, it was identified that NsrFP prevents the cells from nisin-induced pore formation at concentrations between 40 and 60 nM (Reiners *et al.,* 2017). Nonetheless, the exact mechanism and structure of the resistance system need to be investigated in more detail.

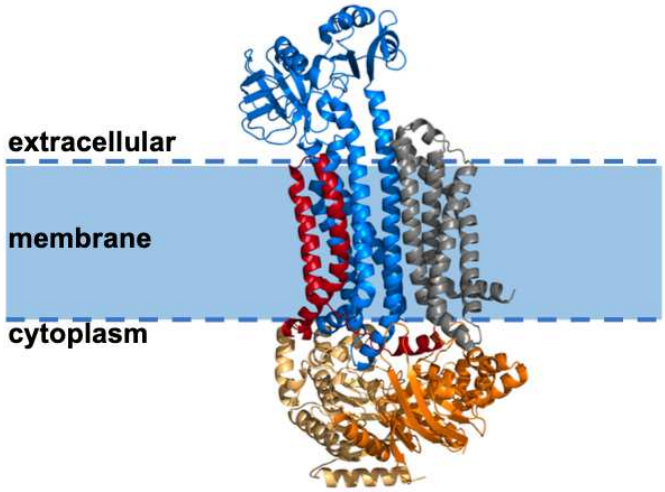

Figure 14: The BceAB-transporter *Sa*NsrFP. TM Helix bundles 1-4 (grey), TM helix bundles 7-10 (blue), TM helices 5 and 6 (red), and NsrF (light orange/ orange). *Sa*NsrFP model was created using AlphaFold2 (Jumper *et al.,* 2021). Image created with PyMOL Version 2.3.0 and Powerpoint 16.72.

2 Aim of the thesis

Bacteria developing antimicrobial resistance are a leading cause of death around the world and challenge global health systems. This emphasizes the urgency of investigating antibiotic alternatives. Lantibiotics are small antimicrobial peptides with high potency against human pathogenic Gram-positive bacteria. Pharmaceutical use of lantibiotics such as nisin is limited due to *Streptococcus agalactiae*, known for causing pneumonia, sepsis, and meningitis. It expresses the nisin resistance operon characterized by the presence of a two-component system and a membrane-embedded ATP-binding cassette (ABC) transporter NsrFP. The latter alone is enough to confer resistance and in combination with the nisin resistance protein (NSR) it is an effective resistance system. The work reported in this thesis is part of a larger effort to characterize the ABC transporter protein *Sa*NsrFP and the characteristic large extracellular domain of NsrP *in vivo* and *in vitro*. Furthermore, to identify high-affinity binding inhibitors, acting specifically against *Sa*NSR and/or *Sa*NsrFP, compounds were screened.

Lantibiotic-producing bacterial strains express two proteins that confer immunity against their own lantibiotic. In the case of *Lactococcus lactis* which produces nisin, these proteins are NisI and NisFEG. By simultaneous expression full immunity is achieved. Since the mechanism of immunity ABC transporter could also be helpful to understand resistance systems, another objective of this thesis was to characterize NisFEG functionally and structurally.

3 Publications

3.1 Chapter I: The Nucleotide-Binding Domain NsrF

Characterization of the nucleotide-binding domain NsrF from the BceAB-type ABC-transporter NsrFP from the human pathogen *Streptococcus agalactiae*

Fabia Furtmann[1,5], Nicola Porta [2,5], Dai Tri Hoang[1], Jens Reiners[3], Julia Schumacher[1], **Julia Gottstein[1],** Holger Gohlke [2,4] & Sander H. J. Smits [1,3*]

[1]Institute of Biochemistry, Heinrich-Heine-University Duesseldorf, Universitätsstrasse 1, 40225 Duesseldorf, Germany.
[2]Institute of Pharmaceutical and Medicinal Chemistry, Heinrich-Heine-University Düsseldorf, Universitätsstrasse 1, 40225 Düsseldorf
[3]Center for Structural Studies, Heinrich-Heine-University Duesseldorf, Universitätsstrasse 1, 40225 Duesseldorf, Germany.
[4]John von Neumann Institute for Computing (NIC), Jülich Supercomputing Centre (JSC), Institute of Biological Information Processing (IBI-7: Structural Biochemistry), Forschungszentrum Jülich GmbH, Wilhelm-Johnen-Straße, 52425 Jülich, Germany.
[5]These authors contributed equally: Fabia Furtmann and Nicola Porta. *email: sander.smits@hhu.de

Published in: Scientific reports (2020)

Impact factor: 4.379

Own proportion of this work: 10%

- Cloning
- Established the purification protocol
- Writing the manuscript

SCIENTIFIC REPORTS
natureresearch

Check for updates

OPEN

Characterization of the nucleotide-binding domain NsrF from the BceAB-type ABC-transporter NsrFP from the human pathogen *Streptococcus agalactiae*

Fabia Furtmann[1,5], Nicola Porta[2,5], Dai Tri Hoang[1], Jens Reiners[3], Julia Schumacher[1], Julia Gottstein[1], Holger Gohlke[2,4] & Sander H. J. Smits[1,3]✉

Treatment of bacterial infections is a great challenge of our era due to the various resistance mechanisms against antibiotics. Antimicrobial peptides are considered to be potential novel compound as antibiotic treatment. However, some bacteria, especially many human pathogens, are inherently resistant to these compounds, due to the expression of BceAB-type ABC transporters. This rather new transporter family is not very well studied. Here, we report the first full characterization of the nucleotide binding domain of a BceAB type transporter from *Streptococcus agalactiae*, namely *Sa*NsrF of the transporter *Sa*NsrFP, which confers resistance against nisin and gallidermin. We determined the NTP hydrolysis kinetics and used molecular modeling and simulations in combination with small angle X-ray scattering to obtain structural models of the *Sa*NsrF monomer and dimer. The fact that the *Sa*NsrF$_{H202A}$ variant displayed no ATPase activity was rationalized in terms of changes of the structural dynamics of the dimeric interface. Kinetic data show a clear preference for ATP as a substrate, and the prediction of binding modes allowed us to explain this selectivity over other NTPs.

Therapeutic compounds against bacterial infections are currently one of the biggest needs worldwide. Among antibiotics, antimicrobial peptides (AMP) offer promising potential for the treatment of bacterial infections, alone or in combination with already known molecules[1,2]. An alarming number of pathogenic multidrug resistant strains have evolved under the selective pressure caused by decades of incorrect antibiotic usage. Among them, methicillin-resistant *Staphylococcus aureus* (MRSA) or vancomycin-resistant *Enterococcus* (VRE) pose a high risk to therapeutic regimens[3]. To include new classes of antibiotics in therapy, studies were performed with lantibiotics, a class of AMPs. These ribosomally-synthesized peptides exhibit high potency against several human pathogenic bacterial strains[2–4] and show high stability to chemical and enzymatic degradation due to multiple intramolecular thioether rings and unsaturated amino acids[4–8].

Most known lantibiotics act similar in that they inhibit cell wall synthesis[9]. A common target for AMPs is the peptidoglycan layer, which exists in Gram-positive as well as Gram-negative bacteria. It is built up by altering amino sugars such as *N*-acetylglucosamine (GlcNAc) and *N*-acetylmuramic acid (MurNAc) and stabilized by a cross-linkage of those polymer chains. The inhibition of the cell wall synthesis results in reduced cell growth

[1]Institute of Biochemistry, Heinrich-Heine-Universität Düsseldorf, Universitätsstraße 1, 40225 Düsseldorf, Germany. [2]Institute for Pharmaceutical and Medicinal Chemistry, Heinrich-Heine-Universität Düsseldorf, Universitätsstraße 1, 40225 Düsseldorf, Germany. [3]Center for Structural Studies, Heinrich-Heine-Universität Düsseldorf, Universitätsstraße 1, 40225 Düsseldorf, Germany. [4]John von Neumann Institute for Computing (NIC), Jülich Supercomputing Centre (JSC), Institute of Biological Information Processing (IBI-7: Structural Biochemistry),, Forschungszentrum Jülich GmbH, Wilhelm-Johnen-Straße, 52425 Jülich, Germany. [5]These authors contributed equally: Fabia Furtmann and Nicola Porta. ✉email: sander.smits@hhu.de

and subsequent cell death. The well-known lantibiotic nisin contains five lanthionine rings and primarily targets the cell wall precursor Lipid II. The initial binding of the first two N-terminal lanthionine rings (A and B) of the lantibiotic to Lipid II is followed by a reorientation of the C-terminus into the membrane, resulting in pore formation and subsequently cell lysis[10,11]. Even though lantibiotics are effective in the nanomolar range, their application is hampered by resistance-conferring mechanisms found in human pathogenic bacteria[7,12,13]. The resistance is mediated by a newly discovered class of ATP binding cassette transporters, called Bacitracin efflux ABC transporters (BceAB), named after their first discovery in the bacitracin resistant strain of *Bacillus subtilis*[14,15]. In *Streptococcus agalactiae* such a BceAB-type ABC transporter is also present, as part of an operon that confers resistance against the lantibiotic nisin[16]. This operon consists of the membrane-associated protease *Sa*Nsr[17], the ABC transporter *Sa*NsrFP[8], and the two-component system comprising the response regulator *Sa*NsrR and the histidine kinase *Sa*NsrK[18]. So far, structural information is known only for *Sa*Nsr[17] and *Sa*NsrR[18].

Like all ABC transporters, BceAB-type transporters are composed of a nucleotide-binding domain (NBD) and a transmembrane domain (TMD). The NBD hydrolyses ATP, which drives conformational changes in the TMD, leading to substrate translocation. The TMD of BceAB-type ABC transporters are characterized by ten predicted transmembrane helices and a large extracellular domain (ECD_L) of ~ 220 amino acids that is the hallmark of this transporter family[4,8,16].

Sequences of the TMD domains from various BceAB-type ABC transporters are not very similar, which explains the large variety of substances they are able to translocate[16]. In contrast, NBDs share sequence and distinct motifs which are highly conserved throughout the ABC transporter superfamily[19–22]. NBDs are mainly L-shaped and comprise a helical signaling domain and a catalytic domain built of α-helices and β-strands[23–25]. The catalytic domain contains the Walker A motif that forms the nucleotide-binding site. A glutamate residue in the Walker B motif takes part in proper nucleotide binding; the γ-phosphate of the ATP molecule is sensed by a conserved histidine (H-loop) which when mutated results in an inactive variant[22,23,26]. Signaling and catalytic domains are connected by the Q- and the P-loop. Within the signaling domain the C-loop is located, which is the signature motif of an ABC transporter (for an alignment see Fig. S6 and Table S2)[22,27,28].

Dimerization of two NBD monomers in a head-to-tail conformation, is needed to enable ATP hydrolysis with the nucleotide binding sites located in the dimer interface. Each ATP molecule is sandwiched between the Walker A motif of one monomer and the C-loop of the second one, which results in a closed, stable complex[24,29–31]. An interaction between the NBD and the nucleotide is supposed to occur by π–π-stacking between the aromatic ring system of the nucleotide and an aromatic residue of the protein (F or Y). Hence, no preference towards any nucleotide-triphosphate (NTP) has been assumed[24], as also observed for example for yeast PDR5[32]. The hydrolysis of ATP is coupled to the presence of a cofactor, almost exclusively Mg^{2+}, which is coordinated by the Walker B motif. The divalent cation participates in the hydrolytic attack on the γ-phosphate of the nucleotide[26,28,31].

Here, we report for the first time biochemical and structural characteristics of the BceA nucleotide binding domain *Sa*NsrF, through NTP hydrolysis assays, molecular modeling and simulations. *Sa*NsrF is part of the BceAB-type ABC transporter NsrFP from *Streptococcus agalactiae*[16]. We show that the NBD *Sa*$NsrF_{WT}$ and its hydrolysis-deficient variant *Sa*$NsrF_{H202A}$ are monomeric in solution. Broad-ranging in vitro ATPase screenings delivered detailed information about the protein's properties with regard to its structure and physiology. We show that the preferred substrate of *Sa*NsrF is ATP as demonstrated by its kinetic parameters. Moreover, we built a structural model of the ATP/Mg^{2+}-bound *Sa*NsrF protein in its monomeric and dimeric form by comparative modeling and molecular dynamics simulations. In all, this constitutes the first biochemical characterization of a BceAB-type NBD.

Results

Cloning, expression and purification. For substrate transport BceAB-type ABC transporters depend on energy supply generated by ATP hydrolysis, which is mediated by the NBD. Here, we characterized the NBD NsrF of the BceAB-type ABC transporter NsrFP from *Streptococcus agalactiae*. To heterologously express *Sa*$NsrF_{WT}$ and *Sa*$NsrF_{H202A}$, we constructed expression vectors using a codon-optimized version of *Sa*NsrF for the heterologous expression in *E. coli* (Gen Bank accession number: WP_000923537). These constructs expressed a *Sa*NsrF protein with an N-terminal His10-tag attached for purification using Metal Ion Affinity Chromatography. The corresponding *Sa*NsrF constructs were expressed under the control of the plasmid-based T7-promoter via induction with Isopropyl-β-D-thiogalactopyranoside (IPTG). *Sa*$NsrF_{WT}$ was purified to high homogeneity (Fig. 1A), and was examined by Size Exclusion Chromatography coupled to Multiangle Light Scattering (SEC-MALS)[33], which revealed a molecular mass of 31.9 ± 0.4 kDa for the *Sa*$NsrF_{WT}$ protein (Fig. 1B). This corresponds nicely with the calculated theoretical molecular mass of the recombinant monomer of 30.9 kDa including the His10-tag. Thus, the conducted SEC-MALS analysis revealed that *Sa*$NsrF_{WT}$ exists as a stable monomer in solution, which is in line with previous observations of other NBDs from different ABC transporter families[34–36].

By sequence alignments, His_{202} was identified to be the essential residue of the H-loop[37–39]. As shown for other NBDs, a point mutation to alanine results in a loss of the ATPase activity of the NBD. We generated this variant of *Sa*NsrF (*Sa*$NsrF_{H202A}$), which indeed displayed no NTP hydrolysis (see below). This variant served as a negative control in all our experiments. The lack of NTP hydrolysis for *Sa*$NsrF_{H202A}$ is in line with in vivo studies that show that this variant abolishes the activity of *Sa*NsrFP[8,40].

Activity of $SaNsrF_{WT}$. After successful purification, we functionally characterized *Sa*$NsrF_{WT}$. To do so, we screened the following parameters for their influence on the ATP hydrolysis velocity: (I) pH, (II) salt concentration, (III) nature of the divalent ion and (IV) temperature (see Supporting Information and Fig. S1). As a result, the optimized conditions were found to be 100 mM HEPES at pH 7 with 0 mM NaCl as an assay buffer. The

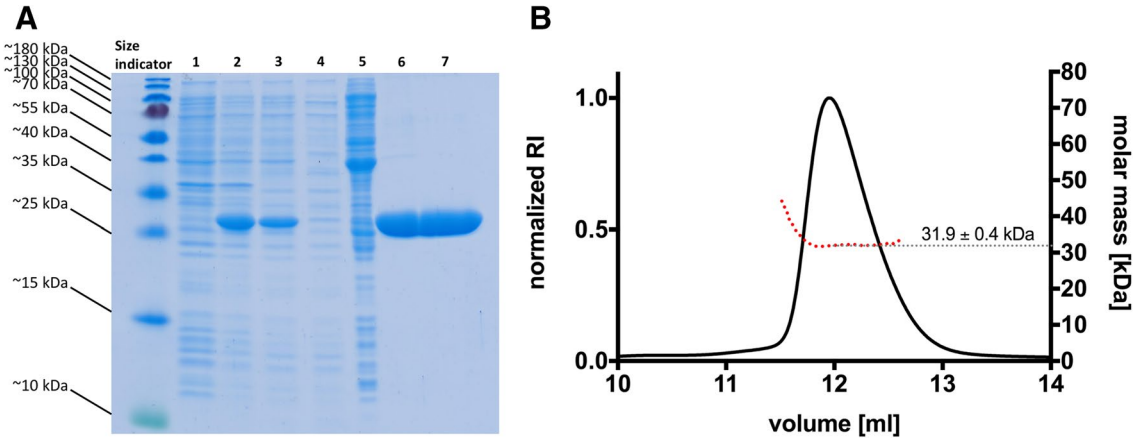

Figure 1. Purification and SEC-MALS of *Sa*NsrF$_{WT}$. (**A**) SDS-PAGE of the *Sa*NsrF$_{WT}$ purification progress. PageRuler Prestained Protein Ladder (size indicator; 10 to 180 kDa), *E. coli* strain before IPTG induction (1), *E. coli* strain after IPTG induction (2), IMAC load (3), IMAC flow-through (4), IMAC wash-fraction (5), IMAC eluate (6), SEC eluate (7). (**B**) Multiangle Light Scattering of *Sa*NsrF$_{WT}$. Freshly purified *Sa*NsrF$_{WT}$ was diluted in MALS-buffer and applied with a concentration of 3 mg mL^{-1} onto a Superdex 75 16/300 increase column. MALS-RI analysis shows that the *Sa*NsrF$_{WT}$ protein elutes with an absolute molecular mass of 31.9 ± 0.4 kDa, consistent with a theoretical monomeric mass in solution.

buffer included 10 mM Mg^{2+} and the reaction was finally performed at 30 °C, with an incubation time of 18 min (Fig S1). These optimized conditions were applied in all following experiments.

Velocity of NTP hydrolysis by SaNsrF$_{WT}$ and SaNsrF$_{H202A}$. Kinetic measurements were performed by quantifying the NTP hydrolysis under increasing concentrations of the respective nucleotide. We determined the NTP hydrolysis behaviour of *Sa*NsrF$_{WT}$ and *Sa*NsrF$_{H202A}$ using increasing amounts of ATP, GTP, CTP or UTP.

As depicted in Fig. 2A, the *Sa*NsrF$_{WT}$ protein demonstrated a nonlinear dependency of ATPase activity over a range of 0–5 mM ATP. The maximal reaction velocity was calculated to be 190.9 ± 10.0 nmol min^{-1} mg^{-1} when using ATP. Moreover, the calculation of the kinetic parameters resulted in a kinetic constant of k_{half} = 0.41 ± 0.05 mM and a Hill coefficient of h = 1.72 ± 0.27 (Fig. 2A and Table 1). A Hill coefficient > 1 demonstrates a cooperative behaviour, and suggests that *Sa*NsrF$_{WT}$ needs to dimerize to hydrolyze ATP, which is in line with other previously characterized NBDs[41–43]. For GTP, the maximal reaction velocity was 221.6 ± 11.1 nmol min^{-1} mg^{-1} with a Hill coefficient of h = 1.82 ± 0.27 and a k_{half} value of 0.69 ± 0.07 mM (Fig. 2B and Table 1). Interestingly, the highest reaction velocity with a value of 339.0 ± 30.4 nmol min^{-1} mg^{-1} was reached using CTP as a substrate with the highest measured k_{half} value of 1.23 ± 0.20 mM and a Hill coefficient of 1.63 ± 0.53 (Fig. 2C and Table 1). The kinetic parameters using UTP as a substrate resulted in comparably high values of v_{max} = 314.8 ± 23.4 nmol min^{-1} mg^{-1}, k_{half} = 0.90 ± 0.13 mM and h = 1.55 ± 0.25 (Fig. 2D and Table 1). The variant *Sa*NsrF$_{H202A}$ displayed no hydrolytic activity for any of the four used NTPs (Fig. 2, dashed lines).

Structural models of SaNsrF monomer and dimer. Since no experimental structure of *Sa*NsrF is available, we generated a structural model of the NBD by comparative modeling. NBDs are the most conserved parts of ABC transporters and in the case of *Sa*NsrF, the templates used for modeling show a sequence identity of ~ 30–40% and a sequence similarity of 84–89% (Table S1). Of these X-ray structures (resolution between 1.7 and 3.4 Å), two constitute NBDs in the functionally active assembly; they were crystallized with the TMD of the macrolide exporter MacAB from *Acinetobacter baumannii* (PDB ID 5GKO[44]) and MacAB-like from *Streptococcus pneumoniae* (PDB ID 5XU1[45]).

The homology model of *Sa*NsrF$_{WT}$ in the monomeric form is of high quality, given the low overall TopScore[46] (TS) value of 0.24 (Fig. 3A). This superimposition-free score evaluates local distance differences[47] of all atoms in a model, and a value closer to zero indicates higher quality. The regions modeled with lower reliability (TS > 0.5), accounting only for ~ 6% of the total sequence, are located at the β-hairpin (residues 15–18) and the two C-terminal helices (residues 229–232, 235–236, 246–250). Both substructures can be found in other NDBs, however, indicating the plausibility of the model. For example, when compared to the structure of ComA from *Streptococcus mutans* (PDB ID 3VX4[48]), the C-terminal helices have a virtually identical fold, with an RMSD of 0.6 Å for the last 50 residues, based on sequence alignment followed by structural superimposition.

The dimeric *Sa*NsrF$_{WT}$ model is structurally similar to other known structures, given RMSD values of ~ 5 Å or lower (RMSD of 3.5 Å, 4.5 Å and 5.2 Å for PDB IDs 1L2T, 5GKO, and 5XU1, respectively), indicating the suitability of the performed protein–protein docking. The reliability of the model is additionally verified by the presence of conserved motifs (Fig. 2B and Table S2), such as the phosphate-binding loop (P-loop or Walker A motif), the cofactor-chelating region (Walker B motif), and a short consensus sequence "LSGGQ" (C-loop or ABC signature motif), which signify ABC transporter family membership at the sequence level. Moreover, the α-helical and RecA-like domains are in the canonical head-to-tail arrangement (Fig. 3C). Interestingly, the

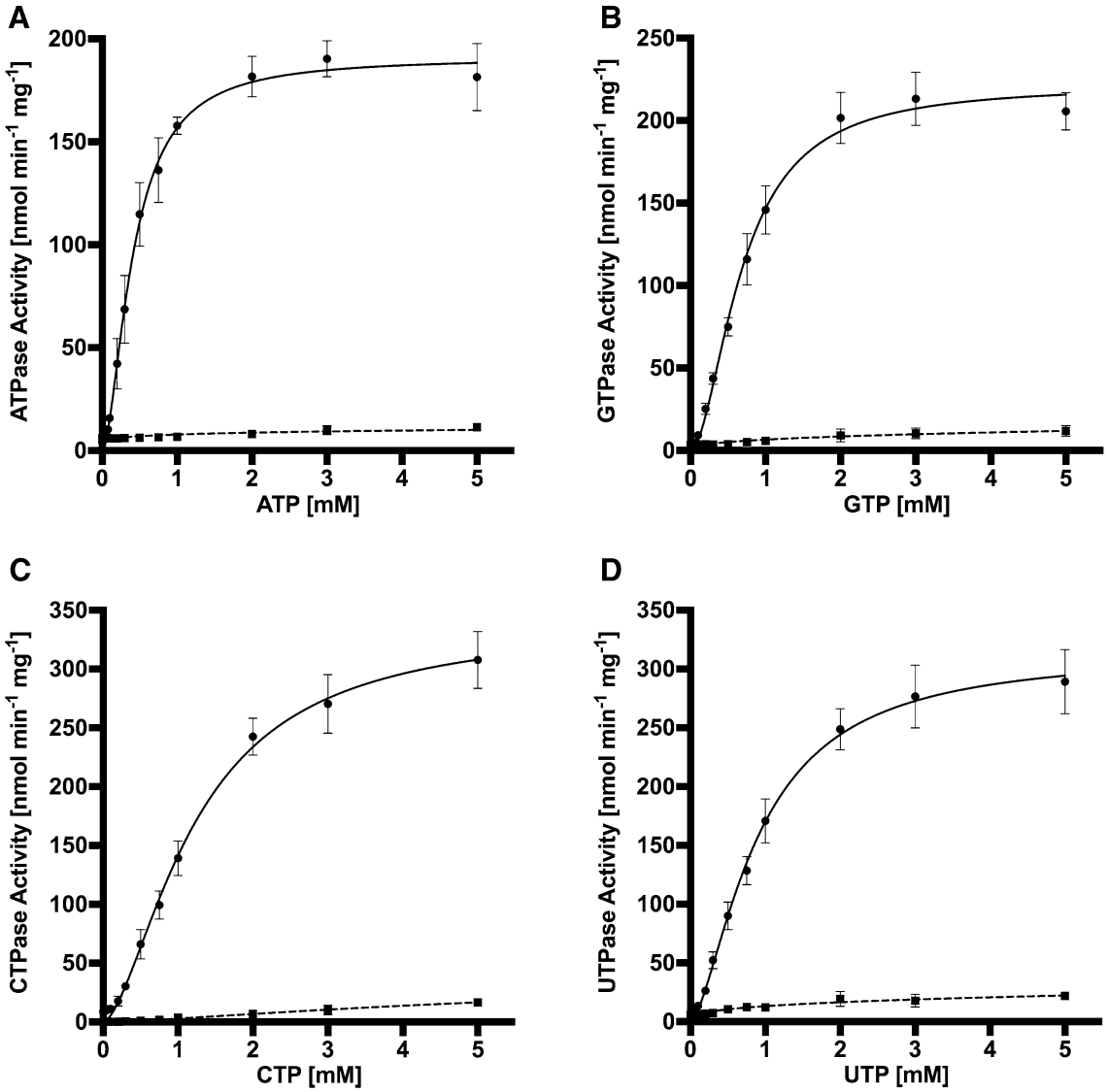

Figure 2. Kinetic measurement of *Sa*NsrF$_{WT}$ (black) and *Sa*NsrF$_{H202A}$ (dashed lines) NTPase Activity [nmol min^{-1} mg^{-1}] after 18 min of incubation. A concentration range of each NTP from 0 to 5 mM was applied on freshly purified *Sa*NsrF or *Sa*NsrF$_{H202A}$ (0.1 mg mL^{-1}; diluted in 100 mM HEPES at pH 7). The reaction was stopped after 18 min and dyed for 7 min. A sigmoidal fit was applied using GraphPad PRISM 8.3.0. (**A**) Kinetic parameters of *Sa*NsrF$_{WT}$ exposed to 0–5 mM ATP: v_{max}: 190.9 ± 10.0 [nmol min^{-1} mg^{-1}], h: 1.72 ± 0.27, k_{half}: 0.41 ± 0.05 [mM]. (**B**) Kinetic parameters of *Sa*NsrF$_{WT}$ exposed to 0–5 mM GTP: v_{max}: 221.6 ± 11.1 [nmol min^{-1} mg^{-1}], h: 1.82 ± 0.27, k_{half}: 0.69 ± 0.07 [mM]. (**C**) Kinetic parameters of *Sa*NsrF$_{WT}$ exposed to 0–5 mM CTP: v_{max}: 339.0 ± 30.4 [nmol min^{-1} mg^{-1}], h: 1.63 ± 0.53, k_{half}: 1.23 ± 0.20 [mM]. (**D**) Kinetic parameters of *Sa*NsrF exposed to 0–5 mM UTP: v_{max}: 314.8 ± 23.4 [nmol min^{-1} mg^{-1}], h: 1.55 ± 0.25, k_{half}: 0.90 ± 0.13 [mM]. All experiments have been performed in at least three biological replicates and are represented as means ± s.d.

NTP	V_{max}	k_{half}	h
ATP	190.9 ± 10.0	0.41 ± 0.05	1.72 ± 0.27
GTP	221.6 ± 11.1	0.69 ± 0.07	1.82 ± 0.27
CTP	339.0 ± 30.4	1.23 ± 0.20	1.63 ± 0.53
UTP	314.8 ± 23.4	0.90 ± 0.13	1.55 ± 0.25

Table 1. Kinetic parameters V_{max} [nmol min^{-1} mg^{-1}], k_{half} [mM] and the Hill-coefficient h resulting from different NTPs as a substrate for *Sa*NsrF$_{WT}$. All experiments have been performed in at least three biological replicates and are represented as means ± s.d.

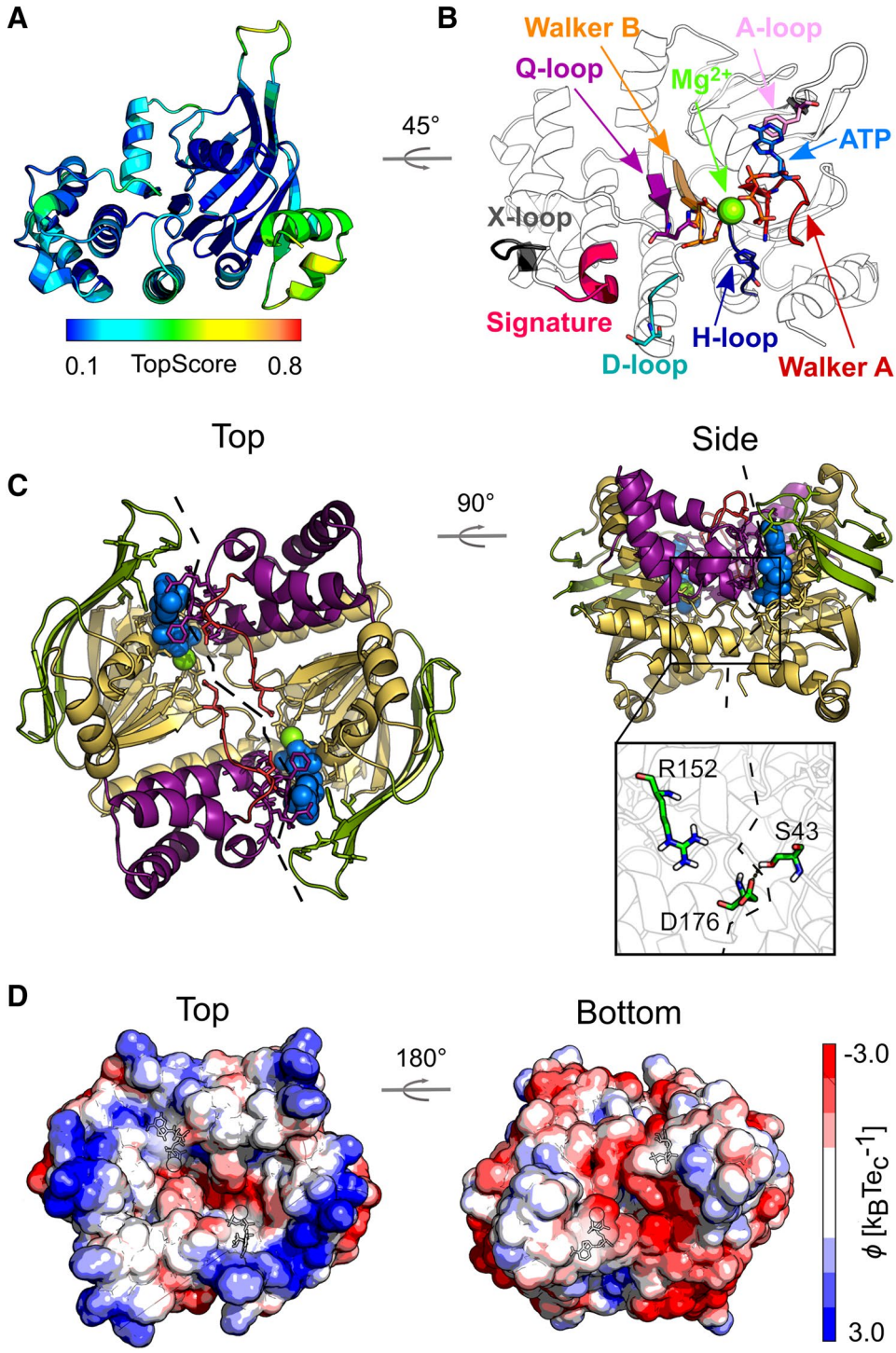

Figure 3. Homology models of *Sa*NsrF$_{WT}$ monomer (**A**, **B**) and dimer (**C**, **D**). (**A**) Structure colored according to the residue-wise TopScore. Green/yellow colors indicate regions with low residue-wise error (< 50%). (**B**) Zoom into the NBD-NBD interface with ATP and Mg^{2+} bound, highlighting the conserved motifs necessary for ATP binding and hydrolysis, and for NBD-NBD and NBD-TM communication. See Table S2 for the location of the conserved motifs in the primary sequence[22]. (**C**) Structure colored according to domain organization and zoom into the NBD–NBD interface, reporting the conserved residues used as restraints for protein–protein docking. The α-helical domain is shown in violet; the RecA-like domain, further subdivided into F1-type ATP binding core, antiparallel β subdomain, and γ-phosphate linker is colored respectively in yellow, green, and red. The bound ATP (blue) and Mg^{2+} (green) are shown in space-filling representation. The dashed line highlights the interface between subunits. (**D**) Electrostatic potential computed for the representative structure of the most populated cluster of conformations obtained by MD simulations. The color scale of the electrostatic potential ranges from − 3.0 (red) to + 3.0 (blue) $k_B Te_c^{-1}$; the potentials were computed with the Adaptive Poisson-Boltzmann Solver (APBS)[49].

calculated electrostatic potential shows a clear polarization (Fig. 3D) with positively charged residues (such as R and K) prevalent on the dimer's side oriented towards the membrane (named "top") and negatively charged residues (such as D and E) on the opposite side (named "bottom") in agreement with the expected topology.

Structural dynamics at the NBD–NBD interface and impact of the SaNsrF$_{H202A}$ substitution. The *Sa*NsrF models were subjected to all-atom MD simulations of in total 10 µs length to investigate the structural dynamics at the NDB-NDB interface and to highlight the impact of the H202A substitution on ATP/Mg^{2+} binding. The RMSD profiles for *Sa*NsrF$_{WT}$ and *Sa*NsrF$_{H202A}$ monomers (Fig. S2) reach almost immediately a plateau at ~ 4 Å, indicating that the overall structure is mostly invariant over simulation times of 0.5 µs for each replica. Additionally, the low variability of ATP/Mg^{2+} coordinates (Fig. S3A,B) suggests that the *Sa*NsrF$_{H202A}$ substitution does not impact ATP/Mg^{2+} binding, at least on the timescale of our simulations.

The RMSD profile for the *Sa*NsrF$_{WT}$ and *Sa*NsrF$_{H202A}$ dimers is mostly invariant (Fig. S4A) when the structures are superimposed onto the two subunits separately (red and blue lines). However, when the superimposition is done with respect to the least mobile regions in the whole dimer (black line), RMSD values reach ~ 6–9 Å in three out of five replicas for *Sa*NsrF$_{WT}$, indicating that the arrangement of the two subunits changes during the simulations. In particular, the interface between the subunits partially opens (Fig. S4B) up to ~ 25 Å (Fig. S5). The change of ATP molecule and Mg^{2+} ion positions relative to the protein is more marked for *Sa*NsrF$_{WT}$ dimer (Fig. S3). Interestingly, this is not happening in the *Sa*NsrF$_{H202A}$ variant, where the interface seems to be more stable.

In terms of structural mobility, the central region of *Sa*NsrF$_{WT}$ and *Sa*NsrF$_{H202A}$ (residues ~ 50–150) shows a different profile in monomers and dimers (Fig. 4). In monomers (Fig. 4A,B), this region is less mobile than in dimers (Fig. 4C,D), with RMSF values lower than 2 Å and up to 4 Å, respectively. Moreover, in the dimeric *Sa*NsrF$_{H202A}$ variant, this region is slightly less mobile than in *Sa*NsrF$_{WT}$. The residues of the central region are oriented towards the TM region of the transporter (Fig. 4E,D). In addition, after the alignment of *Sa*NsrF with NBDs of structures containing the TMD (PDB ID 5XU1, Fig. 4G), most of the residues of this central region are located at < 5 Å distance from the coupling helices (CH1, between TM2 and TM3, and C-terminal CH2) of the transporter, suggesting that this central region is involved in NBD-TMD communication (Fig. 4H). A similar result was found for the HlyB transporter[50], where the X-loop motif (corresponding to residues 137–142 in *Sa*NsrF, located in the central region) has been proposed to be an important part of the NBD-TMD communication. Even though we are considering an ATP-bound pre-hydrolysis state, *Sa*NsrF in the dimer seems to be generally more mobile than in the monomer, in agreement with the idea that a dimeric assembly is needed in order to perform its function.

H-bond analysis in *Sa*NsrF$_{WT}$ and *Sa*NsrF$_{H202A}$ dimers reveals that the number of H-bond interactions between *Sa*NsrF and the ligands (ATP molecules and magnesium ions) is on average higher in the case of the *Sa*NsrF$_{H202A}$ variant (Fig. 5A). This is due to the higher structural stability compared to *Sa*NsrF$_{WT}$. Besides the three residues used as restraints for protein–protein docking (S43–R152–D176), other residues contribute to the stability of the dimer with H-bond occupancies up to 70%, such as R13, T14, R15, E42, E144, and R178 (Fig. 5B,C). Surprisingly, the residue-wise H-bond occupancy in *Sa*NsrF$_{WT}$ is significantly higher ($p < 0.01$) for two specific H-bonds involving both side chains and backbone atoms (D136–R15 and R133–R15), although the interface of the *Sa*NsrF$_{WT}$ dimer is less structurally stable (see above). Indeed, in the initial dimeric model, these interactions are not present, but require the movement of one monomer to the other for them to form.

To conclude, the generated models show a high structural stability over the simulation lengths. In the dimers, the central region is more mobile than in the monomers; in *Sa*NsrF$_{WT}$, the interface between subunits is structurally less stable than in the *Sa*NsrF$_{H202A}$ variant. Since a shift of one monomer to the other is necessary for NDBs to perform their function, these results together suggest that the mutation *Sa*NsrF$_{H202A}$ impacts the structural dynamics at the *Sa*NsrF interface and not only the catalytic mechanism.

Small angle X-ray scattering. Unfortunately, we were not able to crystalize the *Sa*NsrF protein, although extensively tried. In order to experimentally validate this new model, we choose Small Angle X-Ray Scattering (SAXS) to compare the theoretical model with the experimental scattering (Fig. 6A) measured with the Xenocs Xeuss 2. Based on the experimental data, we calculated an ab initio model for *Sa*NsrF$_{WT}$ with the program GASBOR[51] and obtained a χ^2 value of 0.97. Superimposing the ab initio and the TopModel model reveals that the structure and the envelope obtained by the SAXS experiment overlap, but also a density tail at the C-terminus of *Sa*NsrF$_{WT}$ (Fig. 6B) that is not occupied by the model. Scrutinizing the templates used by TopModel[52] shows that this helical part (Fig. 6B, orange helix) is rather unstructured or even missing. This finding indicated that this region might be highly flexible in solution, thereby covering the available free space in the SAXS envelope (Fig. 6B, red helix). With the program CRYSOL[53] we compared the theoretical scattering curve obtained from the TopModel model against the experimental data. The resulting χ^2 value of 1.16 indicates a good agreement between the prediction and the experiment. We uploaded the SAXS data and the corresponding model of *Sa*NsrF to the Small Angle Scattering Biological Data Bank (SASBDB)[54,55] with the accession code SASDJR3.

Molecular docking of other NTPs. In order to rationalize the hydrolysis preference for ATP over other NTPs, we predicted the binding mode of these molecules in complex with the *Sa*NsrF$_{WT}$ dimer. Ten different pocket conformations, obtained from five equilibrated structures used also for MD simulations times two pockets each, were considered. When focusing on the configurations with lowest Coulomb (ecoul) and van der Waals (evdw) energies, ATP is slightly enriched compared to the other NTP (3 × ATP, 2 × UTP, 1 × CTP and 1 × GTP), suggesting that ATP binding is preferred due to enthalpic contributions to binding (Fig. 7A). Residues giving rise to this preference are those interacting with the nucleobase, namely F12, T49, A23 of one subunit and F143′ and

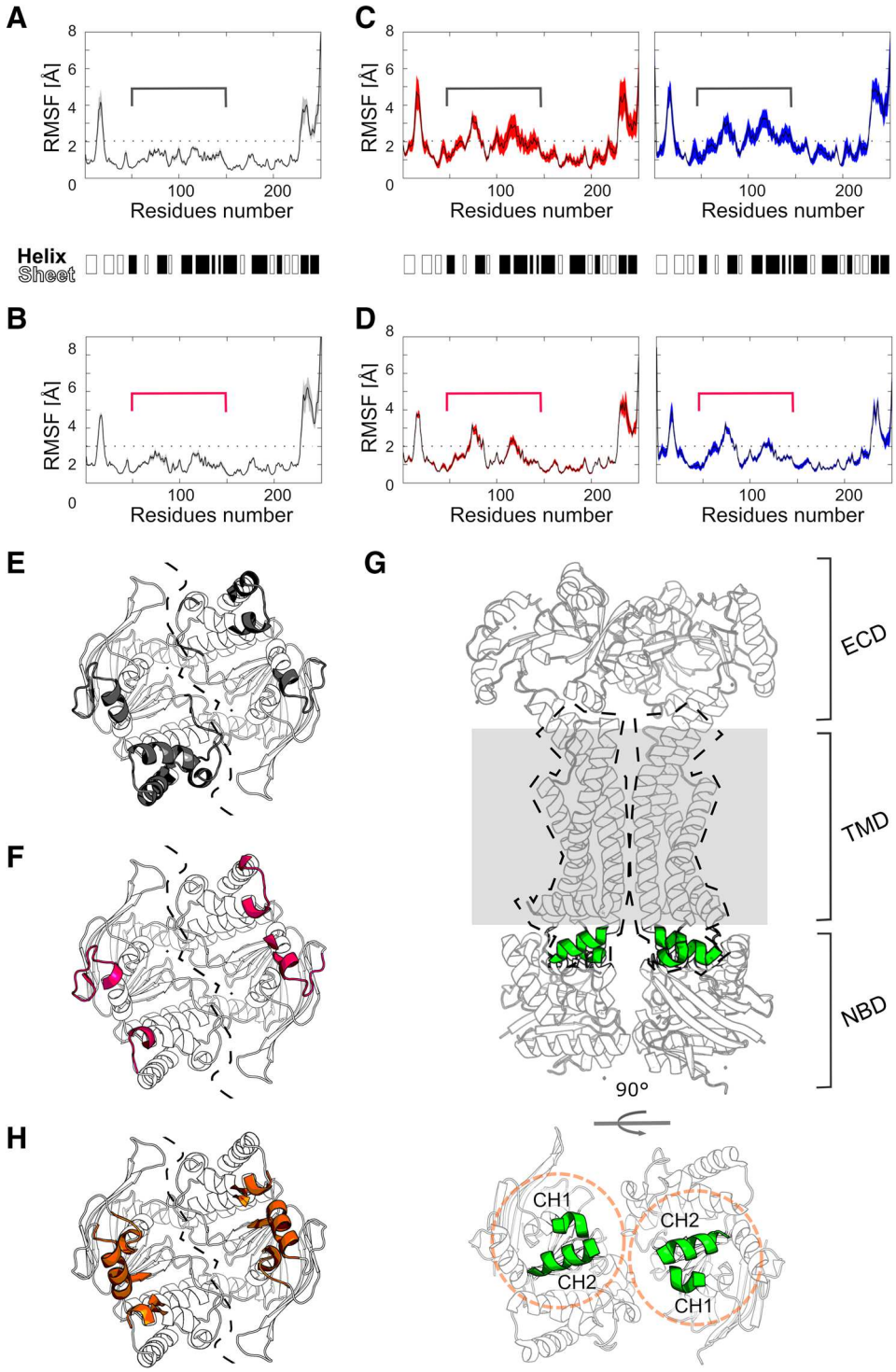

Figure 4. Structural mobility of the *Sa*NsrF$_{WT}$ and *Sa*NsrF$_{H202A}$ systems expressed as RMSF of Cα atoms. Before RMSF calculation, the structures were fitted onto the 15% least mobile residues, averaged over five MD simulation replicas. The variability between replicas is expressed as SEM and shown as colored area (grey for the monomers, red for chain A and blue for chain B). (**A**) *Sa*NsrF$_{WT}$ monomer. (**B**) *Sa*NsrF$_{H202}$ variant monomer. (**C**) *Sa*NsrF$_{WT}$ dimer. (**D**) *Sa*NsrF$_{H202}$ variant dimer. The secondary structure elements of the initial model are shown as black and white bands. The central region of *Sa*NsrF$_{H202}$ (residues ~ 50–150) is highlighted with brackets. Residues of the central region with RMSF > 2 Å are mapped onto the dimer structures. (**E**) For *Sa*NsrF$_{WT}$ (in grey) and (**F**) for *Sa*NsrF$_{H202}$ variant (in pink). The other two regions with RMSF > 2 Å (hairpin of the antiparallel β subdomain and the C-term) are not shown for clarity. The dashed line highlights the interface between subunits. (**G**) Structure of the MacAB-like transporter from *Streptococcus pneumoniae* (PDB ID 5XU1[45]) reported as comparison to highlight the expected orientation of the NBD to the TMD (shown as dashed shape), its coupling helices (CH1 and CH2, highlighted in green) and the membrane (as grey area). (**H**) After superimposition of the NBDs, regions of *Sa*NsrF located at < 5 Å from the coupling helices of the MacAB-like structure, and therefore likely involved in NBD-TMD communication, are highlighted in orange.

A

System	Replica	*Sa*NsrF$_A$-*Sa*NsrF$_B$	*Sa*NsrF-(ATP-Mg^{2+})
*Sa*NsrF$_{wt}$	I	6.29 (2.10)	15.54 (2.21)
	II	10.70 (3.12)	13.94 (2.05)
	III	8.07 (2.35)	15.19 (2.14)
	IV	9.02 (2.90)	13.24 (2.93)
	V	12.62 (3.20)	12.54 (2.05)
	All ± SEM	**9.34 ± 1.57**	**14.09 ± 1.15**
*Sa*NsrF$_{H202A}$	I	8.65 (2.39)	15.33 (2.05)
	II	9.51 (3.01)	14.64 (2.57)
	III	10.95 (2.85)	13.17 (2.41)
	IV	8.39 (2.34)	18.05 (2.39)
	V	18.05 (2.39)	18.66 (2.61)
	All ± SEM	**9.25 ± 1.30**	**15.97 ± 1.42**

**

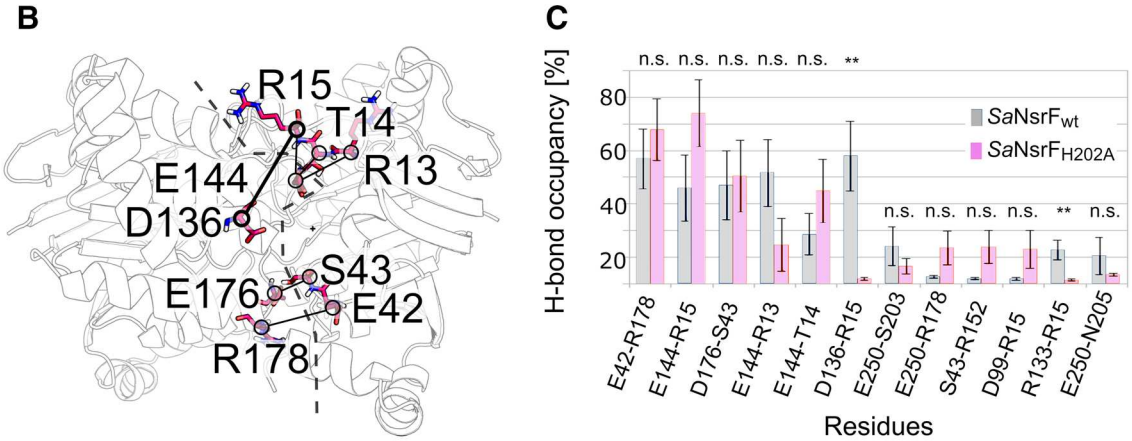

Figure 5. H-bond analysis in *Sa*NsrF$_{WT}$ and *Sa*NsrF$_{H202A}$ dimers. (**A**) The average number of H-bonds between the two proteins and between the protein and the ligands per MD replica. Standard deviations are reported in parentheses. For the numbers in bold, the SEM was computed according to $n = 5$. $^{**}p < 0.01$ according to a two-tailed *t*-test. (**B**) Residues in the interface that predominantly form H-bonds (occupancy > 20%). H-bonds are shown as lines connecting the Cα atoms of these residues. The dashed line highlights the interface between subunits. (**C**) H-bond occupancy for the most prevalent interactions (occupancy in at least one of the systems > 10%). Error bars are showing the SEM. $^{**}p < 0.01$ according to a two-tailed *t*-test for the comparison of *Sa*NsrF$_{WT}$ and *Sa*NsrF$_{H202A}$ variant; n.s.: not significant.

E144′ of the other (Fig. 7B). In particular, the phenylalanines are interacting with the nucleobase by π-π stacking interactions, and the amino groups of CTP and GTP form H-bonds with the backbone oxygen of F143′ and the carboxylate group of E144′, respectively. Since in ATP the amino group has the same orientation as in CTP, a similar kind of H-bond pattern can be expected.

Over respective pockets 1 or 2, which are not symmetric as described above, ATP shows the largest sums of Coulomb and van der Waals energies compared to the other NTPs (Fig. 7C), indicating strongest binding based on enthalpic components, which is in line with the biochemical data where ATP shows the lowest k_{half} value (Fig. 2 and Table 1).

Discussion

A rather novel family of ABC-transporters, the Bacitracin efflux (Bce) type transporters, have been identified to confer high-level resistance against bacitracin as well as against lantibiotics such as nisin and gallidermin in *Bacillus subtilis, Staphylococcus aureus,* and *Streptococcus agalactiae*[8,14,16,57–60]. These transporters have been rudimentarily characterized in vitro. We set out to characterize the NBD of the transporter *Sa*NsrFP; this transporter has been shown to be involved in lantibiotic resistance[8].

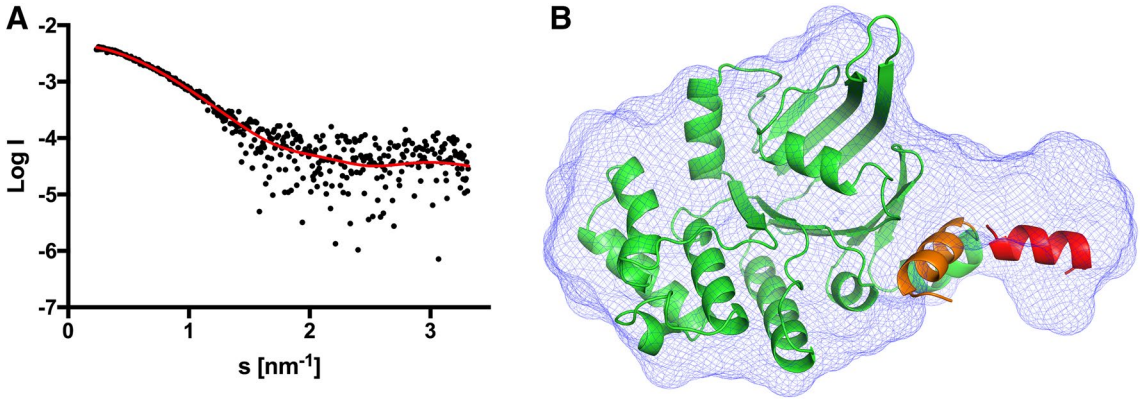

Figure 6. Comparison of the ab initio model with the homology model. (**A**) Experimental scattering data are shown as black dots and the ab initio model fit as red line. The intensity is displayed as a function of momentum transfer *s*. (**B**) Ab initio model of the *Sa*NsrF$_{WT}$. The volumetric envelope from *Sa*NsrF$_{WT}$, calculated from the scattering data using GASBOR[51], is shown by the blue mesh. The homology model of the *Sa*NsrF$_{WT}$ monomer (shown in green) was docked into the volumetric envelope using SUPCOMB[56]. Concerning the flexibility of the C-terminal helix (shown in orange), we show a possible, changed orientation of this helix in red.

We have purified and characterized the *Sa*NsrF$_{WT}$ and *Sa*NsrF$_{H202A}$ proteins regarding their ability of ATP hydrolysis. The results revealed that inorganic phosphate is only released in a pH range of 6–8, where an HEPES buffer at pH 7 was found to yield maximal ATPase activity. Interestingly, 20% difference could be found in a TRIS buffer system at the same pH (Fig S1A). Similar results were obtained by Zaitseva et al. examining the HlyB-NBD[36]. In that study, a correlation between the pH of 6 and the pK$_a$ values of the glutamate residue and/or the γ-phosphate of the nucleotide and between the pH of 8 and the pK$_a$ value of the conserved histidine bound in a salt bridge with the γ-phosphate was made. On that basis, the nucleophilic attack on the γ-phosphate is preceded, originating from a hydrolytic water molecule, which results in the cleavage of the γ-phosphate moiety[26,36,61]. Moreover, the importance of the conserved histidine could be confirmed since the *Sa*NsrF$_{H202A}$ variant was shown to be incapable of hydrolysing ATP. Here, the 'linchpin'-role during ATP-hydrolysis is conducted by the H-loop[22,36,38,62]. Also, this allows a possible explanation for the observed decrease of activity with increasing concentrations of NaCl (Fig. S1B). Since the conserved histidine is in contact with the γ-phosphate of the nucleotide by forming a salt bridge, rising salt concentration could disrupt this existing interaction. In contrast, a buffer system containing 300 mM of NaCl was used for protein storage, which indicates an inverse correlation between protein stability and activity at rising NaCl concentrations[63]. The incapability of *Sa*NsrF$_{H202A}$ to hydrolyse ATP supports in vivo studies where a loss of resistance against the lantibiotic nisin was observed when expressed in *L. lactis* bacterial cells[8].

Like many other NBDs, *Sa*NsrF was observed to be strictly dependent on its cofactor Mg^{2+}[39,64,65], because this is required as a Lewis acid in the catalytic cycle. Mg^{2+} is involved in proton abstraction from the nucleotide and the nucleophilic attack of the catalytic water, which results in the hydrolytic cleavage of its γ-phosphate[36].

Finally, we conducted kinetic measurements including all optimized parameters and the preference of *Sa*NsrF$_{WT}$ and *Sa*NsrF$_{H202A}$ for hydrolysing different NTPs. We propose that the main interaction of the nucleoside triphosphate and the protein occurs by π–π-stacking between the adenine moiety and F12 downstream of the Walker A motif (Fig. 3B,C) as also observed for other NBD's[22,24,25,30]. Also, Mg^{2+}, anchored to the protein through Asp and Glu residues of the Walker B motif, interacts with the phosphate region of ATP. The Walker A motif binds to the other side of the phosphate region (Fig. 3B).

Based on a comparison of docked binding poses of other NTPs, additional interacting residues were predicted (Fig. 7B). Amino group-containing NTPs (ATP, CTP and GTP) can form H-bonds with the backbone oxygen of F143′ and the carboxylate group of E144′, whereas purines in ATP and GTP form more extended π–π stacking interactions with F12 and F143′. ATP shows the largest sums of Coulomb and van der Waals energies compared to the other NTPs in either pocket of the NBD, in line with the biochemical data where ATP displayed the lowest k_{half} value (Fig. 2 and Table 1).

By comparing the measured kinetic parameters of each examined NTP, it becomes obvious that the reactions including UTP or CTP resulted in a significantly higher reaction velocity, respectively, when compared to ATP. Nevertheless, the CTPase and UTPase activities revealed noticeably high kinetic constants (k_{half}) as well. With regards to the substrate affinity represented by the k_{half} value, a minimum of 0.41 ± 0.05 mM was reached using ATP as a substrate, which signifies ATP as the most favoured of all four tested NTPs for *Sa*NsrF$_{WT}$. Hence, ATP has the highest affinity to *Sa*NsrF$_{WT}$ compared to the other examined NTPs, which corresponds with the physiological appearance in vivo of each NTP ([ATP] > [GTP] > [UTP] > [CTP]), which underlines that ATP is the preferred substrate for the protein[32,66–68]. Considering the physiology of purine (ATP, GTP) and pyrimidine (UTP, CTP) nucleotides, we concluded that the involved aromatic ring systems play a major role concerning the substrate affinity and stability of the protein-substrate-complex. Here, pyrimidine bases exhibit a smaller electron density that can be involved in π–π-stacking. Thus, dissociation of pyrimidine nucleotides from the enzyme occurs faster than purine nucleotides. By contrast, the stabilized protein–purine-complex is less liable

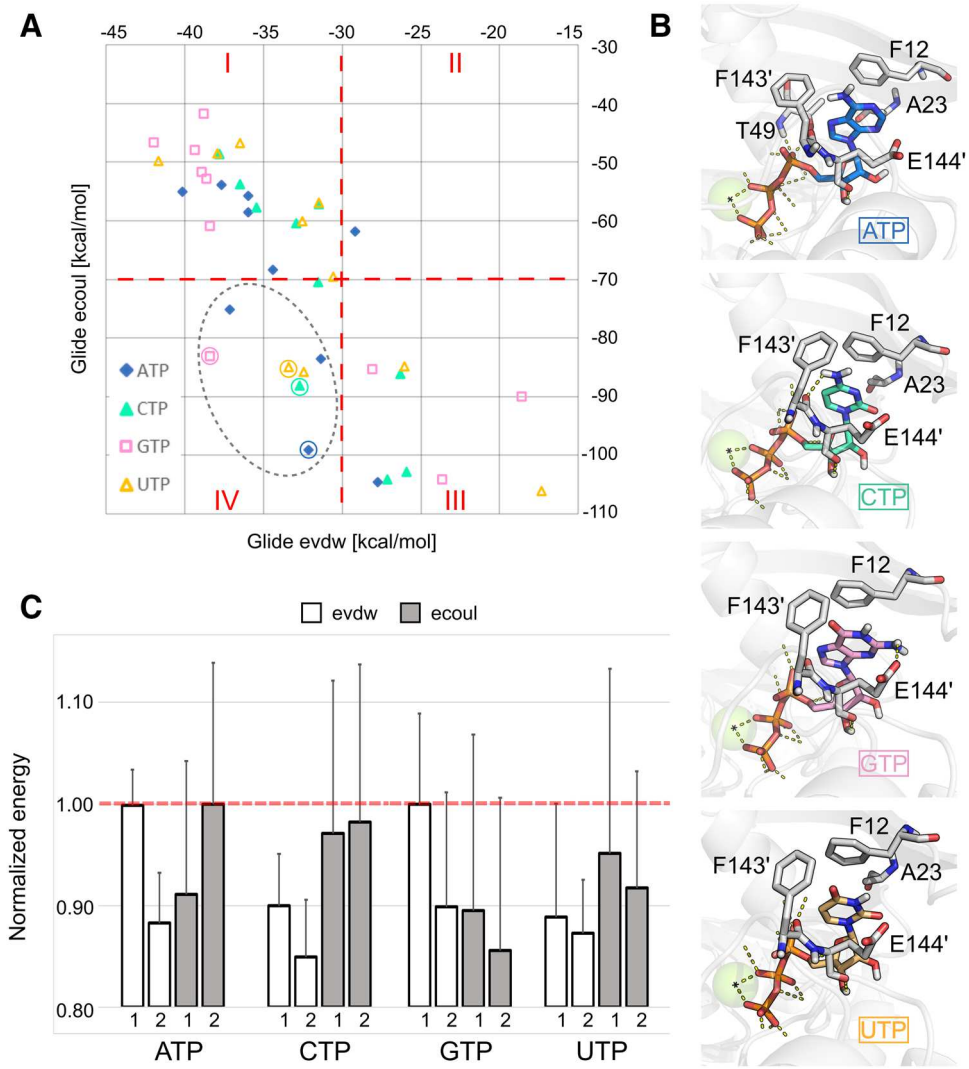

Figure 7. Molecular docking of other NTPs. (**A**) Scatterplot representing the Coulomb (ecoul) versus the van der Waals (evdw) energy terms of the docking score. Each data point represents an NTP configuration inside the two pockets of five different, equilibrated *Sa*NsrF structures. In quadrant IV, NTP configurations with respective lowest energies are circled. (**B**) Representative binding modes of NTPs, referring to the circled data points in section A. Residues at ≤ 4 Å from the nucleobases are shown in sticks and labelled. The Mg^{2+} ion is shown as a green sphere (**C**) Normalized average energy terms for pockets 1 and 2 of each SaNsrF complex. The error is reported as normalized SEM ($n = 5$).

to dissociation. Together, this may explain the small k_{half} values found for ATP and GTP and the high reaction velocities caused by a high turnover of CTP and UTP.

NBDs are assumed to share a large number of properties due to highly conserved sequences and specific motifs (see Fig. 3B,C and Table S2)[22–26,30]. The presence of a certain substrate such as ATP is supposed to induce a dimerization of the two NBD monomers in a typical head-to-tail formation, resulting in two ATP molecules in the dimer interface, sandwiched by the Walker A motif of one monomer and the signature motif of the other one as a cooperative process[22,24,25].

NBDs hydrolyse ATP, which drives substrate translocation by conformational changes of the TMD. In the case of the BceAB-type ABC transporter *Sa*NsrFP, the energy supply is provided by the BceA-domain *Sa*NsrF[16]. By employing SEC-MALS-coupled analysis we were able to confirm a monomeric state of $SaNsrF_{WT}$ and its variant $SaNsrF_{H202A}$ in solution since the measured molecular masses corresponded with the calculated values for each monomer. This agrees with the oligomeric state of other NBDs from other ABC transporter families in the absence of nucleotide[34–36].

Furthermore, this is in line with our SAXS data that allowed the construction of a volumetric envelope of the $SaNsrF_{WT}$ monomer. The experimental structure of *Sa*NsrF has not been published yet. Here, we generated a structural model using TopModel[52] based on five main templates 1F3O_A, 5XU1_B, 2PCL_A, 5GKO_A, 2OLJ_A (Fig. 3A, 6B). We compared this model with the volumetric envelope obtained from SAXS data, showing high

reliability and agreement with experimental data. It is striking that the density of the protein model is partly not occupied. A flexible C-terminus could be the reason, which would make a temporary fit of the versatile C-terminal helix to the proposed model possible. As for well-studied NBDs such as HisP, the modeled *Sa*NsrF dimer exhibits the typical head-to-tail formation including two sandwiched ATP molecules in the dimer interface between the Walker A motif of the first monomer and the C-loop of the second one[22,24,25,30]. Therefore, the *Sa*NsrF protein shares many structural similarities with other known NBDs. As the γ-phosphate moiety of ATP was predicted to be in close proximity of the conserved histidine (H-loop) and the cofactor Mg^{2+}, one can deduce a consensus with the hypothesis of the H-loop acting as a sensor, whereas the cofactor is involved in hydrolytic cleavage while being coordinated by the Walker B motif (Fig. 3B,C)[22,23,26,28]. Furthermore, in *Sa*NsrF$_{WT}$, the interface between subunits is structurally less stable than in *Sa*NsrF$_{H202A}$. Since a shift of one monomer to the other is necessary for NDBs to perform their function, these results suggest that the substitution *Sa*NsrF$_{H202A}$ impacts the structural dynamics at the *Sa*NsrF interface and not only the catalytic mechanism.

Clearly, the *Sa*NsrF protein represent an isolated NBD and we do not know if the kinetic correspond to the ATP hydrolysis that will occur in the presence of the transmembrane protein *Sa*NsrP. However, when comparing the data with known NBDs which has been described before in the presence and absence of the transmembrane segment it can be observed that v_{max} might be changed, the k_m values however remains very similar. For example the ATP hydrolysis kinetics have been described for the HlyB NBD as well as for the purified full length transporter in detergent solution[26,36,38,43,69]. Here the NBD showed a v_{max} of 200 nmol min^{-1} mg^{-1} with a k_m value of 0.31 where as the full length transporter displayed a lower v_{max} of 8.1 nmol min^{-1} mg^{-1} with a k_m value of 0.36. This reduction is likely due to the detergent, which is present to keep the HlyB transporter in solution. Important, however is that in both cases the kinetic displayed cooperativity (Hill coefficient > 1) as in the case of *Sa*NsrF and the corresponding histidine mutation also resulted in an inactive protein. This shows that our NTP analysis of the *Sa*NsrF will likely be similar even when the TMD *Sa*NsrP is present. The same observations were found for the nisin transporter NisT from *L. lactis*[70] and the nukacin ISK-1 transporter NukT from *Staphylococcus arneri* ISK-1[71] albeit in detergent solution.

In summary, the experiments revealed the first detailed insights into biochemical properties of the BceA domain of the BceAB-type ABC transporter *Sa*NsrFP. We showed that *Sa*NsrF$_{WT}$ and its variant *Sa*NsrF$_{H202A}$ exist as monomers in solution and determined several physiological and structural properties of the protein by evaluating its ATPase activity in comprehensive in vitro studies and molecular modelling and simulations. Hence, this study contributes to the mechanistic and structural understanding of the BceAB-type ABC transporter family, which opens up the possibility to pharmacologically target this family in order to combat multidrug-resistant species in the long run. It further confirms in vivo data where the H202A variant of *Sa*NsrF displayed a loss in the activity, which now can be pinpointed to a lack of ATP hydrolysis, and shows that this variant can well serve as a negative control in studies concerning BceAB type transporters since the histidine is conserved throughout the sequence of this family.

Materials and methods

Expression of SaNsrF$_{WT}$ and SaNsrF$_{H202A}$. *E. coli* BL21 (DE3) strains were transformed via heat shock method[72] with pET-16b-NHis$_{10}$-*Sa*NsrF$_{WT}$ or pET-16b-NHis$_{10}$-*Sa*NsrF$_{H202A}$, respectively. Precultures were selectively grown with 20 µg mL^{-1} ampicillin at 37 °C and 180 rpm overnight. Lysogeny Broth (LB) medium was pre-incubated with 20 µg mL^{-1} ampicillin and inoculated with the respective preculture to an OD_{600} of 0.1. The cultures were grown to an OD_{600} of 0.4 at 37 °C and 180 rpm whereupon the temperature was reduced to 18 °C. Protein expression was induced by the addition of 1 mM IPTG at an OD_{600} of 0.8 and the cultures were further grown overnight.

Protein purification. *Sa*NsrF$_{WT}$ and *Sa*NsrF$_{H202A}$ were purified using Immobilized Metal Ion Chromatography (IMAC). Therefore, a 5 mL HiTrap Chelating HP column, loaded with Zn^{2+}, was equilibrated with low IMAC-buffer (100 mM HEPES at pH 8, 300 mM NaCl, 20% glycerol). Protein elution was undertaken with the high IMAC-buffer (low IMAC-buffer plus 125 mM histidine). A washing step of 40-percent high IMAC-buffer was introduced before. The concentrated eluted proteins were then injected onto a Superdex 75 16/60 size exclusion column at a flow rate of 0.5 mL min^{-1}, pre-equilibrated with SEC buffer (100 mM HEPES at pH 8, 300 mM NaCl, 20% glycerol). Protein eluates were collected and stored at 4 °C.

ATPase activity assay. The ATPase activity of *Sa*NsrF$_{WT}$ and *Sa*NsrF$_{H202A}$ (diluted in 100 mM HEPES at pH 8, 100 mM NaCl) was examined by the Malachite Green Phosphate Assay at a protein concentration of 0.1 mg mL^{-1} that was initially undertaken at room temperature (20 °C). Several parameters were screened to determine the optimal buffer and temperature conditions for the protein activity (see Supplementary Information).

Kinetic measurements for *Sa*NsrF$_{WT}$ and *Sa*NsrF$_{H202A}$ were performed under the influence of NTP (ATP, GTP, CTP, UTP) with concentrations ranging from 0 to 5 mM.

Therefore, the kinetics were fitted using the Hill equation:

$$Y = \frac{v_{max} \times X^h}{\left(k_{half}^h + X^h\right)}.$$

Y: ATPase activity [nmol min^{-1} mg^{-1}], X: substrate concentration [mM], k_{half}: substrate concentration at half-maximal reaction velocity [mM], h: Hill coefficient.

All shown data are representing the average of a triple evaluation at least, with the standard deviation reported as errors.

Small angle X-ray scattering (SAXS). We collected all SAXS data on our Xeuss 2.0 Q-Xoom system from Xenocs, equipped with a PILATUS 3 R 300 K detector (Dectris) and a GENIX 3D CU Ultra Low Divergence x-ray beam delivery system (Xenocs). The chosen sample to detector distance for the experiment was 0.55 m, results in an achievable q-range of 0.18–6 nm^{-1}. All measurements were performed at 15 °C with protein concentrations between 0.5 and 4.2 mg mL^{-1}. Samples were injected in the Low Noise Flow Cell (Xenocs) via autosampler. For each sample, twelve frames with an exposer time of ten minutes were collected. By comparing these frames, we excluded the possibility of aggregation and radiation damage during the measurement. Data were scaled to absolute intensity against water. All used programs for data processing were part of the ATSAS Software package (Version 3.0.1), available on the EMBL website[73]. Primary data reduction was performed with the program PRIMUS[74]. With the Guinier approximation we determined the forward scattering $I(0)$ and the radius of gyration (Rg)[75]. The program GNOM was used to estimate the maximum particle dimension (D_{max}) with the pair distribution function $p(r)$[76]. Low resolution ab initio models were calculated using GASBOR[51]. The superposition of a predicted *Sa*NsrF model (see below) was done using the program SUPCOMB[56].

Structural models of SaNsrF complexes. As an experimental *Sa*NsrF structure is not available, a homology model was constructed using the template-based protein structure prediction program TopModel[52] and the *Sa*$NsrF_{WT}$ sequence as input (NCBI Reference Sequence: WP_000923535.1). In order to build a *Sa*NsrF model arranged in a dimeric assembly with substrate (ATP) and cofactor (Mg^{2+}) bound, starting from the *Sa*$NsrF_{WT}$ monomer in the *apo* state, a search for sequence similarity and structural properties was performed on the Protein Data Bank. The results were filtered according to the following criteria: sequence identity ≥ 33% and E-value cutoff 0.001 as determined by BLAST[77]; oligomeric state equals 2; sequence length of 250 ± 50 residues; resolution ≤ 2 Å. Out of six results, only one (PDB ID: 1L2T[28]) is crystallized as a functionally active "ATP sandwich" symmetrical dimer and was therefore used as a reference. Since ATP is bound at the interface of the dimer and its binding is influenced by both protein subunits, both protein–ligand and protein–protein docking would be particularly challenging in this case. Hence, we constructed first the *Sa*$NsrF_{WT}$ dimer in the *apo* form and the ATP/Mg^{2+}-bound form subsequently.

To do so, protein–protein docking was performed with the program HADDOCK[78,79], using distances between respective three residues that bridge the two subunits together with H-bond interactions as restraints (S40/S43, R153/R152 and D177/D176, for PDB ID 1L2T/*Sa*$NsrF_{WT}$ sequences, respectively). The most similar docking solution to the reference PDB ID 1L2T was used for further modeling steps.

Both, *Sa*$NsrF_{WT}$ monomer and dimer structures were preprocessed with the Protein Preparation Wizard[80] of Schrödinger's Maestro Suite. Since the residues at the binding sites are highly conserved, ATP and Mg^{2+} are considered to bind in a very similar way as in PDB ID 1L2T. Thus, their coordinates were copied from the reference into the *Sa*$NsrF_{WT}$ model after alignment to one protein subunit. Residues located ≤ 5 Å away from the ATP molecules were energy-minimized using the OPLS 2005 force field[81] with standard cutoff values for van der Waals, electrostatic, and H-bond interactions, until the average RMSD of non-hydrogen atoms reaches 0.30 Å. Bond orders as well as missing hydrogen atoms were assigned, and the H-bond network was optimized. Finally, residue 202 was substituted to construct the *Sa*$NsrF_{H202A}$ variant of the monomer and dimer.

Molecular dynamics simulations. In order to validate the modeled protein–protein interface and the ATP binding mode, and to investigate the impact of the *Sa*$NsrF_{H202A}$ substitution on structural dynamics, a set of MD simulations was performed using Amber 2019[82]. Four different ATP/Mg^{2+}-bound *Sa*NsrF systems were prepared for this with the LEaP program[83]: monomer and dimer, both for *Sa*$NsrF_{WT}$ and *Sa*$NsrF_{H202A}$.

After establishing charge neutrality by adding sodium counter ions, each system was placed in a truncated octahedral box of TIP3P[84] water with a distance of the nearest atom to the border of the box of ≥ 11 Å. Structural relaxation, thermalization, and production runs of MD simulations were conducted with pmemd.cuda[85] using the ff14SB force field[86] for the protein, Joung-Cheatham parameters[87] for ions, and available ATP parameters[88]. For each starting complex, five independent replicas of 500 ns length each were performed, resulting in a cumulative simulation time of 10 µs. In order to set up independent replicas and obtain slightly different starting structures, the target temperature was set to different values during thermalization (299.8 K, 299.9 K, 300.0 K, 300.1 K, 300.2 K and 300.3 K). A detailed description of the thermalization protocol can be found elsewhere[89]. The analysis of the MD trajectories was carried out with cpptraj[90] on snapshots extracted every 1 ns. All the MD-generated conformations were clustered applying a hierarchical agglomerative approach and an RMSD cutoff value of 4 Å. The representative structure of the *Sa*$NsrF_{WT}$ monomer was compared to the experimentally determined SAXS density.

The representative structure of the most populated cluster for the *Sa*$NsrF_{WT}$ dimer was used to calculate the electrostatic potential with the Adaptive Poisson-Boltzmann Solver (APBS) software package[49] as implemented in PyMOL[91]. Dielectric constants (ε) of 2.0 and 78.0 were used, respectively, for the protein and for water, and the concentration of monovalent cations and anions was set to 0.15 M.

To measure structural mobility, we computed the residue-wise root-mean-square fluctuation (RMSF) of backbone atoms. Structural changes over time, both for the *apo* *Sa*NsrF proteins and the ATP/Mg^{2+}-bound form, were detected calculating the root-mean-square deviation of atomic positions (RMSD) compared to the initial structure. To describe the changes occurring at the level of the interface, we performed two analyses: (I) measurement of the distance between the center of mass of two residues located in opposite subunits at the center of the interface (S43 and S146); (II) H-bond analysis (i) in terms of the total number of interactions between

two subunits (SaNsrF$_A$–SaNsrF$_B$) and between protein and ligands (SaNsrF-(ATP-Mg^{2+})) and ii) residue-wise H-bound occupancy between residues of the two subunits (SaNsrF$_A$–SaNsrF$_B$), allowing to identify which residues perform more frequent H-bonds throughout the simulations. For this analysis, only H-bonds with the following criteria were considered: occupancy between specific donor and acceptor > 1%; H-bond present in at least two replicas of the same system; H-bonds between two residues with residue-wise occupancy > 10% in at least one system.

Molecular docking of other NTPs. To predict the binding mode of other NTPs in complex with the SaNsrF$_{WT}$ dimer, molecular docking was performed. The starting points for these calculations were the five structures resulting from thermalization and equilibration steps, then used also for independent MD simulations replicas (production).

First, for each binding site a cubic grid of 20 Å length centered on the respective ATP molecule was built in the Maestro platform[92], for a total of 10 different grids. Then, starting from the ATP structures, other NTPs were built (GTP, CTP and UTP) by modifying the nucleobase. The generated conformations were refined and scored with the Glide-Extra precision (XP) mode of Glide[93]. Only the best solution for each NTP in each grid was considered. The Coulomb interaction energy (ecoul) and the van der Waals energy (evdw), components of the XP GlideScore scoring function, were computed, and used to describe the enthalpic contribution of binding.

Data availability

We upload the SAXS data and the corresponding model of SaNsrF to the Small Angle Scattering Biological Data Bank (SASBDB)[54,55], with the accession code SASDJR3.

Received: 19 July 2020; Accepted: 27 August 2020
Published online: 16 September 2020

References

1. Gould, K. Antibiotics: from prehistory to the present day. *J. Antimicrob. Chemother.* **71**, 572–575. https://doi.org/10.1093/jac/dkv484 (2016).
2. Meade, E., Slattery, M. A. & Garvey, M. Bacteriocins, potent antimicrobial peptides and the fight against multi drug resistant species: resistance is futile?. *Antibiotics* https://doi.org/10.3390/antibiotics9010032 (2020).
3. Cotter, P. D., Hill, C. & Ross, R. P. Bacterial lantibiotics: strategies to improve therapeutic potential. *Curr. Protein Pept. Sci.* **6**, 61–75. https://doi.org/10.2174/1389203053027584 (2005).
4. Clemens, R., Zaschke-Kriesche, J., Khosa, S. & Smits, S. H. J. Insight into two ABC transporter Families involved in lantibiotic resistance. *Front. Mol. Biosci.* **4**, 91. https://doi.org/10.3389/fmolb.2017.00091 (2017).
5. Bierbaum, G. & Sahl, H. G. Lantibiotics: mode of action, biosynthesis and bioengineering. *Curr. Pharm. Biotechnol.* **10**, 2–18. https://doi.org/10.2174/138920109787048616 (2009).
6. Chatterjee, C., Paul, M., Xie, L. & van der Donk, W. A. Biosynthesis and mode of action of lantibiotics. *Chem. Rev.* **105**, 633–684. https://doi.org/10.1021/cr030105v (2005).
7. Jabes, D. *et al.* Efficacy of the new lantibiotic NAI-107 in experimental infections induced by multidrug-resistant Gram-positive pathogens. *Antimicrob. Agents Chemother.* **55**, 1671–1676. https://doi.org/10.1128/AAC.01288-10 (2011).
8. Reiners, J. *et al.* The N-terminal region of nisin is important for the BceAB-type ABC transporter NsrFP from *Streptococcus agalactiae* COH1. *Front. Microbiol.* **8**, 1643. https://doi.org/10.3389/fmicb.2017.01643 (2017).
9. Malin, J. J. & de Leeuw, E. Therapeutic compounds targeting Lipid II for antibacterial purposes. *Infect. Drug Resist.* **12**, 2613–2625. https://doi.org/10.2147/IDR.S215070 (2019).
10. Breukink, E. *et al.* Use of the cell wall precursor lipid II by a pore-forming peptide antibiotic. *Science* **286**, 2361–2364. https://doi.org/10.1126/science.286.5448.2361 (1999).
11. Hasper, H. E., de Kruijff, B. & Breukink, E. Assembly and stability of nisin-lipid II pores. *Biochemistry* **43**, 11567–11575. https://doi.org/10.1021/bi049476b (2004).
12. AlKhatib, Z. *et al.* The C-terminus of nisin is important for the ABC transporter NisFEG to confer immunity in *Lactococcus lactis*. *Microbiologyopen* **3**, 752–763. https://doi.org/10.1002/mbo3.205 (2014).
13. Draper, L. A., Cotter, P. D., Hill, C. & Ross, R. P. Lantibiotic resistance. *Microbiol. Mol. Biol. Rev.* **79**, 171–191. https://doi.org/10.1128/MMBR.00051-14 (2015).
14. Ohki, R. *et al.* The BceRS two-component regulatory system induces expression of the bacitracin transporter, BceAB, Bacillus subtilis. *Mol. Microbiol.* **49**, 1135–1144. https://doi.org/10.1046/j.1365-2958.2003.03653.x (2003).
15. Podlesek, Z. *et al. Bacillus licheniformis* bacitracin-resistance ABC transporter: relationship to mammalian multidrug resistance. *Mol. Microbiol.* **16**, 969–976. https://doi.org/10.1111/j.1365-2958.1995.tb02322.x (1995).
16. Khosa, S., AlKhatib, Z. & Smits, S. H. NSR from *Streptococcus agalactiae* confers resistance against nisin and is encoded by a conserved nsr operon. *Biol. Chem.* **394**, 1543–1549. https://doi.org/10.1515/hsz-2013-0167 (2013).
17. Khosa, S. *et al.* Structural basis of lantibiotic recognition by the nisin resistance protein from *Streptococcus agalactiae*. *Sci. Rep.* **6**, 18679. https://doi.org/10.1038/srep18679 (2016).
18. Khosa, S., Hoeppner, A., Gohlke, H., Schmitt, L. & Smits, S. H. Structure of the response regulator NsrR from *Streptococcus agalactiae*, which is involved in lantibiotic resistance. *PLoS ONE* **11**, e0149903. https://doi.org/10.1371/journal.pone.0149903 (2016).
19. Kerr, I. D. Structure and association of ATP-binding cassette transporter nucleotide-binding domains. *Biochim. Biophys. Acta* **1561**, 47–64. https://doi.org/10.1016/s0304-4157(01)00008-9 (2002).
20. Lawson, J., O'Mara, M. L. & Kerr, I. D. Structure-based interpretation of the mutagenesis database for the nucleotide binding domains of P-glycoprotein. *Biochim. Biophys. Acta* **1778**, 376–391. https://doi.org/10.1016/j.bbamem.2007.10.021 (2008).
21. Walker, J. E., Saraste, M., Runswick, M. J. & Gay, N. J. Distantly related sequences in the alpha- and beta-subunits of ATP synthase, myosin, kinases and other ATP-requiring enzymes and a common nucleotide binding fold. *EMBO J.* **1**, 945–951 (1982).
22. Szollosi, D., Rose-Sperling, D., Hellmich, U. A. & Stockner, T. Comparison of mechanistic transport cycle models of ABC exporters. *Biochim. Biophys. Acta Biomembr.* **818–832**, 2018. https://doi.org/10.1016/j.bbamem.2017.10.028 (1860).
23. Schmitt, L., Benabdelhak, H., Blight, M. A., Holland, I. B. & Stubbs, M. T. Crystal structure of the nucleotide-binding domain of the ABC-transporter haemolysin B: identification of a variable region within ABC helical domains. *J. Mol. Biol.* **330**, 333–342. https://doi.org/10.1016/s0022-2836(03)00592-8 (2003).
24. Schmitt, L. & Tampe, R. Structure and mechanism of ABC transporters. *Curr. Opin. Struct. Biol.* **12**, 754–760. https://doi.org/10.1016/s0959-440x(02)00399-8 (2002).
25. Wilkens, S. Structure and mechanism of ABC transporters. *F1000Prime Rep* **7**, 14. https://doi.org/10.12703/P7-14 (2015).

26. Hanekop, N., Zaitseva, J., Jenewein, S., Holland, I. B. & Schmitt, L. Molecular insights into the mechanism of ATP-hydrolysis by the NBD of the ABC-transporter HlyB. *FEBS Lett.* **580**, 1036–1041. https://doi.org/10.1016/j.febslet.2005.11.012 (2006).
27. Schmees, G., Stein, A., Hunke, S., Landmesser, H. & Schneider, E. Functional consequences of mutations in the conserved "signature sequence" of the ATP-binding-cassette protein MalK. *Eur J. Biochem.* **266**, 420–430. https://doi.org/10.1046/j.1432-1327.1999.00871.x (1999).
28. Smith, P. C. *et al.* ATP binding to the motor domain from an ABC transporter drives formation of a nucleotide sandwich dimer. *Mol. Cell.* **10**, 139–149 (2002).
29. Chen, J., Lu, G., Lin, J., Davidson, A. L. & Quiocho, F. A. A tweezers-like motion of the ATP-binding cassette dimer in an ABC transport cycle. *Mol. Cell.* **12**, 651–661. https://doi.org/10.1016/j.molcel.2003.08.004 (2003).
30. Locher, K. P. Structure and mechanism of ABC transporters. *Curr. Opin. Struct. Biol.* **14**, 426–431. https://doi.org/10.1016/j.sbi.2004.06.005 (2004).
31. Szollosi, D., Szakacs, G., Chiba, P. & Stockner, T. Dissecting the forces that dominate dimerization of the nucleotide binding domains of ABCB1. *Biophys. J.* **114**, 331–342. https://doi.org/10.1016/j.bpj.2017.11.022 (2018).
32. Wagner, M., Smits, S. H. J. & Schmitt, L. In vitro NTPase activity of highly purified Pdr5, a major yeast ABC multidrug transporter. *Sci. Rep.* **9**, 7761. https://doi.org/10.1038/s41598-019-44327-8 (2019).
33. Sahin, E. & Roberts, C. J. Size-exclusion chromatography with multi-angle light scattering for elucidating protein aggregation mechanisms. *Methods Mol. Biol.* **899**, 403–423. https://doi.org/10.1007/978-1-61779-921-1_25 (2012).
34. Greller, G., Horlacher, R., DiRuggiero, J. & Boos, W. Molecular and biochemical analysis of MalK, the ATP-hydrolyzing subunit of the trehalose/maltose transport system of the hyperthermophilic archaeon *Thermococcus litoralis*. *J. Biol. Chem.* **274**, 20259–20264. https://doi.org/10.1074/jbc.274.29.20259 (1999).
35. Nikaido, K., Liu, P. Q. & Ames, G. F. Purification and characterization of HisP, the ATP-binding subunit of a traffic ATPase (ABC transporter), the histidine permease of *Salmonella typhimurium*. Solubility, dimerization, and ATPase activity. *J. Biol. Chem.* **272**, 27745–27752. https://doi.org/10.1074/jbc.272.44.27745 (1997).
36. Zaitseva, J. *et al.* Functional characterization and ATP-induced dimerization of the isolated ABC-domain of the haemolysin B transporter. *Biochemistry* **44**, 9680–9690. https://doi.org/10.1021/bi0506122 (2005).
37. Kolaczkowski, M., Sroda-Pomianek, K., Kolaczkowska, A. & Michalak, K. A conserved interdomain communication pathway of pseudosymmetrically distributed residues affects substrate specificity of the fungal multidrug transporter Cdr1p. *Biochim Biophys Acta* **479–490**, 2013. https://doi.org/10.1016/j.bbamem.2012.10.024 (1828).
38. Zaitseva, J., Jenewein, S., Jumpertz, T., Holland, I. B. & Schmitt, L. H662 is the linchpin of ATP hydrolysis in the nucleotide-binding domain of the ABC transporter HlyB. *EMBO J.* **24**, 1901–1910. https://doi.org/10.1038/sj.emboj.7600657 (2005).
39. Zhou, Y., Ojeda-May, P. & Pu, J. H-loop histidine catalyzes ATP hydrolysis in the *E. coli* ABC-transporter HlyB. *Phys Chem Chem Phys* **15**, 15811–15815. https://doi.org/10.1039/c3cp50965f (2013).
40. Lagedroste, M., Reiners, J., Smits, S. H. J. & Schmitt, L. Systematic characterization of position one variants within the lantibiotic nisin. *Sci. Rep.* **9**, 935. https://doi.org/10.1038/s41598-018-37532-4 (2019).
41. Davidson, A. L., Laghaeian, S. S. & Mannering, D. E. The maltose transport system of *Escherichia coli* displays positive cooperativity in ATP hydrolysis. *J. Biol. Chem.* **271**, 4858–4863 (1996).
42. Senior, A. E. & Bhagat, S. P-glycoprotein shows strong catalytic cooperativity between the two nucleotide sites. *Biochemistry* **37**, 831–836. https://doi.org/10.1021/bi9719962 (1998).
43. Zaitseva, J. *et al.* A structural analysis of asymmetry required for catalytic activity of an ABC-ATPase domain dimer. *EMBO J.* **25**, 3432–3443. https://doi.org/10.1038/sj.emboj.7601208 (2006).
44. Okada, U. *et al.* Crystal structure of tripartite-type ABC transporter MacB from *Acinetobacter baumannii*. *Nat. Commun.* **8**, 1336. https://doi.org/10.1038/s41467-017-01399-2 (2017).
45. Yang, H. B. *et al.* Structure of a MacAB-like efflux pump from *Streptococcus pneumoniae*. *Nat. Commun.* **9**, 196. https://doi.org/10.1038/s41467-017-02741-4 (2018).
46. Mulnaes, D. & Gohlke, H. TopScore: using deep neural networks and large diverse data sets for accurate protein model quality assessment. *J. Chem. Theory. Comput.* **14**, 6117–6126. https://doi.org/10.1021/acs.jctc.8b00690 (2018).
47. Mariani, V., Biasini, M., Barbato, A. & Schwede, T. lDDT: a local superposition-free score for comparing protein structures and models using distance difference tests. *Bioinformatics* **29**, 2722–2728. https://doi.org/10.1093/bioinformatics/btt473 (2013).
48. Ishii, S., Yano, T., Okamoto, A., Murakawa, T. & Hayashi, H. Boundary of the nucleotide-binding domain of *Streptococcus* ComA based on functional and structural analysis. *Biochemistry* **52**, 2545–2555. https://doi.org/10.1021/bi3017069 (2013).
49. Baker, N. A., Sept, D., Joseph, S., Holst, M. J. & McCammon, J. A. Electrostatics of nanosystems: application to microtubules and the ribosome. *Proc. Natl. Acad. Sci. USA* **98**, 10037–10041. https://doi.org/10.1073/pnas.181342398 (2001).
50. Damas, J. M., Oliveira, A. S., Baptista, A. M. & Soares, C. M. Structural consequences of ATP hydrolysis on the ABC transporter NBD dimer: molecular dynamics studies of HlyB. *Protein Sci.* **20**, 1220–1230. https://doi.org/10.1002/pro.650 (2011).
51. Svergun, D. I., Petoukhov, M. V. & Koch, M. H. Determination of domain structure of proteins from X-ray solution scattering. *Biophys J* **80**, 2946–2953. https://doi.org/10.1016/S0006-3495(01)76260-1 (2001).
52. Mulnaes, D. *et al.* TopModel: template-based protein structure prediction at low sequence identity using top-down consensus and deep neural networks. *J. Chem. Theory Comput.* **16**, 1953–1967. https://doi.org/10.1021/acs.jctc.9b00825 (2020).
53. Svergun, D., Barberato, C. & Koch, M. H. J. CRYSOL: a program to evaluate x-ray solution scattering of biological macromolecules from atomic coordinates. *J. Appl. Crystallogr.* **28**, 768–773. https://doi.org/10.1107/S0021889895007047 (1995).
54. Valentini, E., Kikhney, A. G., Previtali, G., Jeffries, C. M. & Svergun, D. I. SASBDB, a repository for biological small-angle scattering data. *Nucleic Acids Res.* **43**, D357-363. https://doi.org/10.1093/nar/gku1047 (2015).
55. Kikhney, A. G., Borges, C. R., Molodenskiy, D. S., Jeffries, C. M. & Svergun, D. I. SASBDB: towards an automatically curated and validated repository for biological scattering data. *Protein Sci.* **29**, 66–75. https://doi.org/10.1002/pro.3731 (2020).
56. Kozin, M. B. & Svergun, D. I. Automated matching of high- and low-resolution structural models. *J. Appl. Crystallogr.* **34**, 33–41. https://doi.org/10.1107/S0021889800014126 (2001).
57. Collins, B., Curtis, N., Cotter, P. D., Hill, C. & Ross, R. P. The ABC transporter AnrAB contributes to the innate resistance of *Listeria monocytogenes* to nisin, bacitracin, and various beta-lactam antibiotics. *Antimicrob. Agents Chemother.* **54**, 4416–4423. https://doi.org/10.1128/AAC.00503-10 (2010).
58. Hiron, A., Falord, M., Valle, J., Debarbouille, M. & Msadek, T. Bacitracin and nisin resistance in *Staphylococcus aureus*: a novel pathway involving the BraS/BraR two-component system (SA2417/SA2418) and both the BraD/BraE and VraD/VraE ABC transporters. *Mol. Microbiol.* **81**, 602–622. https://doi.org/10.1111/j.1365-2958.2011.07735.x (2011).
59. Popella, P. *et al.* VraH is the third component of the *Staphylococcus aureus* VraDEH system involved in gallidermin and daptomycin resistance and pathogenicity. *Antimicrob. Agents Chemother.* **60**, 2391–2401. https://doi.org/10.1128/AAC.02865-15 (2016).
60. Staron, A., Finkeisen, D. E. & Mascher, T. Peptide antibiotic sensing and detoxification modules of *Bacillus subtilis*. *Antimicrob. Agents Chemother.* **55**, 515–525. https://doi.org/10.1128/AAC.00352-10 (2011).
61. Yang, J., Yu, M., Jan, Y. N. & Jan, L. Y. Stabilization of ion selectivity filter by pore loop ion pairs in an inwardly rectifying potassium channel. *Proc. Natl. Acad. Sci. USA* **94**, 1568–1572. https://doi.org/10.1073/pnas.94.4.1568 (1997).
62. Ramaen, O. *et al.* Structure of the human multidrug resistance protein 1 nucleotide binding domain 1 bound to Mg2+/ATP reveals a non-productive catalytic site. *J. Mol. Biol.* **359**, 940–949. https://doi.org/10.1016/j.jmb.2006.04.005 (2006).

63. Benabdelhak, H. *et al.* Positive co-operative activity and dimerization of the isolated ABC ATPase domain of HlyB from *Escherichia coli*. *Biochem. J.* **386**, 489–495. https://doi.org/10.1042/BJ20041282 (2005).
64. Ramaen, O., Sizun, C., Pamlard, O., Jacquet, E. & Lallemand, J. Y. Attempts to characterize the NBD heterodimer of MRP1: transient complex formation involves Gly771 of the ABC signature sequence but does not enhance the intrinsic ATPase activity. *Biochem. J.* **391**, 481–490. https://doi.org/10.1042/BJ20050897 (2005).
65. Schultz, K. M., Merten, J. A. & Klug, C. S. Characterization of the E506Q and H537A dysfunctional mutants in the *E. coli* ABC transporter MsbA. *Biochemistry* **50**, 3599–3608. https://doi.org/10.1021/bi101666p (2011).
66. Osorio, H. *et al.* H2O2, but not menadione, provokes a decrease in the ATP and an increase in the inosine levels in *Saccharomyces cerevisiae*: an experimental and theoretical approach. *Eur. J. Biochem.* **270**, 1578–1589. https://doi.org/10.1046/j.1432-1033.2003.03529.x (2003).
67. Buckstein, M. H., He, J. & Rubin, H. Characterization of nucleotide pools as a function of physiological state in *Escherichia coli*. *J. Bacteriol.* **190**, 718–726. https://doi.org/10.1128/JB.01020-07 (2008).
68. Bochner, B. R. & Ames, B. N. Complete analysis of cellular nucleotides by two-dimensional thin layer chromatography. *J. Biol. Chem.* **257**, 9759–9769 (1982).
69. Reimann, S. *et al.* Interdomain regulation of the ATPase activity of the ABC transporter haemolysin B from *Escherichia coli*. *Biochem. J.* **473**, 2471–2483. https://doi.org/10.1042/BCJ20160154 (2016).
70. Lagedroste, M., Reiners, J., Smits, S. H. J. & Schmitt, L. Impact of the nisin modification machinery on the transport kinetics of NisT. *Sci. Rep.* **10**, 12295. https://doi.org/10.1038/s41598-020-69225-2 (2020).
71. Zheng, S., Nagao, J. I., Nishie, M., Zendo, T. & Sonomoto, K. ATPase activity regulation by leader peptide processing of ABC transporter maturation and secretion protein, NukT, for lantibiotic nukacin ISK-1. *Appl. Microbiol. Biotechnol.* **102**, 763–772. https://doi.org/10.1007/s00253-017-8645-2 (2018).
72. Hanahan, D. Studies on transformation of *Escherichia coli* with plasmids. *J. Mol. Biol.* **166**, 557–580. https://doi.org/10.1016/s0022-2836(83)80284-8 (1983).
73. Franke, D. *et al.* ATSAS 2.8: a comprehensive data analysis suite for small-angle scattering from macromolecular solutions. *J. Appl. Crystallogr.* **50**, 1212–1225. https://doi.org/10.1107/S1600576717007786 (2017).
74. Konarev, P. V., Volkov, V. V., Sokolova, A. V., Koch, M. H. J. & Svergun, D. I. PRIMUS: a Windows PC-based system for small-angle scattering data analysis. *J. Appl. Crystallogr.* **36**, 1277–1282. https://doi.org/10.1107/S0021889803012779 (2003).
75. Guinier, A. Diffraction of x-rays of very small angles-application to the study of ultramicroscopic phenomenon. *Ann. Phys.* **12**, 161–237 (1939).
76. Svergun, D. I. Determination of the regularization parameter in indirect-transform methods using perceptual criteria. *J. Appl. Crystallogr.* **25**, 495–503. https://doi.org/10.1107/S0021889892001663 (1992).
77. Altschul, S. F., Gish, W., Miller, W., Myers, E. W. & Lipman, D. J. Basic local alignment search tool. *J. Mol. Biol.* **215**, 403–410. https://doi.org/10.1016/S0022-2836(05)80360-2 (1990).
78. Dominguez, C., Boelens, R. & Bonvin, A. M. HADDOCK: a protein-protein docking approach based on biochemical or biophysical information. *J. Am. Chem. Soc.* **125**, 1731–1737. https://doi.org/10.1021/ja026939x (2003).
79. van Zundert, G. C. P. *et al.* The HADDOCK2.2 web server: user-friendly integrative modeling of biomolecular complexes. *J. Mol. Biol.* **428**, 720–725. https://doi.org/10.1016/j.jmb.2015.09.014 (2016).
80. Schrödinger Release 2017-1: Schrödinger Suite 2017-1 Protein Preparation Wizard, Schrödinger, LLC, New York, NY, 2017.
81. Banks, J. L. *et al.* Integrated modeling program, applied chemical theory (IMPACT). *J. Comput. Chem.* **26**, 1752–1780. https://doi.org/10.1002/jcc.20292 (2005).
82. Case, D. A. *et al. Amber* (University of California, San Francisco, 2019).
83. Schafmeister Ceaf, R. W. & Romanovski, V. *LEaP* (University of California, San Francisco, 1995).
84. Jorgensen, W. L., Chandrasekhar, J., Madura, J. D., Impey, R. W. & Klein, M. L. Comparison of simple potential functions for simulating liquid water. *J. Chem. Phys.* **79**, 926–935. https://doi.org/10.1063/1.445869 (1983).
85. Salomon-Ferrer, R., Gotz, A. W., Poole, D., Le Grand, S. & Walker, R. C. Routine microsecond molecular dynamics simulations with AMBER on GPUs 2 explicit solvent particle mesh ewald. *J. Chem. Theory Comput.* **9**, 3878–3888. https://doi.org/10.1021/ct400314y (2013).
86. Maier, J. A. *et al.* ff14SB: improving the accuracy of protein side chain and backbone parameters from ff99SB. *J. Chem. Theory. Comput.* **11**, 3696–3713. https://doi.org/10.1021/acs.jctc.5b00255 (2015).
87. Joung, I. S. & Cheatham, T. E. 3rd. Determination of alkali and halide monovalent ion parameters for use in explicitly solvated biomolecular simulations. *J. Phys. Chem. B* **112**, 9020–9041. https://doi.org/10.1021/jp8001614 (2008).
88. Meagher, K. L., Redman, L. T. & Carlson, H. A. Development of polyphosphate parameters for use with the AMBER force field. *J. Comput. Chem.* **24**, 1016–1025. https://doi.org/10.1002/jcc.10262 (2003).
89. Frieg, B. *et al.* Molecular mechanisms of glutamine synthetase mutations that lead to clinically relevant pathologies. *PLoS Comput. Biol.* **12**, e1004693. https://doi.org/10.1371/journal.pcbi.1004693 (2016).
90. Roe, D. R. & Cheatham, T. E. 3rd. PTRAJ and CPPTRAJ: SOFTWARE for processing and analysis of molecular dynamics trajectory data. *J. Chem. Theory Comput.* **9**, 3084–3095. https://doi.org/10.1021/ct400341p (2013).
91. The PyMOL Molecular Graphics System, Version 2.0 Schrödinger, LLC.
92. Schrödinger Release 2020-2: Maestro, Schrödinger, LLC, New York (2020).
93. Schrödinger Release 2020-2: Schrödinger Suite 2020-2 Glide, Schrödinger, LLC, New York (2020).

Acknowledgements

We thank Lutz Schmitt for his continuous support and the members of the Institute of Biochemistry for valuable discussions. This work has been funded by the Deutsche Forschungsgemeinschaft (DFG, German Research Foundation)—Project number 270650915 (Research Training Group GRK2158, TP4a to H.G. and TP4b to S.S.). The Center for Structural studies is funded by the DFG (Grant Number 417919780 and INST 208/761-1 FUGG to S.S.). H.G. is grateful for computational support by the "Zentrum für Informations und Medientechnologie" at the Heinrich-Heine-Universität Düsseldorf and the computing time provided by the John von Neumann Institute for Computing (NIC) to H.G. on the supercomputer JUWELS at Jülich Supercomputing Centre (JSC) (user IDs: HKF7).

Author contributions

S.H.J.S. conceived and coordinated the study and evaluated all data; F.F performed overexpression, purification and functional characterization of the *Sa*NsrF enzymes and contributed to the writing; J.R. performed the SAXS and data analysis, and contributed to the writing; D.T.H., J.S. and J.G. did the cloning and established the purification protocol; H.G. conceptualized and supervised molecular modeling and simulation, analyzed the

data, and contributed to the writing; N.P. performed molecular modeling and simulation, analyzed the data, and contributed to the writing.

Funding
This work has been funded by the Deutsche Forschungsgemeinschaft (DFG, German Research Foundation)—Project Number 270650915 (Research Training Group GRK2158, TP4a to H.G. and TP4b to S.S.). The Center for Structural studies is funded by the DFG (Grant Number 417919780 and INST 208/761-1 FUGG to S.S.). H.G. is grateful for computational support by the "Zentrum für Informations und Medientechnologie" at the Heinrich-Heine-Universität Düsseldorf and the computing time provided by the John von Neumann Institute for Computing (NIC) to H.G. on the supercomputer JUWELS at Jülich Supercomputing Centre (JSC) (user IDs: HKF7). Open Access funding provided by Projekt DEAL.

Competing interests
The authors declare no competing interests.

Additional information
Supplementary information is available for this paper at https://doi.org/10.1038/s41598-020-72237-7.

Correspondence and requests for materials should be addressed to S.H.J.S.

Reprints and permissions information is available at www.nature.com/reprints.

Publisher's note Springer Nature remains neutral with regard to jurisdictional claims in published maps and institutional affiliations.

Supporting information

Characterization of the Nucleotide-Binding Domain NsrF from the BceAB-type ABC-Transporter NsrFP from the Human Pathogen *Streptococcus agalactiae*

Fabia Furtmann[1*], Nicola Porta[2*], Dai Tri Hoang[1], Jens Reiners[3], Julia Schumacher[1], Julia Gottstein[1], Holger Gohlke[2,4], Sander H. J. Smits[1,3#]

[1]Institute of Biochemistry, Heinrich-Heine-Universität Düsseldorf, Universitätsstraße 1, 40225 Düsseldorf, Germany

[2]Institute for Pharmaceutical and Medicinal Chemistry, Heinrich-Heine-Universität Düsseldorf, Universitätsstraße 1, 40225 Düsseldorf, Germany.

[3]Center for Structural Studies, Heinrich-Heine-Universität Düsseldorf, Universitätsstraße 1, 40225 Düsseldorf, Germany

[4]John von Neumann Institute for Computing (NIC), Jülich Supercomputing Centre (JSC), Institute of Biological Information Processing (IBI-7: Structural Biochemistry), Forschungszentrum Jülich GmbH, Wilhelm-Johnen-Straße, 52425 Jülich, Germany.

*These authors contributed equally

Keywords: antibiotic resistance, lantibiotics, nisin, ABC transporter, molecular dynamics simulations, structural model

Author ORCID
Nicola Porta: 0000-0002-6005-4372
Holger Gohlke: 0000-0001-8613-1447
Sander Smits: 0000-0003-0780-9251

[#] Corresponding author: Sander Smits
Address: Universitätsstr. 1, 40225 Düsseldorf, Germany.
Phone: (+49) 211 81 12647; Fax: (+49) 211 81 15037
E-mail: sander.smits@hhu.de

Materials and Methods

Multiangle Light Scattering (MALS)

To determine the protein's stoichiometry, Multiangle Light Scattering (MALS) was employed. Each protein was diluted in 100 mM HEPES at pH 8 and 300 mM NaCl. An Agilent 1260 HPLC system was used in combination with a triple-angle light scatter detector (miniDAWN TREOS II) and a differential refractive index detector (Optilab T-rEX) (both Wyatt Technology). *Sa*NsrF$_{WT}$ at a concentration of 3 mg/mL were injected onto a Superdex 75 16/300 increase column with a flowrate of 0.6 mL/min. For analysis the ASTRA software package (Astra 7.1) (Wyatt Technology) was used (Fig. 1B).

ATPase Activity Assay

The ATPase activity of *Sa*NsrF$_{WT}$ and *Sa*NsrF$_{H202A}$ (diluted in 100 mM HEPES at pH 8, 100 mM NaCl) was examined by the Malachite Green Phosphate Assay at a protein concentration of 0.1 mg/mL that was initially undertaken at room temperature (20 °C). The initial conditions required a final Mg^{2+}-concentration of 10 mM and an ATP concentration from 0 – 5 mM that was used for the reaction start.

Changes in protein's activity were detected in a time range from 4 – 26 min by stopping a part of the reaction every two minutes, whereupon 18 min were chosen as an optimal time of incubation. An ATP (or NTP) concentration was set at 3 mM for following ATPase screenings. By the addition of EDTA (final concentration: 50 mM) a control was implemented in order to observe the process of autohydrolysis in a Mg^{2+}-free solution.

To determine the maximal possible hydrolysis activity of *Sa*NsrF$_{WT}$, the protein was exposed to various buffer systems including a citrate buffer for pH 4 and 5, MES for pH 6, HEPES for pH 7 and 8, TRIS for pH 7, 8, 9 and CAPS for pH 10 and 11 (100 mM for each). Moreover, the influence of the NaCl concentration on the ATPase-buffer was analysed by determining the ATP hydrolysis of the *Sa*NsrF$_{WT}$ proteins in a buffer with 0, 100, 200, 300, 400, 500 and 1000 mM NaCl. Investigations were made concerning the cofactor choice of *Sa*NsrF$_{WT}$ by introducing Ca^{2+}, Mn^{2+}, Zn^{2+}, Fe^{2+} and Cu^{2+} instead of Mg^{2+} at a final concentration of 10 mM. An identical setup was performed without the addition of protein, which was used as a blank to encounter for autohydrolysis. The reaction including the optimized parameters was performed at 20 °C, 25 °C, 30 °C and 37 °C.

Results

Activity of SaNsrF$_{WT}$

After successful purification, we functionally characterized *Sa*NsrF$_{WT}$. To do so, we screened the following parameters on their influence on the ATP hydrolysis velocity: I) pH, II) salt concentration,

III) nature of the divalent ion, and IV) temperature. This allowed us to obtain optimal conditions for our kinetic measurements

pH dependency of SaNsrF$_{WT}$

We assayed the ATP hydrolysis of the *Sa*NsrF$_{WT}$ protein at different pH conditions in order to determine the optimal buffer composition. Therefore, we used 100 mM of the following buffers: citrate at pH 4.0 – 5.0, MES at pH 6.0, HEPES at pH 7.0 – 8.0, TRIS at pH 7.0 – 9.0 and CAPS at pH 10.0 – 11.0.

We observed a large dependence on the pH of the buffer system (Figure 2A). ATP hydrolysis mediated by *Sa*NsrF$_{WT}$ can only be observed in a pH range from 6.0 – 8.0, and the highest ATPase activity was reached in a HEPES buffer at pH 7.0. Interestingly, a reduction in activity of about 20 – 30 % is observed between HEPES (zwitterionic sulphonic acid) and TRIS (cationic primary amine) buffer systems although the pH was very similar (7.0 and 8.0, respectively).

Influence of salt concentration on the activity of SaNsrF$_{WT}$

Next, we tested the influence of the ionic strengh on the activity of the *Sa*NsrF$_{WT}$ protein. We used 100 mM HEPES at pH 7.0 as the optimal conditions for protein activity and varied the NaCl concentration ranging from 0 – 1 M in steps of 0.1 M (Figure 2B).

With increasing NaCl concentration, the hydrolytic activity strongly decreased. At a concentration of 1 M NaCl, 20% residual activity was recorded when compared to the maximum reached at 0 mM NaCl.

Choice of Cofactor

As a third optimization step, we examined the influence of the cofactor of *Sa*NsrF$_{WT}$ on ATP hydrolysis. We replaced the 10 mM Mg^{2+} used so far with 10 mM Ca^{2+}, Mn^{2+}, Zn^{2+}, Fe^{2+} or Cu^{2+}, respectively. This revealed a clear dependency on the nature of the divalent ion where only for Mg^{2+} a reasonable hydrolytic activity was detected. Besides Mg^{2+}, also Mn^{2+} was taken up as cofactor, with an ATPase activity of about a fourth of the maximally measured value. The other tested divalent ions did not significantly (e.g. Cu^{2+} caused about 15 % of the activity maximum) contribute to the ATPase activity of *Sa*NsrF$_{WT}$ (Fig. S1C).

Temperature dependence

We assayed the ATPase activity of *Sa*NsrF$_{WT}$ within a temperature range from 20 °C – 37 °C including the optimized parameters of 100 mM HEPES assay buffer at pH 7 with no added NaCl (see above). 10 mM Mg^{2+} were used to provide the protein with its cofactor. As illustrated in Figure 2D, the ATPase

activity of *Sa*NsrF$_{WT}$ was maximal at 30 °C. Further increase in the temperature resulted in a significant loss of activity as observed for 37 °C.

In summary, we varied several parameters of the ATPase activity assay in order to obtain the maximal hydrolytic activity for the *Sa*NsrF$_{WT}$ protein. As a result, the optimized conditions were found to be 100 mM HEPES at pH 7 with 0 mM NaCl as an assay buffer. The reaction approach included the addition of 10 mM Mg^{2+} and was finally performed at a temperature of 30 °C. The reaction with the respective NTP was followed for an incubation time of 18 min, then stopped and measured. These optimized conditions were applied in all following experiments.

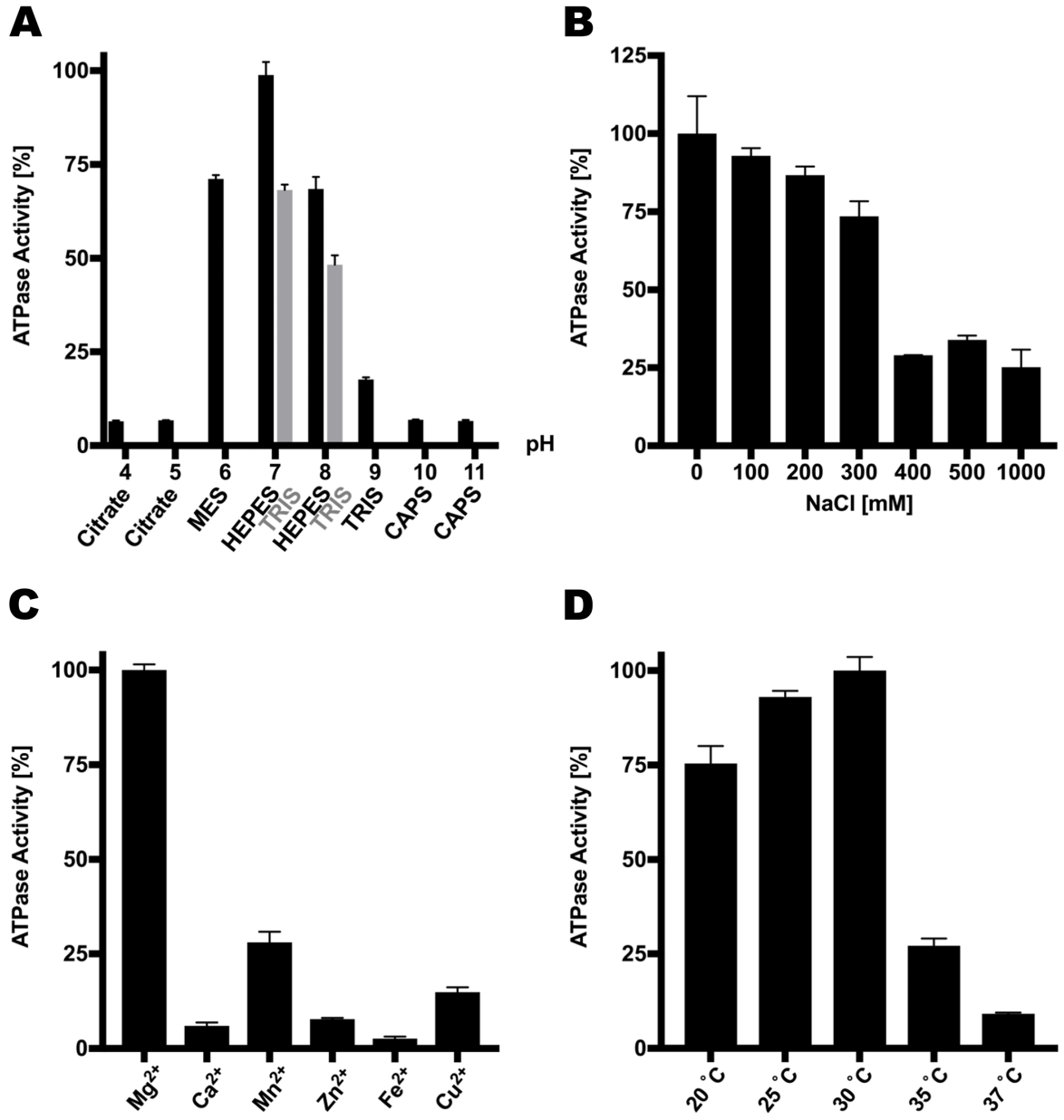

Figure S1. Influence of ATPase activity of *Sa*NsrF$_{WT}$ by parameter variations. (A) ATPase activity [%] of *Sa*NsrF$_{WT}$ dependent on pH and buffer system. 100 mM of citrate, MES, HEPES, TRIS and CAPS were diluted in ddH2O and adjusted to the respective pH. At pH 7 and 8 HEPES as well as TRIS were tested. **(B)** ATPase activity [%] of *Sa*NsrF$_{WT}$ dependent on concentrations of 0 mM to 1 M NaCl. *Sa*NsrF$_{WT}$ was diluted in 100 mM HEPES at pH 7 (0.1 mg/mL). **(C)** ATPase activity [%] of *Sa*NsrF$_{WT}$ dependent on twofold metal ions. *Sa*NsrF$_{WT}$ was exposed to 10 mM of Mg^{2+}, Ca^{2+}, Mn^{2+}, Zn^{2+}, Fe^{2+} or Cu^{2+}. *Sa*NsrF$_{WT}$ was diluted in 100 mM HEPES at pH 7 (0.1 mg/mL). **(D)** ATPase activity [%] of *Sa*NsrF$_{WT}$ dependent on temperature (triple evaluation). A concentration of 3 mM ATP was applied on *Sa*NsrF$_{WT}$ (0.1 mg/mL; diluted in 100 mM HEPES at pH 7). The reaction was incubated at temperatures of 20 °C, 25 °C, 30 °C, 35°C and 37 °C and was stopped after 18 min and dyed as described in ATPase Activity Assay for 7 min. All experiments have been performed in at least three biological replicates and are represented as means ± s.d..

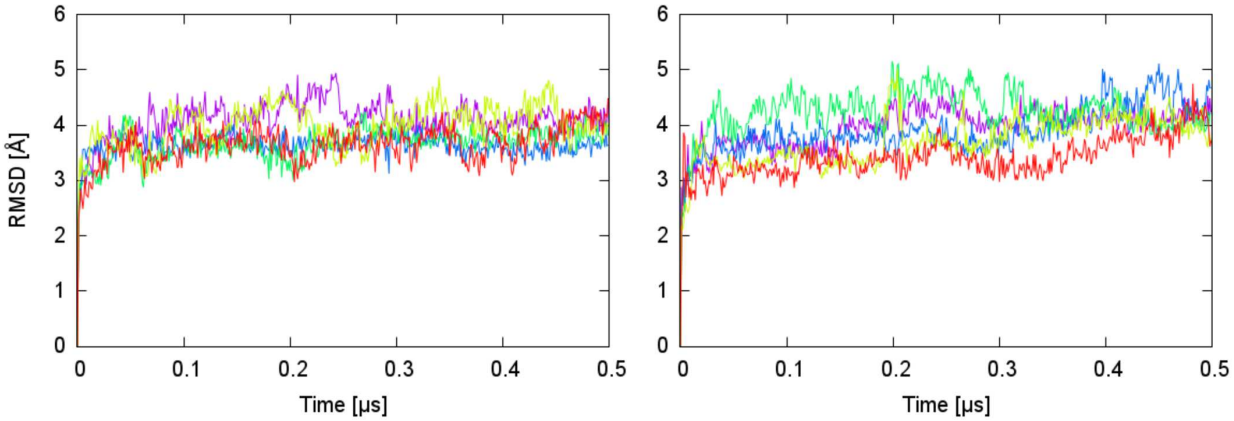

Figure S2: Structural variability of *Sa*NsrF monomers. The RMSD of backbone atoms was calculated after fitting the structures onto the 15% least mobile residues for each replica for *Sa*NsrF$_{WT}$ (left) and for the *Sa*NsrF$_{H202A}$ variant (right). The profiles are reported in a different color for each replica.

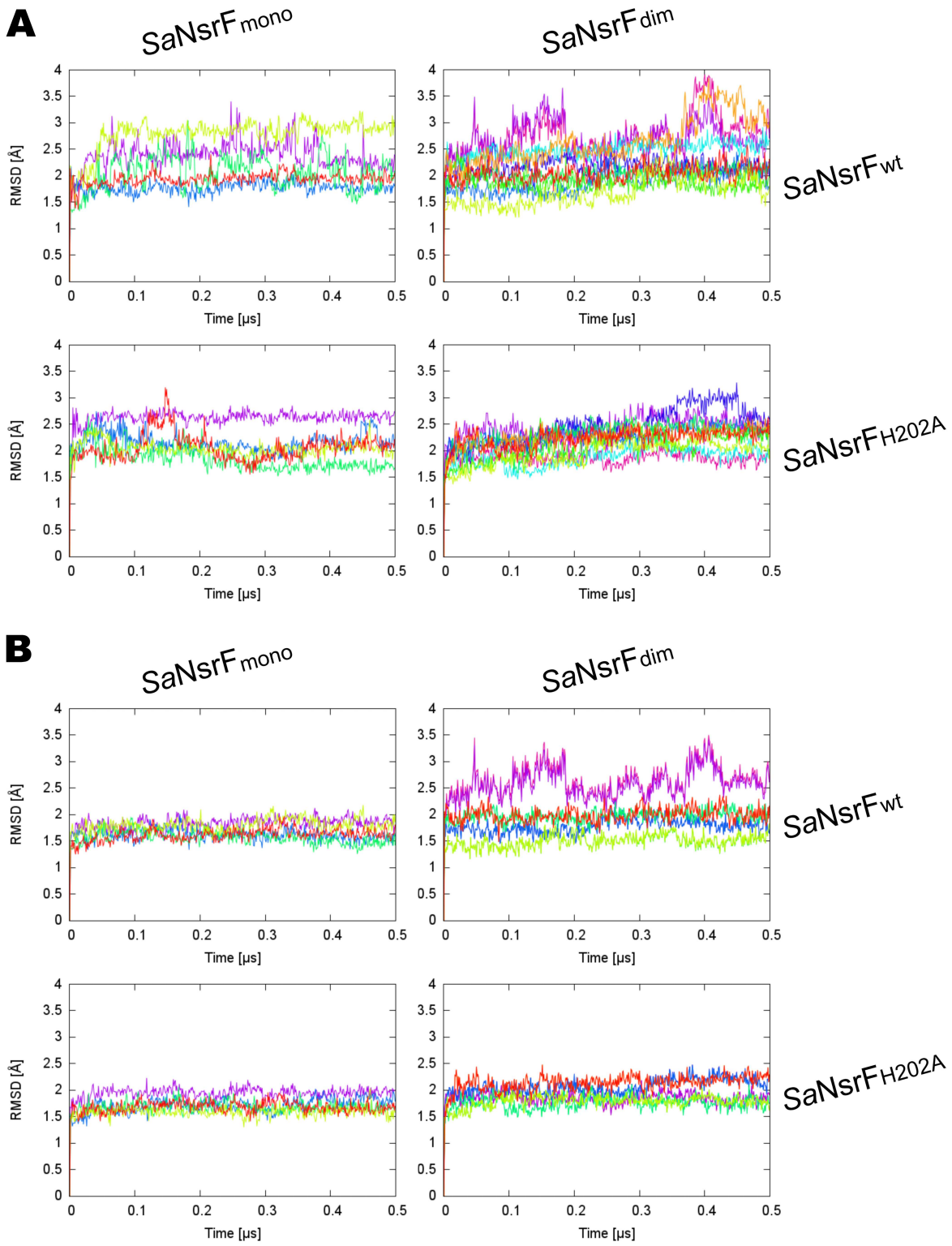

Figure S3: Change of ATP molecule and Mg^{2+} ion positions with respect to the protein for different *Sa*NsrF systems. (A) RMSD of ATP molecules; **(B)** RMSD of Mg^{2+} ions. The RMSD was calculated after fitting the structures onto the 15% least mobile protein residues for each replica. The profiles are shown in a different color for each molecule in each replica.

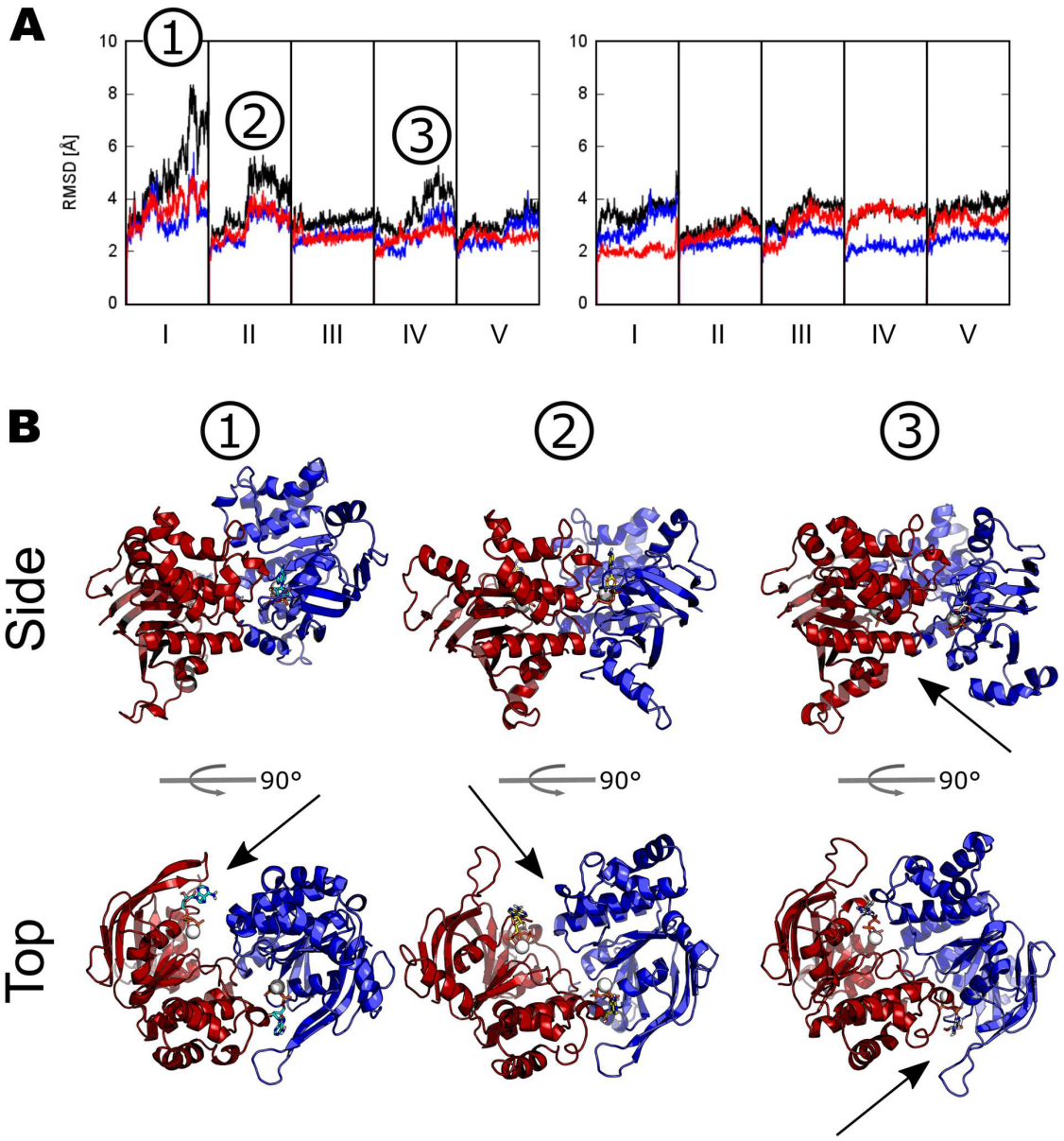

Figure S4: Structural variability of *Sa*NsrF$_{WT}$ and *Sa*NsrF$_{H202A}$ dimers. (A) The RMSD of backbone atoms was calculated for *Sa*NsrF$_{WT}$ (left) and for the *Sa*NsrF$_{H202A}$ variant (right) after fitting the structures onto the 15% least mobile residues for the whole dimer (black) and separately for either subunit A (red) or B (blue). Each box represents a replica of 0.5 µs simulation length (roman numbers). **(B)** Three representative structures of *Sa*NsrF$_{WT}$ with higher RMSD values are displayed from two orientations. Arrows highlight the partial opening of the dimer interface.

A

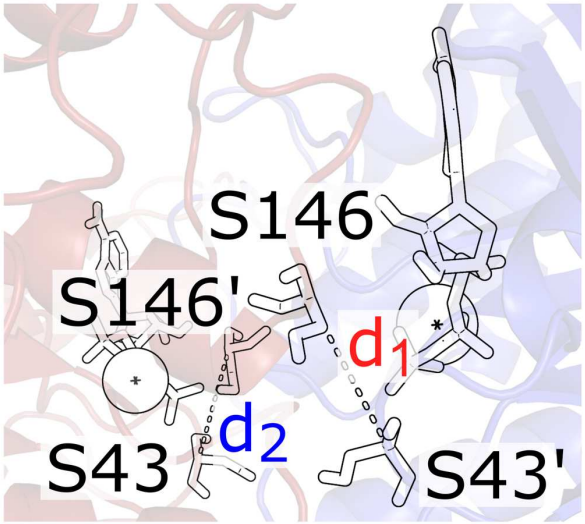

B

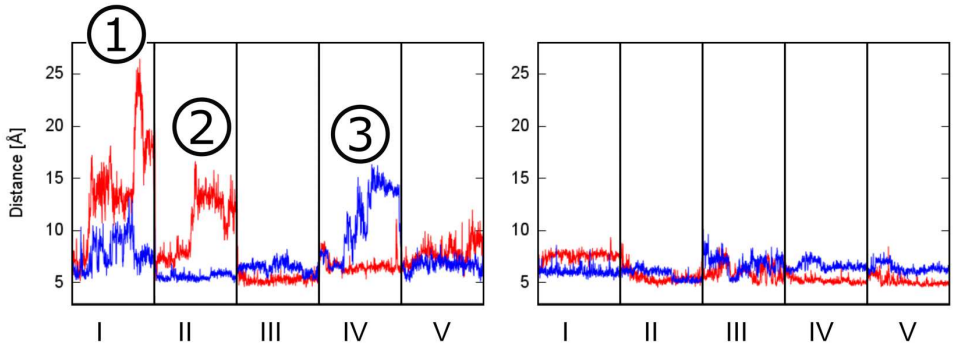

C

Structure$_{time}$ (replica), label	d_1 [Å]	d_2 [Å]
t_0 (I)	6.17	6.72
t_{400} (I), 1	<u>25.13</u>	7.63
t_0 (II)	7.22	7.92
t_{300} (II), 2	<u>13.62</u>	5.58
t_0 (IV)	8.24	7.29
t_{380} (IV), 3	7.06	<u>13.89</u>

Figure S5: Structural variability of dimers, expressed as distance between residues. (A) Representation of the distances *d1* and *d2* between the residues S43 and S146 (centers of mass) located on different monomers. **(B)** Distances for *Sa*NsrF$_{WT}$ dimer (left) and the *Sa*NsrF$_{H202A}$ variant (right). Each box represents a replica of 0.5 µs simulation length (roman numbers). **(C)** Distances for three representative structures with higher RMSD values are reported; these structures are identical to the ones shown in Figure S4. The largest distance values, indicating the separation of the subunits, are underlined.

```
CprA C.difficile                --MSNYILQVKGVSKKF------KEQMAVDNISLAIKSNSIYGLLGPNGAGKSTLLKMIT   52
NisF L.lactis                   -----MQVKIQNLSKTY------KEKQVLQDISFDIKSGTVCGLLGVNGAGKSTLMKILF   49
HisP S.typhimurin               -MMSENKLHVIDLHKRY------GGHEVLKGVSLQARAGDVISIIGSSGSGKSTFLRCIN   53
artP G.stearothermophilus*      ---MLQMIDVHQLKKSF------GSLEVLKGINVHIREGEVVVVIGPSGSGKSTFLRCLN   51
NsrF S.agalactiae               -----MLLEINHLEKVFRTRFSKEETRALQDVDFKVEQGEFIAIMGESGSGKTTLLNILA   55
MbrA S.mutans                   -----MFLEINHLEKVFRTRFSKEETHALQDVDFKVDKGEFIAIMGESGSGKTTLLNILA   55
VraD S.aureus                   ----MTILSVQHVSKTYGKKHTF---QALKDINFDIQKGEFVAIMGPSGSGKTTLLNVLS   53
BceA B.subtilis                 ----MVILEANKIRKSYGNKLNKQ--EVLKGIDIHIEKGEFVSIMGASGSGKTTLLNVLS   54
BcrA B.halodurans               ----MAILEATNIHKSYGTKLNKQ--EVLKGIDIRVEKGEFVSIMGASGSGKTTLLNVLS   54
lolD A.aeolicus*                ---MAEILRAENIKKVI------RGYEILKGISLSVKKGEFVSIIGASGSGKSTLLYILG   51
macB A.baumannii*               ------LEVSNLVREFPAGE--STIQILKGIDLTIYEGELVAIVGQSGSGKSTLMNILG   51
MJ0796 M.jannaschii*            ------MIKLKNVTKTYKMGE--EIIYALKNVNLNIKEGEFVSIMGPSGSGKSTMLNIIG   52
Spr0694-0695 S.pneumoniae*      ---MKQLISLKNIFRSYRNGD--QELQVLKNINLEVNEGEFVAIMGPSGSGKSTLMNTIG   55
NisT L.lactis                   -------VKVINLSYVYPNSN----AFALKNINLSFEKGELAAIVGKNGSGKSTLVKIIS   49
MsbA E.coli                     --RATGDVEFRNVTFTYPGRD----VPALRNINLKIPAGKTVALVGRSGSGKSTIASLIT   54
HlyB E.coli                     -------ITFRNIRFRYKPDS----PVILDNINLSIKQGEVIGIVGRSGSGKSTLTKLIQ   49
                                       :    :               : .:..    .    ::* .*:**:*:   :
consensus                                                                   GxxGxGKST

CprA C.difficile                GILNPTSGKIMFEGHRWTR-----------------KDLSNIGSLIESPAIYENLTARE   94
NisF L.lactis                   GLISADTGKIFFDGQEKTN--------------------NQLGALIEAPAIYMNLSAFD   88
HisP S.typhimurin               FLEKPSEGAIIVNGQNINLVRDKDGQLKVADKNQLR-LLRTRLTMVFQHFNLWSHMTVLE  112
artP G.stearothermophilus*      LLEDFDEGEIIIDGINLKAK-----------DTNLN-KVREEVGMVFQRFNLFPHMTVLN   99
NsrF S.agalactiae               TLEKPTNGQVILNGEDITKIKE----------AKLASFRLKNLGFVFQDFNLLDTLSVRD  105
MbrA S.mutans                   TLEKPTNGAVILNGQDITKIKE----------NNLAKFRLKNLGFVFQEFNLLDTLSVKD  105
VraD S.aureus                   SIDQISSGSVIANGQELNKLNQ----------KALAKFRKESLGFIFQDYSILPTLTVKE  103
BceA B.subtilis                 SIDQVSHGTIHINGNDMTAMKE----------KQLAEFRKQHLGFIFQDYNLLDTLTVKE  104
BcrA B.halodurans               SIDKLSNGSIKIEGSEMTRLKE----------KELAQFRKKHLGFIFQEYNLLDTLTVKE  104
lolD A.aeolicus*                LLDAPTEGKVFLEGKEVDYTNE----------KELSLLRNRKLGFVFQFHYLIPELTALE  101
macB A.baumannii*               CLDRPTSGSYKVNGQETGKLEP----------DQLAQLRREYFGFIFQRYHLLGDLSAEG  101
MJ0796 M.jannaschii*            CLDKPTEGEVYIDNIKTNDLDD----------DELTKIRRDKIGFVFQQFNLIPLLTALE  102
Spr0694-0695 S.pneumoniae*      MLDTPTSGEYYLEGQEVAGLGE----------KQLAKVRNQQIGFVFQQFFLLSKLNALQ  105
NisT L.lactis                   GLYQPTMGIIQYDKMRNSLMPE--------------EFYQKNISVLFQDFVKYE-LTIRE   94
MsbA E.coli                     RFYDIDEGEILMDGHDLREYTL--------------ASLRNQVALVSQNVHLFN-DTVAN   99
HlyB E.coli                     RFYIPENGQVLIDGHDLALADP--------------NWLRRQVGVVLQDNVLLN-RSIID   94
                                 :     *    :                              .  : :         .
consensus                                                                    Q

CprA C.difficile                NLKVHTTLLGL-PD------------SRIEEVLETV---DLRDT---FKKRSGQFSLGMK  135
NisF L.lactis                   NLKTKALLFGI-SD------------KRIHETLEVI---GLAET---GKKRAGKFSLGMK  129
HisP S.typhimurin               NVMEAPIQVLGLSK---HDAR-----ERALKYLAKV---GIDERA--QGKYPVHLSGGQQ  159
artP G.stearothermophilus*      NITLAPMKVRKWPR---EKAE-----AKAMELLDKV---GLKDKA---HAYPDSLSGGQA  145
NsrF S.agalactiae               NIYL-PLVLDRKRY---KEMD-----HRLSELSSHL---RIDDL---LDKRPFELSGGQK  150
MbrA S.mutans                   NIFL-PLVLARKDY---KEME-----KHLYRLAPKL---RIQNL---LEKRPFELSGGQK  150
VraD S.aureus                   NIML-PLSVQKMSK---ATME-----ENYKAITTAL---GIYDL---GNKYPSELSGGQQ  148
BceA B.subtilis                 NILL-PLSITKLSK---KEAN-----RKFEEVAKEL---GIYEL---RDKYPNEISGGQK  149
BcrA B.halodurans               NILL-PLSITKIPR---KAAD-----EKFKQVATEL---GIYEI---KDKYPNEISGGQK  149
lolD A.aeolicus*                NVIV-PMLKMGKPK---KEAK-----ERGEYLLSEL---GLGDK---LSRKPYELSGGEQ  146
macB A.baumannii*               NVEV-PAVYAGVTP---ADRK-----QRATALLTEL---GLGTK---TQNRPSQLSGGQQ  146
MJ0796 M.jannaschii*            NVEL-PLIFKYRGAMSGEERR-----KRALECLKMA---ELEERF--ANHKPNQLSGGQQ  151
Spr0694-0695 S.pneumoniae*      NVEL-PLIYAGV---SSSKRR-----KLAEEYLDKV---ELTER---SHHLPSELSGGQK  150
NisT L.lactis                   NIGLSDLSSQ-WED---EKIIKVLD-NLGLDFLKTNNQYVLDTQLGNWFQEGRQLSGGQW  149
MsbA E.coli                     NIAYARTEQ--YSR---EQIEEAARMAYAMDFINKM-DNGLDTVI---GENGVLLSGGQR  150
HlyB E.coli                     NISLANPG---MSV---EKVIYAAKLAGAHDFISEL-REGYNTIV---GEQGAGLSGGQR  144
                                *:                                                        :* *
consensus                                                                                 LSGGQ(K/R)

CprA C.difficile                QRLGIAIALLNHPKLLILDEPTNGLDPIGIEELRELIRSFPK-QGITVILSSHILSEVEQ  194
NisF L.lactis                   QRLGIGMAILTEPQFLILDEPTNGLDPDGIAELLNLILKLKA-KGVTILISSHQLHEISK  188
HisP S.typhimurin               QRVSIARALAMEPDVLLFDEPTSALDPELVGEVLRIMQQLAE-EGKTMVVVTHEMGFARH  218
artP G.stearothermophilus*      QRVAIARALAMEPKIMLFDEPTSALDPEMVGEVLSVMKQLAN-EGMTMVVVTHEMGFARE  204
NsrF S.agalactiae               QRVAIARSLITNPQILLADEPTAALDYRNSEDLLNLFETINLD-GQTILMVTHSANAASH  209
MbrA S.mutans                   QRVAIARSLITNPQILLADEPTAALDYRNSEDLLNLFEAINND-DQTILMVTHSANAASH  209
VraD S.aureus                   QRTAAARAFVHKPQIIFADEPTGALDSKSANDLLQRLEEMNKSFDTTIVMVTHDPVAASF  208
BceA B.subtilis                 QRTSAGRAFIHDPSIIFADEPTGALDSKSASDLLNKLSQLNQKRNATIIMVTHDPVAASY  209
BcrA B.halodurans               QRASAARAFIHEPSIIFADEPTGALDSKSASDLLGKLQQLNEKLRATIVMVTHDPVAASY  209
lolD A.aeolicus*                QRVAIARALANEPILLFADEPTGNLDSANTKRVMDIFLKINE-GGTSIVMVTHERELAEL  205
macB A.baumannii*               QRVSIARALMNGGDVILADEPTGALDSHSGVEVMRILRELNA-AGHTIILVTHDMQVAKN  205
MJ0796 M.jannaschii*            QRVAIARALANNPPIILADEPTGALDSKTGEKIMQLLKKLNEEDGKTVVVVTHDINVARF  211
Spr0694-0695 S.pneumoniae*      QRVAIARALVNNPSIILADEPTGALDTKTGNQIMQLLVDLNK-EGKTIIMVTHEPEIAAY  209
NisT L.lactis                   QKIALARTFFKKASIYILDEPSAALDPVAEKEIFDYFVALSE--NNISIFISHSLNAARK  207
MsbA E.coli                     QRIAIARALLRDSPILILDEATSALDTESERAIQAALDELQK--NRTSLVIAHRLSTIEK  208
HlyB E.coli                     QRIAIARALVNNPKILIFDEATSALDYESEHVIMRNMHKICK--GRTVIIIAHRLSTVKN  202
                                *: . . ::     . : **    **      :   :  :        :. :*
consensus                       Q              hhhDE  SALD                        H

CprA C.difficile                VVDEIGIISNGVMGYQGEVSKEQNLEKLFMKVVAENRK---RGE----------------  235
NisF L.lactis                   VASQIIILNKGKIRYDHANNKEDDIEQLFFKIVHGGM----------------------  225
HisP S.typhimurin               VSSHVIFLHQGKIEEEGDPEQV------FGNPQSPRLQQFLKGSLK--------------  258
artP G.stearothermophilus*      VGDRVLFMDGGYIIEEGKPEDL------FDRPQHERTKAFLSKVF---------------  243
NsrF S.agalactiae               -AKRVLFIKDGRIFHQLYRGNKN-NSE-FNKDISLTMSAILGGE----------------  250
MbrA S.mutans                   -AKRVLFIKDGRIFHQLYRGNKS-NQE-FSKEISLSMAALLGGE-----------  250
VraD S.aureus                   -AERVIMLKDGQIHTQLYQEGRS-KQA-FYEDIVHLQS-VLGGVSNDI-------  252
BceA B.subtilis                 -CGRVIFIKDGQMYTQLNKGGQD-RQT-FFQDIMKTQG-VLGGVQHEH-------  253
BcrA B.halodurans               -CSRVIFIKDGQIYTQLHKGDES-RQT-FFKDIMKTQG-VLGGVQNDH-------  253
lolD A.aeolicus*                -THRTLEMKDGKVVGEITRV--------------------------------------  224
macB A.baumannii*               -ATRIIEISDGEIISDRPNVPDQSLEE-VKSDPDAAPA----------------------  241
MJ0796 M.jannaschii*            -GERIIYLKDGEVEREEKLRGFDDR---------------------------------  235
Spr0694-0695 S.pneumoniae*      -AKRQIVIRDGVISSDSAQLGKEEN---------------------------------  233
NisT L.lactis                   -ANKIVVMKDGQVEDVGSHDVLLRRCQ-YYQELYYS------------------------  241
MsbA E.coli                     -ADEIVVVEDGVIVERGTHNDLLEHRG-VYAQLHKMQF---GQ-----------------  246
HlyB E.coli                     -ADRIIVMEKGKIVEQGKHKELLSEPESLYSYLYQ-------------------------  236
                                   :   :  * :
```

Figure S6: Sequence alignment of different NBDs. The sequence aligment was done with Clustal Omega [1]. TopModel templates are marked with an asterix (*). The conserved motives are labeled in cyan (Walker A), green (Q-loop), red (C-loop), purple (Walker B), orange (D-loop) and brown (H-loop).

Table S1: Five main templates used by the TopModel software for modeling of *Sa*NsrF.

PDB ID:	Identity [%]	Similarity [%]	Coverage [%]	TM-Score [%]	Note
1F3O [a]	37.7	88.4	88.0	91.9	ADP/Mg^{2+}-bound dimer, not functionally active assembly
5XU1 [b]	39.5	89.4	88.0	90.9	Mg^{2+}-bound dimer with TM domain
2PCL [c]	40.5	84.1	88.8	90.6	Mg^{2+}-bound dimer, not functionally active assembly
5GKO [d]	35.5	83.6	93.6	90.3	Apo dimer with TM domain
2OLI [e]	30.9	76.1	93.2	89.2	α-helical domain only

[a] [2]; [b] [3]; [c] According to RCSB: "To be published"; [d] [4]; [e] According to RCSB: "To be published".

Table S2: Consensus sequence of conserved motifs in the NBDs listed according to their occurrence from N- to C-terminus [5]. For a graphical representation see Fig. 3B.

Motif	Consensus sequence	*Sa*NsrF
A-loop	(F/K)xY	10-KVF-12
Walker A or P-loop	GxxGxGK(S/T)	41-GESGSGKT-48
Q-loop	hV(S/P)Q	90-FVFQ-93
X-loop	TRVGDKGTQ	137-LLDKRP-142
Signature motif or C-loop	LSGGQ(K/R)Q	145-LSGGQKQ-151
Walker B	hhhhDE	165-ILLADE-170
D-loop	SALD	173-AALD-176
H-loop	hAHRL	200-VTH[202]SA-204

Table S3: Overall SAXS Data

SAXS Device	Xenocs Xeuss 2.0 with Q-Xoom
Data collection parameters	
Detector	PILATUS 3 R 300K windowless
Detector distance (m)	0.550
Beam size (mm x mm)	0.8 x 0.8
Wavelength (Å)	1.54 (Cu Source)
Sample environment	Low Noise Flow Cell, 1 mm ø
s range (nm^{-1})‡	0.18 – 6.0
Temperature (K)	288
Exposure time per frame (min)	10
Sample	***Sa*NsrF$_{WT}$**
Mode of measurement	static
Protein concentration (mg/ml)	0.5 – 4.2
Structural parameters	
I(0) from P(r)	0.023
R_g (real-space from P(r)) (nm)	2.46
I(0) from Guinier fit	0.023
s-range for Guinier fit (nm^{-1})	0.23 – 0.54
R_g (from Guinier fit) (nm)	2.40
D_{max} (nm)	7.90
POROD volume estimate (nm^3)	64.37
Molecular mass (kDa)	
From I(0)	31.85
From MoW2 [6]	33.36
From Vc [7]	38.51
From POROD	40.23
From sequence	30.86
Structure Evaluation	
Ambimeter score	0.6990
Crysol χ^2	1.16
Software	
ATSAS Software Version [8]	3.0.1
Primary data reduction	PRIMUS [9]
Data processing	GNOM [10]
Ab initio modelling	GASBOR [11]
Superimposing	SUPCOMB [12]
Structure evaluation	AMBIMETER [13] / CRYSOL [14]
Model visualization	PyMOL [15]

‡s = $4\pi \sin(\theta)/\lambda$, 2θ – scattering angle

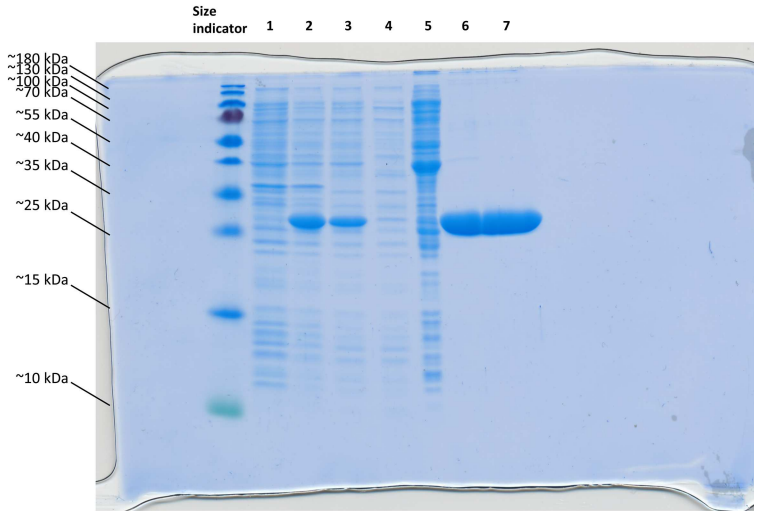

Original Figure 1. Purification and SEC-MALS of *Sa*NsrF$_{WT}$. (A) SDS-PAGE of the *Sa*NsrF$_{WT}$ purification progress. PageRuler Prestained Protein Ladder (size indicator; 10 to 180 kDa), *E. coli* strain before IPTG induction (1), *E. coli* strain after IPTG induction (2), IMAC load (3), IMAC flow-through (4), IMAC wash-fraction (5), IMAC eluate (6), SEC eluate (7).

References:

1 Madeira, F. *et al.* The EMBL-EBI search and sequence analysis tools APIs in 2019. *Nucleic Acids Res* **47**, W636-W641, doi:10.1093/nar/gkz268 (2019).

2 Yuan, Y. R. *et al.* The crystal structure of the MJ0796 ATP-binding cassette. Implications for the structural consequences of ATP hydrolysis in the active site of an ABC transporter. *J Biol Chem* **276**, 32313-32321, doi:10.1074/jbc.M100758200 (2001).

3 Yang, H. B. *et al.* Structure of a MacAB-like efflux pump from *Streptococcus pneumoniae*. *Nat Commun* **9**, 196, doi:10.1038/s41467-017-02741-4 (2018).

4 Okada, U. *et al.* Crystal structure of tripartite-type ABC transporter MacB from *Acinetobacter baumannii*. *Nat Commun* **8**, 1336, doi:10.1038/s41467-017-01399-2 (2017).

5 Szollosi, D., Rose-Sperling, D., Hellmich, U. A. & Stockner, T. Comparison of mechanistic transport cycle models of ABC exporters. *Biochim Biophys Acta Biomembr* **1860**, 818-832, doi:10.1016/j.bbamem.2017.10.028 (2018).

6 Fischer, H., Neto, M. D., Napolitano, H. B., Polikarpov, I. & Craievich, A. F. Determination of the molecular weight of proteins in solution from a single small-angle X-ray scattering measurement on a relative scale. *J Appl Crystallogr* **43**, 101-109, doi:10.1107/S0021889809043076 (2010).

7 Rambo, R. P. & Tainer, J. A. Accurate assessment of mass, models and resolution by small-angle scattering. *Nature* **496**, 477-481, doi:10.1038/nature12070 (2013).

8 Franke, D. *et al.* ATSAS 2.8: a comprehensive data analysis suite for small-angle scattering from macromolecular solutions. *J Appl Crystallogr* **50**, 1212-1225, doi:10.1107/S1600576717007786 (2017).

9 Konarev, P. V., Volkov, V. V., Sokolova, A. V., Koch, M. H. J. & Svergun, D. I. PRIMUS: a Windows PC-based system for small-angle scattering data analysis. *J Appl Crystallogr* **36**, 1277-1282, doi:10.1107/S0021889803012779 (2003).

10 Svergun, D. I. Determination of the Regularization Parameter in Indirect-Transform Methods Using Perceptual Criteria. *J Appl Crystallogr* **25**, 495-503, doi:Doi 10.1107/S0021889892001663 (1992).

11 Svergun, D. I., Petoukhov, M. V. & Koch, M. H. Determination of domain structure of proteins from X-ray solution scattering. *Biophys J* **80**, 2946-2953, doi:10.1016/S0006-3495(01)76260-1 (2001).

12 Kozin, M. B. & Svergun, D. I. Automated matching of high- and low-resolution structural models. *J Appl Crystallogr* **34**, 33-41, doi:Doi 10.1107/S0021889800014126 (2001).

13 Petoukhov, M. V. & Svergun, D. I. Ambiguity assessment of small-angle scattering curves from monodisperse systems. *Acta Crystallogr D Biol Crystallogr* **71**, 1051-1058, doi:10.1107/S1399004715002576 (2015).

14 Svergun, D., Barberato, C. & Koch, M. H. J. CRYSOL - A program to evaluate x-ray solution scattering of biological macromolecules from atomic coordinates. *J Appl Crystallogr* **28**, 768-773, doi:Doi 10.1107/S0021889895007047 (1995).

15 The PyMOL Molecular Graphics System, Version 2.0 Schrödinger, LLC.

3.2 Chapter II: The Antimicrobial Peptide Nisin H

Insights in the Antimicrobial Potential of the Natural Nisin Variant Nisin H

Jens Reiners[1,2†], Marcel Lagedroste[1†], **Julia Gottstein[1]**, Emmanuel T. Adeniyi[3], Rainer Kalscheuer[3], Gereon Poschmann[4], Kai Stühler[4,5], Sander H. J. Smits[1,2*] and Lutz Schmitt[1*]

[1]Institute of Biochemistry, Heinrich-Heine-University Düsseldorf, Düsseldorf, Germany,
[2] Center for Structural Studies, Heinrich-Heine-University Düsseldorf, Düsseldorf, Germany,
[3] Institute of Pharmaceutical Biology and Biotechnology, Heinrich-Heine-University Düsseldorf, Düsseldorf, Germany,
[4] Institute for Molecular Medicine, Medical Faculty, Heinrich-Heine-University Düsseldorf, Düsseldorf, Germany,
[5] Molecular Proteomics Laboratory, BMFZ, Heinrich-Heine-University-Düsseldorf, Düsseldorf, Germany

Published in: Frontiers in Microbiology (2020)

Impact factor: 5.26

Own proportion of this work: 15%

- Performing sytox assays
- Writing the manuscript

frontiers in Microbiology

ORIGINAL RESEARCH
published: 20 October 2020
doi: 10.3389/fmicb.2020.573614

Insights in the Antimicrobial Potential of the Natural Nisin Variant Nisin H

Jens Reiners[1,2†], Marcel Lagedroste[1†], Julia Gottstein[1], Emmanuel T. Adeniyi[3], Rainer Kalscheuer[3], Gereon Poschmann[4], Kai Stühler[4,5], Sander H. J. Smits[1,2] and Lutz Schmitt[1*]*

[1] Institute of Biochemistry, Heinrich-Heine-University Düsseldorf, Düsseldorf, Germany, [2] Center for Structural Studies, Heinrich-Heine-University Düsseldorf, Düsseldorf, Germany, [3] Institute of Pharmaceutical Biology and Biotechnology, Heinrich-Heine-University Düsseldorf, Düsseldorf, Germany, [4] Institute for Molecular Medicine, Medical Faculty, Heinrich-Heine-University Düsseldorf, Düsseldorf, Germany, [5] Molecular Proteomics Laboratory, BMFZ, Heinrich-Heine-University-Düsseldorf, Düsseldorf, Germany

OPEN ACCESS

Edited by:
Des Field,
University College Cork, Ireland

Reviewed by:
Oscar P. Kuipers,
University of Groningen, Netherlands
Stefano Donadio,
Naicons Srl, Italy

***Correspondence:**
Lutz Schmitt
lutz.schmitt@hhu.de
Sander H. J. Smits
sander.smits@hhu.de

† These authors have contributed equally to this work

Specialty section:
This article was submitted to Antimicrobials, Resistance and Chemotherapy, a section of the journal Frontiers in Microbiology

Received: 17 June 2020
Accepted: 25 September 2020
Published: 20 October 2020

Citation:
Reiners J, Lagedroste M, Gottstein J, Adeniyi ET, Kalscheuer R, Poschmann G, Stühler K, Smits SHJ and Schmitt L (2020) Insights in the Antimicrobial Potential of the Natural Nisin Variant Nisin H. Front. Microbiol. 11:573614. doi: 10.3389/fmicb.2020.573614

Lantibiotics are a growing class of antimicrobial peptides, which possess antimicrobial activity against mainly Gram-positive bacteria including the highly resistant strains such as methicillin-resistant *Staphylococcus aureus* or vancomycin-resistant enterococci. In the last decades numerous lantibiotics were discovered in natural habitats or designed with bioengineering tools. In this study, we present an insight in the antimicrobial potential of the natural occurring lantibiotic nisin H from *Streptococcus hyointestinalis* as well as the variant nisin H F_1I. We determined the yield of the heterologously expressed peptide and quantified the cleavage efficiency employing the nisin protease NisP. Furthermore, we analyzed the effect on the modification via mass spectrometry analysis. With standardized growth inhibition assays we benchmarked the activity of pure nisin H and the variant nisin H F_1I, and their influence on the activity of the nisin immunity proteins NisI and NisFEG from *Lactococcus lactis* and the nisin resistance proteins *Sa*NSR and *Sa*NsrFP from *Streptococcus agalactiae* COH1. We further checked the antibacterial activity against clinical isolates of *Staphylococcus aureus*, *Enterococcus faecium* and *Enterococcus faecalis* via microdilution method. In summary, nisin H and the nisin H F_1I variant possessed better antimicrobial potency than the natural nisin A.

Keywords: lantibiotics, nisin, nisin H, MS analysis, antimicrobial activity

INTRODUCTION

Lantibiotics (lanthionine containing antibiotics) are a growing class of antimicrobial peptides (AMPs), which posses antimicrobial activity even against highly resistant strains such as methicillin-resistant *Staphylococcus aureus* (MRSA) or vancomycin-resistant *enterococci* (VRE) and some are already in pre-clinical trials (Mota-Meira et al., 2000; Jabes et al., 2011; Dawson and Scott, 2012; Crowther et al., 2013; Dischinger et al., 2014; Ongey et al., 2017; Brunati et al., 2018; Sandiford, 2019). Lantibiotics are peptides, containing 19–38 amino acids and are mainly produced by Gram-positive bacteria (Klaenhammer, 1993; Sahl and Bierbaum, 1998). In the last decades an increasing number of lantibiotic gene clusters were found by data-mining approaches using tools such as BAGEL4 (van Heel et al., 2018).

The best studied lantibiotic is nisin, which was first discovered in 1928 by Rogers and Whittier and belongs to the class I lantibiotics (Rogers, 1928; Rogers and Whittier, 1928; Arnison et al., 2013). It is used in the food industry since 1953 and obtained the status as generally recognized as safe (GRAS) in 1988 from the Food and Drug Administration (FDA) (Delves-Broughton et al., 1996). The class I lantibiotic nisin contains 34 amino acids and five (methyl)-lanthionine rings. These (methyl)-lanthionine rings require multiple posttranslational modifications (PTMs) which are introduced in the precursor peptide. First, the serine and threonine residues in the core peptide are dehydrated by a specific dehydratase NisB (lantibiotic class I LanB dehydratase) (Kaletta and Entian, 1989; Karakas Sen et al., 1999; Koponen et al., 2002; Ortega et al., 2015; Repka et al., 2017). The next step is a Michael-type condensation of dehydrated residues with the thiol group of a cysteine residue, thereby forming (methyl)-lanthionine rings, guided in a regio- and stereospecific manner by the cyclase NisC (class I lantibiotic cyclase) (Okeley et al., 2003; Li et al., 2006; Li and van der Donk, 2007; Repka et al., 2017). These characteristic (methyl)-lanthionine rings give lantibiotics high heat stability, resistance against proteolytic digestion and are responsible for the nanomolar antimicrobial activity (Gross and Morell, 1967; Rollema et al., 1995; Chan et al., 1996; Lu et al., 2010; Oppedijk et al., 2016).

The sequence of nisin A can be subdivided into three parts (see **Figure 1**). The N-terminal part with ring A, B, and C is responsible for binding to the cell wall precursor lipid II (Hsu et al., 2004). The hinge region is very flexible and allows reorientation of the C-terminal part to insert into the membrane (van Heusden et al., 2002; Hasper et al., 2004; Wiedemann et al., 2004; Medeiros-Silva et al., 2018), while changes in this region have a strong impact on the target antimicrobial activity (Zhou et al., 2015; Zaschke-Kriesche et al., 2019b). After penetrating the membrane, the C-terminal part with ring D and E forms a stable pore with a stoichiometry of eight nisin and four lipid II molecules, which subsequently leads to rapid cell death (Hasper et al., 2004; Wiedemann et al., 2004; Alkhatib et al., 2014a; Medeiros-Silva et al., 2018).

Unfortunately, some bacteria established resistance mechanism against lantibiotics. For instance lantibiotic producing strains express the immunity system LanI and LanFEG (Alkhatib et al., 2014a,b), which prevent a suicidal effect after the lantibiotic is secreted. In the case of nisin A from *Lactococcus lactis* these proteins are called NisI and NisFEG. But also non-lantibiotic producing strains showed resistance against lantibiotics like *Streptococcus agalactiae* COH1, which arises from the expression of the membrane-anchored peptidase *Sa*NSR and the ABC transporter *Sa*NsrFP (Khosa et al., 2013, 2016a,b; Reiners et al., 2017).

Several natural nisin variants have been discovered and up to now eight are known. First of all nisin A from *L. lactis* (Rogers and Whittier, 1928), nisin Z from *L. lactis* NIZO 221 86 (Mulders et al., 1991), nisin F from *L. lactis* F10 (de Kwaadsteniet et al., 2008), nisin Q from *L. lactis* 61-14 (Zendo et al., 2003), nisin O_1 to O_4 from *Blautia obeum* A2-162 (Hatziioanou et al., 2017), nisin U and U2 from *Streptococcus uberis* 42 and D536 (Wirawan et al., 2006), nisin P from *Streptococcus gallolyticus* subsp. *pasteurianus* (Zhang et al., 2012; Wu et al., 2014), nisin J from *Staphylococcus capitis* APC 2923 (O'Sullivan et al., 2020) and nisin H from *Streptococcus hyointestinalis* DPC 6484 (O'Connor et al., 2015).

In this study we focused on the natural nisin H variant (**Figure 1**). We used a standardized workflow for the characterization of lantibiotics, previous described in Lagedroste et al. (2019) to determine the impact on the expression, modification and antimicrobial properties of this nisin variant. We tested further the antimicrobial activity against some pathogen strains from *Staphylococcus aureus*, *Enterococcus faecium,* and *Enterococcus faecalis* using the microdilution method. As a reference we used the wild-type version of nisin A expressed using the same experimental setup. Furthermore, we exchanged the phenylalanine at position one (F_1) of nisin H to isoleucine, which is the natural amino acid of nisin A at this position (**Figure 1**). This position one was previously analyzed in nisin A and showed a major impact on different levels of the characterization (Lagedroste et al., 2019).

MATERIALS AND METHODS

Microorganisms and Culture Conditions

Cultures of *L. lactis* NZ9000 (Kuipers et al., 1997) containing the plasmids for immunity and resistance proteins were grown in M17 medium (Terzaghi and Sandine, 1975) at 30°C supplemented with 0.5% glucose [GM17 and the appropriate antibiotics descripted in Alkhatib et al. (2014a,b), Khosa et al. (2016b), Reiners et al. (2017), Lagedroste et al. (2019)]. For pre-nisin secretion, the *L. lactis* strain NZ9000 was grown in minimal medium (Jensen and Hammer, 1993) at 30°C supplemented with 0.5% glucose and the appropriate antibiotics. All bacteria used for minimum inhibitory concentration (MIC) determination of nisin variants [*Bacillus subtilis* 168; *S. aureus*: MSSA strain ATCC 29213, MRSA/VISA strain ATCC 700699; *E. faecium*: ATCC 35667, ATCC 700221 (vancomycin resistant); *E. faecalis*: ATCC 29212, ATCC 51299 (vancomycin resistant)] were cultivated in Mueller-Hinton broth (MHB) at 37°C and shaking at 150 rpm.

Cloning of Nisin H and the F_1I Variant

Nisin H was created as described in Reiners et al. (2017). The substitution of the phenylalanine at position one (F_1I) to an isoleucine was performed by site-directed mutagenesis. Here, we used the following primers (forward: 5′-GTGCATCACCACGCTTTACAAGTATTTCGC-3′; reverse: 5′-GCGAAATACTTGTAAAGCGTGGTGATGCAC-3′). After sequence analysis a competent *L. lactis* NZ9000 strain was transformed with the resulting plasmid via electroporation (Holo and Nes, 1989). The *L. lactis* NZ9000 strain already contain a vector (pil3-BTC) encoding for the modification and secretion proteins (Rink et al., 2005).

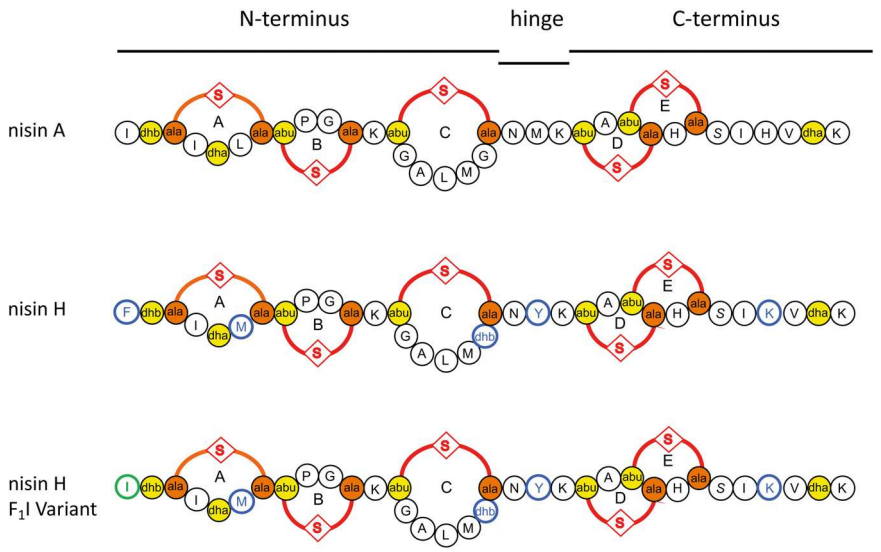

FIGURE 1 | Schematic overview of the used lantibiotics nisin A, nisin H, and the nisin H F_1I variant. Point mutations in nisin H and nisin H F_1I in comparison to nisin A are highlighted in blue. Dehydrated amino acids and cysteine residues involved in (methyl)-lanthionine ring formation (ring A, B, C, D, and E) are labeled in yellow and orange. The mutation of the nisin H F_1I variant is highlighted in green.

Expression, Purification and Activation of Pre-nisin Variants

The precursor of nisin H and its variant were expressed and purified as previously described (Abts et al., 2013; Alkhatib et al., 2014b; Lagedroste et al., 2017, 2019). Briefly, for pre-nisin secretion, the *L. lactis* strain NZ9000 was grown in minimal medium (Jensen and Hammer, 1993) supplemented with 0.5% glucose and 5 μg/ml of each erythromycin and chloramphenicol at 30°C. Cells were induced with 10 ng/ml nisin at an OD_{600} of 0.4 and further grown overnight at 30°C without shaking. After harvesting the cells, the 0.45 μm-filtered supernatant was loaded onto a HiTrap SP HP cation exchange chromatography column. After washing with 50 mM lactic acid, the buffer was changed to 50 mM Hepes pH 7 via gradient and the final elution was done with 50 mM Hepes pH 7, 500 mM NaCl buffer. Elution fractions were concentrated in a 3 kDa cutoff filter. With a soluble version of NisP, the activation of all variants was performed overnight at 8°C (Lagedroste et al., 2017). The yield and cleavage efficiency determination was done by RP-HPLC (Agilent Technologies 1260 Infinity II) with a LiChrospher WP 300 RP-18 end-capped column and an acetonitrile/water solvent system (Abts et al., 2013; Lagedroste et al., 2017, 2019).

MALDI-TOF Analysis: Dehydration and (Methyl)-Lanthionine Ring Analysis

With MALDI-TOF analysis we analyzed the modification state of nisin H and its variant. Dehydrations are directly visible in the spectra, due to the loss of mass (−18 Da). For the determination of the presence of (methyl)-lanthionine rings, we used the organic coupling agent CDAP (1-cyano-4 dimethylaminopyridinium tetrafluoroborate) that binds to free cysteine residues (Wu and Watson, 1998). The reaction of the coupling agent to free cysteine side chains would results in an increased mass in the spectra. The analysis was performed as previously descripted (Lagedroste et al., 2019). The samples were analyzed with MALDI-TOF (UltrafleXtreme, Bruker Daltonics, Bremen, Software: Compass 1.4) in positive mode.

Tandem Mass Spectrometric Analysis of Nisin H and Nisin H F_1I

Nisin H and the nisin H F_1I variant were purified using solid phase extraction (Oasis HLB, Waters) and finally resuspended in 0.1% trifluoroacetic acid. The samples were first subjected to liquid chromatography on a rapid separation liquid chromatography system (Ultimate 3000, Thermo Fisher Scientific) using an 1 h gradient and C18 columns as described (PMID 24646099) and further analyzed by a QExactive Plus mass spectrometer (Thermo Fisher Scientific) coupled via a nano-source electrospray interface. First, a precursor spectrum was acquired at a resolution of 140,000 (advanced gain control target 3E6, maximum ion time 50 ms, scan range 200–2000 m/z, profile data type). Subsequently, up to four 4–6-fold charged precursors were selected by the quadrupole (2 m/z isolation window), fragmented by higher-energy collisional dissociation (normalized collision energy 30) and recorded at a resolution of 35,000 (advanced gain control target 1E5, maximum ion time 50 ms, available scan range 200–2000 m/z, centroid data type).

Recorded spectra were analyzed by the MASCOT search engine (version 2.4.1, Matrix Science) and searches triggered by Proteome Discoverer (version 2.4.0.305, Thermo Fisher Scientific). A database was generated for the searches including 1000 randomly generated sequence entries each 34 amino acid long) and the sequences of nisin H and nisin H F_1I. Methionine oxidation and dehydration of serine and threonine residues were

considered as variable modifications and the precursor mass tolerance set to 10 ppm and the fragment mass tolerance set to 0.02 Da. For peptide validation, the Fixed Value PSM validator was used (1% false discovery rate) and the IMP-ptmRS node for site validation (PMID 22073976). No random sequences were found by the search.

Determination of the Antimicrobial Activity by Growth Inhibition Assay

The determination of the antimicrobial activity of the different nisin variants was tested using a growth inhibition assay. The used strains were described in Alkhatib et al. (2014a,b), Reiners et al. (2017), and Lagedroste et al. (2019).

Briefly, the *L. lactis* NZ9000 strains were grown in M17 medium (Terzaghi and Sandine, 1975) at 30°C supplemented with 0.5% glucose (GM17 and the appropriate antibiotics) overnight with 1 ng/ml nisin. In a 96-well plate, a serial dilution of the nisin variant was applied and incubated with the test strains at a final OD_{600} of 0.1 for 5 h at 30°C. Later on, the optical density was measured at 584 nm via 96-well plate reader BMG. The normalized optical density was plotted against the logarithm of the nisin concentration and the resulting inhibitory concentration (IC_{50}), represents the value where 50% of the cells died in the presence of the different nisin variants. By dividing the IC_{50} values of strains expressing the immunity or resistance proteins from the IC_{50} value of the sensitive strain we calculated the fold of immunity/resistance, which is an indicator for the recognition of nisin H or its variant by the immunity or resistance proteins.

Minimum Inhibitory Concentration Determination of Nisin Variants

Nisin variants were tested for antibacterial capabilities against *B. subtilis* and different strains from *S. aureus*, *E. faecium,* and *E. faecalis* using the microdilution method, according to the recommendations of Clinical and Laboratory Standards Institute (2012). Briefly, fresh cultures prepared from overnight cultures were incubated until exponential phase (OD $\sim$ 0.6) and seeded at 5×10^4 CFU/well in 96-well round-bottom microplates, in a total volume of 100 μL containing twofold serially diluted test peptides. Moxifloxacin was used as a positive control. Plates were incubated statically and aerobically for 24 h at 37°C. MICs were determined macroscopically by identifying the least concentration of peptides that resulted in complete inhibition of bacterial visual growth.

SYTOX Green Nucleic Acids Binding Assay

The cells of NZ9000Cm were grown overnight in GM17 supplemented with 5 mg/ml chloramphenicol. The overnight culture was diluted to an OD_{600} of 0.1 in fresh media and the cultures were grown until the OD_{600} reaches 0.3. The SYTOX green dye was added at a final concentration of 2.5 mM according to the manual of the manufacturer (Invitrogen). After reaching a stable baseline ($\sim$200 s) we added 100 nM of the nisin variants. The fluorescence signal was measured at an excitation wavelength of 504 nm and emission wavelength of 523 nm, respectively (using a fluorolog Horiba III). After a stable baseline was reached, the nisin variant was added and the fluorescence was monitored over an additional time period. The measurement was performed at 30°C.

RESULTS

O'Connor et al. (2015) described a new natural nisin variant from *S. hyointestinalis* DPC 6484 and named it nisin H. In following, we compared nisin A and its natural variant nisin H, both heterologously produced in *L. lactis*, following the protocol of lantibiotic characterization (Lagedroste et al., 2019). We also included the nisin H F_1I variant.

The characterization starts with the expression, secretion and purification of the lantibiotic and its comparison to nisin A. The heterologously expressed and secreted nisin A and the variants nisin H and nisin H F_1I can be purified with high purity as observed on the Tricine-SDS-PAGE gel (**Figure 2A**). Nisin A was purified with a yield of 6.0 ± 0.3 mg/L of cell culture (Lagedroste et al., 2019), nisin H was expressed and purified with a yield of 5.3 ± 0.6 mg/L of cell culture, which is identical within experimental error. The nisin H F_1I variant displayed a slightly reduced yield of 4.9 ± 0.2 mg/L of cell culture (**Figure 2B** and **Table 1**).

An important step prior to the activity assay is the cleavage of the leader sequence form the pre-nisin variants, resulting in biologically active compounds. For the cleavage reaction, we used the peptidase NisP and monitored the cleavage efficiency via RP-HPLC (**Figures 2C–E**).

Intriguingly, the natural variant nisin H showed only a low cleavage efficiency of 15.6 ± 1.4%, compared to nisin A with 94.6 ± 2.0% (**Figure 2C** and **Table 1**). In comparison to nisin A, nisin H contains a phenylalanine at the first position (O'Connor et al., 2015), which apparently leads to a significant reduction in cleavage efficiency. The first residue of nisin A is an isoleucine, and as demonstrated before (Lagedroste et al., 2019), the introduction of aromatic residues at position one results in a clearly reduced cleavage efficiency. To counteract the lower cleavage efficiency of nisin H by NisP, we created a mutant of nisin H, in which the phenylalanine was substituted by isoleucine and termed it nisin H F_1I. For this variant, nisin H F_1I, the cleavage efficiency of the pre-lantibiotic was restored with an efficiency of 91.8 ± 0.8% (**Figure 2C** and **Table 1**), which corresponds to levels previously observed for nisin A. We monitored the cleavage via RP-HPLC, the pre-nisin elutes normally between 18 and 22 min (shown as blue dashed lines, **Figures 2D,E**). After cleavage by NisP, the leader peptide can be detected at 14.5 and 15.5 min in the chromatogram (shown as black lines, **Figures 2D,E**). For nisin H there was a high amount of uncleaved nisin H visible (eluting from 18 to 21 min) and only a small amount of cleaved product at 23–24 min (black lines, **Figure 2D**). For the nisin H F_1I variant, high amounts of leader peptide and cleaved product could be detected in the chromatogram, indicating high cleavage efficiency (black lines, **Figure 2E**). This efficiency was similar as observed for nisin A and in line with previous results that the position

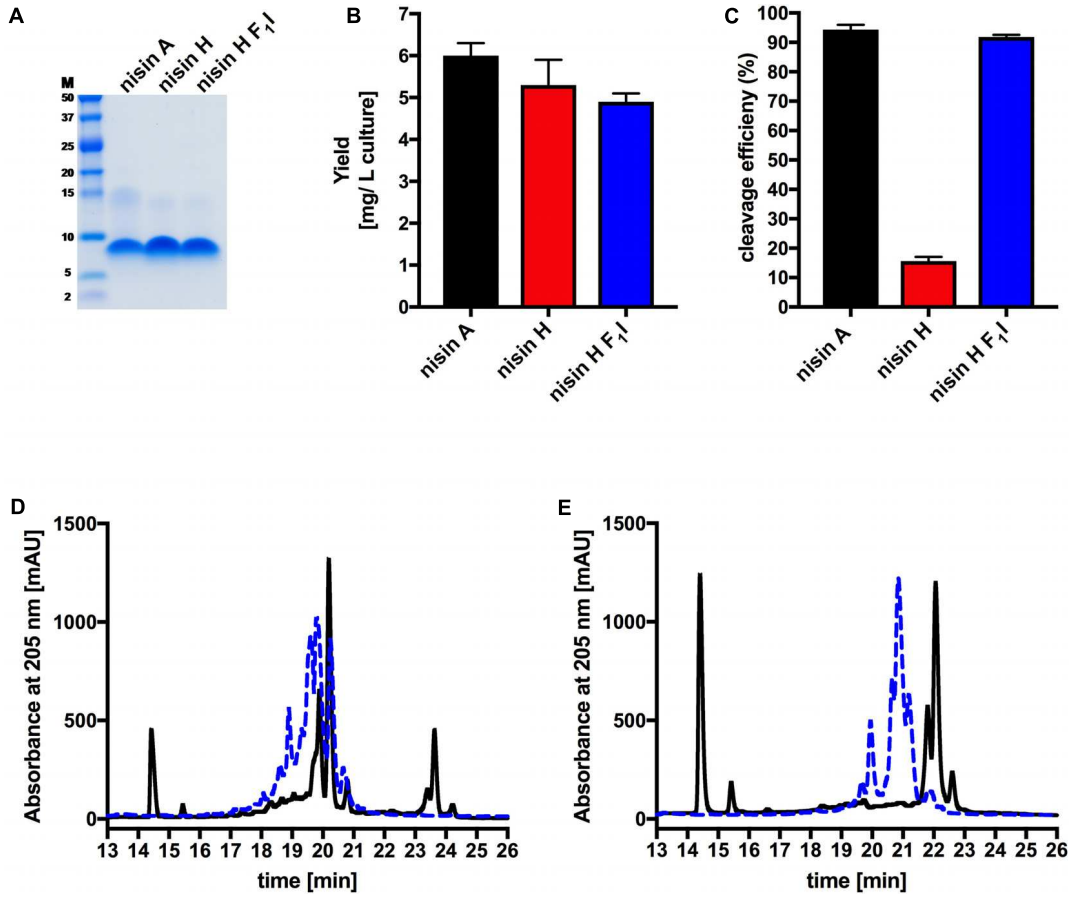

FIGURE 2 | Determination of purity, yield and cleavage efficiency of the pre-nisin variants. **(A)** Purity of the purified nisin A and the variants nisin H and nisin H F_1I (Marker: Precision Plus Protein Dual Xtra standards Bio-Rad). **(B)** Yields after purification of nisin A and their corresponding variants via cation-exchange chromatography. **(C)** Quantification of the cleavage efficiency of NisP. **(D)** Chromatogram of nisin H. **(E)** Chromatogram of the nisin H F_1I variant. The pre-nisin variants before NisP cleavage were shown by blue dashed lines and after NisP cleavage by black lines. Error bars represent the standard deviation of at least three biological replicates.

one is important for the cleavage reaction (Lagedroste et al., 2019). Thus, we assume, that the four other mutations naturally occurring in nisin H (compared to nisin A) do not interfere with cleavage, however the isoleucine at position one does.

The next step was to determine the modification state of the heterologous produced nisin H and its F_1I variant. As the natural variant nisin H contains ten possible residues in the core peptide that can be dehydrated, we were curious to determine if the modification machinery of nisin A was able to modify the peptide as efficiently (O'Connor et al., 2015). In the MALDI-TOF spectra, a dominant species of eightfold dehydrated residues was observed for nisin H, followed by a minor species containing nine- and sevenfold dehydrations. The possible 10-fold dehydrated species however was not observed (**Figure 3A** and **Table 1**). Furthermore no CDAP-coupling products were observed, which indicates that all cysteine residues are linked in (methyl)-lanthionine rings. We proved the functionality of the assay with unmodified pre-nisin A as demonstrated in Lagedroste et al. (2019). Thus, the modification enzymes were able to modify nisin H proving the promiscuity of the nisin modification machinery. Interestingly, the nisin H F_1I variant showed a dominant ninefold dehydrated species in comparison the nisin H wild-type (**Figure 3B** and **Table 1**) and also showed no CDAP-coupling products, indicating that all cysteine residues are closed to (methyl)-lanthionine rings. The difference in the dehydration pattern for the nisin H F_1I variant indicates a different accessibility of the serine and/or threonine residues in the core peptide for at least the dehydratase NisB. To validate which serine or threonine residues is dehydrated, we performed a tandem mass spectrometric

TABLE 1 | Determination of the yield, cleavage efficiency, dehydrations, and (methyl)-lanthionine ring formation for nisin A, nisin H, and nisin H F_1I.

Variant	Yield (mg/L culture)	Cleavage (%)	Dehydrations	Lanthionine rings
Nisin A	6.0 ± 0.3	94.6 ± 2.0	**8**, 7	5
Nisin H	5.3 ± 0.6	15.6 ± 1.4	9, **8**, 7	5
Nisin H F_1I	4.9 ± 0.2	91.8 ± 0.8	**9**, 8, 7, 6	5

Main species found in MALDI-TOF analysis are marked in bold.

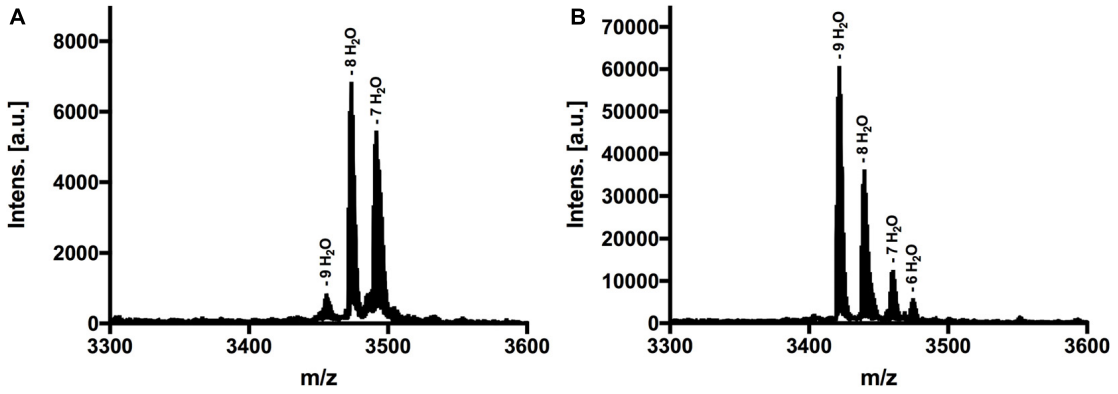

FIGURE 3 | MALDI-TOF analysis to determine dehydrations and (methyl)-lanthionine ring formations. **(A)** MS spectra of nisin H, threated with CDAP. Dominant species was eightfold dehydrated. **(B)** MS spectra of nisin H F_1I variant, threated with CDAP. Dominant species was ninefold dehydrated. Both variants showed no coupling products, indicating that all cysteine residues were involved in (methyl)-lanthionine rings.

analysis of nisin H and the F_1I variant. Here we found that the Thr_2 partially escape the dehydration in nisin H. Only in the small amount of the ninefold dehydrated species the Thr_2 is dehydrated, in all other species we found a mix in the dehydration pattern, where Thr_2 partially escape the dehydration. For example in the eightfold species we have a mix of dehydrated Thr_2 or Ser_{33}. In the nisin H F_1I variant the Thr_2 was in all species dehydrated, which suggests that, the phenylalanine at position one in nisin H is critical for the dehydratase NisB. Ser_{29} was never dehydrated in the found species.

Lantibiotics are very potent and possess an antimicrobial activity in the nanomolar range (Gross and Morell, 1967; Rollema et al., 1995; Chan et al., 1996; Lu et al., 2010; Oppedijk et al., 2016). To verify this potential for nisin H and the nisin H F_1I variant we used a standardized growth inhibition assay and first screened against the nisin sensitive *L. lactis* strain NZ9000Cm. Here, Cm stands for chloramphenicol resistance, which arises from the empty plasmid, which was transformed. In comparison to nisin A (IC_{50} value: 4.8 ± 0.7 nM), the heterologous expressed variant nisin H possessed a comparable IC_{50} value (5.3 ± 1.0 nM) (**Figure 4** and **Table 2**). Both values are in line with previously determined IC_{50} values for the strain NZ9000Cm (Reiners et al., 2017). The effect of the nisin H F_1I variant was more pronounced. For the NZ9000Cm sensitive strain we calculated an IC_{50} value of 14.2 ± 0.2 nM, approximately threefold lower than the wild-type nisin H (**Figure 4** and **Table 2**).

To test the effect of the nisin variants on the immunity proteins NisI (Alkhatib et al., 2014a) and NisFEG (Alkhatib et al., 2014b), as well as the resistance proteins *Sa*NSR (Khosa et al., 2016a) and *Sa*NsrFP (Reiners et al., 2017), we expressed each of them in a plasmid-based system in a *L. lactis* NZ9000 strain. We termed these strains NZ9000NisI, NZ9000NisFEG, NZ9000*Sa*NSR and NZ9000*Sa*NsrFP, respectively.

Nisin A displayed an IC_{50} value of 48.6 ± 6.3 nM against strain NZ9000NisI and 53.0 ± 4.5 nM against strain NZ9000NisFEG. For the resistance strains NZ9000*Sa*NSR and NZ9000*Sa*NsrFP nisin A displayed IC_{50} values of 73.0 ± 3.6 and 82.1 ± 3.1 nM, respectively (**Figure 4** and **Table 2**). By comparing theses values, we calculated the fold of immunity/resistance to 10.1 ± 2.0 for NZ9000NisI, 11.1 ± 1.9 for NZ9000NisFEG, 15.2 ± 2.5 for NZ9000*Sa*NSR and 17.1 ± 2.7 for NZ9000*Sa*NsrFP (**Table 2**). After the first screen against the sensitive strain NZ9000Cm, nisin H and its variant were used to screen against the strains expressing the immunity or resistance proteins.

Nisin H revealed an IC_{50} value of 43.2 ± 8.7 nM against the NZ9000NisI strain, similar to nisin A, and a fold of immunity of 8.1 ± 2.2. Against the NZ9000NisFEG strain we determined an IC_{50} value of 23.4 ± 3.3 nM for nisin H which displayed a fold of resistance of 4.4 ± 1.0. Against the NZ9000*Sa*NSR strain we obtained an IC_{50} value of 52.4 ± 9.9 nM, resulting in a fold of resistance of 9.8 ± 2.6. Nisin H showed an IC_{50} value of 86.4 ± 4.0 nM for the NZ9000*Sa*NsrFP strain, resulting in a fold of resistance of 16.2 ± 3.1 (**Figure 4** and **Table 2**). NZ9000*Sa*NsrFP showed the highest fold of resistance for nisin H [in-line with a previous report (Reiners et al., 2017)]. Intriguingly, strain NZ9000NisFEG showed a reduced immunity and consequently we propose that nisin H is not recognized as efficiently as nisin A. Even NZ9000*Sa*NSR had a reduced resistance. That could be due to the exchange of His_{31} against lysine in the C-terminal part of nisin H (**Figure 1**).

Surprisingly, all strains displayed a reducing resistance/immunity effect for the nisin H F_1I variant in comparison to nisin A and also, with exception of NZ9000FEG for nisin H. Against the NZ9000NisI strain we determined an IC_{50} value of 34.1 ± 0.3 nM for the nisin H F_1I variant, with a fold of resistance 2.4 ± 0.1, which is nearly threefold lower than for nisin A. We obtained an IC_{50} value of 32.1 ± 0.8 nM against the ABC transporter NZ9000NisFEG, with a fold of resistance 2.3 ± 0.1 (**Figure 4** and **Table 2**). Nisin H F_1I showed for the resistance strain NZ9000*Sa*NSR and NZ9000*Sa*NsrFP an IC_{50} value of 44.2 ± 1.3 and 50.2 ± 1.6 nM, respectively. The calculated folds of resistance were 3.1 ± 0.1 and 3.5 ± 0.1, respectively (**Figure 4** and **Table 2**) and both are fivefold less than the observed fold of resistances for nisin A.

Since a similar activity for nisin H and nisin A was observed it became obvious that both exhibit the same mode of action. In

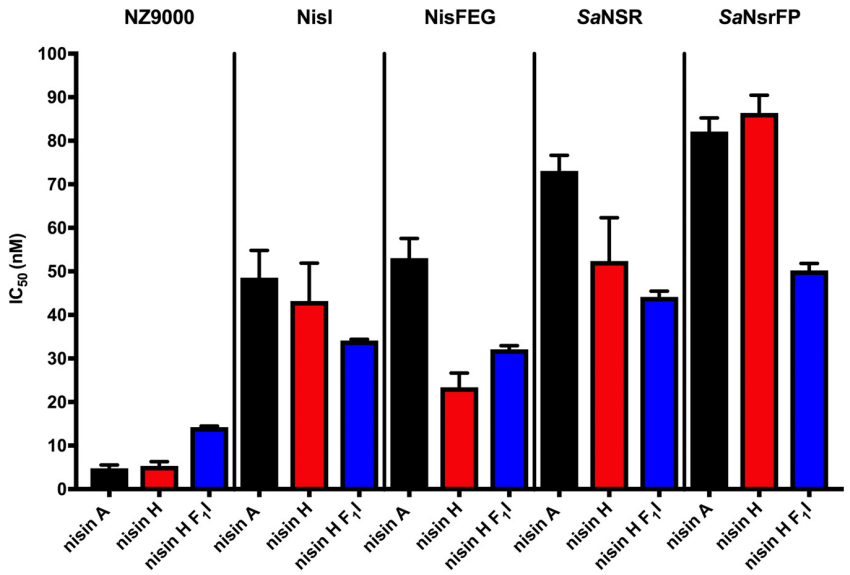

FIGURE 4 | Growth inhibition assays in the presence of nisin A and the nisin H varants. The lantibiotic nisin A (black bars), the heterologous expressed nisin H (red bars) and the position 1 variant of nisin H F_1I (blue bars) were used for growth inhibition (IC_{50}) with the strains NZ9000Cm, NZ9000NisI, NZ9000NisFEG, NZ9000*Sa*NSR, and NZ9000*Sa*NsrFP. Values represent the average of at least five biological independent measurements and the errors report the standard deviation of the mean (SDM).

TABLE 2 | IC_{50} values (nM) for nisin A, nisin H, and nisin H F_1I with the corresponding fold of resistance (FR) against the strains NZ9000Cm, NZ9000NisI, NZ9000NisFEG, NZ9000*Sa*NSR, and NZ9000*Sa*NsrFP.

Variant	NZ9000Cm	NZ9000NisI		NZ9000NisFEG		NZ9000*Sa*NSR		NZ9000*Sa*NsrFP	
		IC_{50}	FR	IC_{50}	FR	IC_{50}	FR	IC_{50}	FR
Nisin A	4.8 ± 0.7	48.6 ± 6.3	10.1 ± 2.0	53.0 ± 4.5	11.1 ± 1.9	73.0 ± 3.6	15.2 ± 2.5	82.1 ± 3.1	17.1 ± 2.7
Nisin H	5.3 ± 1.0	43.2 ± 8.7	8.1 ± 2.2	23.4 ± 3.3	4.4 ± 1.0	52.4 ± 9.9	9.8 ± 2.6	86.4 ± 4.1	16.2 ± 3.1
Nisin H F_1I	14.2 ± 0.2	34.1 ± 0.3	2.4 ± 0.1	32.1 ± 0.8	2.3 ± 0.1	44.2 ± 1.3	3.1 ± 0.1	50.2 ± 1.6	3.5 ± 0.1

the case of nisin A this combines growth inhibition with pore formation in the membrane with subsequent cell death. To test this we performed a SYTOX assay previously used for nisin A (Reiners et al., 2017). Here the SYTOX dye was added to *L. lactis* cells and displayed an increased fluorescence signal upon binding of DNA which is released from the cell upon pore formation (Roth et al., 1997). We use 100 nM of nisin A, nisin H and nisin H F_1I variant respectively and observed an almost instant fluorescence increase similar to the signal increase observed for nisin A (**Figure 5**). This shows that nisin H as well as its F_1I variant form pores in the membrane of *L. lactis* cell.

The nisin variants were further tested for antibacterial capabilities against *B. subtilis* and different pathogenic strains from *S. aureus*, *E. faecium,* and *E. faecalis* using the microdilution method, according to the recommendations of CLSI (2012). Here we found that nisin H and the F_1I variant performed almost identically or in most cases even better than the natural nisin A. Especially against the MSSA and MRSA strains, nisin H had significant lower MIC values of 0.19 and 0.78 μM, in comparison to 0.78 and 6.25 μM for nisin A, respectively (**Table 3**). Also, against *E. faecium* ATCC 35667, *B. subtilis* 168 as well as *E. faecium* ATCC 700221 (VRE), nisin H showed more potency with about two to eightfold lower MIC values than nisin A [0.39, 0.1, and 0.39 μM compared to 1.56, 0.78, and 0.78 μM for nisin A, respectively (**Table 3**)]. While the nisin H F_1I variant and nisin A had similar MIC values against both MSSA and MRSA strains, the nisin H F_1I variant only performed better than nisin A or nisin H against *E. faecalis* ATCC 51299 (VRE) with a MIC value of 0.78 μM compared to 1.56 μM for nisin A and nisin H. Against *E. faecium* ATCC 35667 and *B. subtilis* 168 nisin H F_1I was less efficient than nisin H, but still better than nisin A (**Table 3**).

DISCUSSION

We focused in this study on the natural variant nisin H and the nisin H F_1I mutant. Nisin H was discovered from the gut-derived strain *S. hyointestinalis* DPC6484 in 2015 by O'Connor et al. (2015). Here, we showed the heterologous expression of nisin H and the F_1I variant with the NICE-system in *L. lactis* (Eichenbaum et al., 1998; Mierau and Kleerebezem, 2005; Rink et al., 2005; Zhou et al., 2006; Lagedroste et al., 2019) and extended the characterization in terms of cleavage efficiency by the protease NisP and the antimicrobial activity against

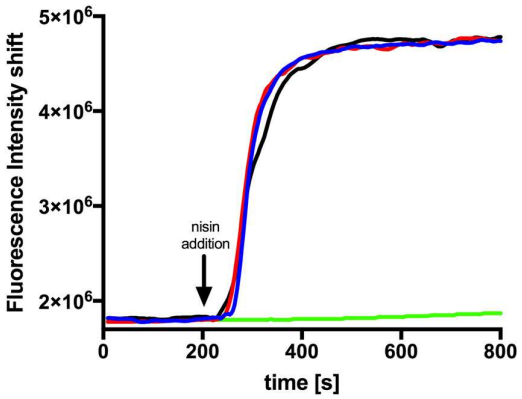

FIGURE 5 | Nisin mediated pore formation, visualized with the SYTOX green assay. The NZ9000Cm strain incubated with the SYTOX dye. After a stable baseline (~200 s), one of the nisin variants (100 nM) was added (indicated with an arrow). The fluorescence signal was measured using a fluorolog (Horiba III). The rapid increase in fluorescence indicates pore formation. The black line represents the addition of nisin A, the red line nisin H, and the blue line nisin H F_1I. As a control we added buffer shown as green line.

the immunity proteins NisFEG (Alkhatib et al., 2014b) and NisI (Alkhatib et al., 2014a), as well as the resistance proteins *Sa*NSR (Khosa et al., 2013; Khosa et al., 2016a,b) and *Sa*NsrFP (Khosa et al., 2016a; Reiners et al., 2017). We further tested for antibacterial capabilities against *B. subtilis* and different pathogenic strains from *S. aureus*, *E. faecium,* and *E. faecalis.*

Both lantibiotics, nisin H and the F_1I variant were purified in high amounts and purity with 5.3 ± 0.6 mg/L of cell culture for nisin H and 4.9 ± 0.2 mg/L of cell culture for nisin H F_1I variant, respectively (**Figure 2B** and **Table 1**). In comparison, the homologous expression of nisin H in *S. hyointestinalis* and nisin A in *L. lactis* NZ9700 results in a very low amount of 0.15 mg/L of cell culture and 0.50 mg/L of cell culture (O'Connor et al., 2015), respectively, which demonstrates the enormous potential of the NICE-system, for lantibiotic and even non-lantibiotic expression (Eichenbaum et al., 1998; Mierau and Kleerebezem, 2005; Rink et al., 2005; Zhou et al., 2006; Lagedroste et al., 2019).

An important step in the maturation of a lantibiotic is the cleavage of the leader peptide to become biological active. The cleavage efficiency of the natural substrate nisin A was determined with 94.6 ± 2.0%. For nisin H the cleaving efficiency was drastically reduced to 15.6 ± 1.4%. The first residue of nisin A is an isoleucine, while the corresponding residue in nisin H is phenylalanine and as demonstrated before (Lagedroste et al., 2019), aromatic residues prevent efficient cleavage likely by interfering with the S1′ binding pocket of NisP. With the nisin H F_1I variant, the cleavage efficiency was restored to 91.8 ± 0.8% (**Figures 1**, **2C** and **Table 1**). This indicated that the other point mutations naturally occurring in nisin H did not affect cleavage by NisP. With respect to other natural nisin variants, NisP cleavage could be a critical step. For example nisin O1 to O4 from *B. obeum* A2-162 (Hatziioanou et al., 2017) has a tyrosine or a threonine, respectively, at position one, which should also result in a low NisP cleavage efficiency. Natural variants such as nisin U (Wirawan et al., 2006), nisin J (O'Sullivan et al., 2019, 2020), nisin Q (Zendo et al., 2003), nisin Z (Mulders et al., 1991) and nisin F (de Kwaadsteniet et al., 2008) have an isoleucine and nisin U2 (Wirawan et al., 2006) and nisin P (Zhang et al., 2012; Wu et al., 2014) a valine at position one, which should result in high NisP cleavage efficiency.

Furthermore, we made a sequence alignment with Clustal Omega (Madeira et al., 2019) for the NshP (the natural protease for the nisin H cleavage) from *S. hyointestinalis* and NisP from *L. lactis* to see if there is any difference in the active site, which could be the reason for the reduced cleavage efficiency (**Figure 6A** and **Supplementary Figure 1**). Here the three important residues His_{306}, Asp_{259}, and Ser_{512} which build up the catalytic triad in NisP are conserved in NshP. We also calculated a homology model of NshP based on the known NisP structure (PDB code 4MZD) using Phyre2 (Kelley et al., 2015; **Figure 6B** and **Supplementary Figure 2**). Here, no significant differences are found within the overall fold as well as the active site which would explain the difference in the cleavage site. This is intriguing since the recognition site within the leader peptide differs between nisin A (sequence is ASPR) and nisin H (sequence is ASTR) (see **Supplementary Figure 3**). This suggests that the proteases NisP and NshP recognize their substrate by small difference in their active site.

Nevertheless, for an efficient cleavage, (methyl)-lanthionine rings have to be present. This even holds true in light of the presence of all (methyl)-lanthionine rings, which is generally assumed as the prerequisite for fast and efficient conversion of the pre-nisin to modified nisin (Plat et al., 2011;

TABLE 3 | MIC values for nisin A, nisin H, and nisin H F_1I against different pathogenic strains.

Organisms	Minimum inhibitory concentration (μM)		
	Nisin A	Nisin H	Nisin H F_1I
Staphylococcus aureus ATCC 29213 (MSSA)	0.78	0.19	0.78
Staphylococcus aureus ATCC 700699 (MRSA)	6.25	0.78	6.25
Enterococcus faecalis ATCC 29212	1.56	1.56	1.56
Enterococcus faecium ATCC 35667	1.56	0.39	0.78
Bacillus subtilis 168	0.78	0.1	0.39
Enterococcus faecalis ATCC 51299 (VRE)	1.56	1.56	0.78
Enterococcus faecium ATCC 700221 (VRE)	0.78	0.39	0.78

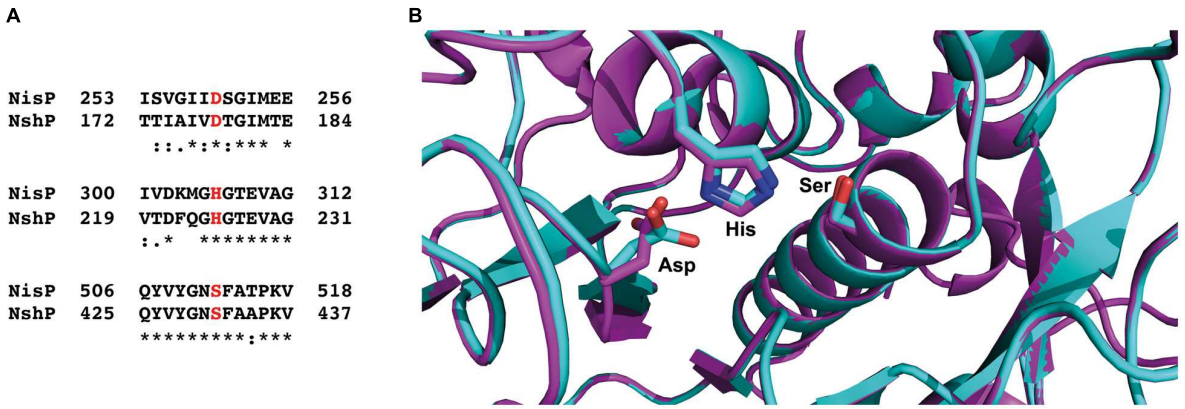

FIGURE 6 | Sequence alignment of NisP from *Lactococcus lactis* and NshP from *Streptococcus hyointestinalis*. **(A)** The important residues from the active site (Asp_{259}, His_{306}, and Ser_{512} for NisP and Asp_{178}, His_{225}, and Ser_{431} for NshP) are marked in red, shown together with the close neighborhood residues. The sequence alignment was done with Clustal Omega (Madeira et al., 2019). **(B)** Zoom-in into the active sites of NshP (magenta) and NisP (cyan). The important residues for the catalytic activity (Asp_{259}, His_{306}, and Ser_{512} for NisP and Asp_{178}, His_{225}, and Ser_{431} for NshP) are shown in stick representation. Figure was generated using Pymol (2015). For a full alignment and a corresponding homology model, please see **Supplementary Material**.

Lagedroste et al., 2017). To check the amount of dehydrations, necessary for (methyl)-lanthionine ring formation we applied MALDI-TOF analysis. The loss of water molecules within the peptide is directly visible in the reduced molecular weight, but not the (methyl)-lanthionine ring formation. Here we used 1-cyano-4 dimethylaminopyridinium tetrafluoroborate (CDAP) (Wu and Watson, 1998), which binds to free cysteine residues, indicating that these cysteines are not involved in a (methyl)-lanthionine ring. For both lantibiotics, nisin H and the nisin H F_1I variant no CDAP coupling products were found, indicating that no (methyl)-lanthionine ring is lacking (**Figure 3** and **Table 1**). Nisin H has 10 possible dehydration sites and is predicated to be ninefold dehydrated when expressed homologous (O'Connor et al., 2015). A minor species of nine dehydrations was found, but the dominant species was eightfold dehydrated. The dehydration pattern of the F_1I variant is changed in comparison to nisin H. Here we determined a dominant ninefold species (**Figure 3** and **Table 1**). This provides a hint, that position two of wild-type nisin H might not have been previously dehydrated, due to steric hindrance of the phenylalanine. To validate which serine or threonine residues is dehydrated, we perform a tandem mass spectrometric analysis of nisin H and the F_1I variant. Here we found that the Thr_2 partially escape the dehydration in nisin H. In the nisin H F_1I variant the Thr_2 was in all species dehydrated, which gives a hint that, the phenylalanine at position one in nisin H is critical for the dehydratase NisB. This is in line with previous data from the I_1F variant of nisin A, where the dominant species was sevenfold dehydrated and not eightfold as wild-type nisin A (Lagedroste et al., 2019). It has also been reported for the natural nisin Z (Mulders et al., 1991), that the I_1W mutation showed a partial inhibition of dehydration of the Thr_2 (Breukink et al., 1998), which could also be the case for nisin H with the aromatic phenylalanine at position one, resulting in eight dehydrations. A dehydration of position Ser_{29} normally goes in line with the lack of ring E (Lubelski et al., 2009), which drastically reduces the antimicrobial activity of nisin A against the sensitive NZ9000Cm strain (Alkhatib et al., 2014b; Khosa et al., 2016a; Reiners et al., 2017). Since the activity was high for nisin H and the F_1I variant, we expected that Ser_{29} was not dehydrated and tandem mass spectrometric analysis supported this.

Nisin H showed nearly the same activity as nisin A against the sensitive NZ9000Cm strain but the nisin H F_1I variant is roughly threefold less active. For the immunity protein NisI, it was revealed that nisin H has an identical activity like nisin A within experimental error. However, the nisin H F_1I variant exhibited a lower IC_{50} value of 34.1 ± 0.3 nM and due to the weaker wild-type activity more than a threefold lower fold of resistance (2.4 ± 0.1 compared to 8.1 ± 2.2) (**Figure 4** and **Table 2**). NisI recognizes the N-terminus of nisin (Wiedemann et al., 2001) and the lower IC_{50} could be due to the fact that Thr_2 is dehydrated in the nisin H F_1I variant in contrast to nisin H. An additional change is the leucine at position 6 against methionine in nisin H and the nisin H F_1I variant, which could be responsible for the better recognition by NisI.

The immunity protein NisFEG, in comparison to nisin A, showed a strong reduction in immunity in the presence of nisin H and the nisin H F_1I variant. NisFEG recognizes the C-terminus of nisin (Alkhatib et al., 2014b), which indicates that the point mutations of nisin H affect NisFEG. So, we suppose that nisin H and the nisin H F_1I variant are not recognized and subsequently transported out of the membrane like nisin A.

The resistance protein *Sa*NSR also recognizes the C-terminus of nisin (Khosa et al., 2016a), and cleaves nisin between the positions 28 and 29. Other studies showed that mutations in this area of the nisin molecule, e.g., $S_{29}P$ or $C_{28}P$ strongly reduce the efficiency of *Sa*NSR (Field et al., 2019; Zaschke-Kriesche et al., 2019a). We assume that the exchange of His_{31} against lysine in nisin H and the nisin H F_1I variant (**Figure 1**) has the same effect on *Sa*NSR thereby lowering the resistance efficiency to an IC_{50} value of 52.4 ± 2.6 nM for nisin H and 44.2 ± 1.3 nM for the nisin H F_1I variant, respectively (**Figure 4** and **Table 2**).

For the resistance protein *Sa*NsrFP, we observed an activity for nisin H identical to nisin A. *Sa*NsrFP recognizes the N-terminus of nisin (Reiners et al., 2017), which is affected due to the different dehydration pattern in wild-type nisin H in comparison to the nisin H F_1I variant. The nisin H F_1I variant showed a lower IC_{50} value of 50.2 ± 1.6 nM, compared to 86.4 ± 4.1 nM for nisin H. This effect is even more pronounced when comparing the fold of resistances of 16.2 ± 3.1 for nisin H to 3.5 ± 0.1 for the nisin H F_1I variant, respectively (**Figure 4** and **Table 2**).

This study demonstrated again that only a complete characterization of a lantibiotic reveals the full antimicrobial potential. Based on the IC_{50} value of the sensitive NZ9000Cm strain the F_1I variant might be classified as weakly antimicrobial active, but with respect to the immunity and resistance proteins, it becomes more interesting, due to its high activity even against the immunity proteins NisI and NisFEG from *L. lactis* and the nisin resistance proteins *Sa*NSR and *Sa*NsrFP from *S. agalactiae* COH1. Against the tested pathogenic bacteria, we found that nisin H and the nisin H F_1I variant performed almost identically or in the most cases even better than the natural nisin A. Nisin H displayed high antimicrobial potential against both methicillin-resistant and –susceptible the *S. aureus* strains, both vancomycin-resistant and -susceptible, *E. faecium* strains, as well as *B. subtilis.*

DATA AVAILABILITY STATEMENT

The raw data supporting the conclusions of this article will be made available by the authors, without undue reservation.

AUTHOR CONTRIBUTIONS

LS and SS conceived and directed this study. JR and ML conducted the expression, purification, MS-analysis, and the growth inhibition experiments. JG performed the SYTOX experiments. GP and KS performed the tandem mass spectrometric analysis. EA and RK performed the MIC experiments. JR, ML, SS, and LS wrote the manuscript. All authors read and approved the manuscript.

FUNDING

This work was supported by the Deutsche Forschungsgemeinschaft (DFG, grant Schm1279/13-1 to LS). The Center for Structural studies is funded by the DFG (Grant number 417919780 to SS). Project number 270650915 (Research Training Group GRK2158, TP2a to RK and TP4a to SS).

ACKNOWLEDGMENTS

We thank all members of the Institute of Biochemistry for fruitful discussions.

SUPPLEMENTARY MATERIAL

The Supplementary Material for this article can be found online at: https://www.frontiersin.org/articles/10.3389/fmicb.2020.573614/full#supplementary-material

REFERENCES

Abts, A., Montalban-Lopez, M., Kuipers, O. P., Smits, S. H., and Schmitt, L. (2013). NisC binds the FxLx motif of the nisin leader peptide. *Biochemistry* 52, 5387–5395. doi: 10.1021/bi4008116

Alkhatib, Z., Lagedroste, M., Fey, I., Kleinschrodt, D., Abts, A., and Smits, S. H. (2014a). Lantibiotic immunity: inhibition of nisin mediated pore formation by NisI. *PLoS One* 9:e102246. doi: 10.1371/journal.pone.0102246

Alkhatib, Z., Lagedroste, M., Zaschke, J., Wagner, M., Abts, A., Fey, I., et al. (2014b). The C-terminus of nisin is important for the ABC transporter NisFEG to confer immunity in *Lactococcus lactis*. *Microbiologyopen* 3, 752–763. doi: 10.1002/mbo3.205

Arnison, P. G., Bibb, M. J., Bierbaum, G., Bowers, A. A., Bugni, T. S., Bulaj, G., et al. (2013). Ribosomally synthesized and post-translationally modified peptide natural products: overview and recommendations for a universal nomenclature. *Nat. Prod. Rep.* 30, 108–160.

Breukink, E., Van Kraaij, C., Van Dalen, A., Demel, R. A., Siezen, R. J., De Kruijff, B., et al. (1998). The orientation of nisin in membranes. *Biochemistry* 37, 8153–8162. doi: 10.1021/bi972797l

Brunati, C., Thomsen, T. T., Gaspari, E., Maffioli, S., Sosio, M., Jabes, D., et al. (2018). Expanding the potential of NAI-107 for treating serious ESKAPE pathogens: synergistic combinations against Gram-negatives and bactericidal activity against non-dividing cells. *J. Antimicrob. Chemother.* 73, 414–424. doi: 10.1093/jac/dkx395

Chan, W. C., Leyland, M., Clark, J., Dodd, H. M., Lian, L. Y., Gasson, M. J., et al. (1996). Structure-activity relationships in the peptide antibiotic nisin: antibacterial activity of fragments of nisin. *FEBS Lett.* 390, 129–132. doi: 10.1016/0014-5793(96)00638-2

Clinical and Laboratory Standards Institute (2012). *Methods for Dilution Antimicrobial Susceptibility Tests for Bacteria that Grow Aerobically; Approved Standard*, 9th Edn. Wayne PA: Clinical and Laboratory Standards Institute.

Crowther, G. S., Baines, S. D., Todhunter, S. L., Freeman, J., Chilton, C. H., and Wilcox, M. H. (2013). Evaluation of NVB302 versus vancomycin activity in an in vitro human gut model of Clostridium difficile infection. *J. Antimicrob. Chemother.* 68, 168–176. doi: 10.1093/jac/dks359

Dawson, M. J., and Scott, R. W. (2012). New horizons for host defense peptides and lantibiotics. *Curr. Opin. Pharmacol.* 12, 545–550. doi: 10.1016/j.coph.2012.06.006

de Kwaadsteniet, M., Ten Doeschate, K., and Dicks, L. M. (2008). Characterization of the structural gene encoding nisin F, a new lantibiotic produced by a *Lactococcus lactis* subsp. lactis isolate from freshwater catfish (*Clarias gariepinus*). *Appl. Environ. Microbiol.* 74, 547–549. doi: 10.1128/aem.01862-07

Delves-Broughton, J., Blackburn, P., Evans, R. J., and Hugenholtz, J. (1996). Applications of the bacteriocin, nisin. *Antonie Van Leeuwenhoek* 69, 193–202. doi: 10.1007/bf00399424

Dischinger, J., Basi Chipalu, S., and Bierbaum, G. (2014). Lantibiotics: promising candidates for future applications in health care. *Int. J. Med. Microbiol.* 304, 51–62. doi: 10.1016/j.ijmm.2013.09.003

Eichenbaum, Z., Federle, M. J., Marra, D., De Vos, W. M., Kuipers, O. P., Kleerebezem, M., et al. (1998). Use of the lactococcal nisA promoter to regulate gene expression in gram-positive bacteria: comparison of induction level and promoter strength. *Appl. Environ. Microbiol.* 64, 2763–2769. doi: 10.1128/aem.64.8.2763-2769.1998

Field, D., Blake, T., Mathur, H., Pm, O. C., Cotter, P. D., Paul Ross, R., et al. (2019). Bioengineering nisin to overcome the nisin resistance protein. *Mol. Microbiol.* 111, 717–731.

Gross, E., and Morell, J. L. (1967). The presence of dehydroalanine in the antibiotic nisin and its relationship to activity. *J. Am. Chem. Soc.* 89, 2791–2792. doi: 10.1021/ja00987a084

Hasper, H. E., De Kruijff, B., and Breukink, E. (2004). Assembly and stability of nisin-lipid II pores. *Biochemistry* 43, 11567–11575. doi: 10.1021/bi049476b

Hatziioanou, D., Gherghisan-Filip, C., Saalbach, G., Horn, N., Wegmann, U., Duncan, S. H., et al. (2017). Discovery of a novel lantibiotic nisin O from Blautia obeum A2-162, isolated from the human gastrointestinal tract. *Microbiology* 163, 1292–1305. doi: 10.1099/mic.0.000515

Holo, H., and Nes, I. F. (1989). High-Frequency transformation, by electroporation, of *Lactococcus lactis* subsp. cremoris grown with glycine in osmotically stabilized media. *Appl. Environ. Microbiol.* 55, 3119–3123. doi: 10.1128/aem.55.12.3119-3123.1989

Hsu, S. T. D., Breukink, E., Tischenko, E., Lutters, M. A. G., De Kruijff, B., Kaptein, R., et al. (2004). The nisin-lipid II complex reveals a pyrophosphate cage that provides a blueprint for novel antibiotics. *Nat. Struct. Mol. Biol.* 11, 963–967. doi: 10.1038/nsmb830

Jabes, D., Brunati, C., Candiani, G., Riva, S., Romano, G., and Donadio, S. (2011). Efficacy of the new lantibiotic NAI-107 in experimental infections induced by multidrug-resistant Gram-positive pathogens. *Antimicrob. Agents Chemother.* 55, 1671–1676. doi: 10.1128/aac.01288-10

Jensen, P. R., and Hammer, K. (1993). Minimal requirements for exponential growth of *Lactococcus lactis*. *Appl. Environ. Microbiol.* 59, 4363–4366. doi: 10.1128/aem.59.12.4363-4366.1993

Kaletta, C., and Entian, K. D. (1989). Nisin, a peptide antibiotic: cloning and sequencing of the nisA gene and posttranslational processing of its peptide product. *J. Bacteriol.* 171, 1597–1601. doi: 10.1128/jb.171.3.1597-1601.1989

Karakas Sen, A., Narbad, A., Horn, N., Dodd, H. M., Parr, A. J., Colquhoun, I., et al. (1999). Post-translational modification of nisin. The involvement of NisB in the dehydration process. *Eur. J. Biochem.* 261, 524–532. doi: 10.1046/j.1432-1327.1999.00303.x

Kelley, L. A., Mezulis, S., Yates, C. M., Wass, M. N., and Sternberg, M. J. (2015). The Phyre2 web portal for protein modeling, prediction and analysis. *Nat. Protoc.* 10, 845–858. doi: 10.1038/nprot.2015.053

Khosa, S., Alkhatib, Z., and Smits, S. H. (2013). NSR from Streptococcus agalactiae confers resistance against nisin and is encoded by a conserved nsr operon. *Biol. Chem.* 394, 1543–1549. doi: 10.1515/hsz-2013-0167

Khosa, S., Frieg, B., Mulnaes, D., Kleinschrodt, D., Hoeppner, A., Gohlke, H., et al. (2016a). Structural basis of lantibiotic recognition by the nisin resistance protein from Streptococcus agalactiae. *Sci. Rep.* 6:18679.

Khosa, S., Lagedroste, M., and Smits, S. H. (2016b). Protein defense systems against the lantibiotic nisin: function of the immunity protein NisI and the resistance protein NSR. *Front. Microbiol.* 7:504. doi: 10.3389/fmicb.2016.00504

Klaenhammer, T. R. (1993). Genetics of bacteriocins produced by lactic acid bacteria. *FEMS Microbiol. Rev.* 12, 39–85. doi: 10.1016/0168-6445(93)90057-g

Koponen, O., Tolonen, M., Qiao, M., Wahlstrom, G., Helin, J., and Saris, P. E. J. (2002). NisB is required for the dehydration and NisC for the lanthionine formation in the post-translational modification of nisin. *Microbiology* 148, 3561–3568. doi: 10.1099/00221287-148-11-3561

Kuipers, O. P., De Ruyter, P. G., Kleerebezem, M., and De Vos, W. M. (1997). Controlled overproduction of proteins by lactic acid bacteria. *Trends Biotechnol.* 15, 135–140. doi: 10.1016/s0167-7799(97)01029-9

Lagedroste, M., Reiners, J., Smits, S. H. J., and Schmitt, L. (2019). Systematic characterization of position one variants within the lantibiotic nisin. *Sci. Rep.* 9:935.

Lagedroste, M., Smits, S. H. J., and Schmitt, L. (2017). Substrate specificity of the secreted nisin leader peptidase NisP. *Biochemistry* 56, 4005–4014. doi: 10.1021/acs.biochem.7b00524

Li, B., and van der Donk, W. A. (2007). Identification of essential catalytic residues of the cyclase NisC involved in the biosynthesis of nisin. *J. Biol. Chem.* 282, 21169–21175. doi: 10.1074/jbc.m701802200

Li, B., Yu, J. P., Brunzelle, J. S., Moll, G. N., Van Der Donk, W. A., and Nair, S. K. (2006). Structure and mechanism of the lantibiotic cyclase involved in nisin biosynthesis. *Science* 311, 1464–1467. doi: 10.1126/science.1121422

Lu, Y., Jiang, L., Chen, M., Huan, L., and Zhong, J. (2010). [Improving heat and pH stability of nisin by site-directed mutagenesis]. *Wei Sheng Wu Xue Bao* 50, 1481–1487.

Lubelski, J., Khusainov, R., and Kuipers, O. P. (2009). Directionality and coordination of dehydration and ring formation during biosynthesis of the lantibiotic nisin. *J. Biol. Chem.* 284, 25962–25972. doi: 10.1074/jbc.m109.026690

Madeira, F., Park, Y. M., Lee, J., Buso, N., Gur, T., Madhusoodanan, N., et al. (2019). The EMBL-EBI search and sequence analysis tools APIs in 2019. *Nucleic Acids Res.* 47, W636–W641.

Medeiros-Silva, J., Jekhmane, S., Paioni, A. L., Gawarecka, K., Baldus, M., Swiezewska, E., et al. (2018). High-resolution NMR studies of antibiotics in cellular membranes. *Nat. Commun.* 9:3963.

Mierau, I., and Kleerebezem, M. (2005). 10 years of the nisin-controlled gene expression system (NICE) in *Lactococcus lactis*. *Appl. Microbiol. Biotechnol.* 68, 705–717. doi: 10.1007/s00253-005-0107-6

Mota-Meira, M., Lapointe, G., Lacroix, C., and Lavoie, M. C. (2000). MICs of mutacin B-Ny266, nisin A, vancomycin, and oxacillin against bacterial pathogens. *Antimicrob. Agents Chemother.* 44, 24–29. doi: 10.1128/aac.44.1.24-29.2000

Mulders, J. W., Boerrigter, I. J., Rollema, H. S., Siezen, R. J., and De Vos, W. M. (1991). Identification and characterization of the lantibiotic nisin Z, a natural nisin variant. *Eur. J. Biochem.* 201, 581–584. doi: 10.1111/j.1432-1033.1991.tb16317.x

O'Sullivan, J. N., O'Connor, P. M., Rea, M. C., O'Sullivan, O., Walsh, C. J., Healy, B., et al. (2020). Nisin J, a novel natural nisin variant, is produced by *Staphylococcus capitis* Sourced from the human skin microbiota. *J. Bacteriol* 202. doi: 10.1128/JB.00639-19

O'Connor, P. M., O'Shea, E. F., Guinane, C. M., O'Sullivan, O., Cotter, P. D., Ross, R. P., et al. (2015). Nisin H is a new nisin variant produced by the gut-derived strain *Streptococcus hyointestinalis* DPC6484. *Appl. Environ. Microbiol.* 81, 3953–3960. doi: 10.1128/aem.00212-15

Okeley, N. M., Paul, M., Stasser, J. P., Blackburn, N., and Van Der Donk, W. A. (2003). SpaC and NisC, the cyclases involved in subtilin and nisin biosynthesis, are zinc proteins. *Biochemistry* 42, 13613–13624. doi: 10.1021/bi0354942

Ongey, E. L., Yassi, H., Pflugmacher, S., and Neubauer, P. (2017). Pharmacological and pharmacokinetic properties of lanthipeptides undergoing clinical studies. *Biotechnol. Lett.* 39, 473–482. doi: 10.1007/s10529-016-2279-9

Oppedijk, S. F., Martin, N. I., and Breukink, E. (2016). Hit 'em where it hurts: the growing and structurally diverse family of peptides that target lipid-II. *Biochim. Biophys. Acta* 1858, 947–957. doi: 10.1016/j.bbamem.2015.10.024

Ortega, M. A., Hao, Y., Zhang, Q., Walker, M. C., Van Der Donk, W. A., and Nair, S. K. (2015). Structure and mechanism of the tRNA-dependent lantibiotic dehydratase NisB. *Nature* 517, 509–512. doi: 10.1038/nature13888

O'Sullivan, J. N., Rea, M. C., O'Connor, P. M., Hill, C., and Ross, R. P. (2019). Human skin microbiota is a rich source of bacteriocin-producing staphylococci that kill human pathogens. *FEMS Microbiol. Ecol.* 95:fiy241.

Plat, A., Kluskens, L. D., Kuipers, A., Rink, R., and Moll, G. N. (2011). Requirements of the engineered leader peptide of nisin for inducing modification, export, and cleavage. *Appl. Environ. Microbiol.* 77, 604–611. doi: 10.1128/aem.01503-10

Pymol (2015). *The PyMOL Molecular Graphics System, Version 2.0*. New York, NY: Schrödinger.

Reiners, J., Lagedroste, M., Ehlen, K., Leusch, S., Zaschke-Kriesche, J., and Smits, S. H. J. (2017). The N-terminal region of nisin is important for the BceAB-Type ABC Transporter NsrFP from *Streptococcus agalactiae* COH1. *Front. Microbiol.* 8:1643. doi: 10.3389/fmicb.2017.01643

Repka, L. M., Chekan, J. R., Nair, S. K., and Van Der Donk, W. A. (2017). Mechanistic understanding of lanthipeptide biosynthetic enzymes. *Chem. Rev.* 117, 5457–5520. doi: 10.1021/acs.chemrev.6b00591

Rink, R., Kuipers, A., De Boef, E., Leenhouts, K. J., Driessen, A. J., Moll, G. N., et al. (2005). Lantibiotic structures as guidelines for the design of peptides that can be modified by lantibiotic enzymes. *Biochemistry* 44, 8873–8882. doi: 10.1021/bi050081h

Rogers, L. A. (1928). The inhibiting effect of streptococcus lactis on Lactobacillus Bulgaricus. *J. Bacteriol.* 16, 321–325. doi: 10.1128/jb.16.5.321-325.1928

Rogers, L. A., and Whittier, E. O. (1928). Limiting factors in the lactic fermentation. *J. Bacteriol.* 16, 211–229. doi: 10.1128/jb.16.4.211-229.1928

Rollema, H. S., Kuipers, O. P., Both, P., De Vos, W. M., and Siezen, R. J. (1995). Improvement of solubility and stability of the antimicrobial peptide nisin by

protein engineering. *Appl. Environ. Microbiol.* 61, 2873–2878. doi: 10.1128/aem.61.8.2873-2878.1995

Roth, B. L., Poot, M., Yue, S. T., and Millard, P. J. (1997). Bacterial viability and antibiotic susceptibility testing with SYTOX green nucleic acid stain. *Appl. Environ. Microbiol.* 63, 2421–2431. doi: 10.1128/aem.63.6.2421-2431.1997

Sahl, H. G., and Bierbaum, G. (1998). Lantibiotics: biosynthesis and biological activities of uniquely modified peptides from gram-positive bacteria. *Annu. Rev. Microbiol.* 52, 41–79. doi: 10.1146/annurev.micro.52.1.41

Sandiford, S. K. (2019). Current developments in lantibiotic discovery for treating Clostridium difficile infection. *Expert Opin. Drug. Discov.* 14, 71–79. doi: 10.1080/17460441.2019.1549032

Terzaghi, B. E., and Sandine, W. E. (1975). Improved medium for lactic Streptococci and Their Bacteriophages. *Appl. Microbiol.* 29, 807–813. doi: 10.1128/aem.29.6.807-813.1975

van Heel, A. J., De Jong, A., Song, C., Viel, J. H., Kok, J., and Kuipers, O. P. (2018). BAGEL4: a user-friendly web server to thoroughly mine RiPPs and bacteriocins. *Nucleic Acids Res.* 46, W278–W281.

van Heusden, H. E., De Kruijff, B., and Breukink, E. (2002). Lipid II induces a transmembrane orientation of the pore-forming peptide lantibiotic nisin. *Biochemistry* 41, 12171–12178. doi: 10.1021/bi026090x

Wiedemann, I., Benz, R., and Sahl, H. G. (2004). Lipid II-mediated pore formation by the peptide antibiotic nisin: a black lipid membrane study. *J. Bacteriol.* 186, 3259–3261. doi: 10.1128/jb.186.10.3259-3261.2004

Wiedemann, I., Breukink, E., Van Kraaij, C., Kuipers, O. P., Bierbaum, G., De Kruijff, B., et al. (2001). Specific binding of nisin to the peptidoglycan precursor lipid II combines pore formation and inhibition of cell wall biosynthesis for potent antibiotic activity. *J. Biol. Chem.* 276, 1772–1779. doi: 10.1074/jbc.m006770200

Wirawan, R. E., Klesse, N. A., Jack, R. W., and Tagg, J. R. (2006). Molecular and genetic characterization of a novel nisin variant produced by *Streptococcus uberis*. *Appl. Environ. Microbiol.* 72, 1148–1156. doi: 10.1128/aem.72.2.1148-1156.2006

Wu, J., and Watson, J. T. (1998). Optimization of the cleavage reaction for cyanylated cysteinyl proteins for efficient and simplified mass mapping. *Anal. Biochem.* 258, 268–276. doi: 10.1006/abio.1998.2596

Wu, Z., Wang, W., Tang, M., Shao, J., Dai, C., Zhang, W., et al. (2014). Comparative genomic analysis shows that *Streptococcus suis* meningitis isolate SC070731 contains a unique 105K genomic island. *Gene* 535, 156–164. doi: 10.1016/j.gene.2013.11.044

Zaschke-Kriesche, J., Behrmann, L. V., Reiners, J., Lagedroste, M., Groner, Y., Kalscheuer, R., et al. (2019a). Bypassing lantibiotic resistance by an effective nisin derivative. *Bioorg. Med. Chem.* 27, 3454–3462. doi: 10.1016/j.bmc.2019.06.031

Zaschke-Kriesche, J., Reiners, J., Lagedroste, M., and Smits, S. H. J. (2019b). Influence of nisin hinge-region variants on lantibiotic immunity and resistance proteins. *Bioorg. Med. Chem.* 27, 3947–3953. doi: 10.1016/j.bmc.2019.07.014

Zendo, T., Fukao, M., Ueda, K., Higuchi, T., Nakayama, J., and Sonomoto, K. (2003). Identification of the lantibiotic nisin Q, a new natural nisin variant produced by *Lactococcus lactis* 61-14 isolated from a river in Japan. *Biosci. Biotechnol. Biochem.* 67, 1616–1619. doi: 10.1271/bbb.67.1616

Zhang, Q., Yu, Y., Velasquez, J. E., and Van Der Donk, W. A. (2012). Evolution of lanthipeptide synthetases. *Proc. Natl. Acad. Sci. U.S.A.* 109, 18361–18366. doi: 10.1073/pnas.1210393109

Zhou, L., Van Heel, A. J., and Kuipers, O. P. (2015). The length of a lantibiotic hinge region has profound influence on antimicrobial activity and host specificity. *Front. Microbiol* 6:11. doi: 10.3389/fmicb.2015.00011

Zhou, X. X., Li, W. F., Ma, G. X., and Pan, Y. J. (2006). The nisin-controlled gene expression system: construction, application and improvements. *Biotechnol. Adv.* 24, 285–295. doi: 10.1016/j.biotechadv.2005.11.001

Conflict of Interest: The authors declare that the research was conducted in the absence of any commercial or financial relationships that could be construed as a potential conflict of interest.

Supplementary Material

Insights in the antimicrobial potential of the natural nisin variant nisin H

Jens Reiners[1,2]*, Marcel Lagedroste[1]*, Julia Gottstein[1], Emmanuel T. Adeniyi[3], Rainer Kalscheuer[3], Gereon Poschmann[4], Kai Stühler[4,5], Sander H.J. Smits[1,2 #] and Lutz Schmitt[1 #]

[1]Institute of Biochemistry, Heinrich-Heine-University Düsseldorf, Universitaetsstrasse 1, 40225, Düsseldorf, Germany.

[2]Center for Structural Studies, Heinrich-Heine-University Düsseldorf, Universitaetsstrasse 1, 40225, Düsseldorf, Germany.

[3]Institute of Pharmaceutical Biology and Biotechnology, Heinrich-Heine-University Düsseldorf, Universitaetsstrasse 1, 40225, Düsseldorf, Germany.

[4]Institute for Molecular Medicine, Medical Faculty, Heinrich-Heine-University Düsseldorf, 40225 Düsseldorf, Germany

[5]Molecular Proteomics Laboratory, BMFZ, Heinrich-Heine-University-Düsseldorf, 40225 Düsseldorf, Germany

*Contributed equally

#Address correspondence to Lutz Schmitt: lutz.schmitt@hhu.de or Sander Smits sander.smits@hhu.de

Key words: lantibiotics, nisin, nisin H, MS analysis, antimicrobial activity

```
NisP      ----MKKILGFLFIVCSLGLSATVHGETTNSQQLLSNNINTELINHNSNAILSSTEGSTT      56
NshP      MGNNVKKFLCLLCMFFTFSITPIVYGEDIS-----------------------------      30
              :**:* :* :. ::.::  *:**  .

NisP      DSINLGAQSPAVKSTTRTELDVTGAAKTLLQTSAVQKEMKVSLQETQVSSEF--SKRDSV      114
NshP      ---------------------------------------LSVDKNEVTTQVSVSSSDEY      50
                                                 :*:::.:*:::.  *. *.

NisP      TNKEAVPVSKDELLEQSEVVVSTSSIQKNKILDNK--------KNRANFVTSSPLIKEKP      166
NshP      QSGDATPQNQYDVTKSSDSYD--NHVGSQSYIDNSNKSDTAEDTINSSYVEDSSIVSEQE      108
           . :*.* .: :: :.*:     . : .:. :**.        . .:.:* .* ::.*:

NisP      SNSKDASGVIDNSASPLSYRKAKEVVSLRQPLKNQKVEAQPLLISNSSEKKASVYTNSHD      226
NshP      S------GE------------SKEVD-SQENFQSDQVQ----TKETTADGNTNNLSASHI      145
          *      *             :***   :: ::.::*:      ..::: ::.  : **

NisP      FWDYQWDMKYVTNNGESYALYQPSKKISVGIIDSGIMEEHPDLSNSLGNYFKNLVPKGGF      286
NshP      FWDKQWDIKNVTNNGESYELYQASKNTTIAIVDTGIMTEHPDLAFSLGDYLKNFVPEGGF      205
          *** ***:* ******** *** **: ::.*:*:*** *****: ***:*:**:**:***

NisP      DNEEPDETGNPSDIVDKMGHGTEVAGQITANGNILGVAPGITVNIYRVFGENLSKSEWVA      346
NshP      DGSEAYEQGNVADVTDFQGHGTEVAGQITANGNMLGVAPGITINIYRVFGESYAKPEWIA      265
          *..*  * ** :*:.*  ***************:********:********. :* **:*

NisP      RAIRRAADDGNKVINISAGQYLMISGSYDDGTNDYQEYLNYKSAINYATAKGSIVVAALG      406
NshP      EAVKQAADDGNRVITISSGQYLMITGSYEDGTNDYQDYLIYKEAVDYATSKGSIVVAALG      325
          .*:::******:**.**:******:***:*******:** **.*::***:**********

NisP      NDSLNIQDNQTMINFLKRFRSIKVPGKVVDAPSVFEDVIAVGGIDGYGNISDFSNIGADA      466
NshP      NEGLNIQDNQALVDYVSTYRNIKVPGVVVDAPSVFDNVVAVGGIDYYNNLSDFSNYSSAA      385
          *:.*******::::::. :*.***** ********::*:****** *.*:***** .: *

NisP      IYAPAGTTANFKKYGQDKFVSQGYYLKDWLFTTTNTGWYQYVYGNSFATPKVSGALALVV      526
NshP      IYAPAGTTANLVKYGEEAFTNQGFYLTDWIFTTSYTGWYQYVYGNSFAAPKVAGALALVA      445
          **********: ***:: *..**:**.**:***: *************:***:******.

NisP      DKYGIKNPNQLKRFLLMNSPEVNGNRVLNIVDLLNGKNKAFSLDTDKGQDDAINHKSMEN      586
NshP      DKYNITDVKQLKEYLISHSPEINSLKILNIVDLLSEDIKTVYTEII-------YKKA---      495
          ***.*.: :***.:*: :***:*. ::*******. . *:.  :          :*:

NisP      LKESRDTMKQEQDKEIQRNTNNNFSIKNDFHNISKEVISVDYNINQKMANNRNSRGAVSV      646
NshP      LIESRVEV-----------SLEVLNMSKKFNDVTPDNYIAKYNSKNSENNKINDRGVVSL      544
          * ***  :           : : :.:.:.*:::: :   ..** ::.  *: *.**.**:

NisP      RSQEILPVTGDGEDFL-PALGIVCISILGILKRKTKN-                            682
NshP      RSCETLPNTGANRDVTYEVLGLFLLAISTSWKKKMKTE                            582
          ** * ** ** ..*.   .**:. ::*    *:* *.
```

Figure S1: Sequence alignment of NispP from *Lactococcus lactis* and NshP from *Streptococcus hyointestinalis*. The important residues of the active site (Asp_{259}, His_{306}, and Ser_{512} for NisP and Asp_{178}, His_{225}, and Ser_{431} for NshP) are highlighted in red. The sequence alignment was done with Clustal Omega [1].

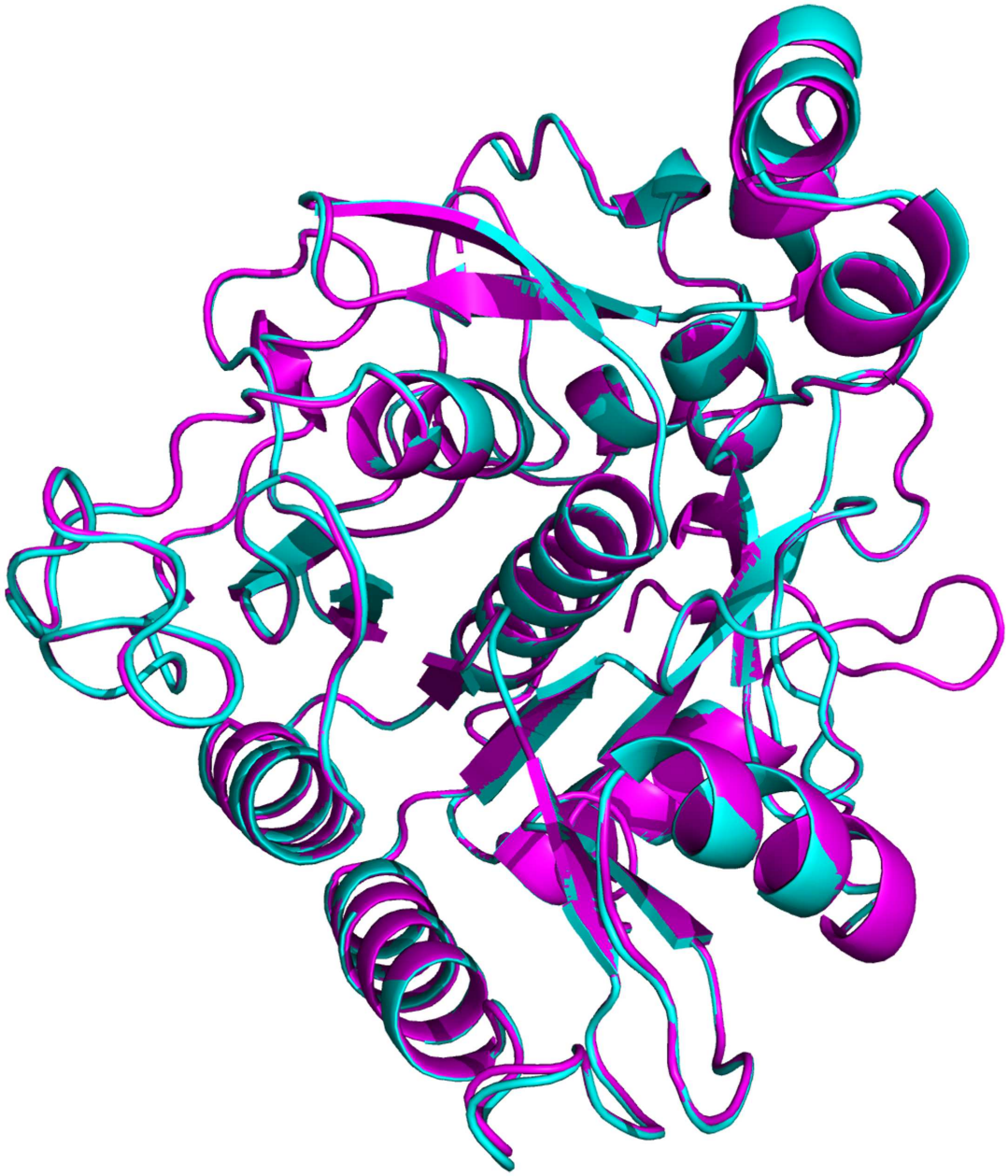

Figure S2: Homology model of NshP from *Streptococcus hyointestinalis*. A homology model of NshP was created using Phyre2 [2]. We used the sequence of the active protein without the self-cleaving part. The NshP model is shown in magenta and NisP (PDB code: 4MZD) in cyan. Figure was generated using PyMol [3].

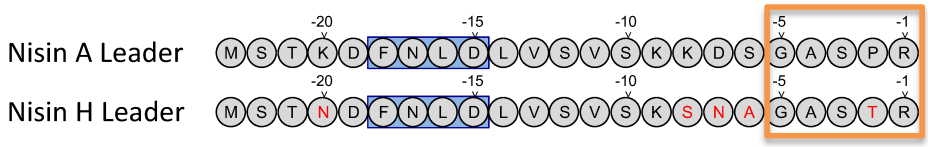

Nisin A Leader MSTKDFNLDLVSVSKKDSGASPR
Nisin H Leader MSTNDFNLDLVSVSKSNAGASTR

Figure S3: Sequence of nisin A and Nisin H leader sequence. Highlighted are the FNLD box (blue box) known to be important for the modification enzymes as well differences in sequence indicated by red letters. The cleavage site within the leader sequence of nisin A and nisin H is highlighted by an orange box.

1. Madeira, F., et al., *The EMBL-EBI search and sequence analysis tools APIs in 2019.* Nucleic Acids Res, 2019. **47**(W1): p. W636-W641.
2. Kelley, L.A., et al., *The Phyre2 web portal for protein modeling, prediction and analysis.* Nat Protoc, 2015. **10**(6): p. 845-58.
3. *The PyMOL Molecular Graphics System, Version 2.0 Schrödinger, LLC.*

3.3 Chapter III: The Resistance Mechanism of *Sa*NsrFP

New insights into the resistance mechanism for the BceAB-type transporter *Sa*NsrFP

Julia Gottstein[1,4], Julia Zaschke-Kriesche[1,4], Sandra Unsleber[2], Irina Voitsekhovskaia[2], Andreas Kulik[2], Lara V. Behrmann[1], Nina Overbeck[3], Kai Stühler[3], Evi Stegmann[2] & Sander H. J. Smits[1]

[1]Institute of Biochemistry, Heinrich-Heine-University Duesseldorf, Universitaetsstrasse 1, 40225 Duesseldorf, Germany. [2]Interfaculty Institute of Microbiology and Infection Medicin, Eberhard Karls University, Auf der Morgenstelle 28, 72076 Tübingen, Germany. [3]Molecular Proteomics Laboratory, Heinrich-Heine-University Duesseldorf, Universitaetsstrasse 1, 40225 Duesseldorf, Germany. [4]These authors contributed equally: Julia Gottstein and Julia Zaschke-Kriesche.[*]email: Sander.Smits@hhu.de

Published in: Scientific reports (2022)

Impact factor: 4.996

Own proportion of this work: 40%

- Biological experiments
- Preparation of figures
- Writing the manuscript

scientific reports

Check for updates

OPEN

New insights into the resistance mechanism for the BceAB-type transporter *Sa*NsrFP

Julia Gottstein[1,4], Julia Zaschke-Kriesche[1,4], Sandra Unsleber[2], Irina Voitsekhovskaia[2], Andreas Kulik[2], Lara V. Behrmann[1], Nina Overbeck[3], Kai Stühler[3], Evi Stegmann[2] & Sander H. J. Smits[1]✉

Treatment of bacterial infections is one of the major challenges of our time due to the evolved resistance mechanisms of pathogens against antibiotics. To circumvent this problem, it is necessary to understand the mode of action of the drug and the mechanism of resistance of the pathogen. One of the most potent antibiotic targets is peptidoglycan (PGN) biosynthesis, as this is an exclusively occurring and critical feature of bacteria. Lipid II is an essential PGN precursor synthesized in the cytosol and flipped into the outer leaflet of the membrane prior to its incorporation into nascent PGN. Antimicrobial peptides (AMPs), such as nisin and colistin, targeting PGN synthesis are considered promising weapons against multidrug-resistant bacteria. However, human pathogenic bacteria that were also resistant to these compounds evolved by the expression of an ATP-binding cassette transporter of the bacitracin efflux (BceAB) type localized in the membrane. In the human pathogen *Streptococcus agalactiae*, the BceAB transporter *Sa*NsrFP is known to confer resistance to the antimicrobial peptide nisin. The exact mechanism of action for *Sa*NsrFP is poorly understood. For a detailed characterization of the resistance mechanism, we heterologously expressed *Sa*NsrFP in *Lactococcus lactis*. We demonstrated that *Sa*NsrFP conferred resistance not only to nisin but also to a structurally diverse group of antimicrobial PGN-targeting compounds such as ramoplanin, lysobactin, or bacitracin/(Zn)-bacitracin. Growth experiments revealed that *Sa*NsrFP-producing cells exhibited normal behavior when treated with nisin and/or bacitracin, in contrast to the nonproducing cells, for which growth was significantly reduced. We further detected the accumulation of PGN precursors in the cytoplasm after treating the cells with bacitracin. This did not appear when *Sa*NsrFP was produced. Whole-cell proteomic protein experiments verified that the presence of *Sa*NsrFP in *L. lactis* resulted in higher production of several proteins associated with cell wall modification. These included, for example, the *N*-acetylmuramic acid-6-phosphate etherase MurQ and UDP-glucose 4-epimerase. Analysis of components of the cell wall of *Sa*NsrFP-producing cells implied that the transporter is involved in cell wall modification. Since we used an ATP-deficient mutant of the transporter as a comparison, we can show that *Sa*NsrFP and its inactive mutant do not show the same phenotype, albeit expressed at similar levels, which demonstrates the ATP dependency of the mediated resistance processes. Taken together, our data agree to a target protection mechanism and imply a direct involvement of *Sa*NsrFP in resistance by shielding the membrane-localized target of these antimicrobial peptides, resulting in modification of the cell wall.

Abbreviations

UDP	Undecaprenyl-phosphate
GlcNAc	*N*-acetylglucosamine
MurNAc	*N*-acetylmuramic acid
MurN	*N*-deacetylated muramic acid
Ala	Alanine

[1]Institute of Biochemistry, Heinrich-Heine-University Duesseldorf, Universitaetsstrasse 1, 40225 Duesseldorf, Germany. [2]Interfaculty Institute of Microbiology and Infection Medicin, Eberhard Karls University, Auf der Morgenstelle 28, 72076 Tübingen, Germany. [3]Molecular Proteomics Laboratory, Heinrich-Heine-University Duesseldorf, Universitaetsstrasse 1, 40225 Duesseldorf, Germany. [4]These authors contributed equally: Julia Gottstein and Julia Zaschke-Kriesche. ✉email: Sander.Smits@hhu.de

iGlu	Isoglutamic acid
iGln	Isoglutamine
Glu	Glutamine
Asp	Aspartate/aspartic acid
Asn	Asparagine
Lys	Lysine

Bacterial infections cause over 150,000 deaths every year and are a major threat for humans[1,2]. The treatment of many infectious diseases is possible due to the development of antibiotics, which have been discovered over the last 100 years, starting with penicillin in 1929. In recent years, however, antibiotic resistance has become a major challenge, as pathogenic bacteria have evolved several resistance mechanisms against antibiotics in use[3].

An Achilles heel of bacteria is the synthesis pathway of peptidoglycan (PGN), the main component of the cell wall[4]. PGN is a heteropolymeric layer that completely encloses the bacterial cell and provides the bacterial shape and integrity. The biosynthesis of PGN requires several steps, which are evolutionarily conserved in all bacterial species but are missing in eukaryotic cells[5]. Therefore, it is an optimal target for antibacterial agents.

PGN synthesis occurs in three distinctive compartments of the bacterial cell, namely, the cytoplasm, the cytoplasmic membrane, and the cell surface[6]: (1) In the cytoplasm, lipid II synthesis takes place; lipid II is a PGN precursor composed of an undecaprenyl pyrophosphate (UPP) anchor, the two amino sugars *N*-acetylglucosamine (GlcNAc) and *N*-acetylmuramic acid (MurNAc) and a covalently attached pentapeptide[7]. (2) Lipid II is afterwards flipped to the extracellular space (or periplasm for gram-negative bacteria) and is still anchored to the membrane via UPP[8]. (3) Following this, the GlcNAc-MurNAc-pentapeptide subunit is incorporated into the nascent PGN, leaving UPP attached to the membrane. UPP is subsequently dephosphorylated to undecaprenyl phosphate (UP), which is flipped back into the cytoplasm and implemented into a new PGN synthesis cycle[9].

This biosynthetic pathway has been shown to be an ideal target for antimicrobial compounds at any stage of (1)–(3)[4,10]. In many cases, the incorporation of lipid II into the nascent PGN layer is prevented; antibiotics either bind directly to lipid II or to enzymes that catalyze its incorporation into PGN. Both types of binding lead to nonrecycling of UP and subsequent inhibition of lipid II synthesis. As a consequence, bacterial cell growth is hindered.

Binding of antibiotics occurs to various moieties of lipid II, e.g., to the pyrophosphate moiety (lantibiotics such as nisin and gallidermin)[11–13] or to the pentapeptide moiety (glycopeptides such as vancomycin)[10,14,15] (Fig. 1). A particular class are small antimicrobial peptides (AMPs) that bind specifically to the pyrophosphate-sugar moiety of lipid II[11], such as the lipoglycodepsipeptide ramoplanin and the acylcyclodepsipeptide lysobactin[10,16–18].

In addition to lipid II binders, antibiotics are known to inhibit PGN biosynthesis at another stage, e.g., the cyclic peptide bacitracin. The binding of bacitracin to UPP inhibits the dephosphorylation of UP and blocks its regeneration, resulting in the accumulation of intracellular PGN precursors[19–21] (Fig. 1). The net effect is the destabilization of the cell wall, leading to cell growth inhibition and subsequently to the death of the bacteria.

Bacitracin has been suggested to form a compact ternary 1:1:1 antibiotic-metal-lipid complex that, with its highly amphipathic structure, enhances membrane-binding affinity[20]. Due to a stabilizing effect and increased antimicrobial activity, a zinc-bacitracin (Zn-bacitracin) complex has been commonly used in human and veterinary medicine in antibiotic formulations[22,23].

Bacitracin has also been used as a growth-promoting additive in animal feed[24]. Additionally, it has been shown to control necrotic enteritis effectively[25] and is therefore used as a drug in many countries. Long-term usage of bacitracin in animals leads to an increase in resistance genes in microorganisms. Some molecular bacitracin resistance mechanisms have been reported in bacteria[26–29].

One of the identified resistance mechanisms against AMP in human pathogens is based on the expression of bacitracin efflux (Bce) transporter, a member of the ABC transporter family. Bce confers high-level resistance to bacitracin and/or lantibiotics such as nisin and gallidermin in *Bacillus subtilis*, *Staphylococcus aureus* and *Streptococcus agalactiae*[27,30–34]. Genomic analysis revealed the presence of homologous transporters (BceAB-type transporters) mostly in bacteria predominantly found in soil and in human pathogenic bacteria[35].

The first BceAB-type transporter was identified in *B. subtilis*. Adjacent to the *bceAB* genes, the *bceRS* genes are located, encoding a two-component system (TCS). The TCS regulates the expression of transporters[27] and it is hypothesized that the detoxification against peptide antibiotics is functionally linked to it[36]. Status quo is that upon substrate binding the BceAB type transporter transfers a signal to the histidine kinase that then phosphorylates its cognate response regulator which induces the expression of the ABC transporter genes. This was described i.e. for the GraRS-VraFG system[37] in *S. aureus* and also for several TCS-ABC transporters in *B. subtilis* (BceRS-AB, YxdJK-LM and YvcPQ-RS)[35,38]. The direct interaction between the BceAB transporter and the BceS histidine kinase was demonstrated in *B. subtilis*[36]. In that study, it was shown that BceAB, which was purified from the membrane, needs to form a complex with BceRS in order to initiate antibiotic resistance signalling[36]. A characteristic feature of these BceAB-type transporters is an extracellular domain (ECD) of roughly 210–230 amino acid located between transmembrane helices 7 and 8. These domains are supposed to be involved in binding the substrate (e.g., bacitracin). This is hypothesized due to the reason that the cognate histidine kinase, consists only of a short loop which is buried almost entirely in the cytoplasmic membrane and thus cannot detect extracellular stimuli[39]. So the binding to the ECD is supposed to trigger simultaneously the histidine kinase (HK)[36]. It has been shown with medically and biotechnologically relevant Gram-positive species that BceS-like HKs require BceAB-type transporters for antibiotic signaling[31,36,40,41]. Moreover, ATP hydrolysis by the ATPase BceA was shown to play an essential role for lantibiotic signaling[23]. Additionally, it was found that the associated sensor kinase BceS is unable to detect bacitracin in the absence of the transporter BceAB, which

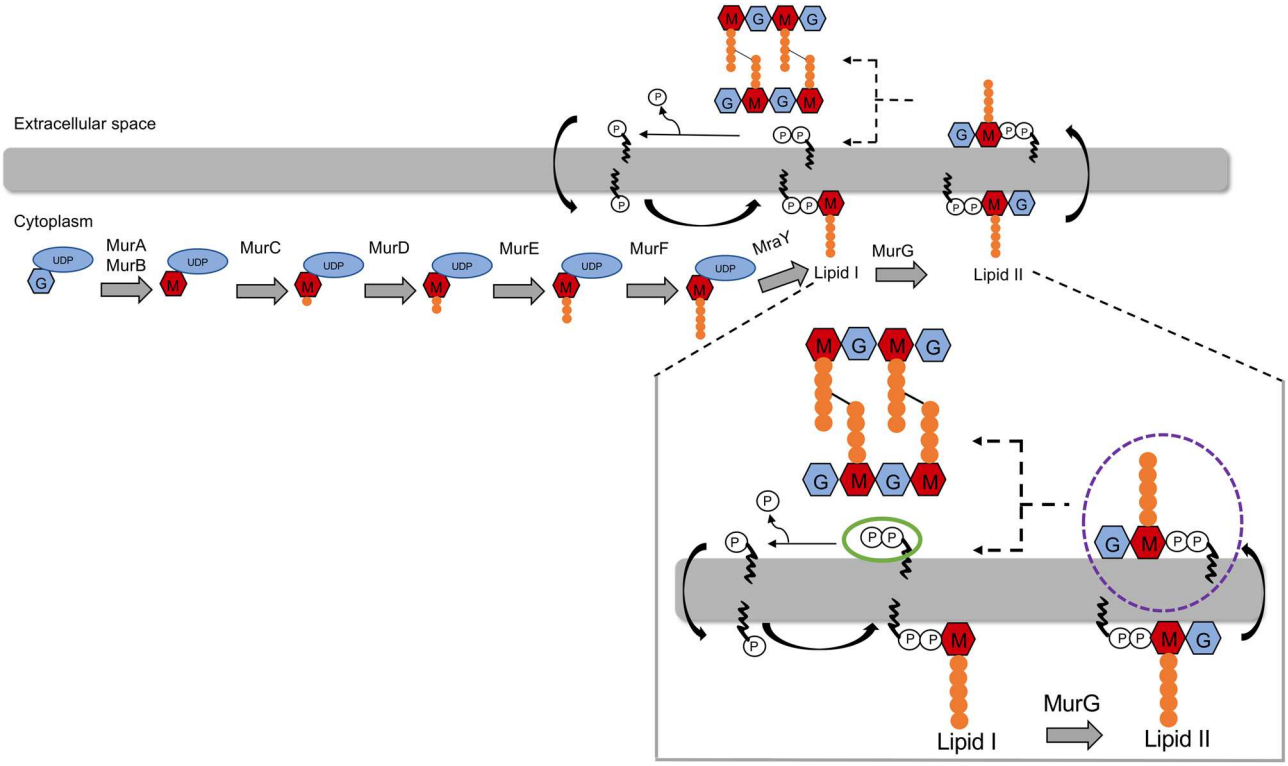

Figure 1. Schematic view of peptidoglycan synthesis. Synthesis of lipid II in the cytoplasm and its incorporation into the peptidoglycan. Phosphates are marked with a P, undecaprenyl as a black curved line, uridine phosphate (UDP) in light blue, GlcNAc in blue, MurNAc in red and amino acids of the pentapeptide in orange. Enlarged step of peptidoglycan synthesis showing targets of bacitracin, which is undecaprenyl pyrophosphate (green circle), and targets of many antimicrobial peptides, such as nisin, gallidermin, lysobactin, and ramoplanin: lipid II (violet, dotted circle). *GlcNAc N*-acetylglucosamine; *MurNAc N*-acetylmuramic acid. The figure was created using Microsoft Powerpoint Version 16.54.

led to proposition that the transporter contains the involved sensory domain of the system[40,42]. More recently, the binding of AMP LL-37 to the ECD of VraG (a BceAB homologous transporter) was described in *B. subtilis*[37].

Similar operon structures have been reported for other BceAB-type transporters, in some cases with an additional gene encoding a membrane-embedding protein such as *Sa*NSR, a BceAB-type transporter in the human pathogen *S. agalactiae*, conferring resistance against lantibiotics such as nisin A, nisin H and gallidermin[32,43]. Using a peptide release assay, it was postulated that *Sa*NsrFP transports these peptides via an efflux mechanism back into the medium[34].

Several putative mechanisms for BceAB-type transporters have been proposed, ranging from AMP removal from the membrane[44], functioning as an exporter[34], to flipping the UPP[21]. Recently, a study proposed a target-AMP dissociative, ATP-hydrolysis-driven mechanism for BceAB-type transporters, in which the target-AMP complex is recognized and UPP physically released from the grip of bacitracin[45].

In our study, in order to elucidate the mechanism of *Sa*NsrFP, we expressed the BceAB-type transporter *Sa*NsrFP in *L. lactis* NZ9000 without its cognate TCS[34]. We hypothesized that the transporter alone is able to sense an AMP in the surrounding since the Bce type transporters are known to play a crucial role in the signalling process[37,42,43,46]. It was shown for the related BceAB transporter that signalling is triggered by the activity of the transporter itself and the transporter can autoregulate its own production[46]. In previous work, it was shown that *Sa*NsrFP is able to confer resistance against nisin without its TCS[34]. As a control for our study, we also analyzed the ATPase-deficient mutant of the ABC transporter that showed no ATPase function in-vitro[47].

Since the BceAB system of *B. subtilis* is known to confer resistance against bacitracin and also other antibiotics i.e. mersacidin, plectasine and actagardine[27,38], we wanted to test whether the *Sa*NsrFP is also able to confer resistance against bacitracin and structurally different antibiotics. By investigating the effect the expression of *sansrfp* has on the proteome level, we gained further insights into the mode of action. Since here it was observed that genes involved in cell wall biosynthesis were downregulated, we also analyzed the composition of the peptidoglycan layer. Cell wall modification is one of several mechanisms of being involved in antibiotic resistance and has been shown to play an important role in the resistance mechanism in *S. aureus*, *C. difficile*, *S. pneumoniae* and *S. agalactiae*[48–50]. Also, in recent studies it is suggested that transporters can have a direct or indirect influence on peptidoglycan biosynthesis or peptidoglycan remodeling as was shown recently for the ABC transporter YtrBCDEF in *B. subtilis*[51].

In this study, we aimed to characterize *Sa*NsrFP in larger detail and analyzed the ability of this transporter to confer resistance against different structurally unrelated compounds, such as lysobactin, ramoplanin, vancomycin

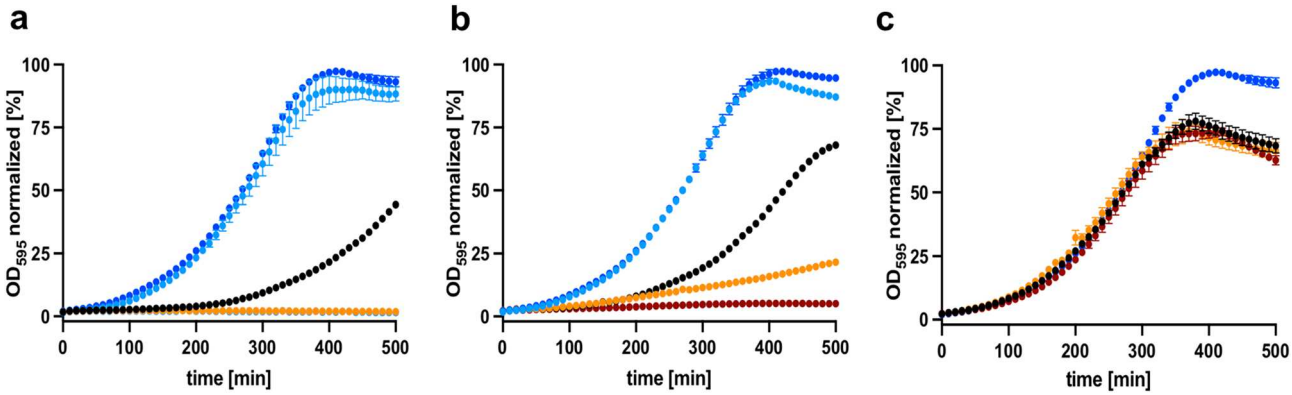

Figure 2. (**a**) Growth curve of the BceAB type ABC transporter expressing strain *L. lactis* NZ9000NsrFP (light blue), the ATP-hydrolysis deficient mutant strain *L. lactis* NZ9000NsrF$_{H202A}$P (orange), the empty plasmid expressing strain *L. lactis* NZ9000Cm (black) and the nisin transporter expressing strain *L. lactis* NZ9000NisT (dark red) were induced with 0.3 nM nisin and treated with 1 µM bacitracin and 1 mM $ZnCl_2$. As a control, *L. lactis* NZ9000NsrFP (dark blue) was induced with 0.3 nM nisin, and 1 mM $ZnCl_2$ was added. (**b**) Growth curve of *L. lactis* NZ9000NsrFP (light blue), *L. lactis* NZ9000NsrF$_{H202A}$P (orange), *L. lactis* NZ9000Cm (black), *L. lactis* NZ9000NisT (dark red) induced with 0.3 nM nisin and treated with an additional 4 µM bacitracin without $ZnCl_2$. As a control, *L. lactis* NZ9000NsrFP (dark blue) was induced with 0.3 nM nisin. (**c**) Growth curve of the control, *L. lactis* NZ9000NsrFP (dark blue), *L. lactis* NZ9000Cm (black) and *L. lactis* NZ9000NisT (dark red) induced with 0.3 nM nisin, and 1 mM $ZnCl_2$ was added. The normalized OD_{600} was plotted against the time using GraphPad Prism version 9.2.0 for Mac, GraphPad Software, San Diego, California USA, www.graphpad.com.

and bacitracin, as well as its zinc complex Zn-bacitracin. Whole-cell proteome and cytosolic PGN precursor analysis supported our hypothesis that the different antibiotics bind to *Sa*NsrFP inducing an altering of the cell wall. This is relying on the ATP hydrolysis of *Sa*NsrFP since the ATP hydrolysis deficient mutant does not show this phenotype. The transporter is able to protect the target via a first-line and second-line defense, and the energy set free by ATP hydrolysis could be the key to resetting the system. Our study provides new insights into the resistance mechanism of the BceAB-type transporter *Sa*NsrFP. The data presented are in agreement with a mechanism of protection by shielding the target of the antimicrobial peptide.

Results

_Sa_NsrFP enables normal growth in the presence of bacitracin. The BceAB-type transporter NsrFP from the human pathogen *S. agalactiae* COH1, *Sa*NsrFP, has been shown to confer resistance against the lantibiotic nisin and structurally related compounds such as nisin H and gallidermin by recognizing and binding to the N-terminus of these lantibiotics[34].

To investigate whether *Sa*NsrFP confers resistance against bacitracin and Zn-bacitracin, binding to the lipid carrier UPP[20,52], we analyzed the influence of the expression of the *sansrfp* gene. The sensitive *L. lactis* strain NZ9000, served as an indicator strain for these studies which was transformed with a plasmid encoding the *nsrfp* gene. We included two controls where the strains were transformed with (I) an empty plasmid (*L. lactis* NZ9000Cm) (II) a plasmid containing a variant of the *nsrfp* gene (*L. lactis* NZ9000*Sa*NsrF$_{H202A}$P)[34]. This NZ9000*Sa*NsrF$_{H202A}$P strain is used since the transporter carries a mutation in the H-loop, a highly conserved region of ABC transporters, and as a result is not able to hydrolyze ATP[47]. This mutation causes loss of ATP hydrolysis and stabilization of the closed conformation[53]. Although the substrate still binds to it as the transporter, it cannot be translocated because the required energy cannot be provided[34,47]. The growth of *L. lactis* NZ9000Cm, *L. lactis* NZ9000*Sa*NsrFP, *L. lactis* NZ9000*Sa*NsrF$_{H202A}$P and *L. lactis* NZ9000NisT was monitored online over a time period of 500 min (Fig. 2a,b). After adding the different antibiotics to the culture, the growth curve was determined.

The expression of the *sansrFP* and *sansrFP*$_{H202}$A genes was induced by adding a sublethal concentration of 0.3 nM nisin to the cells. This subinhibitory concentration of nisin is able to induce the *nisA* promotor in the pIL-SV plasmids which enables the gene expression of the respective protein. Important to note that this low concentration of nisin is not harming the cells as observed by different growth studies[54,55]. Simultaneously, either 1 µM bacitracin in combination with 1 mM $ZnCl_2$ (Fig. 2a) or 4 µM bacitracin without zinc (Fig. 2b) was added. As a control, all strains were only induced with 0.3 nM nisin without receiving any additional supplements (Fig. 2c).

Severe growth inhibition was shown for the *L. lactis* NZ9000Cm *and L. lactis* NZ9000NisT strains. When using the *L. lactis* NZ9000*Sa*NsrFP strain, however, the growth behavior was comparable to that of *L. lactis* NZ9000Cm without the addition of bacitracin (Fig. 2a,b light blue curve and c). Interestingly, *L. lactis* NZ9000*Sa*NsrF$_{H202A}$P cells were unable to grow when treated with (Zn)-bacitracin (Fig. 2a orange), whereas reduced growth was observed when bacitracin was added (Fig. 2b orange). Growth retardation, as observed in *L. lactis* NZ9000Cm upon the addition of bacitracin, has been shown for many bacterial cells, such as methicillin-resistant *S. aureus* and group B streptococci[56,57]. It is caused by the binding of bacitracin to UPP, preventing the dephosphorylation

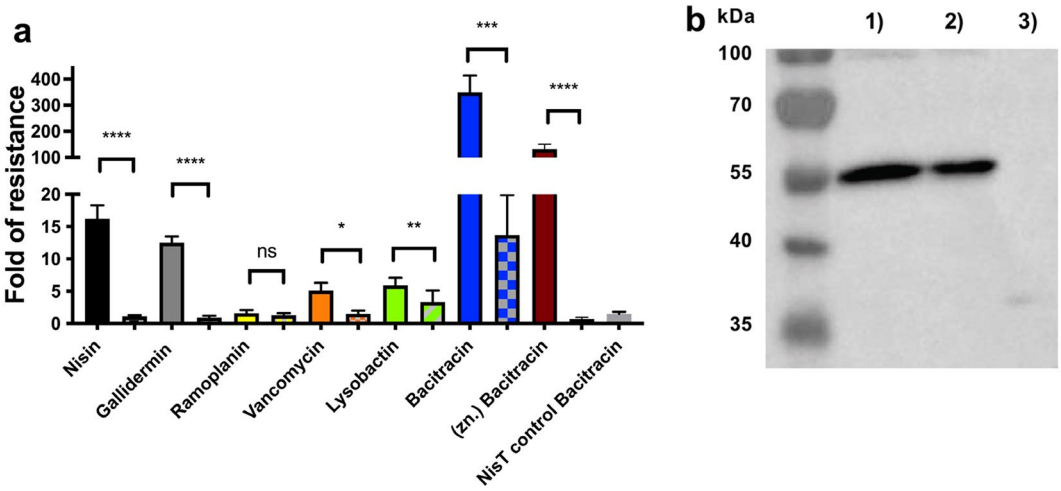

Figure 3. (**a**) Fold of resistance of *L. lactis* NZ9000NsrFP and NZ9000NsrF$_{H202A}$P (hatched bars) against *L. lactis* NZ9000Cm calculated with the determined IC$_{50}$ of ramoplanin A2 (yellow), vancomycin (orange), lysobactin (green), bacitracin (blue) and bacitracin with $ZnCl_2$ (dark red). Values for nisin and gallidermin were taken from Reiners et al.[34] and marked with an asterisk. Values were calculated from at least 4 independent measurements and are also listed in Table 1. A two-sided Students t-test was performed with the IC$_{50}$ data obtained for *Sa*NsrFP and *Sa*NsrF$_{H202A}$P. Significance was marked with an asterisk. p-values were listed in a separate table (SI Table S1) in the supplement. (**b**) Expression of *Sa*NsrFP (1) and *Sa*NsrF$_{H202A}$P (2) and the empty vector pIL-SV (3) in *L. lactis* NZ9000, monitored *via* western blot with a polyclonal antibody against the extracellular domain of *Sa*NsrP. Loaded are purified membranes from the corresponding strains. A nonlinear regression curve fit and a two-sided, unpaired Students t-test was performed using Graphpad Prism version 9.2.0 for Mac, GraphPad Software, San Diego, California USA, www.graphpad.com.

reaction and leading to the interruption of PGN biosynthesis[20]. Intriguingly, *L. lactis* NZ9000*Sa*NsrFP did not show reduced growth (Fig. 2a,b light blue) in the presence of bacitracin in comparison to the control strain *L. lactis* NZ9000*Sa*NsrFP (Fig. 2a,b blue) and the sensitive strain *L. lactis* NZ9000Cm.

These results demonstrated that *Sa*NsrFP is involved in bacitracin resistance with a requirement for ATP hydrolysis. For our study, we expressed *sansrfp* without its TCS, leading us to the conclusion that the transporter alone is directly involved in bacitracin resistance.

_Sa_NsrFP confers resistance against bacitracin, ramoplanin, vancomycin and lysobactin. Since *Sa*NsrFP conferred resistance in addition to lanthipeptides against bacitracin and Zn-bacitracin, we extended the resistance study to a structurally diverse, rather unrelated group of antibiotics, including ramoplanin, vancomycin and lysobactin, all of which bind to different parts of lipid II[10,18].

After adding the different antibiotics to the cultures of the strains *L. lactis* wild type (WT), *L. lactis* NZ9000Cm, *L. lactis* NZ9000*Sa*NsrFP and *L. lactis Sa*NsrF$_{H202A}$P, the IC$_{50}$ was determined. By dividing the IC$_{50}$ obtained for the strains producing *Sa*NsrFP or the inactive variant SaNsrF$_{H202A}$P by the IC$_{50}$ value obtained for the sensitive strain NZ9000Cm, the fold change of resistance was calculated, which was independent of small variations in bacterial cell growth behavior.

Compared to *L. lactis* WT, *L. lactis* NZ9000SaNsrFP exhibited small resistance to the lipid II binders, vancomycin and lysobactin (two to sixfold) (Fig. 3a, SI Fig. S1, Table 1). No significant differences were detected between NZ9000NsrFP and NZ9000NsrFH202AP with ramoplanin. The fold increases of resistance (two, fivefold increases) obtained were significantly lower than the fold changes described for nisin (16-fold) and gallidermin (12-fold)[34], suggesting that nisin is a preferred substrate of the transporter. IC$_{50}$ values decreased to similar levels in *L. lactis* NZ9000SaNsrF$_{H202A}$P (one, two and threefold), as observed for the *L. lactis* NZ9000Cm strain (73.0 nM, 213.5 nM, and 30.7 nM, respectively, Table 1), indicating that resistance was not achieved solely by the expression of the SaNsrF$_{H202A}$P transporter. To ensure that this loss of resistance was not due to different production levels, we performed Western blot analysis on the purified membrane fractions of the transporter expressing cells using a polyclonal antibody against the ECD of *Sa*NsrP (Fig. 3b). We confirmed that comparable levels of transporters were produced in both strains. Since ATP hydrolysis activity was deleted in the SaNsrF$_{H202A}$P mutant, the obtained results suggested that *Sa*NsrFP requires ATP hydrolysis to confer resistance.

However, high-level resistance was observed for *L. lactis* NZ9000SaNsrFP to bacitracin (350-fold) and (Zn)-bacitracin (132-fold) compared to *L. lactis* WT (Fig. 3a, SI Fig. S1, Table 1). In contrast, *L. lactis* NZ9000*Sa*NsrF$_{H202A}$P displayed only moderate resistance (13-fold), which was completely abolished when the cells were treated with (Zn)-bacitracin (0.7-fold). Resistance at a low level against nisin (2.6-fold) was shown in Khosa et al., in which an inactive variant of the protease *Sa*NSR (*Sa*NSR$_{S236A}$) was produced[32]. Even though, it was demonstrated that NZ9000*Sa*NsrF$_{H202A}$P shows no ATPase activity in-vitro[47], it is known that it is difficult to compare in-vitro with in-vivo data since it cannot be excluded that other processes in the bacterial cell might

Antibiotic	*L. lactis* NZ9000Cm	*L. lactis* NZ9000NsrFP		*L. lactis* NZ9000NsrF$_{H202A}$P		*L. lactis* NZ9000NisT	
	IC_{50} (nM)	IC_{50} (nM)	Fold of resistance	IC_{50} (nM)	Fold of resistance	IC_{50} (nM)	Fold of resistance
Ramoplanin A2	73 ± 18	121 ± 34	2 ± 1	92 ± 21	1 ± 0	95	1.3 ± 0
Vancomycin	214 ± 27	1078 ± 264	5 ± 1	325 ± 117	2 ± 1	133 ± 9	1 ± 0
Lysobactin	31 ± 17	182 ± 37	6 ± 1	101.8 ± 52.2	3 ± 2	25 ± 3	1 ± 0
Bacitracin	938 ± 94	327,500 ± 60,884	349 ± 65	12,855 ± 8517	14 ± 9	733	1 ± 0
Bacitracin $ZnCl_2$	81 ± 16	10,694 ± 1541	132± 19	58.7 ± 17.9	1 ± 0	49 ± 16	1 ± 0

Table 1. Measured IC_{50} values and calculated fold of resistance for the antibiotics ramoplanin A2, vancomycin, lysobactin and bacitracin and for the strains NZ9000Cm, NZ9000*Sa*NsrF$_{H202A}$P and NZ9000*Sa*NsrFP. The control strain NZ9000NisT was only treated with bacitracin or (Zn)-bacitracin. Each measurement was performed at least by 3 biological replicated with 3 technical replicates each.

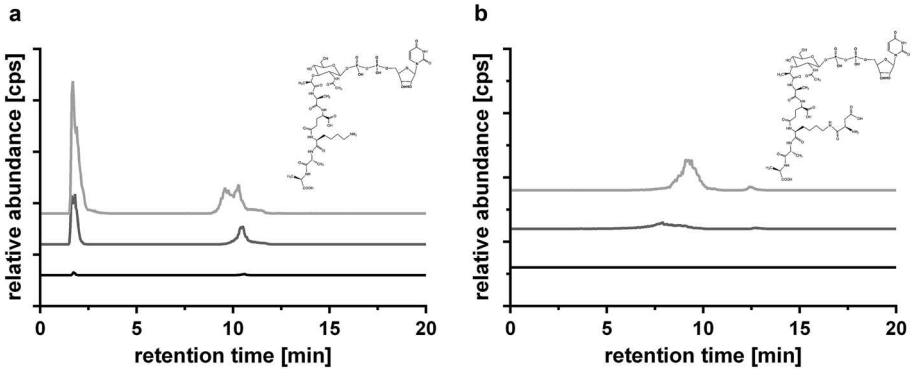

Figure 4. Relative abundance of obtained mass in cps against retention time in min of precursor accumulation after treatment with bacitracin. (**a**) Extracted ion chromatography (EIC) spectrum for UDP-MurNAc-L-Ala-D-iGlu-L-Lys-D-Ala-D-Ala (1148.4 m/z^{-1}) and (**b**) EIC spectrum for UDP-MurNAc-L-Ala-D-iGlu-L-Lys(D-Asp)-D-Ala-D-Ala (1263.4 m/z^{-1}) of the strains NZ9000Cm (light gray), NZ9000*Sa*NsrF$_{H202A}$P (gray) and NZ9000*Sa*NsrFP (black). Extracted ion chromatograms (EICs) in negative ion mode for UDP-MurNAc-L-Ala-D-iGlu-L-Lys-D-Ala-D-Ala (m/z^{-1} 1148.34 ± 0.1) and UDP-MurNAc-L-Ala-D-iGlu-L-Lys-(D-Asp)-D-Ala-D-Ala (m/z^{-1} 1263.37 ± 0.1) were analyzed with Data Analysis (Bruker), exported and presented with GraphPad Prism 6.0, GraphPad Software, San Diego, California USA, www.graphpad.com. *UDP* undecaprenyl-phosphate, *MurNAc N*-acetylmuramic acid, *Ala* alanine, *iGlu* isoglutamic acid, *Glu* glutamine, *Asp* aspartate/aspartic acid, *Lys* lysine.

lead to such a residual bacitracin resistance for *Sa*NsrF$_{H202A}$P. On the other hand, the residual resistance is only observed with bacitracin not with zinc-bacitracin. It has been shown that bacitracin shows a higher attraction to the membranes in the presence of zinc and the target most probably due to the observation that it is forced into an amphiphile conformation[20]. This could explain why only residual resistance is observed with only bacitracin since it cannot access the membrane as easily as with zinc.

To strengthen this hypothesis and to exclude that the resistance to bacitracin in *L. lactis* NZ9000SaNsrF$_{H202A}$P is caused by an altered membrane protein composition due to the overexpression, we performed growth inhibition experiments with another large ABC transporter, namely, NisT from *L. lactis,* which is not present in the genome of the NZ9000 strain used, using the same plasmid backbone. Recently, it was shown that NisT is produced in high amounts in the used strain[58,59]. However, NisT is not relevant to bacitracin resistance, as evidenced by similar IC_{50} values of the strain NZ9000NisT, producing no NisT (Table 1). Therefore, it can be concluded that the production of large membrane proteins, as well as ATP hydrolysis and a possible alteration of the membrane protein composition is not the explanation for the resistant phenotype but is due to the production of *Sa*NsrFP or its inactive variant.

_Sa_NsrFP prevents the accumulation of peptidoglycan precursors after the addition of bacitracin. To further understand the mechanism of action of *Sa*NsrFP, we analyzed PGN precursor accumulation in the cytoplasm of *L. lactis* NZ9000*Sa*NsrFP, *L. lactis* NZ9000Cm and *L. lactis* NZ9000*Sa*NsrF$_{H202A}$P grown in the presence of bacitracin. HPLC/MS analysis of the PGN extracts revealed the presence of the characteristic PGN precursors UDP-MurNAc-L-Ala-D-iGlu-L-Lys-D-Ala-D-Ala (1148.4 m/z^{-1}) and MurNAc-L-Ala-D-iGlu-L-Lys-(D-Asp)-D-Ala-D-Ala (1263.4 m/z^{-1}) in the *L. lactis* NZ9000Cm strain (Fig. 4a,b light gray).

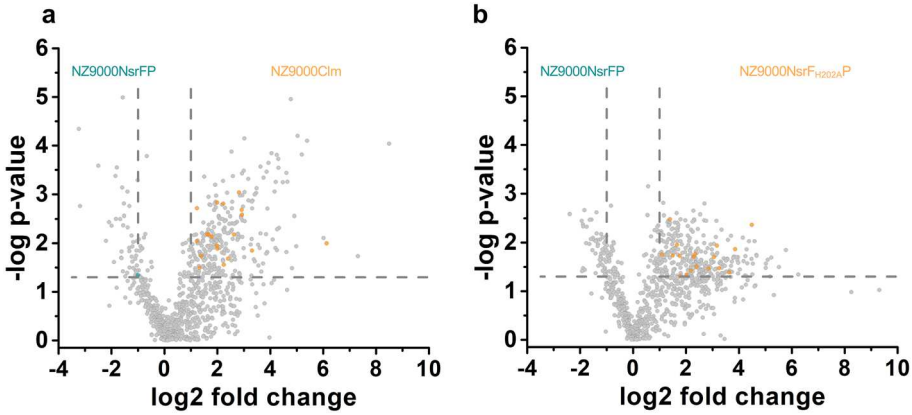

Figure 5. (**a**) Volcano plot of the proteome analysis of NZ9000*Sa*NsrFP against NZ9000Cm and (**b**) NZ9000*Sa*NsrFP against NZ9000SaNsrF$_{H202A}$P. Proteins involved in cell wall synthesis are highlighted in orange if upregulated in NZ9000Cm (**a**) and NZ9000*Sa*NsrF$_{H202A}$P (**b**) and highlighted in blue if upregulated in NZ9000*Sa*NsrFP. Proteins with a p-value ≤ 0.05 and a fold change ≥ 2 were considered as statistically significant. Proteome data was plotted using GraphPad Prism 6.0 for Mac, GraphPad Software, San Diego, California USA, www.graphpad.com.

Interestingly, no accumulation of the PGN precursors was observed in the *L. lactis* NZ9000*Sa*NsrFP strain (Fig. 4a,b black line), whereas *L. lactis* NZ9000*Sa*NsrFP without bacitracin treatment revealed the accumulation of the PGN precursor UDP-MurNAc-L-Ala-D-iGlu-L-Lys-D-Ala-D-Ala (1148.4 m/z^{-1}) (SI Fig. S6a,b). The fact that bacitracin was not able to block UPP recycling, together with the results obtained in the resistance test, clearly suggests that *Sa*NsrFP prevents the binding of bacitracin to UPP and thus the accumulation of PGN precursors. This hypothesis is further supported by the results obtained for the *L. lactis* NZ9000*Sa*NsrF$_{H202A}$P strain. Here, reduced PGN precursor accumulation was observed compared to the bacitracin-sensitive *L. lactis* NZ9000Cm strain (Fig. 4a,b gray line), implicating that the availability of UPP for bacitracin binding is decreased in the *L. lactis* NZ9000*Sa*NsrF$_{H202A}$P strain. Considering that bacitracin did not inhibit PGN synthesis in *L. lactis* NZ9000*Sa*NsrFP, *Sa*NsrFP might protect the bacitracin target and directly interact with a component of PGN, most likely UPP, to evade the accumulation of PGN precursors.

Binding of bacitracin to the UPP or UP normally results in the accumulation of lipid II precursors in the cytosol. The lack of this accumulation in *L. lactis Sa*NsrFP suggests that bacitracin is unable to bind to its membrane-localized target UPP. This, together with the observation that the cell growth of *L. lactis Sa*NsrFP in the presence of bacitracin is similar to that of cells without bacitracin, supports the shielding mechanism proposed by Kobras et al.[45].

***Sa*NsrFP causes downregulation of proteins involved in peptidoglycan synthesis.** To get an insight to the mode of action initiated by *Sa*NsrFP expression, we analyzed the whole proteome of *L. lactis* NZ9000*Sa*NsrFP, *L. lactis* NZ9000Cm and *L. lactis* NZ9000*Sa*NsrF$_{H202A}$P grown under identical growth conditions (at 30 °C in GM17 medium containing 5 µg/ml chloramphenicol and induced with 0.3 nM nisin) by mass spectrometry. The analyses led to the identification of 894 proteins (identified by at least two unique peptides in each strain). The comparison between *L. lactis* NZ9000Cm and NZ9000*Sa*NsrFP revealed 315 with differential abundances (Fig. 5a) and 339 proteins showing differential abundances between the *L. lactis* strains NZ9000*Sa*NsrF$_{H202A}$P and NZ9000*Sa*NsrFP (Fig. 5b). In 231 proteins there was no change of abundance. Here, we took the slightly different OD after 5 h of cell growth into account and adjusted the whole cell protein concentration accordingly. In particular, the latter highlights that these up- or downregulation of the proteins do not arise from the expression of the transporter since they are expressed at similar levels (see Fig. 2b). This high number of differentially produced proteins implied that the *L. lactis* NZ9000*Sa*NsrFP strain has to respond significantly to counteract the effects mediated by the presence and activity of the *Sa*NsrFP BceAB-type ABC transporter.

In-depth analysis showed that the production of proteins involved in PGN synthesis was reduced in *L. lactis* NZ9000*Sa*NsrFP (Fig. 4a,b, SI Fig. S3). Among them the UDP-N-acetylglucosamine 1-carboxyvinyltransferase MurA (ADJ59532), was produced 6.2-fold less in the *L. lactis* NZ9000*Sa*NsrFP compared to *L. lactis* NZ9000Cm; UDP-*N*-acetylmuramate-L-alanine ligase MurC (ADJ61283), 4.0-fold, UDP-*N*-acetylmuramoyl-L-alanyl-D-glutamate synthetase MurD (ADJ59924) the 3.5-fold, UDP-*N*-acetylmuramoylalanyl-D-glutamate-2,6-diaminopimelate ligase MurE (ADJ60966), 4.0-fold less produced in the control strain as well as UDP-*N*-acetylmuramoylalanyl-D-glutamyl-2,6-diaminopimelate-D-alanyl-D-alanine ligase MurF (ADJ59966). Furthermore, proteins involved in the synthesis of components of lipid II synthesis, such as uracil phosphoribosyl transferase or glucosamine-fructose-6-phosphate aminotransferase, responsible for UMP and glucosamine-6-phosphate synthesis, respectively, were downregulated in *L. lactis* NZ9000*Sa*NsrFP (Table 2, SI Fig. S3).

We included in the analysis proteins from other metabolic pathways, such as amino sugar metabolism and translation, represented by α-D-glucosamine-1,6-phosphomutase or phenylalanyl-tRNA synthetase beta subunit in order to show that the expression of the ABC transporter *Sa*NsrFP is not toxic to the cells and has an influence

Protein	Description	Fold of expression of *Sa*NsrFP in comparison to			
		NZ9000Cm	p-value	NZ9000*Sa*NsrF$_{H202A}$P	p-value
ADJ59532	UDP-*N*-acetylglucosamine 1-carboxyvinyltransferase MurA	1.2		2.1	0.018
ADJ61283	UDP-*N*-acetylmuramate-L-alanine ligase MurC	4.0	0.013		
ADJ59924	UDP-*N*-acetylmuramoyl-L-alanyl-D-glutamate synthetase MurD	3.5	0.007	9.0	0.012
ADJ60966	UDP-*N*-acetylmuramoylalanyl-D-glutamate-2, 6-diaminopimelate ligase MurE	4.0	0.001	4.9	0.019
ADJ59382	UDP-*N*-acetylmuramoylalanyl-D-glutamyl-2,6-diaminopimelate-D-alanyl-D-alanine ligase MurF	2.5	0.032	4.5	0.037
ADJ60503	Glucosamine-fructose-6-phosphate aminotransferase	7.6	0.002	12.4	0.041
ADJ61146	Uracil phosphoribosyltransferase	2.4	0.001	2.1	
ADJ59249	UDP-galactopyranose mutase	3.9	0.011	7.2	0.034
ADJ59465	a-D-glucosamine 1,6-phosphomutase	1.0		1.0	
ADJ61162	Phenylalanyl-tRNA synthetase subunit beta	1.0		1.0	

Table 2. Selected proteins of the proteome analysis with their description and their fold of down regulation in NZ9000*Sa*NsrFP compared to NZ9000Cm and NZ9000*Sa*NsrF$_{H202A}$P. The number of replicates were n = 5. We performed an ANOVA test and the p values are also part of the protein lists. Only significant p-values were listed.

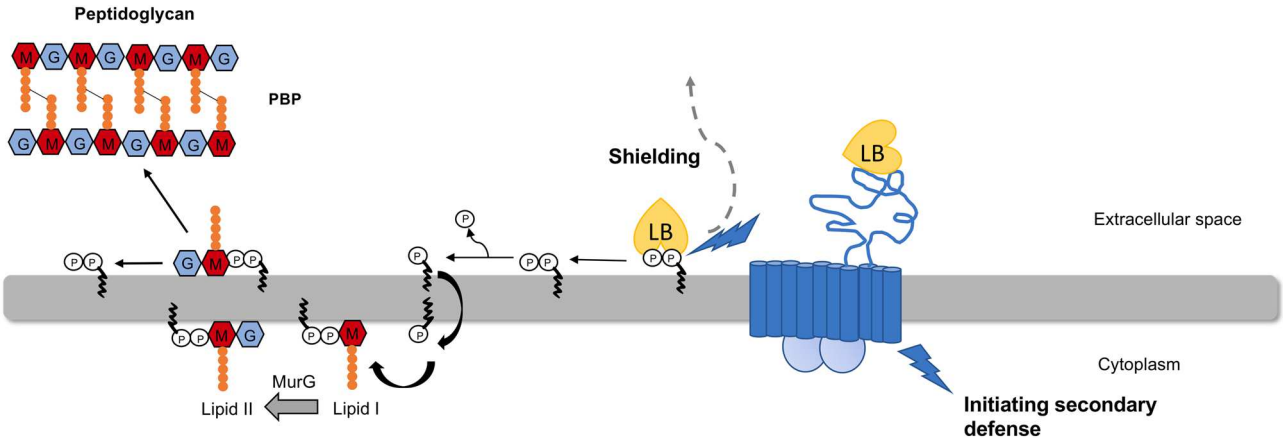

Figure 6. Schematic view of the proposed mechanism of *Sa*NsrFP. Phosphates are marked with a P, undecaprenyl as a black curved line, GlcNAc in blue, MurNAc in red and amino acids of the pentapeptide in orange. The transporter *Sa*NsrFP is shown in blue, showing its functions of sensing antibacterial attack, shielding the target most likely by releasing the target from the grip of bacitracin and initiating a secondary defense leading to possible cell wall thickening, modifying the electrostatic charge of the cell wall by integrating lipoteichoic acids and increasing D-alanylation in the cell wall. Subsequentially, the released target can enter a new cell wall synthesis cycle and be incorporated into the peptidoglycan (not shown fully here but in Fig. 1). *GlcNAc N*-acetylglucosamine, *MurNAc N*-acetylmuramic acid. The figure was created using Microsoft Powerpoint Version 16.54.

on other important cell processes. These proteins did not reveal any differences in production among all three tested strains (Table 2), confirming that the observed differences for the other proteins were due to the expression of the active *Sa*NsrFP transporter.

In summary, upregulated proteins when *Sa*NsrFP was produced, such as UDP-glucose-4-epimerase, *N*-acetylmuramic acid-6-phosphate etherase MurQ and RodA, were found to be associated with AMP resistance and cell wall modification (Fig. 6).

Additionally, the components of the nascent cell wall of *L. lactis* NZ9000Cm-, *Sa*NsrFP- and *Sa*NsrF$_{H202A}$P-expressing *L. lactis* cells were analyzed via LC–MS. The comparison of their chromatograms revealed that some peaks, which are occurring only in the sensitive strain and the inactive mutant (Fig. 7, SI Fig. S5a–f). These peaks correspond to components consisting of GlcNAc-MurNAc-L-Ala-D-iGln-L-Lys-(D-Asn) with *m/z* 938.37 $[M+H]^+$ (RT 27.0–28.3 min) (Fig. 7, SI Fig. S5a, peak 1), to GlcNAc-MurNAc-L-Ala-D-iGln-L-Lys-(D-Asp) with *m/z* 939.37 $[M+H]^+$ (RT 29.8–30.6 and 32.4–33.1 min) (Fig. 7, SI Fig. S5b, peak 2), to GlcNAc-MurNAc-L-Ala-D-iGln-L-Lys-(D-Asn)-D-Ala with *m/z* 1009.45 $[M+H]^+$ (RT 35.8–36.9 min) (Fig. 7, SI Fig. S5c, peak 3), to GlcNAc-MurNAc-L-Ala-D-iGln-L-Lys-(D-Asn)-D-Ala-D-Ala with *m/z* 1080.50 $[M+H]^+$ (RT 38.0–39.3 min) (Fig. 7, SI Fig. S5d, peak 4). The obtained masses are in agreement with the data described in the literature[60,61].

90

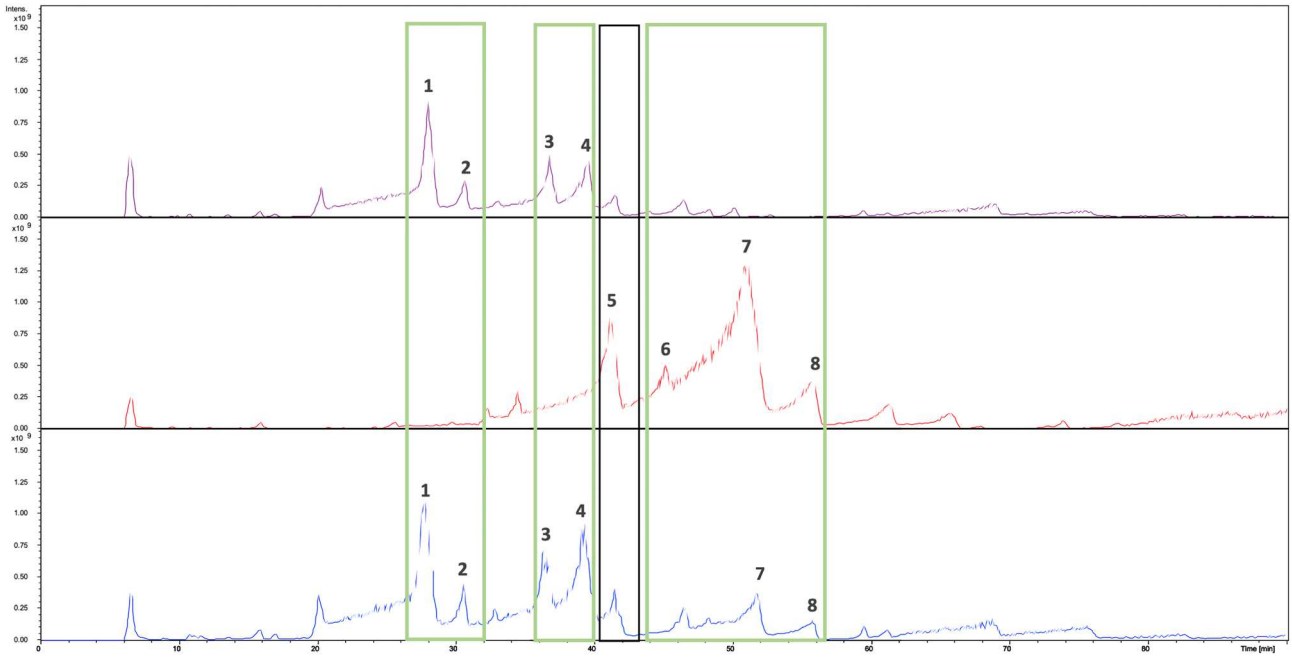

Figure 7. LC–MS chromatogram of isolated muropeptides from *L. lactis* NZ9000Cm (purple), *L. lactis* NZ9000NsrFP (red) and *L. lactis* NZ9000NsrF$_{H202A}$P (blue). The peaks that only occur in *L. lactis* NZ9000Cm and *L. lactis* NZ9000NsrF$_{H202A}$P are framed in green. Black framed is the peak, which can especially be observed in *L. lactis* NZ9000NsrFP. Peak 1: GlcNAc-MurNAc-L-Ala-D-iGln-L-Lys-(D-Asn); peak 2: GlcNAc-MurNAc-L-Ala-D-iGln-L-Lys-(D-Asp); peak 3: GlcNAc-MurNAc-L-Ala-D-iGln-L-Lys-(D-Asn)-D-Ala; peak 4: GlcNAc-MurNAc-L-Ala-D-iGln-L-Lys-(D-Asn)-D-Ala-D-Ala; peak 5: GlcNAc-MurNAc-L-Ala-D-iGln-L-Lys-(Ala)-D-Ala-D-Ala, and peaks 6–8: GlcNAc-MurNAc-L-Ala-D-iGln-L-Lys-(Ala-Ala)-D-Ala-D-Ala. *UDP* undecaprenyl-phosphate, *GlcNAc N*-acetylglucosamine, *MurNAc N*-acetylmuramic acid, *MurN N*-deacetylated muramic acid, *Ala* alanine, *iGlu* isoglutamic acid, *iGln* isoglutamine, *Glu* glutamine, *Asp* aspartate/aspartic acid, *Asn* asparagine, *Lys* lysine.

In contrast, one peak at RT 40.4–41.4 min with mass *m/z* 1037.49 $[M+H]^+$ (Fig. 7, SI Fig. S5e, peak 5) was detected only in *L. lactis Sa*NsrFP-expressing cells. The detected mass may indicate the presence of GlcNAc-MurNAc-L-Ala-D-iGln-L-Lys-(Ala)-D-Ala-D-Ala muropeptide fragment, that could contain an Ala residue attached to Lys, forming the crosslinking bridge. In addition, we detected three peaks (Fig. 7, SI Fig. S5f, peaks 6–8) whose masses presumably corresponded to GlcNAc-MurNAc-L-Ala-D-iGln-L-Lys-(Ala-Ala)-D-Ala-D-Ala (RT 44.4–45.5 min, 47.0–51.8 min and 54.4–55.7 min) with *m/z* 1108.53 $[M+H]^+$.These masses are in accordance with the masses described in the literature[62–64]. Intriguingly, the *Sa*NsrF$_{H202A}$P-expressing strain also showed some double alanine muropeptide species, albeit with a lower percentage than in the active transporter. These findings suggest that the transporter not only confers resistance by defending the target but also induces modulation of the cell wall.

Discussion

To elucidate the mechanism of the *Sa*NsrFP resistance mechanism, we showed that this transporter is able to circumvent reduced cell growth when cells are treated with bacitracin and/or Zn-bacitracin. Furthermore, we determined that resistance occurs against lipid II-binding AMPs. However, the highest resistance was observed for bacitracin and its Zn-bacitracin counterpart. This suggesting that this is the main substrate for NsrFP. The previously observed nisin resistance (Reiners et al.[34]) appears to be a side effect of the resistance mechanism. Here, our data implies that this resistance is ATP hydrolysis dependent and therefore is an active process, something that has been underestimated until now. Bacitracin resistance has been shown for several other BceAB-type transporters and appears to be conserved within this protein family. Examples include the AnrAB transporter from *Listeria monocytogenes*[30], VraDE from *S. aureus*[31,33], and the ABC transporter BceAB from *B. subtilis*[38]. However, similar to *Sa*NsrFP, these transporters additionally exhibited a certain degree of resistance to nisin and gallidermin, suggesting a general resistance mechanism rather than specific resistance to one type or even to specific antibiotics. Therefore, considering that *Sa*NsrFP confers resistance to structurally unrelated compounds, we concluded that *Sa*NsrFP is neither able to inactivate nor bind various compounds but rather that the resistance is based on a more general mechanism, such as shielding PGN biosynthesis components, including lipid II, UPP or UP, which are exposed on the outer surface of the bacterial membrane. The high-level resistance observed for the UPP binders bacitracin and (Zn)-bacitracin suggested that *Sa*NsrFP could shield either UPP or lipid II. (Figs. 1, 3a). Current hypotheses explain the resistance mechanism by the inaccessibility of the target UPP to bacitracin in this strain by either (i) target removal[21], (ii) target protection[45] or (iii) the combination of an active AMP defense mechanism that also mediates a multifactorial AMP defense response. The AMP defense

mechanism does not involve only a higher expression of ABC transporter encoding genes but also modifications of the cell wall structure or the membrane lipid composition, PGN thickening, changes in net charge and degrading enzymes[4]. Given that *L. lactis Sa*NsrFP cells are still growing at high (Zn-) bacitracin concentrations, PGN synthesis was not completely inhibited. Since *Sa*NsrFP cells repel structurally diverse antibiotics, as is known for the related BceAB transporter of *B. subtilis*[27], we hypothesize that *Sa*NsrFP could mediate resistance by shielding UPP and subsequent modification of PGN synthesis. These mechanisms have also been postulated by recent studies[45]. Based on previous studies and transporter activity studies in the presence of accumulated UPP or C35 isoprenoid heptaprenyl diphosphate (HPP), the authors proposed that the BceAB transporter detects UPP-bacitracin complexes and shields the target (e.g., lipid II or UPP or HPP) by severing the bond between them[65]. This further excludes other mechanisms, such as UPP flipping for BceAB in *B. subtilis*[21] and import and inactivation of the target[23].

Current opinion of researchers investigating antibiotic resistance conferring ABC transporters is that detoxification against peptide antibiotics is functionally linked to a two-component system[36]. It is hypothesized that upon sensing the antibiotic, the histidine kinase phosphorylates its cognate response regulator which induces the expression of the ABC transporter genes. Such a scenario was described i.e., for the GraRS-VraFG system[37] in *S. aureus* and also for several TCS-ABC transporters in *B. subtilis* (BceRS-AB, YxdJK-LM and YvcPQ-RS)[36,38]. Moreover, a direct interaction of the BceRS and BceAB was shown in in vitro and in vivo studies[36]. In their study, it is claimed that BceAB and the TCS need to form a complex in order to be able to sense the AMP.

In our study, in order to elucidate the mechanism of the BceAB-type transporter *Sa*NsrFP, we expressed it without its cognate TCS. It has been shown that the ABC transporter without its TCS can confer resistance against nisin[34]. The large extracellular domain is the hallmark of BceAB-type transporter which is hypothesized to be involved in extracellular detection of antibiotics[43]. Interestingly, the cognate histidine kinase consists only of a short loop which is buried almost entirely in the cytoplasmic membrane and thus cannot detect extracellular stimuli[39]. The crucial role of a Bce-type transporter for lantibiotic signalling has been shown in various studies already[23,42]. For the BceAB transporter it was shown that signalling is triggered by the activity of the transporter itself and the transporter can autoregulate its own production[45,46]. This is the reason we hypothesize that the ABC transporter *Sa*NsrFP should also be able to sense the AMP via its large extracellular domain. Therefore, we strived to investigate the role *Sa*NsrFP plays together with its 221 amino acid large extracellular domain in conferring resistance without its cognate TCS.

Since *Sa*NsrFP is able to confer resistance against bacitracin and other AMP's, we can show that the transporter is directly involved in sensing the antibiotic and the resistance process.

By the expression of *sansrfp*, adjustments within the bacterial cells occur. For example, the downregulation of proteins involved in lipid II biosynthesis. The reduced production of the key enzymes of the lipid II cycle was remarkable and suggested that the biosynthesis of new lipid II molecules occurred with less efficiency in the *L. lactis* NZ9000*Sa*NsrFP strain. This could be the case if lipid II or UPP might be the actual substrate of *Sa*NsrFP, but this hypothesis remains controversial, as it does not correspond to the growth behavior observed in the growth analysis. Here, the *Sa*NsrFP-expressing strain showed similar growth to the control strains *L. lactis* NZ9000NisT and *L. lactis* NZ9000Cm (see above Fig. 2c).

This strengthens the idea that BceAB-type transporters interact with precursors of cell wall synthesis or its recycling by binding. Therefore, the lipid II cycle might be inhibited, and the bacteria react by downregulating its lipid II pool. This has been directly shown by the analyses of the cell wall precursors that were clearly reduced in the *Sa*NsrFP strain. This would not only result in growth inhibition but would also lower the number of available targets at the membrane surface. Controversially, we could not see reduced growth in *Sa*NsrFP-expressing cells, and thus far, it was not possible to measure a difference in targets at the membrane surface. Less target on the surface could explain the moderate resistance observed for the lipid II binding AMPs like ramoplanin, vancomycin and others but it is not at all clear if this is a possible scenario since the removal of the target would likely lead to growth inhibition which would be toxic for the cell. Therefore, we cannot entirely exclude that the heterologous expression of the BceAB-type transporter influences the cell wall synthesis of *L. lactis* or whether the transporter itself is responsible for the alteration of its cell wall. Nonetheless, the NICE expression system (nisin-controlled gene expression system) that we used for the overexpression of *Sa*NsrFP is a tightly regulated system which can be turned on by adding a subinhibitory concentration of nisin to the media. It has been shown for the system that genes of closely related Gram-positive organisms (e.g., Streptococcus, Enterococcus, Staphylococcus, and low-GC Lactobacillus) are expressed effectively usually without any problems[66]. Interestingly, in the work of Marreddy et al.[67], overexpression of a membrane protein led to an upregulation of cell wall synthesis in the membrane protein expressing strain. In our data we detected a downregulation of involved proteins of cell wall synthesis but a slight upregulation of cell wall modification proteins. Moreover, we could not observe a significant change of expression of proteins responsible for a general stress response. Nonetheless, we chose the best possible system for heterologous expression of *Sa*NsrFP to overcome possible bottlenecks.

We show evidence that cells expressing *Sa*NsrFP obtain a modified cell wall: instead of an apartate/asparagine bridge in the pentapeptide found for the sensitive mutant, a species with two alanines was detected. In *Sa*NsrF-$_{H202A}$P, a mixture was found, although the two alanine species were present in only minor amounts (Fig. 7). This suggests that the transporter might already sense and mediate a second line of defense ATP-independently. ABC transporters that confer resistance against cationic antimicrobials are hypothesized to be involved or mediate modification processes of peptidoglycan in Gram-positive bacteria. D-alanylation of teichoic acids is assumed to diminish electrostatic attraction based on the observation that a lack of alanylation leads to increased binding to several positively charged molecules, e.g., gallidermin and vancomycin[41]. Additionally, the upregulation of the *gal* operon, especially of UDP-glucose-4-epimerase (GalE), influences the lipoteichoic acid (LTA) structure. GalE is responsible for the synthesis of α-galactose, which is transported across the membrane to become a part of LTA[68].

We can see this in our data with the upregulation of the MurQ which is responsible for the intracellular conversion of MurNAc-6P to *N*-acetylglucosamine-6-phosphate and D-lactate for the *Sa*NsrFP and *Sa*NsrF$_{H202A}$P mutants in comparison to the sensitive strain. For transporter-expressing cells, we also observed an upregulation of proteins associated with antimicrobial resistance, such as UDP-glucose-4-epimerase and RodA[68].

In the case that *Sa*NsrFP might mediate cell wall modifications upon receiving information on the cell wall targeting AMP, altered expression of genes could be the consequence. This finding might also reduce the number of proteins in the cytosol that are involved in lipid II biosynthesis, as seen by the whole proteome data where the expression of the genes is downregulated but not completely abolished. It needs to be verified whether *Sa*NsrFP is directly responsible for this or whether the *L. lactis* strain is reacting since its lipid II cycle is severely changed and, as a consequence, alters its cell wall composition.

Based on all results from this study, a joint activity of the transporter as a first-line defender and initiator for a second-line defense is very likely and results in resistance against compounds targeting the lipid II cycle and thus cell wall synthesis. By shielding the target UPP and lipid II from the extracellular space, e.g., by PGN modification that alters electrostatic attraction, less antibiotic, e.g., bacitracin, can be bound, and increased antibiotic concentrations can be detected in the supernatant. Our findings are in agreement with the previous conclusions for an export mechanism and further assumptions on the removal of AMPs from the membrane[34,44]. The tendency for upregulation of proteins associated with antimicrobial resistance and cell wall modification in *Sa*NsrFP-producing cell proteins indicates the activation of a second-line defense system.

Conclusively, BceAB-type transporters such as *Sa*NsrFP are evolutionarily conserved in human pathogenic and nonpathogenic strains. Although they are less conserved at the sequence level, the topology of the protein and their encoding operons are conserved. The resistance observed in different BceAB-type transporter studies indicates a common mechanism. The findings in this study are in line with a target protection mechanism, as was postulated for the BceAB transporter. Our data implies that AMP resistance is a far more complex process that involves a combination of an active target mechanism, which enables continuous growth, and a second line of defense, which could be initiated after sensing the AMP directly by the *Sa*NsrFP transporter.

Materials and methods

Cloning and expression. The plasmids pIL-SV SaNsrFP and pIL-SV SaNsrF$_{H202A}$P, the latter harboring a point mutation in the H-loop, known to be crucial for ATP hydrolysis, were generated by cloning *nsrfp* from *S. agalactiae* COH1 as described in Alkhatib et al.[69] and Reiners et al.[34]. Each plasmid and the empty vector pIL-SVCm was transformed into electrocompetent *L. lactis* NZ9000 cells[70], and the resulting strains were termed NZ9000*Sa*NsrFP, NZ9000*Sa*NsrF$_{H202A}$P and NZ9000Cm.

All strains used in this study have been described in previous publications[34,69].

The *L. lactis* strains NZ9000*Sa*NsrFP and NZ9000*Sa*NsrF$_{H202A}$P were cultured in GM17 medium containing 5–10 µg/ml chloramphenicol. Expression was induced by adding 0.3 nM nisin, and cultures were grown at 30 °C.

To analyze the expression, cultures were grown for 5 h and subsequently harvested using a centrifugation step for 30 min at 5000×*g*. The pellets were resuspended to an OD_{600} of 200 in resuspension buffer (50 mM HEPES pH 8.0, 150 mM NaCl, 10% glycerol), then 1/3 (w/v) 0.5 mm glass beads were added. The cells were lysed, and the supernatant was separated from cell debris as well as glass beads by centrifuging at 10,000×*g*. Subsequently, the membranes were harvested from the supernatant by a 100,000×*g* centrifugation step. Membrane fractions were mixed with SDS-loading dye (0.2 M Tris–HCl, pH 6.8, 10% (w/v) SDS, 40% (v/v) glycerol, 0.02% (w/v) bromophenol and β-mercaptoethanol) and used for SDS-PAGE and western blot analysis. A polyclonal antibody against the extracellular domain of *Sa*NsrP was used to detect the expressed *Sa*NsrFP protein (Davids Biotechnologie, Regensburg, Germany).

Biological assays. *Purification of nisin.* Nisin was purified with ion-exchange chromatography as previously described[71], and the concentration was determined with RP-HPLC according to Abts et al.[72].

Determination of the half-maximal inhibitory concentration (IC_{50}). The half maximal inhibitory concentration was determined according to Abts et al.[71]. Briefly, *L. lactis* NZ9000Cm, *L. lactis* NZ9000*Sa*NsrFP and *L. lactis* NZ9000*Sa*NsrF$_{H202A}$P cells were grown in GM17 medium containing 5 µg/ml chloramphenicol and 0.3 nM nisin at 30 °C overnight. Fresh GM17Cm medium with a sublethal amount of nisin (0.3 nM) was inoculated with overnight cultures to an OD_{600} of 0.1. A 96-well plate was prepared with a serial dilution of examined antibiotics (concentration ranges ramoplanin 0.014 nM–3.75 µM; lysobactin 0.002 nM–10 µM; vancomycin 0.02 nM–80 µM; nisin 0.0001 nM–0.5 µM) and subsequently the cell culture was added and plates were incubated at 30 °C for 5 h. Afterwards, the optical density was measured, and the IC_{50} values for each strain and antibiotic were calculated[34]. To make those values more comparable, the fold of resistance was determined by dividing the IC_{50} values of *L. lactis* NZ9000*Sa*NsrFP and *L. lactis* NZ9000*Sa*NsrF$_{H202A}$P by the corresponding value for *L. lactis* NZ9000Cm.

Growth curves. To detect the growth behavior of the different strains, precultures of *L. lactis* NZ9000Cm, *L. lactis* NZ9000*Sa*NsrFP and *L. lactis* NZ9000*Sa*NsrF$_{H202A}$P cells were grown in GM17 medium with 5 or 10 µg/ml chloramphenicol and 0.3 nM nisin at 30 °C overnight. Freshly prepared GM17Cm medium with 0.3 nM nisin was inoculated with overnight cultures to an OD_{600} of 0.1 and grown to an OD_{600} of 0.4–0.5 at 30 °C. Afterwards, the cells were diluted to an OD_{600} of 0.05 in GM17Cm medium containing 0.3 nM nisin. Cells were treated with either 1 µM bacitracin and 1 mM $ZnCl_2$ or 4 µM bacitracin without $ZnCl_2$. Growth was detected at OD_{584} every 10 min with a FLUOstar OPTIMA (BMG Lab technology).

Cell wall precursor analysis. *Growth condition and sample preparation.* Cells were grown in M17 medium supplemented with 0.5% glucose and 0.3 nM nisin overnight at 30 °C without shaking. The next day, 100 ml with 0.5% glucose and 0.3 nM nisin was inoculated with overnight cultures to $OD_{600} = 0.1$. When $OD_{600} = 1.2$ bacitracin (100 µg/ml) was added to the cultures to enrich cell wall precursors, and the cultures were incubated for an additional 30 min at 30 °C. This step was repeated once. (As a control, a second culture each was harvested before bacitracin was added at an $OD_{600} = 1.2$, and cell pellets were stored at − 20 °C) After incubation with bacitracin, the cells were harvested, and the cell pellets were stored at − 20 °C. The next day, the cell pellets were resuspended in 25 ml water and cooked for 60 min in boiling water to break the cells. Cell debris was removed by centrifugation (15 min, 500×*g*, 4 °C). The supernatant, containing the cell wall precursors, was lyophilized overnight. Cell pellets were resuspended in 150 µl water and used for LC/MS analysis.

LC/MS analysis of cell wall fragments. Five microliters of each sample were injected into an XCT6330 LC/MSD ultratrap system (Agilent Technologies) equipped with a Nucleosil 100 C18 column (3 µm × 100 mm × 2 mm internal diameter, Dr. Maisch GmbH). The column was used at 40 °C. A linear gradient was performed from 0 to 10% eluent B (0.06% formic acid in acetonitrile) over 25 min with a flow rate of 400 µl/min. The column was re-equilibrated for 10 min with 100% buffer A (0,1% formic acid in water). Ionization alternated between positive and negative ion modes with a capillary voltage of 3.5 kV at 350 °C. Extracted ion chromatograms (EICs) in negative ion mode for UDP-MurNAc-L-Ala-D-iGlu-L-Lys-D-Ala-D-Ala (m/z^{-1} 1148.34 ± 0.1) and UDP-MurNAc-L-Ala-D-iGlu-L-Lys-(D-Asp)-D-Ala-D-Ala (m/z^{-1} 1263.37 ± 0.1) were analyzed with Data Analysis (Bruker), exported and presented with GraphPad Prism 6.0.

Peptidoglycan analysis. *Isolation of peptidoglycan.* 600 ml main culture of *L. lactis* NZ9000Cm, *L. lactis Sa*NsrFP and *L. lactis Sa*NsrF$_{H202A}$P were inoculated with overnight culture and incubated to an OD600 of 0.1 at 30 °C. After reaching the late exponential growth phase, the cells were harvested. To isolate the peptidoglycan, the cells were thawed on ice and resuspended in 15 ml of 50 mM Tris/HCl buffer pH 7.0. The cell suspension was added dropwise to 60 ml of boiling, stirred 4% SDS solution. After boiling for another 15 min, the suspension was cooled to room temperature and centrifuged at 13,000×*g* for 10 min. The pellet was washed twice with 1 M NaCl followed by water until no SDS was detectable in the supernatant. Pellet was resuspended in 1 ml water, and 1/3 volume of glass beads (Æ 0.5 mm) were added. After cell lysis the glass beads were harvested at 2000×*g* for 5 min. The supernatant was centrifuged at 25,000×*g* for 15 min, and the pellet containing the cell walls were resuspended in 100 mM Tris/HCl pH 8.5 buffer with 20 mM $MgSO_4$. After addition of 10 µg/ml DNase I and 50 µg/ml RNase, the samples were incubated at 37 °C with 180 rpm for 2 h. Following the addition of 10 mM $CaCl_2$ and 100 µg/ml trypsin, an 18 h incubation was performed under the same conditions. Enzymatic activities were stopped by the addition of 1% SDS and incubation at 80 °C for 15 min. The suspension was diluted to 20 ml with water and centrifuged at 25,000×*g* for 30 min. The pellet was resuspended and incubated at 37 °C for 15 min with 10 ml 8 M LiCl and 10 ml 100 mM EDTA pH7, respectively. The peptidoglycan pellet was washed with water, acetone and water and was lyophilized.

Samples were treated as follows: 150 µl of resuspended peptidoglycan were mixed with 60 µl of mQ water and with 75 µl of TES buffer (200 mM TES, 4 mM $MgCl_2$, pH 7.0 with final concentration in sample: 150 mM TES, 3 mM $MgCl_2$, pH 7.0) and 15 µl of mutanolysine (75U) (Sigma-Aldrich, 5 kU/ml, dissolved in mQ water). Samples were incubated overnight at 37 °C and then centrifuged at RT for 5 min at 14,000 rpm. 90 µl of the supernatant were used for HPLC–MS analysis.

HPLC–MS analysis of muropeptides. 90 µl of the sample were injected for HPLC–MS analyses (XCT 6330 LC/MSD Ultra Trap system; Agilent Technologies) and Reprosil-Gold 300 C_{18} column (5 µm by 250 mm by 4.6 mm internal diameter). The HPLC parameters were as follows: Holding with 5% of solvent B (methanol + 0.06% HCOOH) for 5 min and then start with a linear gradient from 30% solvent B to 70% solvent A (water + 0.1% HCOOH) for 150 min with additional holding with 30% solvent B over 30 min at a flow rate of 500 µl/min. The MS parameters were as follows: Ionization alternating positive and negative, capillary voltage 3.5 kV, and temperature 350 °C.

Proteome analysis. *Sample preparation.* The *L. lactis* strains NZ9000*Sa*NsrFP and NZ9000*Sa*NsrF$_{H202A}$P were grown at 30 °C in GM17 medium containing 5 µg/ml chloramphenicol and 0.3 nM nisin. Precultures were inoculated to an OD_{600} of 0.1 and grown to the exponential growth phase before a main culture was inoculated to an OD_{600} of 0.1. The cells were harvested using 5000×*g*, and the pellets were resuspended in phosphate buffer pH 7 to an OD_{600} of 200. Then, 1/3 (w/v) 0.5 mm glass beads were added. The cells were lysed, and the supernatant was separated by centrifugation at 10,000×*g*.

Protein concentration was determined by means of a Pierce 660 nm Protein Assay (Fischer Scientific, Schwerte, Germany), and 10 µg protein per sample was loaded on an SDS-PAGE gel for in-gel digestion. The isolated gel pieces were reduced, alkylated and underwent tryptic digestion. The peptides were resolved in 0.1% trifluoracetic acid and subjected to liquid chromatography.

LC–MS analysis. For the LC–MS analysis, a QExactive plus (Thermo Scientific, Bremen, Germany) connected with an Ultimate 3000 Rapid Separation liquid chromatography system (Dionex/Thermo Scientific, Idstein, Germany) equipped with an Acclaim PepMap 100 C18 column (75 µm inner diameter, 25 cm length, 2 mm particle size from Thermo Scientific, Bremen, Germany) was applied. The length of the LC gradient was 120 min. The mass spectrometer was operated in positive mode and coupled with a nano electrospray ionization

source. The capillary temperature was set to 250 °C, and the source voltage was set to 1.4 kV. In the QExactive plus mass spectrometer for the survey scans, a mass range from 200 to 2000 m/z at a resolution of 70,000 was used. The automatic gain control was set to 3,000,000, and the maximum fill time was 50 ms. The 10 most intensive peptide ions were isolated and fragmented by high-energy collision dissociation (HCD).

Computational mass spectrometric data analysis. Proteome Discoverer (version 2.1.0.81, Thermo Fisher Scientific, Bremen, Germany) was applied for peptide/protein identification by applying Mascot (version 2.4, Matrix Science, London, UK) as a search engine employing the EnsemblBacteria database (*Lactococcus lactis* subsp. *cremoris* NZ9000; date 03-11-2019). A false discovery rate of 1% ($p \leq 0.01$) at the peptide level was set as the identification threshold. Proteins were quantified with Progenesis QI for Proteomics (Version 2.0, Nonlinear Dynamics, Waters Corporation, Newcastle upon Tyne, UK). Only proteins containing at least two unique peptides were taken into consideration. For the calculation of enriched proteins in the groups, a 5% false discovery rate and a minimum fold change of two were used.

The mass spectrometry proteomics data have been deposited to the ProteomeXchange Consortium via the PRIDE partner repository with the data set identifier PXD017318.

The protein lists, which have been uploaded to PRIDE, are also provided as Supplementary Material.

Received: 1 September 2021; Accepted: 23 February 2022
Published online: 10 March 2022

References

1. Laxminarayan, R. *et al.* Antibiotic resistance-the need for global solutions. *Lancet Infect. Dis.* **13**, 1057–1098 (2013).
2. Li, B. & Webster, T. J. Bacteria antibiotic resistance: New challenges and opportunities for implant-associated orthopedic infections. *J. Orthop. Res.* **36**, 22–32 (2018).
3. Dever, L. A. & Dermody, T. S. Mechanisms of bacterial resistance to antibiotics. *Arch. Intern. Med.* **151**, 886–895 (1991).
4. Muller, A., Klockner, A. & Schneider, T. Targeting a cell wall biosynthesis hot spot. *Nat. Prod. Rep.* **34**, 909–932 (2017).
5. Bugg, T. D. & Walsh, C. T. Intracellular steps of bacterial cell wall peptidoglycan biosynthesis: Enzymology, antibiotics, and antibiotic resistance. *Nat. Prod. Rep.* **9**, 199–215 (1992).
6. Typas, A., Banzhaf, M., Gross, C. A. & Vollmer, W. From the regulation of peptidoglycan synthesis to bacterial growth and morphology. *Nat. Rev. Microbiol.* **10**, 123–136 (2011).
7. Dik, D. A. *et al.* A synthetic 5,3-cross-link in the cell wall of rod-shaped gram-positive bacteria. *Proc. Natl. Acad. Sci. U.S.A.* **118**, e2100137118 (2021).
8. Kuk, A. C. Y., Hao, A., Guan, Z. & Lee, S. Y. Visualizing conformation transitions of the lipid II flippase MurJ. *Nat. Commun.* **10**, 1736 (2019).
9. Lovering, A. L., Safadi, S. S. & Strynadka, N. C. Structural perspective of peptidoglycan biosynthesis and assembly. *Annu. Rev. Biochem.* **81**, 451–478 (2012).
10. Breukink, E. & de Kruijff, B. Lipid II as a target for antibiotics. *Nat. Rev. Drug Discov.* **5**, 321–332 (2006).
11. Wiedemann, I. *et al.* Specific binding of nisin to the peptidoglycan precursor lipid II combines pore formation and inhibition of cell wall biosynthesis for potent antibiotic activity. *J. Biol. Chem.* **276**, 1772–1779 (2001).
12. Hsu, S. T. *et al.* The nisin-lipid II complex reveals a pyrophosphate cage that provides a blueprint for novel antibiotics. *Nat. Struct. Mol. Biol.* **11**, 963–967 (2004).
13. Bonelli, R. R., Schneider, T., Sahl, H. G. & Wiedemann, I. Insights into *in vivo* activities of lantibiotics from gallidermin and epidermin mode-of-action studies. *Antimicrob. Agents Chemother.* **50**, 1449–1457 (2006).
14. Perkins, H. R. Specificity of combination between mucopeptide precursors and vancomycin or ristocetin. *Biochem. J.* **111**, 195–205 (1969).
15. Malin, J. J. & de Leeuw, E. Therapeutic compounds targeting lipid II for antibacterial purposes. *Infect. Drug Resist.* **12**, 2613–2625 (2019).
16. Hu, Y., Helm, J. S., Chen, L., Ye, X. Y. & Walker, S. Ramoplanin inhibits bacterial transglycosylases by binding as a dimer to lipid II. *J. Am. Chem. Soc.* **125**, 8736–8737 (2003).
17. Hamburger, J. B. *et al.* A crystal structure of a dimer of the antibiotic ramoplanin illustrates membrane positioning and a potential lipid II docking interface. *Proc. Natl. Acad. Sci. U.S.A.* **106**, 13759–13764 (2009).
18. Lee, W. *et al.* The mechanism of action of lysobactin. *J. Am. Chem. Soc.* **138**, 100–103 (2016).
19. Storm, D. R. & Strominger, J. L. Complex formation between bacitracin peptides and isoprenyl pyrophosphates. The specificity of lipid-peptide interactions. *J. Biol. Chem.* **248**, 3940–3945 (1973).
20. Economou, N. J., Cocklin, S. & Loll, P. J. High-resolution crystal structure reveals molecular details of target recognition by bacitracin. *Proc. Natl. Acad. Sci. U.S.A.* **110**, 14207–14212 (2013).
21. Kingston, A. W., Zhao, H., Cook, G. M. & Helmann, J. D. Accumulation of heptaprenyl diphosphate sensitizes *Bacillus subtilis* to bacitracin: Implications for the mechanism of resistance mediated by the BceAB transporter. *Mol. Microbiol.* **93**, 37–49 (2014).
22. Lightbown, J. W., Kogut, M. & Uemura, K. The Second International Standard for Bacitracin. *Bull. World Health Organ.* **31**, 101–109 (1964).
23. Rietkotter, E., Hoyer, D. & Mascher, T. Bacitracin sensing in *Bacillus subtilis*. *Mol. Microbiol.* **68**, 768–785 (2008).
24. Wei, S., Gutek, A., Lilburn, M. & Yu, Z. Abundance of pathogens in the gut and litter of broiler chickens as affected by bacitracin and litter management. *Vet. Microbiol.* **166**, 595–601 (2013).
25. Collinder, E. *et al.* Influence of zinc bacitracin and *Bacillus licheniformis* on microbial intestinal functions in weaned piglets. *Vet. Res. Commun.* **27**, 513–526 (2003).
26. Manson, J. M., Keis, S., Smith, J. M. & Cook, G. M. Acquired bacitracin resistance in *Enterococcus faecalis* is mediated by an ABC transporter and a novel regulatory protein, BcrR. *Antimicrob. Agents Chemother.* **48**, 3743–3748 (2004).
27. Ohki, R. *et al.* The BceRS two-component regulatory system induces expression of the bacitracin transporter, BceAB, in *Bacillus subtilis*. *Mol. Microbiol.* **49**, 1135–1144 (2003).
28. Radeck, J. *et al.* Anatomy of the bacitracin resistance network in *Bacillus subtilis*. *Mol. Microbiol.* **100**, 607–620 (2016).
29. Ma, J. *et al.* Bacitracin resistance and enhanced virulence of *Streptococcus suis* via a novel efflux pump. *BMC Vet. Res.* **15**, 377 (2019).
30. Collins, B., Curtis, N., Cotter, P. D., Hill, C. & Ross, R. P. The ABC transporter AnrAB contributes to the innate resistance of *Listeria monocytogenes* to nisin, bacitracin, and various beta-lactam antibiotics. *Antimicrob. Agents Chemother.* **54**, 4416–4423 (2010).

31. Hiron, A., Falord, M., Valle, J., Debarbouille, M. & Msadek, T. Bacitracin and nisin resistance in *Staphylococcus aureus*: A novel pathway involving the BraS/BraR two-component system (SA2417/SA2418) and both the BraD/BraE and VraD/VraE ABC transporters. *Mol. Microbiol.* **81**, 602–622 (2011).
32. Khosa, S., Lagedroste, M. & Smits, S. H. Protein defense systems against the lantibiotic nisin: Function of the immunity protein nisi and the resistance protein NSR. *Front. Microbiol.* **7**, 504 (2016).
33. Popella, P. *et al.* VraH is the third component of the *Staphylococcus aureus* VraDEH system involved in Gallidermin and Daptomycin resistance and pathogenicity. *Antimicrob. Agents Chemother.* **60**, 2391–2401 (2016).
34. Reiners, J. *et al.* The N-terminal region of nisin is important for the BceAB-type ABC transporter NsrFP from *Streptococcus agalactiae* COH1. *Front. Microbiol.* **8**, 1643 (2017).
35. Dintner, S. *et al.* Coevolution of ABC transporters and two-component regulatory systems as resistance modules against antimicrobial peptides in Firmicutes Bacteria. *J. Bacteriol.* **193**, 3851–3862 (2011).
36. Dintner, S., Heermann, R., Fang, C., Jung, K. & Gebhard, S. A sensory complex consisting of an ATP-binding cassette transporter and a two-component regulatory system controls bacitracin resistance in *Bacillus subtilis*. *J. Biol. Chem.* **289**, 27899–27910 (2014).
37. Cho, J., Costa, S. K., Wierzbicki, R. M., Rigby, W. F. C. & Cheung, A. L. The extracellular loop of the membrane permease VraG interacts with GraS to sense cationic antimicrobial peptides in *Staphylococcus aureus*. *PLoS Pathog.* **17**, e1009338 (2021).
38. Staron, A., Finkeisen, D. E. & Mascher, T. Peptide antibiotic sensing and detoxification modules of *Bacillus subtilis*. *Antimicrob. Agents Chemother.* **55**, 515–525 (2011).
39. Mascher, T. Intramembrane-sensing histidine kinases: A new family of cell envelope stress sensors in Firmicutes bacteria. *FEMS Microbiol. Lett.* **264**, 133–144 (2006).
40. Gebhard, S. ABC transporters of antimicrobial peptides in Firmicutes bacteria—Phylogeny, function and regulation. *Mol. Microbiol.* **86**, 1295–1317 (2012).
41. Revilla-Guarinos, A., Gebhard, S., Mascher, T. & Zuniga, M. Defence against antimicrobial peptides: Different strategies in Firmicutes. *Environ. Microbiol.* **16**, 1225–1237 (2014).
42. Bernard, R., Guiseppi, A., Chippaux, M., Foglino, M. & Denizot, F. Resistance to bacitracin in *Bacillus subtilis*: Unexpected requirement of the BceAB ABC transporter in the control of expression of its own structural genes. *J. Bacteriol.* **189**, 8636–8642 (2007).
43. Clemens, R., Zaschke-Kriesche, J., Khosa, S. & Smits, S. H. J. Insight into two ABC transporter families involved in lantibiotic resistance. *Front. Mol. Biosci.* **4**, 91 (2017).
44. Gebhard, S. & Mascher, T. Antimicrobial peptide sensing and detoxification modules: Unravelling the regulatory circuitry of *Staphylococcus aureus*. *Mol. Microbiol.* **81**, 581–587 (2011).
45. Kobras, C. M. *et al.* BceAB-type antibiotic resistance transporters appear to act by target protection of cell wall synthesis. *Antimicrob. Agents Chemother.* https://doi.org/10.1128/AAC.02241-19 (2020).
46. Fritz, G. *et al.* A new way of sensing: Need-based activation of antibiotic resistance by a flux-sensing mechanism. *MBio* **6**, e00975 (2015).
47. Furtmann, F. *et al.* Characterization of the nucleotide-binding domain NsrF from the BceAB-type ABC-transporter NsrFP from the human pathogen *Streptococcus agalactiae*. *Sci. Rep.* **10**, 15208 (2020).
48. Draper, L. A., Cotter, P. D., Hill, C. & Ross, R. P. Lantibiotic resistance. *Microbiol. Mol. Biol. Rev.* **79**, 171–191 (2015).
49. Poyart, C., Lamy, M. C., Boumaila, C., Fiedler, F. & Trieu-Cuot, P. Regulation of D-alanyl-lipoteichoic acid biosynthesis in *Streptococcus agalactiae* involves a novel two-component regulatory system. *J. Bacteriol.* **183**, 6324–6334 (2001).
50. Peschel, A., Vuong, C., Otto, M. & Gotz, F. The D-alanine residues of *Staphylococcus aureus* teichoic acids alter the susceptibility to vancomycin and the activity of autolytic enzymes. *Antimicrob. Agents Chemother.* **44**, 2845–2847 (2000).
51. Benda, M., Schulz, L. M., Stulke, J. & Rismondo, J. Influence of the ABC transporter YtrBCDEF of *Bacillus subtilis* on competence, biofilm formation and cell wall thickness. *Front. Microbiol.* **12**, 587035 (2021).
52. Storm, D. R. Mechanism of bacitracin action: A specific lipid-peptide interaction. *Ann. N. Y. Acad. Sci.* **235**, 387–398 (1974).
53. Zaitseva, J., Jenewein, S., Jumpertz, T., Holland, I. B. & Schmitt, L. H662 is the linchpin of ATP hydrolysis in the nucleotide-binding domain of the ABC transporter HlyB. *EMBO J.* **24**, 1901–1910 (2005).
54. Alkhatib, Z., Abts, A., Mavaro, A., Schmitt, L. & Smits, S. H. Lantibiotics: How do producers become self-protected? *J. Biotechnol.* **159**, 145–154 (2012).
55. Mierau, I. & Kleerebezem, M. 10 years of the nisin-controlled gene expression system (NICE) in *Lactococcus lactis*. *Appl. Microbiol. Biotechnol.* **68**, 705–717 (2005).
56. Klinzing, D. C. *et al.* The two-component response regulator LiaR regulates cell wall stress responses, pili expression and virulence in group B *Streptococcus*. *Microbiology (Reading)* **159**, 1521–1534 (2013).
57. Vemula, H., Ayon, N. J., Burton, A. & Gutheil, W. G. Antibiotic effects on methicillin-resistant *Staphylococcus aureus* cytoplasmic peptidoglycan intermediate levels and evidence for potential metabolite level regulatory loops. *Antimicrob. Agents Chemother.* **61**, e02253 (2017).
58. Lagedroste, M., Reiners, J., Smits, S. H. J. & Schmitt, L. Impact of the nisin modification machinery on the transport kinetics of NisT. *Sci. Rep.* **10**, 12295 (2020).
59. Lagedroste, M., Smits, S. H. J. & Schmitt, L. Importance of the leader peptide sequence on the lanthipeptide secretion level. *FEBS J.* **288**, 4348 (2021).
60. Courtin, P. *et al.* Peptidoglycan structure analysis of *Lactococcus lactis* reveals the presence of an L, D-carboxypeptidase involved in peptidoglycan maturation. *J. Bacteriol.* **188**, 5293–5298 (2006).
61. Bellais, S. *et al.* Aslfm, the D-aspartate ligase responsible for the addition of D-aspartic acid onto the peptidoglycan precursor of *Enterococcus faecium*. *J. Biol. Chem.* **281**, 11586–11594 (2006).
62. Bouhss, A. *et al.* Synthesis of the L-alanyl-L-alanine cross-bridge of *Enterococcus faecalis* peptidoglycan. *J. Biol. Chem.* **277**, 45935–45941 (2002).
63. Vollmer, W., Blanot, D. & de Pedro, M. A. Peptidoglycan structure and architecture. *FEMS Microbiol. Rev.* **32**, 149–167 (2008).
64. Chapot-Chartier, M. P. & Kulakauskas, S. Cell wall structure and function in lactic acid bacteria. *Microb. Cell Fact* **13**, S9 (2014).
65. Kobras, C. M. *et al.* BceAB-type antibiotic resistance transporters appear to act by target protection of cell wall synthesis. *Antimicrob. Agents Chemother.* https://doi.org/10.1101/835702 (2019).
66. Kunji, E. R., Slotboom, D. J. & Poolman, B. *Lactococcus lactis* as host for overproduction of functional membrane proteins. *Biochim. Biophys. Acta* **1610**, 97–108 (2003).
67. Marreddy, R. K. *et al.* The response of *Lactococcus lactis* to membrane protein production. *PLoS ONE* **6**, e24060 (2011).
68. Kramer, N. E., van Hijum, S. A., Knol, J., Kok, J. & Kuipers, O. P. Transcriptome analysis reveals mechanisms by which *Lactococcus lactis* acquires nisin resistance. *Antimicrob. Agents Chemother.* **50**, 1753–1761 (2006).
69. AlKhatib, Z. *et al.* Lantibiotic immunity: Inhibition of nisin mediated pore formation by NisI. *PLoS ONE* **9**, e102246 (2014).
70. Holo, H. & Nes, I. F. High-frequency transformation, by electroporation, of *Lactococcus lactis* subsp. *cremoris* grown with glycine in osmotically stabilized media. *Appl. Environ. Microbiol.* **55**, 3119–3123 (1989).
71. Abts, A. *et al.* Easy and rapid purification of highly active nisin. *Int. J. Pept.* **2011**, 175145 (2011).
72. Abts, A., Montalban-Lopez, M., Kuipers, O. P., Smits, S. H. & Schmitt, L. NisC binds the FxLx motif of the nisin leader peptide. *Biochemistry* **52**, 5387–5395 (2013).

Acknowledgements
The authors are thankful to Jelle Postma and Stefanie Weidtkamp-Peters from the Center for Advanced Imaging, Heinrich-Heine-University Germany, for valuable suggestions and great support during fluorophore studies. This work was funded by the Deutsche Forschungsgemeinschaft (DFG, German Research Foundation)—270650915/GRK 2158 TP4a to S.S. E.S. gratefully acknowledges financial support from the DFG, TRR261, Project ID 398967434.

Author contributions
J.G. and J.Z.K. performed biological assays and wrote the manuscript. S.U., I.V. and A.K. performed cell wall precursor analysis. L.V.B. performed biological assays. N.O. performed proteome analysis. K.S. and E.S. contributed to the writing. S.H.J.S. initiated and supervised the study. S.H.J.S. and J.G. wrote the manuscript with input of all authors.

Funding
Open Access funding enabled and organized by Projekt DEAL.

Competing interests
The authors declare no competing interests.

Additional information
Supplementary Information The online version contains supplementary material available at https://doi.org/10.1038/s41598-022-08095-2.

Correspondence and requests for materials should be addressed to S.H.J.S.

Reprints and permissions information is available at www.nature.com/reprints.

Publisher's note Springer Nature remains neutral with regard to jurisdictional claims in published maps and institutional affiliations.

New insights into the resistance mechanism for the BceAB-type transporter *Sa*NsrFP

Julia Gottstein[a*], Julia Zaschke-Kriesche[a*], Sandra Unsleber[b], Irina Voitsekhovskaia[b], Andreas Kulik[b], Lara V. Behrmann[a], Nina Overbeck[c], Kai Stühler[c], Evi Stegmann[b] and Sander H.J. Smits[a*]

[a] Institute of Biochemistry, Heinrich-Heine-University Duesseldorf, Universitaetsstrasse 1, 40225 Duesseldorf, Germany.

[b] Interfaculty Institute of Microbiology and Infection Medicin, Eberhard Karls University, Auf der Morgenstelle 28, 72076 Tübingen, Germany.

[c] Molecular Proteomics Laboratory, Heinrich-Heine-University Duesseldorf, Universitaetsstrasse 1, 40225 Duesseldorf, Germany.

*Corresponding author: Sander H. J. Smits, Institute of Biochemistry, Heinrich-Heine-University Duesseldorf, Universitaetsstrasse 1, 40225 Duesseldorf, Germany.

* both authors contributed equally

Email: Sander.Smits@hhu.de

SI Figure 1

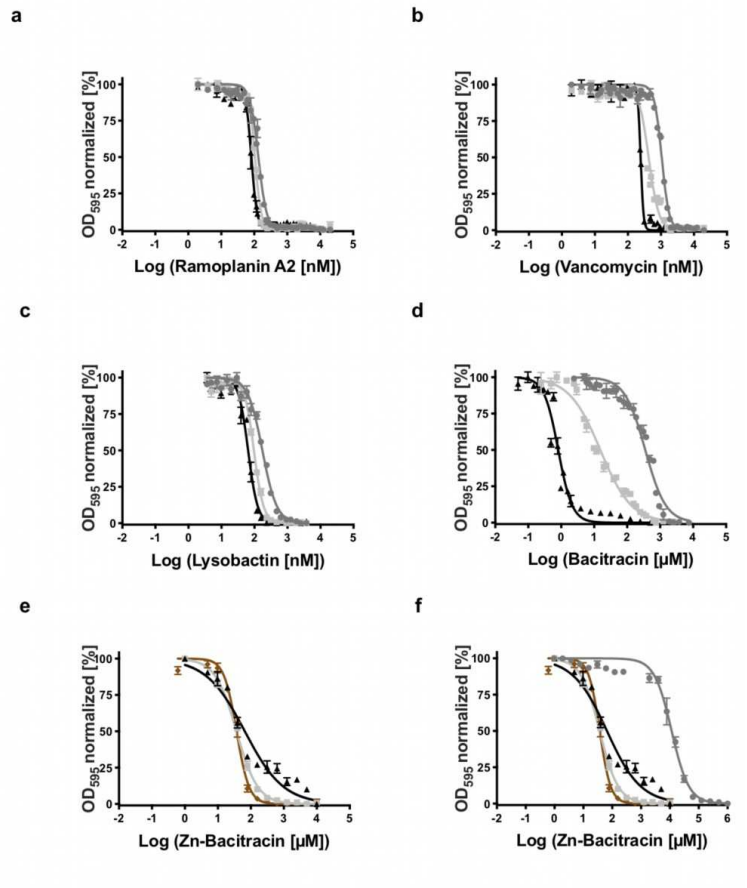

SI Figure 1: Representative inhibitional growth curves of **a) Ramoplanin A2**, **b) Vancomycin**, **c) Lysobactin, d) Bacitracin e) & f) Zn-Bacitracin.** The normalized OD_{595} is plotted against the logarithmic concentration of the antibiotic. NZ9000Cm is demonstrated in black, NZ9000*Sa*NsrF$_{H202A}$P in light grey, NZ9000*Sa*NsrFP in grey and NZ9000NisT in brown.

SI Figure 2.

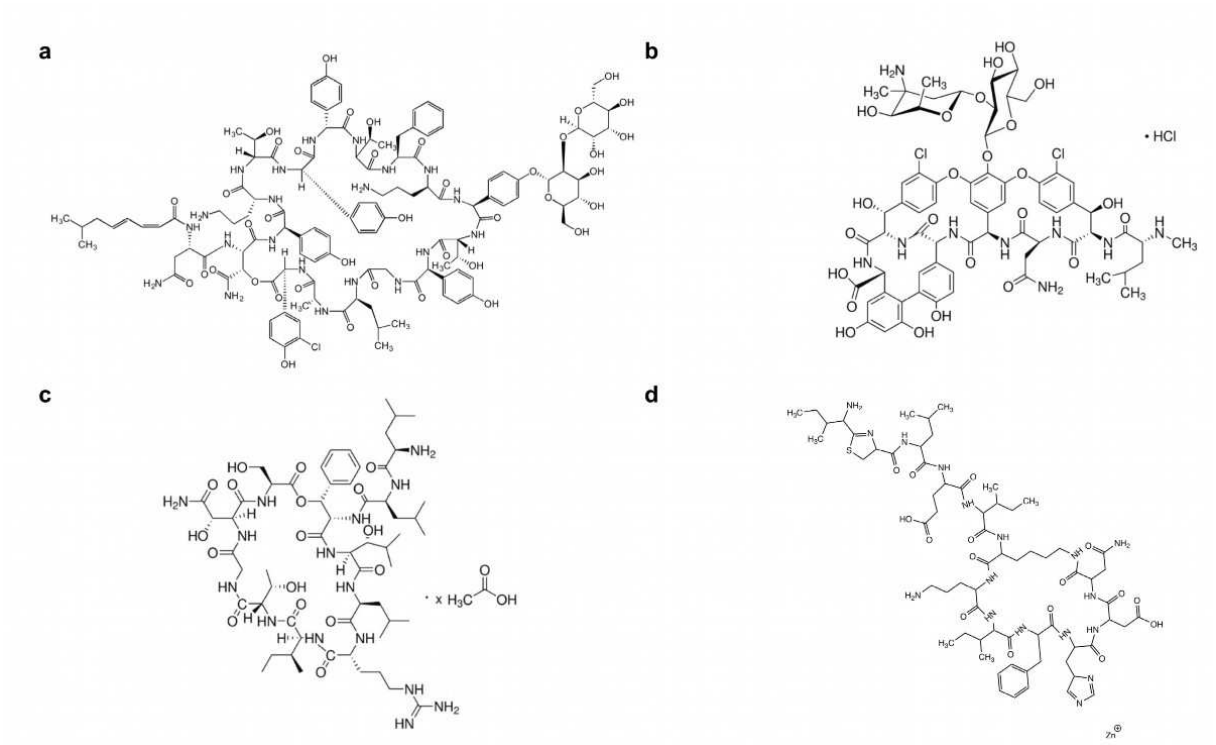

SI Figure 2: Structures of a) Ramoplanin A2 from AdipoGen life sciences, **b) Vancomycin** from Fluka Analytical, **c) Lysobactin** from Sigma life sciences and **d) Bacitracin** from Fisher BioReagents.

ADJ60406

ADJ60417

ADJ60503

ADJ60765

ADJ60806

ADJ60966

ADJ59149

ADJ59249

ADJ59347

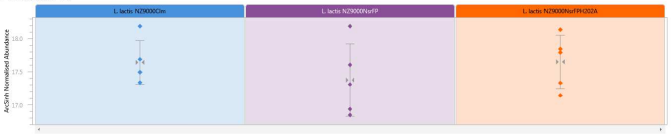

ADJ59379

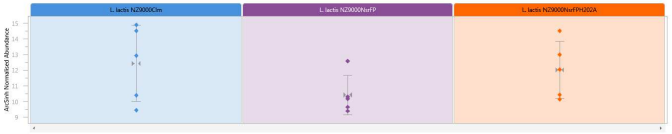

ADJ59381

ADJ59382

ADJ60973

ADJ61030

ADJ61045

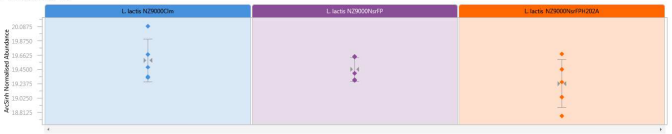

ADJ61135

ADJ61146

ADJ61268

ADJ61283

ADJ61304

ADJ61321

ADJ61415

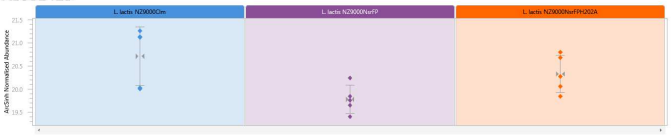

ADJ61465

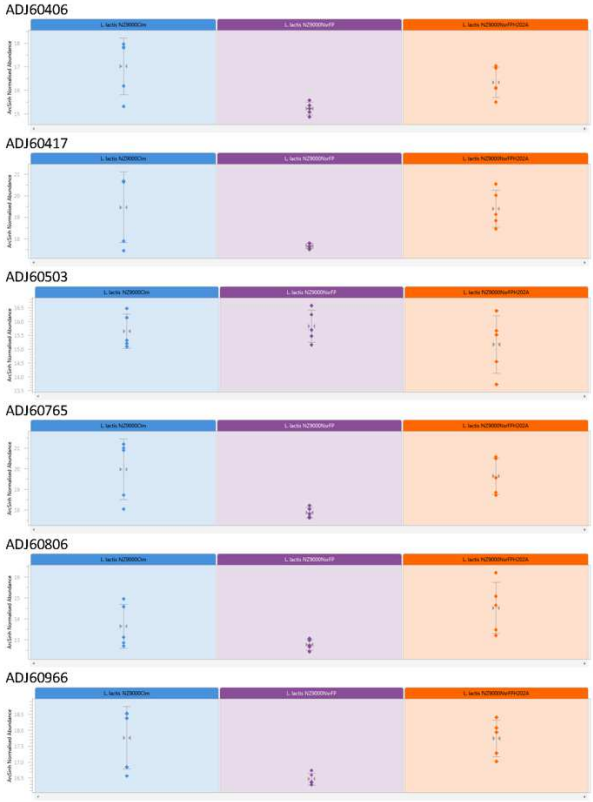

SI Figure 3: Normalized abundance of several proteins of the proteome analysis of *L. lactis* NZ9000Cm (blue), NZ9000NsrFP (violette) and NZ9000NsrF$_{H202A}$P (orange).

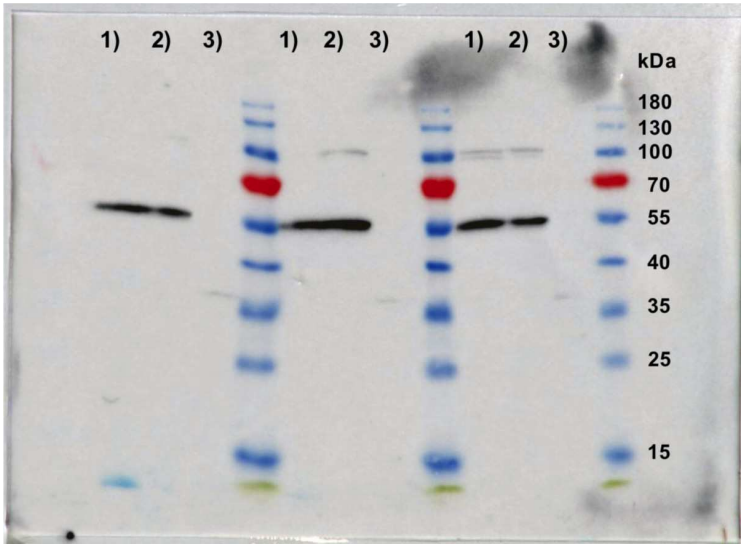

SI Figure 4: Expression of *Sa*NsrFP (1) and *Sa*NsrF$_{H202A}$P (2) and the empty vector pIL-SV (3) in *L. lactis* NZ9000Cm from three different cultures, monitored *via* western blot with a polyclonal antibody against the extracellular domain of *Sa*NsrP**.**

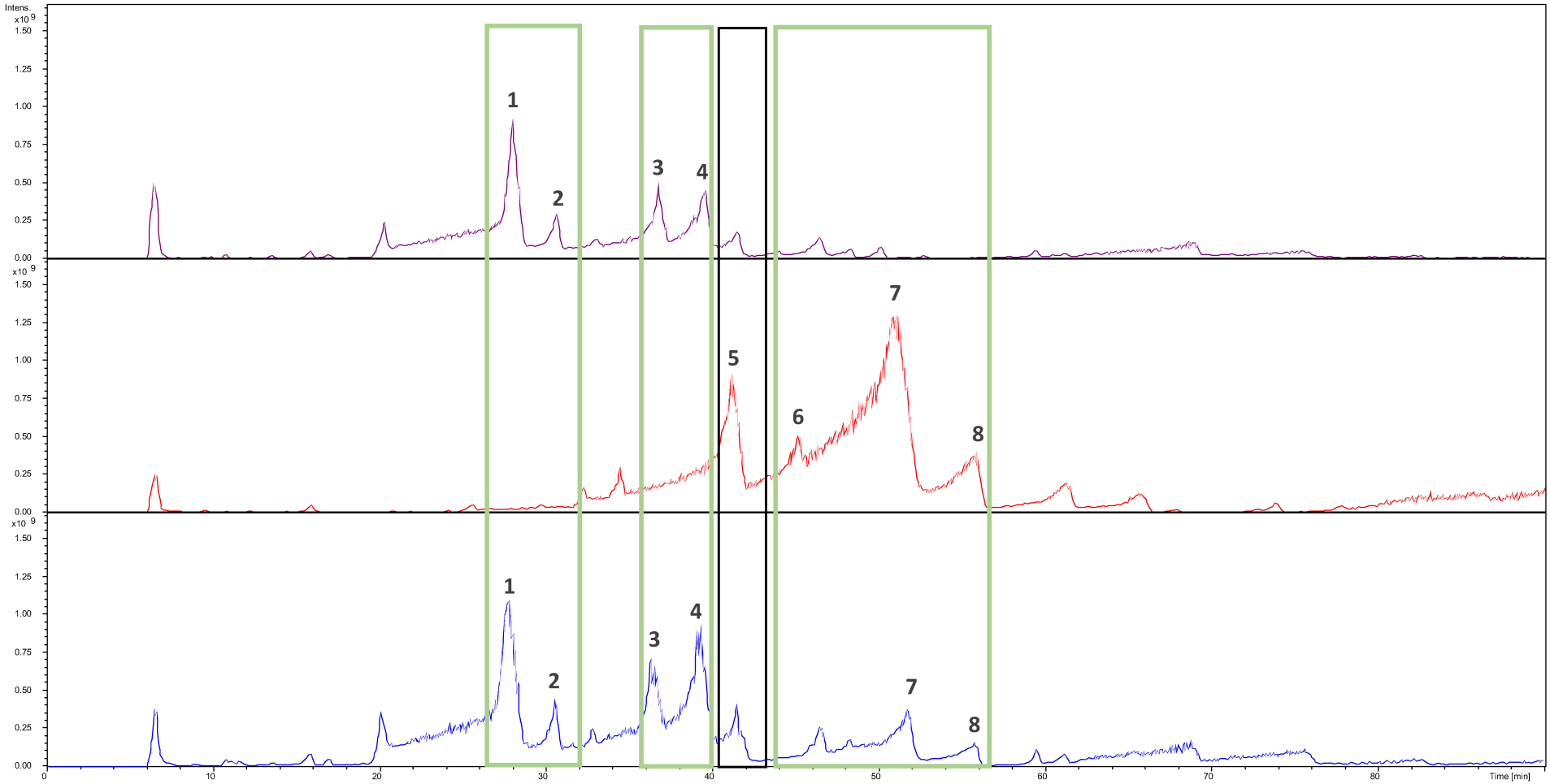

SI Figure 5: LC-MS Chromatogram of isolated muropeptides from *L. lactis* NZ9000Cm (purple), *L. lactis* NZ9000NsrFP (red) and *L. lactis* NZ9000NsrF$_{H202A}$P (blue). Marked peaks in green frames could be related to the mass of GlcNAc-MurNAc-L-Ala-D-iGln-L-Lys-(D-Asn) (peak 1), GlcNAc-MurNAc-L-Ala-D-iGln-L-Lys-(D-Asp) (peak 2), GlcNAc-MurNAc-L-Ala-D-iGln-L-Lys-(D-Asn)-D-Ala (peak 3), GlcNAc-MurNAc-L-Ala-D-iGln-L-Lys-(D-Asn)-D-Ala-D-Ala (peak 4) and GlcNAc-MurNAc-L-Ala-D-iGln-L-Lys-(Ala-Ala)-D-Ala-D-Ala (peaks 6-8). Marked peak 5 in black frame could be related to the mass GlcNac-MurNac-L-Ala-D-iGln-L-Lys-(Ala)-D-Ala-D-Ala.

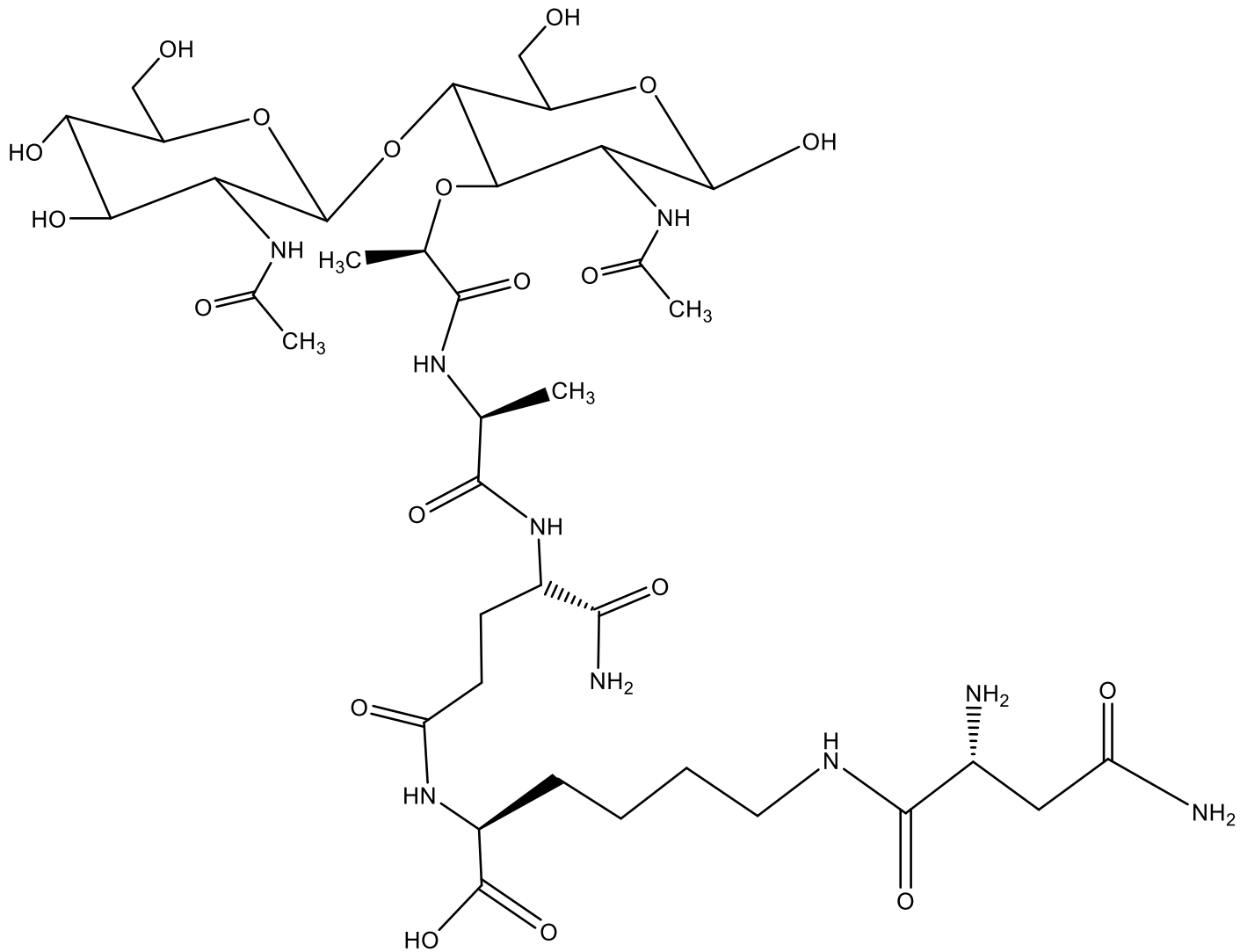

SI Figure 5a: Muropeptide structure corresponding to peak 1.

GlcNAc-MurNAc-L-Ala-D-iGln-L-Lys-(D-Asn) detected in *L. lactis* NZ9000Cm and *L. lactis* NZ9000*Sa*NsrF$_{H202A}$P with *m/z* 938.37 $[M+H]^+$.

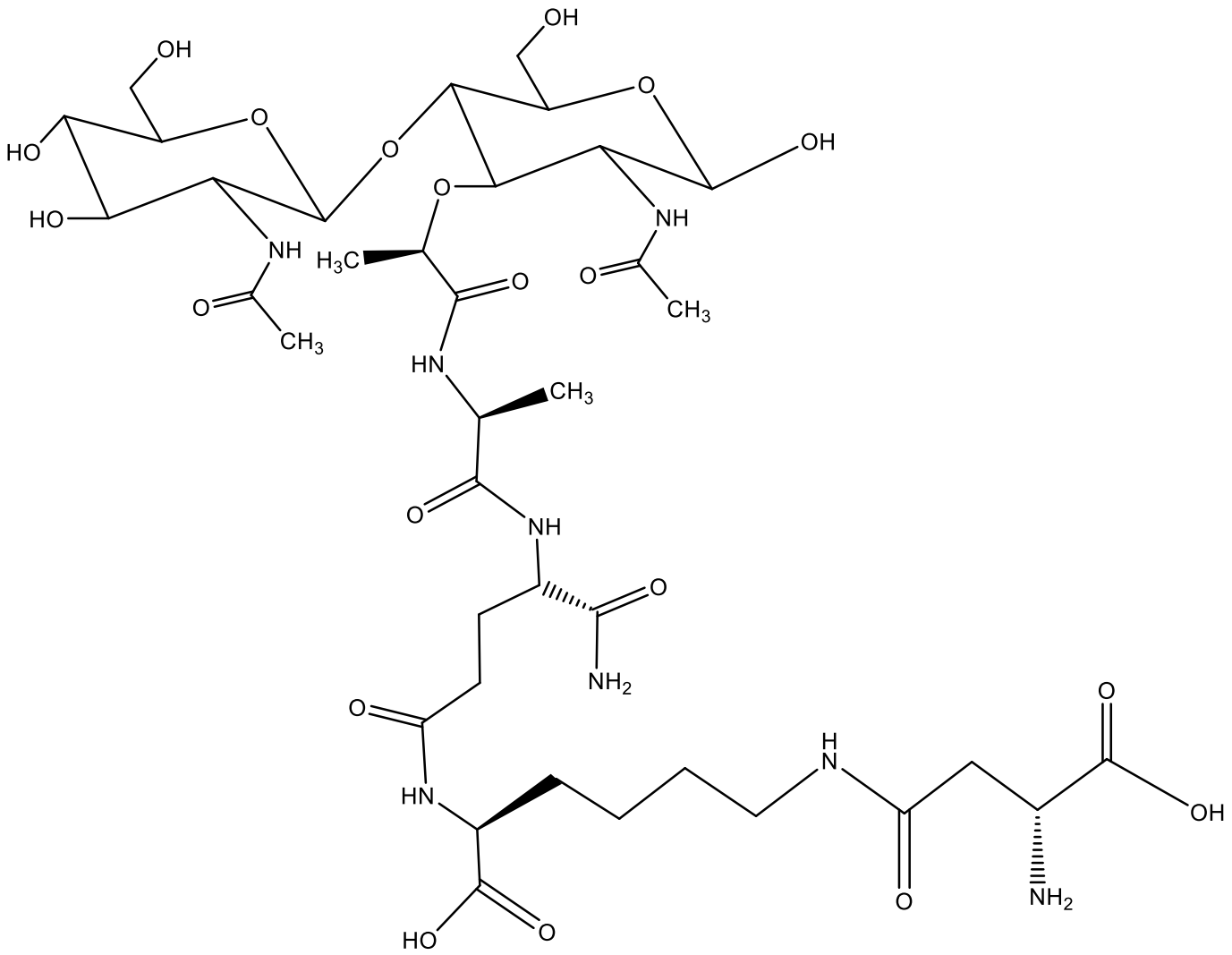

SI Figure 5b: Muropeptide structure corresponding to peak 2.

GlcNAc-MurNAc-L-Ala-D-iGln-L-Lys-(D-Asp) detected in *L. lactis* NZ9000Cm and *L. lactis* NZ9000*Sa*NsrF$_{H202A}$P with *m/z* 939.37 $[M+H]^+$.

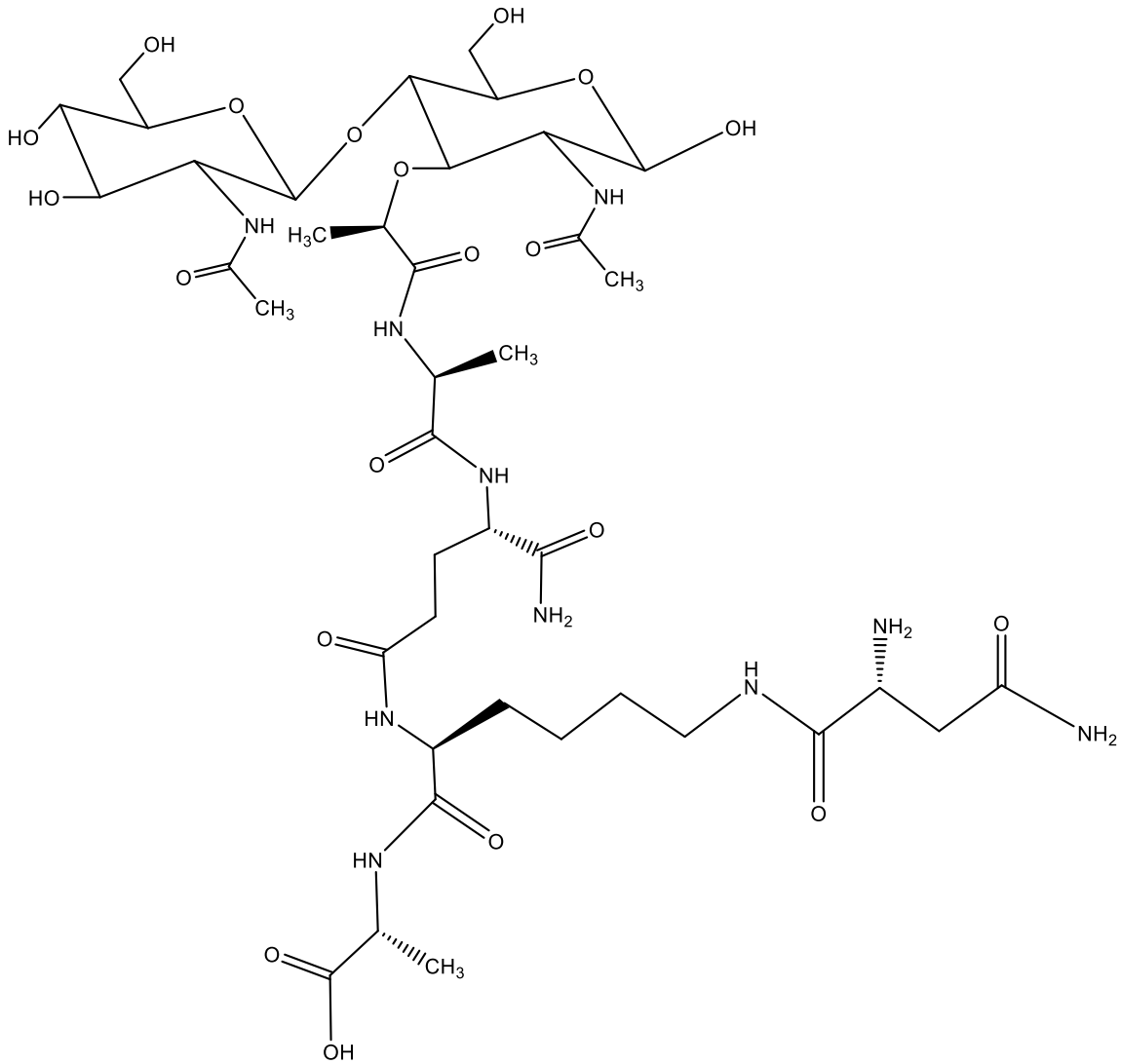

SI Figure 5c: Muropeptide structure corresponding to peak 3.

GlcNAc-MurNAc-L-Ala-D-iGln-L-Lys-(D-Asn)-D-Ala detected in *L. lactis* NZ9000Cm and *L. lactis* NZ9000*Sa*NsrF$_{H202A}$P with *m/z* 1009.45 $[M+H]^+$.

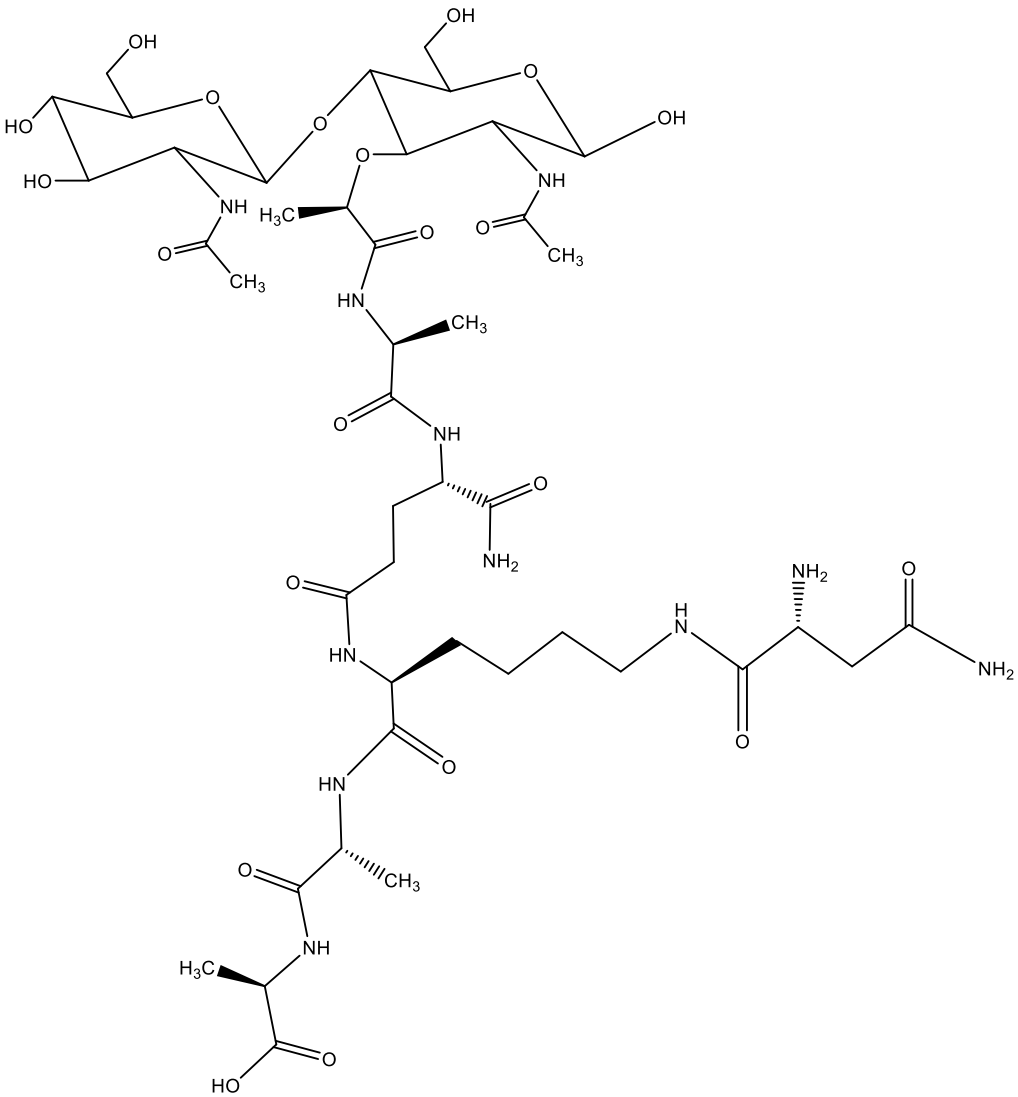

SI Figure 5d: Muropeptide structure corresponding to peak 4.

GlcNAc-MurNAc-L-Ala-D-iGln-L-Lys-(D-Asn)-D-Ala-D-Ala detected in *L. lactis* NZ9000Cm and *L. lactis* NZ9000*Sa*NsrF$_{H202A}$ with *m/z* 1080.50 $[M+H]^+$.

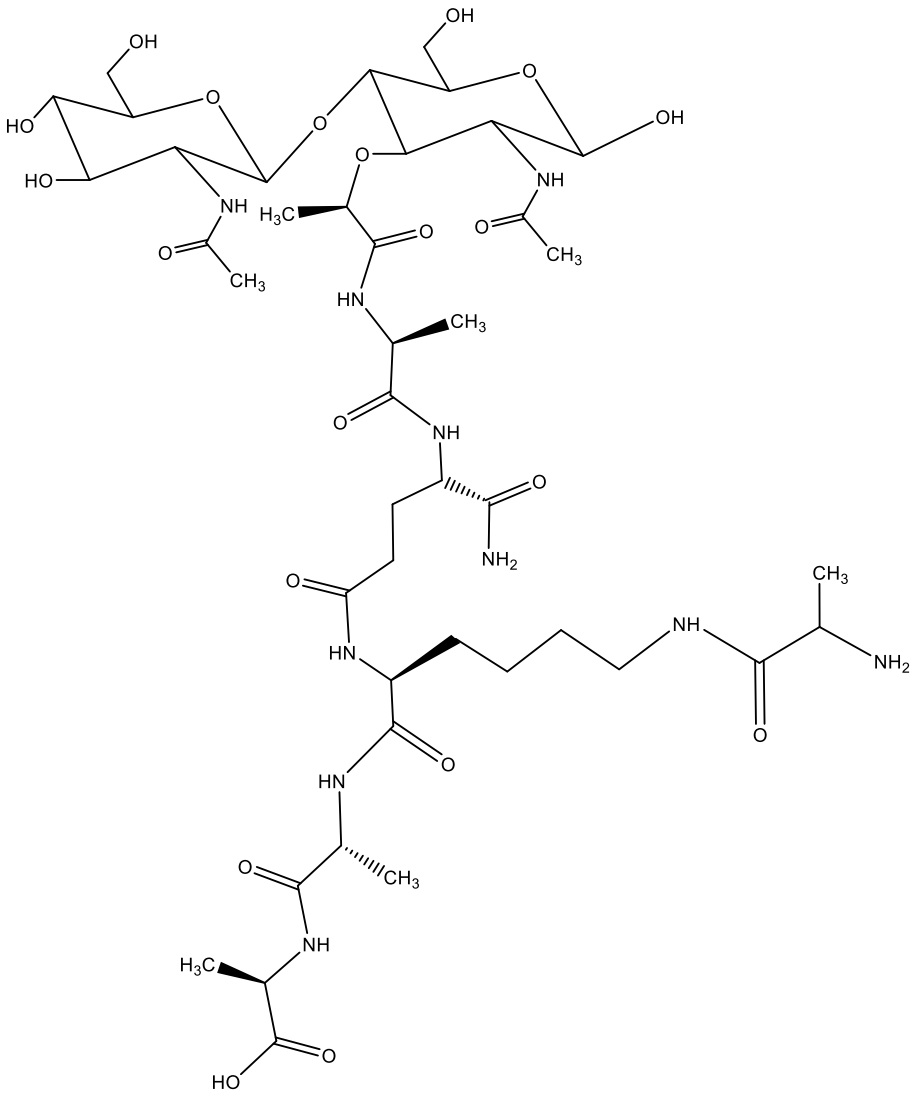

SI Figure 5e: Muropeptide structure corresponding to peak 5.

GlcNAc-MurNAc-L-Ala-D-iGln-L-Lys-(Ala)-D-Ala-D-Ala detected in *L. lactis* NZ9000*Sa*NsrFP with *m/z* 1037.49 $[M+H]^+$.

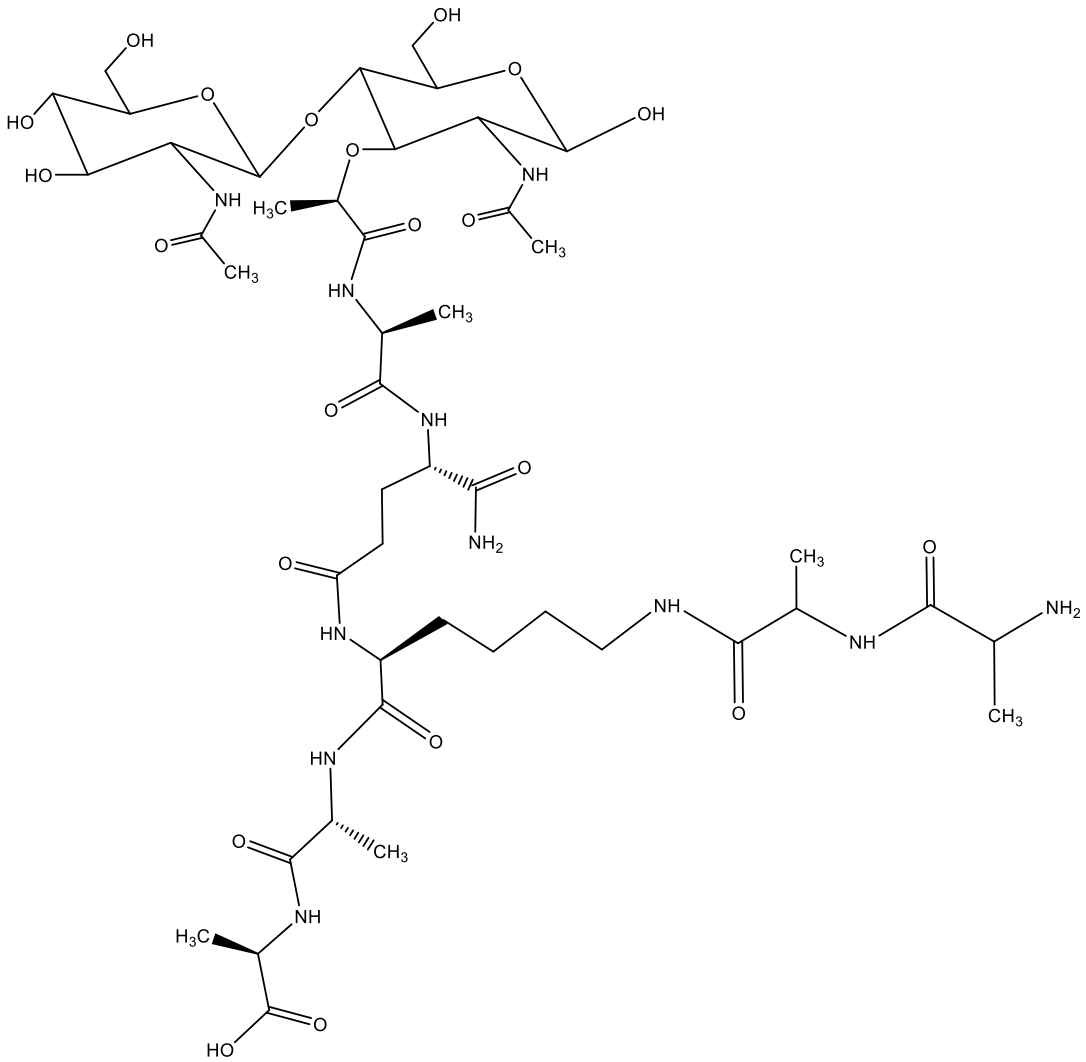

SI Figure 5f: Muropeptide structure corresponding to peaks 6-8.

GlcNAc-MurNAc-L-Ala-D-iGln-L-Lys-(Ala-Ala)-D-Ala-D-Ala detected in *L. lactis* NZ9000*Sa*NsrFP and *L. lactis* NZ9000*Sa*NsrF$_{H202A}$P with *m/z* 1108.53 $[M+H]^+$.

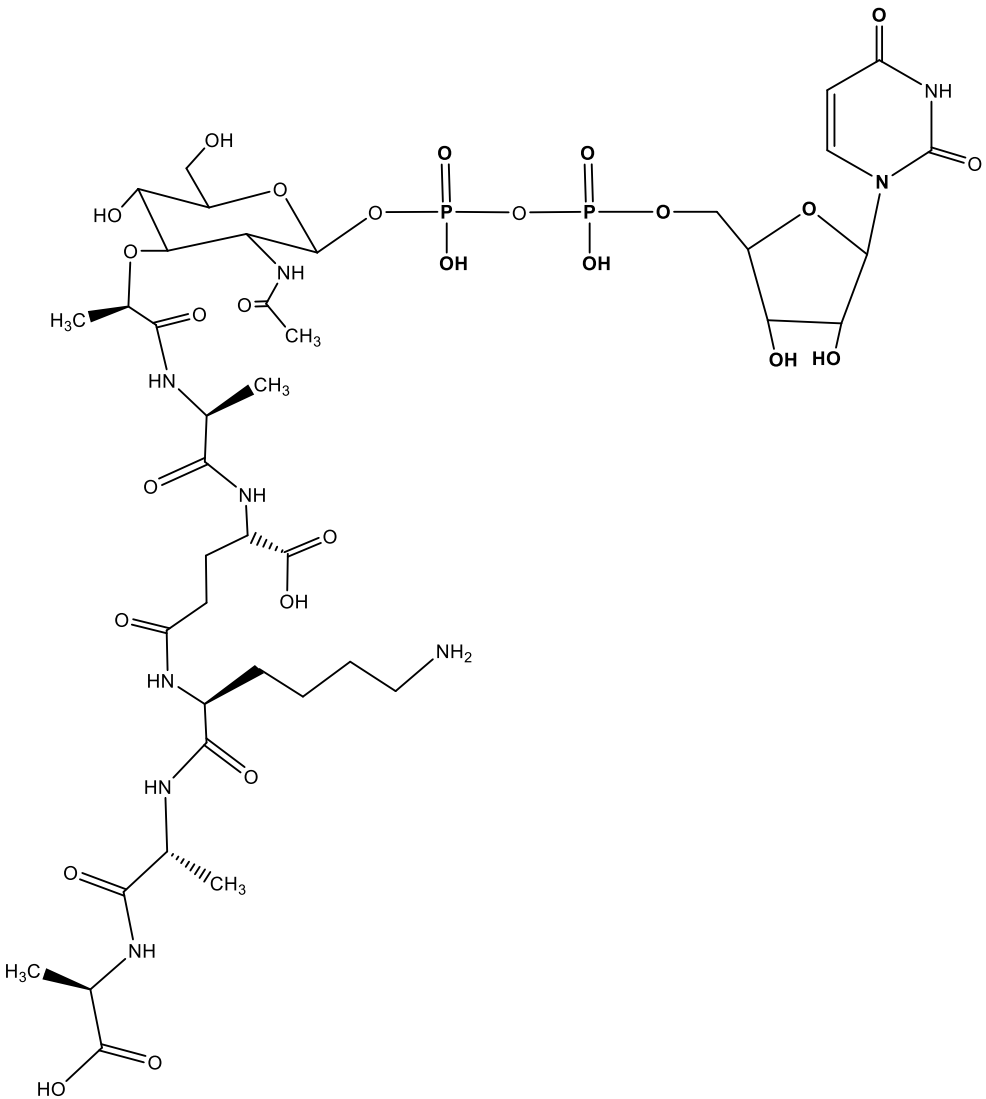

SI Figure 6a: UDP-linked intermediate detected in this study.

UDP-MurNAc-L-Ala-D-iGlu-L-Lys-D-Ala-D-Ala detected in *L. lactis* NZ9000*Sa*NsrF$_{H202A}$P and *L. lactis* NZ9000*Sa*NsrFP with mass m/z-1 (1148.4).

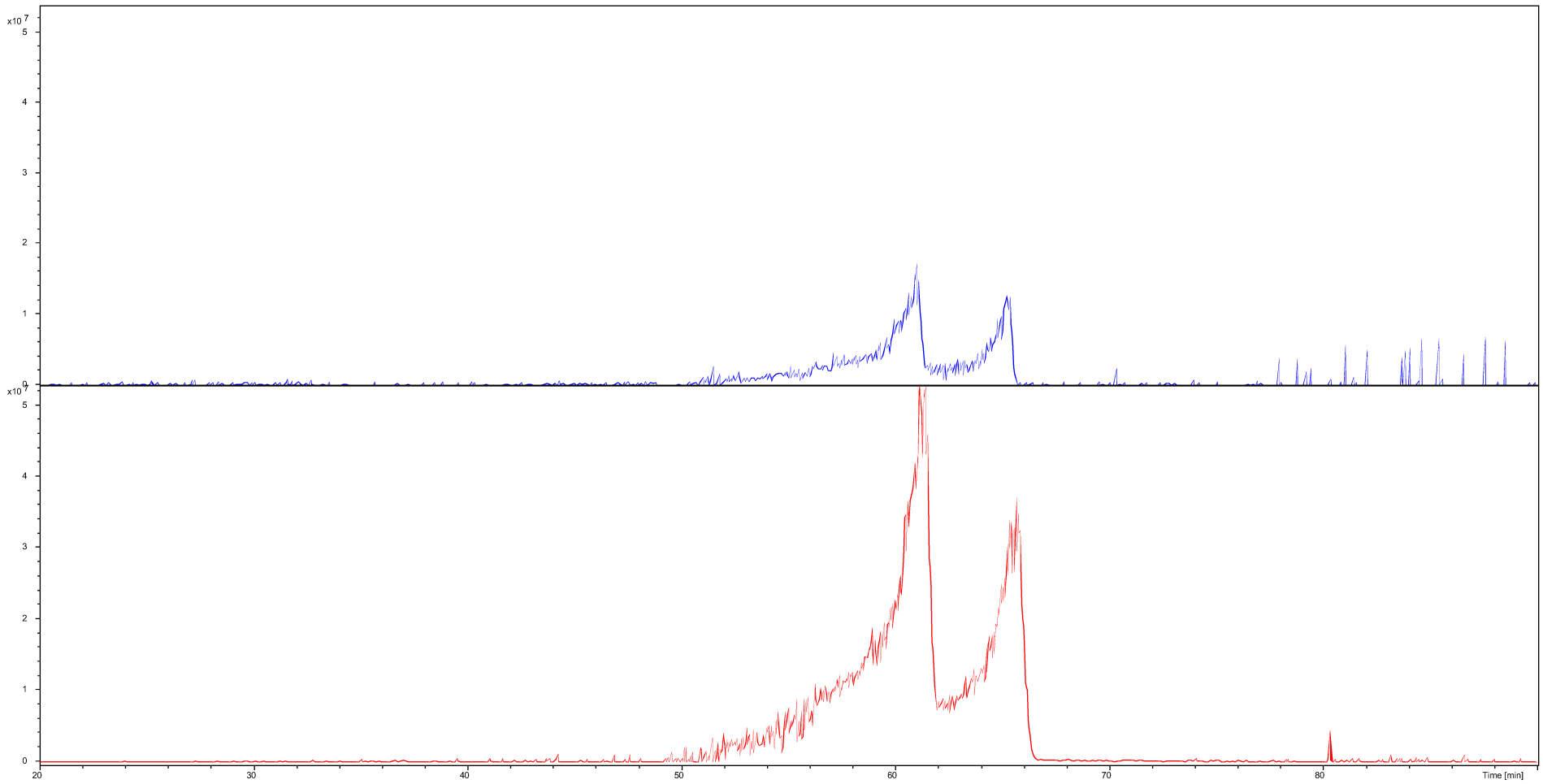

SI Figure 6b: Extracted ion chromatography (EIC) spectrum of UDP-linked intermediate detected in this study.

(EIC) spectrum of UDP-MurNAc-L-Ala-D-iGlu-L-Lys-D-Ala-D-Ala detected in *L. lactis* NZ9000*Sa*NsrF$_{H202A}$P (blue) *L. lactis* NZ9000*Sa*NsrFP (red) with mass m/z-1 (1148.4).

SI Table 1: A two-sided Students t-test was performed using Graphpad Prism version 9.2.0 with the IC_{50} data obtained for *Sa*NsrFP and *Sa*NsrF$_{H202A}$P. P-values were listed. A two-sided, unpaired Students t-test was performed using Graphpad Prism version 9.2.0 for Windows, GraphPad Software, San Diego, California USA, www.graphpad.com".

Antibiotic	p-values ($p<0.05$)
Ramoplanin A2	ns
Vancomycin	0.0228
Lysobactin	0.0076
Bacitracin	0.0001
Bacitracin $ZnCl_2$	<0.0001
Nisin	<0.0001
Gallidermin	<0.0001

3.4 Chapter IV: Lantibiotics

Lantibiotics – Potential Alternative against Antibiotic Resistance
Lantibiotika – hoffnungsvolle Alternative gegen Antibiotikaresistenz

Julia Gottstein[1], Hans Klose[1], C. Vivien Knospe[1], Jens Reiners[2], Sander H. Smits[1,2] & Lutz Schmitt[1]

[1]Institute of Biochemistry, Heinrich-Heine-University Düsseldorf, Düsseldorf, Germany,
[2] Center for Structural Studies, Heinrich-Heine-University Düsseldorf, Düsseldorf, Germany,

Published in: BIOspektrum (2021)

Impact factor: 0.051

Own proportion of this work: 40%

- Writing the manuscript
- Making figures

Antimikrobielle Peptide

Lantibiotika – hoffnungsvolle Alternative gegen Antibiotikaresistenz?

JULIA GOTTSTEIN[1], HANS KLOSE[1], C. VIVIEN KNOSPE[1], JENS REINERS[2], SANDER H. SMITS[1,2], LUTZ SCHMITT[1]
[1] INSTITUT FÜR BIOCHEMIE, UNIVERSITÄT DÜSSELDORF
[2] CENTER FOR STRUCTURAL STUDIES, UNIVERSITÄT DÜSSELDORF

Nisin is one of the most studied lantibiotics which are antimicrobial peptides. Nowadays the knowledge about the Nisin-modification system is profound and can be explored to express and modify lantibiotics with new or specific antimicrobial features. Here we highlight recent advances that include a strategy on bypassing natural occurring resistances against antimicrobial peptides.

DOI: 10.1007/s12268-021-1621-5

Lanthipeptide sind ribosomal synthetisierte und posttranslational modifizierte Peptide, die als Hauptmerkmal (Methyl-)Lanthioninringe besitzen. Im Fall einer antibakteriellen Wirkung werden Lanthipeptide als Lantibiotika bezeichnet [1]. Diese stehen verstärkt im Fokus der Forschung, da oft eine potente, antimikrobielle Wirkung gegenüber humanpathogenen Stämmen vorliegt [2]. Vor dem Hintergrund steigender Antibiotikaresistenzen [3] sind dies wichtige Voraussetzungen für eine Anwendung.

Eines der meist untersuchten Lantibiotika ist Nisin aus dem Gram-positiven Bakterium *Lactococcus lactis*, das seit 1983 (EU) in der Lebensmittelindustrie unter der Bezeichnung E234 [4] verwendet wird. Nisin wirkt, indem es: (I) an Lipid II, eine Zellwandvorstufe, bindet und (II) nach der Bindung Poren in der Membran bildet. Das detaillierte Wissen über das Nisin-Produktionssystem kann daher auch prinzipiell zur Herstellung und Modifikation heterologer Lantibiotika eingesetzt werden [2].

Lantibiotika, generell als LanA bezeichnet, liegen nach ribosomaler Synthese als Vorläuferpeptid vor und bestehen aus einem N-terminalen Signalpeptid (SP) und C-terminalen Kernpeptid (KP). Das SP interagiert mit den Modifikationsenzymen, woraufhin alle Modifikationen im KP stattfinden. Das zweistufige Modifikationssystem des Nisins beinhaltet die Dehydratase NisB sowie die Cyklase NisC (**Abb. 1**). NisB dehydriert die Aminosäuren Serin und Threonin zu Dehydroalanin (Dha) bzw. Dehydrobutyrin (Dhb). Diese dehydrierten Aminosäuren gehen mit räumlich in der Nähe befindlichen Cysteinen eine Michael-Addition ein, die durch NisC katalysiert wird und zur Ausbildung der (Methyl-)Lanthioninringe führt [1, 5]. Nach erfolgreicher Modifikation wird das Peptid mittels eines ABC-Transporters, NisT im Fall von Nisin, exportiert und die Aktivierung erfolgt durch proteolytische Abspaltung des SP durch die Protease NisP (**Abb. 1**, [1, 5]).

Die Aktivierung beinhaltet die Gefahr, dass Nisin zu einem „Selbstmord" des Produzenten führt. Dies wird durch die Immunitätsproteine NisI und NisFEG [6] verhindert. Das Nisinsystem wird durch das Zweikomponentensystem NisR und NisK komplementiert, welches die Expression des Operons reguliert (**Abb. 1**, [7]). Trotz dieser Immunitätsproteine haben sich weitere Resistenzsysteme gegen Lantibiotika entwickelt, die einen möglichen Ansatzpunkt zur Bekämpfung darstellen.

Umgehung der Resistenz gegenüber Lantibiotika

Humanpathogene Bakterien besitzen unterschiedliche Abwehrsysteme gegen Lantibiotika. Ein Beispiel ist das Nsr-Operon aus *Streptococcus agalactiae*. Durch die dort codierten Proteine besitzt das Bakterium zwei Möglichkeiten zur Abwehr: (I) durch Nutzung eines Transporters oder (II) proteolytischen Abbau. Das Nsr-Operon wird durch die Anwesenheit eines Zweikomponentensystems, eines BceAB-Typ-ABC-Transporters (SaNsrFP) und einer Serinprotease (SaNsr) charakterisiert. Nsr erkennt die C-terminalen Ringe D und E des Nisins und inaktiviert es durch Abspaltung der letzten sechs Aminosäuren, welche die antibakterielle Wirkung um den Faktor 10^2 reduzieren [8]. Da diese Resistenzproteine die Wirkung von Lantibiotika inhibieren, wurden zwei Ansätze gewählt, um ihre Funktion zu umgehen: (I) Inhibition der Resistenzproteine und (II) Entwicklung von inerten Varianten.

Spezifische Inhibitoren würden die Resistenz eines humanpathogenen Bakteriums aufheben. Als Startpunkt wurden daher Inhibitoren evaluiert, die vergleichbare Struktureigenschaften wie der Erkennungsbereich des Nisin besitzen. Ein Phenylharnstoffderivat (SaNSR) konnte als spezifischer Nsr-Inhibitor mittels Dosis-Wirkungs-Analysen identifiziert werden (**Abb. 2**, [9]). Dieses Beispiel belegt das Potenzial derartiger Ansätze, um Inhibitoren zu identifizieren.

Ein anderer Ansatz, die Lantibiotikaresistenz zu umgehen, ist die genetische Veränderung bekannter Lantibiotika. Eine Studie konnte zeigen [10], dass die Veränderung einer einzigen Aminosäure in Nisin H (*S. hyotintestinalis* DPC 6484) die Wirksamkeit gegen Resistenzproteine oder resistente Pathogene beeinflussen kann. Hierzu wurde Position 1 durch Valin substituiert und die antimikrobiellen Eigenschaften untersucht (**Abb. 3**). Die Mutante besaß ein leicht gesteigertes Potenzial gegen SaNsr/NsrFP-exprimierende *Lactobacillus lactis*-Stämme. Gegen humane Pathogene wie *Staphylococcus aureus* oder *Enterococcus faecium* konnte sowohl für Nisin H als auch seine Variante im Vergleich zu Nisin eine erhöhte Aktivität nachgewiesen werden. Diese Studie demonstriert, dass biotechnologische Ansätze die Antibiotikaresistenz humanpathogener

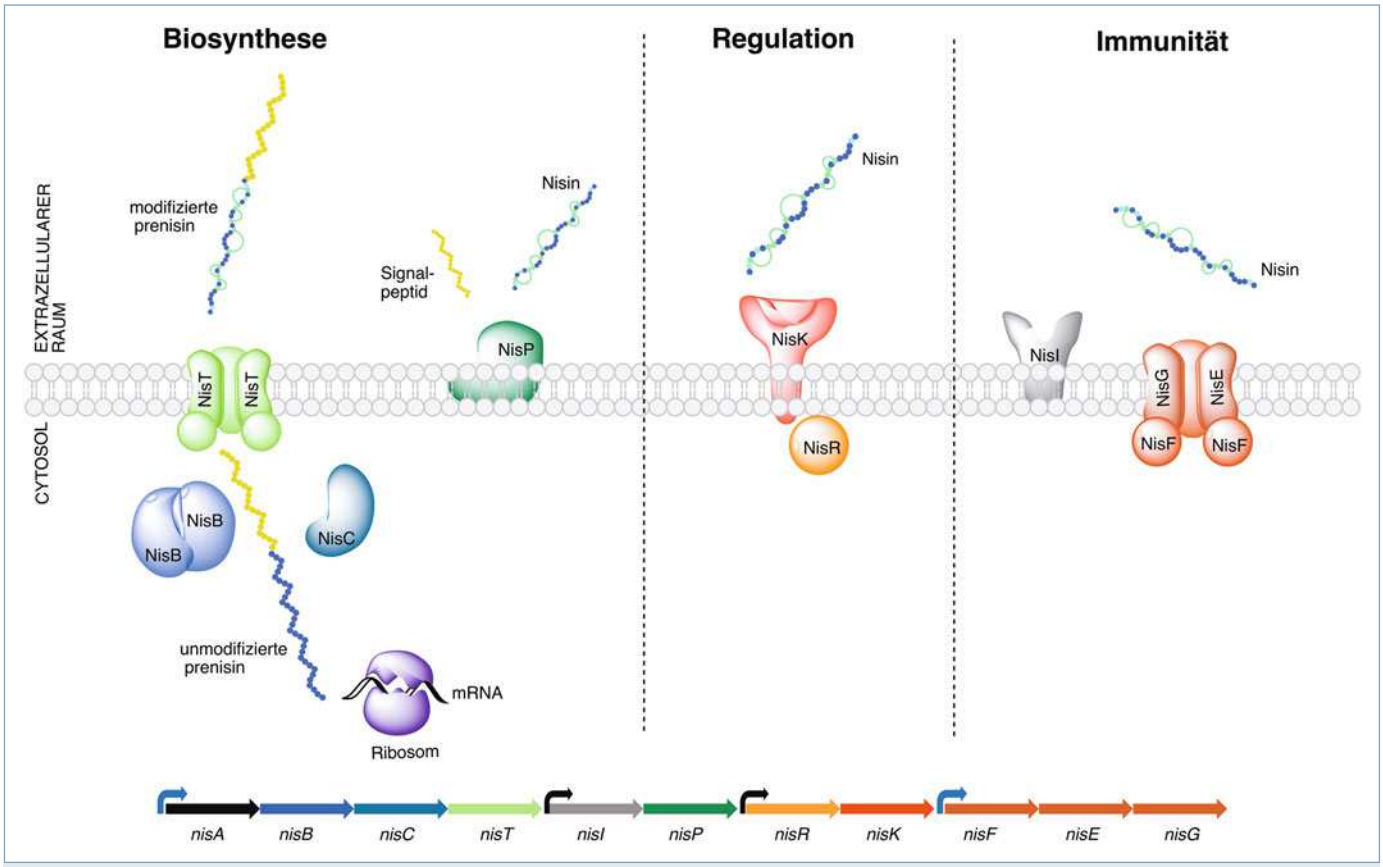

▲ **Abb. 1:** Das Nisin-Operon aus *Lactococcus lactis.* Die Proteine der Biosynthese NisB (blau), NisC (türkis), NisT (grün) und NisP (dunkelgrün) sind links abgebildet. Die Regulationsproteine NisK (rot) und NisR (orange) befinden sich im mittleren Teil, während die Immunitätsproteine NisI (grau) und NisFEG (braun) rechts dargestellt sind. NisB katalysiert die Dehydrierung der Aminosäuren Serin und Threonin innerhalb des Kernpeptids von pre-Nisin, welche in ihrer dehydrierten Form zur Ringbildung durch die Cyclase NisC mit den enthaltenen Cysteinen genutzt werden. Zur vollen Entfaltung der Aktivität wird pre-Nisin mithilfe eines ABC-Transporters (NisT) exportiert und das Signalpeptid durch die Protease (NisP) entfernt. Aktives Nisin wird durch die Immunitätsproteine (NisI und NisFEG) inaktiviert, während das Zweikomponentensystem (NisK und NisR) in Gegenwart ausreichender Konzentration von Nisin die Expression der Proteine des Nisin-Operons induziert.

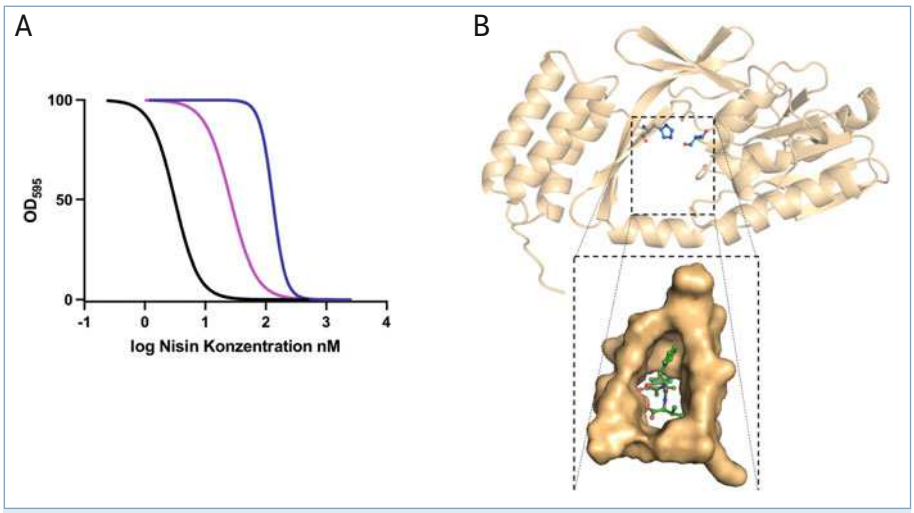

▲ **Abb. 2:** Umgehung der Resistenz durch einen Inhibitor. **A**, Schema der Dosis-Wirkungs-Kurven für einen SaNSR-exprimierenden Stamm (blau) und einen Kontrollstamm (schwarz) im Vergleich zu einem SaNSR-Stamm, der mit einem Inhibitor und Nisin behandelt wurde (pink). **B**, Darstellung der Struktur von SaNsr und seiner Bindetasche (gold) mit dem bindenden Inhibitor NPG9 (grün). SaNsr mit seiner katalytische Dyade His98 und Ser236 ist im Hintergrund gezeigt. Im Ausschnitt ist die Oberflächenstruktur der Bindetasche von SaNsr mit gebundenem Inhibitor (grün) dargestellt.

Bakterien teilweise oder ganz aufgeheben können und eine Alternative darstellen, das akute Problem zunehmender Antibiotikaresistenzen zu umgehen.

Biotechnologische Optimierung von Nisin

Als dritte Möglichkeit kann eine biotechnologische Optimierung durchgeführt werden. Am Beispiel des Nisins wurde hierzu ein rationaler Ansatz mittels Punktmutationen verfolgt. Eine Mutation von Cystein an Position 28 zu Alanin verhindert die Ausbildung des letzten Lantioninrings (Ring E), wodurch die Fähigkeit des Resistenzproteins Nsr, diese Variante zu erkennen, sinkt. Aber auch die antimikrobielle Aktivität war reduziert. In einem zweiten Schritt wurde daher Cystein zu Prolin verändert (**Abb. 3**). In dieser Mutante blieb die antimikrobielle Aktivität erhalten, während die Nsr-Resistenz weiterhin reduziert war. Experimentell konnte zudem gezeigt werden, dass Nisin C28P

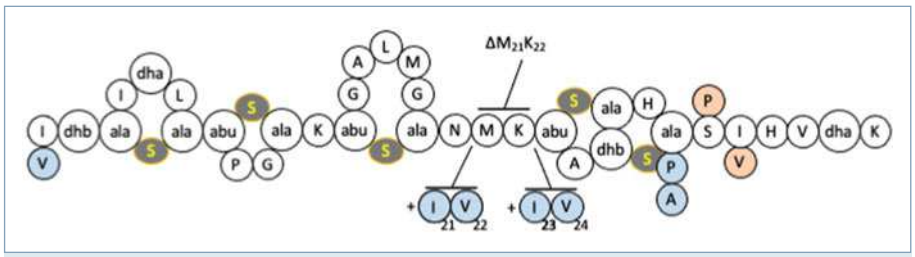

▲ **Abb. 3:** Nisin A. In blau sind die Mutationen durch rationales Design hervorgehoben: Der Austausch von Isoleucin (I) zu Valin (V) an Position 1, die Veränderung von Cystein28 zu Alanin (A) und Prolin (P) sowie die Addition von Isoleucin und Valin in der Scharnier-Region. Reste, die einer Sättigungsmutagenese unterworfen wurden, sind orange dargestellt. Zur Verdeutlichung wurden ebenfalls die deletierten Aminosäuren Methionin (M) und Lysin (K) in der Scharnier-Region markiert.

nicht nur eine antibakterielle Wirkung gegen *L. lactis*, sondern auch gegen nosokomiale *S. aureus* und *E. faecalis* Stämme besaß [11].

Über eine Sättigungsmutagenese an Position 2 konnte die Expression bei gleichbleibender biologischer Aktivität auf das Niveau des Nisins angehoben werden. Diesmal wurde neben Position 29 auch Position 30 verändert (**Abb. 3**). Die beste Variante, NisinA_S29P_I30V, besaß eine 7,5fach höhere Aktivität gegenüber *L. lactis*. Viel wichtiger, diese Variante besaß im Gegensatz zu Nisin eine antimikrobielle Aktivität gegen lantibiotikaresistente *Streptococcus uberis*- und *Enterococcus casseliflavus*-Stämme [12].

Neben Ring E ist die Scharnier-Region von Interesse. Diese Region ist für die Porenbildung von Nisin essenziell und wurde als wichtiger pharmazeutischer Hotspot identifiziert. Deletionsmutanten belegten, dass eine Kürzung der Scharnier-Region zu einer Versteifung von Nisin führt (**Abb. 3**). Dadurch kann nach Bindung an Lipid II keine Pore in der Zellmembran ausgebildet werden. Eine Verlängerung dieser Region durch die Aminosäuren Isoleucin (I) und Valin (V) wies jedoch wie Nisin ein Wirkspektrum im nanomolaren Bereich auf – und Porenbildung, wenn auch verlangsamt, wurde ebenfalls nachgewiesen. Der Einfluss dieser Mutationen auf Resistenzmechanismen wurde anhand zweier Modeltransporter untersucht: NisFEG (Immunität) und SaNsrFP (Resistenz). In beiden Fällen blieb die antimikrobielle Wirkung erhalten, während die Erkennung durch NisFEG und SaNsrFP ineffizient erfolgte [11].

Diese Zusammenfassung belegt hoffentlich, dass Lantibiotika ein enormes Potenzial besitzen, das sicherlich durch biotechnologische Ansätze gesteigert werden kann. Eventuell eröffnet sich damit auch die Möglichkeit, Lantibiotika großflächig gegen Bakterien einzusetzen ohne neue Resistenzen zu generieren.

Danksagung

Wir danken allen Mitarbeitern/innen des Instituts für Biochemie und der DFG für finanzielle Unterstützung (Schm1279/13-1 (L.S.) und GRK2158 (S.S.)). ■

Literatur

[1] Repka LM, Chekan JR, Nair SK, van der Donk WA (2017) Mechanistic understanding of lanthipeptide biosynthetic enzymes. Chem Rev 117: 5457–5520
[2] van Heel AJ, Kloosterman TG, Montalban-Lopez M et al. (2016) Discovery, production and modification of five novel lantibiotics using the promiscuous nisin modification machinery. ACS Synth Biol 5: 1146–1154
[3] Cotter PD, Ross RP, Hill C (2013) Bacteriocins – a viable alternative to antibiotics? Nat Rev Microbiol 11: 95–105
[4] Cotter PD, Hill C, Ross RP (2005) Bacteriocins: developing innate immunity for food. Nat Rev Microbiol 3: 777–788
[5] van den Berg van Saparoea HB, Bakkes PJ, Moll GN, Driessen AJ (2008) Distinct contributions of the nisin biosynthesis enzymes NisB and NisC and transporter NisT to prenisin production by *Lactococcus lactis*. Appl Environ Microbiol 74: 5541–5548
[6] Alkhatib Z, Abts A, Mavaro A et al. (2012) Lantibiotics: how do producers become self-protected? J Biotechnol 159: 145–154
[7] Kuipers OP, Beerthuyzen MM, de Ruyter PG et al. (1995) Autoregulation of nisin biosynthesis in *Lactococcus lactis* by signal transduction. J Biol Chem 270: 27299–27304
[8] Khosa S, Frieg B, Mulnaes D et al. (2016) Structural basis of lantibiotic recognition by the nisin resistance protein from *Streptococcus agalactiae*. Sci Rep 6: 18679
[9] Porta N, Zaschke-Kriesche J, Frieg B et al. (2019) Small-molecule inhibitors of nisin resistance protein NSR from the human pathogen *Streptococcus agalactiae*. Bioorg Med Chem 27: 115079
[10] Reiners J, Lagedroste M, Gottstein J et al. (2020) Insights in the antimicrobial potential of the natural nisin variant nisin H. Front Microbiol 11: 573614
[11] Zaschke-Kriesche J, Reiners J, Lagedroste M, Smits S H J (2019) Influence of nisin hinge-region variants on lantibiotic immunity and resistance proteins. Bioorg Med Chem 27: 3947–3953
[12] Field D, Blake T, Mathur H et al. (2019) Bioengineering nisin to overcome the nisin resistance protein. Mol Microbiol 111: 717–731

Korrespondenzadresse:
Prof. Dr. Lutz Schmitt
Institut Biochemie I
Heinrich-Heine-Universität Düsseldorf
Universitätsstraße 1
D-40225 Düsseldorf
lutz.schmitt@hhu.de
www.biochemistry1.hhu.de

Oben: Lutz Schmitt, Vivien Knospe und Hans Klose (v. l. n. r.), unten: Jens Reiners, Sander Smits und Julia Gottstein (v. l. n. r.).

3.5 Chapter V: BceAB Transporter

BceAB transport is more widely distributed than expected

Julia Gottstein[1], Christian Mammen[1], Pablo Cea Medina[3], Kira Tantsur[1], Jens Reiners[2], Holger Gohlke[3], Sander H. J. Smits[1,2*]

[1]Institute of Biochemistry, Heinrich-Heine-University Duesseldorf, Universitätsstrasse 1, 40225 Duesseldorf, Germany.
[2]Center for Structural Studies, Heinrich-Heine-University Duesseldorf, Universitätsstrasse 1, 40225 Duesseldorf, Germany.
[3]Institute of Pharmaceutical and Medicinal Chemistry, Heinrich-Heine-University Düsseldorf, Universitätsstrasse 1, 40225 Düsseldorf

In preparation

Own proportion of this work: 40%

- Cloning
- Established the purification protocol
- Biological assays
- Preparation of figures
- Writing the manuscript

BceAB transport is more widely distributed than expected

Julia Gottstein[1], Christian Mammen[1], Pablo Cea Medina[3], Kira Tantsur[1], Jens Reiners[2], Holger Gohlke[3], Sander H. J. Smits[1,2*]

[1]Institute of Biochemistry I, Heinrich Heine University Düsseldorf, Düsseldorf, Germany.
[2]Center for Structural Studies, Heinrich Heine University Düsseldorf, Düsseldorf, Germany.
[3]Institute of Pharmaceutical and Medicinal Chemistry, Heinrich-Heine-University Düsseldorf, Düsseldorf, Germany

[*] To whom correspondence should be addressed:

Sander Smits
Institute of Biochemistry
Heinrich Heine University Düsseldorf
Universitätsstr. 1
40225 Düsseldorf, Germany
Phone: +49(0)211-81-12647
Fax: +49(0)211-81-15310
Email: sander.smits@hhu.de

Abstract:

It is of utmost importance for bacteria to sense and adapt rapidly to environmental changes. In the case of an antimicrobial attack, the bacterial cell needs to accurately assess the severity of the situation to react with a minimized metabolic cost and ensure survival. Immediate reactions require most likely two-component systems that induce transcriptional changes, leading to modulation of gene expression

Moreover, in human pathogenic bacteria, gene clusters were identified, encoding for a resistance system, containing membrane-embedded proteins, that include a Bacitracin efflux (BceAB)-type ATP-binding cassette transporter. One example is *Streptococcus agalactiae* which expresses the BceAB-type transporter *Sa*NsrFP that confers resistance against multiple antimicrobial peptides and mainly against bacitracin. The characteristic of BceAB type transporter is a transmembrane consisting of 10 transmembrane helices and between the seventh and the eighth there is a large extracellular domain that is hypothesized to be involved in sensing the antimicrobial peptide. We show that BceAB-type transporter are more widely distributed and that a BceAB-like transporter with an extra ECD between transmembrane helix 1 and 2 (also known as YbbP) can be found in all clinically relevant ESKAPE organisms. By comparing the ECDs of 27 BceB permeases, we could assign them to five subgroups with conserved secondary structures in the SABRE and Porter domains.

To elucidate the structure-function relationship of the ECD and its role for the ABC transporter *Sa*NsrFP, we expressed, purified, and analyzed the ECD of *Sa*NsrP from S. agalactiae via MALS, SAXS and measured intrinsic tyrosine fluorescence. We show that the ECD binds Zn-bacitracin and bacitracin. By performing a docking experiment on the ECD, we found that K481 in the ECD is possibly involved in binding. *In vivo* experiments showed that when an *L. lactis* NZ9000 strain expresses *Sa*NsrFP(K481A) and is treated with bacitracin or Zn-bacitracin, the ABC transporter was not able to confer resistance.

Introduction:

It is of utmost importance for bacteria to sense and adapt rapidly to environmental changes. To survive, microbial cells need to constantly monitor various parameters i.e nutrient supply, the concentration of ions, oxygen levels, pH, temperature, cell densities, and the presence of toxic compounds. In the case of an antimicrobial attack, the bacterial cell needs to accurately assess the severity of the situation to react with a minimized metabolic cost and ensure survival. Immediate reactions require most likely two-component systems that induce transcriptional changes, leading to modulation of gene expression (Fritz *et al*., 2015, Tollerson and Ibba, 2020). There are different methods of how a stimulus can be monitored by the cell: I) i.e in *Bacillus subtilis* cell wall damage is monitored by the cell envelope stress response system LiaRS (Wolf *et al*., 2012) II) in *Streptomyces coelicolor*, the histidine kinase VanS senses vancomycin by binding it via its extracellular domain and induces the expression of resistance genes (Lockey *et al*., 2020).

Moreover, in human pathogenic bacteria, gene clusters were identified, encoding for a resistance system, containing membrane-embedded proteins, that include a Bacitracin efflux (BceAB)-type ATP-binding cassette transporter. Genome analysis revealed the presence of homologous transporters mainly in soil and human pathogenic Gram-positive bacteria (Dintner *et al*., 2011). Recently, the cryo-electron microscopy structure of BceAB was published (George *et al*., 2022). It consists of two nucleotide-binding domains in a complex with a single transmembrane domain. which is composed of 10 transmembrane helices (TMH). TMH 1 to 4 (grey) and TMH 7 to 10 (blue) form bundles that are related by two-fold pseudosymmetry, representing an FtsX-domain fold similar to type VII ABC transporters which are involved in mechanotransmission (Thomas *et al*.,

2020). The overall arrangement of the TMHs of BceB is asymmetrical due to the close position of TMH 5 and 6 to TMH 7 to 10 than to the other TMH bundle (George *et al*., 2022). TM 7 and TM8 form longer and extended stalk helices that lead into the 200-250 amino acid large extracellular domain (ECD) which is the hallmark of Bce-type transporters (Khosa *et al*., 2013). Since BceAB confers resistance against bacitracin, it is proposed that it detects the complex of bacitracin and undecaprenylpyrosphate (UPP). In the structure of BceAB, between its TMH 5,6 and TMH 7,9, a hydrophobic lipid-binding pocket with a suggested bound UPP derivate 4-amino-4-deoxy-L-arabinopyranosyl undecaprenyl phosphate (AUP) (orange) was identified which is situated directly beneath the ECD (George *et al*., 2022). It is proposed that most likely native UPP and other UPP-lipid derivates can bind to this binding site. This suggests that the ECD binds bacitracin when bound to UPP (Kobras *et al*., 2020).

Recently a high level of resistance against bacitracin was observed for the BceAB transporter from *S. agalactiae* COH1, *Sa*NsrFP which was previously found to mediate resistance against lantibiotics like nisin (Gottstein *et al*., 2022, Reiners *et al*., 2020). *Sa*NsrFP shows a very similar structure, while sequence similarity is low (**Permease** cealign RMSD 5.228 (408 atoms), super align with outlier (3.647 (2934 atoms))/ without outlier: 5.452 (3471atoms))

(**TMD**: cealign RMSD 3.233 (416atoms), (outlier rejection) super align RMSD 2.780 (2244atoms), no outlier super align: 3.959 (2611 atoms). *Sa*NsrFP looks structurally very similar to BceAB (Figure 15a).

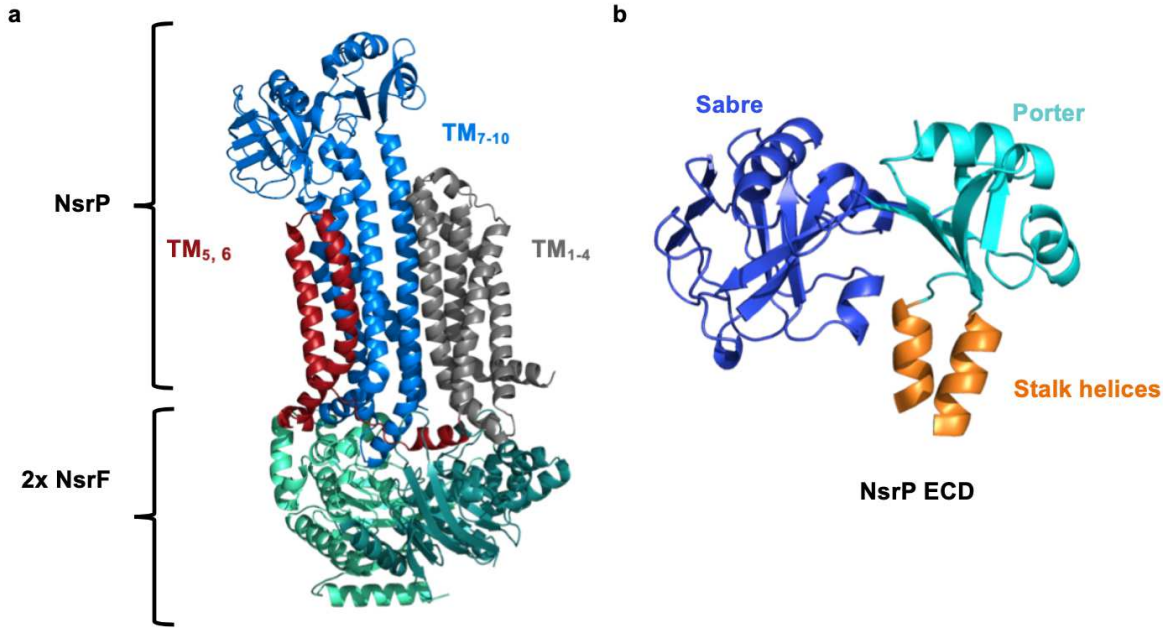

Figure 15 a) Alphafold model of the SaNsrFP transporter. The transporter consists of two nucleotide-binding domains NsrF (greencyan & tealblue) and forms a complex with NsrP which contains 10 transmembrane helices. TMH 5,6 (red) and TMH 7,9 (blue) create a hydrophobic pocket where the substrate of NsrP i.e a lipid could bind. TMH 1 to 4 (grey) are more distant from the extracellular domain. **b:** Alphafold model of NsrP ECD. The ECD of *Sa*NsrFP can be divided into subdomains: in dark blue a small alpha/beta rich extracytoplasmic (SABRE) domain, a porter domain with a repeated motif on either side of the SABRE domain (light blue), and stalk helices (in orange). Structures were modeled using alphafold (Jumper *et al*., 2021).

The transporter consists of two nucleotide-binding domains NsrF (greencyan & tealblue) and forms a complex with NsrP which contains 10 transmembrane helices. TMH 5,6 (red) and TMH 7,9 (blue) create together a hydrophobic pocket where a lipid could bind. TMH 1 to 4 (grey) is more distant from the extracellular domain which creates an asymmetric architecture (Figure 15a).

Part of the *bce* operon is a co-evolved BceRS-type TCS, a response regulator, and an intramembrane-sensing histidine kinase (HK) with a short extracellular domain of ca. 25 amino acids (Mascher et al., 2003, Rietkotter et al., 2008, Mascher, 2006). The function of the TCS has been shown to be associated with the upregulation of the corresponding ABC transporter in the presence of its specific lantibiotic (Staron *et al*., 2011). When the substrate binds, the BceAB type transporter transmits a signal to the histidine kinase which leads to phosphorylation of its cognate response regulator, inducing the expression of the BceAB ABC transporter genes. This process was described for the detoxification system GraRS-VraFG in *S. aureus* (Cho *et al*., 2021) and various TCS-ABC

transporters in *B. subtilis (*BceRS-AB, YxdJK-LM, and YvcPQ-RS) (Dintner *et al*., 2011, Fritz *et al*., 2015). For the BceAB transporter, it was shown that antimicrobial activity depends on ATP-hydrolysis of the ATPase BceA (Rietkotter et al., 2008) as well as the complex formation with BceRS (Dintner *et al*., 2014). The cognate Histidine-kinases of these TCS-ABC transporter systems lack an extracellular domain which disables them to detect extracellular stimuli (Mascher, 2006). Moreover, it has been shown with medically and biotechnologically relevant Gram-positive species that BceS-like HKs require BceAB-type transporters for antibiotic signaling (Gebhard, 2012, Revilla-Guarinos *et al*., 2014). This is supported by the observation that the associated sensor kinase BceS is unable to detect bacitracin in the absence of the transporter BceAB (Bernard *et al*., 2007). By treating a bacterial strain that does not contain BceAB but carries a bceA:lacZ transcriptional fusion with bacitracin, the authors showed that the BceAB transporter is required to trigger transcription from its own promotor in the presence of bacitracin (Bernard *et al*., 2007). This led to the proposition that the transporter contains the involved sensory domain of the system. More recently, the binding of the AMP LL-37 to the ECD of the BceAB homolog VraG was described in *B. subtilis (*Cho *et al.,* 2021*).*

Major efforts have been made to unravel the mechanism for BceAB-type transporters. Proposals ranged from AMP removal from the membrane (Gebhard and Mascher, 2011), functioning as an exporter (Reiners *et al*., 2017), to flipping the UPP (Kingston *et al*., 2014). A more recent study postulated a target-AMP dissociative, ATP-hydrolysis-driven mechanism for BceAB-type transporters, in which the target-AMP complex is recognized and UPP physically released from the grip of bacitracin (Kobras *et al*., 2020).

Current previous work could show that the BceAB-type transporter *Sa*NsrFP from *Streptococcus agalactiae* is able to sense antimicrobial peptides without its cognate two-component system and defend the cell wall by an active process that leads to high bacitracin resistance. Furthermore, a secondary defense mechanism is initiated that leads to the modification of the peptidoglycan, thus repelling positively charged lantibiotics like nisin, gallidermin, lysobactin, and vancomycin (Gottstein *et al*., 2022, Reiners *et al*., 2017). It was proven that these mechanisms are ATP-hydrolysis dependent by using an ATP-hydrolysis deficient

mutant of *Sa*NsrFP termed *Sa*NsrF$_{H202A}$P that showed no ATPase function *in-vitro* (Furtmann *et al*., 2020). To initiate resistance, the 230 amino acids large extracellular domain of *Sa*NsrP, is supposed to be involved in binding the antimicrobial peptide, most likely bacitracin. Mutational experiments replacing the ECD of VraG in *S. aureus* with its counterpart from VraE, responsible for bacitracin resistance, led to enhanced bacitracin resistance in VraG and increasing sensitivity to colistin (Falord *et al*., 2012, Hiron *et al*., 2011, Cho *et al*., 2022). This indicates that the ECD dictates the specificity and resistance against antimicrobial peptides. Moreover, it was demonstrated that the lysine residues play an important role in interacting with the negatively charged residues of the 9 amino acids small ECD of GraS (Cho *et al*., 2022). Especially, the lysine residue K380 of VraG was identified in the same study to be responsible for modulating the sensing of antimicrobial peptides like LL-37.

The role of the ECD is intriguing and we set out to analyze the mode of action in relation to its architecture. Interestingly, the ECD shows only low sequence similarity with other ECDs from BceAB-like ABC transporters (Khosa *et al*., 2013). Thus, we compared the overall structure of various BceAB-like ECDs to each other. The composition of BceAB-type ECDs is comparable to that of Gram-Negative mechanotransmission ABC transporters (George *et al*., 2022). These consist of a small alpha/beta-rich cytoplasmic region, a porter domain with a repeated motif at either side of the SABRE domain, and stalk helices (Crow *et al*., 2017, Bilsing *et al*., 2023). Similarly, the ECD of NsrP contains a small alpha/beta-rich extracytoplasmic region (SABRE) (dark blue), a porter domain showing a ß-a-ßß /turn-alpha-ß (light blue) motif (light blue), and stalk helices (in orange) (Figure 15b).

In this study, we aim to elucidate the structure-function relationship of the ECD and its role in the ABC transporter *Sa*NsrFP via *in vivo* and *in vitro* experiments.

Experimental procedures:

Databank search in structural model data bank from Alphafold.

Alphafold databank was screened for BceAB type ABC transporters. Parameters that were looked for were the characteristic domain architecture found for BceAB transporters of 10 transmembrane helices and a large extracellular domain (150 -250 amino acids) located in between transmembrane helices 7 and 8 (Mascher *et al*., 2008; Collins *et al*., 2010). Furthermore, the nucleotide-binding domain

BceA should be located next to the gene encoding the transmembrane protein. BceB permease models were found under different names such as BceB, Bacitracin-export permease, FtsXlike-Permease, FtsX domain-containing protein, and YbbP.

Cloning and heterologous expression in *Lactococcus lactis* NZ9000.

The plasmids pIL-SV *Sa*NsrFP were generated by cloning *nsrfp* from *S. agalactiae* COH1 as described in (Alkhatib *et al.* 2014) and (Reiners *et al.* 2017). The substitution of lysine at position 481 and 513 to alanine/glutamate was performed by site-directed mutagenesis. Here, we used the following primers

K481A forward: 5´- AAAACCTTTGCAGCATATTTGGATTTGAATAG-3´; K481A reverse: 5´- GGAAAAGTATTGATGTTCTTAG-3´

K481E forward: 5´- AAAACCTTTGAAGCATATTTGGATTTG-3´

K481 E reverse: 5´- GGAAAAGTATTGATGTTCTTAG-3´

K513 A forward: 5´- CGACATAATAGAGGTAGATGGTAAGTATGTT-3´

K513 A reverse: 5´-TATTAGCACTGCACAGAGTTTTCTAAAAG-3´

K513 E forward: 5´- CGACATAATAGAGGTAGATGGTAAGTATGTT-3´

K513 E reverse: 5´-TTTCCAACATACTTACCATC-3´

Each plasmid and the empty vector pIL-SVCm were transformed into electrocompetent *L. lactis* NZ9000 cells (Holo & Nes *et al*., 1989), and the resulting strains were termed NZ9000*Sa*NsrFP, NZ9000*Sa*NsrFP(K481A), NZ9000*Sa*NsrFP(K481E), NZ9000*Sa*NsrFP(K513A), NZ9000*Sa*NsrFP(K513E), NZ9000*Sa*NsrFP(K481A, K513A), NZ9000*Sa*NsrFP(K481E, K513E) and NZ9000Cm.

The strains NZ9000*Sa*NsrFP and NZ9000Cm have been described in previous publications (Reiners *et al*., 2017), (Alkhatib *et al*., 2014). The mutant strains were generated for this study.

The *L. lactis* strains NZ9000*Sa*NsrFP and NZ9000*Sa*NsrFP (mutants) were cultured in GM17 medium containing 5–10 µg/ml chloramphenicol. Expression was induced by adding 0.3 nM nisin, and cultures were grown at 30 °C. To analyze the expression, cultures were grown until an OD_{600} of 1 and subsequently harvested using a centrifugation step for 30 min at 5000×*g*. The pellets were resuspended to an OD_{600} of 300 in resuspension buffer (50 mM HEPES pH 8.0, 150 mM NaCl, 10% glycerol), then 1/3 (w/v) 0.5 mm glass beads were added. The cells were lysed, and the supernatant was separated from cell debris as well

as glass beads by centrifuging at 10,000×*g*. Subsequently, the membranes were harvested from the supernatant by a 100,000×*g* centrifugation step. Membrane fractions were mixed with SDS-loading dye (0.2 M Tris–HCl, pH 6.8, 10% (w/v) SDS, 40% (v/v) glycerol, 0.02% (w/v) bromophenol and β-mercaptoethanol) and used for SDS-PAGE and western blot analysis. A polyclonal antibody against the extracellular domain of *Sa*NsrP was used to detect the expressed *Sa*NsrFP protein Davids Biotechnologie, Regensburg, Germany.

Structural alignments

TMDs of the different BceAB transporters from the structural model server Alphafold (Jumper *et al*., 2021) were cropped so that only the SABRE and Porter domain of the ECD with the first helical turn of the stalk helices remained. The structural alignment was performed by using the cealign tool of Pymol Version 2.5.4. The resulting RMSD matrix was taken to the power of two and subsequently analyzed with the kitsch tool of the phylip program package (V. 3.698) (Felsenstein, 2005). Then, the structural alignment tree was generated with the help of the draw gram tool of the same program package.

Computational predictions of bacitracin binding mode*

A full model of the NsrFP protein (Uniprot: A0A2X2LSF6) was generated with ColabFold (Mirdita *et al*., 2022) using 12 recycling cycles and creating four independent models. A sequence search for MSA construction was performed against Mgnify, UniRef, and PDB70 databases. The final model was chosen based on the resulting pLDDT score. The extracellular domain comprising the residues between the amino acids N307 and L517 was taken for further experiments.

Extensive conformational sampling of bacitracin was carried out using the MacroModel tool in Schrödinger (Mulnaes and Gohlke, 2018) based on the protocol used in previous macrocycle sampling benchmarks (Alogheli *et al*., 2017). The initial structure of bacitracin was taken from the PDB entry 4K7T. Protonation states for side chains were assigned using Propka (Rostkowski *et al*., 2011). 1,000,000 steps of the Monte Carlo Multiple Minimum (MCMM) search were performed incorporating distance restraints between the peptide and the bound zinc ion. Extended sampling was allowed by incorporating the sampling of

*** This subsection is authored by Pablo Cea Medina**

torsional angles of amides, esters, C-N and N-N single bonds, as well as C=N and N=N double bonds. A wide-opening ring criterion was used (0 – 100 Å) avoiding atoms adjacent to stereocenters. 50,000 steps of truncated Newton's conjugate gradient (TNCG) method were performed for energy minimization. Redundancy within the resulting conformers was removed using an RMSD criterion of 0.5 Å for heavy atoms. This resulted in 67,949 unique conformations. The zinc ion was removed before moving on to docking experiments to prevent steric clashes with the receptor.

A putative binding region within the extracellular loop domain was identified using Schrodinger's SiteMap (Halgren, 2009). A 46 Å Grid was manually placed within the site. Rigid docking was carried out using Glide in standard precision (Repasky *et al*., 2007) mode, including a reward for intramolecular hydrogen bonds. The resulting poses were filtered according to their docking energy score. Poses with energies below -6.0 kcal mol^{-1} were kept for further analyses. The final poses were clustered with cpptraj (Roe and Cheatham, 2013) using the DBScan algorithm with an RMSD-based cut-off of 2 Å for heavy atoms and three minimum points.

Biological assays.

Purification of nisin

Nisin was purified with ion-exchange chromatography as previously described by (Abts *et al*., 2011), and the concentration was determined using RP-HPLC according to Abts *et al*. (Abts *et al*., 2013).

Determination of the half-maximal inhibitory concentration (IC_{50}).

The half-maximal inhibitory concentration was determined according to (Abts *et al*., 2011). In short, *L. lactis* NZ9000Cm, *L. lactis* NZ9000*Sa*NsrFP, and *L. lactis* NZ9000*Sa*NsrFP mutant cell lines were grown in GM17 medium containing 5 µg/ml chloramphenicol and 0.3 nM nisin at 30 °C overnight. Fresh GM17Cm medium with a sublethal amount of nisin (0.3 nM) was inoculated with overnight cultures to an OD_{600} of 0.1. A 96-well plate was prepared with a serial dilution of examined antibiotics (concentration ranges nisin 0.0001 nM–0.5 µM; bacitracin 0.2 nM-7.5 mM) and subsequently, the cell culture was added and plates were incubated at 30 °C. After 5 hours of incubation, the optical density

was measured, and the IC_{50} values for each strain and antibiotic were calculated. To make those values more comparable, the fold of resistance was determined by dividing the IC_{50} values of *L. lactis* NZ9000*Sa*NsrFP and *L. lactis* NZ9000*Sa*NsrFP mutant strains by the corresponding value for *L. lactis* NZ9000Cm.

Multi-Angle Light Scattering (MALS)

Purified ECD was concentrated to 2 mg/mL using centrifugal filters with a 3-kDa cut-off (Amicon Ultra-0.5 MERCK/ Millipore) and the samples were centrifuged at 100,000 g, at 4°C for 30min. For the measurement with bacitracin, the protein sample was preincubated with 1mM bacitracin. Superdex 75 Increase 10/300 GL column (GE Healthcare) was pre-equilibrated overnight at 0.1 ml/minute flow rate with buffer (20 mM Tris pH 8.0, 500 mM NaCl). For each analysis, 200 µl of a protein sample at 2.0 mg/ml concentration was loaded onto the column at 0.6 ml/minute flow rate using a 1260 binary pump (Agilent Technologies). The scattered light was measured with a miniDAWN TREOS II light scatterer, (Wyatt Technologies), and the refractive index was measured with an Optilab T-rEX refractometer, (Wyatt Technologies). Data analysis was performed with ASTRA 7.3.2.21 (Wyatt Technologies) (Slotboom *et al*., 2008)

Tyrosine quenching

The measurements were conducted using a Fluorolog Jobin Yvon FL-3-11. 1 ml of NsrPECD solution in SEC buffer (25mM Tris pH 8, 500mM NaCl), with concentrations of NsrPECD in range from 1.3 to 1.7 nM) was prepared in a Hellma Macro-cuvette 100-QS. 10–50 µl of 20 mM bacitracin stock solution in H_2O was added to the cuvette. The cuvette was placed into the fluorolog sample holder and the reaction mixture was incubated for 2 minutes while stirring before measuring the fluorescence intensity. The measurements were conducted for bacitracin concentrations in the range from 0 to 2.8 mM. For measurements with Zn^{2+}, 100 mM of $ZnCl_2$ was added to the 20 mM bacitracin stock solution.

In this experiment, the fluorescence of tyrosine was monitored, due to the fact that *Sa*NsrP ECD lacks tryptophan residues. The excitation wavelength used was 260 nm. The fluorescence was monitored in the range from 303 nm to 450 nm.

The measurements with nisin were conducted using the same procedure. The concentration range was selected based on the IC_{50} of NZ9000*Sa*NsrFP shown in previous work (Gottstein *et al*., 2022).

Small Angle X-ray Scattering

We collected all SAXS data on beamline BM29 at the ESRF Grenoble *(*Pernot *et al*., 2010, Pernot *et al*., 2013). The BM29 beamline was equipped with a PILATUS 2M detector (Dectris) at a fixed distance of 2.812 m. The measurements were performed with a NsrP ECD (without His-tag) concentration of 1.65 mg/ml at 10°C. The corresponding Buffer contains 25 mM MES, pH 6.0, 500 mM NaCl. We collected 10 frames with an exposer time of one second per frame and scaled the Data to absolute intensity against water. We checked each frame for radiation damage using CorMap/ $\chi 2$ test, implemented in PRIMUS (Konarev *et al*., 2003).

All used programs for data processing were part of the ATSAS Software package (Version 3.1.3) (Manalastas-Cantos *et al.*, 2021). Primary data reduction was performed with the program PRIMUS (Konarev *et al*., 2003). With the Guinier approximation (Guinier, 1939), we determine the forward scattering *I(0)* and the radius of gyration (R_g). The program GNOM (Svergun, 1992) was used to estimate the maximum particle dimension (D_{max}) with the pair-distribution function *p(r)*.

Results:

Distribution of BceAB-type transporters

BceAB-like transporters have been identified in non-AMP-producing strains as a protection mechanism of the cell wall. They have been shown to confer resistance against structurally diverse AMPs (Mascher *et al*., 2003, Reiners *et al*., 2017, Gottstein *et al*., 2022). It has been accepted as the status quo that BceAB-like ABC transporters occur almost exclusively in Firmicutes bacteria (Dintner *et al*., 2011, Kobras *et al*., 2020).

With the structural model server Alphafold (Jumper *et al*., 2021, Varadi *et al*., 2022), we strived to investigate these in more detail and searched for other BceAB-type transporters using structural alignments. Here, the characteristic domain architecture found for BceAB transporters is 10 transmembrane helices and a large extracellular domain (150 -250 amino acids) located in between

transmembrane helices 7 and 8 (Mascher *et al*., 2008; Collins *et al*., 2010). Furthermore, the nucleotide-binding domain BceA should be located next to the gene encoding the transmembrane protein. Via this method, we identified several BceAB-type ABC transporters in the genomes of different organisms including opportunistic pathogens as well as medically relevant human pathogens and *ESKAPE* organisms listed by the WHO (Tacconelli *et al*., 2018) such as *C. difficile*, S. *pneumonia*, *MRSA*, *E. faecium* and others (Figure 16).

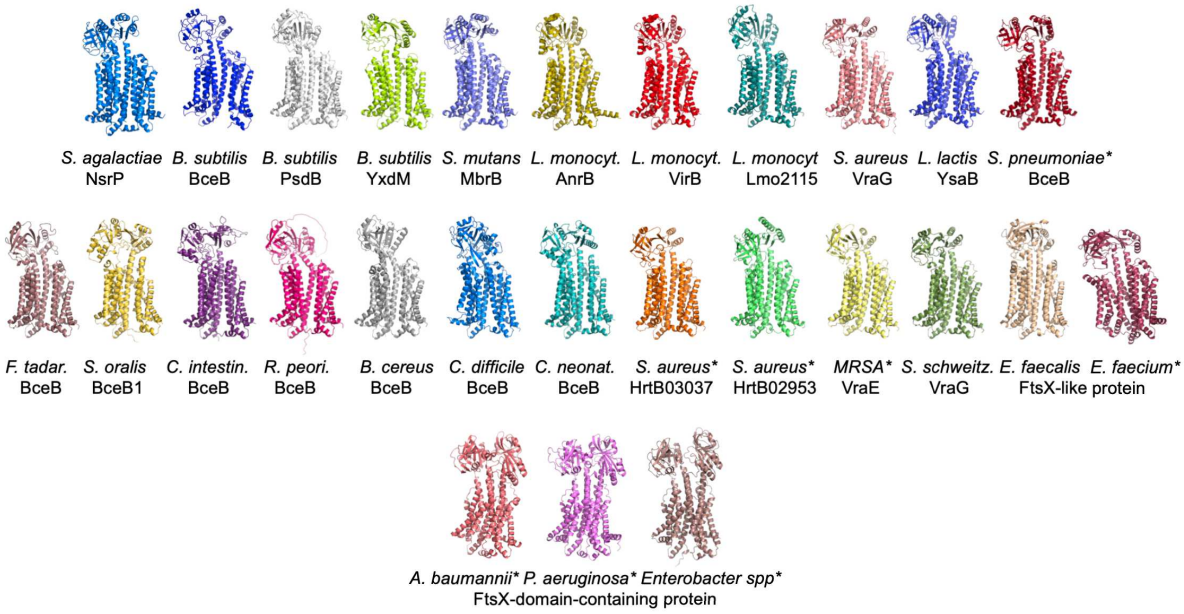

Figure 16: Alpha fold database search shows the presence of BceAB-type transporters and related not only in Firmicutes but also in opportunistic pathogenic and clinically important ESKAPE bacterial strains. A full list of organisms and accession numbers is displayed in the supplement (Table S1). TMD models were found on the structural model server Alphafold (Jumper *et al*., 2021, Varadi *et al*., 2022). The image was created using Pymol Version 2.3.0 and Powerpoint Version 16.76.

The structural comparison revealed that the transmembrane domain is structurally conserved as displayed by a root mean square (RMSD) of 1 to 4 Å. Especially within closely related bacteria i.e. *Streptococcae* the TMDs show a structural high conservation RMSD around 1-2 Å.

Interestingly, we analyzed another set of ABC transporter in Gram-negative bacteria with the typical BceAB-like features but in addition, contains a second extracellular domain between the first and second helix, known as YbbP (Greene *et al*., 2018). Interestingly, the protein MacB also contains an ECD between the first and second ECD. This type of BceAB-like permease can be found in clinically important pathogenic, Gram-negative, bacteria (Figure 16, last row). The topology of the transmembrane helices however is substantially different from the

BceAB type transporter found in Gram-positive bacteria. So far, the function of these type of ABC transporter is unknown.
Altogether, this suggests that the BceAB ABC transporter family appears to be larger than described so far. Furthermore, the models predicted by Alphafold reveal two distinct groups in which the TMDs in the BceAB groups are highly similar- and the TMDs in the BceAB-like group are differently oriented.

Structural alignments of ECDs reveal six distinct groups

Since all the ECDs have a brain-like form and therefore look similar, we strived to analyze and align their structure. Therefore, the TMDs of the different BceAB transporters from the Alpha fold database were cropped so that only the SABRE and Porter domain of the ECD with the first helical turn of the stalk helices remained. ECDs with approximately 200-260 amino acids were used for structural alignments.
Further, the ECDs share very different sequences, making sequential alignment difficult. To gain insight into structurally similar ECDs, we determined RMSD values of the ECDs over 100 – 180 C_α with the cealign tool of PyMOL. The resulting RMSD matrix was used to generate the structural distance tree shown in Figure 17a. Overall, we could assign the ECDs into five distinct classes (I-V).

Interestingly, class I which contains NsrP from *S. agalactiae* is separated early from the other ECDs from the structural distance tree with an average RMSD of 5.7 Å. Further, this group contains other *Streptococcus* species such as *S. mutans*, *S. pneumoniae,* and *L. lactis,* which is closely related to Streptococcus species. This was also shown in a very recent study in a phylogenetic tree based on the alignments of the DNA-dependent RNA polymerase *Streptococcus* species and *Lactococcus lactis* form together their separate lineage in comparison to *Lactobacilli species (Price et al., 2012)*. Additionally, one ECD from the ESKAPE organism *S. aureus* is present in the group. This combination of bacterial strains also clusters together when comparing their TMDs which show RMSDs in the range from 1.1 to 2.0 Å. The RMDs of the ECDs in group I range from 2.6 Å to 4.2 Å (ECD of *S. aureus* Hrt29092: 6.0 Å). The ECD and TMD of *S. aureus* show the highest RMSDs when compared to *S. agalactiae*. This might be due to the fact that *S. aureus* is not part of the *Streptococcae* family, so higher deviations can be expected.

Group two is separated with an average RMSD of 5.2 Å and contains two ECDs of *C. neonatale* and *C. intestinalis* with an RMSD of 3.6 Å. As the largest group, group III is divided from group IVa with an average RMSD of 4.6 Å. This group harbors a total of nine ECDs, ranging from *L. monocytogenes* to *B. cereus*, *B. subtilis*, *E. faecium*, *E. faecalis,* and *C. difficile*. When comparing the ECDs against the ECD of Lmo2115 of *L. monocytogenes,* it becomes evident that ECDs are more similar within the same family (VirAB:3 Å, AnrAB: 3.7 Å). The ECD of VirAB and AnrAB which are both involved in the resistance mechanism from *L. monocytogenes*, share a very high similarity (RMSD of 0.4). The *bacillus* family is closely related to *Listeria (Buchrieser et al., 2003)* which is also reflected in their RMSDs for the ECDs: *B. cereus* 3.7 Å, *B. subtilis* PsdB: 4.1 Å, *B. subtilis* YxdM: 4.7 Å. *E. faecium*, *E. faecalis* and *C. difficile* show the least similar RMSD in this group compared to the ECD of Lmo2115 with RMSDs of approximately 6 Å. It is important to note that *L. monocytogenes* and *B. cereus* are both pathogens causing food-borne diseases while *Enterococci and C. difficile* both infect the gastro-intestinal tract. They can infect patients usually after antibiotics treatment in clinical settings (Wells *et al*., 2023, Zhou *et al*., 2020).

Group IVa features BceB from *B. subtilis* as well as 4 ECDs from the *Staphylococcae* family and one from *F. tadaridae,* a bacterial strain isolated from bat guano. The ECD from Hrt03096 and VraE are the most similar with an RMSD of 0.8, then followed by VraG ECD from *S.aureus* (RMSD: 2.4 Å) and *S. schweitzeri* 2.9 Å, the ECD from BceB from *F. tadaridae* 3.6 Å and lastly the ECD of *B. subtilis* with 5.6 Å compared to VraE but the ECDs more similar to VraG ECDs (approximately 3 Å). In group 4b two ECDs clustered together from *R. peoriensis* and *S. oralis* showed RMSDs of approximately 5Å when compared to each other.

Lastly, ECDs of a new type of ABC transporter that contains all characteristics of a BceAB transporter with an additional ECD between transmembrane helix 1 and 2 (Figure 16 last row) from clinically relevant Gram-negative ESKAPE pathogens are gathered in group five, which show the highest difference to the other groups (RMDs in the range of 8 to 16 Å). Group V is the first group that is split off from the structural distance tree. For a better comparison in the structural distance tree, the ECDs were compared separately from each other. The ECD between TMH 1 and 2 was named “ECD left” and the ECD 7 and 8 “ECD right”.

The Gram-Negative left ECDs are very similar to each other with below 2 Å RMSDs between 1-2 Å. This also holds true for the right ECDs compared to each other. Remarkably, the right ECD of *A. baumannii* is structurally very similar to the ECD of HrtB0292 of *S. aureus* (RMSD of 1.9 Å). However, if left and right ECDs are compared to each other, it becomes evident that they are very different from each other with a mean RMSD of 5.5 Å. Thus, indicating that both left and right ECDs of the Gram-negative are different in structure. More importantly, the average RMSD to all other ECDs is above 6 Å. Overall, RMSD values between each group are above 4.5 Å. An Excel file list of all RMSDs can be found in the supplements.

Throughout the different groups, multiple conserved secondary structure features were found. These features are displayed in the well-known ECD of BceB from *B. subtilis* together with the most prominent ECDs of each group in Figure 17b.

Eight conserved secondary structure elements in the SABRE domain are conserved throughout all ECDs. These secondary structures are presented in the alpha fold model of the ECD of BceB in Figure 17b and consist of two long β-sheets that connect the Porter and SABRE domain, three β-sheets flanking two β-sheets resembling a β-turn and one α-helix with a varying length that connects the SABRE β-sheets with the second long β-sheet leading back to the porter domain.

Within the individual groups, the RMSD values are below 4.5 Å, and characteristic secondary structures supplementing the conserved topology were found for each group. These are depicted in the bottom part of Figure 17b and are with some exceptions present in each member of the designated group.

In group I we found that the three + two β-sheets in the SABRE domain are intersected by one to two short α-helices. Further, the N-terminal β-sheet connection for the Porter and SABRE domain ends in an extended larger loop which contains an additional β-sheet. Thus, changing the overall shape of the ECD in a minor way.

While the ECD of *C. neonatale* of group II does not display major changes in the porter domain, the helical part of the Porter domain is extended and disordered in the ECD from *C. intestinalis*. This might explain the high RMSD value of 3.6 between both ECDs. Further, the three + two β-sheets in the SABRE domain are

extended by large unstructured regions and three to four α-helices, reshaping the SABRE domain at the lower bottom right corner.

As group III is quite large, we noticed the Porter domain of the ECDs from *E. faecium*, *E. faecalis,* and *C. difficile* were extended at the C-terminal stalk helix and harbored either three β-sheets and an α-helix (*E. faecium* and *E. faecalis)* or multiple helices (*C. difficile)*. Additionally, all members of group III show an extended intersection between the three + two β-sheets containing two α-helices and one β-sheet. The extended Porter domain section of the aforementioned ECDs changes the overall shape of the SABRE domain, by adding a region in the upper left corner (Figure 17b, class III). Changes introduced in the SABRE domain are not extensively altering the layout of the SABRE domain.

In contrast to all described groups, the SABRE domain of group IVa is altered in a smaller manner. The three + two β-sheets are intersected with a β-sheet and multiple small α-turns or small β-sheets and unstructured regions. Overall, the ECD profile is not altered in this subgroup.

However, members of group IVb feature a more diverse SABRE domain, containing one to three large α-helices and larger unstructured regions neighboring the three + two β-sheets. Additionally, the ECD from *R. peoriensis* features a large unstructured region in the Porter domain. Notably, the ECD shape of group IVb resembles ECDs of group IVa with added α-helices, leading to an extension at the left side of the SABRE domain.

Lastly, group V containing the ECDs of Gram-negative bacteria shows two to three added α-helices as well as two additional β-sheets surrounding the three plus two β-sheets in the SABRE domain. Thus, extending the SABRE domain in the bottom left corner.

Taken together, the classification reveals, that the addition of secondary structure elements characteristic for each group alters the core structure and determines the overall ECD shape. In most cases, supplementary secondary structures appear to alter the left side of the SABRE domain.

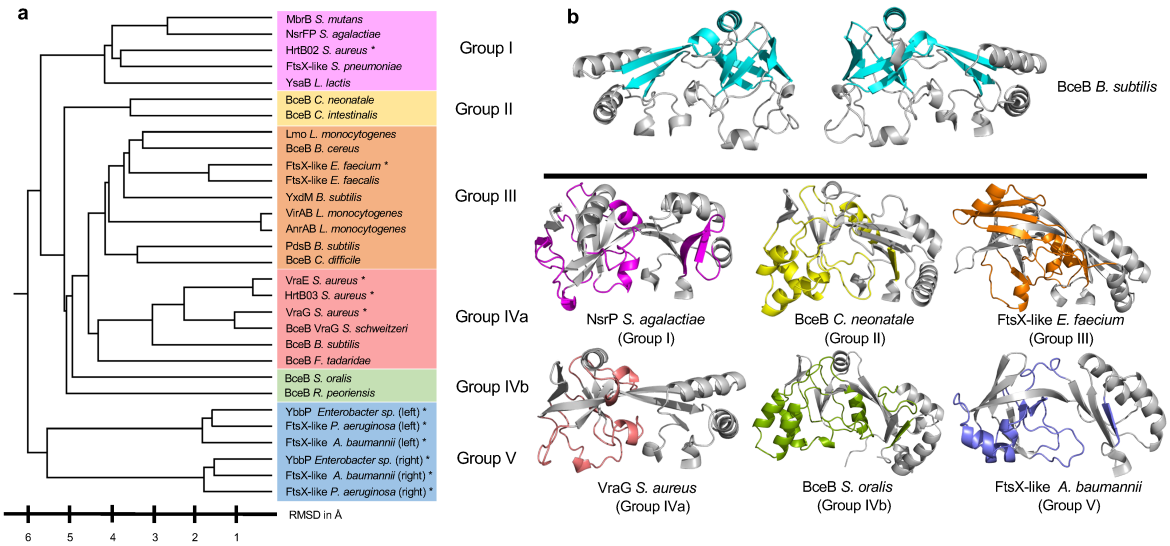

Figure 17 a) Structural distance tree of BceAB-type permeases found searching the alpha fold database. b) ECDs alpha fold models of representative VI groups established by the structural distance tree shown as cartoons. Conserved secondary structures are highlighted in the BceB ECD model, the group defining secondary structures are highlighted in one color for each group. Group I in (pink), group II in yellow, group III in orange, group IV in salmon, group V in green, and group VI in blue. Other helices are colored in grey. TMD models were taken from the structural model server Alphafold (Jumper *et al*., 2021, Varadi *et al*., 2022) and cropped so that only the SABRE-, Porter-domain and first turn of the stalk helix was depicted. Image was created using Pymol Version 2.3.0 and Powerpoint Version 16.76.

Bacitracin binding to ECD

Kobras *et al*. postulated that the ECD of BceAB binds the bacitracin-UPP complex and upon ATP hydrolysis the complex is broken and bacitracin is released (Kobras *et al*., 2020). This intrigued us to see whether we can find a binding mode of bacitracin to the ECD. Here, we have chosen the ECD of NsrP from *S. agalactiae* since this transporter has recently been shown to confer high resistance against bacitracin (Gottstein *et al*., 2022).

Molecular docking prediction of bacitracin binding *

To gain insights into the possible binding mode of bacitracin to NsrP, first, we used SiteMap, which identified two putative binding sites based on properties such as solvent accessibility, potential for hydrogen bond interactions, and polarity (Halgren, 2009). One is located in the transmembrane region matching the putative lipid II binding site described for BceAB (George *et al*., 2022) and the second is located in a central cleft within the extracellular domain (Supplementary Figure 1). As our experimental characterization showed that the NsrFP ECD domain alone can interact with bacitracin, we considered the second site a likely

*** This subsection is authored by Pablo Cea Medina**

binding region. Thus, we performed docking into this identified region using the structural model of the ECD.

Given the large size and high amount of rotable bonds present in bacitracin conventional flexible docking is unviable. Therefore, we decided to combine rigid docking with extensive conformational sampling of the ligand.

We generated over 60,000 unique ligand conformations and docked them into the EC domain of NsrFP. The resulting poses were filtered according to their docking energy (<-6 kcal mol^{-1}) and clustered according to their RMSD. The experimental characterization of the K481A mutant highlighted the importance of K481 in the binding of bacitracin, therefore, we expected that this residue is part of the interaction interface between the lantibiotic and the protein. From the clustered docked poses, we found three clusters where K481 is forming non-covalent interactions with bacitracin: Clusters N°1, N°6, and N°8, according to their indexes.

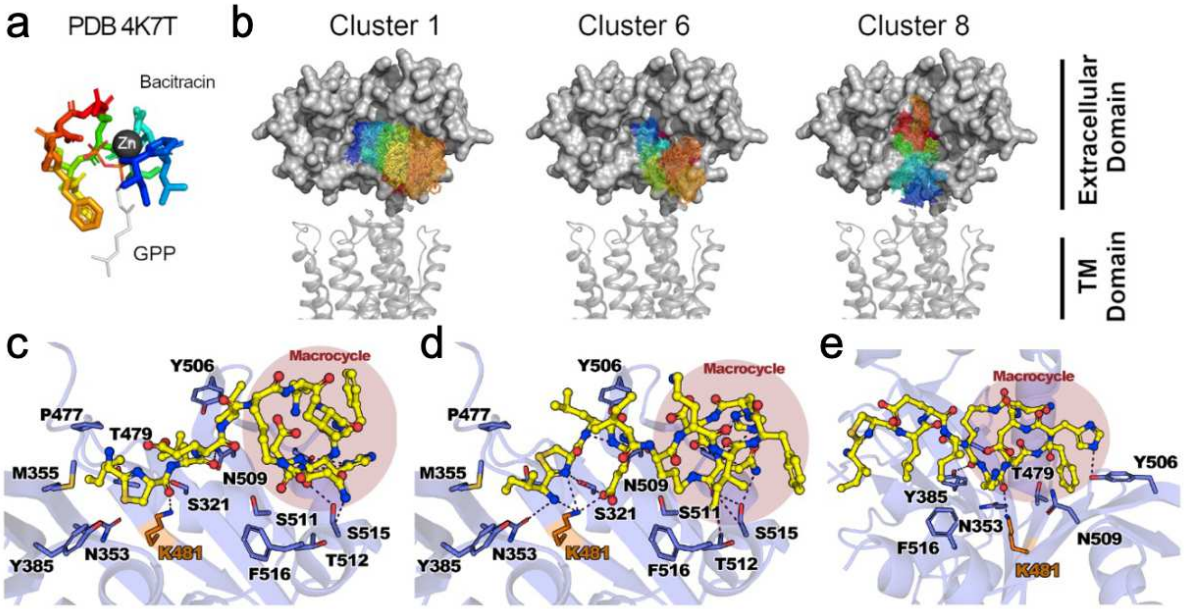

Figure 18: **Bound poses from rigid docking**. **a)** Bacitracin bound to a target analog (GPP). The structure is colored from the N-terminus (blue) to the C-terminus (red). **b)** Docked poses belonging to clusters in agreement with experimental results. The extracellular domain of NsrP is shown as a surface while the transmembrane region is shown as cartoon. Lower panels show the best scoring poses from clusters in agreement with experimental results. The mutated lysine residue is highlighted in orange, and the macrocyclic region of bacitracin is highlighted with a red circle for Cluster 1 **(c)**, Cluster 6 **(d)**, and Cluster 8 **(e).** Image created by Pablo Cea Medina.

In all three clusters, bacitracin is in an extended conformation, with the N- and C-terminus apart from each other. These conformational states differ from the one

in which bacitracin binds its lipidic target, where both ends come close together, leading to a compact conformation (Figure 18a). Cluster 1 is most populated with 207 poses, followed by Cluster 6 with 32 poses, and Cluster 8 with 23. In terms of energy, Cluster 8 has the best median score of -8.04 kcal mol^{-1}, followed by Cluster 1 with a median score of -7.44 kcal mol^{-1}, and Cluster 8 with a median score of -7. 33 kcal mol^{-1} (Supplementary Figure 2).

In Clusters 1 and 6, bacitracin is similarly oriented within the ECD (Figure 18b). The N-terminus — which contains the thiazoline ring — is positioned in the center of the binding cleft, while the cyclic region of the peptide is located at the edge of the protein. On the other hand, bacitracin in Cluster 8 is located perpendicularly to the membrane plane, extending over the central cleft along its vertical axis (Figure 18b). The N-terminal group points towards the transmembrane region, at the lower edge of the ECD.

To analyze the details of the putative binding mode, we took the best scoring pose from each cluster and mapped out the interactions between the protein and the bacitracin. In Cluster 1, K481 interacts with the carbonyl group adjacent to the thiazoline ring, while the rest of the macrocyclic ring interacts with polar residues such as S515 (Figure 18c). In the representative binding pose for Cluster 6, we observe a more complex network of interactions formed around K481 (Figure 18d). In this case, the nitrogen of the thiazoline ring plus an aspartic acid residue and the free N-terminus of bacitracin are in direct contact with these residues, resembling how these moieties coordinate zinc when bacitracin is free. Meanwhile, the backbone of the macrocyclic part of bacitracin forms hydrogen bond interactions with S525 and T512. Finally, in the pose derived from Cluster 8, K481 interacts with the backbone of the macrocyclic region of bacitracin, also involving Y385 and Y506 (Figure 18e). However, no direct interactions between the N-terminus of bacitracin and the protein were observed.

Lysin K481 and K513 in *Sa*NsrFP are important residues for bacitracin resistance.

To verify our computational results, we performed *in vivo* experiments by determining the growth behavior of our *L. lactis* strain with and without *Sa*NsrFP and two Lysine variants in the presence and absence of bacitracin. To characterize the contribution of important lysins 481 and 513 to bacitracin

resistance in the complete BceAB transporter, alanine, and glutamine (introducing a negatively charged residue) mutations were generated. *Sa*NsrFP single and double mutants were cloned in a pIL-SV*Cm* shuttle vector, transformed, and expressed in *L. lactis* NZ9000 by inducing expression with a sublethal amount of nisin (0.3 nM) (Reiners *et al*., 2017, Gottstein *et al*., 2022). This sub-inhibitory nisin concentration can induce the nisA promotor in the pILSV plasmid, allowing gene expression of the respective protein. All measurements were compared to the ATP-deficient *Sa*NsrF$_{H202A}$P mutant that cannot hydrolyze ATP and the sensitive control strain, which was transformed with an empty vector and treated in the same way as the mutant strains.

The activity of nisin, bacitracin, and Zn-bacitracin against the *Sa*NsrFP lysin mutants, WT, and control strains was determined by treating the strains with different concentrations of one antimicrobial peptide.

Upon treatment with bacitracin, strains expressing the BceAB transporter mutants exhibited a strong decrease in resistance although not more sensitive than for the empty vector control strain (Figure 19a left plot). When treated with Zn-bacitracin, the cells expressing the mutated *Sa*NsrFP displayed a loss of resistance with a lower IC_{50} than for bacitracin (Figure 19a right plot).

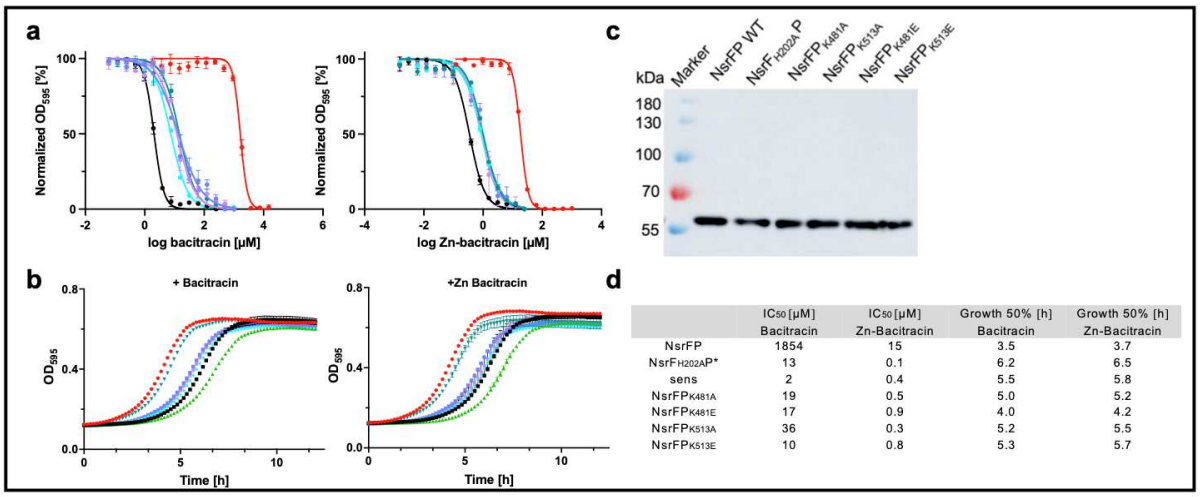

	IC50 [µM] Bacitracin	IC50 [µM] Zn-Bacitracin	Growth 50% [h] Bacitracin	Growth 50% [h] Zn-Bacitracin
NsrFP	1854	15	3.5	3.7
NsrFH202AP*	13	0.1	6.2	6.5
sens	2	0.4	5.5	5.8
NsrFPK481A	19	0.5	5.0	5.2
NsrFPK481E	17	0.9	4.0	4.2
NsrFPK513A	36	0.3	5.2	5.5
NsrFPK513E	10	0.8	5.3	5.7

Figure 19 a) IC_{50} measurements of *L. lactis* NZ9000NsrFP (red), NZ9000pILSVsens (empty vector) (black), NZ9000NsrFP(K481A) (purple), NZ9000NsrFP(K513A) (pink), NZ9000NsrFP(K481E) (teal), NZ9000NsrFP(K513E) (lightblue). Cells were treated with either 7.5 mM – 30 nM bacitracin, or 2 mM – 0.7 nM Zn-bacitracin and monitored for up to 7 hours. Curves were fitted using GraphPad Prism version 9.5.1 for MacOS, GraphPad Software, San Diego, California USA, www.graphpad.com. **b)** Growth curves of the same strains induced with 0.3 nM nisin and treatment of 4 mM bacitracin or 1 mM Zn-bacitracin. The cell density was monitored overnight. **c)** Purified membrane fractions of *Sa*NsrFP and its lysin mutants in *L. lactis* NZ9000 monitored by Western Blot using a polyclonal antibody against the extracellular

domain. The expression levels of the *Sa*NsrFP mutants were similar in all cases. **d)** IC_{50} and $Growth_{50\%}$ values from performed growth inhibition experiments in a) and b).

This is due to the conformational change of bacitracin in the presence of Zn^{2+} which allows higher affinity to membranes (Economou *et al*., 2013). The wildtype strain showed resistance towards the tested antimicrobial peptides as was shown in previous work by (Reiners *et al*., 2017, Gottstein *et al*., 2022). On the contrary, the empty vector strain and the ATP-deficient ABC transporter strain control showed expected sensitivity toward all antimicrobial peptides (Figure 19d). *Sa*NsrFP K to A mutants and K to E mutants did not display any significant differences in their IC_{50} (Figure 19d).

To test if the lysine-alanine or lysine-glutamate mutants influenced bacterial growth of the *Sa*NsrFP mutant expressing strain, growth assays were performed (Figure 19b). The strains were treated with either 4 mM bacitracin (Figure 19b left plot) or 1 mM Zn-bacitracin (Figure 19b right plot) and the OD_{600} was monitored online for 12h. The wildtype strain, the sensitive as well as the ATP-deficient ABC transporter strain were tested as controls. The K481E strain showed a similar rapid growth as the *Sa*NsrFP WT strain reaching 50% of its maximal growth after 4 hours (Figure 19b teal and Figure 19d). All other mutant strains showed a slower growth similar to the sensitive strain reaching 50% of its optical density after approximately 5 hours (Figure 19b left plot) and approximately 6 hours in the presence of Zn-bacitracin (Figure 19b right plot). These results suggest that lysins 481 and 513 in *Sa*NsrFP seem to influence growth which could be explained by the loss of activity. On the contrary, the charged amino acid glutamate at position 481 seems to rescue the ability for more rapid growth while still displaying low IC_{50} values when treated with both bacitracin variants. It has been shown also in previous work that the strain expressing *Sa*NsrF$_{H202A}$P (green curve) shows slow growth when treated with both bacitracin variants (Gottstein *et al*., 2022). The growth retardation as observed for the mutant strains and control strains upon the addition of bacitracin has been shown for many bacterial cells such as group B streptococci and methicillin-resistant *S. aureus* (Klinzing *et al*., 2013, Vemula *et al*., 2017).

To confirm that the loss of resistance was not caused by differences in production levels, we performed Western blot analysis on purified membrane fractions of *Sa*NsrFP-mutant-expressing cells using a polyclonal antibody against the ECD

of *Sa*NsrP (Figure 19c). We were able to prove that comparable levels of transporters were produced in all used strains. This indicates that K481 and K513 play an important role in establishing bacitracin resistance.

***In vitro* characterization of the ECD of *Sa*NsrP.**

*Sa*NsrFP consists of a large extracellular domain (ECD) that is hypothesized to be involved in binding an antibiotic most likely bacitracin/Zn-Bacitracin. To characterize its function and express the protein in sufficient amounts for further characterization, the stalk helices of the ECD were removed via cloning. This led to a stable protein, successfully expressed in *E. coli* BL21 and purified by a three-step purification protocol. For all further functional *in-vitro* analysis, the Histag was cleaved off the ECD, applied to another Ni-chromatography to separate it from the uncleaved protein and subsequently analyzed by size exclusion chromatography (SEC). The success of the purification was monitored via SDS-PAGE (Figure 20a).

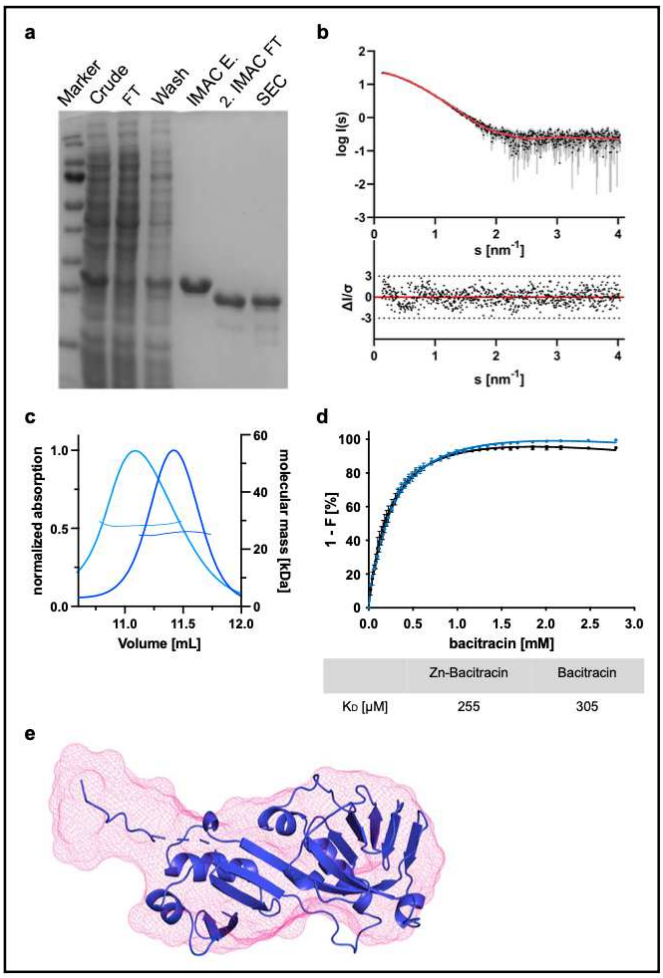

Figure 20 a) 15% SDS gel showing the different fraction samples from the purification of the short construct of the ECDsh of *Sa*NsrP. Lane 1 shows the standard protein marker.

Lanes 2-4 represent samples taken from crude extract, flowthrough, and wash fraction. Lane 5 shows the IMAC eluate at 300 mM of imidazole, Lane 6 the flowthrough sample of the second IMAC after Thrombin digestion, and Lane 7 the eluate sample of the SEC b) SAXS scattering data for monomeric NsrP ECD without His-tag. Experimental data are shown in black dots, with grey error bars. The GNOM fit is shown as a red line and below is the residual plot of the data. c) MALS measurement of *Sa*NsrPECD (blue) and *Sa*NsrPECD with the addition of Zn-Bacitracin (light blue). The normalized UV absorption at 280 nm and molecular mass were plotted against the elution volume. d) Relative quenching of tyrosine fluorescence intensity of *Sa*NsrPECD with bacitracin (blue) and Zn-bacitracin (black). The measurements were conducted in the range of 303 to 450 nm and 0-2.79 mM bacitracin was added subsequently to the protein. Dissociation constants were calculated and graphs were fitted using GraphPad Prism version 9.5.1 for MacOS, GraphPad Software, San Diego, California USA, www.graphpad.com". e) Representation of the SAXS envelope (pink) fitted with the model of the short ECD construct (blue).

The ECD construct eluted at 300 mM in the third peak without contaminations. This is reflected by the thick band in lane 4 on the SDS-gel at 25 kDa which matches the theoretically calculated mass for the ECD with Histidine tag (25.3 kDa). After cleaving the Histag the protein was subjected to another IMAC to separate the cleaved protein from the uncleaved one. The cleaved protein eluted in the flowthrough fractions (Figure 20a, lane 5). On the SDS-gel a band lower than 25 kDa was observed, matching the theoretical mass of 23.8 kDa of cleaved protein without tag (Figure 20a). After SEC chromatography, the cleaved ECD eluted in a single peak. Thus, for the first time, we can show the stable and successful expression and purification of the extracellular domain of *Sa*NsrP.

To confirm the molecular weight and oligomeric state of the protein sample Small-Small-angle X-ray spectroscopy (SAXS) was performed. SAXS experimental scattering data for the ECD without its His-tag are shown in Figure 20b, confirming that the ECD of *Sa*NsrP is a monomer. Table 1 gives an overview of all collected data via SAXS, which supports that the ECD is monomeric. Figure 6e shows the monomeric ECD.

Table 1: Overall SAXS data.

SAXS Device	**BM29, ESRF Grenoble (Pernot *et al.*, 2010, Pernot *et al.*, 2013)**
Data collection parameters	
Detector	PILATUS 2 M
Detector distance (m)	2.827
Beam size	200 µm x 200 µm
Wavelength (nm)	0.099
Sample environment	Quartz capillary,1 mm ø
s range (nm^{-1})‡	0.025–5.0
Exposure time per frame (s)	1 (10 frames)
Sample	**NsrP ECD**
Organism	*Streptococcus agalactiae* COH1
UniProt ID	Q8DZX0

Mode of measurement	Batch
Temperature (°C)	10
Protein concentration (mg/ml)	1.65
Protein buffer	25mM MES pH 6.0, 500 mM NaCl
Structural parameters	
I(0) from P(r)	22.70
R_g (real-space from P(r)) (nm)	2.41
s-range for GNOM fit (nm^{-1})	0.134 – 4.033
I(0) from Guinier fit	22.94
s-range for Guinier fit (nm^{-1})	0.134 – 0.524
R_g (from Guinier fit) (nm)	2.43
points from Guinier fit	1 - 77
D_{max} (nm)	7.47
POROD volume estimate (nm^3)	50.23
Molecular mass (kDa)	
From *I*(0)	22.82
From Qp (Porod, 1951)	24.92
From MoW2 (Fischer *et al.*, 2010)	23.87
From Vc (Rambo and Tainer, 2013)	27.39
From Bayesian Inference (Hajizadeh *et al.*, 2018)	24.33
From GNNOM (Molodenskiy *et al.*, 2022)	24.80
From POROD	25.12 – 31.39
From sequence	23.38
Structure Evaluation	
GASBOR fit χ^2	1.093
CRYSOLfit χ^2	3.159
Ambimeter score	1.204
Software	
ATSAS Software Version (Manalastas-Cantos *et al.*, 2021)	3.1.3
Primary data reduction	PRIMUS (Konarev *et al.*, 2003)
Data processing	GNOM (Svergun, 1992)
Ab initio modelling	GASBOR (Svergun *et al.*, 2001)
Superimposing	SUPCOMB (Kozin and Svergun, 2001)
Structure evaluation	AMBIMETER (Petoukhov and Svergun, 2015) / CRYSOL (Svergun *et al.*, 1995)
Model visualization	PyMOL (PyMOL, 2015)

‡s = 4πsin(θ)/λ, 2θ – scattering angle, λ – Xray-wavelength, n.d. not determined

It is known from previous work that *Sa*NsrFP has been shown to confer resistance to a structurally unrelated group of antibiotics, including nisin, gallidermin, vancomycin, lysobactin, and 100-/350-fold against Zn-bacitracin/bacitracin (Reiners *et al.*, 2017, Gottstein *et al.*, 2022). Due to the absence of an extracellular domain in the histidine kinase *Sa*NsrK, its function (i.e., sensing of

antibiotics was hypothesized to be taken over by the BceAB transporter with its large extracellular domain. So far, the direct binding of an antimicrobial peptide to the extracellular domain of a BceAB transporter was only reported for the related VraG from *S.aureus* (Cho *et al*., 2021). To unveil the interaction partner for the ECD of *S. agalactiae*, we used two independent methods 1) Multi-Angle Light Scattering (MALS) and 2) monitoring the intrinsic tyrosine fluorescence of the ECD, taking advantage of 9 tyrosines and 0 tryptophans.

The binding of Zinc-bacitracin to the ECD of *Sa*NsrP was confirmed via the MALS measurement (Figure 20c). The peak of the ECD without Zn-bacitracin (blue) shows a molecular weight of 25.8 kDa, while the peak of the ECD with Zn-bacitracin (light blue) contains particles with 28 kDa. Thus, the difference of 2.2 kDa and the peak shift correlate with the expected size of Zn-bacitracin (1.5 kDa). Using a second independent method by monitoring the tyrosine fluorescence of *Sa*NsrP upon the addition of bacitracin or Zn-bacitracin, we could measure the change of tyrosine fluorescence with increasing concentrations of the antibiotic peptide (Figure 20d). For Zn-bacitracin a K_D of 255 µM was obtained and for bacitracin, a K_D of 300 µM was obtained. This could be expected since bacitracin is supposed to be repelled from the cell wall after ATP-dependently releasing its grip from its substrate UPP (Kobras *et al*., 2020). Controversially, it was shown for the complete permease BceB that bacitracin is bound with a K_D of 60 nM (Dintner *et al*., 2014). Loss of binding force for the ECD of *Sa*NsrP could be explained by using an ECD construct without its stalk helices. Furthermore, it could be hypothesized that the stalk helices might also be involved in stabilizing the bound bacitracin. Finally, we are the first to show stable expression and purification of an ECD and demonstrate via two independent experiments the interaction of the ECD of *Sa*NsrP with the antimicrobial peptides Zn-bacitracin and bacitracin.

Discussion:

To elucidate the structure-function relationship of the ECD and its role for the ABC transporter *Sa*NsrFP in conferring resistance against antimicrobial peptides, we are the first to successfully express and purify an ECD and demonstrate via SEC-MALS and via measuring intrinsic tyrosine fluorescence that it binds Zn-bacitracin/bacitracin and not nisin. In recent previous work, we show that *L. lactis*

NZ9000 cells expressing *Sa*NsrFP showed the highest resistance against Zn-bacitracin and bacitracin while conferring less fold resistance against cationic antimicrobial peptides such as nisin in comparison to the sensitive empty vector control strain (Gottstein *et al*., 2022). Due to the high difference of fold of resistance, it was concluded in the same study that there must be a first-line mechanism resulting in high bacitracin resistance and a general second-line defense, leading to modifications of the cell wall that wards off several structurally diverse cationic antimicrobial peptides. Thus, our data confirms this since only Zn-bacitracin/bacitracin can bind to the ECD of *Sa*NsrP. Furthermore, we analyzed putative binding sites in the ECD of NsrP. The analysis of putative binding sites in NsrP through SiteMap revealed two sites in the transmembrane region and the ECD. The presence of two binding sites is consistent with the mechanistic model proposed for the homologous protein BceAB, which postulates that this family of proteins detaches the lantibiotic from its lipidic target by first sequestering the complex through interactions with the transmembrane domain and then forming a direct interaction with the lantibiotic through the ECD (George *et al*., 2022).

Our docking results showed that bacitracin only yields good scoring poses and an interface consistent with the mutagenesis studies when it extends over the surface of the ECD. This might imply that the binding of bacitracin would prevent NsrP from adopting its active conformation. Moreover, the fact that two of the possible poses involve an interaction with the thiazoline moiety, which is essential for zinc coordination and, hence, antibiotic activity, suggests that the binding of bacitracin to NsrP and to lipid II are mutually exclusive, thus, making the ECD an effective inhibitor of the formation of a lipid II:bacitracin complex.

Out of the three bacitracin : NsrP complexes proposed, Cluster 8 was the least frequent solution and had the worst docking score and, therefore, is the least likely binding pose. On the other hand, Cluster 1 and Cluster 6 were the most frequent and best-scoring solutions, respectively. Despite displaying a similar relative orientation of bacitracin within the ECD, the interaction networks formed in each pose are different. The predicted network of interactions involving K481 is more complex for Cluster 6 than Cluster 1, which might result in an increased enthalpic contribution and, therefore, a better score. K481 likely is an essential component of the binding interface, since mutating it to alanine hindered

significantly the activity of NsrP. Overall, Cluster 6 is in better agreement with our experimental results.
Nonetheless, major conformational rearrangements in the ECD might occur upon bacitracin binding, which would limit the accuracy of our docking experiments. Still, our results constitute the first atomistic-level prediction of a binding mechanism between a protein belonging to the BceAB family of transporters and a lantibiotic target. Further research is needed to unravel the role of the conformational changes triggered by ATP hydrolysis in the process of decoupling bacitracin from Lipid II.

Bacitracin resistance has been displayed for several other BceAB-type transporter e.g. in *B*. *subtilis*, *L*. *monocytogenes*, *S*. *mutans*, *S*. *aureus (Gebhard, 2012),* and *S*. *pneumoniae* (Diagne *et al*., 2022). We furthermore show that BceAB transporters can be found in opportunistic pathogenic, clinically pathogenic, and a possibly related BceAB transporter of the YbbP type can be found even in Gram-negative ESKAPE organisms such as *A*. *baumannii* and *P*. *aeruginosa*. We postulate that it is highly likely that these BceAB transporters also confer resistance against bacitracin. This means that bacteria with bacitracin resistance can not only be found in soil bacteria, animals such as the gastrointestinal tract of bats but in human mucus bacteria (*S. mutans*), human gut bacteria, and excrement (*S. intestinalis, E. faecalis),* infection-causing bacteria in animals (*R. peoriensis*) and in humans (*E. faecium*, *S.aureus*, MRSA, *S. schweitzeri*, *C. difficile*, *C. neonatale*, *S. pneumoniae*, *S. agalactiae*, *B. cereus*, *L. monocytogenes*. If YbbP type BceAB transporter could also confer resistance against bacitracin then the list of clinical pathogens gets extended to the Gram-negative ESKAPE organisms *A. baumanni*, *Enterobacter,* and *P. aeruginosa.* The question remains how and why Gram-negative bacteria should have developed a resistance mechanism against bacitracin since bacitracin is not able to reach the cell wall due to the outer membrane. On the other side, to control Gram-positive as well as Gram-negative bacteria in minor wounds, ointments containing bacitracin plus polymyxin are prescribed and used (Cartotto, 2017). Thus, in the case that the outer membrane was destroyed by polymyxin, bacitracin could reach the peptidoglycan layer. Other methods also have been explored e.g., attaching bacitracin to biodegradable hydrophobic copolymers of

poly (D, L-lactide-coglycolide (PLGA) which can bring the nanoantibiotic to the periplasmic space of bacteria (Hong *et al*., 2017). It has been shown in the same study that this bioengineered molecule is active against Gram-negative bacteria. MacAB is one example of a Gram-negative bacteria-originating protein that has shown resistance against bacitracin (Crow *et al*., 2017). MacB is part of a tripartite efflux pump (MacAB-TolC) that confers antibiotic resistance. It is not at all clear if the bacitracin resistance mechanism is a side effect mechanism in Gram-negative bacteria or if it was actively developed.

Furthermore, we could assign ECDs from BceB structures from different bacteria in five groups, identifying conserved secondary structures in all (a set of 2 **β**-sheets over a set of three **β**-sheets and individual secondary structures for each group. In a previous study by (Dintner *et al*., 2011), ECDs were analyzed and grouped into 8 different groups. Within their tested BceAB transporters they identified a conserved arrangement of secondary structures in the order α-β- α-$\beta_{2\text{-}3}$ -α- $\beta_{3\text{-}4}$- α-β- $\alpha_{1\text{-}2}$ however some groups showed deviations from this (Dintner *et al*., 2011). In addition, the authors found that ECDs in their assigned group 2 contained a large number of both positively and negatively charged conserved residues, while in their groups 7 and 8 several conserved aromatic side chains were discovered. To date, a correlation of the sequence of the ECD with its substrate range has not been possible.

Conclusively, BceAB-type transporters such as *Sa*NsrFP are evolutionarily conserved in clinically relevant human pathogenic strains and nonpathogenic strains. Although less conserved at the sequence level, the topology of the protein and its cognate encoding operons are conserved. The results of this study are consistent with previous observations that *Sa*NsrFP confers resistance against bacitracin and now we were able to show that the ECD indeed binds bacitracin.

Acknowledgment

The authors thank Eymen Hachani for performing the MALS experiment.

The authors thank the Institute of Biochemistry for fruitful discussions and are thankful to the CSS for performing SAXS measurements. This work was funded by the Deutsche Forschungsgemeinschaft (DFG, German Research Foundation)—270650915/ GRK 2158 to S.S and HG. The Center for Structural Studies is funded by the Deutsche Forschungsgemeinschaft (DFG Grant number 417919780)

.

References

ABTS, A., MAVARO, A., STINDT, J., BAKKES, P. J., METZGER, S., DRIESSEN, A. J., SMITS, S. H. & SCHMITT, L. 2011. Easy and rapid purification of highly active nisin. *Int J Pept,* 2011**,** 175145.

ABTS, A., MONTALBAN-LOPEZ, M., KUIPERS, O. P., SMITS, S. H. & SCHMITT, L. 2013. NisC binds the FxLx motif of the nisin leader peptide. *Biochemistry,* 52**,** 5387-95.

ALOGHELI, H., OLANDERS, G., SCHAAL, W., BRANDT, P. & KARLEN, A. 2017. Docking of Macrocycles: Comparing Rigid and Flexible Docking in Glide. *J Chem Inf Model,* 57**,** 190-202.

BERNARD, R., GUISEPPI, A., CHIPPAUX, M., FOGLINO, M. & DENIZOT, F. 2007. Resistance to bacitracin in Bacillus subtilis: unexpected requirement of the BceAB ABC transporter in the control of expression of its own structural genes. *J Bacteriol,* 189**,** 8636-42.

BILSING, F. L., ANLAUF, M. T., HACHANI, E., KHOSA, S. & SCHMITT, L. 2023. ABC Transporters in Bacterial Nanomachineries. *Int J Mol Sci,* 24.

BUCHRIESER, C., RUSNIOK, C., KUNST, F., COSSART, P., GLASER, P. & LISTERIA, C. 2003. Comparison of the genome sequences of Listeria monocytogenes and Listeria innocua: clues for evolution and pathogenicity. *FEMS Immunol Med Microbiol,* 35**,** 207-13.

CARTOTTO, R. 2017. Topical antimicrobial agents for pediatric burns. *Burns Trauma,* 5**,** 33.

CHO, J., COSTA, S. K., WIERZBICKI, R. M., RIGBY, W. F. C. & CHEUNG, A. L. 2021. The extracellular loop of the membrane permease VraG interacts with GraS to sense cationic antimicrobial peptides in Staphylococcus aureus. *PLoS Pathog,* 17**,** e1009338.

CHO, J., RIGBY, W. F. C. & CHEUNG, A. L. 2022. The thematic role of extracellular loop of VraG in activation of the membrane sensor GraS in a cystic fibrosis MRSA strain differs in nuance from the CA-MRSA strain JE2. *PLoS One,* 17**,** e0270393.

CROW, A., GREENE, N. P., KAPLAN, E. & KORONAKIS, V. 2017. Structure and mechanotransmission mechanism of the MacB ABC transporter superfamily. *Proc Natl Acad Sci U S A,* 114**,** 12572-12577.

DIAGNE, A. M., PELLETIER, A., DURMORT, C., FAURE, A., KANONENBERG, K., FRETON, C., PAGE, A., DELOLME, F., VORAC, J., VALLET, S., BELLARD, L., VIVES, C., FIESCHI, F., VERNET, T., ROUSSELLE, P., GUIRAL, S., GRANGEASSE, C., JAULT, J. M. & ORELLE, C. 2022. Identification of a two-component regulatory system involved in antimicrobial peptide resistance in Streptococcus pneumoniae. *PLoS Pathog,* 18**,** e1010458.

DINTNER, S., HEERMANN, R., FANG, C., JUNG, K. & GEBHARD, S. 2014. A sensory complex consisting of an ATP-binding cassette transporter and a two-component regulatory system controls bacitracin resistance in Bacillus subtilis. *J Biol Chem,* 289**,** 27899-910.

DINTNER, S., STARON, A., BERCHTOLD, E., PETRI, T., MASCHER, T. & GEBHARD, S. 2011. Coevolution of ABC transporters and two-component regulatory systems as resistance modules against antimicrobial peptides in Firmicutes Bacteria. *J Bacteriol,* 193**,** 3851-62.

FALORD, M., KARIMOVA, G., HIRON, A. & MSADEK, T. 2012. GraXSR proteins interact with the VraFG ABC transporter to form a five-component system required for cationic antimicrobial peptide sensing and resistance in Staphylococcus aureus. *Antimicrob Agents Chemother,* 56**,** 1047-58.

FELSENSTEIN, J. 2005. PHYLIP (Phylogeny Inference Package) version 3.6. *Distributed by the author. Department of Genome Sciences, University of Washington, Seattle*.

FISCHER, H., NETO, M. D., NAPOLITANO, H. B., POLIKARPOV, I. & CRAIEVICH, A. F. 2010. Determination of the molecular weight of proteins in solution from a single small-angle X-ray scattering measurement on a relative scale. *Journal of Applied Crystallography,* 43**,** 101-109.

FRITZ, G., DINTNER, S., TREICHEL, N. S., RADECK, J., GERLAND, U., MASCHER, T. & GEBHARD, S. 2015. A New Way of Sensing: Need-Based Activation of Antibiotic Resistance by a Flux-Sensing Mechanism. *mBio,* 6**,** e00975.

FURTMANN, F., PORTA, N., HOANG, D. T., REINERS, J., SCHUMACHER, J., GOTTSTEIN, J., GOHLKE, H. & SMITS, S. H. J. 2020. Characterization of the nucleotide-binding domain NsrF from the BceAB-type ABC-transporter NsrFP from the human pathogen Streptococcus agalactiae. *Sci Rep,* 10**,** 15208.

GEBHARD, S. 2012. ABC transporters of antimicrobial peptides in Firmicutes bacteria - phylogeny, function and regulation. *Mol Microbiol,* 86**,** 1295-317.

GEBHARD, S. & MASCHER, T. 2011. Antimicrobial peptide sensing and detoxification modules: unravelling the regulatory circuitry of Staphylococcus aureus. *Mol Microbiol,* 81**,** 581-7.

GEORGE, N. L., SCHILMILLER, A. L. & ORLANDO, B. J. 2022. Conformational snapshots of the bacitracin sensing and resistance transporter BceAB. *Proc Natl Acad Sci U S A,* 119**,** e2123268119.

GOTTSTEIN, J., ZASCHKE-KRIESCHE, J., UNSLEBER, S., VOITSEKHOVSKAIA, I., KULIK, A., BEHRMANN, L. V., OVERBECK, N., STUHLER, K., STEGMANN, E. & SMITS, S. H. J. 2022. New insights into the resistance mechanism for the BceAB-type transporter SaNsrFP. *Sci Rep,* 12**,** 4232.

GREENE, N. P., KAPLAN, E., CROW, A. & KORONAKIS, V. 2018. Antibiotic Resistance Mediated by the MacB ABC Transporter Family: A Structural and Functional Perspective. *Front Microbiol,* 9**,** 950.

HAJIZADEH, N. R., FRANKE, D., JEFFRIES, C. M. & SVERGUN, D. I. 2018. Consensus Bayesian assessment of protein molecular mass from solution X-ray scattering data. *Sci Rep,* 8**,** 7204.

HALGREN, T. A. 2009. Identifying and Characterizing Binding Sites and Assessing Druggability. *Journal of Chemical Information and Modeling,* 49**,** 377-389.

HIRON, A., FALORD, M., VALLE, J., DEBARBOUILLE, M. & MSADEK, T. 2011. Bacitracin and nisin resistance in Staphylococcus aureus: a novel pathway involving the BraS/BraR two-component system (SA2417/SA2418) and both the BraD/BraE and VraD/VraE ABC transporters. *Mol Microbiol,* 81**,** 602-22.

HONG, W., GAO, X., QIU, P., YANG, J., QIAO, M., SHI, H., ZHANG, D., TIAN, C., NIU, S. & LIU, M. 2017. Synthesis, construction, and evaluation of self-assembled nano-bacitracin A as an efficient antibacterial agent in vitro and in vivo. *Int J Nanomedicine,* 12**,** 4691-4708.

JUMPER, J., EVANS, R., PRITZEL, A., GREEN, T., FIGURNOV, M., RONNEBERGER, O., TUNYASUVUNAKOOL, K., BATES, R., ZIDEK, A., POTAPENKO, A., BRIDGLAND, A., MEYER, C., KOHL, S. A. A., BALLARD, A. J., COWIE, A., ROMERA-PAREDES, B., NIKOLOV, S., JAIN, R., ADLER, J., BACK, T., PETERSEN, S., REIMAN, D., CLANCY, E., ZIELINSKI, M., STEINEGGER, M., PACHOLSKA, M., BERGHAMMER, T., BODENSTEIN, S., SILVER, D., VINYALS, O., SENIOR, A. W., KAVUKCUOGLU, K., KOHLI, P. & HASSABIS, D. 2021. Highly accurate protein structure prediction with AlphaFold. *Nature,* 596**,** 583-589.

KHOSA, S., ALKHATIB, Z. & SMITS, S. H. 2013. NSR from Streptococcus agalactiae confers resistance against nisin and is encoded by a conserved nsr operon. *Biol Chem,* 394**,** 1543-9.

KINGSTON, A. W., ZHAO, H., COOK, G. M. & HELMANN, J. D. 2014. Accumulation of heptaprenyl diphosphate sensitizes Bacillus subtilis to bacitracin: implications for the mechanism of resistance mediated by the BceAB transporter. *Mol Microbiol,* 93**,** 37-49.

KOBRAS, C. M., PIEPENBREIER, H., EMENEGGER, J., SIM, A., FRITZ, G. & GEBHARD, S. 2020. BceAB-Type Antibiotic Resistance Transporters Appear To Act by Target Protection of Cell Wall Synthesis. *Antimicrob Agents Chemother,* 64.

KONAREV, P. V., VOLKOV, V. V., SOKOLOVA, A. V., KOCH, M. H. J. & SVERGUN, D. I. 2003. PRIMUS: a Windows PC-based system for small-angle scattering data analysis. *Journal of Applied Crystallography,* 36**,** 1277-1282.

KOZIN, M. B. & SVERGUN, D. I. 2001. Automated matching of high- and low-resolution structural models. *Journal of Applied Crystallography,* 34**,** 33-41.

LOCKEY, C., EDWARDS, R. J., ROPER, D. I. & DIXON, A. M. 2020. The Extracellular Domain of Two-component System Sensor Kinase VanS from Streptomyces coelicolor Binds Vancomycin at a Newly Identified Binding Site. *Sci Rep,* 10**,** 5727.

MANALASTAS-CANTOS, K., KONAREV, P. V., HAJIZADEH, N. R., KIKHNEY, A. G., PETOUKHOV, M. V., MOLODENSKIY, D. S., PANJKOVICH, A., MERTENS, H. D. T., GRUZINOV, A., BORGES, C., JEFFRIES, C. M., SVERGUN, D. I. & FRANKE, D. 2021. ATSAS 3.0: expanded functionality and new tools for small-angle scattering data analysis. *Journal of Applied Crystallography,* 54.

MASCHER, T. 2006. Intramembrane-sensing histidine kinases: a new family of cell envelope stress sensors in Firmicutes bacteria. *FEMS Microbiol Lett,* 264**,** 133-44.

MASCHER, T., MARGULIS, N. G., WANG, T., YE, R. W. & HELMANN, J. D. 2003. Cell wall stress responses in Bacillus subtilis: the regulatory network of the bacitracin stimulon. *Molecular Microbiology,* 50**,** 1591-1604.

MIRDITA, M., SCHUTZE, K., MORIWAKI, Y., HEO, L., OVCHINNIKOV, S. & STEINEGGER, M. 2022. ColabFold: making protein folding accessible to all. *Nat Methods,* 19**,** 679-682.

MOLODENSKIY, D. S., SVERGUN, D. I. & KIKHNEY, A. G. 2022. Artificial neural networks for solution scattering data analysis. *Structure,* 30**,** 900-908 e2.

MULNAES, D. & GOHLKE, H. 2018. TopScore: Using Deep Neural Networks and Large Diverse Data Sets for Accurate Protein Model Quality Assessment. *J Chem Theory Comput,* 14**,** 6117-6126.

NISINRIETKOTTER, E., HOYER, D. & MASCHER, T. 2008. Bacitracin sensing in Bacillus subtilis. *Mol Microbiol,* 68**,** 768-85.

PERNOT, P., ROUND, A., BARRETT, R., DE MARIA ANTOLINOS, A., GOBBO, A., GORDON, E., HUET, J., KIEFFER, J., LENTINI, M., MATTENET, M., MORAWE, C., MUELLER-DIECKMANN, C., OHLSSON, S., SCHMID, W., SURR, J., THEVENEAU, P., ZERRAD, L. & MCSWEENEY, S. 2013. Upgraded ESRF BM29 beamline for SAXS on macromolecules in solution. *J Synchrotron Radiat,* 20**,** 660-4.

PERNOT, P., THEVENEAU, P., GIRAUD, T., FERNANDES, R. N., NURIZZO, D., SPRUCE, D., SURR, J., MCSWEENEY, S., ROUND, A., FELISAZ, F., FOEDINGER, L., GOBBO, A., HUET, J., VILLARD, C. & CIPRIANI, F. 2010. New beamline dedicated to solution scattering from biological macromolecules at the ESRF. *Journal of Physics: Conference Series,* 247**,** 012009.

PETOUKHOV, M. V. & SVERGUN, D. I. 2015. Ambiguity assessment of small-angle scattering curves from monodisperse systems. *Acta Crystallogr D Biol Crystallogr,* 71**,** 1051-8.

POROD, G. 1951. Die Röntgenkleinwinkelstreuung Von Dichtgepackten Kolloiden Systemen - 1 Teil. *Kolloid-Zeitschrift and Zeitschrift Fur Polymere,* 124**,** 83-114.

PRICE, C. E., ZEYNIYEV, A., KUIPERS, O. P. & KOK, J. 2012. From meadows to milk to mucosa - adaptation of Streptococcus and Lactococcus species to their nutritional environments. *FEMS Microbiol Rev,* 36**,** 949-71.

PYMOL 2015. The PyMOL Molecular Graphics System, Version 2.0 Schrödinger, LLC.

RAMBO, R. P. & TAINER, J. A. 2013. Accurate assessment of mass, models and resolution by small-angle scattering. *Nature,* 496**,** 477-81.

REINERS, J., LAGEDROSTE, M., EHLEN, K., LEUSCH, S., ZASCHKE-KRIESCHE, J. & SMITS, S. H. J. 2017. The N-terminal Region of Nisin Is Important for the BceAB-Type ABC Transporter NsrFP from Streptococcus agalactiae COH1. *Front Microbiol,* 8**,** 1643.

REINERS, J., LAGEDROSTE, M., GOTTSTEIN, J., ADENIYI, E. T., KALSCHEUER, R., POSCHMANN, G., STUHLER, K., SMITS, S. H. J. & SCHMITT, L. 2020. Insights in the Antimicrobial Potential of the Natural Nisin Variant Nisin H. *Front Microbiol,* 11**,** 573614.

REPASKY, M. P., SHELLEY, M. & FRIESNER, R. A. 2007. Flexible ligand docking with Glide. *Curr Protoc Bioinformatics,* Chapter 8**,** Unit 8 12.

REVILLA-GUARINOS, A., GEBHARD, S., MASCHER, T. & ZUNIGA, M. 2014. Defence against antimicrobial peptides: different strategies in Firmicutes. *Environ Microbiol,* 16**,** 1225-37.

ROE, D. R. & CHEATHAM, T. E., 3RD 2013. PTRAJ and CPPTRAJ: Software for Processing and Analysis of Molecular Dynamics Trajectory Data. *J Chem Theory Comput,* 9**,** 3084-95.

ROSTKOWSKI, M., OLSSON, M. H., SONDERGAARD, C. R. & JENSEN, J. H. 2011. Graphical analysis of pH-dependent properties of proteins predicted using PROPKA. *BMC Struct Biol,* 11**,** 6.

SLOTBOOM, D. J., DUURKENS, R. H., OLIEMAN, K. & ERKENS, G. B. 2008. Static light scattering to characterize membrane proteins in detergent solution. *Methods,* 46**,** 73-82.

STARON, A., FINKEISEN, D. E. & MASCHER, T. 2011. Peptide antibiotic sensing and detoxification modules of Bacillus subtilis. *Antimicrob Agents Chemother,* 55**,** 515-25.

SVERGUN, D., BARBERATO, C. & KOCH, M. H. J. 1995. CRYSOL - A program to evaluate x-ray solution scattering of biological macromolecules from atomic coordinates. *Journal of Applied Crystallography,* 28**,** 768-773.

SVERGUN, D. I. 1992. Determination of the Regularization Parameter in Indirect-Transform Methods Using Perceptual Criteria. *Journal of Applied Crystallography,* 25**,** 495-503.

SVERGUN, D. I., PETOUKHOV, M. V. & KOCH, M. H. 2001. Determination of domain structure of proteins from X-ray solution scattering. *Biophys J,* 80**,** 2946-53.

TACCONELLI, E., CARRARA, E., SAVOLDI, A., HARBARTH, S., MENDELSON, M., MONNET, D. L., PULCINI, C., KAHLMETER, G., KLUYTMANS, J., CARMELI, Y., OUELLETTE, M., OUTTERSON, K., PATEL, J., CAVALERI, M., COX, E. M., HOUCHENS, C. R., GRAYSON, M. L., HANSEN, P., SINGH, N., THEURETZBACHER, U., MAGRINI, N. & GROUP, W. H. O. P. P. L. W. 2018. Discovery, research, and development of new antibiotics: the WHO priority list of antibiotic-resistant bacteria and tuberculosis. *Lancet Infect Dis,* 18**,** 318-327.

THOMAS, C., ALLER, S. G., BEIS, K., CARPENTER, E. P., CHANG, G., CHEN, L., DASSA, E., DEAN, M., DUONG VAN HOA, F., EKIERT, D., FORD, R., GAUDET, R., GONG, X., HOLLAND, I. B., HUANG, Y., KAHNE, D. K., KATO, H., KORONAKIS, V., KOTH, C. M., LEE, Y., LEWINSON, O., LILL, R., MARTINOIA, E., MURAKAMI, S., PINKETT, H. W., POOLMAN, B., ROSENBAUM, D., SARKADI, B., SCHMITT, L., SCHNEIDER, E., SHI, Y., SHYNG, S. L., SLOTBOOM, D. J., TAJKHORSHID, E., TIELEMAN, D. P., UEDA, K., VARADI, A., WEN, P. C., YAN, N., ZHANG, P., ZHENG, H., ZIMMER, J. & TAMPE, R. 2020. Structural and functional diversity calls for a new classification of ABC transporters. *FEBS Lett,* 594**,** 3767-3775.

TOLLERSON, R., 2ND & IBBA, M. 2020. Translational regulation of environmental adaptation in bacteria. *J Biol Chem,* 295**,** 10434-10445.

VARADI, M., ANYANGO, S., DESHPANDE, M., NAIR, S., NATASSIA, C., YORDANOVA, G., YUAN, D., STROE, O., WOOD, G., LAYDON, A., ZIDEK, A., GREEN, T., TUNYASUVUNAKOOL, K., PETERSEN, S., JUMPER, J., CLANCY, E., GREEN, R., VORA, A., LUTFI, M., FIGURNOV, M., COWIE, A., HOBBS, N., KOHLI, P., KLEYWEGT, G., BIRNEY, E., HASSABIS, D. & VELANKAR, S. 2022. AlphaFold Protein Structure Database: massively expanding the structural coverage of protein-sequence space with high-accuracy models. *Nucleic Acids Res,* 50**,** D439-D444.

WELLS, K. M., CIFTCI, Y., PEDDINTI, B. S. T., GHILADI, R. A., VEDIYAPPAN, G., SPONTAK, R. J. & GOVIND, R. 2023. Preventing the spread of life-threatening gastrointestinal microbes on the surface of a continuously self-disinfecting block polymer. *J Colloid Interface Sci,* 652**,** 718-726.

WOLF, D., DOMINGUEZ-CUEVAS, P., DANIEL, R. A. & MASCHER, T. 2012. Cell envelope stress response in cell wall-deficient L-forms of Bacillus subtilis. *Antimicrob Agents Chemother,* 56**,** 5907-15.

ZHOU, X., WILLEMS, R. J. L., FRIEDRICH, A. W., ROSSEN, J. W. A. & BATHOORN, E. 2020. Enterococcus faecium: from microbiological insights to practical recommendations for infection control and diagnostics. *Antimicrob Resist Infect Control,* 9**,** 130.

Supplementary information:

BceAB transport is more widely distributed than expected

Julia Gottstein[1], Christian Mammen[1], Pablo Cea Medina[3], Kira Tantsur[1], Jens Reiners[2], Holger Gohlke[3], Sander H. J. Smits[1,2*]

[1]Institute of Biochemistry I, Heinrich Heine University Düsseldorf, Düsseldorf, Germany.
[2]Center for Structural Studies, Heinrich Heine University Düsseldorf, Düsseldorf, Germany.
[3]Institute of Pharmaceutical and Medicinal Chemistry, Heinrich-Heine-University Düsseldorf, Düsseldorf, Germany

[*] To whom correspondence should be addressed:

Sander Smits
Institute of Biochemistry
Heinrich Heine University Düsseldorf
Universitätsstr. 1
40225 Düsseldorf, Germany
Phone: +49(0)211-81-12647
Fax: +49(0)211-81-15310
Email: sander.smits@hhu.de

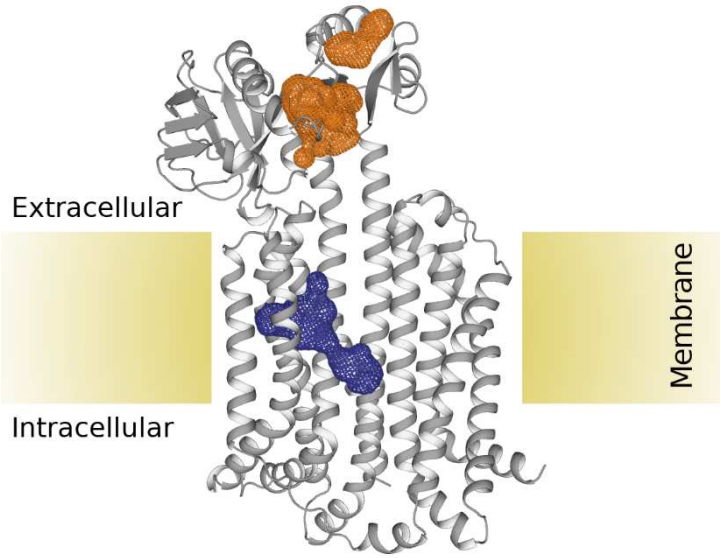

Supplementary Figure 1AKHG. Putative ligand binding sites on NsrFP. The putative binding site located in the transmembrane domain is shown as a blue mesh, whereas the putative binding site on the extracellular domain is shown as an orange mesh.

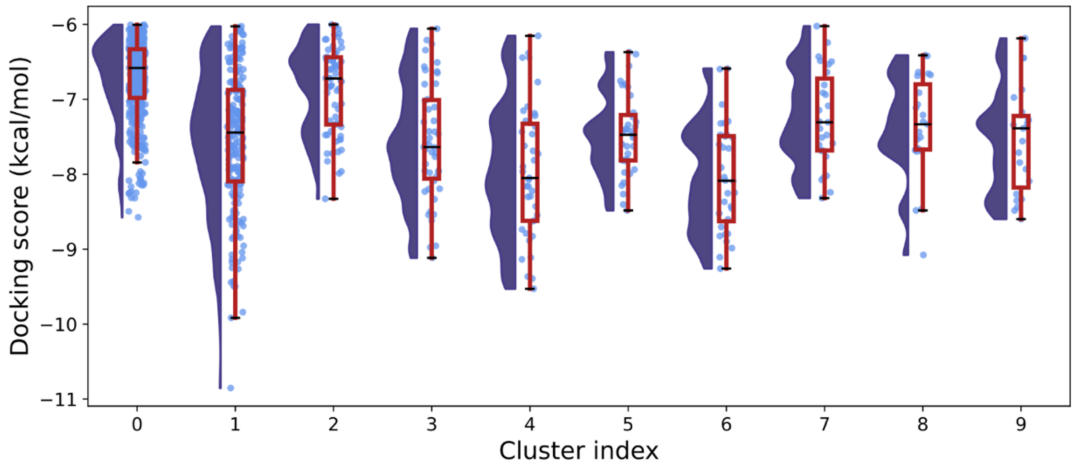

Supplementary Figure 2AKHG. Rain cloud plots showing the energy score distribution per cluster. The half-violin plots show the data density distribution (dark blue), each data point is shown in light blue. A box plot is overlayed on top (red). Its center line indicates the median of the distribution, the edges of the box show the lower and upper quartile and the whiskers show the minimum and maximum values of the distribution, excluding outliers (defined as points 1.5 times outside the difference between the lower and upper quartile).

Supplement Table S1: Overview of RMSDs and atoms of the structural alignment for BceB ECDs of different bacterial strains

RMSD in Å	NsrFP agalactiae (310 - 516)	BceB subtilis (321 - 516)	BceB peoriensis (321- 568)	BceB oralis (315 - 540)	BceB intestinalis (326 - 588)	BceB cereus (319 - 519)	BceB difficile (315 - 567)	BceB neonatale (320 - 541)	BceB tadaridae (316 - 518)	VraG schweitzeri (316 - 498)	FtsX faecalis (326 - 552)	FtsX baumannii right (495 - 679)	FtsX baumannii left (51 - 245)
NsrFP agalactiae (310 - 516)		6.286	5.542	6.088	5.913	5.823	5.94	5.645	6.601	5.667	5.913	5.802	5.254
BceB subtilis (321 - 516)	6.286		5.098	4.694	5.766	4.591	5.001	4.573	3.829	2.798	4.363	5.642	6.908
BceB peoriensis (321- 568)	5.542	5.098		5.506	5.318	5.563	5.197	6.38	4.836	5.185	4.799	5.742	6.333
BceB oralis (315 - 540)	6.088	4.694	5.506		5.124	4.648	6.487	5.09	5.53	4.563	4.555	6.732	5.94
BceB intestinalis (326 - 588)	5.913	5.766	5.318	5.124		4.063	6.005	3.557	5.749	5.423	5.25	6.673	6.063
BceB cereus (319 - 519)	5.823	4.591	5.563	4.648	4.063		3.987	4.347	3.6653	5	3.019	6.033	6.288
BceB difficile (315 - 567)	5.94	5.001	5.197	6.487	6.005	3.987		4.88	5.439	5.724	5.335	6.015	6.643
BceB neonatale (320 - 541)	5.645	4.573	6.38	5.09	3.557	4.347	4.88		5.577	5.389	5.086	6.335	6.004
BceB tadaridae (316 - 518)	6.601	3.829	4.836	5.53	5.749	3.6653	5.439	5.577		4.6743	3.838	5.761	6.503
BceB VraG schweitzeri (316 - 498)	5.667	2.798	5.185	4.563	5.423	5	5.724	5.389	4.6743		3.363	6.121	5.926
FtsX faecalis (326 - 552)	5.913	4.363	4.799	4.555	5.25	3.019	5.335	5.086	3.838	3.363		6.398	6.54
FtsX baumannii right (495 - 679)	5.802	5.642	5.742	6.732	6.673	6.033	6.015	6.335	5.761	6.121	6.398		5.3
FtsX baumannii left (51 - 245)	5.254	6.908	6.333	5.94	6.063	6.288	6.643	6.004	6.503	5.926	6.54	5.3	
FtsX aeruginosa (501 - 697) right	6.533	5.587	5.274	6.354	6.593	5.743	6.947	6.765	7.085	6.084	6.246	1.986	6.615
FtsX aeruginosa (59 - 252) left	4.908	6.886	6.582	6.101	6.316	6.83	7.507	6.305	7.128	6.166	6.463	5.257	1.846
FtsX faecium (326 - 553)	5.963	3.585	5.12	4.722	5.507	4.085	5.134	5.227	4.358	4.207	1.657	6.628	7.306
FtsX pneumoniae (314 - 527)	4.434	5.354	7.983	5.182	6.154	5.527	5.828	6.134	6.115	5.436	5.033	5.395	5.707
YbbP (482 - 665) sp right	5.048	6.69	5.321	6.611	6.68	6.148	5.722	6.171	6.853	5.957	6.338	1.524	5.575
YbbP (48 - 235) sp left	4.928	7.401	5.85	6.43	6.957	6.587	6.706	6.341	7.261	6.812	7.876	5.128	1.781
VraG aureus (320 - 502)	5.619	2.912	5.631	4.52	5.471	5.011	5.661	5.249	4.61	1.028	4.565	5.87	6.21
HrtB03 aureus (320 - 496)	5.192	3.321	6.108	4.922	5.713	4.466	5.145	4.856	4.63	2.165	4.39	5.85	5.317
HrtB02 aureus (315 - 528)	3.995	5.834	5.903	6.75	6.574	5.535	5.567	6.711	7.031	5.072	6.066	6.313	5.818
VraE aureus (320- 496)	6.468	3.181	4.959	5.054	4.358	4.359	5.936	5.2	4.215	2.417	4.259	5.84	5.529
Lmo monocytogenes (320 - 516)	5.681	4.082	4.902	4.717	4.758	3.253	4.275	5.614	4.586	4.393	3.857	5.96	6.715
AnrAB monocytogenes (330 - 540)	6.801	4.642	5.029	5.084	5.363	4.824	4.494	6.18	5.367	5.115	4.438	5.327	6.649
VirAB monocytogenes (319 - 528)	6.248	5.149	5.418	5.158	5.294	4.789	4.346	5.414	5.385	5.142	4.503	5.554	6.709
PsdB subtilis (313 - 516)	6.099	3.88	4.639	5.497	6.186	3.92	3.396	5.206	4.111	4.513	4.569	5.861	6.776
YxdM subtilis (301 - 495)	5.892	4.924	4.647	5.717	4.935	3.52	3.792	4.702	4.548	5.358	3.548	5.517	6.389
MbrB mutans (310 - 532)	2.66	5.471	5.998	5.773	6.759	5.451	5.539	5.141	6.571	5.194	5.735	6.202	5.172
YsaB lactis (310 - 532)	4.196	6.611	6.066	6.239	6.002	5.945	5.878	5.796	6.807	5.926	6.017	5.993	6.377
ABC3 pneumonie right (482 - 665)	5.673	6.681	6.387	5.909	6.686	6.453	6.371	6.183	6.846	5.803	7.114	1.698	5.615
ABC3 pneumonie left (48 - 234)	4.964	7.368	5.836	6.421	6.906	6.609	7.545	6.266	7.236	6.647	7.208	5.161	1.737

Number of atoms in alignment	NsrFP agalactiae (310 - 516)	BceB subtilis (321 - 516)	BceB peoriensis (321- 568)	BceB oralis (315 - 540)	BceB intestinalis (326 - 588)	BceB cereus (319 - 519)	BceB difficile (315 - 567)	BceB neonatale (320 - 541)	BceB tadaridae (316 - 518)	VraG schweitzeri (316 - 498)	FtsX faecalis (326 - 552)	FtsX baumannii right (495 - 679)	FtsX baumannii left (51 - 245)
NsrFP agalactiae (310 - 516)		168	144	168	176	168	160	176	160	160	128	160	160
BceB subtilis (321 - 516)	168		144	176	160	168	168	168	184	176	168	152	152
BceB peoriensis (321- 568)	144	144		152	152	160	144	160	152	144	136	144	144
BceB oralis (315 - 540)	168	176	152		200	168	168	192	184	168	168	160	152
BceB intestinalis (326 - 588)	176	160	152	200		160	128	208	152	160	152	144	168
BceB cereus (319 - 519)	168	168	160	168	160		176	176	176	160	160	152	152
BceB difficile (315 - 567)	160	168	144	168	128	176		112	168	160	168	104	144
BceB neonatale (320 - 541)	176	168	160	192	208	176	112		184	160	168	168	168
BceB tadaridae (316 - 518)	160	184	152	184	152	176	168	184		176	168	136	136
BceB VraG schweitzeri (316 - 498)	160	176	144	168	160	160	160	160	176		160	144	152
FtsX faecalis (326 - 552)	128	168	136	168	152	160	168	168	168	160		136	136
FtsX baumannii right (495 - 679)	160	152	144	160	144	152	104	168	136	144	136		152
FtsX baumannii left (51 - 245)	160	152	144	152	168	152	144	168	136	152	136	152	
FtsX aeruginosa (501 - 697) right	128	152	136	160	160	152	136	168	160	144	144	184	152
FtsX aeruginosa (59 - 252) left	160	152	136	152	160	160	136	160	144	160	144	152	184
FtsX faecium (326 - 553)	152	160	152	168	160	168	168	152	168	160	224	144	136
FtsX pneumoniae (314 - 527)	184	160	144	168	168	176	168	184	160	168	152	152	168
YbbP (482 - 665) sp right	160	160	136	152	160	152	144	160	160	152	128	176	160
YbbP (48 - 235) sp left	168	136	128	144	160	160	136	160	144	152	136	160	184
VraG aureus (320 - 502)	160	176	144	168	160	160	160	160	176	176	168	152	160
HrtB03 aureus (320 - 496)	152	168	136	160	168	152	152	152	168	168	160	144	136
HrtB02 aureus (315 - 528)	184	160	128	168	120	168	176	168	176	160	160	144	160
VraE aureus (320- 496)	144	168	128	160	152	152	152	152	168	168	160	144	136
Lmo monocytogenes (320 - 516)	168	176	168	176	176	176	160	176	184	160	160	160	152
AnrAB monocytogenes (330 - 540)	160	176	176	176	144	184	176	176	184	160	176	152	136
VirAB monocytogenes (319 - 528)	152	176	176	176	144	184	176	168	184	160	176	152	136
PsdB subtilis (313 - 516)	168	168	160	184	152	176	176	184	184	168	168	160	168
YxdM subtilis (301 - 495)	152	160	144	152	144	176	168	168	168	152	152	152	120
MbrB mutans (310 - 532)	200	168	152	160	184	176	168	184	184	168	160	160	176
YsaB lactis (310 - 532)	192	176	144	168	152	176	168	168	168	160	160	160	176
ABC3 pneumonie right (482 - 665)	160	160	144	160	160	152	152	160	160	152	136	176	160
ABC3 pneumonie left (48 - 234)	168	136	128	144	160	160	136	160	136	152	144	160	184

Supplement Table S1: Overview of RMSDs and atoms of the structural alignment for BceB ECDs of different bacterial strains

RMSD in Å	FtsX aeruginosa right (501 - 697)	FtsX aeruginosa left (59 - 252)	FtsX faecium (326 - 553)	FtsX pneumoniae (314 - 527)	YbbP sp right (482 - 665)	YbbP sp left (48 - 235)	VraG aureus (320 - 502)	HrtB03 aureus (320 - 496)	HrtB02 aureus (315 - 528)	VraE aureus (320- 496)	Lmo monocytogenes (320 - 516)	AnrAB monocytogenes (330 - 540)	VirAB monocytogenes (319 - 528)
NsrFP agalactiae (310 - 516)	6.533	4.908	5.963	4.434	5.048	4.928	5.619	5.192	3.995	6.468	5.681	6.801	6.248
BceB subtilis (321 - 516)	5.587	6.886	3.585	5.354	6.69	7.401	2.912	3.321	5.834	3.181	4.082	4.642	5.149
BceB peoriensis (321- 568)	5.274	6.582	5.12	7.983	5.321	5.85	5.631	6.108	5.903	4.959	4.902	5.029	5.418
BceB oralis (315 - 540)	6.354	6.101	4.722	5.182	6.611	6.43	4.52	4.922	6.75	5.054	4.717	5.084	5.158
BceB intestinalis (326 - 588)	6.593	6.316	5.507	6.154	6.68	6.957	5.471	5.713	6.574	4.358	4.758	5.363	5.294
BceB cereus (319 - 519)	5.743	6.83	4.085	5.527	6.148	6.587	5.011	4.466	5.535	4.359	3.253	4.824	4.789
BceB difficile (315 - 567)	6.947	7.507	5.134	5.828	5.722	6.706	5.661	5.145	5.567	5.936	4.275	4.494	4.346
BceB neonatale (320 - 541)	6.765	6.305	5.227	6.134	6.171	6.341	5.249	4.856	6.711	5.2	5.614	6.18	5.414
BceB tadaridae (316 - 518)	7.085	7.128	4.358	6.115	6.853	7.261	4.61	4.63	7.031	4.215	4.586	5.367	5.385
BceB VraG schweitzeri (316 - 498)	6.084	6.166	4.207	5.436	5.957	6.812	1.028	2.165	5.072	2.417	4.393	5.115	5.142
FtsX faecalis (326 - 552)	6.246	6.463	1.657	5.033	6.338	7.876	4.565	4.39	6.066	4.259	3.857	4.438	4.503
FtsX baumannii right (495 - 679)	1.986	5.257	6.628	5.395	1.524	5.128	5.87	5.85	6.313	5.84	5.96	5.327	5.554
FtsX baumannii left (51 - 245)	6.615	1.846	7.306	5.707	5.575	1.781	6.21	5.317	5.818	5.529	6.715	6.649	6.709
FtsX aeruginosa (501 - 697) right		7.425	5.849	6.387	1.621	6.211	5.592	5.064	6.383	5.85	5.476	5.226	5.365
FtsX aeruginosa (59 - 252) left	7.425		6.608	5.319	5.048	1.571	6.277	5.448	6.566	5.682	6.056	7.071	6.762
FtsX faecium (326 - 553)	5.849	6.608		5.009	6.774	7.451	4.315	4.28	5.2	4.57	3.772	3.665	3.724
FtsX pneumoniae (314 - 527)	6.387	5.319	5.009		5.62	6.541	5.409	5.199	3.8	5.277	5.719	5.267	5.911
YbbP (482 - 665) sp right	1.621	5.048	6.774	5.62		5.176	5.58	5.987	6.17	6	5.848	5.831	5.317
YbbP (48 - 235) sp left	6.211	1.571	7.451	6.541	5.176		6.68	5.789	5.997	5.803	6.65	7.162	7.12
VraG aureus (320 - 502)	5.592	6.277	4.315	5.409	5.58	6.68		2.142	4.994	2.359	4.572	5.256	4.896
HrtB03 aureus (320 - 496)	5.064	5.448	4.28	5.199	5.987	5.789	2.142		4.698	0.589	4.222	5.824	5.546
HrtB02 aureus (315 - 528)	6.383	6.566	5.2	3.8	6.17	5.997	4.994	4.698		4.945	4.965	5.914	5.719
VraE aureus (320- 496)	5.85	5.682	4.57	5.277	6	5.803	2.359	0.589	4.945		4.303	5.383	5.399
Lmo monocytogenes (320 - 516)	5.476	6.056	3.772	5.719	5.848	6.65	4.572	4.222	4.965	4.303		3.675	3.771
AnrAB monocytogenes (330 - 540)	5.226	7.071	3.665	5.267	5.831	7.162	5.256	5.824	5.914	5.383	3.675		0.391
VirAB monocytogenes (319 - 528)	5.365	6.762	3.724	5.911	5.317	7.12	4.896	5.546	5.719	5.399	3.771	0.391	
PsdB subtilis (313 - 516)	6.183	6.675	3.951	6.415	5.962	6.969	4.323	4.223	5.899	4.133	4.422	3.931	3.974
YxdM subtilis (301 - 495)	5.156	6.438	3.733	5.862	5.838	6.479	5.198	5.581	5.147	5.317	4.194	4.147	4.088
MbrB mutans (310 - 532)	6.258	5.485	5.406	3.804	5.744	5.125	5.153	6.721	3.902	4.678	5.851	5.918	5.859
YsaB lactis (310 - 532)	5.631	5.691	5.664	4.585	5.918	5.875	6.785	6.115	4.246	5.792	6.179	6.51	6.13
ABC3 pneumonie right (482 - 665)	1.6	5.241	6.08	5.498	0.466	5.392	5.631	5.976	5.786	6.097	5.007	5.859	5.478
ABC3 pneumonie left (48 - 234)	6.242	1.537	7.465	6.559	5.783	0.403	6.512	5.755	6.296	5.769	6.731	6.952	7.008

Number of atoms in alignment	FtsX aeruginosa right (501 - 697)	FtsX aeruginosa left (59 - 252)	FtsX faecium (326 - 553)	FtsX pneumoniae (314 - 527)	YbbP sp right (482 - 665)	YbbP sp left (48 - 235)	VraG aureus (320 - 502)	HrtB03 aureus (320 - 496)	HrtB02 aureus (315 - 528)	VraE aureus (320- 496)	Lmo monocytogenes (320 - 516)	AnrAB monocytogenes (330 - 540)	VirAB monocytogenes (319 - 528)
NsrFP agalactiae (310 - 516)	128	160	152	184	160	168	160	152	184	144	168	160	152
BceB subtilis (321 - 516)	152	152	160	160	160	136	176	168	160	168	176	176	176
BceB peoriensis (321- 568)	136	136	152	144	136	128	144	136	128	128	168	176	176
BceB oralis (315 - 540)	160	152	168	168	152	144	168	160	168	160	176	176	176
BceB intestinalis (326 - 588)	160	160	160	168	160	160	160	168	120	152	176	144	144
BceB cereus (319 - 519)	152	160	168	176	152	160	160	152	168	152	176	184	184
BceB difficile (315 - 567)	136	136	168	168	144	136	160	152	176	152	160	176	176
BceB neonatale (320 - 541)	168	160	152	184	160	160	160	152	168	152	176	176	168
BceB tadaridae (316 - 518)	160	144	168	160	160	144	176	168	176	168	184	184	184
BceB VraG schweitzeri (316 - 498)	144	160	160	168	152	152	176	168	160	168	160	160	160
FtsX faecalis (326 - 552)	144	144	224	152	128	136	168	160	160	160	160	176	176
FtsX baumannii right (495 - 679)	184	152	144	152	176	160	152	144	144	144	160	152	152
FtsX baumannii left (51 - 245)	152	184	136	168	160	184	160	136	160	136	152	136	136
FtsX aeruginosa (501 - 697) right		128	144	152	184	152	144	136	144	144	160	152	160
FtsX aeruginosa (59 - 252) left	128		128	168	152	184	160	136	152	136	152	152	120
FtsX faecium (326 - 553)	144	128		152	136	128	160	152	152	160	160	176	176
FtsX pneumoniae (314 - 527)	152	168	152		160	168	160	152	176	152	176	152	160
YbbP (482 - 665) sp right	184	152	136	160		152	152	152	144	152	160	152	152
YbbP (48 - 235) sp left	152	184	128	168	152		144	136	160	128	152	120	120
VraG aureus (320 - 502)	144	160	160	160	152	144		168	160	168	168	168	160
HrtB03 aureus (320 - 496)	136	136	152	152	152	136	168		152	176	152	168	160
HrtB02 aureus (315 - 528)	144	152	152	176	144	160	160	152		152	176	168	168
VraE aureus (320- 496)	144	136	160	152	152	128	168	176	152		152	160	160
Lmo monocytogenes (320 - 516)	160	152	160	176	160	152	168	152	176	152		184	184
AnrAB monocytogenes (330 - 540)	152	152	176	152	152	120	168	168	168	160	184		208
VirAB monocytogenes (319 - 528)	160	120	176	160	152	120	160	160	168	160	184	208	
PsdB subtilis (313 - 516)	160	160	168	168	152	160	168	160	176	160	182	184	184
YxdM subtilis (301 - 495)	152	112	152	144	160	112	152	144	152	144	160	176	176
MbrB mutans (310 - 532)	152	168	160	200	152	168	168	152	192	152	184	168	168
YsaB lactis (310 - 532)	152	168	160	192	160	168	168	152	192	160	184	176	168
ABC3 pneumonie right (482 - 665)	184	152	136	152	184	152	152	152	160	152	160	160	160
ABC3 pneumonie left (48 - 234)	152	184	128	168	152	184	160	136	160	128	152	128	120

Supplement Table S1: Overview of RMSDs and atoms of the structural alignment for BceB ECDs of different bacterial strains

RMSD in Å	PsdB subtilis (313 - 516)	YxdM subtilis (301 - 495)	MbrB mutans (310 - 532)	YsaB lactis (310 - 532)	ABC3 pneumonie right (482 - 665)	ABC3 pneumonie left (48 - 234)
NsrFP agalactiae (310 - 516)	6.099	5.892	2.66	4.196	5.673	4.964
BceB subtilis (321 - 516)	3.88	4.924	5.471	6.611	6.681	7.368
BceB peoriensis (321- 568)	4.639	4.647	5.998	6.066	6.387	5.836
BceB oralis (315 - 540)	5.497	5.717	5.773	6.239	5.909	6.421
BceB intestinalis (326 - 588)	6.186	4.935	6.759	6.002	6.686	6.906
BceB cereus (319 - 519)	3.92	3.52	5.451	5.945	6.453	6.609
BceB difficile (315 - 567)	3.396	3.792	5.539	5.878	6.371	7.545
BceB neonatale (320 - 541)	5.206	4.702	5.141	5.796	6.183	6.266
BceB tadaridae (316 - 518)	4.111	4.548	6.571	6.807	6.846	7.236
BceB VraG schweitzeri (316 - 498)	4.513	5.358	5.194	5.926	5.803	6.647
FtsX faecalis (326 - 552)	4.569	3.548	5.735	6.017	7.114	7.208
FtsX baumannii right (495 - 679)	5.861	5.517	6.202	5.993	1.698	5.161
FtsX baumannii left (51 - 245)	6.776	6.389	5.172	6.377	5.615	1.737
FtsX aeruginosa (501 - 697) right	6.183	5.156	6.258	5.631	1.6	6.242
FtsX aeruginosa (59 - 252) left	6.675	6.438	5.485	5.691	5.241	1.537
FtsX faecium (326 - 553)	3.951	3.733	5.406	5.664	6.08	7.465
FtsX pneumoniae (314 - 527)	6.415	5.862	3.804	4.585	5.498	6.559
YbbP (482 - 665) sp right	5.962	5.838	5.744	5.918	0.466	5.783
YbbP (48 - 235) sp left	6.969	6.479	5.125	5.875	5.392	0.403
VraG aureus (320 - 502)	4.323	5.198	5.153	6.785	5.631	6.512
HrtB03 aureus (320 - 496)	4.223	5.581	6.721	6.115	5.976	5.755
HrtB02 aureus (315 - 528)	5.899	5.147	3.902	4.246	5.786	6.296
VraE aureus (320- 496)	4.133	5.317	4.678	5.792	6.097	5.769
Lmo monocytogenes (320 - 516)	4.422	4.194	5.851	6.179	5.007	6.731
AnrAB monocytogenes (330 - 540)	3.931	4.147	5.918	6.51	5.859	6.952
VirAB monocytogenes (319 - 528)	3.974	4.088	5.859	6.13	5.478	7.008
PsdB subtilis (313 - 516)		3.617	5.718	5.662	5.923	6.988
YxdM subtilis (301 - 495)	3.617		5.918	5.656	5.675	6.463
MbrB mutans (310 - 532)	5.718	5.918		3.834	5.999	5.308
YsaB lactis (310 - 532)	5.662	5.656	3.834		4.966	5.902
ABC3 pneumonie right (482 - 665)	5.923	5.675	5.999	4.966		6.001
ABC3 pneumonie left (48 - 234)	6.988	6.463	5.308	5.902	6.001	

Number of atoms in alignment	PsdB subtilis (313 - 516)	YxdM subtilis (301 - 495)	MbrB mutans (310 - 532)	YsaB lactis (310 - 532)	ABC3 pneumonie right (482 - 665)	ABC3 pneumonie left (48 - 234)
NsrFP agalactiae (310 - 516)	168	152	200	192	160	168
BceB subtilis (321 - 516)	168	160	168	176	160	136
BceB peoriensis (321- 568)	160	144	152	144	144	128
BceB oralis (315 - 540)	184	152	160	168	160	144
BceB intestinalis (326 - 588)	152	144	184	152	160	160
BceB cereus (319 - 519)	176	176	176	176	152	160
BceB difficile (315 - 567)	176	168	168	168	152	136
BceB neonatale (320 - 541)	184	168	184	168	160	160
BceB tadaridae (316 - 518)	184	168	184	168	160	136
BceB VraG schweitzeri (316 - 498)	168	152	168	160	152	152
FtsX faecalis (326 - 552)	168	152	160	160	136	144
FtsX baumannii right (495 - 679)	160	152	160	160	176	160
FtsX baumannii left (51 - 245)	168	120	176	176	160	184
FtsX aeruginosa (501 - 697) right	160	152	152	152	184	152
FtsX aeruginosa (59 - 252) left	160	112	168	168	152	184
FtsX faecium (326 - 553)	168	152	160	160	136	128
FtsX pneumoniae (314 - 527)	168	144	200	192	152	168
YbbP (482 - 665) sp right	152	160	152	160	184	152
YbbP (48 - 235) sp left	160	112	168	168	152	184
VraG aureus (320 - 502)	168	152	168	168	152	160
HrtB03 aureus (320 - 496)	160	144	152	152	152	136
HrtB02 aureus (315 - 528)	176	152	192	192	160	160
VraE aureus (320- 496)	160	144	152	160	152	128
Lmo monocytogenes (320 - 516)	182	160	184	184	160	152
AnrAB monocytogenes (330 - 540)	184	176	168	176	160	128
VirAB monocytogenes (319 - 528)	184	176	168	168	160	120
PsdB subtilis (313 - 516)		176	184	184	152	160
YxdM subtilis (301 - 495)	176		176	152	160	112
MbrB mutans (310 - 532)	184	176		208	160	168
YsaB lactis (310 - 532)	184	152	208		160	168
ABC3 pneumonie right (482 - 665)	152	160	160	160		152
ABC3 pneumonie left (48 - 234)	160	112	168	168	152	

3.6 Chapter VI: The Immunity Transporter NisFEG

Characterization of the immunity transporter NisFEG

Pablo Cea-Medina[1], **Julia Gottstein[2]**, Holger Gohlke[1] & Sander H. J. Smits[2,3]

[1]*Institute of Pharmaceutical and Medicinal Chemistry, Heinrich-Heine-University Düsseldorf, Universitätsstrasse 1, 40225 Düsseldorf*
[2]*Institute of Biochemistry, Heinrich-Heine-University Düsseldorf, Universitätsstrasse 1, 40225 Düsseldorf*
[3]Center for Structural Studies, Heinrich-Heine-Universität Düsseldorf, Universitätsstraße 1, 40225 Düsseldorf, Germany

In preparation

Own proportion of this work: 30%

- Cloning
- Biological assays
- Preparation of figures
- Writing the manuscript

Characterization of the immunity transporter NisFEG

Pablo Cea-Medina[1], **Julia Gottstein[2]**, Holger Gohlke[1] & Sander H. J. Smits[2,3]

[1]*Institute of Pharmaceutical and Medicinal Chemistry, Heinrich-Heine-University Düsseldorf, Universitätsstrasse 1, 40225 Düsseldorf*
[2]*Institute of Biochemistry, Heinrich-Heine-University Düsseldorf, Universitätsstrasse 1, 40225 Düsseldorf*
[3]Center for Structural Studies, Heinrich-Heine-Universität Düsseldorf, Universitätsstraße 1, 40225 Düsseldorf, Germany

Abstract

Lantibiotics are small antimicrobial peptides, ribosomally synthesized as a pre-peptide in Gram-positive bacteria. Their genes are encoded on highly structured operons containing all the genes required for the peptides as well as for the proteins involved in maturation, transport, immunity, and synthesis. The most prominent and best-characterized lantibiotic is nisin from *Lactococcus lactis.* Nisin is active against other Gram-positive bacteria by binding Lipid II and its ability to form pores. To protect itself from self-killing, the producer strain is expressing an ABC transporter called NisFEG, which confers 6 to 8-fold immunity. Furthermore, nisin constructs missing either the last six amino acids or the last lanthionine ring did not result in full immunity exhibited by NisFEG in comparison to the complete nisin molecule, demonstrating that the ABC transporter recognizes the C-terminus of nisin. Although the exact mechanism is still unknown, LanFEG-type transporters are hypothesized to confer immunity by extruding the antimicrobial peptide from the cell membrane. NisFEG is part of the LanFEG-type ABC transporters consisting of the heterodimers NisE and NisG together with the homodimer of NisF. By characterizing the structure of NisFEG via homology modeling and its function by mutating specific amino acids, and assessing its effect by checking the influence on immunity, a new insight into the mechanism can be given.

Introduction

Lantibiotics belong to the class of ribosomally synthesized, small antimicrobial peptides produced by Gram-positive bacteria. They are produced as precursor peptides that undergo posttranslational modification, are transported out of the cell, and subsequently are activated by cleaving off the lantibiotic-specific leader sequence (Kuipers *et al.,* 2004). The activated lantibiotic shows activity against Gram-positive bacteria as well as a limited number of Gram-negative bacteria by

targeting cell wall synthesis (Wiedemann *et al.,* 2001, Chatterjee *et al.,* 2005). Even lantibiotic-producing bacteria would be affected if not immunity proteins such as the lipoprotein LanI and an ATP-binding cassette (ABC) transporter LanFEG would be expressed (Kuipers *et al.,* 1993, Siezen *et al.,* 1996, Alkhatib *et al.,* 2012, Smits *et al.,* 2020). If a lantibiotic only forms pores, only *lanI* is present in the biosynthetic cluster, which is the case for example for Pep5 (Reis *et al*., 1994, Pag *et al*., 1999) and lactocin S (Skaugen *et al*., 1997). LanFEG-type transporter genes are present in bacterial strains, producing peptides that target cell wall synthesis (Altena *et al.,* 2000) modify the lipid composition of membranes (Marki *et al.,* 1991), or bind to a specific receptor (Peschel and Gotz, 1996, Alkhatib *et al.,* 2012, Ra *et al.,* 1996, Klein and Entian, 1994). Both genes can be found in the biosynthetic cluster of e.g. epidermin (Peschel and Gotz, 1996), subtilin (Klein and Entian, 1994), and nisin (Ra *et al*., 1996).

Nisin is produced by various *Lactococcus lactis* strains and is the most extensively studied lantibiotic. Due to its high bactericidal activity in the nanomolar range and low toxicity in humans, nisin is explored as a promising therapeutic compound (De Kwaadsteniet *et al.,* 2009, Aranha *et al.,* 2004, Valenta *et al.,* 1996, Cotter *et al.,* 2013, Barbosa *et al.,* 2021, Geitani *et al.,* 2019, Rana *et al.,* 2019, Santos *et al.,* 2019). It is synthesized as a precursor peptide, consisting of a leader peptide and a core peptide, which is modified prior to its transport out of the cell. Nisin is activated by the protease NisP which cleaves off the leader peptide. The resulting peptide consists of 34 amino acids and contains five lanthionine rings. The N-terminal two rings are important for binding the cell wall precursor Lipid II and are connected via a flexible hinge region with the last two lanthionine rings which have been shown to be important for pore formation (AlKhatib *et al.,* 2014b, Rink *et al.,* 2007). In order not to be affected by their lantibiotic, nisin-producing *L. lactis* strains express the lipoprotein NisI and the ABC transporter NisFEG which provide together full immunity, with an IC_{50} of 990 nM against nisin (Ra *et al.,* 1996). When each protein is expressed alone, they confer with an IC_{50} of 60 to -70 nM only 8-20% of immunity against nisin, thus this indicates a cooperative immunity mechanism (Ra *et al.,* 1996, Stein *et al.,* 2003, AlKhatib *et al.,* 2014b). Both proteins contribute together to immunity, NisI binds up to 1 µmol/L nisin at the surface of the cytoplasmic membrane, preventing it from inserting into the membrane (AlKhatib *et al*., 2014a). Furthermore, NisI-

expressing strains form long-chain cluster of *L. lactis* cells which protects against high nisin concentrations (AlKhatib *et al*., 2014a). In addition, NisFEG exports nisin molecules that have already entered the cytoplasmic membrane before or during pore formation (Stein *et al.*, 2003).

ABC transporter, such as NisFEG, belong to one of the largest families of membrane proteins which can be found in fungi, plants, archaea, and bacteria (Holland, 2003). They can have multiple functions, including uptake of nutrients, transport of signaling molecules, and also conferring multi-drug resistance through various mechanisms e.g., by exporting toxic metabolites or compounds like xenobiotics (Beis, 2015, Thomas and Tampe, 2018). The general architecture of ABC transporter consists of two transmembrane domains (TMDs) and two nucleotide-binding domains (NBDs)(Beis, 2015). The NBDs exhibit the characteristic sequence motifs like Walker A, Walker B, the H-loop, the ABC transporter signature motif (LSGGQ) (Schmitt and Tampe, 2002) and the D-loop (van der Does and Tampe, 2004, Zaitseva *et al.,* 2006). By binding and hydrolyzing ATP, the NBDs provide the energy for the specific function of the ABC transporter e.g. transporting a substrate across the membrane.

NisFEG forms a functional immunity transporter when assembled as a complex with two NBDs NisF and the heterodimeric TMDs NisE and NisG (Alkhatib *et al.,* 2012).

NisE is a 28 kDa integral membrane protein consisting of six TM helices, similarily NisG consists also of six TM helices with a molecular weight of 24 kDa. Deletion of either TMD resulted in a complete loss of immunity against nisin, highlighting their importance for function (Siegers and Entian, 1995). Furthermore, it is known that the C-terminus of nisin is recognized by NisFEG, since, compared to the full-length peptide its immunity is reduced in the presence of nisin constructs lacking either the last six amino acids or the last lanthionine ring (AlKhatib *et al*., 2014b). Nonetheless, the exact mechanism behind the conferred immunity by LanFEG transporters is still unknown, however, it has been proposed for several lantibiotics like subtilin, epidermin, and nisin that the lantibiotic is extruded from the cell membrane (Stein *et al.,* 2003, Peschel and Gotz, 1996, Otto *et al.,* 1998). To characterize the role of the ABC transporter NisFEG, a homologous expression system based on the plasmid pILSV was used which permits the expression of NisFEG dependent on the *nisA* promotor in *L. lactis* NZ9000.

By introducing specific point mutations in NisFEG, we sought to elucidate the amino acid's role in conferring immunity against nisin. For that, we determined IC_{50} values for the generated mutant strains and compared them to the wild-type strain NisFEG and an ATP-hydrolysis deficient mutant $NisF_{H181A}EG$ strain.

Material and Methods

Cloning of *nisFEG, nisF$_{H181A}$EG, nisFEG mutants*

The pILSV-nisFEG and pILSV-$nisF_{H181A}EG$ plasmid were generated as described by (AlKhatib *et al.,* 2014b). In order to generate alanine, cysteine, and tryptophan NisFEG mutants, single-point or double mutations were introduced via site-directed mutagenesis into the pILSV-nisFEG plasmid. The successfully mutated plasmids were transformed into *L. lactis* NZ9000 by electroporation at 1 kV, 25 µF, 5.0 msec, and the corresponding strain were termed NZ9000NisFEG (mutant). The primers, plasmids, and control strains that were used are listed in Tables 2 and 3.

Table 2: Primers used in this study. The following primers were used to generate pILSVNisFEG cysteine- alanine- and tryptophan- mutants.

Primer Name	Primer Sequence (5`- 3`)
NisF(L95C)EG_fwd	AACTAAGGCTTGCCTTTTTGGAA
NisF(L95C)EG_rev	TTAAGATTATCGAAAGCAGATAAATTCATAT
NisF(L96C)_fwd	TAAGGCTTTGTGTTTTGGAATTTCAGATAAG
NisF(L96C)_rev	GTTTTAAGATTATCGAAAGCAG
NisF(T92C)_fwd	TAATCTTAAATGTAAGGCTTTGCTTTTTGGAATTTC
NisF(T92C)_rev	TCGAAAGCAGATAAATTCATATATATTGCTGG
NisFE(I10C)G_fwd	ATCAGAAGCATGCAAATTAAAAAAATCAGGAACTC
NisFE(I10C)G_rev	GCTATTATTCTTTTCATATCACATTCATCCATG
NisFE(F172C)G_fwd	TGTTGCCCCTTGCGTTGCACAAAC
NisFE(F172C)G_rev	ATTAAACAAATCAAGGTATTCGCAGCTAACAAT
NisFEG(S4C)_fwd	CATGATAAGATGTGAATGTCTCAAATTAAAAAATAG
NisFEG(S4C)_rev	TTCTATCACTCCTTTAAGTAAATACGAAACTCC
NisFEG(N165C)_fwd	TTTTGCCAGTTGTAAAGTTTTATTAGCAG
NisFEG(N165C)_fwd	ATAATGAGTAATATTTCAATAATCGCGAT

NisFE(Q76A)G_fwd	TGGAAATTTTGCAAATGTGAAATGGAAAAAG
NisFE(Q76AG)_rev	GCTTGCTCCTCTGATTTTATATC
NisFE(W80A)G_fwd	AAATGTGAAAGCGAAAAAGCTGAGTTGG
NisFE(W80A)G_rev	TGAAAATTTCCAGCTTGC
NisFE(K67A)G_fwd	TTATGATATAGCATCAGAGGAGCAAGC
NisFE(K67A)G_rev	AGAAAAAGCAAACTCATCAAAAG
NisFEG(E66A)_fwd	TCTAATCTTTGCACAGGAGAGTC
NisFEG(E66A)_rev	ATAGACAAAATTGTAACCAG
NisFEG(E76A)_fwd	TCGTTTCCAAGCAATAAATGTAAATAAAAAAAGTAG
NisFEG(E76A)_rev	TTGGCCAGACTCTCCTGT
NisFEG(N72A)_fwd	GAGTCTGGCCGCACGTTTCCAAG
NisFEG(N72A)_rev	TCCTGTTCAAAGATTAGAATAG
NisFE(A102W)G_fwd	AGGTATACTATGGAGCATAGTCTTGATTATTTTG
NisFE(A102W)G_rev	CTTAGCCAAATCAACAAC
NisFE(A139W)G_fwd	ATTACTAGCATGGTCTTGGAATTTACCCTTTATATAC
NisFE(A139W)G_rev	ATAGCAATCAATGCCACAC
NisFE(L233W)G_fwd	TTCGTATTTATGGAAAGGAGTGATAGAACATG
NisFE(L233W)G_rev	ACTCCTATCGTTACAACTATG
NisFE(I104W)G_fwd	ACTAGCGAGCTGGGTCTTGATTATTTTG
NisFE(I104W)G_rev	ATACCTCTTAGCCAAATC
NisFE(I133W)G_fwd	TGTGGCATTGTGGGCTATATTACTAGC
NisFE(I133W)G_rev	CTTACTTTCATAAAATCCACC
NisFE(V224W)G_fwd	ACTTTCCATATGGGTAACGATAGGAGTTTC
NisFE(V224W)G_rev	CCAAATGGTAATAAAACTTCC
NisFEG(V29W)_fwd	GCTTTTAACGTGGCCTATTTATTTAGCTTTTG
NisFEG(V29W)_rev	TCTAATAAAGTAAAGAGAAAAACTAAATAAAAC
NisFEG(L98W)_fwd	GGATTTCCTTTGGTTCTTTCCATC
NisFEG(L98W)_rev	ACTACTATTAGCTTTCATAAC
NisFEG(L205W)_fwd	CACAATAATTTGGGTAGCATTATCTAAAAAAAAG
NisFEG(L205W)_rev	GATAAAACAATCCACCCTAC

NisFEG(L27W)_fwd	ATTAGAGCTTTGGACGGTTCCTATTTATTTAG
NisFEG(L27W)_rev	AAAGTAAAGAGAAAAACTAAATAAAAC
NisFEG(F96W)_fwd	AGTAGTGGATTGGCTTTTGTTCTTTC
NisFEG(F96W)_rev	ATTAGCTTTGATAACCAAATTC
NisFEG(I203W)_fwd	GTTTTATCCACAATAATTCTGGTAGCATTATC
NisFEG(I203W)_rev	AATCCACCCTACGGCAG

Table 3: Control strains used in this study. Mutant strains were generated based on the plasmid pILSV NisFEG.

Strain	Plasmid	Reference
NZ9000sens	pILSV (empty)	(de Ruyter *et al.,* 1996)
NZ9000NisFEG	pILSV-NisFEG	(AlKhatib *et al.,* 2014b)
NZ9000NisF$_{H181A}$EG	pILSV- NisF$_{H181A}$EG	(AlKhatib *et al.,* 2014b)

Expression of NisFEG and NisFEG mutants in L. lactis NZ9000.

The NZ9000NisFEG, NZ9000NisFEG mutants, and control strains were grown in GM17 media supplemented with 10 µg/mL chloramphenicol and induced with a final concentration of 1 ng/mL and were further grown overnight. On the next day, the cells were diluted to an OD_{600} of 0.1 in fresh media supplemented with 10 µg/mL chloramphenicol with the inducer nisin (20 ng/mL). Cells were grown to an OD_{600} of 1 and subsequently harvested at 5000x g for 30 min. The resulting pellet was resuspended with a resuspension buffer (50 mM HEPES pH 7, 150 mM NaCl, 10% (w/v) glycerol) to an OD_{600} of 300. Further 1/3 (w/v) glass beads (0.3 mm) were added and cells were lysed. A cycle of 1 min disruption and 2 min cooling the sample on ice was repeated five times. To collect the cytoplasmic fraction the sample was centrifuged at 10,000 x g. Subsequently, the supernatant was subjected to centrifugation at 100,000 x g to harvest the membranes. To purified membrane fractions, SDS-loading dye (0.2M Tris-HCl, pH 6.8, 10% (w/v) SDS, 40% (v/v) glycerol, 0.02% (w/v) bromophenol, and β-mercaptoethanol) was added and samples were further used for SDS-PAGE and Western Blot analysis (5µL loaded).

Purification of nisin

Nisin was purified as described in (Abts *et al.,* 2011). The concentration of nisin was measured by using RP-HPLC as previously described in (Abts *et al.,* 2013).

Determination of the activity of nisin by growth inhibition experiments (IC_{50}).

The control strains NZ9000sens, and NZ9000NisFEG as well as the alanine and tryptophan mutant strains of NisFEG were grown overnight in GM17 media supplemented with 10 µg/mL chloramphenicol in the presence of 1 ng/mL of nisin. The following day, the cells were diluted to an OD_{600} of 0.1 in fresh GM17 media and incubated at 30°C for 30 minutes. In a 96-well plate, 50 µL of dilutions of either nisin or bacitracin (Zn-bacitracin) were prepared. Then, 150 µL of *L. lactis* NZ9000NisFEG, NZ9000sens, or NZ9000NisFEG mutants were added. After 5-7 hours of incubation at 30°C, the optical density was measured, and the fold of resistance was calculated by comparing the normalized values for *L. lactis* NZ9000NisFEG/ and its mutants against the sensitive strain NZ9000sens.

Crosslinking experiments with generated NisFEG cysteine mutants.

Cysteine mutants were generated in order to confirm if during the transport of nisin specific helices of the ABC transporter NisFEG move in proximity to other hypothesized helices of the same proteins.

NisFEG cysteine mutants were expressed and membranes were isolated as described above. Membranes were suspended in R-buffer (50 mM HEPES pH 7, 150 mM NaCl, 10% (w/v) glycerol) containing 10 mM $MgCl_2$. Then membranes were either preincubated 30 min at 4°C in the presence of 5mM ATP or without any additive. Subsequently, the membranes were incubated with 0.2 mM 1,3-propanediyl bismethanethiosulfonate crosslinker (M3M) (6.5 Å) or the control reagent Copper-phenanthroline (Cu-Phe). M3M was selected based on calculated distances between the domains of interest in a model of NisFEG. The M3M compound was prepared as 100 mM stock solutions in DMSO. The reactions were stopped by the addition of an equal volume of SDS sample buffer (0.2M Tris-HCl, pH 6.8, 10% (w/v) SDS, 40% (v/v) glycerol, 0,02% (w/v) bromophenol + 10mM N-ethylmaleimide). Samples were further analyzed via SDS PAGE and Western Blotting.

Results

The activity of NisFEG mutants against Nisin

Nisin was purified as previously described by (Abts *et al.,* 2011). The generated pILSV plasmid with a single point mutation or double mutation in NisFEG was transformed into *L. lactis NZ9000*. The expression of the *nisFEG* genes was induced by adding a sublethal concentration of 0.3 nM nisin to the cells. This subinhibitory dose of nisin is able to trigger the nisA promotor in the pIL-SV plasmids, enabling the gene expression of the respective protein. It has been shown by different growth studies that this low centration of nisin is not harming the cells (Mierau and Kleerebezem, 2005, Alkhatib *et al.,* 2012, de Ruyter *et al.,* 1996). NisFEG confers immunity against nisin by extruding nisin from the membranes. However, the exact mechanism is unknown. In order to validate the NisFEG structure model and to get insight into the role of selected amino acids in conferring immunity against nisin, six NisFEG alanine mutants were generated. Q76 and W80 are located at the NisE-NisF interface. K67 and E66 are part of the NisG-NisE interface while E76 and N72 are found at the NisG-NisF interface (Figure 21a). After adding nisin to the cultures of the NisFEG mutant strains, WT, and the sensitive empty vector control strain, the IC_{50} was determined using Prism 9 Version 9.5.1. The fold of change, which is independent of small variations in bacterial growth behavior, was obtained by dividing the IC_{50} of the NisFEG WT or mutant strain by the IC_{50} value obtained for the sensitive strain. To address the activity of nisin against the mutant strains of NZ9000NisFEG, the IC_{50} of NisFEG for nisin was set as 100% activity and based on this the activity for the NisFEG mutants was calculated (Figure 21b). All calculated values are summarized in Table 3.

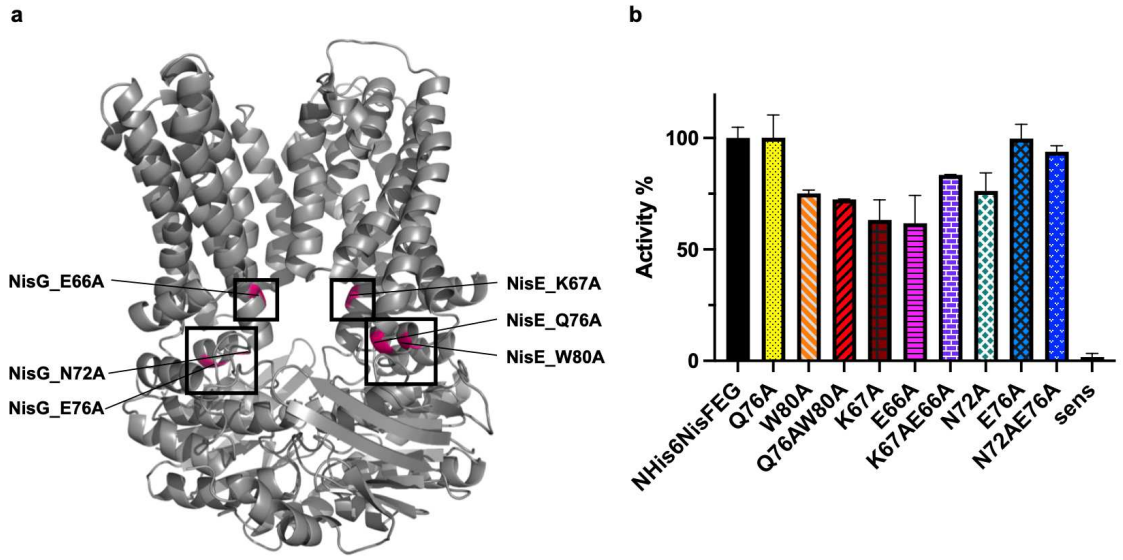

Figure 21: Generated alanine mutants in NisFEG. a) Model of NisFEG showing the location of the introduced alanine mutations (red). Q76 and W80 are located at the NisE-NisF interface. K67 and E66 are part of the NisG-NisE interface of the ABC transporter. Amino acids E76 and N72 are at the NisG-NisF interface. Model calculated with Topmodel (Mulnaes *et al*., 2020) of NisFEG and was provided by Pablo Cea Medina. **b)** Nisin activity of *L. lactis* NZ9000NisFEG mutants compared to the wild type strain NZ9000NisFEG and the empty vector control strain (sens) in %.

The mutant strains NZ9000NisFE$_{(K67A)}$G and NZ9000NisFEG$_{(E66A)}$ exhibited only 63/62% of activity against nisin in comparison to the wild type. This could indicate that K67 and E66 might be involved in the nisin export mechanism but are not crucial amino acids since 60% of activity was retained. The double mutant, on the contrary, showed 20% more activity than the single mutants. For the NisE-NisF interface alanine mutants Q76A and W80A, no loss of activity and a 25% loss of activity were observed, respectively. The double mutant showed a similarly reduced activity of 72%. Furthermore, a 25% reduction of activity was observed for the NisFEG$_{(N72A)}$ mutant in comparison to the wild-type while the NisFEG$_{(E76A)}$ strain showed wild-type activity against nisin. The double mutant NisFEG$_{(N72A, E76A)}$ exhibited 94% of nisin activity, restoring 18% of activity in comparison to the N72A mutant strain. None of the alanine mutations lead to a complete loss of nisin activity compared to the sensitive empty control vector strain with an IC_{50} of 12 nM (Table 4)

Table 4: Calculated IC_{50} values, fold of resistance, and activity in percent for the NisFEG alanine mutants and the control strains NZ9000NisFEG and NZ9000sens.

Nisin	NHis6 NisFEG	Q76A	W80A	W80A-Q76A	K67A	E66A	K67A-E66A	N72A	E76A	N72A-E76A	sens
IC_{50} [nM]	118	118	91	88	78	77	100	93	118	112	12
F.o.R	10	10	8	7	7	6	8	8	10	9	1
Activity %	100	100	75	72	63	62	83	76	100	94	0

Furthermore, NisFEG Trp mutants were generated to explore the role of the selected ten amino acids on the stability and the activity of the ABC transporter NisFEG by mutating them to tryptophans. For this Trp-scanning experiment, buried residues in NisE and NisG as well as solvent-exposed residues were mutated (Figure 22a). After generated NZ9000 NisFEG mutant strains were treated with nisin, the IC_{50} was determined as described previously (Table 5). Furthermore, the fold of resistance and the activity in percent were calculated using Prism 9 version 9.5.1 (Table 5).

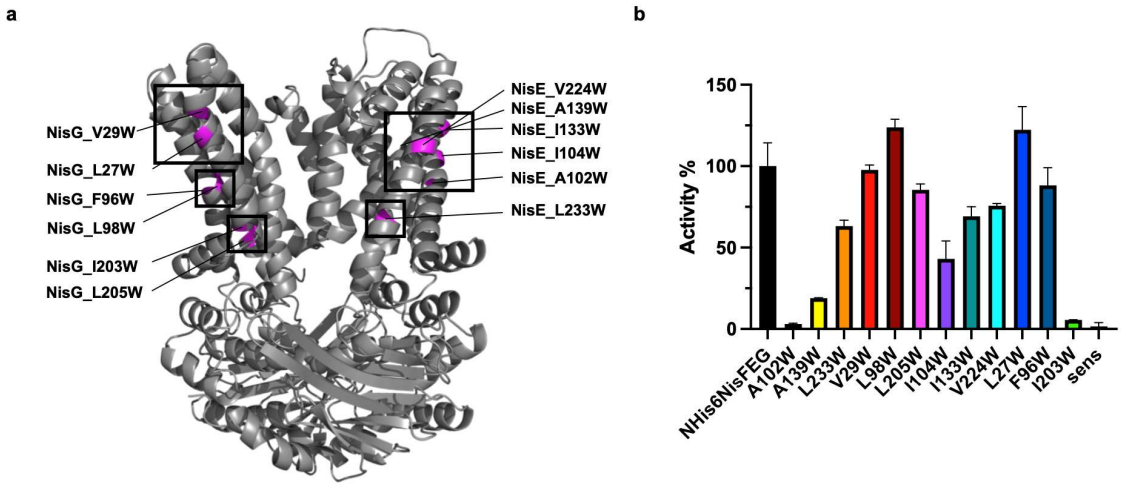

Figure 22: NisFEG model displaying the location of the Trp mutants (pink). Model was calculated with Topmodel (Mulnaes *et al*., 2020) of NisFEG and was provided by Pablo Cea Medina. **a)** The following residues of NisE A102, A139, and L233 represent buried amino acids. Solvent-exposed residues in NisE are I104, I133, and V224. In NisG V29, L98 and L205 are buried residues while L27, F96, and I203 are solvent-exposed. The model was provided by Pablo Cea Medina. **b)** Nisin activity of *L. lactis* NZ9000NisFEG mutants compared to the wild type strain NZ9000NisFEG and the empty vector control strain (sens) in percent.

After treatment with nisin, the NZ9000NisFE$_{(A102W)}$G and NZ9000NisFE$_{(I203W)}$G, mutant strains displayed a complete loss of resistance (3%, 5% respectively) (Figure 22b and Table 5) in the same range as the nisin-sensitive empty vector control strain (sens). Also, NZ9000NisFE$_{(A139W)}$G displayed a reduced activity of 19%. This indicates that the substituted amino acids destabilize NisFEG,

disrupting the ability to confer immunity. The mutant strain NZ9000NisFE$_{(I104W)}$G displayed a residual activity of 43% while the activity of the L233W-, I133W-, and V224W-mutant strains 63%, 69%, and 76% range in the middle field. In contrast, the mutation of amino acids L205, F96, and V29 lead to a reduction of activity of 14%, 12%, or 2% respectively. These amino acids seem not to be involved in stabilizing NisFEG. Mutations in NisG are with the exception of the I203W mutant strain mostly tolerated. For the strains L27W and L98W an increase in nisin activity by 20% was observed (Table 5). This implies that the exchange to tryptophan possibly stabilized the ABC transporter. The potential role of Trp contributing to membrane protein stability by interacting with lipids has been shown in several studies (Situ *et al.,* 2018, McDonald and Fleming, 2016, Hong *et al.,* 2007).

Table 5: Calculated IC_{50} values, fold of resistance, and activity in percent for the NisFEG tryptophan mutants and the control strains NZ9000NisFEG and NZ9000sens.

Nisin	NHis6 NisFEG	A102W	A139W	L233W	V29W	L98W	V224W	L205W	I104W	I133W	L27W	F96W	I203W	sens
IC_{50} [nM]	119	12	30	78	116	145	103	56	85	92	143	106	15	11
F.o.R	11	1	3	7	11	13	9	5	8	8	13	10	1	1
Activity %	100	3	19	63	98	124	76	86	43	69	122	88	5	1

Transport in ABC transporter involves often the movement of certain domains and rearrangement of helices that lead to a change of conformation (Husada *et al*., 2018, Lewinson *et al*., 2020). In order to prove the movement of certain helices, several amino acids were substituted with cysteine in different helices in NisFEG that are hypothesized to move toward each other (Figure 23a). In order to be able to analyze the proteins on Western Blot a C-terminal-His6-tag was introduced in the construct pILSVNHis6-NisFEG. The effect of the additional C-terminal Histidine tag was tested by determining its nisin activity (IC_{50}) via growth inhibition experiments.

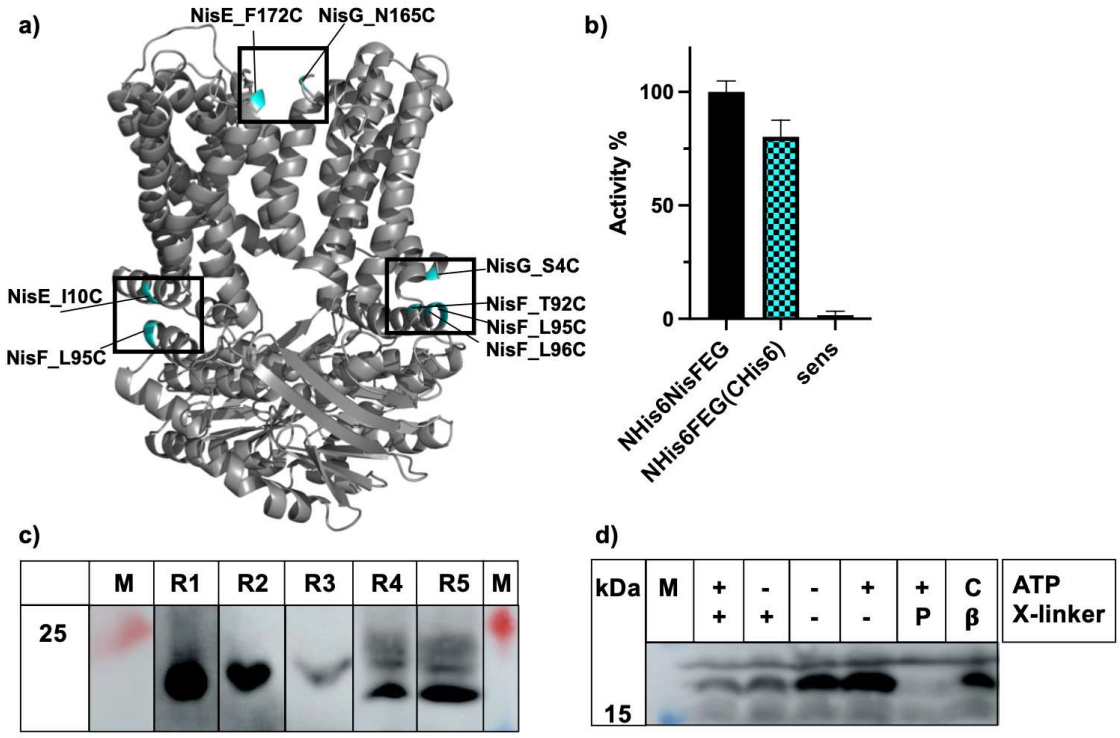

Figure 23 a) NisFEG Model showing the positions of cystein substitutions (cyan) Model was calculated with Topmodel (Mulnaes *et al.*, 2020) of NisFEG and was provided by Pablo Cea Medina. **b)** Nisin activity of the *L. lactis* NZ9000NisFEG mutant in comparison to the wild type strain NZ9000NisFEG and the empty vector control strain (sens) in percent. **c)** The expression of the NisFEG mutants $NisF_{(L95C)}E_{(I10C)}G$ (R1), $NisF_{(L96C)}EG_{(S4C)}$ (R2), $NisF_{(T92C)}EG_{(S4C)}$ (R3), $NisFE_{(F172C)}G_{(N165C)}$ (R4) and $NisF_{(L95C)}EG_{(S4C)}$ (R5) in *L. lactis* NZ9000 was monitored by Western Blot using an anti-Histidine-tag antibody. **d)** As a preliminary control experiment membranes from the strain expressing the wild-type NisFEG were treated with either the M3M crosslinker (X-linker) in the presence of ATP (++) or no ATP (+-). As negative controls, buffer (50 mM HEPES, 150 mM NaCl, 10% glycerol pH 7) (--) or only ATP (+-) or β-Mercaptoethanol (Cβ) was added to the membranes. As a positive control copper phenanthroline was used which triggers disulfide bridge formation (+P).

After the generated NisFEG mutant strain was treated with nisin, the IC_{50} was determined as previously described. For the strain with the new construct, a reduction of 20% nisin activity in comparison to the NHis6-NisFEG construct expressing strain was displayed (Figure 23b). This new construct was used to generate the new cysteine mutants. Following NZ9000NisFEG double mutants were generated: $NisF_{(L95C)}E_{(I10C)}G$, $NisF_{(L96C)}EG_{(S4C)}$, $NisF_{(T92C)}EG_{(S4C)}$, $NisFE_{(F172C)}G_{(N165C)}$ and $NisF_{(L95C)}EG_{(S4C)}$. In the next step, NisFEG mutants were successfully transformed and expressed in *L. lactis* NZ9000. Subsequently, the membrane fraction was isolated for Western blot analysis. The proteins were detected with an anti-histidine antibody at approximately 20 kDa and thus were successfully expressed (Figure 23c). Subsequently, the membrane fraction was purified for Western Blot analysis. The proteins were detected with an anti-

histidine-tag antibody at approximately 20 kDa (Figure 23c). Thus, NisG runs lower than its actual molecular weight (24 kDa).

To validate the NisFEG structural model, an MTS crosslinker was chosen as a molecular ruler to estimate whether the cysteines introduced into NisFEG are in close proximity to be cross-linked. Thiol-reactive MTS cross-linkers have the ability to crosslink cysteine residues which allows them to be used to determine distances between neighboring helices. Previously, the distance between new cysteines in the NisFEG model was determined using Pymol Version 2.3.0. For three of the double cysteine mutants, a distance of approximately 6 Å was measured. Due to possible uncertainties of the model a slightly longer crosslinker, 1,3-propanediyl bismethanethiosulfonate, which measures 6.5 Å (M3M) was used. M3M was described among other MTS crosslinkers in the study by (Loo and Clarke, 2001, Loo and Clarke, 2002).

The control experiment was performed using purified membranes from wild-type NisFEG. Copper-phenanthroline (Cu-Phe), which triggers disulfide formation, was used as a negative control. Since wild-type NisFEG contains seven endogenous cysteines that are not in close proximity to form disulfide bridges or be crosslinked with the chosen cross-linker, treatment with Cu-Phe should not lead to a mass shift of the protein on the Western Blot. To test this, membranes were suspended in a resuspension buffer (50 mM HEPES pH 7, 150 mM NaCl, 10% (w/v) glycerol) containing 10 mM $MgCl_2$. Subsequently, the membranes were incubated with either 0.2 mM 1,3-propanediyl-bismethanethiosulfonate crosslinker (M3M) (6.5 Å) or 1 mM of Cu-Phe or without for 30 minutes at 4°C in the presence of 5 mM ATP or without. Reactions were stopped by adding an equal volume of SDS sample buffer (0.2 M Tris-HCl, pH 6.8, 10% (w/v) SDS, 40% (v/v) glycerol, 0,02% (w/v) bromophenol, and 10 mM N-ethylmaleimide) and analyzed by SDS-PAGE and subsequent Western Blotting.

For the five reactions with wild-type NisFEG membranes treated with either ATP and M3M (++), or without ATP and M3M (-+), or only buffer (--), or ATP without M3M (+-), or with β-Mercaptoethanol (β-M) a thick band at 20 kDa was detected (Figure 23d). Since wild-type NisFEG does not contain cysteine residues in a distance of 6.5 Å, it was to be expected that M3M should not be able to produce crosslinks. Controversially, the negative control (NisFEG membranes treated with

Cu-Phe) showed no band at the molecular weight of NisG. This indicates that Cu-Phe induced disulfide formation in wild-type NisFEG, shifting the protein band to a higher molecular weight that is not visible on the Western blot.

The same experiment with the same conditions was conducted with membranes of the NisFEG mutant NisF$_{(L95C)}$E$_{(I10C)}$G. Similarly, to wild-type NisFEG, treatment with the crosslinking agent M3M did not result in crosslinks. Further experiments to optimize the crosslinking conditions or different lengths of crosslinkers need to be tested for more insight.

Discussion

Transport in ABC transporter involves, after binding of the substrate, often the movement of certain domains and rearrangement of helices that lead to a change of conformation (Husada *et al*., 2018, Lewinson *et al*., 2020). To elucidate the transport mechanism and validate a model of NisFEG, calculated with Topmodel (Mulnaes et al., 2020) and provided by Pablo Cea Medina, specifically selected amino acids in NisFEG were substituted with alanines or tryptophans to determine their role in nisin immunity. Furthermore, to prove the movement of certain helices of the NisE, NisG, and NisF domain interfaces of the ABC transporter, several amino acids were substituted with cysteine residues in NisFEG that are hypothesized to move toward each other. Figure 24 gives an overview of all mutants and their activity (red = loss of activity; yellow = low reduction of activity; green = no loss of reduction or enhanced resistance).

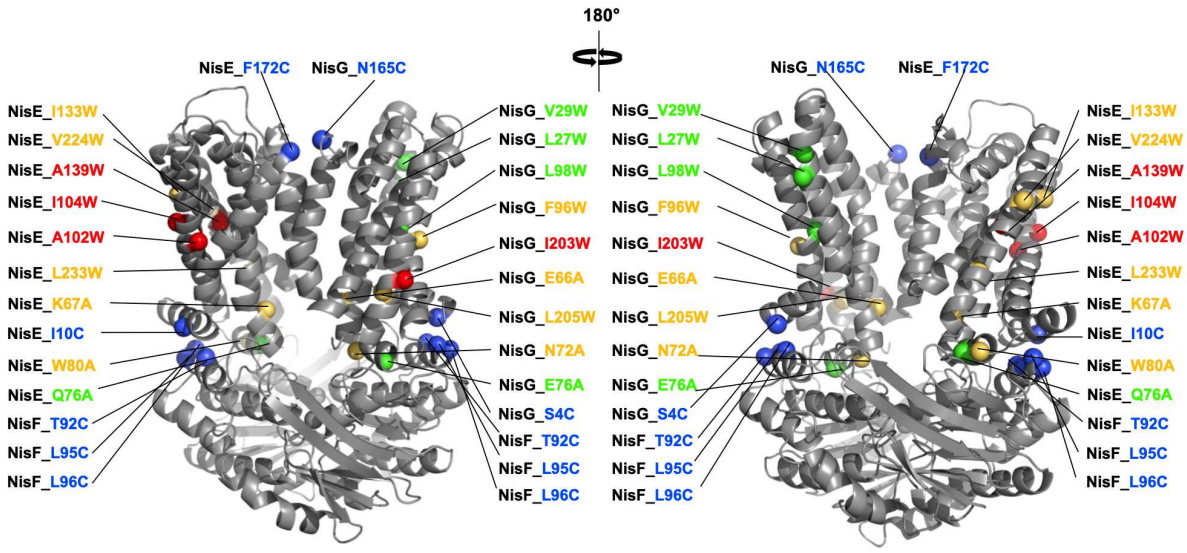

Figure 24: Mapping of Ala and Trp mutations of NisFEG. Front and back views are shown. Mutations are highlighted as colored spheres centered on the Cα of the residue.

Mutations that lead to a complete loss or reduction of nisin activity up to 50 % are labeled in red. Mutations that lead to a low reduction of nisin activity (50-99% of residual activity) are labeled in yellow. All mutations that do not lead to loss of nisin activity or enhance activity are labeled in green. Cysteine mutants are marked in blue. Model calculated with Topmodel (Mulnaes *et al*., 2020) of NisFEG and was provided by Pablo Cea Medina. The figure was created using Powerpoint Version 16.76.

The highest loss of resistance (38-25%) within the alanine mutants in comparison to the wild-type NisFEG-expressing strain was observed for the $NisFE_{(K67A)}G$ and $NisFEG_{(E66A)}$ at the NisE- NisG interface as well as for $NisFE_{(W80A)}G$ at the NisF-NisE interface. Mutating these amino acids to alanine removed all sidechain atoms past the **β**-carbon, allowing to test for their role at their specific position. Since the mutation to alanine did not change the protein backbone, therefore did not influence the helix bundle arrangement, and did not lead to a complete loss of activity, it can be speculated that these amino acids are involved in substrate binding or substrate transport. Due to the change to the charge-less amino acid alanine, nisin cannot bind to its binding site in NisFEG as effectively. It is known that residues like arginine, aspartate, glutamate, and lysine act as gate-keepers on the flanks of hydrophobic regions that are prone to aggregation (Reumers *et al*., 2009). E66 and K67 could act as a gate to prevent the hydrophobic core of NisE and NisG to aggregate during folding, therefore these amino acids contribute also to the stability of the protein.

Tryptophans are the least abundant amino acids in proteins and several studies on membrane proteins have shown that tryptophan residues act as anchors along the lipid bilayer interface, stabilizing membrane-spanning proteins (Granseth *et al.,* 2005, Barik, 2020). Thus, it can be hypothesized that W80 is involved in the stabilization of NisFEG but is not a critical amino acid.

The A102W and I203W substitutions resulted in a complete loss of activity, indicating their importance for the stability of the transporter. It has been shown that mutations in NisG often do not lead to a strong loss of nisin activity while strains expressing NisE mutations show a more severe loss (Siegers and Entian, 1995).

To validate the NisFEG structural model, specific selected amino acids on either side of each domain interface that are hypothesized to interact during substrate transport were replaced with cysteine residues. The mutants were successfully expressed in *L. lactis NZ9000.* NisG is detected at a lower molecular weight than

its theoretical molecular weight (24 kDa). This is a phenomenon frequently observed in membrane proteins that migrate anomalously due to the increased charge of the SDS-protein complex or so-called SDS-resistant helix-helix interactions which could result in residual tertiary structure (Rath and Deber, 2013, Rath *et al.*, 2009, Rais *et al.*, 2004, Ra *et al.*, 1999). In a study by Rath *et al.,* it was observed that membrane proteins, migrating faster on the SDS-gel were detected at 82% of their relative molecular mass (Rath and Deber, 2013). This also holds true for NisG.

Wild-type NisFEG contains seven endogenous cysteine residues that, according to our NisFEG model, should be too distant from each other to form disulfide bridges. Thus, it would have been expected that after treatment with Cu-Phe, the protein NisFEG stays unchanged. Controversially, our results show the contrary. This might imply that NisFEG changes its conformation in the presence of ATP, allowing disulfide bridge formation. Thus, a different negative control is necessary for future experiments. In the study by Loo *et al.*, the authors demonstrated that dependent on ATP hydrolyzation different residues became exposed to the drug binding site of the human multidrug resistance P-glycoprotein, strongly emphasizing that substrate transport can rearrange helices of the ABC transporter (Loo and Clarke, 2002). This could have been the case for NisFEG and thus disulfide-bridge formation could occur.

A potential approach to this problem could be to generate an endogenous cysteine-free and active mutant of NisFEG to increase the likelihood of crosslinks between exogenous cysteines. This was shown for the ABC transporter P-gp (Loo *et al.*, 2004). By treating P-gp carrying exogenous cysteines on transmembrane segments five and eight with Cu-phenanthroline, the authors validated the proximity of these transmembrane helices.

Furthermore, treatment with the selected cross-linker M3M did not lead to crosslinks in the tested mutant strain. Since molecular distances between cysteine mutations were estimated from a theoretical model, it is possible that M3M with a length of 6.5 Å did not fit. A screen of different-sized cross-linkers needs to be conducted to result in a better readout. On the other hand, applied assay conditions might need to be further improved even though similar conditions as stated in (Loo and Clarke, 2002) were used.

Acknowledgments

The authors would like to thank Pablo Cea Medina and Prof. Dr. Holger Gohlke for providing the Topmodel of NisFEG and for the nice collaboration. The authors thank the Institute of Biochemistry for fruitful discussions. This work was funded by the Deutsche Forschungsgemeinschaft (DFG, German Research Foundation)—270650915/ GRK 2158 TP4 to S.S and H.G. The Center for Structural Studies is funded by the Deutsche Forschungsgemeinschaft (DFG Grant number 417919780)

References

ABTS, A., MAVARO, A., STINDT, J., BAKKES, P. J., METZGER, S., DRIESSEN, A. J., SMITS, S. H. & SCHMITT, L. 2011. Easy and rapid purification of highly active nisin. *Int J Pept,* 2011**,** 175145.

ABTS, A., MONTALBAN-LOPEZ, M., KUIPERS, O. P., SMITS, S. H. & SCHMITT, L. 2013. NisC binds the FxLx motif of the nisin leader peptide. *Biochemistry,* 52**,** 5387-95.

ALKHATIB, Z., ABTS, A., MAVARO, A., SCHMITT, L. & SMITS, S. H. 2012. Lantibiotics: how do producers become self-protected? *J Biotechnol,* 159**,** 145-54.

ALKHATIB, Z., LAGEDROSTE, M., FEY, I., KLEINSCHRODT, D., ABTS, A. & SMITS, S. H. 2014a. Lantibiotic immunity: inhibition of nisin mediated pore formation by NisI. *PLoS One,* 9**,** e102246.

ALKHATIB, Z., LAGEDROSTE, M., ZASCHKE, J., WAGNER, M., ABTS, A., FEY, I., KLEINSCHRODT, D. & SMITS, S. H. 2014b. The C-terminus of nisin is important for the ABC transporter NisFEG to confer immunity in Lactococcus lactis. *Microbiologyopen,* 3**,** 752-63.

ALTENA, K., GUDER, A., CRAMER, C. & BIERBAUM, G. 2000. Biosynthesis of the lantibiotic mersacidin: organization of a type B lantibiotic gene cluster. *Appl Environ Microbiol,* 66**,** 2565-71.

ARANHA, C., GUPTA, S. & REDDY, K. V. 2004. Contraceptive efficacy of antimicrobial peptide Nisin: in vitro and in vivo studies. *Contraception,* 69**,** 333-8.

BARBOSA, A. A. T., DE MELO, M. R., DA SILVA, C. M. R., JAIN, S. & DOLABELLA, S. S. 2021. Nisin resistance in Gram-positive bacteria and approaches to circumvent resistance for successful therapeutic use. *Crit Rev Microbiol,* 47**,** 376-385.

BARIK, S. 2020. The Uniqueness of Tryptophan in Biology: Properties, Metabolism, Interactions and Localization in Proteins. *Int J Mol Sci,* 21.

BEIS, K. 2015. Structural basis for the mechanism of ABC transporters. *Biochem Soc Trans,* 43**,** 889-93.

CHATTERJEE, C., MILLER, L. M., LEUNG, Y. L., XIE, L., YI, M., KELLEHER, N. L. & VAN DER DONK, W. A. 2005. Lacticin 481 synthetase phosphorylates its substrate during lantibiotic production. *J Am Chem Soc,* 127**,** 15332-3.

COTTER, P. D., ROSS, R. P. & HILL, C. 2013. Bacteriocins - a viable alternative to antibiotics? *Nat Rev Microbiol,* 11**,** 95-105.

DE KWAADSTENIET, M., DOESCHATE, K. T. & DICKS, L. M. 2009. Nisin F in the treatment of respiratory tract infections caused by Staphylococcus aureus. *Lett Appl Microbiol,* 48**,** 65-70.

DE RUYTER, P. G., KUIPERS, O. P. & DE VOS, W. M. 1996. Controlled gene expression systems for Lactococcus lactis with the food-grade inducer nisin. *Appl Environ Microbiol,* 62**,** 3662-7.

GEITANI, R., AYOUB MOUBARECK, C., TOUQUI, L. & KARAM SARKIS, D. 2019. Cationic antimicrobial peptides: alternatives and/or adjuvants to antibiotics active against methicillin-resistant Staphylococcus aureus and multidrug-resistant Pseudomonas aeruginosa. *BMC Microbiol,* 19**,** 54.

GRANSETH, E., VON HEIJNE, G. & ELOFSSON, A. 2005. A study of the membrane-water interface region of membrane proteins. *J Mol Biol,* 346**,** 377-85.

HOLLAND, I. B., COLE, S.P.C., KUCHLER, K. AND HIGGINS, C.F. 2003. ABC Proteins from Bacteria to Man. *Chapter 2. Academic Press, London*.

HONG, H., PARK, S., JIMENEZ, R. H., RINEHART, D. & TAMM, L. K. 2007. Role of aromatic side chains in the folding and thermodynamic stability of integral membrane proteins. *J Am Chem Soc,* 129**,** 8320-7.

HUSADA, F., BOUNTRA, K., TASSIS, K., DE BOER, M., ROMANO, M., REBUFFAT, S., BEIS, K. & CORDES, T. 2018. Conformational dynamics of the ABC transporter McjD seen by single-molecule FRET. *EMBO J,* 37.

KLEIN, C. & ENTIAN, K. D. 1994. Genes involved in self-protection against the lantibiotic subtilin produced by Bacillus subtilis ATCC 6633. *Appl Environ Microbiol,* 60**,** 2793-801.

KUIPERS, A., DE BOEF, E., RINK, R., FEKKEN, S., KLUSKENS, L. D., DRIESSEN, A. J., LEENHOUTS, K., KUIPERS, O. P. & MOLL, G. N. 2004. NisT, the transporter of the lantibiotic nisin, can transport fully modified, dehydrated, and unmodified prenisin and fusions of the leader peptide with non-lantibiotic peptides. *J Biol Chem,* 279**,** 22176-82.

KUIPERS, O. P., BEERTHUYZEN, M. M., SIEZEN, R. J. & DE VOS, W. M. 1993. Characterization of the nisin gene cluster nisABTCIPR of Lactococcus lactis. Requirement of expression of the nisA and nisI genes for development of immunity. *Eur J Biochem,* 216**,** 281-91.

LEWINSON, O., ORELLE, C. & SEEGER, M. A. 2020. Structures of ABC transporters: handle with care. *FEBS Lett,* 594**,** 3799-3814.

LOO, T. W., BARTLETT, M. C. & CLARKE, D. M. 2004. Disulfide cross-linking analysis shows that transmembrane segments 5 and 8 of human P-glycoprotein are close together on the cytoplasmic side of the membrane. *J Biol Chem,* 279**,** 7692-7.

LOO, T. W. & CLARKE, D. M. 2001. Determining the dimensions of the drug-binding domain of human P-glycoprotein using thiol cross-linking compounds as molecular rulers. *J Biol Chem,* 276**,** 36877-80.

LOO, T. W. & CLARKE, D. M. 2002. Vanadate trapping of nucleotide at the ATP-binding sites of human multidrug resistance P-glycoprotein exposes different residues to the drug-binding site. *Proc Natl Acad Sci U S A,* 99**,** 3511-6.

MARKI, F., HANNI, E., FREDENHAGEN, A. & VAN OOSTRUM, J. 1991. Mode of action of the lanthionine-containing peptide antibiotics duramycin, duramycin B and C, and cinnamycin as indirect inhibitors of phospholipase A2. *Biochem Pharmacol,* 42**,** 2027-35.

MCDONALD, S. K. & FLEMING, K. G. 2016. Aromatic Side Chain Water-to-Lipid Transfer Free Energies Show a Depth Dependence across the Membrane Normal. *J Am Chem Soc,* 138**,** 7946-50.

MIERAU, I. & KLEEREBEZEM, M. 2005. 10 years of the nisin-controlled gene expression system (NICE) in Lactococcus lactis. *Appl Microbiol Biotechnol,* 68**,** 705-17.

MULNAES, D., PORTA, N., CLEMENS, R., APANASENKO, I., REINERS, J., GREMER, L., NEUDECKER, P., SMITS, S. H. J. & GOHLKE, H. 2020. TopModel: Template-Based Protein Structure Prediction at Low Sequence Identity Using Top-Down Consensus and Deep Neural Networks. *J Chem Theory Comput,* 16**,** 1953-1967.

OTTO, M., PESCHEL, A. & GOTZ, F. 1998. Producer self-protection against the lantibiotic epidermin by the ABC transporter EpiFEG of Staphylococcus epidermidis Tu3298. *FEMS Microbiol Lett,* 166**,** 203-11.

PAG, U., HEIDRICH, C., BIERBAUM, G. & SAHL, H. G. 1999. Molecular analysis of expression of the lantibiotic pep5 immunity phenotype. *Appl Environ Microbiol,* 65**,** 591-8.

PESCHEL, A. & GOTZ, F. 1996. Analysis of the Staphylococcus epidermidis genes epiF, -E, and -G involved in epidermin immunity. *J Bacteriol,* 178**,** 531-6.

RA, R., BEERTHUYZEN, M. M., DE VOS, W. M., SARIS, P. E. J. & KUIPERS, O. P. 1999. Effects of gene disruptions in the nisin gene cluster of Lactococcus lactis on nisin production and producer immunity. *Microbiology (Reading),* 145 (Pt 5)**,** 1227-1233.

RA, S. R., QIAO, M., IMMONEN, T., PUJANA, I. & SARIS, P. E. J. 1996. Genes responsible for nisin synthesis, regulation and immunity form a regulon of two operons and are induced by nisin in Lactoccocus lactis N8. *Microbiology (Reading),* 142 (Pt 5)**,** 1281-1288.

RAIS, I., KARAS, M. & SCHAGGER, H. 2004. Two-dimensional electrophoresis for the isolation of integral membrane proteins and mass spectrometric identification. *Proteomics,* 4**,** 2567-71.

RANA, K., SHARMA, R. & PREET, S. 2019. Augmented therapeutic efficacy of 5-fluorouracil in conjunction with lantibiotic nisin against skin cancer. *Biochem Biophys Res Commun,* 520**,** 551-559.

RATH, A. & DEBER, C. M. 2013. Correction factors for membrane protein molecular weight readouts on sodium dodecyl sulfate-polyacrylamide gel electrophoresis. *Anal Biochem,* 434**,** 67-72.

RATH, A., GLIBOWICKA, M., NADEAU, V. G., CHEN, G. & DEBER, C. M. 2009. Detergent binding explains anomalous SDS-PAGE migration of membrane proteins. *Proc Natl Acad Sci U S A,* 106**,** 1760-5.

REIS, M., ESCHBACH-BLUDAU, M., IGLESIAS-WIND, M. I., KUPKE, T. & SAHL, H. G. 1994. Producer immunity towards the lantibiotic Pep5: identification of the immunity gene pepI and localization and functional analysis of its gene product. *Appl Environ Microbiol,* 60**,** 2876-83.

REUMERS, J., MAURER-STROH, S., SCHYMKOWITZ, J. & ROUSSEAU, F. 2009. Protein sequences encode safeguards against aggregation. *Hum Mutat,* 30**,** 431-7.

RINK, R., WIERENGA, J., KUIPERS, A., KLUSKENS, L. D., DRIESSEN, A. J., KUIPERS, O. P. & MOLL, G. N. 2007. Dissection and modulation of the four distinct activities of nisin by mutagenesis of rings A and B and by C-terminal truncation. *Appl Environ Microbiol,* 73**,** 5809-16.

SANTOS, R., RUZA, D., CUNHA, E., TAVARES, L. & OLIVEIRA, M. 2019. Diabetic foot infections: Application of a nisin-biogel to complement the activity of conventional antibiotics and antiseptics against Staphylococcus aureus biofilms. *PLoS One,* 14**,** e0220000.

SCHMITT, L. & TAMPE, R. 2002. Structure and mechanism of ABC transporters. *Curr Opin Struct Biol,* 12**,** 754-60.

SIEGERS, K. & ENTIAN, K. D. 1995. Genes involved in immunity to the lantibiotic nisin produced by Lactococcus lactis 6F3. *Appl Environ Microbiol,* 61**,** 1082-9.

SIEZEN, R. J., KUIPERS, O. P. & DE VOS, W. M. 1996. Comparison of lantibiotic gene clusters and encoded proteins. *Antonie Van Leeuwenhoek,* 69**,** 171-84.

SITU, A. J., KANG, S. M., FREY, B. B., AN, W., KIM, C. & ULMER, T. S. 2018. Membrane Anchoring of alpha-Helical Proteins: Role of Tryptophan. *J Phys Chem B,* 122**,** 1185-1194.

SKAUGEN, M., ABILDGAARD, C. I. & NES, I. F. 1997. Organization and expression of a gene cluster involved in the biosynthesis of the lantibiotic lactocin S. *Mol Gen Genet,* 253**,** 674-86.

SMITS, S. H. J., SCHMITT, L. & BEIS, K. 2020. Self-immunity to antibacterial peptides by ABC transporters. *FEBS Lett,* 594**,** 3920-3942.

STEIN, T., HEINZMANN, S., SOLOVIEVA, I. & ENTIAN, K. D. 2003. Function of Lactococcus lactis nisin immunity genes nisI and nisFEG after coordinated expression in the surrogate host Bacillus subtilis. *J Biol Chem,* 278**,** 89-94.

THOMAS, C. & TAMPE, R. 2018. Multifaceted structures and mechanisms of ABC transport systems in health and disease. *Curr Opin Struct Biol,* 51**,** 116-128.

VALENTA, C., BERNKOP-SCHNURCH, A. & RIGLER, H. P. 1996. The antistaphylococcal effect of nisin in a suitable vehicle: a potential therapy for atopic dermatitis in man. *J Pharm Pharmacol,* 48**,** 988-91.

VAN DER DOES, C. & TAMPE, R. 2004. How do ABC transporters drive transport? *Biol Chem,* 385**,** 927-33.

WIEDEMANN, I., BREUKINK, E., VAN KRAAIJ, C., KUIPERS, O. P., BIERBAUM, G., DE KRUIJFF, B. & SAHL, H. G. 2001. Specific binding of nisin to the peptidoglycan precursor lipid II combines pore formation and inhibition of cell wall biosynthesis for potent antibiotic activity. *J Biol Chem,* 276**,** 1772-9.

ZAITSEVA, J., OSWALD, C., JUMPERTZ, T., JENEWEIN, S., WIEDENMANN, A., HOLLAND, I. B. & SCHMITT, L. 2006. A structural analysis of asymmetry required for catalytic activity of an ABC-ATPase domain dimer. *EMBO J,* 25**,** 3432-43.

3.7 Chapter VI: Natural Compounds

Natural compounds against antimicrobial resistance

Julia Gottstein[1], Pablo Cea Medina[3], Lars Seifert[3], Holger Stark[3], Holger Gohlke[3] & Sander H. J. Smits[1,2]

[1]*Institute of Biochemistry, Heinrich-Heine-University Düsseldorf, Universitätsstrasse 1, 40225 Düsseldorf*
[2]Center for Structural Studies, Heinrich-Heine-University Duesseldorf, Universitätsstrasse 1, 40225 Duesseldorf, Germany.
[3]*Institute of Pharmaceutical and Medicinal Chemistry, Heinrich-Heine-University Düsseldorf, Universitätsstrasse 1, 40225 Düsseldorf*

In preparation

Own proportion of this work: 40%

- Biological assays
- Preparation of figures
- Writing the manuscript

Natural compounds against antimicrobial resistance

Julia Gottstein[1], Pablo Cea Medina[3], Lars Seifert[3], Holger Stark[3], Holger Gohlke[3] & Sander H. J. Smits[1,2]

[1]*Institute of Biochemistry, Heinrich-Heine-University Düsseldorf, Universitätsstrasse 1, 40225 Düsseldorf*
[2]Center for Structural Studies, Heinrich-Heine-University Duesseldorf, Universitätsstrasse 1, 40225 Duesseldorf, Germany.
[3]*Institute of Pharmaceutical and Medicinal Chemistry, Heinrich-Heine-University Düsseldorf, Universitätsstrasse 1, 40225 Düsseldorf*

Abstract

A major challenge of our time is the treatment of life-threatening bacterial infections due to the evolved resistance mechanisms of pathogens against antibiotics. To counteract this problem, it is necessary to understand the drug's mode of action and the pathogen's resistance mechanism. The biosynthesis of the peptidoglycan (PGN), which is a critical feature of bacteria is one of the most potent antibiotic targets. Antimicrobial peptides (AMPs), such as nisin and colistin, targeting PGN synthesis are considered promising weapons against multidrug-resistant bacteria. However, human pathogenic bacteria conferring resistance to these compounds evolved by the expression of resistance proteins: a serine protease NSR cleaving nisin and an ATP-binding cassette transporter of the Bacitracin efflux (BceAB) type that is localized in the membrane. In *Streptococcus agalactiae*, the BceAB transporter *Sa*NsrFP is known to confer resistance to a wide variety of structurally diverse antimicrobial peptides. In previous studies, it has been demonstrated that it is possible to bypass this resistance system e.g. by modifying the target and also by screening for small molecule inhibitors that sensitize the strains to nisin. In this study latter method was used to identify a compound that is able to inhibit *L. lactis* strains that express one of the nisin resistance proteins while not inhibiting the empty vector control strains. For this, 95 compounds were tested and screened for specific inhibition against *Sa*NSR and *Sa*NsrFP. Two compounds were identified that could inhibit both nisin resistance proteins specifically without inhibiting the sensitive control strain. Further optimization of the compounds is necessary to reduce the concentration needed to inhibit 50 % of the cells.

Introduction

Natural products derived from bacteria, fungi, or plants constitute an abundant source of bioactive drugs, accounting for almost half of all released pharmaceuticals in the past forty years (Newman and Cragg, 2020, Miethke *et al.,* 2021). Their rich scaffold diversity and structural complexity is an asset that has enabled scientists to find treatments for cancer, cardiovascular disease, multiple sclerosis, and infections. Today, life-threatening bacterial infections caused by multidrug-resistant pathogens pose major challenges to the global health system and drive growing demand for new antimicrobial drugs.

Antimicrobial peptides are promising alternatives to antibiotics. They are natural products that can be isolated from organisms across all kingdoms of life (Malmsten, 2014, Chen and Lu, 2020) and most importantly, they are gene-encoded which facilitates genetic manipulation. Antimicrobial peptides are of high pharmaceutical interest due to their diverse activity including antibacterial, antifungal, antiviral, antitumor, antinociceptive, and more (Diep and Nes, 2002, Green and Olivera, 2016, Buda De Cesare *et al.,* 2020, Fu *et al.,* 2021, Liu *et al.,* 2022, Rojas-Pirela *et al.,* 2023). The mode of action of these peptides ranges from inhibiting transcription, translation, or functioning as chalco- or siderophores to targeting the membrane (Schmidt *et al.,* 2005, Arnison *et al.,* 2013, Ongpipattanakul *et al.,* 2022).

Peptides that kill other bacteria, so-called lantibiotics, are produced by mainly Gram-positive bacteria (Klaenhammer, 1993, Sahl and Bierbaum, 1998). They are produced as precursor peptides which undergo a maturation process leading to the formation of lanthionine rings, important for activity and stability (Oman and van der Donk, 2010, Arnison et al., 2013, Chatterjee *et al*., 2005). They are then transported out of the cell and activated (Lagedroste *et al*., 2021). The most prominent example of a lantibiotic is nisin, produced by *Lactococcus lactis*. The high antimicrobial activity of nisin is based on two modes of action. First, nisin specifically binds the cell wall precursor lipid II with its first three lanthionine rings and thereby inhibits cell wall synthesis (Wiedemann *et al*., 2001). The second functionality is facilitated by the flexible hinge region which allows nisin to insert its rings D and E into the membrane resulting in the formation of pores (Hasper et al., 2004). Eight molecules of nisin and four molecules of lipid II constitute one

pore of 2-2.5nm diameter, allowing rapid efflux of cell content and eventually cell death (Hsu *et al*., 2004, Breukink and de Kruijff, 2006).

However, the pharmaceutical applications of nisin and other lantibiotics are challenged by resistance mechanisms in human pathogenic bacteria (Gebhard, 2012, Draper *et al*., 2015, Kobras *et al*., 2020, Gottstein *et al*., 2022). *Streptococcus agalactiae* COH1 is one example, conferring resistance against nisin (Khosa *et al*., 2013, Sun *et al*., 2009) and other structurally diverse antimicrobial peptides (Reiners *et al.,* 2017, Gottstein *et al*., 2022) by expressing the nisin resistance operon (nsr). It consists of genes encoding a two-component system NsrRK, an ABC transporter NsrFP, and a serine protease NSR (Khosa *et al*., 2013). The latter belongs to the S41 peptidase family which is characterized by a catalytic dyad consisting of a serine and a histidine residue (Khosa *et al*., 2016a, Rawlings *et al*., 2018). The resistance mechanism of NSR involves the enzymatic inactivation of nisin by cleaving the last six amino acid residues. The resulting peptide fragment exhibits a 100-fold reduced antibacterial activity and lower affinity towards bacterial membranes (Sun *et al*., 2009). In a previous study, it was shown that heterologous expression of the NSR protein in a nisin-sensitive *L. lactis* strain conferred a 20-fold resistance against nisin (Khosa et al., 2013, Khosa et al., 2016c, Khosa et al., 2016a).

Part of the *nsr* operon is a gene encoding for the BceAB-type transporter *Sa*NsrFP consisting of a nucleotide-binding domain NsrF and a transmembrane domain NsrP (Clemens *et al*., 2017, Reiners *et al*., 2017). Similar to BceAB, the TM helices 1 to 4 and 7 to 10 form individual bundles, representing an FtsX-domain fold like that observed in type VII mechanotransmission ABC transporters (Thomas *et al.,* 2020). Furthermore, TM helices 5 and 6 interact with each other and are positioned closer to helices 7-10 than to the other bundle, creating an asymmetrical arrangement. Between helix 7 and 8 is a large ECD of 221 amino acids. This ECD, characteristic of BceAB-type transporters, is hypothesized to be involved in substrate binding and recognition (Ohki *et al.,* 2003, Clemens *et al.,* 2017, Khosa *et al.,* 2013). *Sa*NsrFP was shown to recognize the N-terminus of nisin and its heterologous expression in the nisin-sensitive *L. lactis* NZ9000 strain resulted in a 16-fold resistance against nisin A, and a 12-fold resistance against nisin H and gallidermin (Reiners *et al*., 2017). Additionally, previous work has shown that *Sa*NsrFP protects against a structurally diverse group of antimicrobial

peptides by actively shielding the cell wall and initiating a second line of defense, resulting in cell wall modification (Gottstein *et al*., 2022). The nisin resistance system is one of many types of antimicrobial resistance systems that has emerged as a complex and multi-faceted mechanism that requires further investigation.

One method to overcome the nisin resistance system is to find and screen for potent small molecule inhibitors that potentially inhibit the nisin resistance proteins *Sa*NSR and *Sa*NsrFP from *S. agalactiae.* In a previous study, a halogenated phenyl-urea derivative (NPG9) that specifically inhibits NSR was identified by virtual screening based on a structural model of the NSR/nisin complex (Porta *et al*., 2019) (Figure 25). Based on this molecule, a new generation of small molecules was designed by the research group of Prof. Dr. Gohlke and tested in this study.

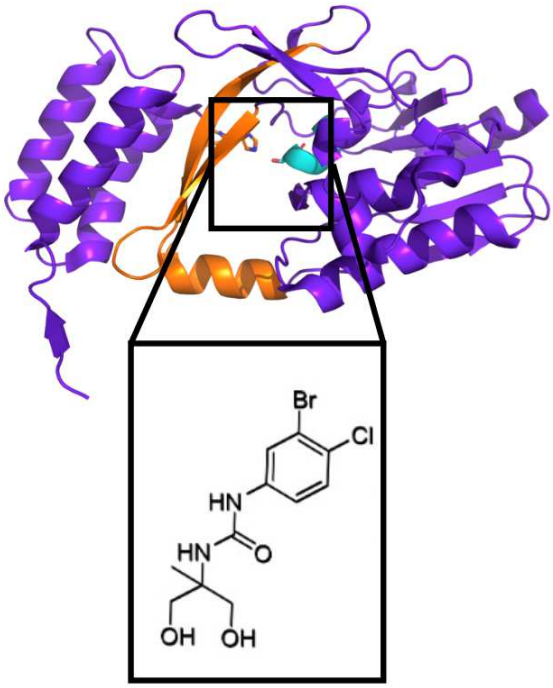

Figure 25: NSR- the nisin resistance protein (PDB ID: 4Y68) and its inhibitor NPG9. The structure of the serine protease NSR is shown. The residues around the active site are highlighted in light blue and the protease cap in orange. The catalytically active His98 and Ser236 are shown as sticks. NPG9 was designed to fit the active site of NSR (Porta *et al.*, 2019). Image created with PyMOL Version 2.3.0 and Powerpoint 16.72.

Material and Methods

Molecular dynamics simulation

Molecular dynamics simulation was performed by taking NPG9 as a model inhibitor as described in previous works by (Porta *et al*., 2019).

Compound acquisition

The tested compounds were either custom-synthetized or purchased from different suppliers as a powder (Table S9). The compounds were dissolved in 100% sterile DMSO to make a stock of 100mM. To ensure that compounds are pure enough to be used for the screening assays of this study their purity was assessed via LC-MS. For the specific growth inhibition assay the compounds were diluted with media. A list of all compounds is attached in the supplementary of this chapter.

Purity assessment using LC-MS

For the LC-MS measurement, the compound-stock solutions were diluted with sterile methanol (hypergrade) to concentrations of 0.1-0.2 mg/mL. A volume of 2 µL was injected for each measurement. The relative purity of the compounds was determined as a ratio of the area under the curve. The following LC system was used: Elute SP LC System (Bruker Daltonics, Bremen, Germany) with a vacuum degasser, binary pump, autosampler, and column oven. Furthermore, the following column was used: Intensity Solo 2 C18 (100 mm *2.1 mm). Parameters were set as described in the following: Temperature: 50°C; Mobile phase: A. Water hypergrade with 0.1% formic acid (v/v) (Merck); B. Acetonitrile hypergrade (Merck); Flow rate: 0.2 mL/min. Method 1: 0-4 min 95% A, 4-16 min gradient 95% to 5% A, 16-17 min gradient 5% to 0% A, reconditioning: 17-18 min gradient 0% to 95% A, 18-21 min 95% A. Method 2: 0-4 min 98% A, 4-5 min gradient 98% to 95% A, 5-9 min 95% A, 9-16 min gradient 95% to 5% A, 16-17 min gradient 5% to 0% A, reconditioning: 17-18 min gradient 0% to 98% A, 18-21 min 98% A. MS-System: amazon speed ETD ion Trap LC/MSn System (Bruker Daltonics, Bremen, Germany); Ionisation: electronspray; Polarity: positive; Alternating ion-polarity: on; Scan range: *m/z*: 80-1200; Nebulizer: Nitrogen, 15 Psi; Dry Gas: Nitrogen, 8L/min, 200°C; Massrange mode: UltraScan.

Cloning of the proteins SaNSR and SaNsrF

Cloning was performed as described in previous work by (Khosa *et al*., 2013) and (Reiners *et al*., 2017). The respective plasmid (pNZ-SV*Sa*NSR) or (pIL-SV*Sa*NsrFP) was transformed using electro-competent *L. lactis* NZ9000. Thus, the cells were electroporated, using a pulse-setting of 1 kV, 25 µF, 200 Ω, for 4.5-5.0 ms (Holo and Nes, 1989). Subsequently, 950 µL GM17 media was added, and the cells were incubated at 30°C for 3h. In the last step, cells were plated on SMGG-agar plates containing either 5 µg/mL erythromycin (for pNZ-SV) or 10 µg/mL chloramphenicol.

Purification of nisin

Nisin was purified with cation exchange chromatography and its concentration was determined by RP-HPLC as described in previous work by (Abts et al., 2011, Abts et al., 2013).

Compound growth inhibition assay

To verify whether the selected compounds specifically inhibit the growth of strains expressing *Sa*NSR or *Sa*NsrFP, a growth inhibition assay was performed as previously described in (Porta *et al*., 2019). *L. lactis* strains expressing the resistance proteins were grown in GM17 medium with 1 ng/mL nisin with either 5 µg/mL erythromycin for *Sa*NSR-expressing strains or 10 µg/mL chloramphenicol for *Sa*NsrFP-expressing *L. lactis* strains. The cells were grown overnight at 30°C. The next day, cells were diluted in fresh media to an OD_{600nm} of =.1 and incubated for 30 min at 30°C. 50 µL of the selected compound and the DMSO control (20%) were added to a 96-well plate. 150 µL of the empty vector-control NZ9000senspNZ-SV/ NZ9000senspIL-SV without nisin and NZ9000pNZ-SV*Sa*NSR, and NZ9000pIL-SV*Sa*NsrFP supplemented respectively with 30 nM nisin, was added. After 5 h-7 h at 30°C, the optical density was measured and the relative growth inhibition was calculated by comparing the normalized values for *L. lactis* NZ9000 pNZ-SV-*Sa*NSR or pIL-SV *Sa*NsrFP.

Measurement of nisin activity (IC_{50})

The control strains NZ9000senspNZ, NZ9000senspIL, and strains expressing the resistance proteins were grown overnight in GM17 media supplemented with either 5 µg/mL erythromycin (pNZ-SV*Sa*NSR) or 10 µg/mL chloramphenicol (pIL-SV*Sa*NsrFP) in the presence of 1 ng/mL of nisin. The following day, the cells

were diluted to an OD_{600} of 0.1 in fresh GM17 media with respective antibiotics and incubated at 30°C for 30 minutes. In a 96-well plate, 50 µL of dilutions of nisin were prepared. Then, 150 µL of each strain supplemented with 30 nM nisin was added to the plate. After 5 to 7 hours of incubation at 30°C, the optical density was measured, and the IC_{50} was calculated.

Results

Experimental validation of the compounds was performed using a modified growth inhibition assay that allows screening for specific inhibition against the nisin resistance proteins bacterial cells tested *in vivo*. With this assay, the compounds were examined on specific inhibition of *L. lactis* strains expressing either *Sa*NSR or *Sa*NsrFP. This was possible due to supplementing each strain with 30 nM of nisin which is the concentration that was determined in previous work to kill nisin-sensitive cells but not the resistance protein-expressing cells (dashed line in Figure 26). Thus, susceptibility to nisin by a resistance protein-expressing *L. lactis* strain in the presence of the compound was taken as a direct indication of specific inhibition of nisin resistance proteins (Figure 26). As a control, a sensitive *L. lactis* strain, expressing the empty vector (pNZ-SV or pIL-SV) was used in the assay. Figure 26 shows exemplary growth inhibition curves for the sensitive control strain (black), the resistance protein-expressing strain without compound (purple), and the resistance strain treated with different concentrations of compound and 30 nM of nisin (pink) which is shifted toward the sensitive strain. This shift indicates that the compound inhibits the respective resistance protein, due to its susceptibility against a low nisin concentration of 30 nM (the dashed line in Figure 26 represents 30 nM).

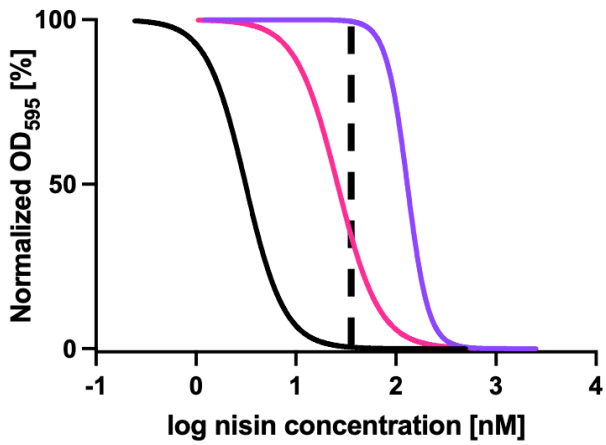

Figure 26: Exemplary growth inhibition curves. The normalized OD_{595nm} was plotted against the logarithmic nisin concentrations in nanomolar for the sensitive control strain *L. lactis* NZ9000 (black) treated with nisin, *L. lactis* NZ9000 expressing a resistance protein (purple) treated with nisin, and *L. lactis* NZ9000 with a resistance protein treated with different concentrations of an inhibitor in the presence of 30 nM nisin (pink). The dashed line shows that at a concentration of approximately 30 nM nisin, the sensitive strain is killed but the resistance protein-expressing strain survives. In the presence of 30 nM of nisin and an inhibitor, specifically inhibiting the resistance protein, a shift of the growth inhibition curves can be observed.

Screening for specific small molecule inhibitors against *Sa*NSR and *Sa*NsrFP

53 newly designed and purchased compounds were provided by the research group of Prof. Dr. Gohlke and 43 newly synthesized compounds by the research group of Prof. Dr. Stark. Compounds that precipitated during the preparation of the assay were omitted. This was the case for all compounds provided by the research group of Prof. Dr. Stark and compounds 4 and 25 from the research group of Prof. Dr. Gohlke. The remaining stable compounds were tested for specific inhibition against *Sa*NSR and *Sa*NsrFP. For this purpose, the bacterial cells expressing either *Sa*NSR or *Sa*NsrFP were treated with a concentration of 150 µM, 75 µM, and 37.5 µM of a compound in the presence of 30 nM of nisin. After 5 hours of incubation, the OD_{600nm} was measured. The sensitive control strain was treated with the compound alone as 30 nM nisin would directly kill the strain. Furthermore, all strains were also treated with DMSO as a control. To calculate the specific inhibition against one of the resistance proteins, the OD_{600nm} was normalized against the DMSO control. In the next step, the normalized ODs for the strain expressing a resistance protein were subtracted from the ODs of the respective sensitive strain and this value was multiplied by 100. The specific inhibition was plotted against the concentration of the tested compound. Since

NPG9 showed 67% of specific inhibition against NSR in previous work, this value was set as a threshold (dashed line in Figure 27) for compounds screened for specific inhibition against NSR (Figure 27). Figures 27 and 28 display the results for the compounds tested on *L. lactis* NZ9000 pNZ-SV-*Sa*NSR and *L. lactis* NZ9000 pNZ-SV-*Sa*NsrFP.

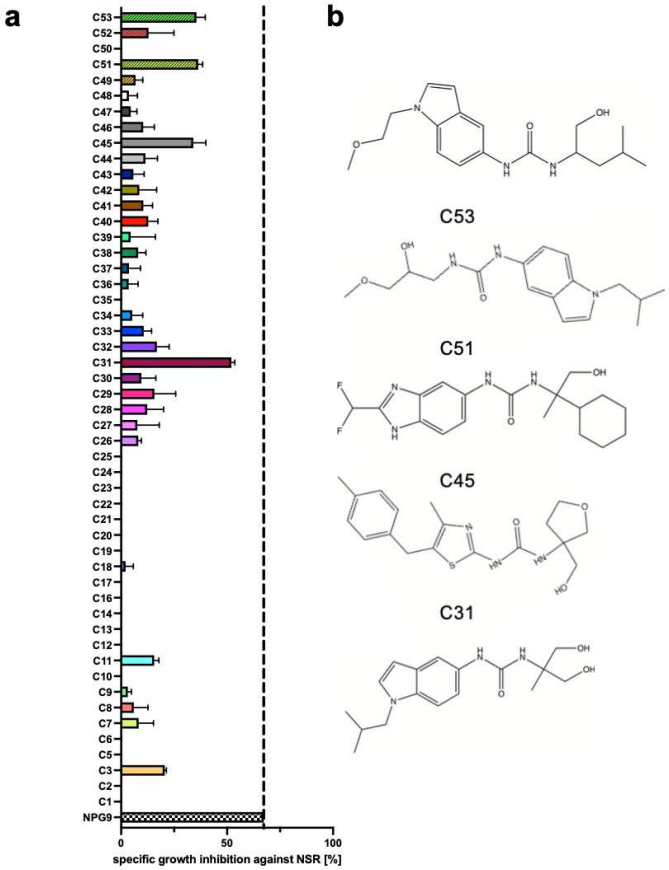

Figure 27 a) Screen of compounds on *L. lactis* NZ9000 pNZ-SV-*Sa*NSR. The bacterial cells were treated with 150 µM of the compound and screened on their potential of specifically inhibiting *Sa*NSR in the presence of 30 nM nisin. The line at 67% percent represents the specific growth inhibition of NPG9 which was taken as a threshold. Compounds 4 and 15 were omitted due to precipitation in the assay. All compounds from the research group Prof.Dr. Stark had to be omitted due to precipitation in the assay. Compounds without specific inhibition activity are shown in the graph without a bar. **b)** Molecular structures of the compounds with the highest specific inhibition against *Sa*NSR. The graph was plotted using Prism Version 10.0.2, molecules were drawn using ChemDraw 20.1, and the figure was arranged using Powerpoint 16.72.

Compounds that showed the highest specific inhibition against the *Sa*NSR-expressing strain were C3 (21%), C31 (45%), C45 (34%), C51 (26%), and C53 (36%). However, none of the tested compounds reached the minimal threshold of 67% set by NPG9 (Figure 27).

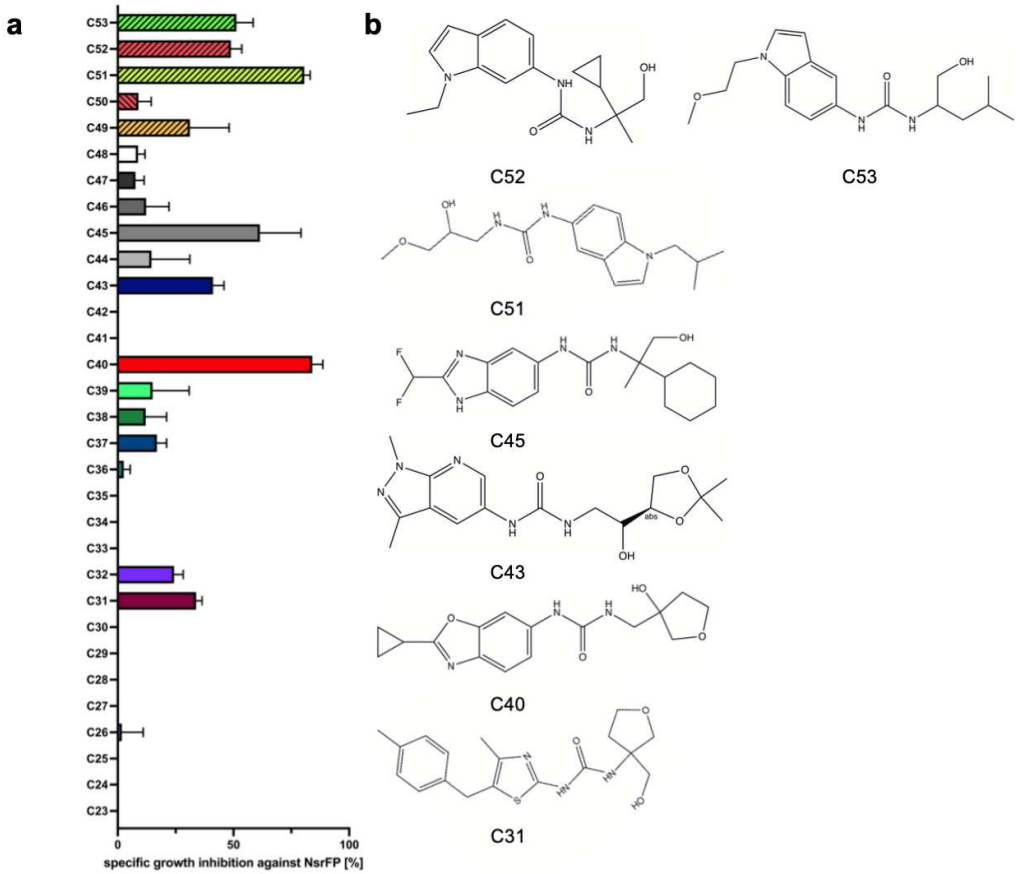

Figure 28 a) Screen of compounds on *L. lactis* NZ9000 pNZ-SV-*Sa*NsrFP. The bacterial cells were treated with 150 µM of compound and screened on their potential of specifically inhibiting *Sa*NsrFP in the presence of 30 nM nisin. Compounds without specific inhibition activity are shown in the graph without a bar. **b)** Molecular structures of the compounds with highest specific inhibition against *Sa*NsrFP. The graph was plotted using Prism Version 10.0.2, molecules were drawn using ChemDraw 20.1, and the figure was arranged using Powerpoint 16.72.

For the *Sa*NsrFP-expressing strain, compounds C31 (33%), C40 (84%), C43 (41%), C45 (61%), C51 (80%), C52 (49%), and C53 (51%) exhibited the highest specific inhibition against *Sa*NsrFP within the tested compounds (Table 6).

Table 6: Overview of the compounds with the highest specific inhibition against the resistance proteins *Sa*NSR and *Sa*NsrFP. The horizontal line indicates low activity and n.t indicates not tested at this stage.

Specific inhibition [%]	C3	C31	C40	C43	C45	C51	C52	C53
NSR	21% ± 1	45% ± 8	-	-	34% ± 6	36% ± 2	-	36% ± 4
NsrFP	n.t	34% ± 3	84% ± 5	41% ± 5	72% ± 3	81% ± 3	49% ± 5	51% ± 7

The most promising compounds were then analyzed to determine an IC_{50}. Due to the unavailability of the compounds C40, C43, C45, C51, C52, and C53 from Molport, only C3 and C31 could be purchased and were tested further. To determine the IC_{50} of the compounds, bacterial cells expressing either *Sa*NSR or *Sa*NsrFP were treated with a concentration of different concentrations of the compound in the presence of 30 nM nisin. After 5 to 7 hours of incubation, the OD_{600nm} was measured and the IC_{50} value was determined.

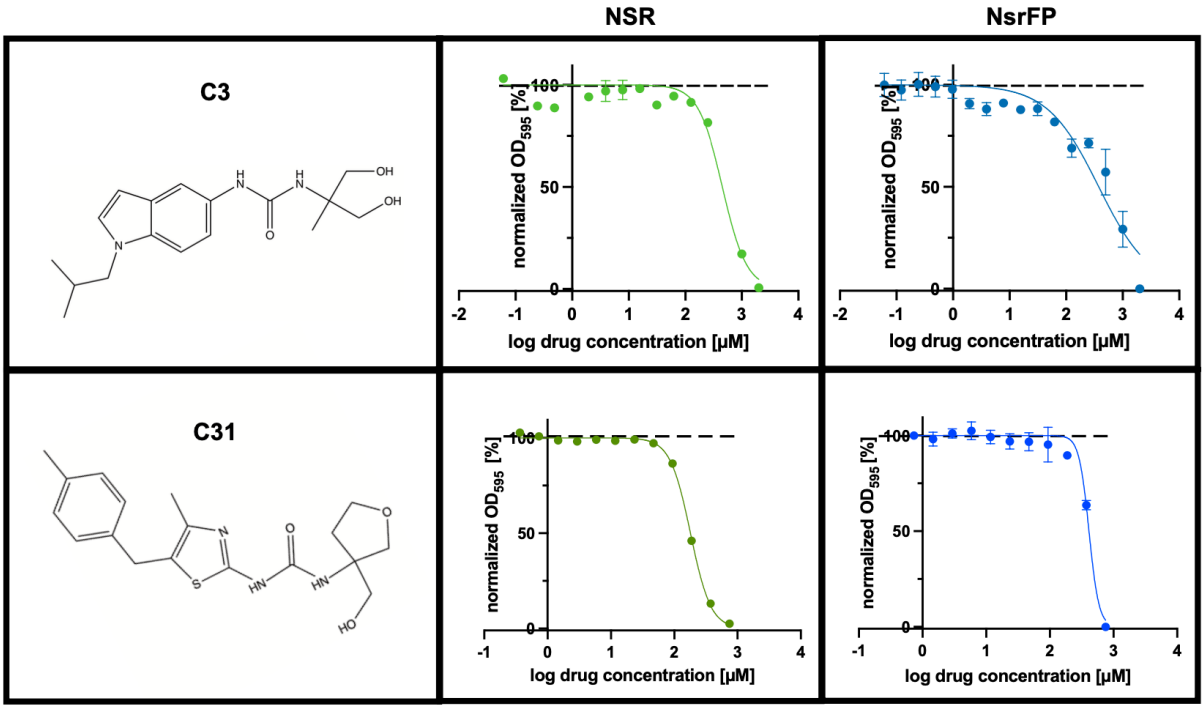

Figure 29: Structure of compounds and growth inhibition curves. *L. lactis* NZ9000 pNZ-SV-NSR were treated with either C3 (limegreen) or C31 (darkgreen) in presence of 30 nM nisin and growth inhibition curves *L. lactis* NZ9000 pIL-SV-NsrFP treated with either C3 (darkblue) or C31 (blue) in presence of 30 nM nisin. The black dotted line represents the sensitive strain *L. lactis* NZ9000 pNZ-SV or *L. lactis* NZ9000 pIL-SV that was treated also with each compound. The curves were plotted using Prism Version 10.0.2, molecules were drawn using ChemDraw 20.1, and the figure was arranged using Powerpoint 16.72.

C3 and C31 inhibited the nisin resistance protein in the presence of 30 nM of nisin with IC_{50} values of 455 µM and 180 µM, respectively (Table 7), wheras they did

not inhibit the sensitive control strain (dashed black line in Figure 29). Furthermore, both compounds were also able to inhibit the ABC transporter *Sa*NsrFP in the presence of nisin, while not inhibiting the sensitive strain (dashed black line in Figure 29). C31 shows a lower IC_{50} for *Sa*NsrFP with 151 µM than C3 with 363 µM (Table 7). Thus, two urea derivatives were identified as potential inhibitors against the nisin resistance proteins NSR and NsrFP of *S. agalactiae*.

Table 7: IC_{50} values of the tested compounds against the resistance proteins *Sa*NSR and *Sa*NsrFP.

Compound IC_{50} [µM]	IUPAC	NSR	NsrFP
C3	3-(1,3-dihydroxy-2-methylpropan-2-yl)-1-[1-(2-methylpropyl)-1H-indol-5-yl]urea	455± 51	363 ± 43
C31	1-[3-(hydroxymethyl)-oxolan-3-yl]-3-(4-methyl-5-[(4-methylphenyl)methyl]-1,3-thiazol-2-yl)urea	180 ± 3	151 ± 8

Discussion

From preliminary 96 compounds, two urea derivatives were identified as potential inhibitors against the resistance-conferring proteins from *S. agalactiae*: 3-(1,3-dihydroxy-2-methylpropan-2-yl)-1-(1-(2-methylpropyl)-1H-indol-5-yl]urea (C3) and 1-(3-(hydroxymethyl)-oxolan-3-yl]-3-(4-methyl-5-((4-methylphenyl)methyl]-1,3-thiazol-2-yl)urea (C31). C31 showed 2.5 times higher inhibition of both resistance proteins than compound C3. Structural differences are the oxolan or thiazol moiety of C31 and the indole moiety of C3 but more experiments and data are needed for more insight. Both compounds exhibited an IC_{50} value in the micromolar range, insufficient to be used in clinical applications. Therefore, optimization of both molecules is necessary to reduce the amount needed to inhibit 50 % of bacterial cells. The question that remains is how these two compounds can inhibit two structurally very different resistance proteins, *Sa*NSR (a serine protease) and *Sa*NsrFP (a membrane-bound ABC transporter). While structurally different, they have a common basis, as both proteins potentially interact with nisin. Thus, hypothetically, the compounds could bind to such a nisin binding site but this remains to be elucidated in detail.

The compounds that selectively inhibited the ABC transporter *Sa*NsrFP with a high specific inhibition of 50% to 84% were C40, C43, C45, C51, and C53. These

compounds could not be tested further due to limited availability. However, it is important to examine them as possible inhibitors in future experiments. Furthermore, a potent inhibitor was identified in previous work (Zaschke-Kriesche *et al.,* 2019), with a very different molecular structure compared to the compounds of this study here. Cerebroside C was shown to have a lipid-like structure consisting of a fatty acid and sphingosine which form together a ceramide and finally a monosaccharide. This compound was able to inhibit *Sa*NsrFP with a specific inhibition of 83 % (Zaschke-Kriesche *et al.,* 2019). Indeed, a close relative of this inhibitor, Cerebroside D, did not show inhibition towards *Sa*NsrFP, indicating highly specific binding of Cerebroside C (Zaschke-Kriesche *et al.,* 2019). A recent study described the structure of the related ABC transporter BceAB, which showed a lipid-binding pocket between its transmembrane helices 5 and 6 and 7 and 9 (George *et al*., 2022). *Sa*NsrFP as a homolog of BceAB is hypothesized to have a similar lipid-binding pocket between its TM helices 5,6 and 7,9. This could be the potential binding site for the previously identified compound Cerebroside C.

In previous work, a halogenated phenyl-urea derivative, NPG9, was identified as a potent inhibitor against the nisin resistance protein (NSR). So far, all NPG9-derived compounds in this study here failed to improve inhibitory activity or reach the nanomolar concentration range. This could be due to the specific chemical properties of the inhibitor NPG9 which was modeled to fit the active site of NSR (Porta *et al*., 2019). In the same study, it was observed that the inhibition activity required a linear molecular shape in combination with one or two hydrophobic regions separated by an amide-like moiety similar to nisin (Porta *et al*., 2019, Graham *et al*., 2014). Nisin´s hydrophobic regions are reflected by methyl-lanthionine and isoleucine residues. Additionally, a hydroxyl group as shown in NPG9, or an aromatic polar group (Porta *et al*., 2019), mimicking Ser29 and His28 of the NSR active site could result in stronger inhibitory activity in the compounds. Several publications have shown that urea derivatives play an important role as pharmacologically active drugs (Listro *et al*., 2022, Patil *et al*., 2019, Ommi *et al*., 2023, Poonia *et al*., 2022, Ghosh and Brindisi, 2020). The bioactivity of drugs depends on molecular recognition through interactions between the drug and the target protein. Hydrogen bonding, among other forces, can stabilize drug-

receptor interactions (Kuhn *et al*., 2010) thus, compounds with this capability can show biological activity. Urea derivatives act as hydrogen bond donors or acceptors which allows them to be involved in diverse interactions (Ghosh and Brindisi, 2020). They can have a diverse spectrum of activities including antiviral, anticonvulsant, and antibacterial (Venkatachalam *et al*., 2004, Ghosh and Brindisi, 2020, Ommi *et al.*, 2023, Patil *et al*., 2019). Furthermore, they can inhibit enzymes (Porta *et al*., 2019), be used as a sedative, or act as an anticancer drug (Listro *et al*., 2022, Ghosh and Brindisi, 2020).

As shown in this study, small molecule inhibitors represent a powerful method to bypass resistance systems in bacteria such as the nisin resistance system in *S. agalactiae*. One of the major advantages of this method of combating antibiotic resistance mechanisms is that pathogenic bacteria become susceptible to potent and well-known antimicrobial peptides such as nisin. Screening for potential small molecule inhibitors against antimicrobial resistance is therefore very promising and important for combating antibiotic resistance in other clinically relevant pathogens as well.

Acknowledgment

We thank to Dr. Aleksandra Zivkovic for the HPLC-MS analysis. This work was funded by the German Research Foundation (DFG) – GRK 2158.

References

ABTS, A., MAVARO, A., STINDT, J., BAKKES, P. J., METZGER, S., DRIESSEN, A. J., SMITS, S. H. & SCHMITT, L. 2011. Easy and rapid purification of highly active nisin. *Int J Pept,* 2011**,** 175145.

ABTS, A., MONTALBAN-LOPEZ, M., KUIPERS, O. P., SMITS, S. H. & SCHMITT, L. 2013. NisC binds the FxLx motif of the nisin leader peptide. *Biochemistry,* 52**,** 5387-95.

ARNISON, P. G., BIBB, M. J., BIERBAUM, G., BOWERS, A. A., BUGNI, T. S., BULAJ, G., CAMARERO, J. A., CAMPOPIANO, D. J., CHALLIS, G. L., CLARDY, J., COTTER, P. D., CRAIK, D. J., DAWSON, M., DITTMANN, E., DONADIO, S., DORRESTEIN, P. C., ENTIAN, K. D., FISCHBACH, M. A., GARAVELLI, J. S., GORANSSON, U., GRUBER, C. W., HAFT, D. H., HEMSCHEIDT, T. K., HERTWECK, C., HILL, C., HORSWILL, A. R., JASPARS, M., KELLY, W. L., KLINMAN, J. P., KUIPERS, O. P., LINK, A. J., LIU, W., MARAHIEL, M. A., MITCHELL, D. A., MOLL, G. N., MOORE, B. S., MULLER, R., NAIR, S. K., NES, I. F., NORRIS, G. E., OLIVERA, B. M., ONAKA, H., PATCHETT, M. L., PIEL, J., REANEY, M. J., REBUFFAT, S., ROSS, R. P., SAHL, H. G., SCHMIDT, E. W., SELSTED, M. E., SEVERINOV, K., SHEN, B., SIVONEN, K., SMITH, L., STEIN, T.,

SUSSMUTH, R. D., TAGG, J. R., TANG, G. L., TRUMAN, A. W., VEDERAS, J. C., WALSH, C. T., WALTON, J. D., WENZEL, S. C., WILLEY, J. M. & VAN DER DONK, W. A. 2013. Ribosomally synthesized and post-translationally modified peptide natural products: overview and recommendations for a universal nomenclature. *Nat Prod Rep,* 30**,** 108-60.

BREUKINK, E. & DE KRUIJFF, B. 2006. Lipid II as a target for antibiotics. *Nat Rev Drug Discov,* 5**,** 321-32.

BUDA DE CESARE, G., CRISTY, S. A., GARSIN, D. A. & LORENZ, M. C. 2020. Antimicrobial Peptides: a New Frontier in Antifungal Therapy. *mBio,* 11.

CHATTERJEE, C., MILLER, L. M., LEUNG, Y. L., XIE, L., YI, M., KELLEHER, N. L. & VAN DER DONK, W. A. 2005. Lacticin 481 synthetase phosphorylates its substrate during lantibiotic production. *J Am Chem Soc,* 127**,** 15332-3.

CHEN, C. H. & LU, T. K. 2020. Development and Challenges of Antimicrobial Peptides for Therapeutic Applications. *Antibiotics (Basel),* 9.

CLEMENS, R., ZASCHKE-KRIESCHE, J., KHOSA, S. & SMITS, S. H. J. 2017. Insight into Two ABC Transporter Families Involved in Lantibiotic Resistance. *Front Mol Biosci,* 4**,** 91.

DIEP, D. B. & NES, I. F. 2002. Ribosomally synthesized antibacterial peptides in Gram positive bacteria. *Curr Drug Targets,* 3**,** 107-22.

DRAPER, L. A., COTTER, P. D., HILL, C. & ROSS, R. P. 2015. Lantibiotic resistance. *Microbiol Mol Biol Rev,* 79**,** 171-91.

FU, Y., JAARSMA, A. H. & KUIPERS, O. P. 2021. Antiviral activities and applications of ribosomally synthesized and post-translationally modified peptides (RiPPs). *Cell Mol Life Sci,* 78**,** 3921-3940.

GEBHARD, S. 2012. ABC transporters of antimicrobial peptides in Firmicutes bacteria - phylogeny, function and regulation. *Mol Microbiol,* 86**,** 1295-317.

GEORGE, N. L., SCHILMILLER, A. L. & ORLANDO, B. J. 2022. Conformational snapshots of the bacitracin sensing and resistance transporter BceAB. *Proc Natl Acad Sci U S A,* 119**,** e2123268119.

GHOSH, A. K. & BRINDISI, M. 2020. Urea Derivatives in Modern Drug Discovery and Medicinal Chemistry. *J Med Chem,* 63**,** 2751-2788.

GOTTSTEIN, J., ZASCHKE-KRIESCHE, J., UNSLEBER, S., VOITSEKHOVSKAIA, I., KULIK, A., BEHRMANN, L. V., OVERBECK, N., STUHLER, K., STEGMANN, E. & SMITS, S. H. J. 2022. New insights into the resistance mechanism for the BceAB-type transporter SaNsrFP. *Sci Rep,* 12**,** 4232.

GRAHAM, T. H., SHU, M., VERRAS, A., CHEN, Q., GARCIA-CALVO, M., LI, X., LISNOCK, J., TONG, X., TUNG, E. C., WILTSIE, J., HALE, J. J., PINTO, S. & SHEN, D. M. 2014. Pyrazoles as non-classical bioisosteres in prolylcarboxypeptidase (PrCP) inhibitors. *Bioorg Med Chem Lett,* 24**,** 1657-60.

GREEN, B. R. & OLIVERA, B. M. 2016. Venom Peptides From Cone Snails: Pharmacological Probes for Voltage-Gated Sodium Channels. *Curr Top Membr,* 78**,** 65-86.

HASPER, H. E., DE KRUIJFF, B. & BREUKINK, E. 2004. Assembly and stability of nisin-lipid II pores. *Biochemistry,* 43**,** 11567-75.

HOLO, H. & NES, I. F. 1989. High-Frequency Transformation, by Electroporation, of Lactococcus lactis subsp. cremoris Grown with Glycine in Osmotically Stabilized Media. *Appl Environ Microbiol,* 55**,** 3119-23.

HSU, S. T., BREUKINK, E., TISCHENKO, E., LUTTERS, M. A., DE KRUIJFF, B., KAPTEIN, R., BONVIN, A. M. & VAN NULAND, N. A. 2004. The nisin-lipid II complex reveals a pyrophosphate cage that provides a blueprint for novel antibiotics. *Nat Struct Mol Biol,* 11**,** 963-7.

KHOSA, S., ALKHATIB, Z. & SMITS, S. H. 2013. NSR from Streptococcus agalactiae confers resistance against nisin and is encoded by a conserved nsr operon. *Biol Chem,* 394**,** 1543-9.

KHOSA, S., FRIEG, B., MULNAES, D., KLEINSCHRODT, D., HOEPPNER, A., GOHLKE, H. & SMITS, S. H. 2016a. Structural basis of lantibiotic recognition by the nisin resistance protein from Streptococcus agalactiae. *Sci Rep,* 6**,** 18679.

KHOSA, S., LAGEDROSTE, M. & SMITS, S. H. 2016b. Protein Defense Systems against the Lantibiotic Nisin: Function of the Immunity Protein NisI and the Resistance Protein NSR. *Front Microbiol,* 7**,** 504.

KLAENHAMMER, T. R. 1993. Genetics of bacteriocins produced by lactic acid bacteria. *FEMS Microbiol Rev,* 12**,** 39-85.

KOBRAS, C. M., PIEPENBREIER, H., EMENEGGER, J., SIM, A., FRITZ, G. & GEBHARD, S. 2020. BceAB-Type Antibiotic Resistance Transporters Appear To Act by Target Protection of Cell Wall Synthesis. *Antimicrob Agents Chemother,* 64.

KUHN, B., MOHR, P. & STAHL, M. 2010. Intramolecular hydrogen bonding in medicinal chemistry. *J Med Chem,* 53**,** 2601-11.

LAGEDROSTE, M., SMITS, S. H. J. & SCHMITT, L. 2021. Importance of the leader peptide sequence on the lanthipeptide secretion level. *FEBS J*.

LISTRO, R., ROSSINO, G., PIAGGI, F., SONEKAN, F. F., ROSSI, D., LINCIANO, P. & COLLINA, S. 2022. Urea-based anticancer agents. Exploring 100-years of research with an eye to the future. *Front Chem,* 10**,** 995351.

LIU, S. X., ZHOU, Y., ZHAO, L., ZHOU, L. S., SUN, J., LIU, G. J., DU, Y. S. & ZHOU, Y. N. 2022. Thiostrepton confers protection against reactive oxygen species-related apoptosis by restraining FOXM1-triggerred development of gastric cancer. *Free Radic Biol Med,* 193**,** 385-404.

MALMSTEN, M. 2014. Antimicrobial peptides. *Ups J Med Sci,* 119**,** 199-204.

MIETHKE, M., PIERONI, M., WEBER, T., BRONSTRUP, M., HAMMANN, P., HALBY, L., ARIMONDO, P. B., GLASER, P., AIGLE, B., BODE, H. B., MOREIRA, R., LI, Y., LUZHETSKYY, A., MEDEMA, M. H., PERNODET, J. L., STADLER, M., TORMO, J. R., GENILLOUD, O., TRUMAN, A. W., WEISSMAN, K. J., TAKANO, E., SABATINI, S., STEGMANN, E., BROTZ-OESTERHELT, H., WOHLLEBEN, W., SEEMANN, M., EMPTING, M., HIRSCH, A. K. H., LORETZ, B., LEHR, C. M., TITZ, A., HERRMANN, J., JAEGER, T., ALT, S., HESTERKAMP, T., WINTERHALTER, M., SCHIEFER, A., PFARR, K., HOERAUF, A., GRAZ, H., GRAZ, M., LINDVALL, M., RAMURTHY, S., KARLEN, A., VAN DONGEN, M., PETKOVIC, H., KELLER, A., PEYRANE, F., DONADIO, S., FRAISSE, L., PIDDOCK, L. J. V., GILBERT, I. H., MOSER, H. E. & MULLER, R. 2021. Towards the sustainable discovery and development of new antibiotics. *Nat Rev Chem,* 5**,** 726-749.

NEWMAN, D. J. & CRAGG, G. M. 2020. Natural Products as Sources of New Drugs over the Nearly Four Decades from 01/1981 to 09/2019. *J Nat Prod,* 83**,** 770-803.

OHKI, R., GIYANTO, TATENO, K., MASUYAMA, W., MORIYA, S., KOBAYASHI, K. & OGASAWARA, N. 2003. The BceRS two-component regulatory system induces expression of the bacitracin transporter, BceAB, in Bacillus subtilis. *Mol Microbiol,* 49**,** 1135-44.

OMAN, T. J. & VAN DER DONK, W. A. 2010. Follow the leader: the use of leader peptides to guide natural product biosynthesis. *Nat Chem Biol,* 6**,** 9-18.

OMMI, O., NAIYAZ AHMAD, M., GAJULA, S. N. R., WANJARI, P., SAU, S., AGNIVESH, P. K., SAHOO, S. K., KALIA, N. P., SONTI, R., NANDURI, S., DASGUPTA, A., CHOPRA, S. & YADDANAPUDI, V. M. 2023. Synthesis and pharmacological evaluation of 1,3-diaryl substituted pyrazole based (thio)urea derivatives as potent antimicrobial agents against multi-drug resistant Staphylococcus aureus and Mycobacterium tuberculosis. *RSC Med Chem,* 14**,** 1296-1308.

ONGPIPATTANAKUL, C., DESORMEAUX, E. K., DICAPRIO, A., VAN DER DONK, W. A., MITCHELL, D. A. & NAIR, S. K. 2022. Mechanism of Action of Ribosomally Synthesized and Post-Translationally Modified Peptides. *Chem Rev*.

PATIL, M., NOONIKARA-POYIL, A., JOSHI, S. D., PATIL, S. A., PATIL, S. A. & BUGARIN, A. 2019. New Urea Derivatives as Potential Antimicrobial Agents: Synthesis, Biological Evaluation, and Molecular Docking Studies. *Antibiotics (Basel),* 8.

POONIA, N., LAL, K., KUMAR, A., KUMAR, A., SAHU, S., BAIDYA, A. T. K. & KUMAR, R. 2022. Urea-thiazole/benzothiazole hybrids with a triazole linker: synthesis, antimicrobial potential, pharmacokinetic profile and in silico mechanistic studies. *Mol Divers,* 26**,** 2375-2391.

PORTA, N., ZASCHKE-KRIESCHE, J., FRIEG, B., GOPALSWAMY, M., ZIVKOVIC, A., ETZKORN, M., STARK, H., SMITS, S. H. J. & GOHLKE, H. 2019. Small-molecule inhibitors of nisin resistance protein NSR from the human pathogen Streptococcus agalactiae. *Bioorg Med Chem,* 27**,** 115079.

RAWLINGS, N. D., BARRETT, A. J., THOMAS, P. D., HUANG, X., BATEMAN, A. & FINN, R. D. 2018. The MEROPS database of proteolytic enzymes, their substrates and inhibitors in 2017 and a comparison with peptidases in the PANTHER database. *Nucleic Acids Res,* 46**,** D624-D632.

REINERS, J., LAGEDROSTE, M., EHLEN, K., LEUSCH, S., ZASCHKE-KRIESCHE, J. & SMITS, S. H. J. 2017. The N-terminal Region of Nisin Is Important for the BceAB-Type ABC Transporter NsrFP from Streptococcus agalactiae COH1. *Front Microbiol,* 8**,** 1643.

ROJAS-PIRELA, M., KEMMERLING, U., QUINONES, W., MICHELS, P. A. M. & ROJAS, V. 2023. Antimicrobial Peptides (AMPs): Potential Therapeutic Strategy against Trypanosomiases? *Biomolecules,* 13.

SAHL, H. G. & BIERBAUM, G. 1998. Lantibiotics: biosynthesis and biological activities of uniquely modified peptides from gram-positive bacteria. *Annu Rev Microbiol,* 52**,** 41-79.

SCHMIDT, E. W., NELSON, J. T., RASKO, D. A., SUDEK, S., EISEN, J. A., HAYGOOD, M. G. & RAVEL, J. 2005. Patellamide A and C biosynthesis by a microcin-like pathway in Prochloron didemni, the cyanobacterial symbiont of Lissoclinum patella. *Proc Natl Acad Sci U S A,* 102**,** 7315-20.

SUN, Z., ZHONG, J., LIANG, X., LIU, J., CHEN, X. & HUAN, L. 2009. Novel mechanism for nisin resistance via proteolytic degradation of nisin by the nisin resistance protein NSR. *Antimicrob Agents Chemother,* 53**,** 1964-73.

THOMAS, C., ALLER, S. G., BEIS, K., CARPENTER, E. P., CHANG, G., CHEN, L., DASSA, E., DEAN, M., DUONG VAN HOA, F., EKIERT, D., FORD, R., GAUDET, R., GONG, X., HOLLAND, I. B., HUANG, Y., KAHNE, D. K., KATO, H., KORONAKIS, V., KOTH, C. M., LEE, Y., LEWINSON, O., LILL, R., MARTINOIA, E., MURAKAMI, S., PINKETT, H. W., POOLMAN, B., ROSENBAUM, D., SARKADI, B., SCHMITT, L., SCHNEIDER, E., SHI, Y., SHYNG, S. L., SLOTBOOM, D. J., TAJKHORSHID, E., TIELEMAN, D. P., UEDA, K., VARADI, A., WEN, P. C., YAN, N., ZHANG, P., ZHENG, H., ZIMMER, J. & TAMPE, R. 2020. Structural and functional diversity calls for a new classification of ABC transporters. *FEBS Lett,* 594**,** 3767-3775.

VENKATACHALAM, T. K., MAO, C. & UCKUN, F. M. 2004. Effect of stereochemistry on the anti-HIV activity of chiral thiourea compounds. *Bioorg Med Chem,* 12**,** 4275-84.

WIEDEMANN, I., BREUKINK, E., VAN KRAAIJ, C., KUIPERS, O. P., BIERBAUM, G., DE KRUIJFF, B. & SAHL, H. G. 2001. Specific binding of nisin to the peptidoglycan precursor lipid II combines pore formation and inhibition of cell wall biosynthesis for potent antibiotic activity. *J Biol Chem,* 276**,** 1772-9.

Supporting information

Natural compounds against antimicrobial resistance

Julia Gottstein[1], Pablo Cea Medina[3], Lars Seifert[3], Holger Stark[3], Holger Gohlke[3] & Sander H. J. Smits[1,2]

[1]*Institute of Biochemistry, Heinrich-Heine-University Düsseldorf, Universitätsstrasse 1, 40225 Düsseldorf*
[2]Center for Structural Studies, Heinrich-Heine-University Duesseldorf, Universitätsstrasse 1, 40225 Duesseldorf, Germany.
[3]*Institute of Pharmaceutical and Medicinal Chemistry, Heinrich-Heine-University Düsseldorf, Universitätsstrasse 1, 40225 Düsseldorf*

Table S8*: *Following 53 compounds were provided by the research group of Prof. Dr. Gohlke and 43 compounds were provided by the research group of Prof.Dr.Stark to be examined on their ability of specific inhibition against the nisin resistance proteins.

Internal ID, structure	Mol-Port ID	MW	IUPAC
#1 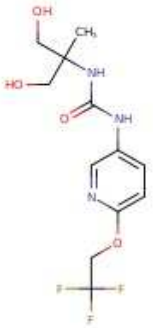	MolPort-027-929-772	323.27	3-(1,3-dihydroxy-2-methylpropan-2-yl)-1-[6-(2,2,2-trifluoroethoxy)pyridin-3-yl]urea C12H16F3N3O4
#2 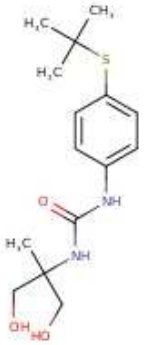	MolPort-027-929-777	312.43	1-[4-(tert-butylsulfanyl)phenyl]-3-(1,3-dihydroxy-2-methylpropan-2-yl)urea C15H24N2O3S
#3 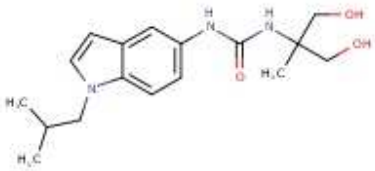	MolPort-028-782-031	319.41	3-(1,3-dihydroxy-2-methylpropan-2-yl)-1-[1-(2-methylpropyl)-1H-indol-5-yl]urea C17H25N3O3

#4 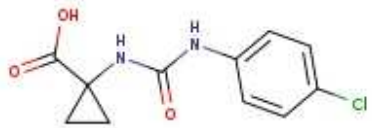	MolPort-035-830-065	254.67	1-{[(4-chlorophenyl)carbamoyl]amino}cyclopropane-1-carboxylic acid C11H11ClN2O3
#5 	MolPort-038-962-886	333.61	1-(2-bromo-5-chloro-4-methylphenyl)-3-[1-(hydroxymethyl)cyclopropyl]urea C12H14BrClN2O2
#6 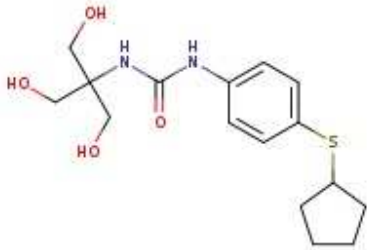	MolPort-039-310-041	340.44	1-[4-(cyclopentylsulfanyl)phenyl]-3-[1,3-dihydroxy-2-(hydroxymethyl)propan-2-yl]urea C16H24N2O4S
#7 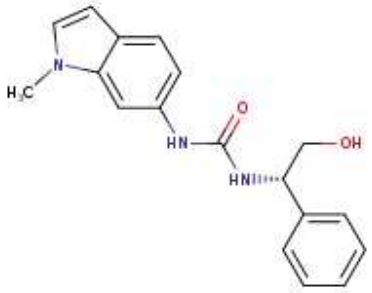	MolPort-042-598-883	309.37	1-[(1S)-2-hydroxy-1-phenylethyl]-3-(1-methyl-1H-indol-6-yl)urea C18H19N3O2

#8 	MolPort-042-604-826	336.19	3-(5-bromopyridin-3-yl)-1-(2-hydroxy-1-phenylethyl)urea C14H14BrN3O2
#9 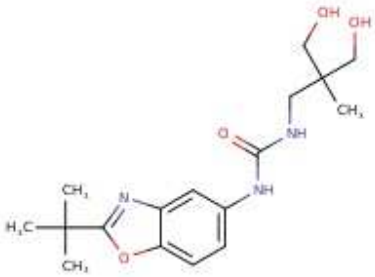	MolPort-044-226-201	335.40	1-(2-tert-butyl-1,3-benzoxazol-5-yl)-3-[3-hydroxy-2-(hydroxymethyl)-2-methylpropyl]urea C17H25N3O4
#10 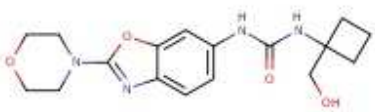	MolPort-044-490-349	349.39	3-[1-(hydroxymethyl)cyclobutyl]-1-[2-(morpholin-4-yl)-1,3-benzoxazol-6-yl]urea C17H22N4O4
#11 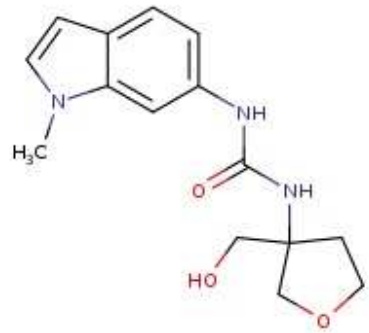	MolPort-044-499-524	289.34	1-[3-(hydroxymethyl)oxolan-3-yl]-3-(1-methyl-1H-indol-6-yl)urea C15H19N3O3

#12 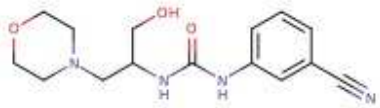	MolPort-044-542-265	304.35	1-(3-cyanophenyl)-3-[1-hydroxy-3-(morpholin-4-yl)propan-2-yl]urea C15H20N4O3
#13 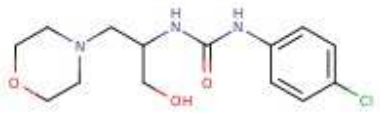	MolPort-044-601-547	313.78	1-(4-chlorophenyl)-3-[1-hydroxy-3-(morpholin-4-yl)propan-2-yl]urea C14H20ClN3O3
#14 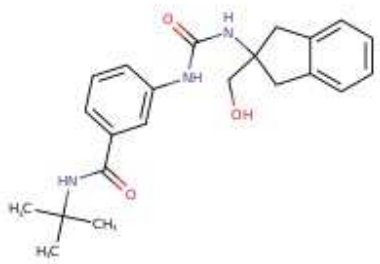	MolPort-046-080-232	381.48	N-tert-butyl-3-({[2-(hydroxymethyl)-2,3-dihydro-1H-inden-2-yl]carbamoyl}amino)benzamide C22H27N3O3
#15 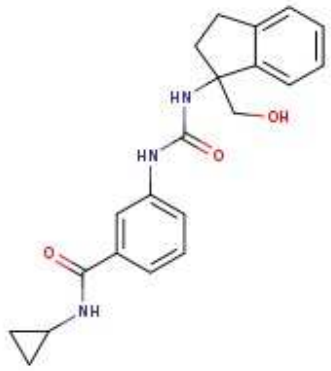	MolPort-046-452-058	365.43	N-cyclopropyl-3-({[1-(hydroxymethyl)-2,3-dihydro-1H-inden-1-yl]carbamoyl}amino)benzamide C21H23N3O3

#16 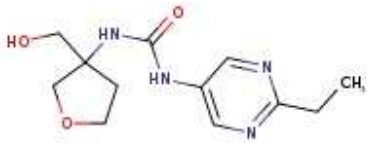	MolPort-046-533-255	266.30	1-(2-ethylpyrimidin-5-yl)-3-[3-(hydroxymethyl)oxolan-3-yl]urea C12H18N4O3
#17 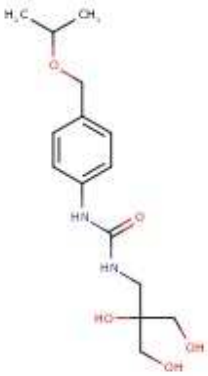	MolPort-046-539-915	312.37	3-[2,3-dihydroxy-2-(hydroxymethyl)propyl]-1-{4-[(propan-2-yloxy)methyl]phenyl}urea C15H24N2O5
#18 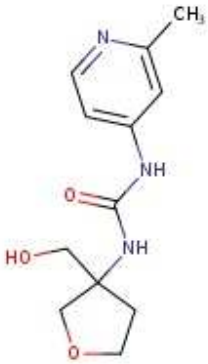	MolPort-046-633-670	251.29	3-[3-(hydroxymethyl)oxolan-3-yl]-1-(2-methylpyridin-4-yl)urea C12H17N3O3
#19 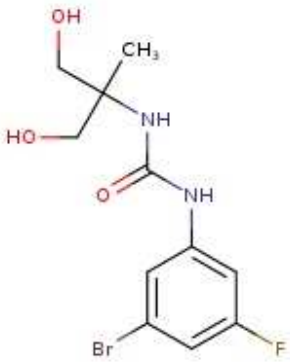	MolPort-028-906-665	321.15	1-(3-bromo-5-fluorophenyl)-3-(1,3-dihydroxy-2-methylpropan-2-yl)urea C11H14BrFN2O3

#20 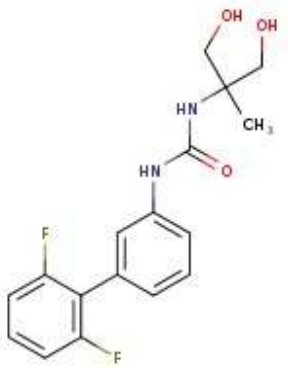	MolPort-028-906-666	336.34	1-{2',6'-difluoro-[1,1'-biphenyl]-3-yl}-3-(1,3-dihydroxy-2-methylpropan-2-yl)urea C17H18F2N2O3
#21 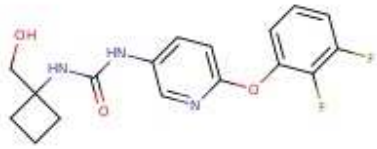	MolPort-039-318-707	349.34	1-[6-(2,3-difluorophenoxy)pyridin-3-yl]-3-[1-(hydroxymethyl)cyclobutyl]urea C17H17F2N3O3
#22 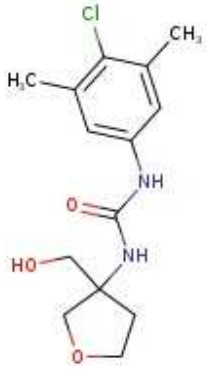	MolPort-039-319-880	298.77	1-(4-chloro-3,5-dimethylphenyl)-3-[3-(hydroxymethyl)oxolan-3-yl]urea C14H19ClN2O3

New number for figure	Internal ID, structure	MolPort ID	MW	IUPAC
#23	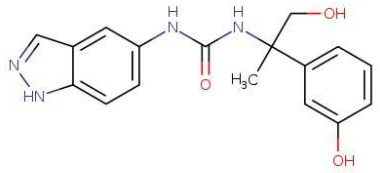 #2	MolPort-046-714-890	326.356	1-[1-hydroxy-2-(3-hydroxyphenyl)propan-2-yl]-3-(1H-indazol-5-yl)urea C17H18N4O3
#24	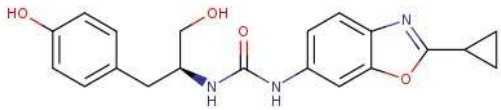 #3	MolPort-028-802-683	367.405	3-(2-cyclopropyl-1,3-benzoxazol-6-yl)-1-[(2S)-1-hydroxy-3-(4-hydroxyphenyl)propan-2-yl]urea C20H21N3O4
#25	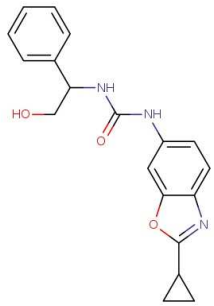 #4	MolPort-027-678-616	337.379	3-(2-cyclopropyl-1,3-benzoxazol-6-yl)-1-(2-hydroxy-1-phenylethyl)urea C19H19N3O3
#26	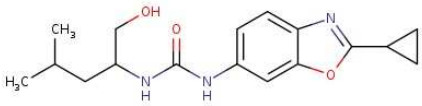 #5	MolPort-023-241-287	317.389	1-(2-cyclopropyl-1,3-benzoxazol-6-yl)-3-(1-hydroxy-4-methylpentan-2-yl)urea C17H23N3O3

#27	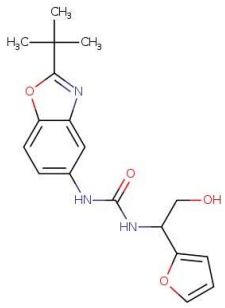 #6	MolPort-023-171-165	343.383	3-(2-tert-butyl-1,3-benzoxazol-5-yl)-1-[1-(furan-2-yl)-2-hydroxyethyl]urea C18H21N3O4
#28	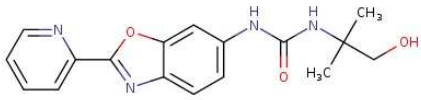 #7	MolPort-028-793-290	326.356	3-(1-hydroxy-2-methylpropan-2-yl)-1-[2-(pyridin-2-yl)-1,3-benzoxazol-6-yl]urea C17H18N4O3
#29	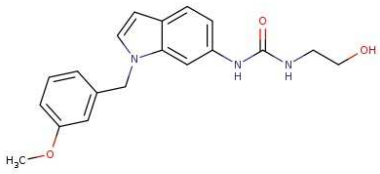 #8	MolPort-028-781-481	339.395	3-(2-hydroxyethyl)-1-{1-[(3-methoxyphenyl)methyl]-1H-indol-6-yl}urea C19H21N3O3
#30	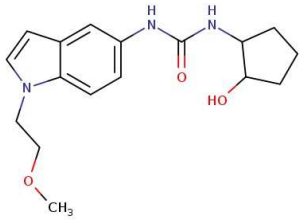 #9	MolPort-023-158-450	317.389	1-(2-hydroxycyclopentyl)-3-[1-(2-methoxyethyl)-1H-indol-5-yl]urea C17H23N3O3
#31	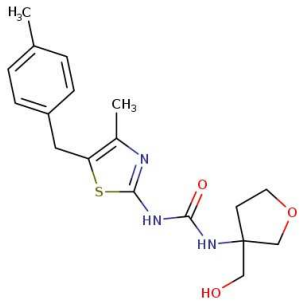 #10	MolPort-044-499-379	361.46	1-[3-(hydroxymethyl)oxolan-3-yl]-3-{4-methyl-5-[(4-methylphenyl)methyl]-1,3-thiazol-2-yl}urea C18H23N3O3S

#32	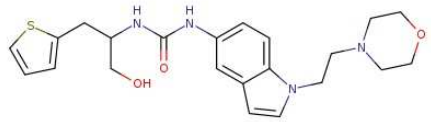 #11	MolPort-047-337-210	428.55	3-[1-hydroxy-3-(thiophen-2-yl)propan-2-yl]-1-{1-[2-(morpholin-4-yl)ethyl]-1H-indol-5-yl}urea C22H28N4O3S
#33	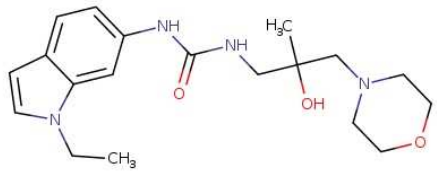 #12	MolPort-023-171-283	360.458	3-(1-ethyl-1H-indol-6-yl)-1-[2-hydroxy-2-methyl-3-(morpholin-4-yl)propyl]urea C19H28N4O3
#34	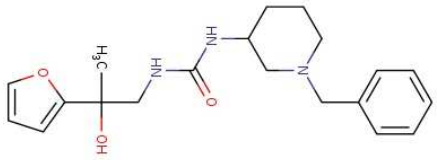 #13	MolPort-046-533-596	357.454	1-(1-benzylpiperidin-3-yl)-3-[2-(furan-2-yl)-2-hydroxypropyl]urea C20H27N3O3
#35	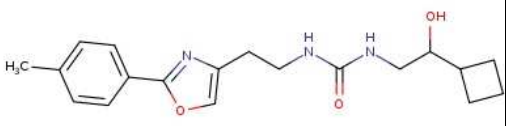 #14	MolPort-046-459-037	343.427	3-(2-cyclobutyl-2-hydroxyethyl)-1-{2-[2-(4-methylphenyl)-1,3-oxazol-4-yl]ethyl}urea C19H25N3O3
#36	 #15	MolPort-044-579-351	317.389	3-(2-ethyl-1,3-benzoxazol-5-yl)-1-[(1-hydroxycyclohexyl)methyl]urea C17H23N3O3
#37	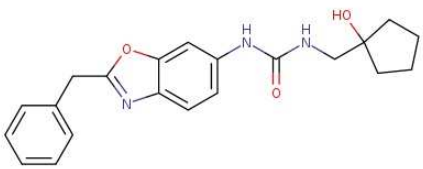 #16	MolPort-044-502-368	365.433	1-(2-benzyl-1,3-benzoxazol-6-yl)-3-[(1-hydroxycyclopentyl)methyl]urea C21H23N3O3

#38	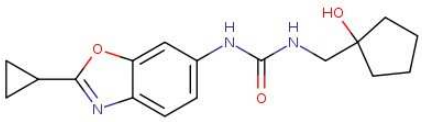 #17	MolPort-044-584-414	315.373	1-(2-cyclopropyl-1,3-benzoxazol-6-yl)-3-[(1-hydroxycyclopentyl)methyl]urea C17H21N3O3
#39	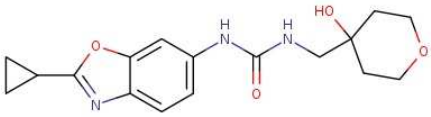 #18	MolPort-044-501-544	331.372	3-(2-cyclopropyl-1,3-benzoxazol-6-yl)-1-[(4-hydroxyoxan-4-yl)methyl]urea C17H21N3O4
#40	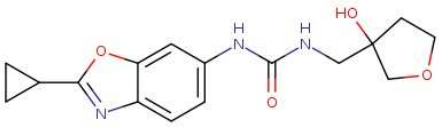 #19	MolPort-044-573-923	317.345	1-(2-cyclopropyl-1,3-benzoxazol-6-yl)-3-[(3-hydroxyoxolan-3-yl)methyl]urea C16H19N3O4
#41	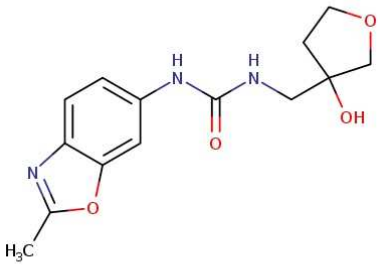 #20	MolPort-044-573-920	291.307	1-[(3-hydroxyoxolan-3-yl)methyl]-3-(2-methyl-1,3-benzoxazol-6-yl)urea C14H17N3O4
#42	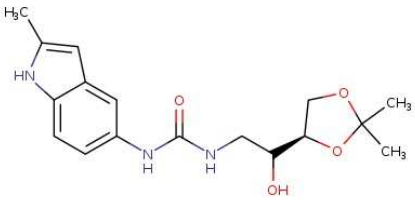 #21	MolPort-047-331-865	333.388	1-{2-[(4R)-2,2-dimethyl-1,3-dioxolan-4-yl]-2-hydroxyethyl}-3-(2-methyl-1H-indol-5-yl)urea C17H23N3O4
#43	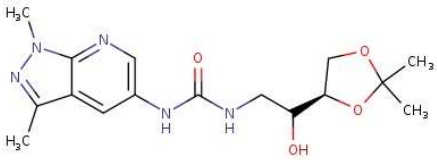 #22	MolPort-047-331-863	349.391	1-{2-[(4R)-2,2-dimethyl-1,3-dioxolan-4-yl]-2-hydroxyethyl}-3-{1,3-dimethyl-1H-

				pyrazolo[3,4-b]pyridin-5-yl}urea C16H23N5O4
#44	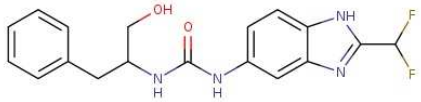 #23	MolPort-027-927-603	360.365	3-[2-(difluoromethyl)-1H-1,3-benzodiazol-5-yl]-1-(1-hydroxy-3-phenylpropan-2-yl)urea C18H18F2N4O2
#45	 #24	MolPort-044-505-114	366.413	1-(2-cyclohexyl-1-hydroxypropan-2-yl)-3-[2-(difluoromethyl)-1H-1,3-benzodiazol-5-yl]urea C18H24F2N4O2
#46	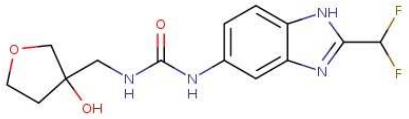 #25	MolPort-044-502-403	326.304	1-[2-(difluoromethyl)-1H-1,3-benzodiazol-5-yl]-3-[(3-hydroxyoxolan-3-yl)methyl]urea C14H16F2N4O3
#47	 #26	MolPort-046-632-537	344.415	3-[1-(3,5-dimethylphenyl)-5-methyl-1H-pyrazol-3-yl]-1-[(3-hydroxyoxolan-3-yl)methyl]urea C18H24N4O3
#48	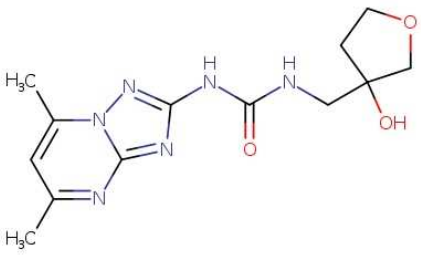 #27	MolPort-046-803-128	306.326	3-{5,7-dimethyl-[1,2,4]triazolo[1,5-a]pyrimidin-2-yl}-1-[(3-hydroxyoxolan-3-yl)methyl]urea C13H18N6O3

#49	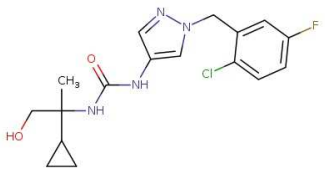 #28	MolPort-046-464-744	366.82	1-{1-[(2-chloro-5-fluorophenyl)methyl]-1H-pyrazol-4-yl}-3-(2-cyclopropyl-1-hydroxypropan-2-yl)urea C17H20ClFN4O2
#50	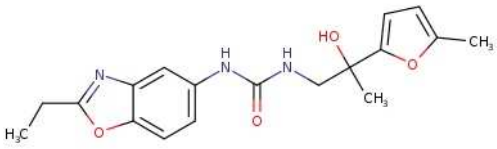 #29	MolPort-028-294-478	343.383	3-(2-ethyl-1,3-benzoxazol-5-yl)-1-[2-hydroxy-2-(5-methylfuran-2-yl)propyl]urea C18H21N3O4
#51	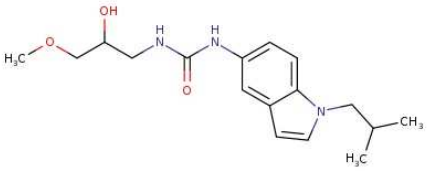 #30	MolPort-028-276-164	319.405	3-(2-hydroxy-3-methoxypropyl)-1-[1-(2-methylpropyl)-1H-indol-5-yl]urea C17H25N3O3
#52	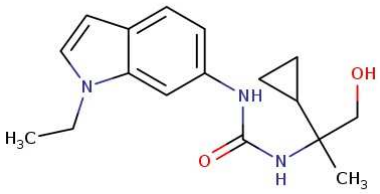 #31	MolPort-028-312-944	301.39	3-(2-cyclopropyl-1-hydroxypropan-2-yl)-1-(1-ethyl-1H-indol-6-yl)urea C17H23N3O2
#53	 #32	MolPort-028-275-566	333.432	3-(1-hydroxy-4-methylpentan-2-yl)-1-[1-(2-methoxyethyl)-1H-indol-5-yl]urea C18H27N3O3

Internal ID	Structure	Molecular Weight
ST-2396	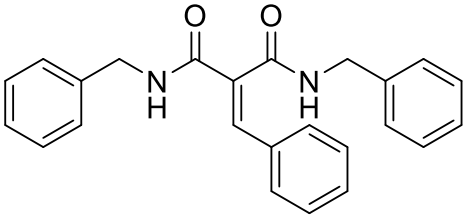	370.2
ST-2397	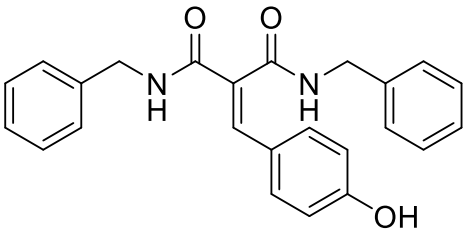	386.2
ST-2398	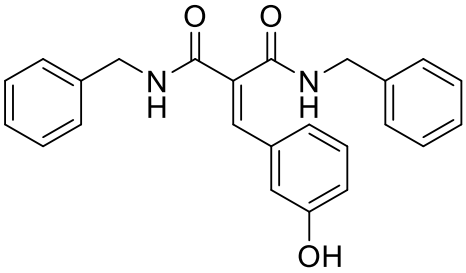	386.2
ST-2399	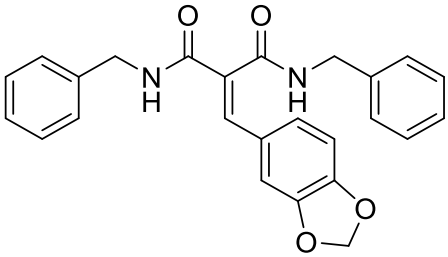	414.2
ST-2400	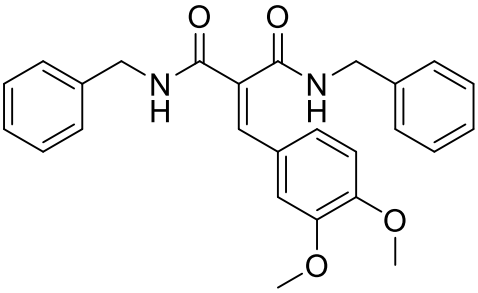	430.2
ST-2401	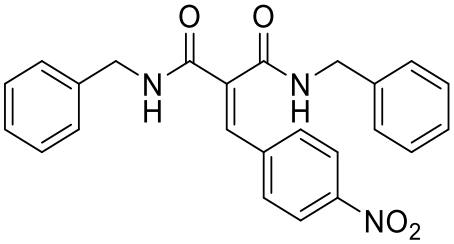	415.5

ST-2302	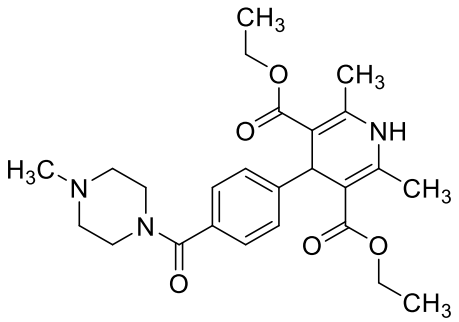	455.6
ST-2147	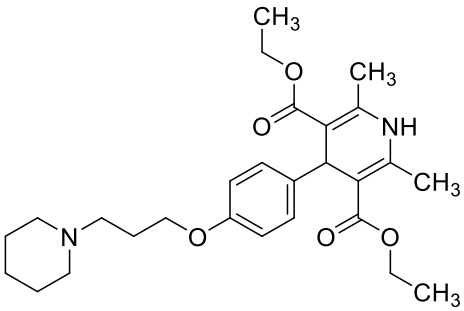	470.6
ST-2301	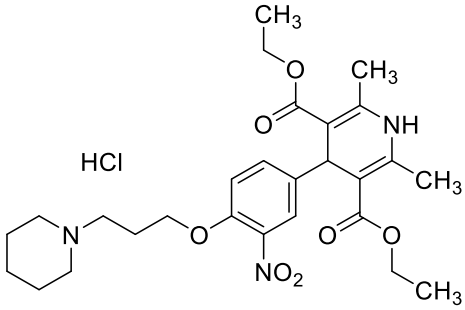	552.1
ST-2186	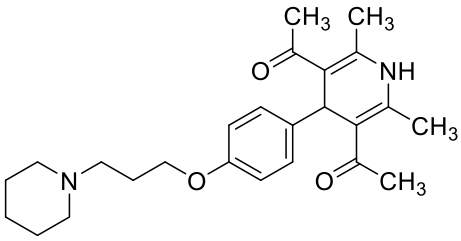	410.6
ST-2146	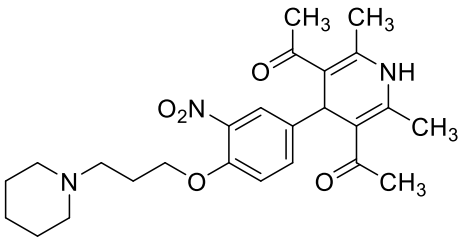	455.6
ST-2267	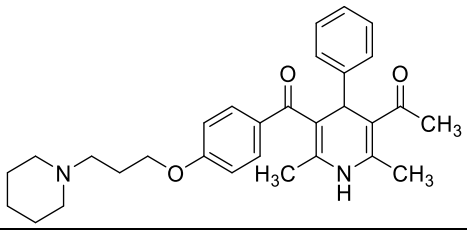	472.6

ST-2390	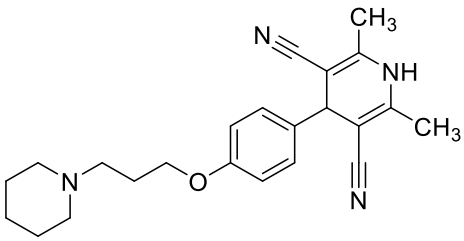	376.5
ST-2403	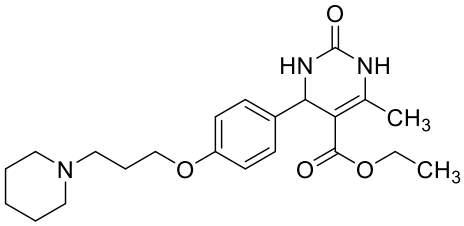	401.5
ST-2402	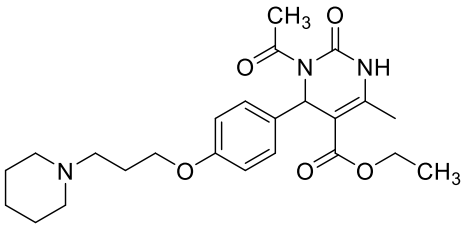	443.5
ST-2404	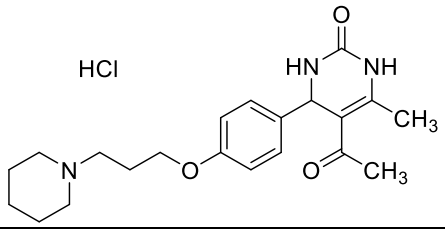	407.9
ST-2360	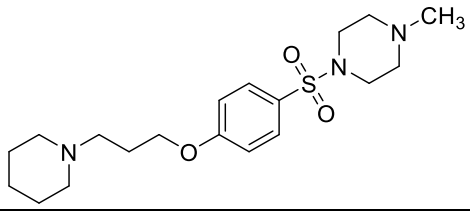	381.5
ST-2450	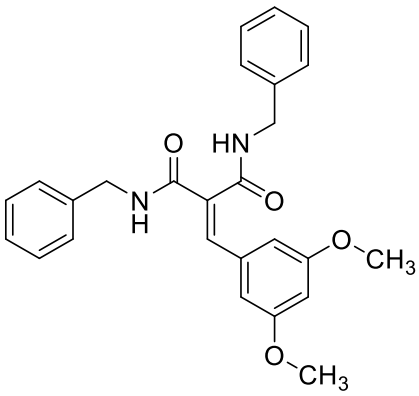	430.2

ST-2451	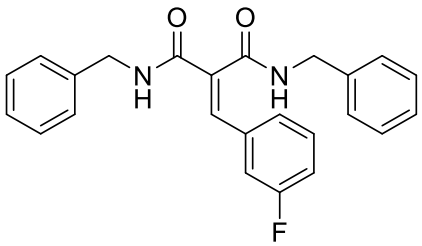	388.2
ST-2452	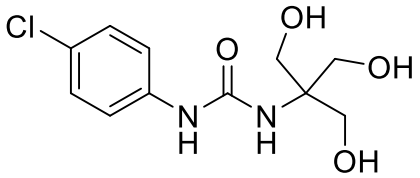	274.1
ST-2453	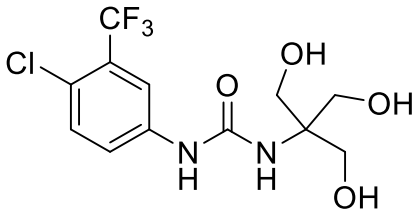	342.1
HG008	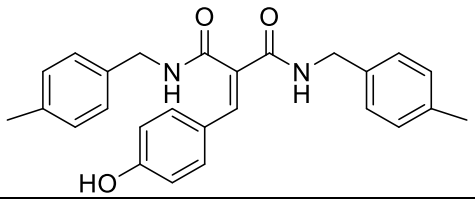	414.2

ST-2478	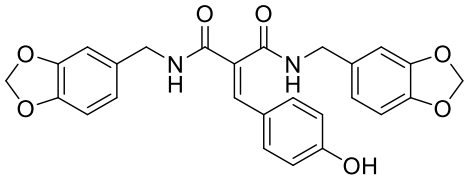	474.2
ST-2479	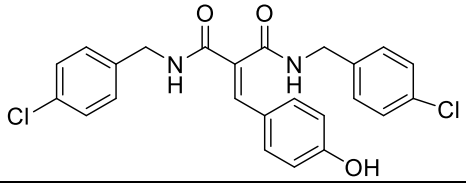	454.1
ST-2480	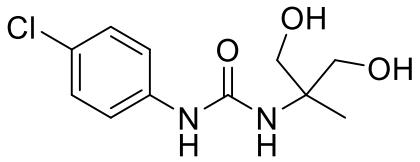	258.1
LSE-064	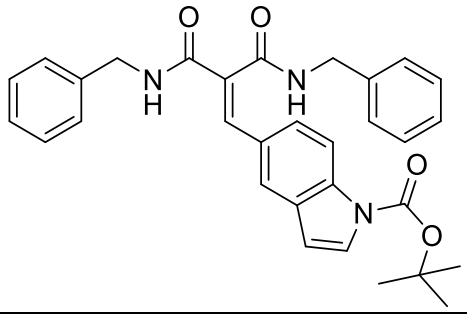	509.2

LSE070	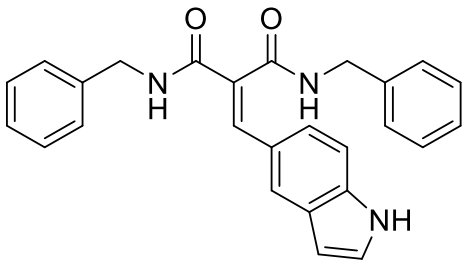	409.2

ST-2542	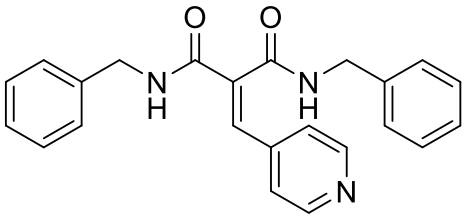	371.4
ST-2547	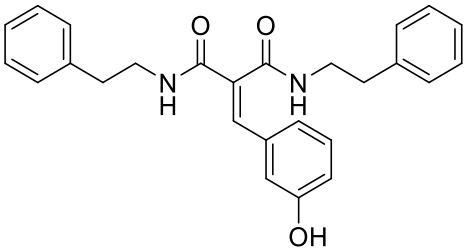	414.29
ST-2543	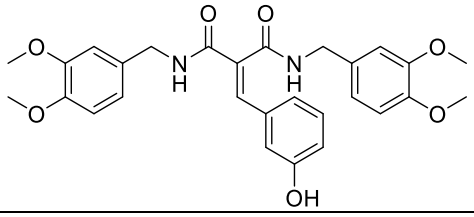	506.6
ST-2546	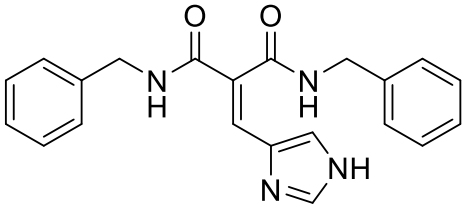	360.4

LSE-106	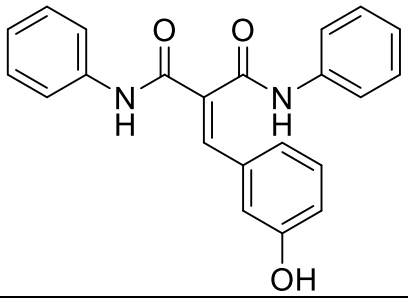	358.40

LSE-110	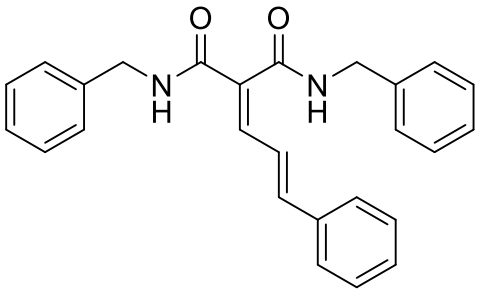	396.49
LSE117	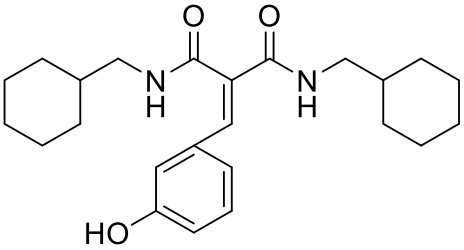	398.55
LSE119	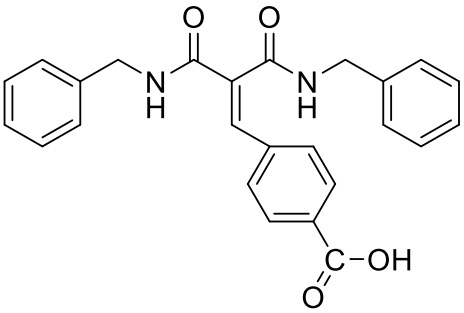	414.46
LSE121	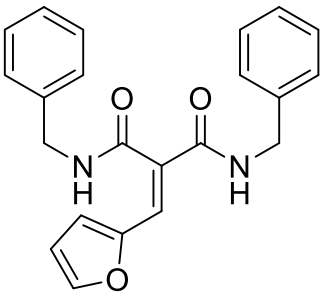	360.41
LSE122	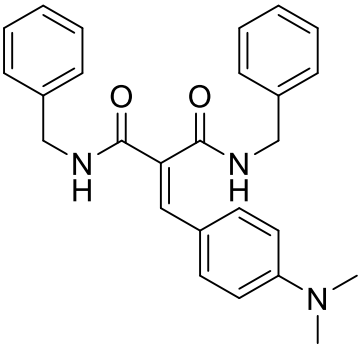	413.52

LSE123	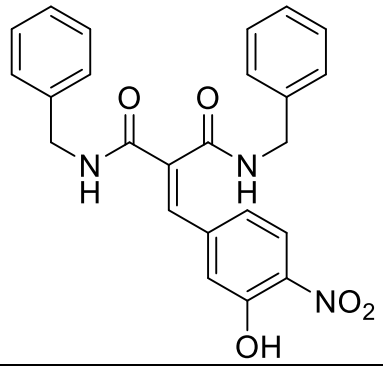	431.45

LSE-124	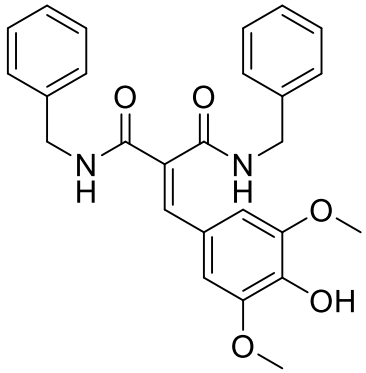	446.50
LSE125	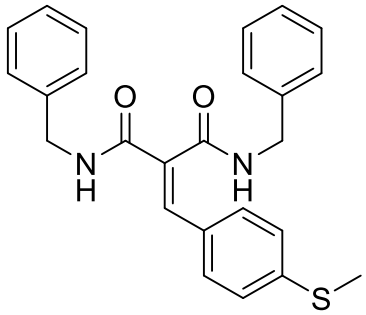	416.54
LSE134	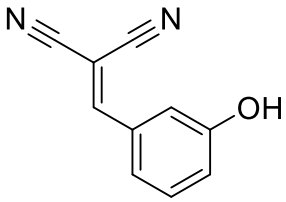	170.17
LSE141	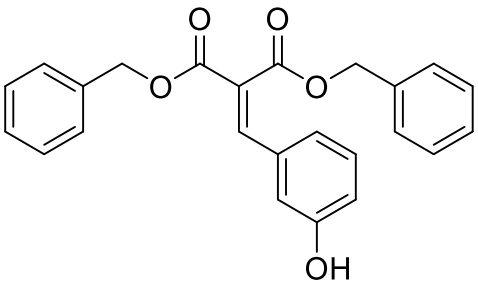	388.42

LSE138	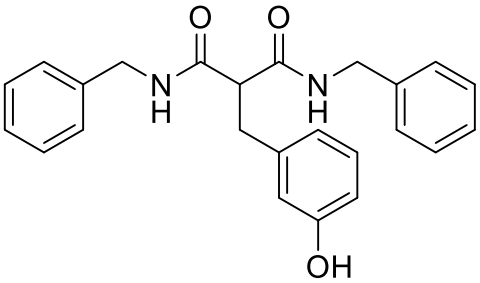	388.46

4 Discussion

Antimicrobial peptides such as nisin represent important alternatives to antibiotics in the face of increasing multi-drug resistance in pathogenic bacteria that threaten the global health system. Thus, to tackle this crisis efforts have to be made to elucidate and characterize resistance systems in human pathogens. One such resistance system is the nisin resistance operon of *Streptococcus agalactiae* COH1 consisting of the nisin resistance protein (NSR), a BceAB-type transporter NsrFP and a two-component system (TCS) (Khosa *et al*., 2013). Expressing this operon confers resistance against multiple antimicrobial peptides, including nisin. In this thesis the BceAB transporter *Sa*NsrFP and its large extracellular domain were characterized *in vivo* and *in vitro*, elucidating the involved mechanism of resistance.

Resistance gene clusters similar to the nisin resistance operon are found in *Firmicutes* and also in clinically relevant pathogenic bacteria (Chapter V) (Gebhard, 2012). They mostly contain a BceAB-type ABC transporter and a coevolved cognate TCS (Dintner *et al*., 2011). The hallmark of BceAB-type transporters is a large extracellular domain (ECD) that is hypothesized to be involved in sensing antimicrobial peptides instead of the cognate histidine kinase. This cognate histidine kinase is part of the intramembrane histidine kinase family, thus lacks an extracellular sensor domain (Mascher, 2014, Clemens *et al*., 2017). Therefore, it is postulated that the BceAB-type transporter takes over the sensor function of the histidine kinase while also conferring resistance against AMPs (Fritz *et al*., 2015). In very recent work the complex of BceAB and BceS was published, showing an interaction phase that is mediated by lipids (Figure 30) (George and Orlando, 2023). It is evident, that the histidine kinase is dependent on the BceAB transporter for sensing extracellular stimuli.

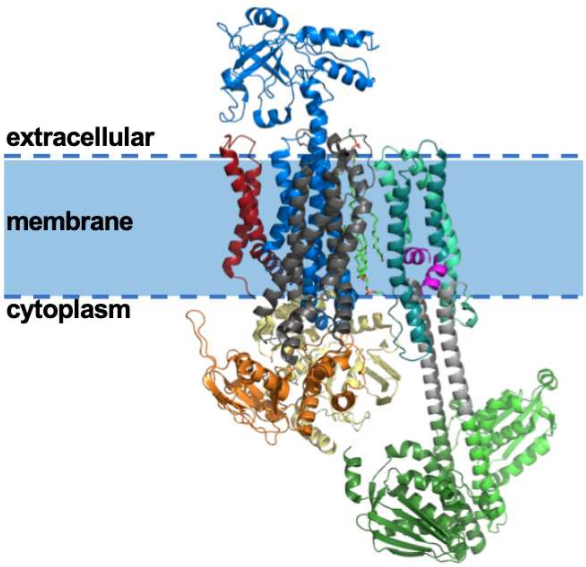

Figure 30: Architecture of the BceAB-BceS ABC transporter (George and Orlando, 2023) (PDB 8G3A). TM Helix bundles 1-4 (grey), TM helix bundles 7-10 (blue), TM helices 5 and 6 (red), and NsrF (light orange/ orange). The intra-histidine kinase BceS can be subdivided into three domains: TM domain (greenteal & teal) containing the characteristic HAMP transfer domain, a linker domain (grey), and a catalytic domain (lightgreen & green), containing the cytoplasmic dimerization and histidine phosphotransfer domain (DHp). A short amphipathic helix at the N-terminus of the TMD (pink) is conserved in intramembrane histidine kinases (Bhate *et al.,* 2018). Image created with PyMOL Version 2.3.0 and Powerpoint 16.72.

In contrast to other resistance-conferring transporters, BceAB-type transporters confer resistance against structurally diverse AMPs (Gebhard and Mascher, 2011, Reiners *et al*., 2017, Gottstein *et al*., 2022), regulate their own production, thus finetuning antimicrobial resistance of a bacterial cell (Bernard *et al*., 2007, Fritz *et al*., 2015). Elucidating the resistance mechanism and the role of the ECD, BceAB and TCS in conferring resistance is crucial to combat antimicrobial resistance also in other pathogenic bacteria.

Lantibiotic-producing bacteria such as *L. lactis* have a different mechanism to protect themselves from suicide by their own lantibiotic. Within the biosynthetic cluster of nisin, also the immunity genes are located. By producing the immunity lipoprotein NisI, an immunity-conferring ABC transporter NisFEG, and its cognate TCS NisRK, *L. lactis* survives nisin production. The immunity response is characterized by the interplay between NisI which binds nisin and NisFEG, extruding nisin from the cytoplasmic membrane into the extracellular medium (Stein *et al.*, 2003, Peschel and Gotz, 1996, Otto *et al.*, 1998, Alkhatib *et al.,* 2012).

In this thesis, the BceAB transporter NsrFP with its extracellular domain was elucidated structurally and functionally. Here I will discuss and compare the role of resistance transporters such as NsrFP, the interplay between TCS and BceAB transporters, and compare it to immunity transporters like NisFEG. Lastly, I discuss the importance of designing and finding small molecule inhibitors to inhibit resistance system such as the nisin resistance system.

4.1 The BceAB-type transporter *Sa*NsrFP

The ABC transporter NsrFP originating from *Streptococcus agalactiae* COH1 is part of the BceAB-type transporter family. BceAB-type ABC transporters are characterized by a TMD consisting of 10 transmembrane helices and by a large extracellular domain between the 7th and the 8th transmembrane helix (Ohki *et al.,* 2003*,* Clemens *et al.,* 2017*)*. Furthermore, BceAB-type transporters are known to confer resistance against a spectrum of different antimicrobial peptides (Ohki *et al*., 2003, Staron *et al*., 2011, Hiron *et al*., 2011, Yang *et al*., 2012, Cho *et al*., 2021). It was also shown for *Sa*NsrFP that it confers resistance against nisin A, nisin H and gallidermin (Reiners *et al*., 2017). In Chapter III I show that *Sa*NsrFP confers resistance against a group of structurally diverse antimicrobial peptides (Gottstein *et al*., 2022). Furthermore, I unravel the resistance mechanism of *Sa*NsrFP. Several putative mechanisms were proposed for BceAB-type transporters, ranging from AMP export, AMP removal from the membrane, flipping UPP to an ATP hydrolysis-dependent target protection mechanism, in which the target-AMP complex is recognized by the BceAB transporter and UPP is physically released from the bound bacitracin (Gebhard and Mascher, 2011, Kingston *et al*., 2014, Kobras *et al*., 2020).

4.2 Spectrum of Antimicrobial Resistance of *Sa*NsrFP

In Chapter III, a different set of cell wall targeting antimicrobial peptides were used to treat *L. lactis* strains expressing the ABC transporter *Sa*NsrFP. Expressing the active ABC transporter conferred resistance against vancomycin (targets the D-Ala D-Ala residues of lipid II), lysobactin (targets the sugar-pyrophosphate-lipid region of lipid II) (Figure 31a) and most importantly against Zn-bacitracin and bacitracin which target the diphosphate group of UPP (Figure 31b).

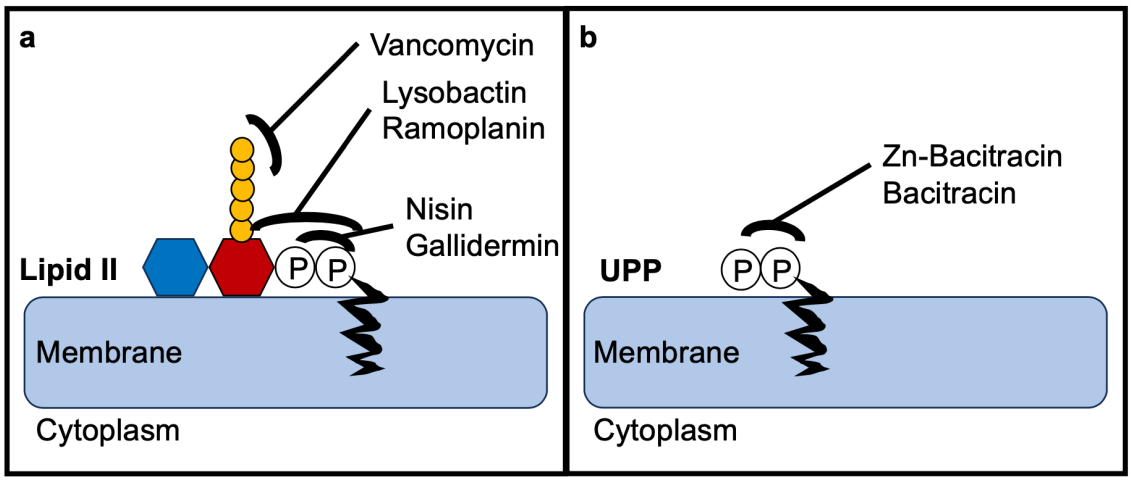

Figure 31 a: Schematic representation of Lipid II. Phosphates are marked with a P, undecaprenyl as a black curved line, GlcNAc in blue, MurNAc in red and amino acids of the pentapeptide in orange. Different domains of Lipid II are targeted by the antimicrobial peptides used in the study by (Gottstein *et al*., 2022). Vancomycin targets the D-Ala D-Ala residues of lipid II, lysobactin and ramoplanin recognize the sugar-pyrophosphate-lipid domain of lipid II and the target region of nisin and gallidermin is the pyrophosphate domain of lipid II. **b:** Zn-bacitracin and bacitracin target the pyrophosphate domain of undecaprenylpyrophosphate.

*Sa*NsrFP showed the highest resistance against Zn-bacitracin and bacitracin with a 350-fold and 132-fold of resistance which is 26 to 70 times higher than the resistance against vancomycin and lysobactin. The difference in resistance is remarkable between these antimicrobial peptides and the question remains, why there is this difference and how can the ABC transporter defend the cell wall against so many different antimicrobial peptides? Also for the BceAB transporter AnrAB from *Listeria monocytogenes* such a similar phenomenon was observed, in which the ABC transporter showed 21-fold to 85-fold higher resistance against bacitracin in comparison to nisin (Collins *et al*., 2010). A difference of the antimicrobial peptides in comparison to bacitracin is that bacitracin targets UPP while vancomycin, lysobactin, and gallidermin are lipid II binders. These results indicate that the mechanism most likely involves bacitracin and UPP as the main target of *Sa*NsrFP as was also described for BceAB from *B. subtilis*. Several other BceAB-type transporters have been shown to confer resistance against lantibiotics and bacitracin (Table 8). Remarkably, bacitracin resistance seems to be conferred by almost all BceAB transporters in this list as can be seen by the MIC values (Table 8) and it can be hypothesized that further BceAB-type transporters are able to confer resistance against bacitracin. In comparison, almost all transporters confer less resistance against nisin. Thus, it can be presumed that these transporters share a common mechanism. Nonetheless,

since most of the studies have not tested the effect of the BceAB without their TCS, more in-depth studies are needed to confirm this.

Table 9: Examples of BceAB transporter, their substrates, and MIC values for Bacitracin and Nisin.

BceAB transporter	Organism	Substrate	Reference	MIC Bacitracin	MIC Nisin
BceAB	*Bacillus subtilis*	Bacitracin, actagardine, mersacidin	(Ohki et al., 2003, Rietkotter et al., 2008, Staron et al., 2011)	351 µM	-
AnrAB	*Listeria monocytogenes*	Nisin, gallidermin, bacitracin, penicillin, (others)	(Collins *et al.*, 2010)	180 µM	0.3 µM
BraDE	*Staphylococcus aureus*	Bacitracin, nisin	(Hiron *et al.*, 2011, Blake *et al.*, 2011, Kolar *et al.*, 2011)	33.7 µM	>38 µM
MbrAB	*Streptococcus mutans*	Bacitracin	(Tsuda *et al.*, 2002, Ouyang *et al.*, 2010)	4U/ml 48 U/mL	30 µM 0.1 µM
PsdAB	*Bacillus subtilis*	Nisin, subtilin, gallidermin, enduracidin	(Staron *et al.*, 2011)	211 µM	0.8 µM
VraDE	*Staphylococcus aureus*	Bacitracin, nisin, gallidermin, daptomycin,	(Yoshida *et al.*, 2011, Popella *et al.*, 2016)	24 µM	12 µM
VraFG	*Staphylococcus aureus*	Nisin, colistin, bacitracin, vancomycin, indolicidin, LL-37, hBD3	(Meehl et al., 2007, Falord et al., 2012, Cho et al., 2021)	24 µM	>24.4 µM
YxdLM	*Bacillus subtilis*	LL-37	(Pietiainen *et al.*, 2005)	-	-
BceAB	*Streptococcus pneumoniae*	Actagardin, bacitracin, nisin, planosporicin	(Diagne *et al.*, 2022)	6 µM	0.08 µM

4.3 The Mechanism of *Sa*NsrFP

To elucidate the mechanism of *Sa*NsrFP, we showed in Chapter III that bacterial cells expressing the transporter are able to resist bacitracin and/or Zn-bacitracin and show unaffected growth (Gottstein *et al.*, 2022). Furthermore, we determined that the highest resistance occurs against bacitracin/Zn-bacitracin, binding UPP which is a cell wall precursor. This suggests that bacitracin is the main substrate for *Sa*NsrFP. The previously reported resistance against nisin appears to be a side effect of the resistance mechanism (Reiners *et al.*, 2017). Since other BceAB transporter also confer resistance against bacitracin and lantibiotics such as nisin, gallidermin, vancomycin, it suggests that a general mechanism is responsible to ward off cationic antimicrobial peptides (Section 4.2, Table 8). Thus, it was concluded that *Sa*NsrFP is neither able to inactivate nor bind various

compounds but that resistance is provided by shielding peptidoglycan precursors, including lipid II, UPP or UP, which are located at the outer surface of the bacterial membrane. In contrast to the lower resistance against lipid II binders, high-level resistance was observed for the UPP binders Zn-bacitracin/ bacitracin suggesting that *Sa*NsrFP shields UPP. Current hypotheses explain the resistance mechanism as a process that protects the cell wall by either target removal (Kingston *et al*., 2014), target protection (Kobras *et al*., 2020) or the combination of an active AMP defense mechanism that mediates a multifactorial defense response against cationic antimicrobial peptides (Gottstein *et al*., 2022). Other cell wall defense mechanisms are modification of the cell wall structure or membrane lipid composition, peptidoglycan thickening, changes in net charge and production of proteases (Draper *et al*., 2015).

Since *Sa*NsrFP was expressed without its cognate TCS system in our study, however is still able to confer resistance against bacitracin and other AMP's, we can show that the transporter is directly involved in sensing the antibiotic and the resistance process.

The expression of *sansrfp*, causes adjustments within the bacterial cells. For example, we observed the downregulation of proteins involved in lipid II biosynthesis (Gottstein *et al*., 2022) by whole cell mass spectrometry. The reduced production of the key enzymes of the lipid II cycle was remarkable and suggested that the biosynthesis of new lipid II molecules occurred with less efficiency in the *L. lactis* NZ9000*Sa*NsrFP strain. This could be the case if lipid II or UPP might be the actual substrate of *Sa*NsrFP, but this hypothesis remains controversial, as it does not correspond to the growth behavior observed in the growth analysis. In Chapter III, the *Sa*NsrFP-expressing strain showed comparable growth as the control strains (Chapter III, Figure 2c).

Furthermore, we showed evidence that cells expressing *Sa*NsrFP obtain a modified cell wall: instead of an aspartate/asparagine bridge in the pentapeptide found for the sensitive mutant, a species with two alanines was detected. In *Sa*NsrF$_{H202A}$P, a mixture was found, although the two alanine species were present in only minor amounts (Chapter III Figure 7). This indicates that the transporter might already sense and mediate a second line of defense ATP-independently. ABC transporters that confer resistance against cationic

antimicrobials are hypothesized to be involved or mediate modification processes of peptidoglycan in Gram-positive bacteria (Rismondo and Schulz, 2021). D-alanylation of teichoic acids is assumed to diminish electrostatic attraction based on the observation that a lack of alanylation leads to increased binding to several positively charged molecules, e.g., gallidermin and vancomycin (Revilla-Guarinos *et al.*, 2014). Additionally, the upregulation of the *gal* operon, especially of UDP-glucose-4-epimerase (GalE), influences the lipoteichoic acid (LTA) structure. GalE is responsible for the synthesis of α-galactose, which is transported across the membrane to become a part of LTA (Kramer *et al.*, 2006).

The experimentally derived data supports this with the observation of upregulation of the MurQ which is responsible for the intracellular conversion of MurNAc-6P to *N*-acetylglucosamine-6-phosphate and D-lactate for the *Sa*NsrFP and *Sa*NsrF$_{H202A}$P mutants in comparison to the sensitive strain. For transporter-expressing cells, we furthermore observed an upregulation of as UDP-glucose-4-epimerase and RodA which are proteins associated with antimicrobial resistance (Kramer *et al.*, 2006).

In the case that *Sa*NsrFP is able to mediate cell wall modifications upon receiving information on the cell wall targeting AMP, altered expression of genes could be the consequence. This would result in a reduction of the number of proteins in the cytosol that are involved in lipid II biosynthesis, as seen by the whole proteome data where the expression of the genes is downregulated but not completely abolished. However, it needs to be verified whether *Sa*NsrFP is directly responsible for this or whether the *L. lactis* strain is reacting since its lipid II cycle is severely changed and, as a consequence, alters its cell wall composition.

Based on all results from the study presented in Chapter III, a joint activity of the transporter as a first-line defender and initiator for a second-line defense is very likely and builds up resistance against compounds targeting the lipid II cycle and thus cell wall synthesis (Figure 32). By shielding the target UPP and lipid II from the extracellular space, e.g., by PGN modification that alters electrostatic attraction, less antibiotic, e.g., bacitracin, can be bound, and increased antibiotic concentrations can be detected in the supernatant. These results are in agreement with the previous conclusions for an export mechanism and further assumptions on the removal of AMPs from the membrane (Reiners *et al.*, 2017,

Kobras *et al*., 2020). The tendency for upregulation of proteins associated with antimicrobial resistance and cell wall modification in *Sa*NsrFP-producing cell proteins indicates the activation of a second-line defense system.

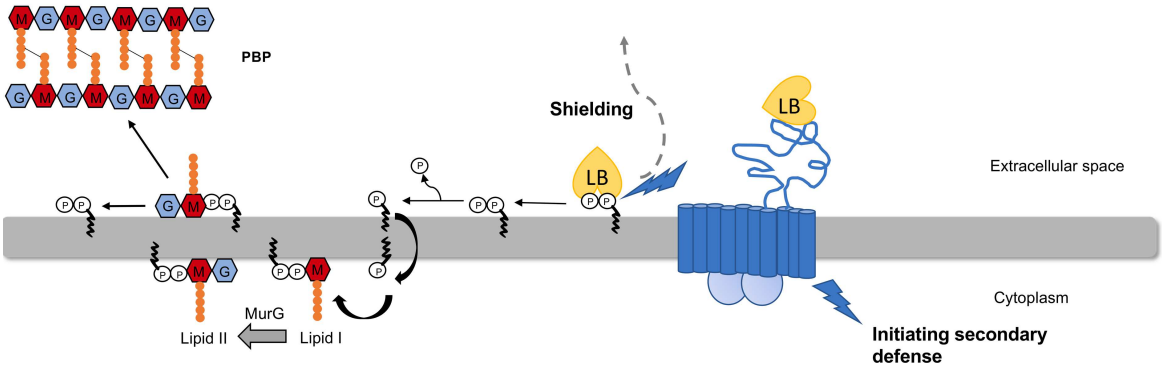

Figure 32: Schematic view of the proposed mechanism of *Sa*NsrFP (Gottstein *et al*., 2022). Phosphates are indicated with a P, undecaprenyl as a black wavy line, GlcNAc in blue, MurNAc in red and amino acids of the pentapeptide in orange. The transporter *Sa*NsrFP is shown in blue, showing its functions of sensing the antibacterial attack, shielding the target most likely by releasing the target from bound bacitracin and initiating a secondary defense resulting in possible cell wall thickening, modification of the electrostatic charge of the cell wall by integrating lipoteichoic acids and increasing d-alanylation in the cell wall. Subsequentially, the released target can enter a new cell wall synthesis cycle and be incorporated into the peptidoglycan. The figure was created using Microsoft Powerpoint Version 16.54.

4.4 The role of the TCS and the ECD for AMP resistance

Current opinion of researchers investigating BceAB transporters such as NsrFP is that detoxification against peptide antibiotics is functionally linked to a two-component system (Dintner *et al*., 2011). It is presumed that upon sensing the antibiotic, the histidine kinase phosphorylates its cognate response regulator which induces the expression of the ABC transporter genes. Such a process was described i.e., for the GraRS-VraFG system (Cho *et al*., 2021) in *S. aureus* and also for several TCS-ABC transporters in *B. subtilis* (BceRS-AB, YxdJK-LM and YvcPQ-RS) (Dintner *et al*., 2014, Staron *et al*., 2011). Moreover, a direct interaction of the BceRS and BceAB was shown in in vitro and in vivo studies (Dintner *et al*., 2011). In their study, it is claimed that BceAB and the TCS need to form a complex in order to be able to sense the AMP. Controversially, the cognate histidine kinase of BceAB transporter consists only of a short loop which is buried almost entirely in the cytoplasmic membrane and thus cannot detect extracellular stimuli (Mascher, 2006).

In Chapter III, in order to elucidate the mechanism of the BceAB-type transporter, *Sa*NsrFP without its cognate TCS was expressed. Previously, it was shown that

the ABC transporter without its TCS can confer resistance against nisin (Reiners *et al*., 2017). This is possible due to the large extracellular domain which is the hallmark of BceAB-type transporter hypothesized to sense antimicrobial peptides (Clemens *et al*., 2017). The essential role of a Bce-type transporter for lantibiotic signalling has been shown in various studies already (Rietkotter et al., 2008). For the BceAB transporter of *B. subtilis* it was reported that signalling is triggered by the activity of the transporter itself and the transporter can autoregulate its own production (Fritz *et al*., 2015, Kobras *et al*., 2020). Thus, the ABC transporter *Sa*NsrFP should also be able to sense the AMP via its large extracellular domain. In Chapter V, direct proof is shown via two independent methods using MALS and measuring tyrosine fluorescence that the ECD of *Sa*NsrFP binds bacitracin and Zn-bacitracin. Surprisingly, determined K_D values for bacitracin and Zn-bacitracin are in the micromolar range. Since for the ECD construct of the study in Chapter V the stalk helices were deleted, bacitracin might not have tightly bound. In a different study it was postulated that the closely related BceAB transporter detects and binds bacitracin-UPP complexes (Kobras *et al*., 2020). In a very recent study, the structure of BceAB was solved, revealing a lipid pocket with a bound lipid right under the extracellular domain (George *et al*., 2022). This lipid reaches near the stalk helices making it plausible that bacitracin would be ankered via UPP to the transmembrane domain of BceAB. More studies have to be conducted in order to confirm the dissociation constant for different constructs in order to exclude a bias of instability. Thus, we can show that *Sa*NsrFP acts as a sensor for antimicrobial peptides and that antimicrobial resistance is not dependent on the cognate TCS. On the contrary, it has been shown for the intramembrane kinase NsaS from *S. aureus* that it controls several genes associated with cell wall synthesis, lipid-modifying enzymes, proteases and several membrane transporters (Mensa *et al*., 2014, Bhate *et al*., 2018). One key structural feature of a IMHK as was reported for NsaS is a short N-terminal amphiphilic helix that anchors its four TM helices into the inner leaflet of the lipid bilayer, thus sensing membrane stress such as antibiotic attacks that deform the bilayer or to interact with accessory proteins such as membrane transporters (Bhate *et al*., 2018). In contrast to that in our study from Chapter III modified cell wall was found in *Sa*NsrFP expressing strains without its cognate TCS, furthermore the ATP hydrolysis deficient mutant showed mainly unmodified cell

wall. In *S. pneumoniae* TCS01 contributes to pneumococcal virulence and it was shown that it co-operates with a BceAB-type ABC transporter not located in the same gene cluster (Diagne *et al*., 2022). It could be hypothesized that *Sa*NsrFP in this study without a TCS could interact also with other TCS that might substitute for the missing one. More in-depth study is necessary to explain how the ABC transporter without its cognate two component system is able to initiate the secondary defense mechanisms.

In a recent study, the cryo-EM structure of the BceAB transporter of *B. subtilis* together with its TCS was published (Figure 30). The authors show that BceS and BceAB interact mediated by lipids near the N-terminal region (TM1-4) of BceB (George and Orlando, 2023). In an earlier study, the authors showed that ATP binding induced full closure of the BceA NBDs of BceAB and a subsequent closure of the BceB TM helices resulting in a tilted extracellular domain (George *et al*., 2022). When BceS and ATP bind within the complete BceAB-S complex, the partial closing of BceA is induced disabling ATP hydrolysis (George and Orlando, 2023). Thus, this was taken as indication that both proteins regulate each other.

It is evident that to date there is not much knowledge on the function of the two component system of BceAB type transporter and how it is involved in the multifactorial process of antimicrobial resistance.

For *Sa*NsrFP, we provided insight that the sole ABC transporter confers resistance by actively freeing bound cell wall precursor from the grip of bacitracin while also initiating a secondary defense mechanism resulting in cell wall modification (Chapter III). Furthermore, we show that *Sa*NsrFP conferred antimicrobial resistance is independent of its cognate histidine kinase NsrK. Also, we are the first to successfully purify the ECD of NsrP and demonstrate that it binds to bacitracin and Zn-bacitracin (Chapter V). In addition, we show that BceAB transporter occur in opportunistic pathogenic and pathogenic bacteria. Finally, we could identify a new ABC transporter that is possibly related to BceAB type transporters that are characterized by 10 TMH and an ECD between helix 7 and 8 but additionally contains an extracellular domain between helix 1 and 2 (Chapter V).

In future experiments the interaction of *Sa*NsrK and *Sa*NsrFP should be elucidated to unravel the role the histidine kinase plays in the process of antimicrobial resistance. The first preliminary steps to elucidate the complete ABC transporter *Sa*NsrFP have already been conducted (Figure 33). Two NsrP constructs were generated in C41dd *E.coli* strains: pET16b Nter10x NsrP and pET26b NsrP C-terminal 6x Histag. Both were successfully expressed (Figure 33a) and membranes were isolated (Figure 33b). Bands are shown at 55 kDa which was expected since NsrP runs lower than its actual molecular weight.

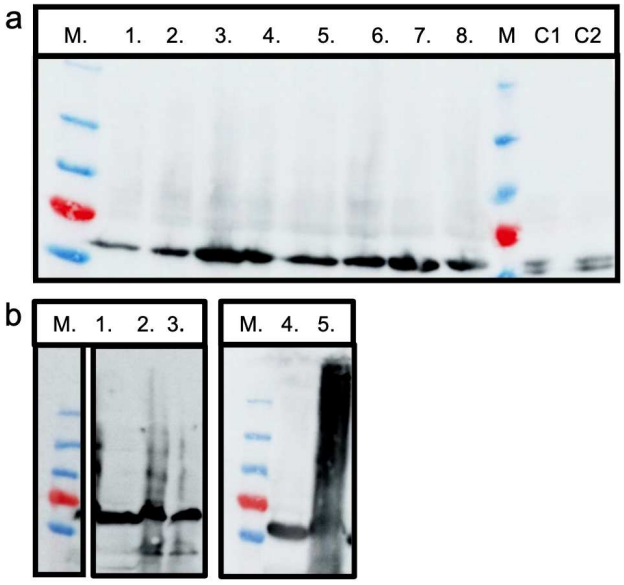

Figure 33 a) Expression of NsrP in *E.coli* C41dd (pET16b Nter10x NsrP and pET26b NsrP C-terminal 6x Histag). NHis-NsrP: lanes 1,2: before induction; lanes 3,4: 4 hours after induction; CHis-NsrP: lanes 5,6: before induction; lanes 7,8: 4 hours after induction. C1 and C2 present positive controls. An antibody against the extracellular domain of NsrP was used. **b)** Isolated membranes of NsrP from *E.coli* C41dd Nter10xHisNsrP construct: Lane 1: supernatant after centrifugation; Lane 2&3 membranes of Nter10xHisNsrP. Isolated membranes of NsrP from *E.coli* C41dd Cter6xHisNsrP construct: Lane 4: supernatant after centrifugation; Lane 5: membrane fraction Cter6xHisNsrP.

4.5 Comparison of *Sa*NsrFP and NisFEG.

Bacteria depend on their ability to sense and adapt rapidly to environmental changes and defend against competitors. To survive, bacterial cells need to constantly assess various parameters such as nutrient supply ion concentration, oxygen levels, pH, temperature, cell density and the presence of toxic compounds e.g. antimicrobial peptides. Different types of bacterial strains have developed protein systems that enable them to survive. Bacteria producing lantibiotics e.g., the nisin producer *Lactococcus lactis* contain an immunity

system to prevent suicide. This immunity system is encoded on the same operon as the genes for nisin biosynthesis and consists of a lipoprotein NisI and an ABC transporter NisFEG. Bacteria that are non-antimicrobial peptide producers have developed a different resistance system. One example is *Streptococcus agalactiae* expressing the nisin resistance operon consisting of the nisin resistance protein (NSR), a serine protease that cleaves nisin and an BceAB transporter *Sa*NsrFP.

Both ABC transporter differ structurally and functionally from each other (Figure 34).

NisFEG is conserved in all species producing nisin and shows similarity with other LanFEG transporters from producer strains of other lantibiotics such as subtilin. The immunity transporter consists of NisF, the NBD of 25 kDa. The TMD consists of the proteins NisE (28 kDa) and NisG (24 kDa), each containing six predicted TM helices. On the contrary, BceAB transporters are found in opportunistic pathogenic as well as pathogenic bacterial strains (Chapter V). Structurally BceAB type transporter resemble each other however most display a rather low sequence identity (20-40%) (Chapter V) (Gebhard, 2012). *Sa*NsrFP consists of an NBD *Sa*NsrF (28 kDa) which contains the typical ABC transporter signature motifs (Khosa *et al.,* 2013). The TMD domain comprises 10 TM helices (74 kDa). Similar to BceAB, the TM helices 1 to 4 and 7 to 10 form individual bundles, each representing an FtsX-domain fold like that observed in type VII mechanotransmission ABC transporters (Thomas *et al*., 2020, George *et al*., 2022). TM helices 5 and 6 interact with one another and are positioned closer to helices 7-10 than to the other bundle, therefore creating an asymmetric arrangement. Between helix 7 and 8, there is a large ECD of 221 amino acids that acts as a sensor for antimicrobial peptides.

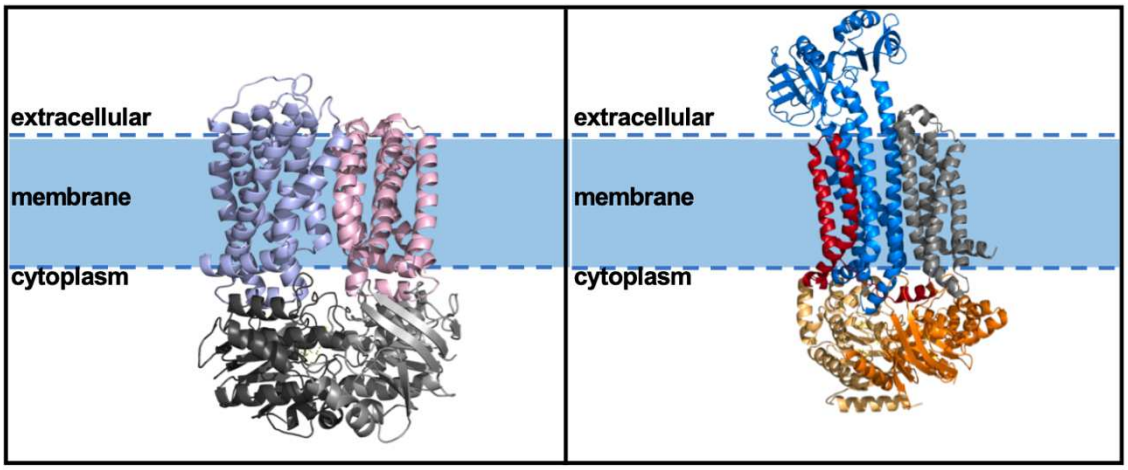

Figure 34: Model of NisFEG calculated using TopModel (Mulnaes *et al.*, 2020) and alphafold model of *Sa*NsrFP. Left: Subdomains are highlighted: NisE in light blue, NisG light pink, and the NBDs in black and grey. Right: TM Helix bundles 1-4 (grey), TM helix bundles 7-10 (blue), TM helices 5 and 6 (red), and NsrF (light orange/ orange). *Sa*NsrFP model was created using AlphaFold2 (Jumper *et al.,* 2021). Image created with PyMOL Version 2.3.0 and Powerpoint 16.72.

Thus*, Sa*NsrFP senses bacitracin via its ECD and initiates a first line defense that ATP-dependently releases UPP from bacitracin. Subsequently, the ABC transporter is able to trigger cell wall modification which results in cell wall thickening, change of electrostatic attraction and other (Chapter III) (Gottstein *et al.,* 2022). This enables the bacterial cell to additionally ward off cationic antimicrobial peptides like nisin, gallidermin, vancomycin and lysobactin (Gottstein *et al*., 2022). Due to the cell wall modifications and processes such as cell wall thickening possibly initiated by *Sa*NsrFP, cell wall precursors in the cell wall become less accessible to antimicrobial peptides such as the aforementioned (Gottstein *et al*., 2022). Thus, *Sa*NsrFP shields indirectly lipid II by initiating these processes and nisin and other antimicrobial peptides do not need to interact with the ABC transporter in order to be expelled from the cell wall. This is how the slight increase of resistance against multiple structurally diverse antimicrobial peptides could be explained.

In contrast to this, NisFEG mainly confers immunity against nisin by extruding it from the inner cell membrane leaflet to the extracellular space. So far it has not been investigated if production of NisFEG can influence the cell wall composition. Furthermore, NisFEG production is regulated via NisK/NisR (Ra *et al*., 1996, van der Meer *et al.*, 1993). It has been shown that NisFEG recognizes the last ring and the last 6 amino acids of nisin. When expressed in *L. lactis NZ9000* NisFEG confers 8-fold immunity against nisin (AlKhatib *et al.*, 2014b). However, when NisI

and NisFEG are expressed together they reach full immunity (AlKhatib *et al*., 2014b). By expressing *Sa*NsrFP in *L. lactis NZ9000* 15-fold resistance against nisin was conferred, however most importantly 132 to 350 fold resistance against Zn-bacitracin and bacitracin (Gottstein *et al*., 2022). To date, it is not clear if *Sa*NsrFP and *Sa*NSR show cooperativity in conferring resistance. This has to be yet determined in future experiments.

4.6 Small molecule inhibitors against AMP resistance.

One of the major challenges of our time is the treatment of life-threatening bacterial infections due to the rapid evolving resistance mechanisms of pathogens against antibiotics. To counteract this problem, it is crucial to understand the drug's mode of action and the pathogen's resistance mechanism. The biosynthesis of the peptidoglycan (PGN), which is a critical feature of bacteria is one of the most effective antibiotic targets. Antimicrobial peptides (AMPs), targeting PGN synthesis such as nisin and colistin, are considered as promising weapons against multidrug-resistant bacteria. However, human pathogenic bacteria conferring resistance to these compounds evolved. They survive by expressing resistance proteins such as e.g. a serine protease NSR cleaving nisin and an ATP-binding cassette transporter of the Bacitracin efflux (BceAB) type that is localized in the membrane. In *Streptococcus agalactiae*, the BceAB transporter *Sa*NsrFP is known to confer resistance to a wide variety of structurally diverse antimicrobial peptides (Gottstein *et al*., 2022). In previous studies, it has been demonstrated that it is possible to bypass this resistance system e.g. by modifying the target (Zaschke-Kriesche *et al*., 2019a) and also by screening for small molecule inhibitors that sensitize the strains to nisin (Porta et al., 2019). In Chapter VII latter method was used to identify a compound that is able to inhibit *L. lactis* strains that express one of the nisin resistance proteins while not inhibiting the empty vector control strains. For this, 95 compounds were tested and screened for specific inhibition against *Sa*NSR and *Sa*NsrFP. Two compounds were identified that could inhibit both nisin resistance proteins specifically without inhibiting the sensitive control strain. The first one C3 was a indolurea derivative and C31 a thiazolurea derivative. C31 showed 2.5 times higher inhibition of both resistance proteins than compound C3. Structural differences are the oxolan or thiazol moiety of C31 and the indole moiety of C3

but more experiments and data are needed for more insight. Both compounds exhibited an IC_{50} value in the micromolar range, insufficient to be used in clinical applications. Therefore, optimization of both molecules is necessary to reduce the amount needed to inhibit 50 % of bacterial cells. The question that still remains to be answered is how these two compounds inhibit two structurally very different resistance proteins, *Sa*NSR (a serine protease) and *Sa*NsrFP (a membrane-bound ABC transporter). While structurally different, both proteins have a common basis, they potentially interact with nisin. Thus, hypothetically, the compounds could bind to such a nisin binding site but this remains to be elucidated in detail.

In previous work, a potent inhibitor was identified (Zaschke-Kriesche *et al.,* 2019), with a very different molecular structure compared to the compounds of this study here. Cerebroside C was shown to have a lipid-like structure consisting of a fatty acid and sphingosine which form together a ceramide and finally a monosaccharide. This compound was able to inhibit *Sa*NsrFP with a specific inhibition of 83 % (Zaschke-Kriesche *et al.,* 2019). Remarkably, a close relative of this inhibitor, Cerebroside D, did not show inhibition towards *Sa*NsrFP, indicating highly specific binding of Cerebroside C (Zaschke-Kriesche *et al.,* 2019). In a recent study the structure of the related ABC transporter BceAB was published, which showed a lipid-binding pocket between its transmembrane helices 5 and 6 and 7 and 9 (George *et al*., 2022) The homolog of BceAB, *Sa*NsrFP is hypothesized to have a similar lipid-binding pocket between its TM helices 5,6 and 7,9. This might be the potential binding site for the previously identified inhibitor Cerebroside C.

In another previous study, a halogenated phenyl-urea derivative, NPG9, was identified as a potent inhibitor against the nisin resistance protein (NSR) (Porta *et al.*, 2019). In contrast, all NPG9-derived compounds in this study described in Chapter VII failed to improve inhibitory activity or reach the nanomolar concentration range. This could be due to the specific chemical properties of the inhibitor NPG9 which was modeled to fit the active site of NSR (Porta *et al*., 2019). In the same study, it was observed that the inhibition activity required a linear molecular shape in combination with one or two hydrophobic regions separated by an amide-like moiety similar to nisin (Porta *et al*., 2019, Graham *et al*., 2014). Nisin´s hydrophobic regions are reflected by methyl-lanthionine and isoleucine

residues. Additionally, a hydroxyl group as shown in NPG9, or an aromatic polar group (Porta *et al*., 2019), mimicking Ser29 and His28 of the NSR active site could result in stronger inhibitory activity in the compounds. Figure 35 displays potent inhibitors of previous work and this current work.

Several publications have shown that urea derivatives play an important role as pharmacologically active drugs (Listro *et al*., 2022, Patil *et al.*, 2019, Ommi *et al*., 2023, Poonia *et al*., 2022, Ghosh and Brindisi, 2020). The bioactivity of drugs depends on molecular recognition through interactions between the drug and the target protein. Hydrogen bonding, among other forces, can stabilize drug-receptor interactions (Kuhn *et al*., 2010) thus, compounds with this capability can show biological activity. Urea derivatives act as hydrogen bond donors or acceptors which allows them to be involved in diverse interactions (Ghosh and Brindisi, 2020). They can have a diverse spectrum of activities including antiviral, anticonvulsant, and antibacterial (Venkatachalam *et al*., 2004, Ghosh and Brindisi, 2020, Ommi *et al.*, 2023, Patil *et al*., 2019). Furthermore, they can inhibit enzymes (Porta *et al*., 2019), be used as a sedative, or act as an anticancer drug (Listro *et al*., 2022, Ghosh and Brindisi, 2020).

As shown in Chapter VII, small molecule inhibitors represent a powerful method to bypass resistance systems in bacteria such as the nisin resistance system in *S. agalactiae*. One of the major advantages of this method of combating antibiotic resistance mechanisms is that pathogenic bacteria become susceptible to potent and well-known antimicrobial peptides such as nisin. This is a great advantage, considering that if the inhibitor specifically inhibits the pathogenic protein, then benign bacteria will not be harmed which is important in a clinical setting for the patient. Furthermore, by using small molecule inhibitors it will not be necessary to urgently find new antibiotics due to the fact that inhibited bacterial cells become sensitized to well-known “old” lantibiotics such as nisin (see Chapter VII).

It is important to understand that Bce resistance systems are evolutionarily conserved. In Chapter V, it was shown that BceAB type transporters and related are found in non-pathogenic bacteria and pathogenic clinically-relevant ESKAPE bacteria such as *E. faecium, MRSA, C. difficile, P. aeruginosa, Enterobacter spp.*, *A. baumannii, S. pneumoniae*, *S. agalactiae* (see Chapter V). ESKAPE bacteria challenge the global health system due to their multi-resistance against clinically used antibitoics and even last resort antibiotics. In 2019 infections by resistant

bacteria were responsible for approximately 4,95 million deaths (Antimicrobial Resistance, 2022). Thus, it becomes evident how crucial the elucidation of resistance systems such as the nisin resistance system of *S. agalactiae* helps to understand the resistance mechanism of MRSA and other multiresistant strains causing yearly global deaths. Small molecule inhibitors active against antimicrobial resistance-conferring protein systems are therefore powerful weapons to combat antibiotic resistance and most importantly save human lives.

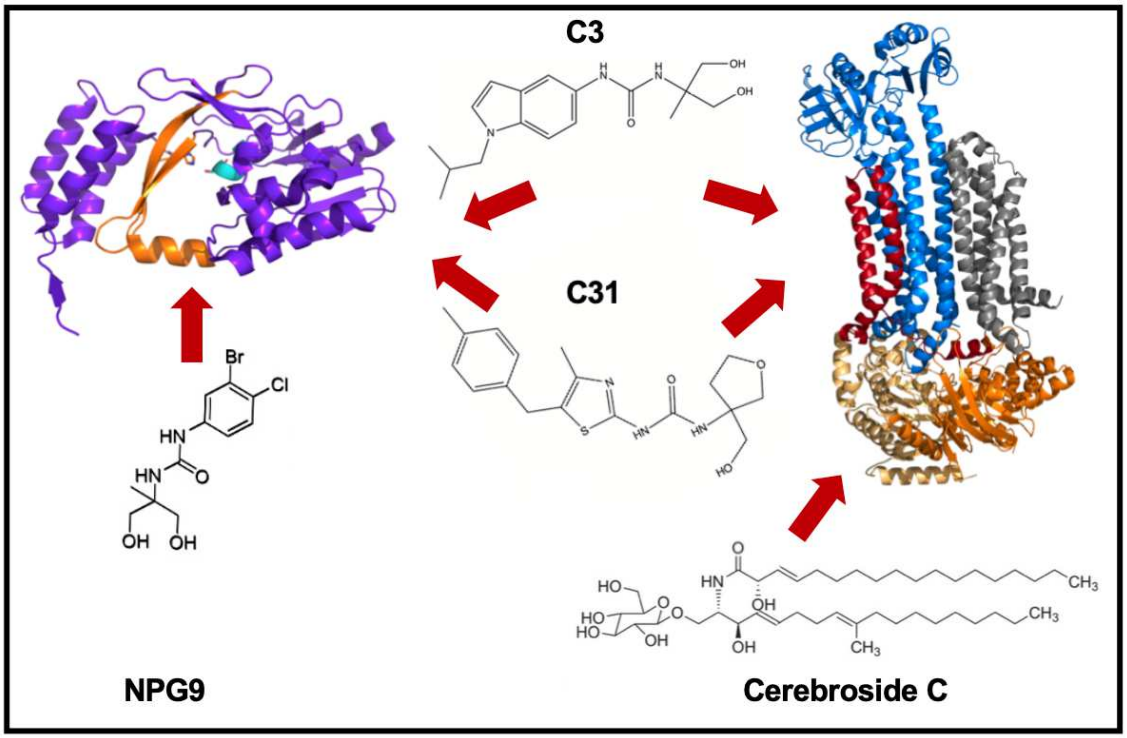

Figure 35: Inhibitors of *Sa*NSR (Khosa *et al*., 2016a) PDB ID: 4Y68 and *Sa*NsrFP. Selective inhibitors from previous work: NPG9 inhibits *Sa*NSR (Porta *et al.*, 2019) and Cerebroside C inhibits *Sa*NsrFP (Doctoral thesis by Zaschke-Kriesche, 2019). In this work compounds C3 and C31 were found as selective inhibitors against both resistance-conferring proteins. Red arrows indicate inhibition. The structure of the serine protease NSR is shown. The residues around the active site are highlighted in light blue, and the protease cap in orange. Image created with PyMOL Version 2.3.0 and Powerpoint 16.72. Alphafold model of *Sa*NsrFP. Right: TM Helix bundles 1-4 (grey), TM helix bundles 7-10 (blue), TM helices 5 and 6 (red), and NsrF (light orange/ orange). *Sa*NsrFP model was created using AlphaFold2 (Jumper *et al.,* 2021). Image created with PyMOL Version 2.3.0 and Powerpoint 16.72.

5 Literature

ABTS, A. 2014. The Nisin ABC-Investigating the maturation process of the lanthipeptide nisin.

ABTS, A., MAVARO, A., STINDT, J., BAKKES, P. J., METZGER, S., DRIESSEN, A. J., SMITS, S. H. & SCHMITT, L. 2011. Easy and rapid purification of highly active nisin. *Int J Pept,* 2011**,** 175145.

ABTS, A., MONTALBAN-LOPEZ, M., KUIPERS, O. P., SMITS, S. H. & SCHMITT, L. 2013. NisC binds the FxLx motif of the nisin leader peptide. *Biochemistry,* 52**,** 5387-95.

ALKHATIB, Z., ABTS, A., MAVARO, A., SCHMITT, L. & SMITS, S. H. 2012. Lantibiotics: how do producers become self-protected? *J Biotechnol,* 159**,** 145-54.

ALKHATIB, Z., LAGEDROSTE, M., FEY, I., KLEINSCHRODT, D., ABTS, A. & SMITS, S. H. 2014a. Lantibiotic immunity: inhibition of nisin mediated pore formation by NisI. *PLoS One,* 9**,** e102246.

ALKHATIB, Z., LAGEDROSTE, M., ZASCHKE, J., WAGNER, M., ABTS, A., FEY, I., KLEINSCHRODT, D. & SMITS, S. H. 2014b. The C-terminus of nisin is important for the ABC transporter NisFEG to confer immunity in Lactococcus lactis. *Microbiologyopen,* 3**,** 752-63.

ALOGHELI, H., OLANDERS, G., SCHAAL, W., BRANDT, P. & KARLEN, A. 2017. Docking of Macrocycles: Comparing Rigid and Flexible Docking in Glide. *J Chem Inf Model,* 57**,** 190-202.

ALTENA, K., GUDER, A., CRAMER, C. & BIERBAUM, G. 2000. Biosynthesis of the lantibiotic mersacidin: organization of a type B lantibiotic gene cluster. *Appl Environ Microbiol,* 66**,** 2565-71.

ALVAREZ-SIEIRO, P., MONTALBAN-LOPEZ, M., MU, D. & KUIPERS, O. P. 2016. Bacteriocins of lactic acid bacteria: extending the family. *Appl Microbiol Biotechnol,* 100**,** 2939-51.

ANTIMICROBIAL RESISTANCE, C. 2022. Global burden of bacterial antimicrobial resistance in 2019: a systematic analysis. *Lancet,* 399**,** 629-655.

ANTOSHINA, D. V., BALANDIN, S. V. & OVCHINNIKOVA, T. V. 2022. Structural Features, Mechanisms of Action, and Prospects for Practical Application of Class II Bacteriocins. *Biochemistry (Mosc),* 87**,** 1387-1403.

ARANHA, C., GUPTA, S. & REDDY, K. V. 2004. Contraceptive efficacy of antimicrobial peptide Nisin: in vitro and in vivo studies. *Contraception,* 69**,** 333-8.

ARNISON, P. G., BIBB, M. J., BIERBAUM, G., BOWERS, A. A., BUGNI, T. S., BULAJ, G., CAMARERO, J. A., CAMPOPIANO, D. J., CHALLIS, G. L., CLARDY, J., COTTER, P. D., CRAIK, D. J., DAWSON, M., DITTMANN, E., DONADIO, S., DORRESTEIN, P. C., ENTIAN, K. D., FISCHBACH, M. A., GARAVELLI, J. S., GORANSSON, U., GRUBER, C. W., HAFT, D. H., HEMSCHEIDT, T. K., HERTWECK, C., HILL, C., HORSWILL, A. R., JASPARS, M., KELLY, W. L., KLINMAN, J. P., KUIPERS, O. P., LINK, A. J., LIU, W., MARAHIEL, M. A., MITCHELL, D. A., MOLL, G. N., MOORE, B. S., MULLER, R., NAIR, S. K., NES, I. F., NORRIS, G. E., OLIVERA, B. M., ONAKA, H., PATCHETT, M. L., PIEL, J., REANEY, M. J., REBUFFAT, S., ROSS, R. P., SAHL, H. G., SCHMIDT, E. W., SELSTED, M. E.,

SEVERINOV, K., SHEN, B., SIVONEN, K., SMITH, L., STEIN, T., SUSSMUTH, R. D., TAGG, J. R., TANG, G. L., TRUMAN, A. W., VEDERAS, J. C., WALSH, C. T., WALTON, J. D., WENZEL, S. C., WILLEY, J. M. & VAN DER DONK, W. A. 2013. Ribosomally synthesized and post-translationally modified peptide natural products: overview and recommendations for a universal nomenclature. *Nat Prod Rep,* 30**,** 108-60.

BARBOSA, A. A. T., DE MELO, M. R., DA SILVA, C. M. R., JAIN, S. & DOLABELLA, S. S. 2021. Nisin resistance in Gram-positive bacteria and approaches to circumvent resistance for successful therapeutic use. *Crit Rev Microbiol,* 47**,** 376-385.

BARIK, S. 2020. The Uniqueness of Tryptophan in Biology: Properties, Metabolism, Interactions and Localization in Proteins. *Int J Mol Sci,* 21.

BARTHOLOMAE, M., BUIVYDAS, A., VIEL, J. H., MONTALBAN-LOPEZ, M. & KUIPERS, O. P. 2017. Major gene-regulatory mechanisms operating in ribosomally synthesized and post-translationally modified peptide (RiPP) biosynthesis. *Mol Microbiol,* 106**,** 186-206.

BEGLEY, M., COTTER, P. D., HILL, C. & ROSS, R. P. 2009. Identification of a novel two-peptide lantibiotic, lichenicidin, following rational genome mining for LanM proteins. *Appl Environ Microbiol,* 75**,** 5451-60.

BEIS, K. 2015. Structural basis for the mechanism of ABC transporters. *Biochem Soc Trans,* 43**,** 889-93.

BERARDI, A., ROSSI, C., LUGLI, L., CRETI, R., BACCHI REGGIANI, M. L., LANARI, M., MEMO, L., PEDNA, M. F., VENTURELLI, C., PERRONE, E., CICCIA, M., TRIDAPALLI, E., PIEPOLI, M., CONTIERO, R., FERRARI, F. & GBS PREVENTION WORKING GROUP, E.-R. 2013. Group B streptococcus late-onset disease: 2003-2010. *Pediatrics,* 131**,** e361-8.

BERNARD, R., GUISEPPI, A., CHIPPAUX, M., FOGLINO, M. & DENIZOT, F. 2007. Resistance to bacitracin in Bacillus subtilis: unexpected requirement of the BceAB ABC transporter in the control of expression of its own structural genes. *J Bacteriol,* 189**,** 8636-42.

BHATE, M. P., LEMMIN, T., KUENZE, G., MENSA, B., GANGULY, S., PETERS, J. M., SCHMIDT, N., PELTON, J. G., GROSS, C. A., MEILER, J. & DEGRADO, W. F. 2018. Structure and Function of the Transmembrane Domain of NsaS, an Antibiotic Sensing Histidine Kinase in Staphylococcus aureus. *J Am Chem Soc,* 140**,** 7471-7485.

BIERBAUM, G. & SAHL, H. G. 2009. Lantibiotics: mode of action, biosynthesis and bioengineering. *Curr Pharm Biotechnol,* 10**,** 2-18.

BILSING, F. L., ANLAUF, M. T., HACHANI, E., KHOSA, S. & SCHMITT, L. 2023. ABC Transporters in Bacterial Nanomachineries. *Int J Mol Sci,* 24.

BLAKE, K. L., RANDALL, C. P. & O'NEILL, A. J. 2011. In vitro studies indicate a high resistance potential for the lantibiotic nisin in Staphylococcus aureus and define a genetic basis for nisin resistance. *Antimicrob Agents Chemother,* 55**,** 2362-8.

BONELLI, R. R., SCHNEIDER, T., SAHL, H. G. & WIEDEMANN, I. 2006. Insights into in vivo activities of lantibiotics from gallidermin and epidermin mode-of-action studies. *Antimicrob Agents Chemother,* 50**,** 1449-57.

BREUKINK, E. & DE KRUIJFF, B. 2006. Lipid II as a target for antibiotics. *Nat Rev Drug Discov,* 5**,** 321-32.

BROTZ, H., BIERBAUM, G., LEOPOLD, K., REYNOLDS, P. E. & SAHL, H. G. 1998. The lantibiotic mersacidin inhibits peptidoglycan synthesis by targeting lipid II. *Antimicrob Agents Chemother,* 42**,** 154-60.

BUCHRIESER, C., RUSNIOK, C., KUNST, F., COSSART, P., GLASER, P. & LISTERIA, C. 2003. Comparison of the genome sequences of Listeria monocytogenes and Listeria innocua: clues for evolution and pathogenicity. *FEMS Immunol Med Microbiol,* 35**,** 207-13.

BUDA DE CESARE, G., CRISTY, S. A., GARSIN, D. A. & LORENZ, M. C. 2020. Antimicrobial Peptides: a New Frontier in Antifungal Therapy. *mBio,* 11.

CAO, L. T., WU, J. Q., XIE, F., HU, S. H. & MO, Y. 2007. Efficacy of nisin in treatment of clinical mastitis in lactating dairy cows. *J Dairy Sci,* 90**,** 3980-5.

CARTOTTO, R. 2017. Topical antimicrobial agents for pediatric burns. *Burns Trauma,* 5**,** 33.

CASCALES, E., BUCHANAN, S. K., DUCHE, D., KLEANTHOUS, C., LLOUBES, R., POSTLE, K., RILEY, M., SLATIN, S. & CAVARD, D. 2007. Colicin biology. *Microbiol Mol Biol Rev,* 71**,** 158-229.

CASTIGLIONE, F., LAZZARINI, A., CARRANO, L., CORTI, E., CICILIATO, I., GASTALDO, L., CANDIANI, P., LOSI, D., MARINELLI, F., SELVA, E. & PARENTI, F. 2008. Determining the structure and mode of action of microbisporicin, a potent lantibiotic active against multiresistant pathogens. *Chem Biol,* 15**,** 22-31.

CHATTERJEE, C., MILLER, L. M., LEUNG, Y. L., XIE, L., YI, M., KELLEHER, N. L. & VAN DER DONK, W. A. 2005. Lacticin 481 synthetase phosphorylates its substrate during lantibiotic production. *J Am Chem Soc,* 127**,** 15332-3.

CHEN, C. H. & LU, T. K. 2020. Development and Challenges of Antimicrobial Peptides for Therapeutic Applications. *Antibiotics (Basel),* 9.

CHEN, L., HOU, W. T., FAN, T., LIU, B., PAN, T., LI, Y. H., JIANG, Y. L., WEN, W., CHEN, Z. P., SUN, L., ZHOU, C. Z. & CHEN, Y. 2020. Cryo-electron Microscopy Structure and Transport Mechanism of a Wall Teichoic Acid ABC Transporter. *mBio,* 11.

CHEN, M., LIN, N., LIU, X., TANG, X., WANG, Z. & ZHANG, D. 2023a. A novel antimicrobial peptide screened by a Bacillus subtilis expression system, derived from Larimichthys crocea Ferritin H, exerting bactericidal and parasiticidal activities. *Front Immunol,* 14**,** 1168517.

CHEN, X., CAO, S., FU, X., NI, Y., HUANG, B., WU, J., CHEN, L., HUANG, S., CAO, J., YU, W. & YE, H. 2023b. The risk factors for Group B Streptococcus colonization during pregnancy and influences of intrapartum antibiotic prophylaxis on maternal and neonatal outcomes. *BMC Pregnancy Childbirth,* 23**,** 207.

CHO, J., COSTA, S. K., WIERZBICKI, R. M., RIGBY, W. F. C. & CHEUNG, A. L. 2021. The extracellular loop of the membrane permease VraG interacts with GraS to sense cationic antimicrobial peptides in Staphylococcus aureus. *PLoS Pathog,* 17**,** e1009338.

CHO, J., RIGBY, W. F. C. & CHEUNG, A. L. 2022. The thematic role of extracellular loop of VraG in activation of the membrane sensor GraS in a cystic fibrosis MRSA strain differs in nuance from the CA-MRSA strain JE2. *PLoS One,* 17**,** e0270393.

CLEMENS, R., ZASCHKE-KRIESCHE, J., KHOSA, S. & SMITS, S. H. J. 2017. Insight into Two ABC Transporter Families Involved in Lantibiotic Resistance. *Front Mol Biosci,* 4**,** 91.

COLE, T. J., PARKER, J. K., FELLER, A. L., WILKE, C. O. & DAVIES, B. W. 2022. Evidence for Widespread Class II Microcins in Enterobacterales Genomes. *Appl Environ Microbiol,* 88**,** e0148622.

COLLINS, B., CURTIS, N., COTTER, P. D., HILL, C. & ROSS, R. P. 2010. The ABC transporter AnrAB contributes to the innate resistance of Listeria monocytogenes to nisin, bacitracin, and various beta-lactam antibiotics. *Antimicrob Agents Chemother,* 54**,** 4416-23.

CORVEY, C., STEIN, T., DUSTERHUS, S., KARAS, M. & ENTIAN, K. D. 2003. Activation of subtilin precursors by Bacillus subtilis extracellular serine proteases subtilisin (AprE), WprA, and Vpr. *Biochem Biophys Res Commun,* 304**,** 48-54.

COTTER, P. D., ROSS, R. P. & HILL, C. 2013. Bacteriocins - a viable alternative to antibiotics? *Nat Rev Microbiol,* 11**,** 95-105.

CRETI, R., IMPERI, M., BERARDI, A., LINDH, E., ALFARONE, G., PATARACCHIA, M., RECCHIA, S., THE ITALIAN NETWORK ON, N. & INFANT GBS, I. 2021. Invasive Group B Streptococcal Disease in Neonates and Infants, Italy, Years 2015-2019. *Microorganisms,* 9.

CROW, A., GREENE, N. P., KAPLAN, E. & KORONAKIS, V. 2017. Structure and mechanotransmission mechanism of the MacB ABC transporter superfamily. *Proc Natl Acad Sci U S A,* 114**,** 12572-12577.

CROWTHER, G. S., BAINES, S. D., TODHUNTER, S. L., FREEMAN, J., CHILTON, C. H. & WILCOX, M. H. 2013. Evaluation of NVB302 versus vancomycin activity in an in vitro human gut model of Clostridium difficile infection. *J Antimicrob Chemother,* 68**,** 168-76.

DAWSON, R. J. & LOCHER, K. P. 2006. Structure of a bacterial multidrug ABC transporter. *Nature,* 443**,** 180-5.

DE KWAADSTENIET, M., DOESCHATE, K. T. & DICKS, L. M. 2009. Nisin F in the treatment of respiratory tract infections caused by Staphylococcus aureus. *Lett Appl Microbiol,* 48**,** 65-70.

DE KWAADSTENIET, M., TEN DOESCHATE, K. & DICKS, L. M. 2008. Characterization of the structural gene encoding nisin F, a new lantibiotic produced by a Lactococcus lactis subsp. lactis isolate from freshwater catfish (Clarias gariepinus). *Appl Environ Microbiol,* 74**,** 547-9.

DE RUYTER, P. G., KUIPERS, O. P. & DE VOS, W. M. 1996. Controlled gene expression systems for Lactococcus lactis with the food-grade inducer nisin. *Appl Environ Microbiol,* 62**,** 3662-7.

DELVES-BROUGHTON, J., BLACKBURN, P., EVANS, R. J. & HUGENHOLTZ, J. 1996. Applications of the bacteriocin, nisin. *Antonie Van Leeuwenhoek,* 69**,** 193-202.

DESMOND, A., O'HALLORAN, F., COTTER, L., HILL, C. & FIELD, D. 2022. Bioengineered Nisin A Derivatives Display Enhanced Activity against Clinical Neonatal Pathogens. *Antibiotics (Basel),* 11.

DIAGNE, A. M., PELLETIER, A., DURMORT, C., FAURE, A., KANONENBERG, K., FRETON, C., PAGE, A., DELOLME, F., VORAC, J., VALLET, S., BELLARD, L., VIVES, C., FIESCHI, F., VERNET, T., ROUSSELLE, P., GUIRAL, S., GRANGEASSE, C., JAULT, J. M. & ORELLE, C. 2022. Identification of a two-component regulatory system involved in

antimicrobial peptide resistance in Streptococcus pneumoniae. *PLoS Pathog,* 18**,** e1010458.

DIEP, D. B. & NES, I. F. 2002. Ribosomally synthesized antibacterial peptides in Gram positive bacteria. *Curr Drug Targets,* 3**,** 107-22.

DINTNER, S., HEERMANN, R., FANG, C., JUNG, K. & GEBHARD, S. 2014. A sensory complex consisting of an ATP-binding cassette transporter and a two-component regulatory system controls bacitracin resistance in Bacillus subtilis. *J Biol Chem,* 289**,** 27899-910.

DINTNER, S., STARON, A., BERCHTOLD, E., PETRI, T., MASCHER, T. & GEBHARD, S. 2011. Coevolution of ABC transporters and two-component regulatory systems as resistance modules against antimicrobial peptides in Firmicutes Bacteria. *J Bacteriol,* 193**,** 3851-62.

DISCHINGER, J., BASI CHIPALU, S. & BIERBAUM, G. 2014. Lantibiotics: promising candidates for future applications in health care. *Int J Med Microbiol,* 304**,** 51-62.

DRAPER, L. A., COTTER, P. D., HILL, C. & ROSS, R. P. 2015. Lantibiotic resistance. *Microbiol Mol Biol Rev,* 79**,** 171-91.

DRAPER, L. A., GRAINGER, K., DEEGAN, L. H., COTTER, P. D., HILL, C. & ROSS, R. P. 2009. Cross-immunity and immune mimicry as mechanisms of resistance to the lantibiotic lacticin 3147. *Mol Microbiol,* 71**,** 1043-54.

DRAPER, L. A., ROSS, R. P., HILL, C. & COTTER, P. D. 2008. Lantibiotic immunity. *Curr Protein Pept Sci,* 9**,** 39-49.

DUBOIS, A. 1995. Spiral bacteria in the human stomach: the gastric helicobacters. *Emerg Infect Dis,* 1**,** 79-85.

ECONOMOU, N. J., COCKLIN, S. & LOLL, P. J. 2013. High-resolution crystal structure reveals molecular details of target recognition by bacitracin. *Proc Natl Acad Sci U S A,* 110**,** 14207-12.

EKKELENKAMP, M. B., HANSSEN, M., DANNY HSU, S. T., DE JONG, A., MILATOVIC, D., VERHOEF, J. & VAN NULAND, N. A. 2005. Isolation and structural characterization of epilancin 15X, a novel lantibiotic from a clinical strain of Staphylococcus epidermidis. *FEBS Lett,* 579**,** 1917-22.

FALORD, M., KARIMOVA, G., HIRON, A. & MSADEK, T. 2012. GraXSR proteins interact with the VraFG ABC transporter to form a five-component system required for cationic antimicrobial peptide sensing and resistance in Staphylococcus aureus. *Antimicrob Agents Chemother,* 56**,** 1047-58.

FELSENSTEIN, J. 2005. PHYLIP (Phylogeny Inference Package) version 3.6. *Distributed by the author. Department of Genome Sciences, University of Washington, Seattle*.

FIELD, D., BLAKE, T., MATHUR, H., PM, O. C., COTTER, P. D., PAUL ROSS, R. & HILL, C. 2019. Bioengineering nisin to overcome the nisin resistance protein. *Mol Microbiol,* 111**,** 717-731.

FIELD, D., FERNANDEZ DE ULLIVARRI, M., ROSS, R. P. & HILL, C. 2023. After a century of nisin research - where are we now? *FEMS Microbiol Rev,* 47.

FISCHER, H., NETO, M. D., NAPOLITANO, H. B., POLIKARPOV, I. & CRAIEVICH, A. F. 2010. Determination of the molecular weight of proteins in solution from a single small-angle X-ray scattering measurement on a relative scale. *Journal of Applied Crystallography,* 43**,** 101-109.

FRITZ, G., DINTNER, S., TREICHEL, N. S., RADECK, J., GERLAND, U., MASCHER, T. & GEBHARD, S. 2015. A New Way of Sensing: Need-Based Activation of Antibiotic Resistance by a Flux-Sensing Mechanism. *mBio,* 6**,** e00975.

FROSETH, B. R. & MCKAY, L. L. 1991. Molecular characterization of the nisin resistance region of Lactococcus lactis subsp. lactis biovar diacetylactis DRC3. *Appl Environ Microbiol,* 57**,** 804-11.

FU, Y., JAARSMA, A. H. & KUIPERS, O. P. 2021. Antiviral activities and applications of ribosomally synthesized and post-translationally modified peptides (RiPPs). *Cell Mol Life Sci,* 78**,** 3921-3940.

FUJINAMI, D., MAHIN, A. A., ELSAYED, K. M., ISLAM, M. R., NAGAO, J. I., ROY, U., MOMIN, S., ZENDO, T., KOHDA, D. & SONOMOTO, K. 2018. The lantibiotic nukacin ISK-1 exists in an equilibrium between active and inactive lipid-II binding states. *Commun Biol,* 1**,** 150.

FURTMANN, F., PORTA, N., HOANG, D. T., REINERS, J., SCHUMACHER, J., GOTTSTEIN, J., GOHLKE, H. & SMITS, S. H. J. 2020. Characterization of the nucleotide-binding domain NsrF from the BceAB-type ABC-transporter NsrFP from the human pathogen Streptococcus agalactiae. *Sci Rep,* 10**,** 15208.

GARCIA-GUTIERREZ, E., MAYER, M. J., COTTER, P. D. & NARBAD, A. 2019. Gut microbiota as a source of novel antimicrobials. *Gut Microbes,* 10**,** 1-21.

GEBHARD, S. 2012. ABC transporters of antimicrobial peptides in Firmicutes bacteria - phylogeny, function and regulation. *Mol Microbiol,* 86**,** 1295-317.

GEBHARD, S. & MASCHER, T. 2011. Antimicrobial peptide sensing and detoxification modules: unravelling the regulatory circuitry of Staphylococcus aureus. *Mol Microbiol,* 81**,** 581-7.

GEIGER, C., KORN, S. M., HASLER, M., PEETZ, O., MARTIN, J., KOTTER, P., MORGNER, N. & ENTIAN, K. D. 2019. LanI-Mediated Lantibiotic Immunity in Bacillus subtilis: Functional Analysis. *Appl Environ Microbiol,* 85.

GEITANI, R., AYOUB MOUBARECK, C., TOUQUI, L. & KARAM SARKIS, D. 2019. Cationic antimicrobial peptides: alternatives and/or adjuvants to antibiotics active against methicillin-resistant Staphylococcus aureus and multidrug-resistant Pseudomonas aeruginosa. *BMC Microbiol,* 19**,** 54.

GEORGE, N. L. & ORLANDO, B. J. 2023. Architecture of a complete Bce-type antimicrobial peptide resistance module. *Nat Commun,* 14**,** 3896.

GEORGE, N. L., SCHILMILLER, A. L. & ORLANDO, B. J. 2022. Conformational snapshots of the bacitracin sensing and resistance transporter BceAB. *Proc Natl Acad Sci U S A,* 119**,** e2123268119.

GHOBRIAL, O. G., DERENDORF, H. & HILLMAN, J. D. 2009. Pharmacodynamic activity of the lantibiotic MU1140. *Int J Antimicrob Agents,* 33**,** 70-4.

GHOSH, A. K. & BRINDISI, M. 2020. Urea Derivatives in Modern Drug Discovery and Medicinal Chemistry. *J Med Chem,* 63**,** 2751-2788.

GOTO, Y., LI, B., CLAESEN, J., SHI, Y., BIBB, M. J. & VAN DER DONK, W. A. 2010. Discovery of unique lanthionine synthetases reveals new mechanistic and evolutionary insights. *PLoS Biol,* 8**,** e1000339.

GOTTSTEIN, J., ZASCHKE-KRIESCHE, J., UNSLEBER, S., VOITSEKHOVSKAIA, I., KULIK, A., BEHRMANN, L. V., OVERBECK, N., STUHLER, K., STEGMANN, E. & SMITS, S. H. J. 2022. New insights into the resistance mechanism for the BceAB-type transporter SaNsrFP. *Sci Rep,* 12**,** 4232.

GRAHAM, T. H., SHU, M., VERRAS, A., CHEN, Q., GARCIA-CALVO, M., LI, X., LISNOCK, J., TONG, X., TUNG, E. C., WILTSIE, J., HALE, J. J., PINTO, S. & SHEN, D. M. 2014. Pyrazoles as non-classical bioisosteres in

prolylcarboxypeptidase (PrCP) inhibitors. *Bioorg Med Chem Lett,* 24**,** 1657-60.

GRANSETH, E., VON HEIJNE, G. & ELOFSSON, A. 2005. A study of the membrane-water interface region of membrane proteins. *J Mol Biol,* 346**,** 377-85.

GREEN, B. R. & OLIVERA, B. M. 2016. Venom Peptides From Cone Snails: Pharmacological Probes for Voltage-Gated Sodium Channels. *Curr Top Membr,* 78**,** 65-86.

GREENE, N. P., KAPLAN, E., CROW, A. & KORONAKIS, V. 2018. Antibiotic Resistance Mediated by the MacB ABC Transporter Family: A Structural and Functional Perspective. *Front Microbiol,* 9**,** 950.

GROSS, E. & MORELL, J. L. 1967. The presence of dehydroalanine in the antibiotic nisin and its relationship to activity. *J Am Chem Soc,* 89**,** 2791-2.

GROSS, E. & MORELL, J. L. 1968. The number and nature of alpha,beta-unsaturated amino acids in nisin. *FEBS Lett,* 2**,** 61-64.

GUINIER, A. 1939. Small-angle X-ray diffraction: application to the study of ultramicroscopic
phenomena. *Annales de Physique,* 11**,** 161-237.

HACKER, C., CHRIST, N. A., DUCHARDT-FERNER, E., KORN, S., GOBL, C., BERNINGER, L., DUSTERHUS, S., HELLMICH, U. A., MADL, T., KOTTER, P., ENTIAN, K. D. & WOHNERT, J. 2015. The Solution Structure of the Lantibiotic Immunity Protein NisI and Its Interactions with Nisin. *J Biol Chem,* 290**,** 28869-86.

HAJIZADEH, N. R., FRANKE, D., JEFFRIES, C. M. & SVERGUN, D. I. 2018. Consensus Bayesian assessment of protein molecular mass from solution X-ray scattering data. *Sci Rep,* 8**,** 7204.

HALGREN, T. A. 2009. Identifying and Characterizing Binding Sites and Assessing Druggability. *Journal of Chemical Information and Modeling,* 49**,** 377-389.

HALL, J., ADAMS, N. H., BARTLETT, L., SEALE, A. C., LAMAGNI, T., BIANCHI-JASSIR, F., LAWN, J. E., BAKER, C. J., CUTLAND, C., HEATH, P. T., IP, M., LE DOARE, K., MADHI, S. A., RUBENS, C. E., SAHA, S. K., SCHRAG, S., SOBANJO-TER MEULEN, A., VEKEMANS, J. & GRAVETT, M. G. 2017. Maternal Disease With Group B Streptococcus and Serotype Distribution Worldwide: Systematic Review and Meta-analyses. *Clin Infect Dis,* 65**,** S112-S124.

HASPER, H. E., DE KRUIJFF, B. & BREUKINK, E. 2004. Assembly and stability of nisin-lipid II pores. *Biochemistry,* 43**,** 11567-75.

HATZIIOANOU, D., GHERGHISAN-FILIP, C., SAALBACH, G., HORN, N., WEGMANN, U., DUNCAN, S. H., FLINT, H. J., MAYER, M. J. & NARBAD, A. 2017. Discovery of a novel lantibiotic nisin O from Blautia obeum A2-162, isolated from the human gastrointestinal tract. *Microbiology (Reading),* 163**,** 1292-1305.

HEILBRONNER, S., KRISMER, B., BROTZ-OESTERHELT, H. & PESCHEL, A. 2021. The microbiome-shaping roles of bacteriocins. *Nat Rev Microbiol,* 19**,** 726-739.

HIRON, A., FALORD, M., VALLE, J., DEBARBOUILLE, M. & MSADEK, T. 2011. Bacitracin and nisin resistance in Staphylococcus aureus: a novel pathway involving the BraS/BraR two-component system (SA2417/SA2418) and

both the BraD/BraE and VraD/VraE ABC transporters. *Mol Microbiol,* 81**,** 602-22.

HOLLAND, I. B., COLE, S.P.C., KUCHLER, K. AND HIGGINS, C.F. 2003. ABC Proteins from Bacteria to Man. *Chapter 2. Academic Press, London*.

HOLO, H. & NES, I. F. 1989. High-Frequency Transformation, by Electroporation, of Lactococcus lactis subsp. cremoris Grown with Glycine in Osmotically Stabilized Media. *Appl Environ Microbiol,* 55**,** 3119-23.

HONG, H., PARK, S., JIMENEZ, R. H., RINEHART, D. & TAMM, L. K. 2007. Role of aromatic side chains in the folding and thermodynamic stability of integral membrane proteins. *J Am Chem Soc,* 129**,** 8320-7.

HONG, W., GAO, X., QIU, P., YANG, J., QIAO, M., SHI, H., ZHANG, D., TIAN, C., NIU, S. & LIU, M. 2017. Synthesis, construction, and evaluation of self-assembled nano-bacitracin A as an efficient antibacterial agent in vitro and in vivo. *Int J Nanomedicine,* 12**,** 4691-4708.

HSU, S. T., BREUKINK, E., TISCHENKO, E., LUTTERS, M. A., DE KRUIJFF, B., KAPTEIN, R., BONVIN, A. M. & VAN NULAND, N. A. 2004. The nisin-lipid II complex reveals a pyrophosphate cage that provides a blueprint for novel antibiotics. *Nat Struct Mol Biol,* 11**,** 963-7.

HUDSON, G. A. & MITCHELL, D. A. 2018. RiPP antibiotics: biosynthesis and engineering potential. *Curr Opin Microbiol,* 45**,** 61-69.

HUSADA, F., BOUNTRA, K., TASSIS, K., DE BOER, M., ROMANO, M., REBUFFAT, S., BEIS, K. & CORDES, T. 2018. Conformational dynamics of the ABC transporter McjD seen by single-molecule FRET. *EMBO J,* 37.

INGRAM, L. C. 1969. Synthesis of the antibiotic nisin: formation of lanthionine and beta-methyl-lanthionine. *Biochim Biophys Acta,* 184**,** 216-9.

IORIO, M., SASSO, O., MAFFIOLI, S. I., BERTORELLI, R., MONCIARDINI, P., SOSIO, M., BONEZZI, F., SUMMA, M., BRUNATI, C., BORDONI, R., CORTI, G., TAROZZO, G., PIOMELLI, D., REGGIANI, A. & DONADIO, S. 2014. A glycosylated, labionin-containing lanthipeptide with marked antinociceptive activity. *ACS Chem Biol,* 9**,** 398-404.

JABES, D., BRUNATI, C., CANDIANI, G., RIVA, S., ROMANO, G. & DONADIO, S. 2011. Efficacy of the new lantibiotic NAI-107 in experimental infections induced by multidrug-resistant Gram-positive pathogens. *Antimicrob Agents Chemother,* 55**,** 1671-6.

JEONG, J. H. & HA, S. C. 2018. Crystal Structure of NisI in a Lipid-Free Form, the Nisin Immunity Protein, from Lactococcus lactis. *Antimicrob Agents Chemother,* 62.

JOHNSON, B. A., ANKER, H. & MELENEY, F. L. 1945. Bacitracin: A New Antibiotic Produced by a Member of the B. Subtilis Group. *Science,* 102**,** 376-7.

JORDAN, S., JUNKER, A., HELMANN, J. D. & MASCHER, T. 2006. Regulation of LiaRS-dependent gene expression in bacillus subtilis: identification of inhibitor proteins, regulator binding sites, and target genes of a conserved cell envelope stress-sensing two-component system. *J Bacteriol,* 188**,** 5153-66.

JUMPER, J., EVANS, R., PRITZEL, A., GREEN, T., FIGURNOV, M., RONNEBERGER, O., TUNYASUVUNAKOOL, K., BATES, R., ZIDEK, A., POTAPENKO, A., BRIDGLAND, A., MEYER, C., KOHL, S. A. A., BALLARD, A. J., COWIE, A., ROMERA-PAREDES, B., NIKOLOV, S., JAIN, R., ADLER, J., BACK, T., PETERSEN, S., REIMAN, D., CLANCY, E., ZIELINSKI, M., STEINEGGER, M., PACHOLSKA, M.,

BERGHAMMER, T., BODENSTEIN, S., SILVER, D., VINYALS, O., SENIOR, A. W., KAVUKCUOGLU, K., KOHLI, P. & HASSABIS, D. 2021. Highly accurate protein structure prediction with AlphaFold. *Nature,* 596**,** 583-589.

KAMIMOTO, Y., TERASAKA, K., HAMAMOTO, M., TAKANASHI, K., FUKUDA, S., SHITAN, N., SUGIYAMA, A., SUZUKI, H., SHIBATA, D., WANG, B., POLLMANN, S., GEISLER, M. & YAZAKI, K. 2012. Arabidopsis ABCB21 is a facultative auxin importer/exporter regulated by cytoplasmic auxin concentration. *Plant Cell Physiol,* 53**,** 2090-100.

KASAHARA, K., BALTUS, A. J., LEE, S. H., EDELSTEIN, M. A. & EDELSTEIN, P. H. 2010. Prevalence of non-penicillin-susceptible group B streptococcus in Philadelphia and specificity of penicillin resistance screening methods. *J Clin Microbiol,* 48**,** 1468-9.

KHOSA, S., ALKHATIB, Z. & SMITS, S. H. 2013. NSR from Streptococcus agalactiae confers resistance against nisin and is encoded by a conserved nsr operon. *Biol Chem,* 394**,** 1543-9.

KHOSA, S., FRIEG, B., MULNAES, D., KLEINSCHRODT, D., HOEPPNER, A., GOHLKE, H. & SMITS, S. H. 2016a. Structural basis of lantibiotic recognition by the nisin resistance protein from Streptococcus agalactiae. *Sci Rep,* 6**,** 18679.

KHOSA, S., HOEPPNER, A., GOHLKE, H., SCHMITT, L. & SMITS, S. H. 2016b. Structure of the Response Regulator NsrR from Streptococcus agalactiae, Which Is Involved in Lantibiotic Resistance. *PLoS One,* 11**,** e0149903.

KHOSA, S., HOEPPNER, A., KLEINSCHRODT, D. & SMITS, S. H. 2015. Overexpression, purification, crystallization and preliminary X-ray diffraction of the nisin resistance protein from Streptococcus agalactiae. *Acta Crystallogr F Struct Biol Commun,* 71**,** 671-5.

KHOSA, S., LAGEDROSTE, M. & SMITS, S. H. 2016c. Protein Defense Systems against the Lantibiotic Nisin: Function of the Immunity Protein NisI and the Resistance Protein NSR. *Front Microbiol,* 7**,** 504.

KIM, S. G., BECATTINI, S., MOODY, T. U., SHLIAHA, P. V., LITTMANN, E. R., SEOK, R., GJONBALAJ, M., EATON, V., FONTANA, E., AMORETTI, L., WRIGHT, R., CABALLERO, S., WANG, Z. X., JUNG, H. J., MORJARIA, S. M., LEINER, I. M., QIN, W., RAMOS, R., CROSS, J. R., NARUSHIMA, S., HONDA, K., PELED, J. U., HENDRICKSON, R. C., TAUR, Y., VAN DEN BRINK, M. R. M. & PAMER, E. G. 2019. Microbiota-derived lantibiotic restores resistance against vancomycin-resistant Enterococcus. *Nature,* 572**,** 665-669.

KIM, T. S., HUR, J. W., YU, M. A., CHEIGH, C. I., KIM, K. N., HWANG, J. K. & PYUN, Y. R. 2003. Antagonism of Helicobacter pylori by bacteriocins of lactic acid bacteria. *J Food Prot,* 66**,** 3-12.

KINGSTON, A. W., ZHAO, H., COOK, G. M. & HELMANN, J. D. 2014. Accumulation of heptaprenyl diphosphate sensitizes Bacillus subtilis to bacitracin: implications for the mechanism of resistance mediated by the BceAB transporter. *Mol Microbiol,* 93**,** 37-49.

KLAENHAMMER, T. R. 1993. Genetics of bacteriocins produced by lactic acid bacteria. *FEMS Microbiol Rev,* 12**,** 39-85.

KLEIN, C. & ENTIAN, K. D. 1994. Genes involved in self-protection against the lantibiotic subtilin produced by Bacillus subtilis ATCC 6633. *Appl Environ Microbiol,* 60**,** 2793-801.

KOBRAS, C. M., PIEPENBREIER, H., EMENEGGER, J., SIM, A., FRITZ, G. & GEBHARD, S. 2020. BceAB-Type Antibiotic Resistance Transporters Appear To Act by Target Protection of Cell Wall Synthesis. *Antimicrob Agents Chemother,* 64.

KODANI, S., HUDSON, M. E., DURRANT, M. C., BUTTNER, M. J., NODWELL, J. R. & WILLEY, J. M. 2004. The SapB morphogen is a lantibiotic-like peptide derived from the product of the developmental gene ramS in Streptomyces coelicolor. *Proc Natl Acad Sci U S A,* 101**,** 11448-53.

KOLAR, S. L., NAGARAJAN, V., OSZMIANA, A., RIVERA, F. E., MILLER, H. K., DAVENPORT, J. E., RIORDAN, J. T., POTEMPA, J., BARBER, D. S., KOZIEL, J., ELASRI, M. O. & SHAW, L. N. 2011. NsaRS is a cell-envelope-stress-sensing two-component system of Staphylococcus aureus. *Microbiology (Reading),* 157**,** 2206-2219.

KONAREV, P. V., VOLKOV, V. V., SOKOLOVA, A. V., KOCH, M. H. J. & SVERGUN, D. I. 2003. PRIMUS: a Windows PC-based system for small-angle scattering data analysis. *Journal of Applied Crystallography,* 36**,** 1277-1282.

KONZ, D., KLENS, A., SCHORGENDORFER, K. & MARAHIEL, M. A. 1997. The bacitracin biosynthesis operon of Bacillus licheniformis ATCC 10716: molecular characterization of three multi-modular peptide synthetases. *Chem Biol,* 4**,** 927-37.

KOPONEN, O., TAKALA, T. M., SAARELA, U., QIAO, M. & SARIS, P. E. 2004. Distribution of the NisI immunity protein and enhancement of nisin activity by the lipid-free NisI. *FEMS Microbiol Lett,* 231**,** 85-90.

KOPONEN, O., TOLONEN, M., QIAO, M., WAHLSTROM, G., HELIN, J. & SARIS, P. E. J. 2002. NisB is required for the dehydration and NisC for the lanthionine formation in the post-translational modification of nisin. *Microbiology (Reading),* 148**,** 3561-3568.

KORDEL, M., SCHULLER, F. & SAHL, H. G. 1989. Interaction of the pore forming-peptide antibiotics Pep 5, nisin and subtilin with non-energized liposomes. *FEBS Lett,* 244**,** 99-102.

KORKHOV, V. M., MIREKU, S. A. & LOCHER, K. P. 2012. Structure of AMP-PNP-bound vitamin B12 transporter BtuCD-F. *Nature,* 490**,** 367-72.

KOZIN, M. B. & SVERGUN, D. I. 2001. Automated matching of high- and low-resolution structural models. *Journal of Applied Crystallography,* 34**,** 33-41.

KRAMER, N. E., VAN HIJUM, S. A., KNOL, J., KOK, J. & KUIPERS, O. P. 2006. Transcriptome analysis reveals mechanisms by which Lactococcus lactis acquires nisin resistance. *Antimicrob Agents Chemother,* 50**,** 1753-61.

KUHN, B., MOHR, P. & STAHL, M. 2010. Intramolecular hydrogen bonding in medicinal chemistry. *J Med Chem,* 53**,** 2601-11.

KUIPERS, A., DE BOEF, E., RINK, R., FEKKEN, S., KLUSKENS, L. D., DRIESSEN, A. J., LEENHOUTS, K., KUIPERS, O. P. & MOLL, G. N. 2004. NisT, the transporter of the lantibiotic nisin, can transport fully modified, dehydrated, and unmodified prenisin and fusions of the leader peptide with non-lantibiotic peptides. *J Biol Chem,* 279**,** 22176-82.

KUIPERS, O. P., BEERTHUYZEN, M. M., DE RUYTER, P. G., LUESINK, E. J. & DE VOS, W. M. 1995. Autoregulation of nisin biosynthesis in Lactococcus lactis by signal transduction. *J Biol Chem,* 270**,** 27299-304.

KUIPERS, O. P., BEERTHUYZEN, M. M., SIEZEN, R. J. & DE VOS, W. M. 1993. Characterization of the nisin gene cluster nisABTCIPR of Lactococcus

lactis. Requirement of expression of the nisA and nisI genes for development of immunity. *Eur J Biochem,* 216**,** 281-91.

LAGEDROSTE, M., REINERS, J., KNOSPE, C. V., SMITS, S. H. J. & SCHMITT, L. 2020. A Structural View on the Maturation of Lanthipeptides. *Front Microbiol,* 11**,** 1183.

LAGEDROSTE, M., REINERS, J., SMITS, S. H. J. & SCHMITT, L. 2019. Systematic characterization of position one variants within the lantibiotic nisin. *Sci Rep,* 9**,** 935.

LAGEDROSTE, M., SMITS, S. H. J. & SCHMITT, L. 2017. Substrate Specificity of the Secreted Nisin Leader Peptidase NisP. *Biochemistry,* 56**,** 4005-4014.

LAGEDROSTE, M., SMITS, S. H. J. & SCHMITT, L. 2021. Importance of the leader peptide sequence on the lanthipeptide secretion level. *FEBS J*.

LAWRENCE, G. W., GARCIA-GUTIERREZ, E., WALSH, C. J., O'CONNOR, P. M., BEGLEY, M., P.D., C. & C.M., G. 2022. Nisin G is a novel nisin variant produced by a gut-derived
Streptococcus salivarius *bioRxiv*.

LEWINSON, O., ORELLE, C. & SEEGER, M. A. 2020. Structures of ABC transporters: handle with care. *FEBS Lett,* 594**,** 3799-3814.

LI, B., SHER, D., KELLY, L., SHI, Y., HUANG, K., KNERR, P. J., JOEWONO, I., RUSCH, D., CHISHOLM, S. W. & VAN DER DONK, W. A. 2010. Catalytic promiscuity in the biosynthesis of cyclic peptide secondary metabolites in planktonic marine cyanobacteria. *Proc Natl Acad Sci U S A,* 107**,** 10430-5.

LI, Q., MONTALBAN-LOPEZ, M. & KUIPERS, O. P. 2018. Increasing the Antimicrobial Activity of Nisin-Based Lantibiotics against Gram-Negative Pathogens. *Appl Environ Microbiol,* 84.

LIGHTBOWN, J. W., KOGUT, M. & UEMURA, K. 1964. The Second International Standard for Bacitracin. *Bull World Health Organ,* 31**,** 101-9.

LISTRO, R., ROSSINO, G., PIAGGI, F., SONEKAN, F. F., ROSSI, D., LINCIANO, P. & COLLINA, S. 2022. Urea-based anticancer agents. Exploring 100-years of research with an eye to the future. *Front Chem,* 10**,** 995351.

LIU, S. X., ZHOU, Y., ZHAO, L., ZHOU, L. S., SUN, J., LIU, G. J., DU, Y. S. & ZHOU, Y. N. 2022. Thiostrepton confers protection against reactive oxygen species-related apoptosis by restraining FOXM1-triggerred development of gastric cancer. *Free Radic Biol Med,* 193**,** 385-404.

LOCKEY, C., EDWARDS, R. J., ROPER, D. I. & DIXON, A. M. 2020. The Extracellular Domain of Two-component System Sensor Kinase VanS from Streptomyces coelicolor Binds Vancomycin at a Newly Identified Binding Site. *Sci Rep,* 10**,** 5727.

LOO, T. W., BARTLETT, M. C. & CLARKE, D. M. 2004. Disulfide cross-linking analysis shows that transmembrane segments 5 and 8 of human P-glycoprotein are close together on the cytoplasmic side of the membrane. *J Biol Chem,* 279**,** 7692-7.

LOO, T. W. & CLARKE, D. M. 2001. Determining the dimensions of the drug-binding domain of human P-glycoprotein using thiol cross-linking compounds as molecular rulers. *J Biol Chem,* 276**,** 36877-80.

LOO, T. W. & CLARKE, D. M. 2002. Vanadate trapping of nucleotide at the ATP-binding sites of human multidrug resistance P-glycoprotein exposes

different residues to the drug-binding site. *Proc Natl Acad Sci U S A,* 99**,** 3511-6.

MA, J., LIU, J., ZHANG, Y., WANG, D., LIU, R., LIU, G., YAO, H. & PAN, Z. 2019. Bacitracin resistance and enhanced virulence of Streptococcus suis via a novel efflux pump. *BMC Vet Res,* 15**,** 377.

MADRID, L., SEALE, A. C., KOHLI-LYNCH, M., EDMOND, K. M., LAWN, J. E., HEATH, P. T., MADHI, S. A., BAKER, C. J., BARTLETT, L., CUTLAND, C., GRAVETT, M. G., IP, M., LE DOARE, K., RUBENS, C. E., SAHA, S. K., SOBANJO-TER MEULEN, A., VEKEMANS, J., SCHRAG, S. & INFANT, G. B. S. D. I. G. 2017. Infant Group B Streptococcal Disease Incidence and Serotypes Worldwide: Systematic Review and Meta-analyses. *Clin Infect Dis,* 65**,** S160-S172.

MAFFIOLI, S. I., CRUZ, J. C., MONCIARDINI, P., SOSIO, M. & DONADIO, S. 2016. Advancing cell wall inhibitors towards clinical applications. *J Ind Microbiol Biotechnol,* 43**,** 177-84.

MAKWANA, P., RAHUL, K., ITO, K. & SUBHADRA, B. 2023. Diversity of Antimicrobial Peptides in Silkworm. *Life (Basel),* 13.

MALMSTEN, M. 2014. Antimicrobial peptides. *Ups J Med Sci,* 119**,** 199-204.

MANALASTAS-CANTOS, K., KONAREV, P. V., HAJIZADEH, N. R., KIKHNEY, A. G., PETOUKHOV, M. V., MOLODENSKIY, D. S., PANJKOVICH, A., MERTENS, H. D. T., GRUZINOV, A., BORGES, C., JEFFRIES, C. M., SVERGUN, D. I. & FRANKE, D. 2021. ATSAS 3.0: expanded functionality and new tools for small-angle scattering data analysis. *Journal of Applied Crystallography,* 54.

MANSON, J. M., KEIS, S., SMITH, J. M. & COOK, G. M. 2004. Acquired bacitracin resistance in Enterococcus faecalis is mediated by an ABC transporter and a novel regulatory protein, BcrR. *Antimicrob Agents Chemother,* 48**,** 3743-8.

MARAHIEL, M. A. & ESSEN, L. O. 2009. Chapter 13. Nonribosomal peptide synthetases mechanistic and structural aspects of essential domains. *Methods Enzymol,* 458**,** 337-51.

MARKI, F., HANNI, E., FREDENHAGEN, A. & VAN OOSTRUM, J. 1991. Mode of action of the lanthionine-containing peptide antibiotics duramycin, duramycin B and C, and cinnamycin as indirect inhibitors of phospholipase A2. *Biochem Pharmacol,* 42**,** 2027-35.

MARKOVIC, K. G., GRUJOVIC, M. Z., KORACEVIC, M. G., NIKODIJEVIC, D. D., MILUTINOVIC, M. G., SEMEDO-LEMSADDEK, T. & DJILAS, M. D. 2022. Colicins and Microcins Produced by Enterobacteriaceae: Characterization, Mode of Action, and Putative Applications. *Int J Environ Res Public Health,* 19.

MASCHER, T. 2006. Intramembrane-sensing histidine kinases: a new family of cell envelope stress sensors in Firmicutes bacteria. *FEMS Microbiol Lett,* 264**,** 133-44.

MASCHER, T. 2014. Bacterial (intramembrane-sensing) histidine kinases: signal transfer rather than stimulus perception. *Trends Microbiol,* 22**,** 559-65.

MASCHER, T., MARGULIS, N. G., WANG, T., YE, R. W. & HELMANN, J. D. 2003. Cell wall stress responses in Bacillus subtilis: the regulatory network of the bacitracin stimulon. *Molecular Microbiology,* 50**,** 1591-1604.

MAVARO, A., ABTS, A., BAKKES, P. J., MOLL, G. N., DRIESSEN, A. J., SMITS, S. H. & SCHMITT, L. 2011. Substrate recognition and specificity of the

NisB protein, the lantibiotic dehydratase involved in nisin biosynthesis. *J Biol Chem,* 286**,** 30552-60.

MCDONALD, S. K. & FLEMING, K. G. 2016. Aromatic Side Chain Water-to-Lipid Transfer Free Energies Show a Depth Dependence across the Membrane Normal. *J Am Chem Soc,* 138**,** 7946-50.

MEEHL, M., HERBERT, S., GOTZ, F. & CHEUNG, A. 2007. Interaction of the GraRS two-component system with the VraFG ABC transporter to support vancomycin-intermediate resistance in Staphylococcus aureus. *Antimicrob Agents Chemother,* 51**,** 2679-89.

MENGIST, H. M., ZEWDIE, O., BELEW, A. & DABSU, R. 2017. Prevalence and drug susceptibility pattern of group B Streptococci (GBS) among pregnant women attending antenatal care (ANC) in Nekemte Referral Hospital (NRH), Nekemte, Ethiopia. *BMC Res Notes,* 10**,** 388.

MENSA, B., HOWELL, G. L., SCOTT, R. & DEGRADO, W. F. 2014. Comparative mechanistic studies of brilacidin, daptomycin, and the antimicrobial peptide LL16. *Antimicrob Agents Chemother,* 58**,** 5136-45.

MIERAU, I. & KLEEREBEZEM, M. 2005. 10 years of the nisin-controlled gene expression system (NICE) in Lactococcus lactis. *Appl Microbiol Biotechnol,* 68**,** 705-17.

MIETHKE, M., PIERONI, M., WEBER, T., BRONSTRUP, M., HAMMANN, P., HALBY, L., ARIMONDO, P. B., GLASER, P., AIGLE, B., BODE, H. B., MOREIRA, R., LI, Y., LUZHETSKYY, A., MEDEMA, M. H., PERNODET, J. L., STADLER, M., TORMO, J. R., GENILLOUD, O., TRUMAN, A. W., WEISSMAN, K. J., TAKANO, E., SABATINI, S., STEGMANN, E., BROTZ-OESTERHELT, H., WOHLLEBEN, W., SEEMANN, M., EMPTING, M., HIRSCH, A. K. H., LORETZ, B., LEHR, C. M., TITZ, A., HERRMANN, J., JAEGER, T., ALT, S., HESTERKAMP, T., WINTERHALTER, M., SCHIEFER, A., PFARR, K., HOERAUF, A., GRAZ, H., GRAZ, M., LINDVALL, M., RAMURTHY, S., KARLEN, A., VAN DONGEN, M., PETKOVIC, H., KELLER, A., PEYRANE, F., DONADIO, S., FRAISSE, L., PIDDOCK, L. J. V., GILBERT, I. H., MOSER, H. E. & MULLER, R. 2021. Towards the sustainable discovery and development of new antibiotics. *Nat Rev Chem,* 5**,** 726-749.

MIRDITA, M., SCHUTZE, K., MORIWAKI, Y., HEO, L., OVCHINNIKOV, S. & STEINEGGER, M. 2022. ColabFold: making protein folding accessible to all. *Nat Methods,* 19**,** 679-682.

MITROPHANOV, A. Y. & GROISMAN, E. A. 2008. Signal integration in bacterial two-component regulatory systems. *Genes Dev,* 22**,** 2601-11.

MOLODENSKIY, D. S., SVERGUN, D. I. & KIKHNEY, A. G. 2022. Artificial neural networks for solution scattering data analysis. *Structure,* 30**,** 900-908 e2.

MONTALBAN-LOPEZ, M., DENG, J., VAN HEEL, A. J. & KUIPERS, O. P. 2018. Specificity and Application of the Lantibiotic Protease NisP. *Front Microbiol,* 9**,** 160.

MONTALBAN-LOPEZ, M., SCOTT, T. A., RAMESH, S., RAHMAN, I. R., VAN HEEL, A. J., VIEL, J. H., BANDARIAN, V., DITTMANN, E., GENILLOUD, O., GOTO, Y., GRANDE BURGOS, M. J., HILL, C., KIM, S., KOEHNKE, J., LATHAM, J. A., LINK, A. J., MARTINEZ, B., NAIR, S. K., NICOLET, Y., REBUFFAT, S., SAHL, H. G., SAREEN, D., SCHMIDT, E. W., SCHMITT, L., SEVERINOV, K., SUSSMUTH, R. D., TRUMAN, A. W., WANG, H., WENG, J. K., VAN WEZEL, G. P., ZHANG, Q., ZHONG, J., PIEL, J., MITCHELL, D. A., KUIPERS, O. P. & VAN DER DONK, W. A. 2021. New

developments in RiPP discovery, enzymology and engineering. *Nat Prod Rep,* 38**,** 130-239.

MOTA-MEIRA, M., LAPOINTE, G., LACROIX, C. & LAVOIE, M. C. 2000. MICs of mutacin B-Ny266, nisin A, vancomycin, and oxacillin against bacterial pathogens. *Antimicrob Agents Chemother,* 44**,** 24-9.

MULDERS, J. W., BOERRIGTER, I. J., ROLLEMA, H. S., SIEZEN, R. J. & DE VOS, W. M. 1991. Identification and characterization of the lantibiotic nisin Z, a natural nisin variant. *Eur J Biochem,* 201**,** 581-4.

MULNAES, D. & GOHLKE, H. 2018. TopScore: Using Deep Neural Networks and Large Diverse Data Sets for Accurate Protein Model Quality Assessment. *J Chem Theory Comput,* 14**,** 6117-6126.

MULNAES, D., PORTA, N., CLEMENS, R., APANASENKO, I., REINERS, J., GREMER, L., NEUDECKER, P., SMITS, S. H. J. & GOHLKE, H. 2020. TopModel: Template-Based Protein Structure Prediction at Low Sequence Identity Using Top-Down Consensus and Deep Neural Networks. *J Chem Theory Comput,* 16**,** 1953-1967.

NAKANO, M. M. & ZUBER, P. 1990. Molecular biology of antibiotic production in Bacillus. *Crit Rev Biotechnol,* 10**,** 223-40.

NEWMAN, D. J. & CRAGG, G. M. 2020. Natural Products as Sources of New Drugs over the Nearly Four Decades from 01/1981 to 09/2019. *J Nat Prod,* 83**,** 770-803.

NEWTON, G. G., ABRAHAM, E. P. & BERRIDGE, N. J. 1953. Sulphur-containing amino-acids of nisin. *Nature,* 171**,** 606.

NIKAIDO, H. & VAARA, M. 1985. Molecular basis of bacterial outer membrane permeability. *Microbiol Rev,* 49**,** 1-32.

NISSEN-MEYER, J., ROGNE, P., OPPEGARD, C., HAUGEN, H. S. & KRISTIANSEN, P. E. 2009. Structure-function relationships of the non-lanthionine-containing peptide (class II) bacteriocins produced by gram-positive bacteria. *Curr Pharm Biotechnol,* 10**,** 19-37.

O'CONNOR, P. M., O'SHEA, E. F., GUINANE, C. M., O'SULLIVAN, O., COTTER, P. D., ROSS, R. P. & HILL, C. 2015. Nisin H Is a New Nisin Variant Produced by the Gut-Derived Strain Streptococcus hyointestinalis DPC6484. *Appl Environ Microbiol,* 81**,** 3953-60.

O'SULLIVAN, J. N., O'CONNOR, P. M., REA, M. C., O'SULLIVAN, O., WALSH, C. J., HEALY, B., MATHUR, H., FIELD, D., HILL, C. & ROSS, R. P. 2020. Nisin J, a Novel Natural Nisin Variant, Is Produced by Staphylococcus capitis Sourced from the Human Skin Microbiota. *J Bacteriol,* 202.

OHKI, R., GIYANTO, TATENO, K., MASUYAMA, W., MORIYA, S., KOBAYASHI, K. & OGASAWARA, N. 2003. The BceRS two-component regulatory system induces expression of the bacitracin transporter, BceAB, in Bacillus subtilis. *Mol Microbiol,* 49**,** 1135-44.

OKUDA, K., YANAGIHARA, S., SUGAYAMA, T., ZENDO, T., NAKAYAMA, J. & SONOMOTO, K. 2010. Functional significance of the E loop, a novel motif conserved in the lantibiotic immunity ATP-binding cassette transport systems. *J Bacteriol,* 192**,** 2801-8.

OLDHAM, M. L., DAVIDSON, A. L. & CHEN, J. 2008. Structural insights into ABC transporter mechanism. *Curr Opin Struct Biol,* 18**,** 726-33.

OLDHAM, M. L., KHARE, D., QUIOCHO, F. A., DAVIDSON, A. L. & CHEN, J. 2007. Crystal structure of a catalytic intermediate of the maltose transporter. *Nature,* 450**,** 515-21.

OMAN, T. J. & VAN DER DONK, W. A. 2010. Follow the leader: the use of leader peptides to guide natural product biosynthesis. *Nat Chem Biol,* 6**,** 9-18.

OMMI, O., NAIYAZ AHMAD, M., GAJULA, S. N. R., WANJARI, P., SAU, S., AGNIVESH, P. K., SAHOO, S. K., KALIA, N. P., SONTI, R., NANDURI, S., DASGUPTA, A., CHOPRA, S. & YADDANAPUDI, V. M. 2023. Synthesis and pharmacological evaluation of 1,3-diaryl substituted pyrazole based (thio)urea derivatives as potent antimicrobial agents against multi-drug resistant Staphylococcus aureus and Mycobacterium tuberculosis. *RSC Med Chem,* 14**,** 1296-1308.

ONGPIPATTANAKUL, C., DESORMEAUX, E. K., DICAPRIO, A., VAN DER DONK, W. A., MITCHELL, D. A. & NAIR, S. K. 2022. Mechanism of Action of Ribosomally Synthesized and Post-Translationally Modified Peptides. *Chem Rev*.

ORTIZ-LOPEZ, F. J., CARRETERO-MOLINA, D., SANCHEZ-HIDALGO, M., MARTIN, J., GONZALEZ, I., ROMAN-HURTADO, F., DE LA CRUZ, M., GARCIA-FERNANDEZ, S., REYES, F., DEISINGER, J. P., MULLER, A., SCHNEIDER, T. & GENILLOUD, O. 2020. Cacaoidin, First Member of the New Lanthidin RiPP Family. *Angew Chem Int Ed Engl,* 59**,** 12654-12658.

OTTO, M., PESCHEL, A. & GOTZ, F. 1998. Producer self-protection against the lantibiotic epidermin by the ABC transporter EpiFEG of Staphylococcus epidermidis Tu3298. *FEMS Microbiol Lett,* 166**,** 203-11.

OUYANG, J., TIAN, X. L., VERSEY, J., WISHART, A. & LI, Y. H. 2010. The BceABRS four-component system regulates the bacitracin-induced cell envelope stress response in Streptococcus mutans. *Antimicrob Agents Chemother,* 54**,** 3895-906.

PAG, U., HEIDRICH, C., BIERBAUM, G. & SAHL, H. G. 1999. Molecular analysis of expression of the lantibiotic pep5 immunity phenotype. *Appl Environ Microbiol,* 65**,** 591-8.

PANDIT, B., BHAT, U. G. & GARTEL, A. L. 2011. Proteasome inhibitory activity of thiazole antibiotics. *Cancer Biol Ther,* 11**,** 43-7.

PATIL, M., NOONIKARA-POYIL, A., JOSHI, S. D., PATIL, S. A., PATIL, S. A. & BUGARIN, A. 2019. New Urea Derivatives as Potential Antimicrobial Agents: Synthesis, Biological Evaluation, and Molecular Docking Studies. *Antibiotics (Basel),* 8.

PEI, Z. F., ZHU, L., SARKSIAN, R., VAN DER DONK, W. A. & NAIR, S. K. 2022. Class V Lanthipeptide Cyclase Directs the Biosynthesis of a Stapled Peptide Natural Product. *J Am Chem Soc,* 144**,** 17549-17557.

PERNOT, P., ROUND, A., BARRETT, R., DE MARIA ANTOLINOS, A., GOBBO, A., GORDON, E., HUET, J., KIEFFER, J., LENTINI, M., MATTENET, M., MORAWE, C., MUELLER-DIECKMANN, C., OHLSSON, S., SCHMID, W., SURR, J., THEVENEAU, P., ZERRAD, L. & MCSWEENEY, S. 2013. Upgraded ESRF BM29 beamline for SAXS on macromolecules in solution. *J Synchrotron Radiat,* 20**,** 660-4.

PERNOT, P., THEVENEAU, P., GIRAUD, T., FERNANDES, R. N., NURIZZO, D., SPRUCE, D., SURR, J., MCSWEENEY, S., ROUND, A., FELISAZ, F., FOEDINGER, L., GOBBO, A., HUET, J., VILLARD, C. & CIPRIANI, F. 2010. New beamline dedicated to solution scattering from biological macromolecules at the ESRF. *Journal of Physics: Conference Series,* 247**,** 012009.

PESCHEL, A. & GOTZ, F. 1996. Analysis of the Staphylococcus epidermidis genes epiF, -E, and -G involved in epidermin immunity. *J Bacteriol,* 178**,** 531-6.

PETOUKHOV, M. V. & SVERGUN, D. I. 2015. Ambiguity assessment of small-angle scattering curves from monodisperse systems. *Acta Crystallogr D Biol Crystallogr,* 71**,** 1051-8.

PIETIAINEN, M., GARDEMEISTER, M., MECKLIN, M., LESKELA, S., SARVAS, M. & KONTINEN, V. P. 2005. Cationic antimicrobial peptides elicit a complex stress response in Bacillus subtilis that involves ECF-type sigma factors and two-component signal transduction systems. *Microbiology (Reading),* 151**,** 1577-1592.

PIPER, C., COTTER, P. D., ROSS, R. P. & HILL, C. 2009. Discovery of medically significant lantibiotics. *Curr Drug Discov Technol,* 6**,** 1-18.

POONIA, N., LAL, K., KUMAR, A., KUMAR, A., SAHU, S., BAIDYA, A. T. K. & KUMAR, R. 2022. Urea-thiazole/benzothiazole hybrids with a triazole linker: synthesis, antimicrobial potential, pharmacokinetic profile and in silico mechanistic studies. *Mol Divers,* 26**,** 2375-2391.

POPELLA, P., KRAUSS, S., EBNER, P., NEGA, M., DEIBERT, J. & GOTZ, F. 2016. VraH Is the Third Component of the Staphylococcus aureus VraDEH System Involved in Gallidermin and Daptomycin Resistance and Pathogenicity. *Antimicrob Agents Chemother,* 60**,** 2391-401.

POROD, G. 1951. Die Röntgenkleinwinkelstreuung Von Dichtgepackten Kolloiden Systemen - 1 Teil. *Kolloid-Zeitschrift and Zeitschrift Fur Polymere,* 124**,** 83-114.

PORTA, N., ZASCHKE-KRIESCHE, J., FRIEG, B., GOPALSWAMY, M., ZIVKOVIC, A., ETZKORN, M., STARK, H., SMITS, S. H. J. & GOHLKE, H. 2019. Small-molecule inhibitors of nisin resistance protein NSR from the human pathogen Streptococcus agalactiae. *Bioorg Med Chem,* 27**,** 115079.

PRICE, C. E., ZEYNIYEV, A., KUIPERS, O. P. & KOK, J. 2012. From meadows to milk to mucosa - adaptation of Streptococcus and Lactococcus species to their nutritional environments. *FEMS Microbiol Rev,* 36**,** 949-71.

PUOPOLO, K. M., LYNFIELD, R., CUMMINGS, J. J., COMMITTEE ON, F., NEWBORN & COMMITTEE ON INFECTIOUS, D. 2019. Management of Infants at Risk for Group B Streptococcal Disease. *Pediatrics,* 144.

PYMOL 2015. The PyMOL Molecular Graphics System, Version 2.0 Schrödinger, LLC.

QIAO, M. & SARIS, P. E. 1996. Evidence for a role of NisT in transport of the lantibiotic nisin produced by Lactococcus lactis N8. *FEMS Microbiol Lett,* 144**,** 89-93.

QUAZI, F., LENEVICH, S. & MOLDAY, R. S. 2012. ABCA4 is an N-retinylidene-phosphatidylethanolamine and phosphatidylethanolamine importer. *Nat Commun,* 3**,** 925.

QURESHI, N. K., YIN, S. & BOYLE-VAVRA, S. 2014. The role of the Staphylococcal VraTSR regulatory system on vancomycin resistance and vanA operon expression in vancomycin-resistant Staphylococcus aureus. *PLoS One,* 9**,** e85873.

RA, R., BEERTHUYZEN, M. M., DE VOS, W. M., SARIS, P. E. J. & KUIPERS, O. P. 1999. Effects of gene disruptions in the nisin gene cluster of Lactococcus lactis on nisin production and producer immunity. *Microbiology (Reading),* 145 (Pt 5)**,** 1227-1233.

RA, S. R., QIAO, M., IMMONEN, T., PUJANA, I. & SARIS, P. E. J. 1996. Genes responsible for nisin synthesis, regulation and immunity form a regulon of two operons and are induced by nisin in Lactoccocus lactis N8. *Microbiology (Reading),* 142 (Pt 5), 1281-1288.

RAABE, V. N. & SHANE, A. L. 2019. Group B Streptococcus (Streptococcus agalactiae). *Microbiol Spectr,* 7.

RADECK, J., GEBHARD, S., ORCHARD, P. S., KIRCHNER, M., BAUER, S., MASCHER, T. & FRITZ, G. 2016. Anatomy of the bacitracin resistance network in Bacillus subtilis. *Mol Microbiol,* 100, 607-20.

RAIS, I., KARAS, M. & SCHAGGER, H. 2004. Two-dimensional electrophoresis for the isolation of integral membrane proteins and mass spectrometric identification. *Proteomics,* 4, 2567-71.

RAMBO, R. P. & TAINER, J. A. 2013. Accurate assessment of mass, models and resolution by small-angle scattering. *Nature,* 496, 477-81.

RANA, K., SHARMA, R. & PREET, S. 2019. Augmented therapeutic efficacy of 5-fluorouracil in conjunction with lantibiotic nisin against skin cancer. *Biochem Biophys Res Commun,* 520, 551-559.

RATH, A. & DEBER, C. M. 2013. Correction factors for membrane protein molecular weight readouts on sodium dodecyl sulfate-polyacrylamide gel electrophoresis. *Anal Biochem,* 434, 67-72.

RATH, A., GLIBOWICKA, M., NADEAU, V. G., CHEN, G. & DEBER, C. M. 2009. Detergent binding explains anomalous SDS-PAGE migration of membrane proteins. *Proc Natl Acad Sci U S A,* 106, 1760-5.

RAWLINGS, N. D., BARRETT, A. J., THOMAS, P. D., HUANG, X., BATEMAN, A. & FINN, R. D. 2018. The MEROPS database of proteolytic enzymes, their substrates and inhibitors in 2017 and a comparison with peptidases in the PANTHER database. *Nucleic Acids Res,* 46, D624-D632.

REINERS, J., LAGEDROSTE, M., EHLEN, K., LEUSCH, S., ZASCHKE-KRIESCHE, J. & SMITS, S. H. J. 2017. The N-terminal Region of Nisin Is Important for the BceAB-Type ABC Transporter NsrFP from Streptococcus agalactiae COH1. *Front Microbiol,* 8, 1643.

REINERS, J., LAGEDROSTE, M., GOTTSTEIN, J., ADENIYI, E. T., KALSCHEUER, R., POSCHMANN, G., STUHLER, K., SMITS, S. H. J. & SCHMITT, L. 2020. Insights in the Antimicrobial Potential of the Natural Nisin Variant Nisin H. *Front Microbiol,* 11, 573614.

REIS, M., ESCHBACH-BLUDAU, M., IGLESIAS-WIND, M. I., KUPKE, T. & SAHL, H. G. 1994. Producer immunity towards the lantibiotic Pep5: identification of the immunity gene pepI and localization and functional analysis of its gene product. *Appl Environ Microbiol,* 60, 2876-83.

REPASKY, M. P., SHELLEY, M. & FRIESNER, R. A. 2007. Flexible ligand docking with Glide. *Curr Protoc Bioinformatics,* Chapter 8, Unit 8 12.

REPKA, L. M., CHEKAN, J. R., NAIR, S. K. & VAN DER DONK, W. A. 2017. Mechanistic Understanding of Lanthipeptide Biosynthetic Enzymes. *Chem Rev,* 117, 5457-5520.

REUMERS, J., MAURER-STROH, S., SCHYMKOWITZ, J. & ROUSSEAU, F. 2009. Protein sequences encode safeguards against aggregation. *Hum Mutat,* 30, 431-7.

REVILLA-GUARINOS, A., GEBHARD, S., MASCHER, T. & ZUNIGA, M. 2014. Defence against antimicrobial peptides: different strategies in Firmicutes. *Environ Microbiol,* 16, 1225-37.

RIETKOTTER, E., HOYER, D. & MASCHER, T. 2008. Bacitracin sensing in Bacillus subtilis. *Mol Microbiol,* 68**,** 768-85.

RINK, R., WIERENGA, J., KUIPERS, A., KLUSKENS, L. D., DRIESSEN, A. J., KUIPERS, O. P. & MOLL, G. N. 2007. Dissection and modulation of the four distinct activities of nisin by mutagenesis of rings A and B and by C-terminal truncation. *Appl Environ Microbiol,* 73**,** 5809-16.

RISMONDO, J. & SCHULZ, L. M. 2021. Not Just Transporters: Alternative Functions of ABC Transporters in Bacillus subtilis and Listeria monocytogenes. *Microorganisms,* 9.

ROE, D. R. & CHEATHAM, T. E., 3RD 2013. PTRAJ and CPPTRAJ: Software for Processing and Analysis of Molecular Dynamics Trajectory Data. *J Chem Theory Comput,* 9**,** 3084-95.

ROGERS, L. A. 1928. The Inhibiting Effect of Streptococcus Lactis on Lactobacillus Bulgaricus. *J Bacteriol,* 16**,** 321-5.

ROJAS-PIRELA, M., KEMMERLING, U., QUINONES, W., MICHELS, P. A. M. & ROJAS, V. 2023. Antimicrobial Peptides (AMPs): Potential Therapeutic Strategy against Trypanosomiases? *Biomolecules,* 13.

ROSTKOWSKI, M., OLSSON, M. H., SONDERGAARD, C. R. & JENSEN, J. H. 2011. Graphical analysis of pH-dependent properties of proteins predicted using PROPKA. *BMC Struct Biol,* 11**,** 6.

RUSHWORTH, D. D., CHRISTL, I., KUMAR, N., HOFFMANN, K., KRETZSCHMAR, R., LEHMANN, M. F., SCHENKEVELD, W. D. C. & KRAEMER, S. M. 2022. Copper mobilisation from Cu sulphide minerals by methanobactin: Effect of pH, oxygen and natural organic matter. *Geobiology,* 20**,** 690-706.

SAAR-DOVER, R., BITLER, A., NEZER, R., SHMUEL-GALIA, L., FIRON, A., SHIMONI, E., TRIEU-CUOT, P. & SHAI, Y. 2012. D-alanylation of lipoteichoic acids confers resistance to cationic peptides in group B streptococcus by increasing the cell wall density. *PLoS Pathog,* 8**,** e1002891.

SADOWY, E., MATYNIA, B. & HRYNIEWICZ, W. 2010. Population structure, virulence factors and resistance determinants of invasive, non-invasive and colonizing Streptococcus agalactiae in Poland. *J Antimicrob Chemother,* 65**,** 1907-14.

SAHL, H. G. & BIERBAUM, G. 1998. Lantibiotics: biosynthesis and biological activities of uniquely modified peptides from gram-positive bacteria. *Annu Rev Microbiol,* 52**,** 41-79.

SANDIFORD, S. K. 2020. An overview of lantibiotic biosynthetic machinery promiscuity and its impact on antimicrobial discovery. *Expert Opin Drug Discov,* 15**,** 373-382.

SANTOS, R., RUZA, D., CUNHA, E., TAVARES, L. & OLIVEIRA, M. 2019. Diabetic foot infections: Application of a nisin-biogel to complement the activity of conventional antibiotics and antiseptics against Staphylococcus aureus biofilms. *PLoS One,* 14**,** e0220000.

SCHMIDT, E. W., NELSON, J. T., RASKO, D. A., SUDEK, S., EISEN, J. A., HAYGOOD, M. G. & RAVEL, J. 2005. Patellamide A and C biosynthesis by a microcin-like pathway in Prochloron didemni, the cyanobacterial symbiont of Lissoclinum patella. *Proc Natl Acad Sci U S A,* 102**,** 7315-20.

SCHMITT, L. & TAMPE, R. 2002. Structure and mechanism of ABC transporters. *Curr Opin Struct Biol,* 12**,** 754-60.

SCHRAG, S. J., FARLEY, M. M., PETIT, S., REINGOLD, A., WESTON, E. J., PONDO, T., HUDSON JAIN, J. & LYNFIELD, R. 2016. Epidemiology of Invasive Early-Onset Neonatal Sepsis, 2005 to 2014. *Pediatrics,* 138.

SCHWARZER, D., FINKING, R. & MARAHIEL, M. A. 2003. Nonribosomal peptides: from genes to products. *Nat Prod Rep,* 20**,** 275-87.

SEVERINOV, K., SEMENOVA, E., KAZAKOV, A., KAZAKOV, T. & GELFAND, M. S. 2007. Low-molecular-weight post-translationally modified microcins. *Mol Microbiol,* 65**,** 1380-94.

SHENKAREV, Z. O., FINKINA, E. I., NURMUKHAMEDOVA, E. K., BALANDIN, S. V., MINEEV, K. S., NADEZHDIN, K. D., YAKIMENKO, Z. A., TAGAEV, A. A., TEMIROV, Y. V., ARSENIEV, A. S. & OVCHINNIKOVA, T. V. 2010. Isolation, structure elucidation, and synergistic antibacterial activity of a novel two-component lantibiotic lichenicidin from Bacillus licheniformis VK21. *Biochemistry,* 49**,** 6462-72.

SHIN, J. M., GWAK, J. W., KAMARAJAN, P., FENNO, J. C., RICKARD, A. H. & KAPILA, Y. L. 2016. Biomedical applications of nisin. *J Appl Microbiol,* 120**,** 1449-65.

SIEGERS, K. & ENTIAN, K. D. 1995. Genes involved in immunity to the lantibiotic nisin produced by Lactococcus lactis 6F3. *Appl Environ Microbiol,* 61**,** 1082-9.

SIEVERS, F., WILM, A., DINEEN, D., GIBSON, T. J., KARPLUS, K., LI, W., LOPEZ, R., MCWILLIAM, H., REMMERT, M., SODING, J., THOMPSON, J. D. & HIGGINS, D. G. 2011. Fast, scalable generation of high-quality protein multiple sequence alignments using Clustal Omega. *Mol Syst Biol,* 7**,** 539.

SIEZEN, R. J., KUIPERS, O. P. & DE VOS, W. M. 1996. Comparison of lantibiotic gene clusters and encoded proteins. *Antonie Van Leeuwenhoek,* 69**,** 171-84.

SITU, A. J., KANG, S. M., FREY, B. B., AN, W., KIM, C. & ULMER, T. S. 2018. Membrane Anchoring of alpha-Helical Proteins: Role of Tryptophan. *J Phys Chem B,* 122**,** 1185-1194.

SKAUGEN, M., ABILDGAARD, C. I. & NES, I. F. 1997. Organization and expression of a gene cluster involved in the biosynthesis of the lantibiotic lactocin S. *Mol Gen Genet,* 253**,** 674-86.

SLOTBOOM, D. J., DUURKENS, R. H., OLIEMAN, K. & ERKENS, G. B. 2008. Static light scattering to characterize membrane proteins in detergent solution. *Methods,* 46**,** 73-82.

SMITS, S. H. J., SCHMITT, L. & BEIS, K. 2020. Self-immunity to antibacterial peptides by ABC transporters. *FEBS Lett,* 594**,** 3920-3942.

SOKOLOVE, P. M., WESTPHAL, P. A., KESTER, M. B., WIERWILLE, R. & SIKORA-VANMETER, K. 1989. Duramycin effects on the structure and function of heart mitochondria. I. Structural alterations and changes in membrane permeability. *Biochim Biophys Acta,* 983**,** 15-22.

STARON, A., FINKEISEN, D. E. & MASCHER, T. 2011. Peptide antibiotic sensing and detoxification modules of Bacillus subtilis. *Antimicrob Agents Chemother,* 55**,** 515-25.

STEIN, T., HEINZMANN, S., DUSTERHUS, S., BORCHERT, S. & ENTIAN, K. D. 2005. Expression and functional analysis of the subtilin immunity genes spaIFEG in the subtilin-sensitive host Bacillus subtilis MO1099. *J Bacteriol,* 187**,** 822-8.

STEIN, T., HEINZMANN, S., SOLOVIEVA, I. & ENTIAN, K. D. 2003. Function of Lactococcus lactis nisin immunity genes nisI and nisFEG after coordinated expression in the surrogate host Bacillus subtilis. *J Biol Chem,* 278**,** 89-94.

STEVENS, K. A., SHELDON, B. W., KLAPES, N. A. & KLAENHAMMER, T. R. 1991. Nisin treatment for inactivation of Salmonella species and other gram-negative bacteria. *Appl Environ Microbiol,* 57**,** 3613-5.

STOCK, A. M., ROBINSON, V. L. & GOUDREAU, P. N. 2000. Two-component signal transduction. *Annu Rev Biochem,* 69**,** 183-215.

STORM, D. R. 1974. Mechanism of bacitracin action: a specific lipid-peptide interaction. *Ann N Y Acad Sci,* 235**,** 387-98.

STORM, D. R. & STROMINGER, J. L. 1973. Complex formation between bacitracin peptides and isoprenyl pyrophosphates. The specificity of lipid-peptide interactions. *J Biol Chem,* 248**,** 3940-5.

SUGRUE, I., HILL, D., O'CONNOR, P. M., DAY, L., STANTON, C., HILL, C. & ROSS, R. P. 2023. Nisin E Is a Novel Nisin Variant Produced by Multiple Streptococcus equinus Strains. *Microorganisms,* 11.

SUN, Z., ZHONG, J., LIANG, X., LIU, J., CHEN, X. & HUAN, L. 2009. Novel mechanism for nisin resistance via proteolytic degradation of nisin by the nisin resistance protein NSR. *Antimicrob Agents Chemother,* 53**,** 1964-73.

SVERGUN, D., BARBERATO, C. & KOCH, M. H. J. 1995. CRYSOL - A program to evaluate x-ray solution scattering of biological macromolecules from atomic coordinates. *Journal of Applied Crystallography,* 28**,** 768-773.

SVERGUN, D. I. 1992. Determination of the Regularization Parameter in Indirect-Transform Methods Using Perceptual Criteria. *Journal of Applied Crystallography,* 25**,** 495-503.

SVERGUN, D. I., PETOUKHOV, M. V. & KOCH, M. H. 2001. Determination of domain structure of proteins from X-ray solution scattering. *Biophys J,* 80**,** 2946-53.

TACCONELLI, E., CARRARA, E., SAVOLDI, A., HARBARTH, S., MENDELSON, M., MONNET, D. L., PULCINI, C., KAHLMETER, G., KLUYTMANS, J., CARMELI, Y., OUELLETTE, M., OUTTERSON, K., PATEL, J., CAVALERI, M., COX, E. M., HOUCHENS, C. R., GRAYSON, M. L., HANSEN, P., SINGH, N., THEURETZBACHER, U., MAGRINI, N. & GROUP, W. H. O. P. P. L. W. 2018. Discovery, research, and development of new antibiotics: the WHO priority list of antibiotic-resistant bacteria and tuberculosis. *Lancet Infect Dis,* 18**,** 318-327.

TAKALA, T. M. & SARIS, P. E. J. 2006. C terminus of NisI provides specificity to nisin. *Microbiology (Reading),* 152**,** 3543-3549.

TAYLOR, W. R. 1997. Residual colours: a proposal for aminochromography. *Protein Eng,* 10**,** 743-6.

TERASAKA, K., BLAKESLEE, J. J., TITAPIWATANAKUN, B., PEER, W. A., BANDYOPADHYAY, A., MAKAM, S. N., LEE, O. R., RICHARDS, E. L., MURPHY, A. S., SATO, F. & YAZAKI, K. 2005. PGP4, an ATP binding cassette P-glycoprotein, catalyzes auxin transport in Arabidopsis thaliana roots. *Plant Cell,* 17**,** 2922-39.

THOMAS, C., ALLER, S. G., BEIS, K., CARPENTER, E. P., CHANG, G., CHEN, L., DASSA, E., DEAN, M., DUONG VAN HOA, F., EKIERT, D., FORD, R., GAUDET, R., GONG, X., HOLLAND, I. B., HUANG, Y., KAHNE, D. K., KATO, H., KORONAKIS, V., KOTH, C. M., LEE, Y., LEWINSON, O., LILL, R., MARTINOIA, E., MURAKAMI, S., PINKETT, H. W., POOLMAN, B., ROSENBAUM, D., SARKADI, B., SCHMITT, L., SCHNEIDER, E., SHI, Y.,

SHYNG, S. L., SLOTBOOM, D. J., TAJKHORSHID, E., TIELEMAN, D. P., UEDA, K., VARADI, A., WEN, P. C., YAN, N., ZHANG, P., ZHENG, H., ZIMMER, J. & TAMPE, R. 2020. Structural and functional diversity calls for a new classification of ABC transporters. *FEBS Lett,* 594**,** 3767-3775.

THOMAS, C. & TAMPE, R. 2018. Multifaceted structures and mechanisms of ABC transport systems in health and disease. *Curr Opin Struct Biol,* 51**,** 116-128.

TOLLERSON, R., 2ND & IBBA, M. 2020. Translational regulation of environmental adaptation in bacteria. *J Biol Chem,* 295**,** 10434-10445.

TRACANNA, V., DE JONG, A., MEDEMA, M. H. & KUIPERS, O. P. 2017. Mining prokaryotes for antimicrobial compounds: from diversity to function. *FEMS Microbiol Rev,* 41**,** 417-429.

TSUDA, H., YAMASHITA, Y., SHIBATA, Y., NAKANO, Y. & KOGA, T. 2002. Genes involved in bacitracin resistance in Streptococcus mutans. *Antimicrob Agents Chemother,* 46**,** 3756-64.

TUNG, L. & VAN DER DONK, W. A. 2021. Mechanisms and Evolution of Diversity-Generating RiPP Biosynthesis. *Trends in Chemistry*.

TWOMEY, E., HILL, C., FIELD, D. & BEGLEY, M. 2020. Bioengineered Nisin Derivative M17Q Has Enhanced Activity against Staphylococcus epidermidis. *Antibiotics (Basel),* 9.

UPATISSA, S. & MITCHELL, R. J. 2023. The "Cins" of Our Fathers: Rejuvenated Interest in Colicins to Combat Drug Resistance. *J Microbiol,* 61**,** 145-158.

URMI, U. L., VIJAY, A. K., KUPPUSAMY, R., ISLAM, S. & WILLCOX, M. D. P. 2023. A review of the antiviral activity of cationic antimicrobial peptides. *Peptides,* 166**,** 171024.

VALENTA, C., BERNKOP-SCHNURCH, A. & RIGLER, H. P. 1996. The antistaphylococcal effect of nisin in a suitable vehicle: a potential therapy for atopic dermatitis in man. *J Pharm Pharmacol,* 48**,** 988-91.

VAN DE VEN, F. J. M., VAN DEN HOOVEN, H.W., HILBERS, C.W., KONINGS, R.N.H. 1992. NMR Studies of Lantibiotics: The Three-Dimensional Structure of Nisin in Aqueous Solution. *James, R., Lazdunski, C., Pattus, F. (eds) Bacteriocins, Microcins and Lantibiotics. NATO ASI Series,* 65.

VAN DER DOES, C. & TAMPE, R. 2004. How do ABC transporters drive transport? *Biol Chem,* 385**,** 927-33.

VAN DER MEER, J. R., POLMAN, J., BEERTHUYZEN, M. M., SIEZEN, R. J., KUIPERS, O. P. & DE VOS, W. M. 1993. Characterization of the Lactococcus lactis nisin A operon genes nisP, encoding a subtilisin-like serine protease involved in precursor processing, and nisR, encoding a regulatory protein involved in nisin biosynthesis. *J Bacteriol,* 175**,** 2578-88.

VAN DER MEER, J. R., ROLLEMA, H. S., SIEZEN, R. J., BEERTHUYZEN, M. M., KUIPERS, O. P. & DE VOS, W. M. 1994. Influence of amino acid substitutions in the nisin leader peptide on biosynthesis and secretion of nisin by Lactococcus lactis. *J Biol Chem,* 269**,** 3555-62.

VAN HEEL, A. J., DE JONG, A., SONG, C., VIEL, J. H., KOK, J. & KUIPERS, O. P. 2018. BAGEL4: a user-friendly web server to thoroughly mine RiPPs and bacteriocins. *Nucleic Acids Res,* 46**,** W278-W281.

VAN HEEL, A. J., KLOOSTERMAN, T. G., MONTALBAN-LOPEZ, M., DENG, J., PLAT, A., BAUDU, B., HENDRIKS, D., MOLL, G. N. & KUIPERS, O. P. 2016. Discovery, Production and Modification of Five Novel Lantibiotics Using the Promiscuous Nisin Modification Machinery. *ACS Synth Biol,* 5**,** 1146-1154.

VARADI, M., ANYANGO, S., DESHPANDE, M., NAIR, S., NATASSIA, C., YORDANOVA, G., YUAN, D., STROE, O., WOOD, G., LAYDON, A., ZIDEK, A., GREEN, T., TUNYASUVUNAKOOL, K., PETERSEN, S., JUMPER, J., CLANCY, E., GREEN, R., VORA, A., LUTFI, M., FIGURNOV, M., COWIE, A., HOBBS, N., KOHLI, P., KLEYWEGT, G., BIRNEY, E., HASSABIS, D. & VELANKAR, S. 2022. AlphaFold Protein Structure Database: massively expanding the structural coverage of protein-sequence space with high-accuracy models. *Nucleic Acids Res,* 50**,** D439-D444.

VENKATACHALAM, T. K., MAO, C. & UCKUN, F. M. 2004. Effect of stereochemistry on the anti-HIV activity of chiral thiourea compounds. *Bioorg Med Chem,* 12**,** 4275-84.

VESTERGAARD, M., BERGLUND, N. A., HSU, P. C., SONG, C., KOLDSO, H., SCHIOTT, B. & SANSOM, M. S. P. 2019. Structure and Dynamics of Cinnamycin-Lipid Complexes: Mechanisms of Selectivity for Phosphatidylethanolamine Lipids. *ACS Omega,* 4**,** 18889-18899.

WANG, X., WANG, Z., DONG, Z., YAN, Y., ZHANG, Y. & HUO, L. 2023. Deciphering the Biosynthesis of Novel Class I Lanthipeptides from Marine Pseudoalteromonas Reveals a Dehydratase PsfB with Dethiolation Activity. *ACS Chem Biol,* 18**,** 1218-1227.

WATERHOUSE, A. M., PROCTER, J. B., MARTIN, D. M., CLAMP, M. & BARTON, G. J. 2009. Jalview Version 2--a multiple sequence alignment editor and analysis workbench. *Bioinformatics,* 25**,** 1189-91.

WELLS, K. M., CIFTCI, Y., PEDDINTI, B. S. T., GHILADI, R. A., VEDIYAPPAN, G., SPONTAK, R. J. & GOVIND, R. 2023. Preventing the spread of life-threatening gastrointestinal microbes on the surface of a continuously self-disinfecting block polymer. *J Colloid Interface Sci,* 652**,** 718-726.

WEST, A. H. & STOCK, A. M. 2001. Histidine kinases and response regulator proteins in two-component signaling systems. *Trends Biochem Sci,* 26**,** 369-76.

WIEDEMANN, I., BOTTIGER, T., BONELLI, R. R., SCHNEIDER, T., SAHL, H. G. & MARTINEZ, B. 2006a. Lipid II-based antimicrobial activity of the lantibiotic plantaricin C. *Appl Environ Microbiol,* 72**,** 2809-14.

WIEDEMANN, I., BOTTIGER, T., BONELLI, R. R., WIESE, A., HAGGE, S. O., GUTSMANN, T., SEYDEL, U., DEEGAN, L., HILL, C., ROSS, P. & SAHL, H. G. 2006b. The mode of action of the lantibiotic lacticin 3147--a complex mechanism involving specific interaction of two peptides and the cell wall precursor lipid II. *Mol Microbiol,* 61**,** 285-96.

WIEDEMANN, I., BREUKINK, E., VAN KRAAIJ, C., KUIPERS, O. P., BIERBAUM, G., DE KRUIJFF, B. & SAHL, H. G. 2001. Specific binding of nisin to the peptidoglycan precursor lipid II combines pore formation and inhibition of cell wall biosynthesis for potent antibiotic activity. *J Biol Chem,* 276**,** 1772-9.

WIENER, M., FREYMANN, D., GHOSH, P. & STROUD, R. M. 1997. Crystal structure of colicin Ia. *Nature,* 385**,** 461-4.

WIRAWAN, R. E., KLESSE, N. A., JACK, R. W. & TAGG, J. R. 2006. Molecular and genetic characterization of a novel nisin variant produced by Streptococcus uberis. *Appl Environ Microbiol,* 72**,** 1148-56.

WOLF, D., DOMINGUEZ-CUEVAS, P., DANIEL, R. A. & MASCHER, T. 2012. Cell envelope stress response in cell wall-deficient L-forms of Bacillus subtilis. *Antimicrob Agents Chemother,* 56**,** 5907-15.

WU, Z., WANG, W., TANG, M., SHAO, J., DAI, C., ZHANG, W., FAN, H., YAO, H., ZONG, J., CHEN, D., WANG, J. & LU, C. 2014. Comparative genomic analysis shows that Streptococcus suis meningitis isolate SC070731 contains a unique 105K genomic island. *Gene,* 535**,** 156-64.

XU, K., ZHANG, M., ZHAO, Q., YU, F., GUO, H., WANG, C., HE, F., DING, J. & ZHANG, P. 2013. Crystal structure of a folate energy-coupling factor transporter from Lactobacillus brevis. *Nature,* 497**,** 268-71.

XU, M., ZHANG, F., CHENG, Z., BASHIRI, G., WANG, J., HONG, J., WANG, Y., XU, L., CHEN, X., HUANG, S. X., LIN, S., DENG, Z. & TAO, M. 2020. Functional Genome Mining Reveals a Class V Lanthipeptide Containing a d-Amino Acid Introduced by an F(420) H(2) -Dependent Reductase. *Angew Chem Int Ed Engl,* 59**,** 18029-18035.

YANG, S. J., BAYER, A. S., MISHRA, N. N., MEEHL, M., LEDALA, N., YEAMAN, M. R., XIONG, Y. Q. & CHEUNG, A. L. 2012. The Staphylococcus aureus two-component regulatory system, GraRS, senses and confers resistance to selected cationic antimicrobial peptides. *Infect Immun,* 80**,** 74-81.

YOSHIDA, Y., MATSUO, M., OOGAI, Y., KATO, F., NAKAMURA, N., SUGAI, M. & KOMATSUZAWA, H. 2011. Bacitracin sensing and resistance in Staphylococcus aureus. *FEMS Microbiol Lett,* 320**,** 33-9.

ZAITSEVA, J., OSWALD, C., JUMPERTZ, T., JENEWEIN, S., WIEDENMANN, A., HOLLAND, I. B. & SCHMITT, L. 2006. A structural analysis of asymmetry required for catalytic activity of an ABC-ATPase domain dimer. *EMBO J,* 25**,** 3432-43.

ZASCHKE-KRIESCHE, J., BEHRMANN, L. V., REINERS, J., LAGEDROSTE, M., GRONER, Y., KALSCHEUER, R. & SMITS, S. H. J. 2019a. Bypassing lantibiotic resistance by an effective nisin derivative. *Bioorg Med Chem,* 27**,** 3454-3462.

ZASCHKE-KRIESCHE, J., REINERS, J., LAGEDROSTE, M. & SMITS, S. H. J. 2019b. Influence of nisin hinge-region variants on lantibiotic immunity and resistance proteins. *Bioorg Med Chem,* 27**,** 3947-3953.

ZENDO, T., FUKAO, M., UEDA, K., HIGUCHI, T., NAKAYAMA, J. & SONOMOTO, K. 2003. Identification of the lantibiotic nisin Q, a new natural nisin variant produced by Lactococcus lactis 61-14 isolated from a river in Japan. *Biosci Biotechnol Biochem,* 67**,** 1616-9.

ZENDO, T., OHASHI, C., MAENO, S., PIAO, X., SALMINEN, S., SONOMOTO, K. & ENDO, A. 2020. Kunkecin A, a New Nisin Variant Bacteriocin Produced by the Fructophilic Lactic Acid Bacterium, Apilactobacillus kunkeei FF30-6 Isolated From Honey Bees. *Front Microbiol,* 11**,** 571903.

ZHANG, Q., YU, Y., VELASQUEZ, J. E. & VAN DER DONK, W. A. 2012. Evolution of lanthipeptide synthetases. *Proc Natl Acad Sci U S A,* 109**,** 18361-6.

ZHENG, Y., DU, Y., QIU, Z., LIU, Z., QIAO, J., LI, Y. & CAIYIN, Q. 2022. Nisin Variants Generated by Protein Engineering and Their Properties. *Bioengineering (Basel),* 9.

ZHOU, L., VAN HEEL, A. J. & KUIPERS, O. P. 2015. The length of a lantibiotic hinge region has profound influence on antimicrobial activity and host specificity. *Front Microbiol,* 6**,** 11.

ZHOU, L., VAN HEEL, A. J., MONTALBAN-LOPEZ, M. & KUIPERS, O. P. 2016. Potentiating the Activity of Nisin against Escherichia coli. *Front Cell Dev Biol,* 4**,** 7.

ZHOU, X., WILLEMS, R. J. L., FRIEDRICH, A. W., ROSSEN, J. W. A. & BATHOORN, E. 2020. Enterococcus faecium: from microbiological insights to practical recommendations for infection control and diagnostics. *Antimicrob Resist Infect Control,* 9**,** 130.

ZIMINA, M., BABICH, O., PROSEKOV, A., SUKHIKH, S., IVANOVA, S., SHEVCHENKO, M. & NOSKOVA, S. 2020. Overview of Global Trends in Classification, Methods of Preparation and Application of Bacteriocins. *Antibiotics (Basel),* 9.

6 Curriculum vitae

Personal Data	
Name	Julia Gottstein
Date of Birth	25.03.1992 (Bonn)
Nationality	German

Education & Work Experience	
2019 - 2023	Ph.D. student at the Institute of Biochemistry, Heinrich Heine University, Duesseldorf Germany with Prof. Dr. Sander Smits
2019	Research assistant (WHK) at the Center for Familial Breast and Ovarian Cancer of the University Hospital Cologne in the research Department Molecular Gynecologic Oncology led by Univ. Prof. Dr. med. Rita Schmutzler
2017	Master thesis at the Department of Gynecology and Obstetrics of the University Hospital in Duesseldorf. Title: Activated Signal Transduction Pathways in Therapy-resistant Ovarian Cancer Treated with Estrogen and Progesterone.
2014 - 2017	Master studies of Biochemistry at the Heinrich-Heine-University in Duesseldorf
2014	Bachelor thesis at the transplantation Diagnostics and Cell therapeutics in Duesseldorf. Title: Comparison of different generation protocols of stromal cells.
2011 - 2014	Bachelor studies of Biochemistry at the Heinrich-Heine-University in Duesseldorf
2002-2003; 2007-2011	Abitur, Erzbischöfliches Liebfrauen Gymnasium Bonn
2003-2007	German School of Washington D.C, USA

Internships	
2019	Center for Familial Breast and Ovarian Cancer of the University Hospital Cologne in the research Department Molecular Gynecologic Oncology
2014, 2016	Three internship modules at the Jülich Research Center
2015	Institute of Biochemistry I (HHU) 4 months
2011	German Center for Neurodegenerative Diseases DZNE (Bonn)

Professional Memberships	
2019-present	Member of Interdisciplinary Graduate and Research Academy
2019-present	Member of the Research Training Group GRK2158:

	Natural products and natural product analogs against therapy-resistant tumors and microorganisms: new lead structures and modes of action
2019 - present	Junior Member of „Gesellschaft für Biochemie and Molekularbiologie“ (GBM)

Conferences

2023	Opening Symposium Center for System-based Antibiotic Research – Bochum
2023	Multi Drug Efflux Systems GRC – Galveston, Texas (USA) (Poster Pitch and Poster)
	Poster Award
2022	7th International Symposium on Antimicrobial Peptides (AMP) -Paris (Poster)
2022	5th International Conference in Caparica on Antibiotic Resistance I2CAR -Lisbon (Poster)
2022	GBM Falls Conference Duesseldorf (Poster)
2022	Annual Conference of the Association for General and Applied Microbiology (Poster)
2022	Annual GRK2158 Symposium Duesseldorf (Poster and talk)
2022	GRK2158 Scientific Retreat in Radevormwald (Short talk and poster)
2021	Annual GRK2158 Symposium (online)
2020	Annual GRK2158 Symposium (online)

Workshops

2023	Method Course: Structural Studies in Modern Biology - Center for Structural Studies (CSS)
2022	Project Management Workshop “Getting it done” by impulsplus
2022	Good Manufacturing Practice Grundlagen Kurs – GMP Academy **(Certificate)**
2022	Our Diversity- Our Success for Diverse Scientific Teams
2021	Gentechnisches Arbeiten in gentechnischen Anlagen (accredited training §15 Abs. 2 S.1 Nr.3 GenTSV) (**Certificate**: Projektleiter und Beauftragter für die Biologische Sicherheit)
2019/2020	Out with it: Training for voice, speech, and body language (basic level & advanced level)
2020	Good Scientific Practice for Doctoral Researchers
2020	Research Data Management
2020	Personal Development

7 List of publications

- Furtmann F., Porta N., Hoang D.T., Reiners J., Schumacher J., **Gottstein J.**, Gohlke H., Smits S.H.J**.** (2020) Characterization of the Nucleotide-Binding Domain NsrF from the BceAB-type ABC-Transporter NsrFP from the Human Pathogen *Streptococcus agalactiae* Sci. Rep. (1):15208. doi: 10.1038/s41598-020-72237-7.

- Reiners, J., Lagedroste, M., **Gottstein, J.**, Adeniyi, E. T., Kalscheuer, R., Poschmann, G., Stuhler, K., Smits, S. H. J., and Schmitt, L. (2020) Insights in the Antimicrobial Potential of the Natural Nisin Variant Nisin H, *Front Microbiol 11*, 573614.

- **Gottstein, J.**, Zaschke-Kriesche, J.**,** Unsleber, S., Voitsekhovskaiab, I., Kulik, A., Behrmann, L. V., Overbeck, N., Stühler, K., Stegmann, E., Smits, S. H. (**2022**) New insights into the resistance mechanism for the BceAB-type transporter SaNsrFP. *SciRep* 12, 4232. https://doi.org/10.1038/s41598-022-08095-2

- **Gottstein J.**, Klose H., Knospe C.V., Reiners J., Smits S.H., Schmitt L. (2021) Lantibiotika – hoffnungsvolle Alternative gegen Antibiotikaresistenz? Biospektrum

Acknowledgment

Zum Schluss meiner Dissertation möchte ich mich bei all denjenigen Personen bedanken, die mich durch alle Höhen und Tiefen in dieser Zeit begleitet und unterstützt haben.

Ich danke Sander, dass er mir dieses tolle Projekt anvertraut hat. Es hat mir sehr viel Spaß gemacht an den verschiedenen Themen zu forschen und ich danke ihm für die gute Zusammenarbeit, die vielen Ratschläge, wertvolle Feedbacks, Tipps und Tricks für tolle Präsentationen. Ich danke Sander für die Inspiration, Ideen und Motivation in der Forschung und für die tollen Erlebnisse (die tollen Konferenzen VAAM, I2CAR in Lissabon, GBMFalls, AMP in Paris, Gordon Texas, Bochum), die er und das GRK2158 mir ermöglicht haben. Das waren unvergessliche Erlebnisse, die ich nicht vergessen werde! Dank Sander habe ich gelernt, dass man Freude an der Forschung haben kann und wie man diese Freude vermittelt. Zudem danke ich ihm für seine Geduld und Vertrauen in mich und den Optimismus, den er mir entgegengebracht hat. Ich danke ihm dazu noch für die Freiheit, die er mir in meiner Arbeitszeit gegeben hat, die es mir ermöglicht hat auf meine Gesundheit zu achten und mit maximaler Energie in den Arbeitstag zu starten.
Zudem möchte ich mich bei ihm für die tolle, offene, konstruktive und fröhliche Arbeitsatmosphäre bedanken. Es macht einen großen Unterschied, wenn man schallendes Gelächter beim Arbeiten hört oder man untereinander Witze reißen kann.
Ich danke ihm für das Verständnis und die Unterstützung, die er mir in den schweren Zeiten, die meine Familie durchlebt hat entgegengebracht hat, das werde ich nie vergessen. Ich danke Sander dafür, dass er Supervisor, Mentor, Betreuer, Motivator und kreative Inspiration für mich war. Danke für die tolle Zeit.

Vielen Dank an Lutz Schmitt für die Möglichkeit meine Promotion im Institut für Biochemie machen zu können und vor allem für gute Feedbacks während der Gruppenmeetings. Zudem möchte ich mich bei ihm für die tolle Möglichkeit bedanken auf die Gordon Konferenz nach Galveston Texas zu fahren! Das war einmalig.

Vielen Dank auch an PD Ulrich Schulte. Er war für mich Betreuer, Mentor und Ansprechperson während meines Studiums und konnte, wenn es Probleme gab sofort helfen. Er hat uns als junge Naturwissenschaftler bei unserer Ausbildung als Biochemiker begleitet, unterstützt und geprägt, dafür bin ich sehr dankbar. Ulrich Schulte war mein Zweitbetreuer sowohl in der Bachelor- als auch in der Masterarbeit. Er war auch bei beiden Abschlussvorträgen von mir anwesend und hat interessiert Fragen gestellt. Als ich meine Doktorarbeit angefangen hatte und Praktika betreut habe, habe ich ihn als einen hilfsbereiten und großzügigen Arbeitskollegen kennengelernt, der den Studenten und allen anderen auch immer freundlich gesinnt war. Ein für mich prägender Moment war die „Pizzaparty“ auf dem Dach des alten Instituts, die Ulrich für die Praktikumsbetreuer nach Beendigung des Praktikums organisiert hatte. So konnte ich wahrnehmen, dass auch durch seinen Einfluss eine kollegiale und freundliche Arbeitsatmosphäre geschaffen wurde. Als Doktorandin habe ich diese gute Arbeitsstimmung auch

zwischen den Chefs miterlebt: oft konnte man die Chefs zusammen (Lutz, Sander und Ulrich) schallend Lachen hören…was einen auch selbst angesteckt hat zu lachen.

Ich möchte mich bei Professor Dr. Holger Gohlke für die Übernahme des Koreferats und die gute Zusammenarbeit im GRK2158 bedanken.

Vielen Dank an Jan für die gute Übernahme der Koordination der Praktika und für witzige Gespräche zwischendurch.

Ich danke auch Julia Schumacher für die Start-Hilfe im Labor und der Einarbeitung im Labor. Danke auch, dass ich dich bei Fragen erreichen konnte.

I now want to thank my favorite ladies from our “international office”. You were and still are my support, inspiration, food buddies, cappuccino buddies, and female scientist role models. It was such a fun time with you and I am forever grateful for meeting you, being with me, and rocking the science world: I love you very dearly and I will never forget you!

I thank Zohreh for being my support at the beginning year of my Ph.D. when I had questions, doubts, or just needed someone to talk to. Thank you for being patient, and teaching me how to use the PCR cycler, and thanks for listening to my curious questions! I enjoyed our scientific and non-scientific conversations about different topics, our little trip to the Café in Bilk, and our office girls outing to the Persian restaurant! You are one of my inspirations for hard and diligent work. You have made my Ph.D. start fun and enjoyable! I am so grateful to have met you and I am glad to have you as a friend.

I thank Feby for all the good and long conversations, for the support as a great friend, to listen to my stories, and for laughing and crying with me during these years. For all the shared food and new knowledge about South Indian culture, for dancing and making jokes with me. I love how we can laugh about random things and how we can overcome little and big problems. It was also really comforting to have a friend in the same (late) shift as kind, loving, and positive as you. We have spent so much time together and thanks to you these roller coaster three years have been the most fun and enjoyable time.

A big thank you goes to Sakshi for being my motivation, and inspiration, and for being a great kind, and loving friend. Thank you for listening to my problems, worries, and stories, and for being there during the good and the difficult times. I learned so much from you be it project-related knowledge, how to work hard, what it means to be a scientist, to roam around and be hungry for good food, to discover new places, and how to enjoy and learn the most at conferences. Thank you for accompanying me on a lot of late-night after-work dinners. All discussions with you are really valuable and thanks to you I feel I came to cherish and understand science life.

Another big thank you goes to Athanasios for being one of my first good friends in the lab, for listening to my problems when something didn´t work, and for giving helpful advice. Especially, I want to thank him for sharing valuable knowledge, for inspiring me to become a hard worker and to teach me what it means to have grit

in science. Thank you for all the support you have shown during this time, be it a motivational talk when I was in doubt, for sharing food unexpectedly, in moments I really needed it, or for offering a ride when I had to stay late. Thank you for being the role model that inspired me to go beyond my comfort zone and really invest my time into science. You are a great scientist and truly a genius of hard work. I am looking forward to your scientific future.

I express my thanks to Martina who supports our institute like no other. Thank you for your patient explanations to naïve questions in the beginning and sometimes on other occasions. Thank you for knowing about the most important things and for always helping out whenever something breaks. Also thank you for the rides you offered.
I am also thanking Silke for finding cryos and plasmids and helping out with the data documentation.
I also thank Corinna for every issue concerning things that were not taken over the GRK2158.

I also sincerely thank Jens who supervised me during my master's internship, taught me a lot, and also helped me when the machines broke or were not properly working (HPLC, Äkta etc…). Thank you for your advice at all times and for the spontaneous rides home when you found me working in the lab in the middle of the night. Also, thanks for measuring SAXS!

I also thank Alex for the fun pickup rides to Korean restaurants or any restaurants during Corona times. It was a fun time working numerous weekends in the lab, at least we cooked/ ordered and ate good food!

I thank Eymen for the fun late shift time and long conversations. Joking around with him and the bro, and talking about interesting things made working in the lab always a nice experience. Thanks also for the scientific input and MALS measurements!

I also want to thank Marten for very good input on science, life philosophy, and good conversations!! Thanks for the pep talks and for lots of laughter and jokes in between!

I am also thanking my Nisin subgroup members Hans and Vivi for their scientific input and fun conversations. It was an awesome time working with them, going to the AMP conference, making fun memories, and even founding the Japanese Course for PhDs and also ordering lots of food. It was always a nice atmosphere in the lab.

A sincere thank you also goes to the AKTA team Florestan and Manuel who saved various experiments/ solving Äkta issues or gave advice on purification results. Thanks for the helpful discussions!

Big thanks go to Martina Holz who coordinated everything concerning my 3.5 years PhD in the GRK2158. Thanks for organizing nice events, symposia and for giving me advice on how to do all the paperwork concerning conferences. Also, I am grateful to have had the opportunity to go to so many conferences which would not have been possible without funding from the GRK2158.

I also thank Stefanie and Violetta from the CSS for the nice collaboration and crystallization attempts with the ECD!

I also thank Lea for being a fun conference company and being organized and prepared. It was a really nice time in Galveston Texas.
I also thank Steffi for the nice conversations about food during lunch break.

I want to thank Maryna, Michael, Max, and Alexej for the fun conversations, making jokes, and giving nice scientific advice, meeting sometimes on the weekend on the way to work. It has been a fun time!

Then I also want to thank Sergiy for the fun conversations, the exchange of newly acquired knowledge in science, and the fun bus rides. You are a smart and bright person; I know you can do it!

I want to thank the new Ph.D. Kira, Cigdem, Neele, Christian, Sergiy, and Max. You are a cool and bright group and I am sure you will rock your projects.

I thank all my students: Sophie, Maike, Claire, Nhi, and Kira for contributing nicely to my projects! I really enjoyed supervising you. I hope you experienced how fun and interesting science can be! All the best on your path!

I also want to thank my soon-to-be supervisor, Miriam Kutsch! The short time I have known you has been fun and made me look forward to a great time working in the lab together!

I am very grateful to my dear best friends who accepted my crazy scientific life and supported me during the ups and downs, the busy days, and the difficult days and celebrated the successful days with me. Life with you is a colorful burst of energy …it never gets boring. Thank you for being there for me, and accepting me as I am.

From the bottom of my heart, I want to thank my family for all the love, support, care packages, motivation, and phone calls that helped me endure the up and downs of the Ph.D. Without them, this journey would have been impossible for me. I am grateful to be granted the trust and belief that everything will be all right, that I can do everything, and that they will be proud no matter the result. It is empowering to know that they are believing in me and supporting my dreams.

Lastly, I want to commemorate my dear grandmother in Peru and grandparents in Germany who sadly passed away during my path to becoming a scientist. They have supported my curiosity and creativity and showed great interest in my life. Thank you for supporting my dreams and believing in me.

Declaration

Ich, Julia Gottstein, versichere an Eides statt, dass die vorliegende Dissertation von mir selbstständig und ohne unzulässige fremde Hilfe unter Beachtung der „Grundsätze zur Sicherung guter wissenschaftlicher Praxis an der Heinrich-Heine-Universität Düsseldorf“ erstellt worden ist.
Diese Dissertation wurde in der vorgelegten oder in ähnlicher Form noch bei keiner anderen Institution eingereicht. Ich habe bisher keine erfolglosen Promotionsversuche unternommen.

Düsseldorf, den

(Julia Gottstein)